frontiers | Research Topics

Innate immunity and intercellular communication

Edited by
Toshiyuki Shimizu and Hang Yin

Published in
Frontiers in Immunology

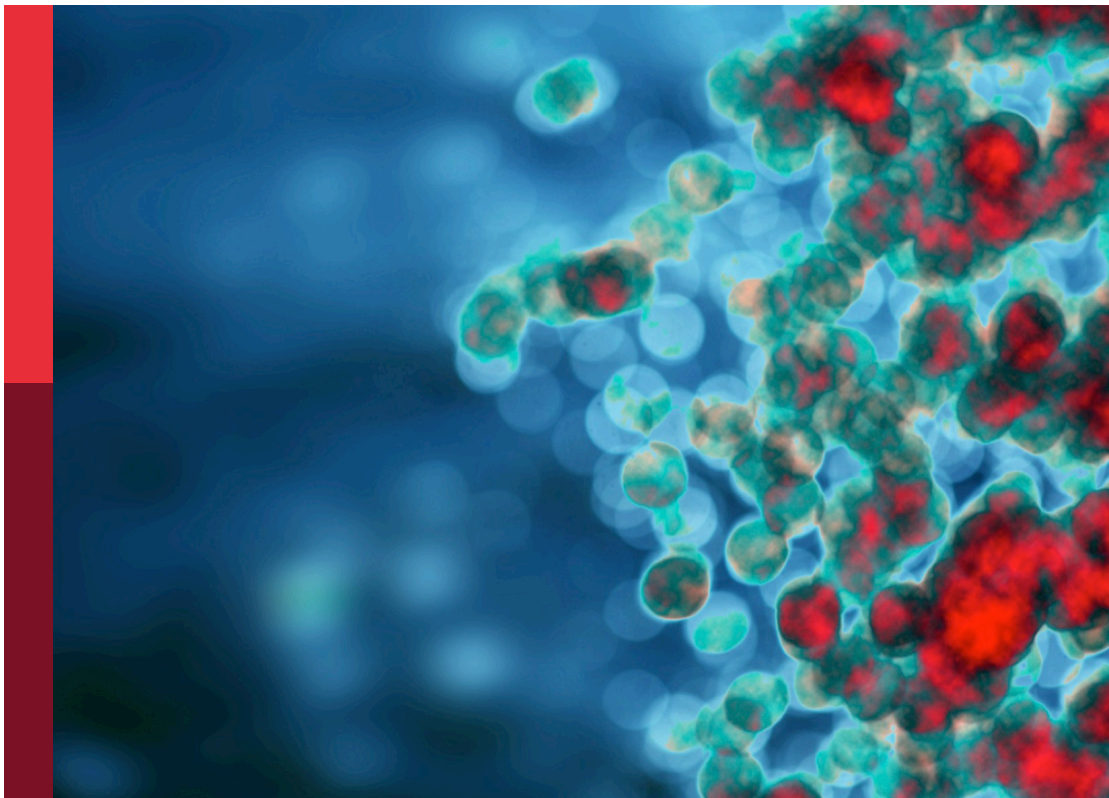

ISSN 1664-8714
ISBN 978-2-83251-209-8
DOI 10.3389/978-2-83251-209-8

About Frontiers

Frontiers is more than just an open access publisher of scholarly articles: it is a pioneering approach to the world of academia, radically improving the way scholarly research is managed. The grand vision of Frontiers is a world where all people have an equal opportunity to seek, share and generate knowledge. Frontiers provides immediate and permanent online open access to all its publications, but this alone is not enough to realize our grand goals.

Frontiers journal series

The Frontiers journal series is a multi-tier and interdisciplinary set of open-access, online journals, promising a paradigm shift from the current review, selection and dissemination processes in academic publishing. All Frontiers journals are driven by researchers for researchers; therefore, they constitute a service to the scholarly community. At the same time, the *Frontiers journal series* operates on a revolutionary invention, the tiered publishing system, initially addressing specific communities of scholars, and gradually climbing up to broader public understanding, thus serving the interests of the lay society, too.

Dedication to quality

Each Frontiers article is a landmark of the highest quality, thanks to genuinely collaborative interactions between authors and review editors, who include some of the world's best academicians. Research must be certified by peers before entering a stream of knowledge that may eventually reach the public - and shape society; therefore, Frontiers only applies the most rigorous and unbiased reviews. Frontiers revolutionizes research publishing by freely delivering the most outstanding research, evaluated with no bias from both the academic and social point of view. By applying the most advanced information technologies, Frontiers is catapulting scholarly publishing into a new generation.

What are Frontiers Research Topics?

Frontiers Research Topics are very popular trademarks of the *Frontiers journals series*: they are collections of at least ten articles, all centered on a particular subject. With their unique mix of varied contributions from Original Research to Review Articles, Frontiers Research Topics unify the most influential researchers, the latest key findings and historical advances in a hot research area.

Find out more on how to host your own Frontiers Research Topic or contribute to one as an author by contacting the Frontiers editorial office: frontiersin.org/about/contact

Innate immunity and intercellular communication

Topic editors
Toshiyuki Shimizu — The University of Tokyo, Japan
Hang Yin — Tsinghua University, China

Topic Coordinator
Ying Zhang — Tsinghua University, China

Citation
Shimizu, T., Yin, H., eds. (2023). *Innate immunity and intercellular communication*. Lausanne: Frontiers Media SA. doi: 10.3389/978-2-83251-209-8

The authors declare that the research was conducted in the absence of any commercial or financial relationships that could be construed as a potential conflict of interest.

Table of contents

frontiers | Frontiers in Immunology

TYPE Editorial
PUBLISHED 19 December 2022
DOI 10.3389/fimmu.2022.1102776

OPEN ACCESS

EDITED AND REVIEWED BY
Francesca Granucci,
University of Milano-Bicocca, Italy

*CORRESPONDENCE
Toshiyuki Shimizu
shimizu@mol.f.u-tokyo.ac.jp
Hang Yin
yin_hang@tsinghua.edu.cn
Ying Zhang
z_ying@mail.tsinghua.edu.cn

SPECIALTY SECTION
This article was submitted to Molecular Innate Immunity, a section of the journal Frontiers in Immunology

RECEIVED 19 November 2022
ACCEPTED 08 December 2022
PUBLISHED 19 December 2022

CITATION
Xiao Y, Zhang Y, Yin H and Shimizu T (2022) Editorial: Frontiers on innate immunity and intercellular communication.
Front. Immunol. 13:1102776.
doi: 10.3389/fimmu.2022.1102776

Editorial: Frontiers on innate immunity and intercellular communication

Yu Xiao[1,2], Ying Zhang[2*], Hang Yin[2*] and Toshiyuki Shimizu[3*]

[1]Department of Laboratory Medicine, Zhujiang Hospital, Southern Medical University Guangzhou, Guangdong, China, [2]School of Pharmaceutical Sciences, Tsinghua University, Beijing, China, [3]Graduate School of Pharmaceutical Sciences, The University of Tokyo, Tokyo, Japan

KEYWORDS

innate immunity, intercellular communication, extracellular vesicle, TLR, nod like receptor

Editorial on the Research Topic
Innate immunity and intercellular communication

Introduction

As one of the important components of the primary defense system, the innate immune system can be rapidly deployed in organisms against microbial infections upon activation. Both pathogen-associated molecular patterns (PAMPs) and damage-associated molecular patterns (DAMPs) activate innate immune pattern recognition receptors to trigger downstream inflammatory responses and other immune responses. Therefore, elaborating more detailed mechanisms for the precise regulation of innate immunity has important implications for the treatment of human diseases.

Various soluble factors and particles in body fluids mediate immunological, long-distance intercellular communication. In the past decades, the investigation of extracellular vesicles (EVs), a group of nano-size particles with lipid bilayer membranes that carry particular cellular contents of parent cells, is a paradigm shift for traditional intercellular communication mechanisms and ushers in a new research interest for cell-to-cell communication mechanisms. EVs may raise the alarm for innate immune responses or silence them *via* the transfer of cargo biomolecules between cells to affect intracellular communication (1).

This Research Topic encompasses a collection of reviews, opinions, perspectives, as well as primary research articles investigating Innate Immunity and Intercellular Communication.

Exploration of the unknown in innate immunity

Although innate immune signaling pathways have been well investigated, there are still have many aspects in this area that need more in-depth study. The scientific researchers involved in the current Research Topic introduce us to some interesting research directions, pointing towards future research possibilities.

Pathogen constituents, including microbial lipids and nucleic acids (NAs), are able to activate Toll-like receptor (TLR) signaling pathways. To prevent unnecessary autoimmune responses, NA-sensing TLRs are localized in the endosomal compartment. With the degradation of NAs in endosomal compartment, TLR subfamilies are less activated by self-derived NAs. Surprisingly, NA degradation products were found to be effective TLRs ligands. Miyake et al. summarize recent findings of how dysregulation of NA metabolism affects TLR responses and their relationship with diseases.

Unlike the TLR family, nucleotide-binding and oligomerization domain (NOD)-like receptors (NLRs) have different subcellular localization and complex caspase reaction signals. However, limited structural evidence restrained the understanding of NLR activation mechanism. Ohto's review introduces the mechanisms of activity regulation and signal transduction as revealed by structural biology studies conducted over the past decade. These detailed structural biology studies are expected to aid further development of therapeutic agents.

Ym1 is a widely confirmed M2 polarization marker, but there is still a lack of research on its function. Kang et al.'s review highlights the relationship between Ym1 and diseases such as allergic lung inflammation, parasitic infection, autoimmune diseases and nervous system diseases.

Protein tyrosine phosphatases (PTPs) remove phosphates from tyrosine residues in some proteins. Luo et al. found an SH2-domain-containing PTP named LvPTPN6 in *Litopenaeus vannamei* and reveal the mechanism whereby LvPTPN6 enhances the antiviral immunity of shrimp *via* the JAK/STAT signaling pathway.

Extracellular traps (ETs) of neutrophils are widely reported in both animals and plants, where they play a vital role in killing invading microbes. Liao et al.'s review summarize the mechanism through which bacteria, fungal pathogens and parasites use nucleases to evade the ETs of the host.

Both innate and adaptive immune processes involve hemichannels (HC)/gap junctions (GJs) and immunoglobulin (Ig)-like domain-containing proteins (IGLDCPs). Meng et al. summarize the current understanding of HC-released immune signaling factors that influence IGLDCPs in regulating innate/adaptive immunity.

HMGB1 can function as a DAMP outside the cell, activating the immune system and promoting inflammation. Gao et al. show that HMGB1 mobilization was completely inhibited by selective H1-receptor antagonists, suggesting that histamine induces HMGB1 release from vascular endothelial cells through H1 receptor stimulation. Anti-HMGB1 antibodies may become a new therapeutic option.

Development of disease therapy strategies

Cannabidivarin (CBDV) is a non-psychoactive phytocannabinoid found in plants of the *Cannabis* species. Wang et al. demonstrate that CBDV has anti-neuroinflammatory effects through direct binding to MD2, possibly acting as an antagonist of TLR4. CBDV further mediates analgesic effects by inhibiting morphine-induced glial activation. CBDV could be a potential agent for improving morphine-mediated analgesia.

ACT001 was proven to be an anti-tumor drug. In Tianshu Zhang et al.'s work, ACT001 effectively reduced the peripheral injury and activation of microglia and astrocyte *via* inhibiting the formation of TLR4/MD2/MyD88 complex. Their work provides strong evidence for ACT001's potential in the treatment of neuropathic pain.

Investigating roles of EVs in innate immunity

EVs are known as a novel carrier of MAMPS and DAMPs. Therefore, studying isolation methods and mechanisms for EVs is helpful for the investigation of the function of EVs in innate immunity.

Although gut bacteria cannot easily cross the complex gut-blood barrier into circulation, a large number of studies have shown that both gram-positive and -negative EVs can be detected in circulation. Wei et al. presents a new bioanalytical technology for the purification of bacterial extracellular vesicles (BEVs), which contain various bioactive compounds and thus can be further used as therapeutic approaches for modulating innate immune responses of host cells. Epsilon-poly-L-lysin (ϵ-PL) is useful for collecting BEVs, and BEVs purified by ϵ-PL (ϵ-PL BEVs) are comparable to those concentrated by ultracentrifugation.

In aging individuals, chronic inflammation is widely observed, but the biological functions of EVs are still beyond investigation. Xiao et al. found that senescent fibroblasts in the aging microenviroments release larger amounts of miR-30b-5p containing EVs. These EVs can specifically activate the classical NF-kB signaling pathway *via* releasing miR-30b-5p into recipient cells.

Conclusion

The Research Topic of 'Innate Immunity and Intercellular Communication' has gathered numerous worthy investigations

and contributions on the subject of innate immune signaling pathways and intercellular communication, offering us research tactics and insights into new research direction on new players in signaling pathways. The articles in this collection highlight important interrelated topics and will hopefully serve as a catalyst for further studies such as elucidation of mechanisms involved in signaling pathways in innate immune responses. Ultimately, we trust that these efforts may eventually lead to the development of new anti-inflammatory drugs and bioengineering techniques for theranostics.

Author contributions

YX and TS completed the draft manuscript. And all authors listed have made a substantial, direct, and intellectual contribution to the work and approved it for publication.

Funding

This work was supported by the National Natural Science Foundation of China Grant (21825702, 22137004, 21977061), Beijing Advanced Innovation Center for Structural Biology Funding no. 20151551402, Beijing Outstanding Young Scientist Program Grant (BJJWZYJH01201910003013) and National Key R&D Program of China no. 2021YFE0109300.

Acknowledgments

We thank the participation and attention to this research topics of all authors and readers.

Conflict of interest

The authors declare that the research was conducted in the absence of any commercial or financial relationships that could be construed as a potential conflict of interest.

Publisher's note

References

1. Xiao Y, Driedonks T, Witwer KW, Wang Q, Yin H. How does an RNA selfie work? EV-associated RNA in innate immunity as self or danger. *J Extracell Vesicles* (2022) 9(1):1793515.

frontiers | Frontiers in Immunology

ORIGINAL RESEARCH
published: 09 June 2022
doi: 10.3389/fimmu.2022.873054

ACT001 Inhibits TLR4 Signaling by Targeting Co-Receptor MD2 and Attenuates Neuropathic Pain

Tianshu Zhang[1,2,3], *Cong Lin*[1,2*], *Siru Wu*[1,2], *Sha Jin*[4], *Xiaodong Li*[5], *Yinghua Peng*[6*] *and Xiaohui Wang*[1,2,3,7*]

[1] Laboratory of Chemical Biology, Changchun Institute of Applied Chemistry, Chinese Academy of Sciences, Changchun, China, [2] School of Applied Chemistry and Engineering, University of Science and Technology of China, Hefei, China, [3] State Key Laboratory of Natural and Biomimetic Drugs, Peking University, Beijing, China, [4] State Key Laboratory of Polymer Physics and Chemistry, Changchun Institute of Applied Chemistry, Chinese Academy of Sciences, Changchun, China, [5] Beijing Changping Huayou Hospital, Beijing, China, [6] Institute of Special Animal and Plant Sciences, Chinese Academy of Agricultural Sciences, Changchun, China, [7] Beijing National Laboratory for Molecular Sciences, Beijing, China

OPEN ACCESS

Edited by:
Hang Hubert Yin,
Tsinghua University, China

Reviewed by:
Yinan Wang,
The First Hospital of Jilin University, China
Shun-Fen Tzeng,
National Cheng Kung University, Taiwan

***Correspondence:**
Cong Lin
cong.lin@ciac.ac.cn
Yinghua Peng
pengyinghua@caas.cn
Xiaohui Wang
xiaohui.wang@ciac.ac.cn

Specialty section:
This article was submitted to Molecular Innate Immunity, a section of the journal Frontiers in Immunology

Received: *10 February 2022*
Accepted: *03 May 2022*
Published: *09 June 2022*

Citation:
Zhang T, Lin C, Wu S, Jin S, Li X, Peng Y and Wang X (2022) ACT001 Inhibits TLR4 Signaling by Targeting Co-Receptor MD2 and Attenuates Neuropathic Pain. Front. Immunol. 13:873054. doi: 10.3389/fimmu.2022.873054

Neuropathic pain is a common and challenging neurological disease, which renders an unmet need for safe and effective new therapies. Toll-like receptor 4 (TLR4) expressed on immune cells in the central nervous system arises as a novel target for treating neuropathic pain. In this study, ACT001, an orphan drug currently in clinical trials for the treatment of glioblastoma, was identified as a TLR4 antagonist. *In vitro* quenching titrations of intrinsic protein fluorescence and saturation transfer difference (STD)-NMR showed the direct binding of ACT001 to TLR4 co-receptor MD2. Cellular thermal shift assay (CETSA) showed that ACT001 binding affected the MD2 stability, which implies that MD2 is the endogenous target of ACT001. *In silico* simulations showed that ACT001 binding decreased the percentage of hydrophobic area in the buried solvent-accessible surface areas (SASA) of MD2 and rendered most regions of MD2 to be more flexible, which is consistent with experimental data that ACT001 binding decreased MD2 stability. In keeping with targeting MD2, ACT001 was found to restrain the formation of TLR4/MD2/MyD88 complex and the activation of TLR4 signaling axes of NF-κB and MAPKs, therefore blocking LPS-induced TLR4 signaling downstream pro-inflammatory factors NO, IL-6, TNF-α, and IL-1β. Furthermore, systemic administration of ACT001 attenuated allodynia induced by peripheral nerve injury and activation of microglia and astrocyte *in vivo*. Given the well-established role of neuroinflammation in neuropathic pain, these data imply that ACT001 could be a potential drug candidate for the treatment of chronic neuropathic pain.

Keywords: neuropathic pain, toll-like receptor 4, myeloid differentiation protein 2, chronic constriction injury, ACT001

1 INTRODUCTION

Neuropathic pain is a chronic and pathological disease resulting from nerve injury or inflammation which remains poorly managed by currently available therapeutics (1). Most of these therapeutics target neurons (2). Recently considerable investigations demonstrate that glia also plays a key role in neuropathic pain outcomes (3, 4). Once the peripheral nerve is injured, glial cells become activated and release pro-inflammatory cytokines, chemokines, and other inflammatory mediators such as nitric oxide (NO), which contributes to the maintenance of neuronal central sensitization (4, 5). Therefore, resetting the activated glia to the resting state and blocking the neuroinflammation would be a useful intervention strategy for treating neuropathic pain.

Toll-like receptor 4 (TLR4) is a pattern recognition receptor (PRR), which is responsible for the recognition of pathogen-associated molecular patterns (PAMPs), damage-associated molecular patterns (DAMPs), and xenobiotic-associated molecular patterns (XMAPs) (6). Lipopolysaccharide (LPS), a component of the outer membrane of Gram-negative bacteria, is a natural ligand of TLR4 (6). In the central nervous system (CNS), TLR4 is primarily expressed on microglia (7), functioning mainly in the regulation of pro-inflammatory factors production. Injured sensory neurons may release extracellular matrix molecules and DAMPs, which are detected by TLR4 thus activating immunocompetent cells and exerting the influence on the neural pain (7, 8). Therefore, TLR4 antagonists could be potential therapeutics for treating neuropathic pain. However, there are rare TLR4 antagonist that cross the blood-brain barrier (BBB).

ACT001 (also known as dimethylaminomicheliolide, DMAMCL), derived from parthenolide (9), displays anti-tumor activities in various cancers, including hepatocellular carcinoma, breast cancer, and glioblastoma (10–13). As a promising drug for the treatment of glioblastoma, ACT001 has an excellent effect on restraining the growth of glioblastoma in Phase I clinical trials and now it is currently undergoing Phase II clinical trials (14, 15). ACT001, which can penetrate the blood–brain barrier (BBB) and accumulate in the brain, alleviates glial activation and neuroinflammation (16, 17). As a foreign substance in CNS, it is not surprising that ACT001 would perturb the CNS immunity (16, 17). TLR4 is the key PRR of innate immune system, which detects PAMPs (18), DAMPs (19) and XMAPs (20, 21). It would be interesting to explore whether ACT001 acts as a XAMP and can be sensed by myeloid differentiation 2 (MD2), an accessory protein of TLR4 responsible for the recognition of ligand. This study found that ACT001 bound to MD2 and inhibited LPS-induced formation of TLR4/MD2/MyD88 complex and the activation NF-κB and MAPKs, therefore suppressing LPS-induced pro-inflammatory factors. Moreover, intravenous injection of ACT001 attenuated allodynia induced by peripheral nerve injury and lumbar spinal cord dorsal horn expression of Iba-1 (a microglial activation marker) and GFAP (an astrocyte activation marker) *in vivo*. These data implicate that ACT001 has the potential for treating neuropathic pain.

2 MANUSCRIPT FORMATTING

2.1 Materials and Methods

2.1.1 Materials

ACT001 was kindly provided by Tianjin Shangde Pharmaceutical Margin Technology Co., Ltd. Microglial BV-2 cells were obtained from China Center for Type Culture Collection. Ultrapure lipopolysaccharide (LPS), HEK Blue TLR4 293 cells, and HEK-Blue Selection were obtained from Invivogen. Phospha-Light™ SEAP Reporter Gene Assay System was purchased from Applied Biosystems. Dual-Glo Luciferase Assay System was purchased from Promega. Crystal violet, 2,3-diaminonaphthalene, protease inhibitor cocktails, and anti-β-actin antibodies were purchased from Sigma-Aldrich. Dulbecco's Modified Eagle Medium (DMEM), TRIzol, RIPA buffer were purchased from Thermo Fisher Scientific. Fetal bovine serum was purchased from PAN-Seratech. RNeasy Mini Kit, RT² Easy First Strand cDNA Synthesis Kit, PCR primers and SYBR Green PCR Master Mix were obtained from Qiagen. Primary MD2 antibody, anti-Iba1 antibody, anti-TLR4 antibody and anti-GFAP antibody were purchased from Abcam. Primary antibodies targeting MyD88, p38 MAPK, NF-κB p65, ERK (1/2), IKK-β, SAPK/JNK, phospho-NF-κB p65, phospho-ERK(1/2), phospho-SAPK/JNK, phospho-IKK-α/β, and phospho-p38 MAPK antibodies were obtained from Cell Signaling Technology.

2.1.2 Fluorescence Titrations of MD2 With ACT001

MD2 expression and purification were performed as described previously (22, 23). Fluorescence titrations of MD2 with ACT001 were performed on a Cary Eclipse spectrofluorometer. All measurements were carried out at room temperature using a 2×10 mm quartz cell with MD2. The fluorescence titration was carried out at a wavelength of 280 nm to excite the Tyr and Trp residues in MD2. Emission at 310-450 nm was measured. 0.5 μM MD2 was titrated with different concentrations of ACT001 and fluorescence intensity at 337 nm was plotted against ACT001 concentration.

2.1.3 Saturation Transfer Difference (STD) NMR Measurement

MD2 was prepared in a phosphate buffer in D_2O (75 mM potassium phosphate, 150 mM sodium chloride, pH 7.5)and ACT001 was dissolved in DMSO-d6 (50 mM) as stock solution. Saturation transfer difference NMR spectroscopy experiments were performed to investigate ligand-protein interactions. NMR spectra were acquired at 25 °C in a Bruker Avance III-600 MHz (proton frequency) spectrometer with a conventional inverse 5 mm probe head with z-gradients using standard Bruker pulse programs. Samples containing 400 μM ACT001 in the absence or presence of MD2 (4 μM) in D_2O buffer were used for NMR spectra data acquisition.

2.1.4 Cellular Thermal Shift Assay (CETSA)

Cellular thermal shift assay (CETSA) was performed as described (21).

2.1.5 *In Silico* Simulations

2.1.5.1 System Preparation and Docking

The structure of ACT001 was drawn through Gauss View 6 (24) and optimized by Gaussian 09 (25) software using the B3LYP density functional method and 6-31G (d,p) basis set. The X-ray structure of MD2 was extracted from TLR4/MD2 complex (PDB ID: 2Z64) and was used for molecular docking and molecular dynamics simulations. Missing hydrogen atoms of MD2 were added by Maestro under pH 7.0 (26). Molecular docking was conducted through AutodockVina 1.1.2 in a box of $50 \times 60 \times 50$ $Å^3$, which covers MD2 protein completely (27). The most favorable binding site was searched and located by the Iterated Local Search Globule Optimizer (28, 29). MD2 was considered rigid and ACT001 was regarded as semi-flexible during molecular docking. Ten docking poses were generated by AutodockVina 1.1.2 and ranked according to their affinity with MD2. Of all the docking poses, the pose with the best affinity to MD2 was chosen for further simulations.

2.1.5.2 Molecular Dynamics Simulation

MD2 alone (apo-MD2) and the best docking pose of MD2 interacting with ACT001 were further studied through molecular dynamics simulations by the NAMD2.12 package (30) with AMBER ff03 force field (31, 32). R.E.D was used to optimize and fit the atomic charges of ACT001 based on the quantum mechanics calculations (33). The general AMBER force field (GAFF) was used to treat other atomic parameters (32). A TIP3P model of a water box was used to solvate all solutes with a distance of 10 Å between the protein and the edge of the box. Na^+ and Cl^- ions were added to neutralize the system with a concentration of 0.15 M. Energy minimization was performed for 5000 steps first and the system was heated to 310 K in 310 ps with 1 ns equilibration. The system was further run in the isothermal-isobaric (NPT) ensemble at a temperature of 310 K for 400 ns. SHAKE algorithm was used to restrain all bonds involving hydrogen (29). Calculations of long-range electrostatic interactions were performed by the Particle-mesh Ewald (PME) summation method (34). Langevin dynamics was used to keep the temperature of the system at 310 K with the collision frequency of 5 ps^{-1} and the pressure was set at 1 atm with Nosé–Hoover Langevin piston method (35).

The RMSD (root-mean-square deviation) and RMSF (root-mean-square fluctuation) analyses were performed through VMD (36) and Bio3D package (37), respectively. The interactions between MD2 and ACT001 were analyzed by $LigPlot^+$ (38) and PyMol (39) software. The ratio of hydrophobic SASA (solvent accessible surface areas) in buried SASA was calculated as specified before (20).

2.1.6 Nitric Oxide (NO) Assay

BV-2 cells were cultured in supplemented DMEM (10% FBS, 50 U/mL penicillin, and 50 μg/mL streptomycin) and seeded at a density of 4×10^4 cells per well in 96-well plates. After overnight incubation, media was aspirated and changed to DMEM media without FBS. Cells were then treated with LPS (200 ng/mL) and the indicated concentrations of ACT001. The NO concentration in the culture supernatant was determined by the 2,3-diaminonaphthalene-based fluorescent method as described (23).

2.1.7 BV-2 Cells Morphology

BV-2 cells were cultured as above and treated with LPS (200 ng/mL) and 100 μM ACT001 for 6 h. Cell morphology images were collected by a Nikon microscope.

2.1.8 Cell Viability Assay

Cellular viability was determined by the crystal violet staining method and CCK-8 Kit as described (23, 40).

2.1.9 Secreted Embryonic Alkaline Phosphatase (SEAP) Assay

SEAP assay was performed as described (40).

2.1.10 Dual-Luciferase NF-κB Reporter Assay

Dual-luciferase NF-κB reporter assay was performed as described (40).

2.1.11 Co-Immunoprecipitation (Co-IP)

BV-2 cells were seeded at 4×10^6 cells/dish in 100 mm culture dishes. After 24 h incubation, cells were stimulated by LPS (200 ng/mL) and indicated concentrations of ACT001 for 1 h. Cells were washed twice with ice-cold PBS and lysed in 1 mL Co-IP lysis buffer (25 mM Tris pH 8.0, 150 mM KCl, 5 mM EDTA, 0.5% NP-40) with a complete protease inhibitor cocktail, 1 mM DTT, and 1 mM PMSF by incubating on ice for 30 min. Cell supernatant was collected *via* centrifugation at 12,000 g at 4 °C for 12 min and incubated with corresponding primary antibody at 4 °C overnight. Washed magnetic beads were then incubated with the samples at room temperature for 1 h. The magnetic beads were washed twice with PBS and boiled with 50 μL 2 × SDS sample buffer at 100 °C for 8 min for immunoblotting.

2.1.12 Immunoblotting

Immunoblotting was performed as described (23).

2.1.13 qRT-PCR

BV-2 cells were seeded at a density of 4×10^5 cells/well in 6-well plates. After overnight incubation, BV-2 cells were treated with LPS (200 ng/mL) and indicated concentrations of ACT001 for 6 h. Total RNA was isolated from BV-2 cells using TRIzol reagent and cDNA was generated with an oligo (dT) primer. Primer sequences are shown in **Table 1**. The ribosomal protein L27 gene RPL27 was used as the internal control. qPCR was performed on a TOptical Real-Time qPCR Thermal Cycler (Analytik Jena, Thuringia, Germany) using the SYBR Green method. The data were analyzed by the $2^{-\Delta\Delta CT}$ method and were normalized to RPL27.

2.1.14 *In Vivo* Study

2.1.14.1 Animals and Drug Treatment

Pathogen-free adult male Sprague-Dawley rats (300-350 g) were used in all experiments (Liaoning Changsheng Biotechnology, China). Rats were housed in temperature-controlled (20 ± 2 °C) and light-controlled (12-h light-dark cycle; lights on at 7:00 am)

TABLE 1 | Primer sequences of iNOS, IL-1β, TNF-α, IL-6 and RPL27.

Gene		Sequence (5'-3')
iNOS	Forward	GGGCTGTCACGGAGATCAATG
	Reverse	GCCCGGTACTCATTCTGCATG
IL-1β	Forward	CCACCTTTTGACAGTGATGA
	Reverse	GAGATTTGAAGCTGGATGCT
IL-6	Forward	TAGTCCTTCCTACCCCAATTTCC
	Reverse	TTGGTCCTTAGCCACTCCTTC
TNF-α	Forward	CCCTCCAGAAAAGACACCATG
	Reverse	GCCACAAGCAGGAATGAGAAG
RPL27	Forward	AAGCCGTCATCGTGAAGAACA
	Reverse	CTTGATCTTGGATCGCTTGGC

rooms with standard rodent food and water available ad libitum and allowed to habituate to the holding facility for ≥1 week before experimentation. All the animal-handling procedures were approved by the Institutional Animal Care and Use Committee (IACUC) of Changchun Institute of Applied Chemistry, Chinese Academy of Sciences (CIAC2021-0026).

Animals were randomly divided into three groups. Rats in sham group (n = 6) and CCI group (n = 9) were intravenously administrated with 0.9% saline, while rats in the CCI + ACT001 group (n = 9) were intravenously administrated with 50 mg/kg ACT001 (dissolved in 0.9% saline), once a day from the 2nd day to 42nd day after surgery.

2.1.14.2 CCI Induced Neuropathic Pain

Neuropathic pain was induced using chronic constriction injury (CCI) surgery as described previously (41). Briefly, rats were anesthetized and maintained with isoflurane. The left sciatic nerve was gently exposed. Four ligations were tied loosely around the sciatic nerve with sterile chromic gut sutures. The sham group animals were treated with the same surgery but without the ligation. All animals were monitored postoperatively until fully ambulatory before returning to their home cage and checked daily for any sign of infection. No such cases occurred in this study.

2.1.14.3 Mechanical Allodynia

Animals received at least two days of habituation in the test environment before baseline testing. The nociceptive behavior was monitored 1 day before surgery and 10, 14, 17, 21, 24, 28, 31, 35, and 42 days after surgery. Rats' weight was collected every two weeks to monitor animal health state. The stimulus with Von Frey filaments, ranging from 0.6 to 26 g, was applied to the plantar surface of the hind paw. The paw withdrawal threshold was accessed *via* the up-down method using the Chaplan formula (42).

2.1.14.4 Immunofluorescence

Following the final behavioral testing, rats were anesthetized and perfused through the ascending aorta first with isotonic saline and then with fresh 4% paraformaldehyde in 0.1 M phosphate buffer (pH 7.4). The rat was decapitated, and the lumbar spinal cords (L4-L6) were removed immediately, immersed continuously in the 4% paraformaldehyde at 4 °C overnight. The spinal cord tissue was dehydrated with ethanol gradient, embedded in paraffin, and then sliced at a thickness of 4 μm. Paraffin-processed tissues were deparaffinized in xylene and rehydrated with a graded alcohol solution. The sections were placed in 0.01 M citrate buffer (pH 6.0) and heated in a microwave oven for hot repair antigen (43, 44). These sections were incubated with goat serum at 37 °C for 20 min and then with a mixture of rabbit-anti-Iba-1 monoclonal antibody and mouse-anti-GFAP monoclonal antibody at 4 °C overnight. After three washes with PBS, the sections were incubated with secondary antibody conjugated with Alexa-488 or 647 for 1 h in the dark. Ultimately, followed by three washes with PBS twice for 5 min each, the sections were counterstained with DAPI and examined under a confocal microscope.

2.1.15 Statistical Analysis

Origin 8 was used for the plotting of the data and statistical analysis. Non-linear Logistic regression was used to plot and analyze concentration-response curves and to obtain IC_{50}. For the analyses of qRT-PCR data, immunoblotting data, von Frey test and quantification of immunofluorescence, an unpaired Student t-test was used for comparisons between two groups. Data are presented as mean ± SEM. P-value summary is mentioned on the bar of each figure. # P< 0.05; ## P< 0.01; ### P< 0.001 *versus* the control/sham group; *P < 0.05; **P < 0.01; ***P < 0.001 *versus* the LPS/CCI group. ns, not significant. P< 0.05 was considered statistically significant in all analyses.

2.2 Results

2.2.1 Biophysical Binding of ACT001 With MD2

Besides its anticancer action, ACT001 (**Figure 1A**) has also been reported to alleviate neuroinflammatory responses in the CNS (16). However, the molecular target responsible for the immunosuppressive effects of ACT001 is not known. Herein the acting of ACT001 is hypothesized to be, at least in part, mediated by TLR4, which plays a fundamental role in regulating innate immunity. MD2, a co-receptor of TLR4, is responsible for ligand recognition (45). Fluorescence quenching titration of MD2 was first performed to explore the possible interaction of ACT001 with MD2 as the potential target for the inhibition of innate immune signaling. ACT001 caused the quenching of MD2 intrinsic fluorescence (**Figure 1B**). A dissociation constant K_d of 2.8 ± 0.3 μM was derived by the nonlinear least-square fitting of the titration curve of MD2-ACT001 interaction. Moreover, saturation transfer difference (STD) nuclear magnetic resonance (NMR) was employed to characterize transient receptor-ligand interaction. Only ligand protons that are in close contact with the receptor-binding site and receive magnetization transfer will appear in the difference spectrum (46, 47). As the difference spectra shown in **Figure 1C**, hydrogens of methyl at positions 8, 19, 20 and 21 exhibited the most favorable binding characteristics, which confirm the direct interaction between ACT001 and MD2. To explore whether MD2 is the endogenous target of ACT001, cellular thermal shift assay (CETSA) was performed. CETSA is based on the principle that drug binding leads to the thermal stability change of the target protein as reflected by the shift of its melting temperature (T_m). ACT001 binding decreased the T_m value of

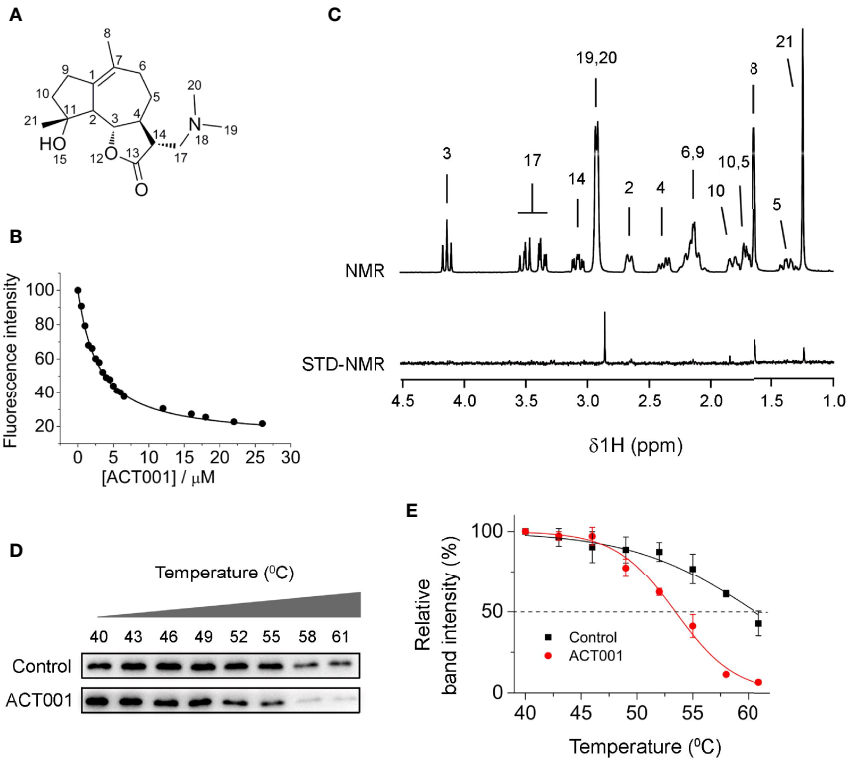

FIGURE 1 | ACT001 binds to MD2. **(A)** The chemical structure of ACT001. **(B)** Titration curve of MD2 intrinsic fluorescence with the increasing ACT001. 280 nm was chosen as the excitation and emission at 337 nm (peak position) was plotted against the titrated ACT001 concentration. A value of K_d = 2.8 ± 0.3 μM was derived by nonlinear least-square fit a one-site-binding model for the MD2-ACT001 interaction. **(C)** The upper panel corresponds to the NMR assignments of ACT001; the lower panel is the saturation transfer difference spectrum recorded for 400 μM ACT001 in the presence of MD2 (4 μM). **(D)** Cellular thermal shift assay of MD2 with ACT001. **(E)** Quantification of MD2 shown in panel **(D)** was made using immunoblotting. Three independent cell culture preparations were performed. All data are given as the mean ± SEM.

MD2 by 6.4 ± 0.9 °C (**Figures 1D, E**), which indicates ACT001 directly binds to MD2 in the cellular context. Taken together, these biophysical binding characterizations show MD2 is a direct target of ACT001.

2.2.2 Computational Simulations of ACT001 Binding to MD2

In order to investigate how ACT001 interacts with MD2, molecular docking and molecular dynamics simulation were conducted. ACT001 was found to dock into the conserved hydrophobic cavity and overlap with the space of R2', R3 and R2" chains of Lipid A in MD2, therefore hindering the binding of LPS to MD2 (**Figure 2A**). The best docking pose was refined using molecular dynamics simulations. The root-mean-square deviation (RMSD) analysis of backbone atoms of apo-MD2 and MD2 bound with ACT001 showed that both systems reached stable states during 400 ns simulations (**Figure 2B**). To investigate the flexibility changes caused by ACT001, the root-mean-square fluctuation (RMSF) analysis was conducted with the last 100 ns equilibrated trajectories. The binding of ACT001 rendered most regions of MD2 to be more flexible (**Figure 2C**), indicating that ACT001 destabilizes MD2. This result is consistent with the experimental CETSA data. The exposed solvent-accessible surface areas (SASA) of MD2 (**Figure 2D**) did not change upon interacting with ACT001. Interestingly, further analysis showed that ACT001 binding decreased the percentage of hydrophobic area in the buried SASA of MD2 (**Figure 2E**). It should be noted that the hydrophobic residues prefer to be buried inside owing to the hydrophobic interactions to stabilize the apo-MD2 (48). These *in silico* simulation results explicitly explain that ACT001 binding decreases MD2 stability.

The detailed binding mode of ACT001 with MD2 was subsequently investigated. **Figure 2F** shows the representative pose of ACT001 binding to MD2 after the molecular dynamic equilibration. ACT001 formed hydrogen bonds with surrounding water molecules and formed hydrophobic interactions with residues of MD2. Specifically, methyl at position 8 of ACT001 interacted with Ile97 and Pro98; methyl groups at positions 19 and 20 of ACT001 formed interactions with Val73; methyl at position 21 of ACT001 interacted with Phe101 and Cys113. These are consistent with STD-NMR results. In addition, Phe56, Leu58, Glu72, Phe99 and Phe131 were also found to form hydrophobic

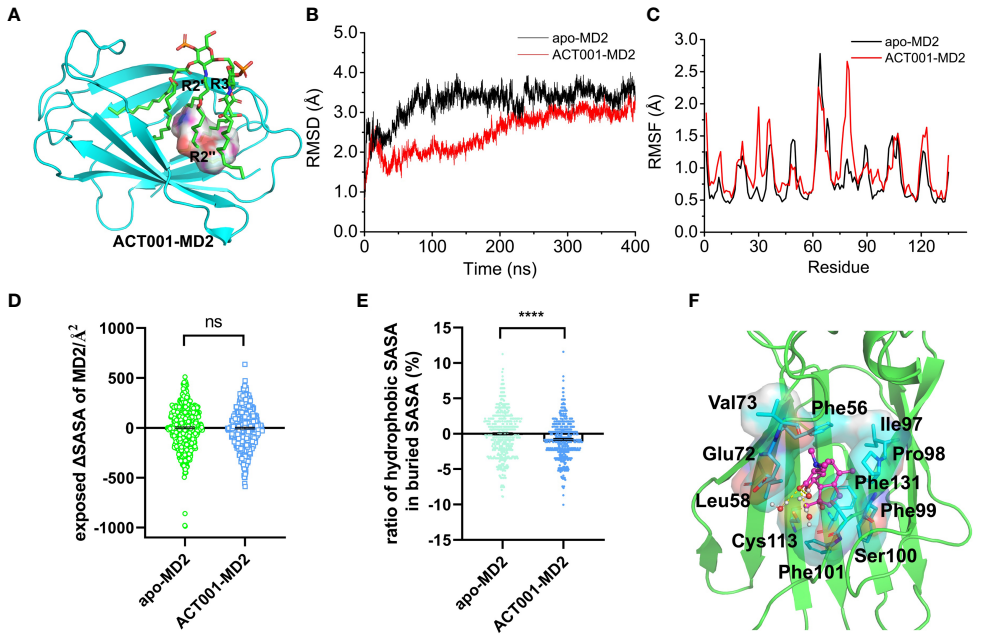

FIGURE 2 | *In silico* simulation of ACT001 interacting with MD2. **(A)** Overlap of the best docking pose of ACT001 and lipid A in MD2. ACT001 occupied the LPS binding location (acyl chains R3, R2' and R2''). Lipid A was extracted from the active state of TLR4/MD2/LPS complex (PDB ID: 3VQ2) after aligning with ACT001-docked MD2. MD2 was shown as a cyan cartoon, lipid A as green sticks, and ACT001 as surface. **(B)** Time evolution of the RMSD of MD2 (apo-MD2) and ACT001 bound MD2 (ACT001-MD2) during the MD simulations at 310 K. **(C)** Time evolution of RMSF of MD2 and ACT001 bound MD2 during the MD simulations at 310 K. **(D)** The changes of the exposed SASA of MD2 upon binding with ACT001. Data were calculated based on the last 20 ns equilibrated MD trajectories at 310 K. ns, not statistically significant. **(E)** The ratio of the hydrophobic SASA in the buried SASA of MD2. Data were calculated based on the last 100 ns equilibrated MD trajectories at 310 K ****P< 0.0001. **(F)** The representative binding mode of ACT001 with MD2 at 310 K after molecular dynamics simulation.ACT001 was shown as a balls-stick model. MD2 was shown as a cartoon model. Key residues of MD2 in interacting with ligands were shown as stick and surface models labeled with residue names. Hydrogen bonds were shown as dashed lines in yellow. Water molecule interacting with ACT001 was represented as a balls-stick model.

interactions with ACT001. All these *in silico* simulation results confirmed that ACT001 interacted with MD2 and decreased the stability of MD2.

2.2.3 ACT001 Inhibits TLR4 Signaling and LPS-Induced Pro-Inflammatory Factors

TLR4 activation leads to the recruitment of myeloid differentiation primary response protein 88 (MyD88) to activate NF-κB and MAPKs. Immunoprecipitation and immunoblotting were employed to measure the effect of ACT001 on TLR4 downstream signaling. As shown in **Figures 3A-C**, ACT001 inhibited LPS-induced MyD88 recruitment of TLR4 and significantly suppressed the formation of TLR4/MD2/MyD88 complex. LPS induced the phosphorylation of IKKβ, p65, JNK, ERK as well as p38 and ACT001 significantly inhibited LPS induced phosphorylation of these TLR4 signaling factors in a concentration-dependent manner (**Figures 3D-I**).

To further quantitatively investigate the effect of ACT001 on TLR4 signaling NF-κB activity, HEK TLR4 cell line with a SEAP reporter gene, under the control of NF-κB responsive element, was used. ACT001 was found to inhibit LPS-induced NF-κB activation in a dose-dependent manner, with an IC_{50} of 22.4 ± 0.3 μM while no apparent cellular toxicity of ACT001 was observed within 200 μM (**Figure 4A**). In addition to HEK based NF-κB reporter cell, the effect of ACT001 on NF-κB activity in BV-2 cells, which reproduces many of the responses of immunocompetent primary microglia with high fidelity (49), was also examined. ACT001 inhibited LPS-induced NF-κB activation in BV-2 cells in a dose-dependent manner with an IC_{50} of 24.1 ± 1.3 μM without apparent cellular toxicity within 200 μM (**Figure 4B**). These data clearly show that ACT001 inhibits TLR4 signaling NF-κB activation.

The pro-inflammatory mediators are downstream effectors of TLR4 innate immune responses. ACT001 inhibited LPS induced nitric oxide (NO) overproduction in BV-2 cells in a concentration-dependent manner with an IC_{50} of 16.0 ± 1.2 μM (**Figure 5A**). No apparent cellular toxicity of ACT001 was observed, even at the concentration of 100 μM, which eliminates the possibility of the observed inhibition of TLR4 signaling by ACT001 was owing to cell death (**Figure 5A**). qRT-PCR was performed to measure the effect of ACT001 on LPS-induced pro-inflammatory factors iNOS, IL-1β, IL-6 and TNF-α mRNAs expression. ACT001 suppressed LPS-induced iNOS (**Figure 5B**), IL-1β (**Figure 5C**), IL-6 (**Figure 5D**) and TNF-α (**Figure 5E**) mRNA expression in a concentration-dependent

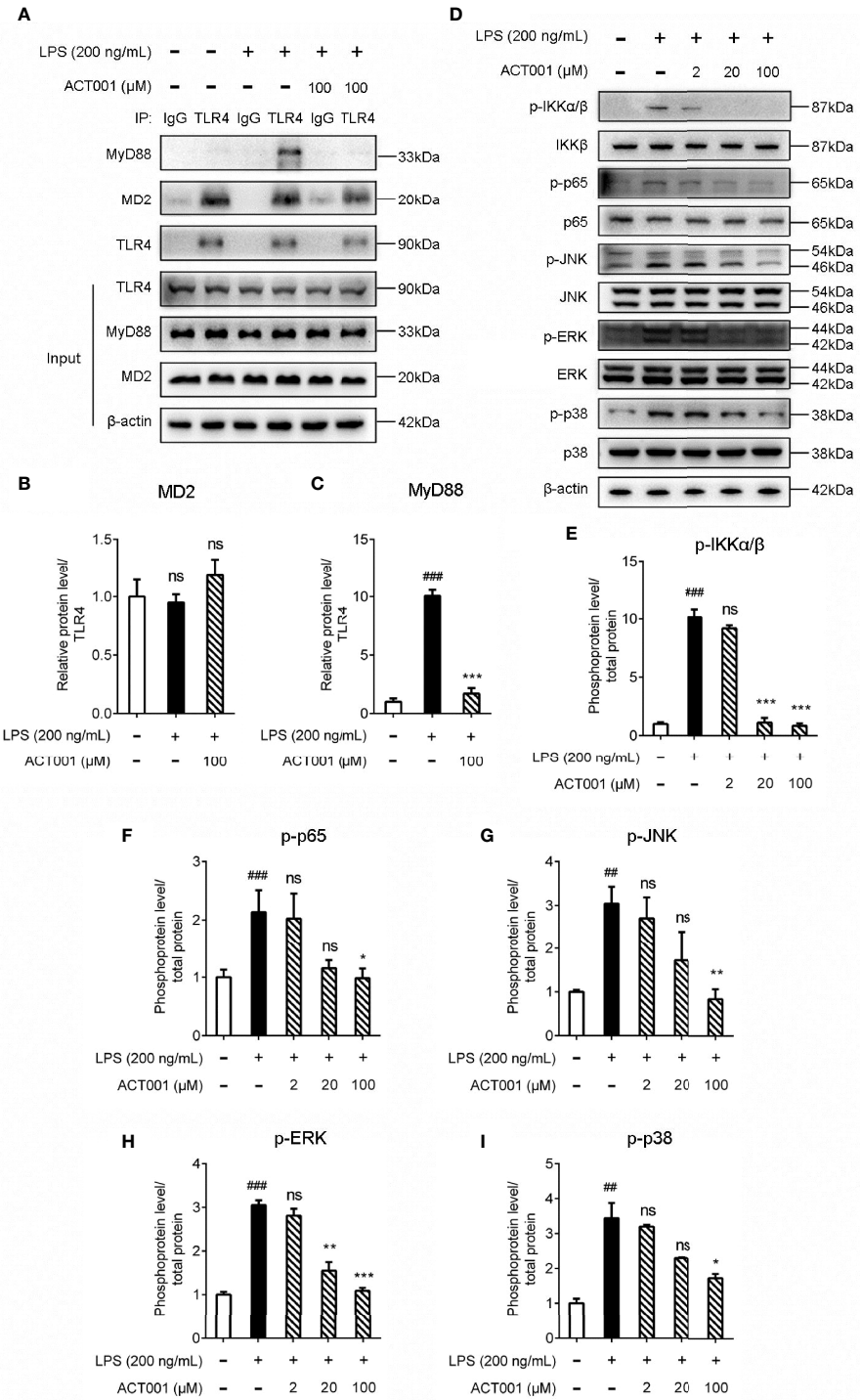

FIGURE 3 | Cellular characterizations of ACT001 on TLR4 signaling. BV-2 cells were administered with 200 ng/mL LPS and the indicated concentration of ACT001 for 1 h. **(A-C)** Co-immunoprecipitation of anti-TLR4 antibody, MD2, TLR4, and MyD88 were detected by immunoblotting. **(D-I)** The effect of ACT001 on LPS-induced phosphorylation of IKKβ, p65 and MAPKs. The total protein level of IKKβ, p65 and MAPKs was set as reference. All experiments were performed three times independently, and data were given as the mean ± SEM. $^{\#\#}$P< 0.01, $^{\#\#\#}$P< 0.001 *versus* the control; *P< 0.05, **P< 0.01, ***P< 0.001 *versus* the LPS group; ns, not significant.

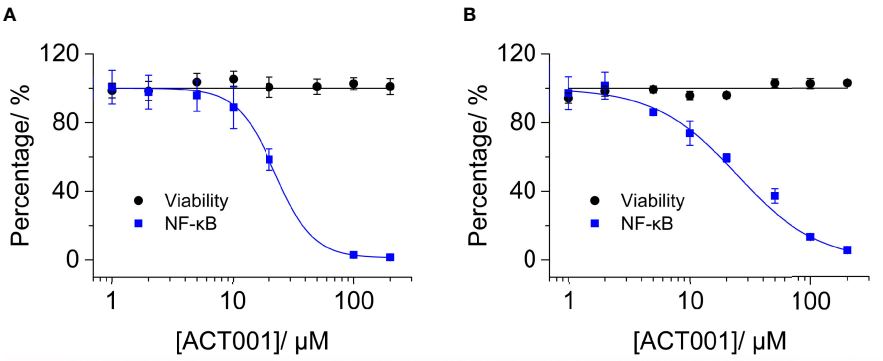

FIGURE 4 | ACT001 inhibits LPS-induced NF-κB activation. **(A)** HEK Blue TLR4 293 cells, which over-express human CD14, TLR4, and MD2, were stimulated with 20 ng/mL LPS and indicated concentrations of ACT001. The NF-κB activity was determined by SEAP assay and cellular viability was measured by CCK-8 Kit. **(B)** BV-2 NF-κB luciferase reporter cells were treated with 200 ng/mL LPS and the indicated concentrations of ACT001. After 24 h of incubation, the NF-κB activity was determined by the Dual-Glo luciferase assay and cellular viability was measured by crystal violet staining. All experiments were performed 3 times independently and data were given as the mean ± SEM.

manner. The LPS-induced cell body was enlarged, and the percentage of amoeboid-like microglia increased significantly, while ACT001 markedly reversed the LPS induced morphological changes in BV-2 cells (**Supplementary Figure 1**). Together, these cellular signaling characterizations demonstrate that ACT001 inhibits the formation of TLR4/MD2/MyD88 complex and LPS-induced activation of NF-κB and MAPKs, therefore inhibiting TLR4 signaling downstream pro-inflammatory factors.

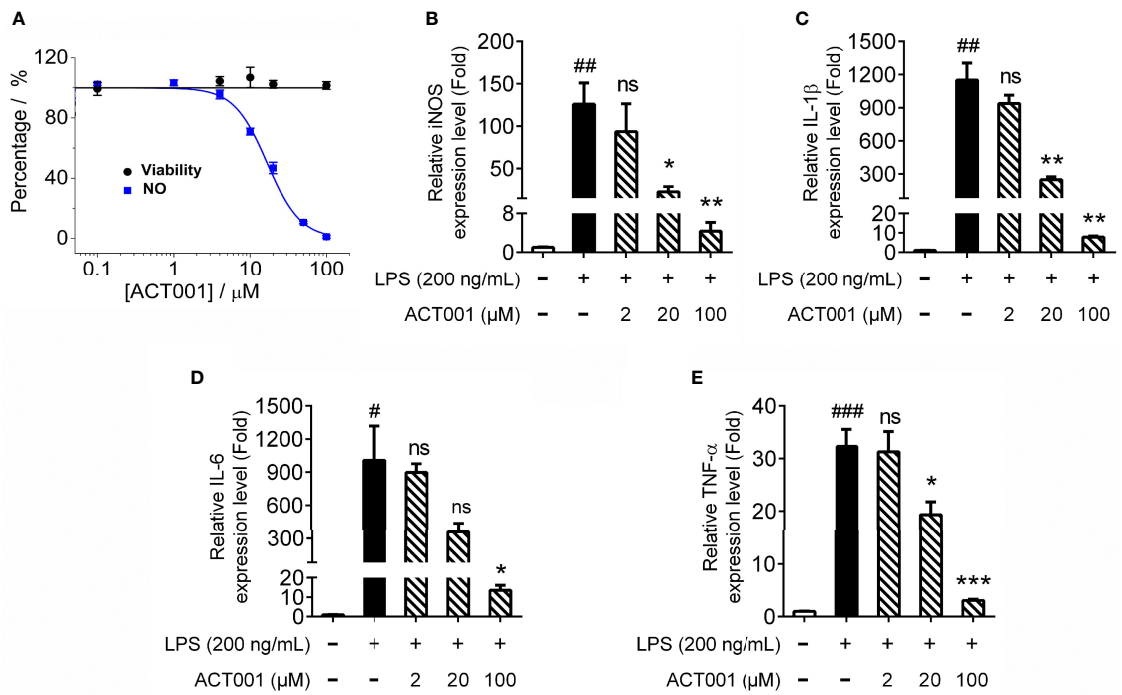

FIGURE 5 | ACT001 inhibits LPS-induced pro-inflammatory factors overproduction. **(A)** BV-2 cells were administered with LPS and indicated concentrations of ACT001. After 24 h incubation, the effects of ACT001 on LPS-induced NO and cellular viability were measured. **(B-E)** BV-2 cells were administered with 200 ng/mL LPS and indicated concentrations of ACT001. After 6 h incubation, the effects of ACT001 on LPS induced iNOS **(B)**, IL-1β **(C)**, IL-6 **(D)** and TNF-α **(E)** mRNA were measured. All the data represented the mean ± SEM; n, number of independent cell culture preparations = 3. $^{\#}P< 0.05$, $^{\#\#}P< 0.01$, $^{\#\#\#}P< 0.001$ versus the control; $^{*}P< 0.05$,$^{**}P< 0.01$, $^{***}P< 0.001$ *versus* the LPS group; ns, not significant.

2.2.4 ACT001 Attenuates Neuropathic Pain and Glial Activation

Chronic constriction injury (CCI)-induced allodynia is associated with up-regulated TLR4 expression in spinal cord and TLR4 antagonism has been shown to attenuate neuropathic pain (41).The mechanical threshold of ipsilateral hind paw of the CCI group decreased significantly compared to the sham group (**Figure 6**). Repeated systemic administration of ACT001 resulted in significant attenuation of allodynia since the 21stday after CCI surgery without interrupting weight gain in animals (**Figure 6** and **Supplementary Figure 2**). To further analyze whether the attenuation of allodynia by ACT001 was associated with a decrease in the expression of glial activation markers, the lumbar spinal cords (L4-L6) of three group animals were collected following the final behavioral testing. These tissues were stained for microglia and astrocyte activation markers Iba-1 and GFAP, respectively. The expression of Iba-1 and GFAP in the ipsilateral spinal dorsal horn segments in the CCI group significantly increased when compared to the sham group (**Figures 7**, **8**). Moreover, the number and size of glia were also elevated in CCI group compared to sham group. ACT001 significantly inhibited the CCI-induced overexpression of glial markers as well as the Iba1- and GFAP-positive area and the cell number (**Figures 7**, **8**). These results show ACT001 attenuates neuropathic pain and glial activation.

2.3 Discussion

ACT001 has been proved to exert anti-tumor functions through a variety of pharmacological activities. Hou*et al* and Tong *et al.* reported that ACT001 inhibited glioblastoma growth by inhibiting AEBP1/PI3K/AKT and signal transducer and activator of transcription 3 (STAT3) signaling pathways (12, 50). Xu et al. found that ACT001 had an anti-growth effect on rhabdomyosarcoma, which was mediated by Bim protein up-regulation and ROS overproduction (51). Ba et al. and Yao et al. discovered that ACT001 repressed hepatocellular carcinoma and osteosarcoma proliferation and triggered cell cycle arrest *via* the intrinsic apoptotic pathway (13, 52). Moreover, ACT001 was found to alleviate NLRP3-mediated neuroinflammation (16). In this study, *in vitro* quenching titrations of MD2 intrinsic fluorescence and STD-NMR demonstrated the direct binding of ACT001 to TLR4 co-receptor MD2. CETSA validated that MD2 is the endogenous target of ACT001 in the cellular context. The RMSF analysis indicated that ACT001 destabilized MD2, which is consistent with CETSA data. In brief, ACT001 was found to bind to MD2 directly and inhibited the formation of TLR4/MD2/MyD88 complex and the TLR4 signaling NF-κB and MAPKs, therefore suppressing neuroinflammation. This study demonstrates that ACT001 is a TLR4 antagonist for the first time, which at least in part accounts for its anti-neuroinflammatory activity. However, it should be acknowledged that most likely ACT001 has other unknown non-MD2 targets, which deserves further investigations.

Neuropathic pain has affected 7%-10% of the general population (53). Despite several therapeutics are available for treating neuropathic pain, they have serious side effects. For example, opioids are less effective in treating neuropathic pain as the negative effects of tolerance and addiction may prevent their long-term use (54). Ion channel blockers such as gabapentin and pregabalin could relieve neuropathic pain, but there are dose limitations concerning efficacy and side effects like dizziness, sedation, and weight gain (55). Ziconotide is an effective analgesic for severe chronic pain refractory to other treatments but only can be delivered intrathecally (55). Therefore, there is an

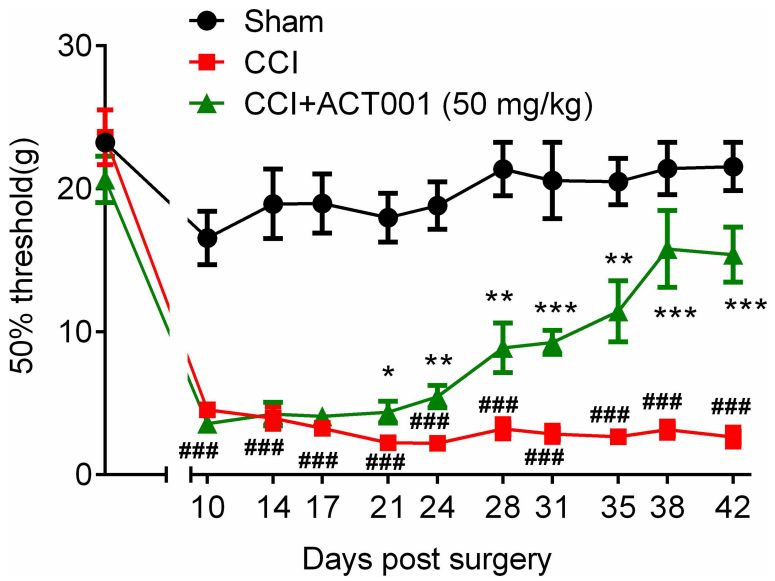

FIGURE 6 | ACT001 attenuates neuropathic pain induced by CCI. All the data represented mean ± SEM. ###P< 0.001 *versus* the sham group; *P< 0.05, **P< 0.01, ***P<0.001 versus the CCI group.

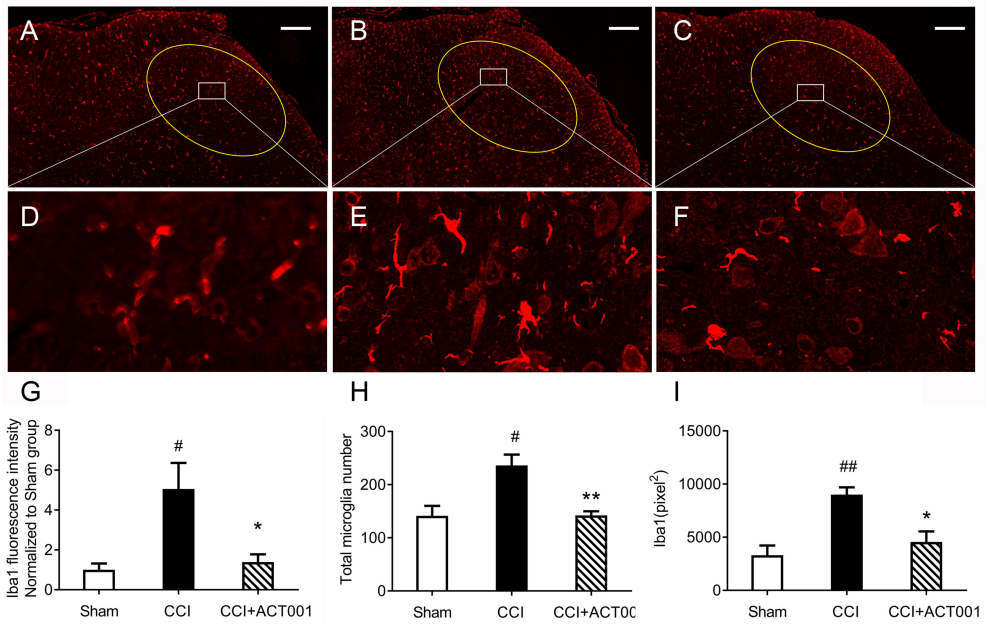

FIGURE 7 | ACT001 inhibits microglial activation markers expression induced by CCI. The lumbar spinal cords (L4-L6) were collected following the final behavioral testing shown in **Figure 6**. These tissues were stained for microglial activation markers. **(A-C)** Representative immunofluorescence Iba1 images for the sham group **(A)**, CCI group **(B)**, and CCI + ACT001 group **(C)**. **(D-F)** Representative images for sham group **(D)**, CCI group **(E),** and CCI + ACT001 group **(F)** with high magnification (×60). **(G-I)** The quantification of Iba1 expression was shown as normalized fluorescence intensity **(G)**, number **(H)**, and size of **(I)** microglia. Scale bar = 200 μm. All the data represented mean ± SEM. $^{\#}$P< 0.05, $^{\#\#}$P< 0.01 *versus* the sham group; *P< 0.05, **P< 0.01 *versus* the CCI group.

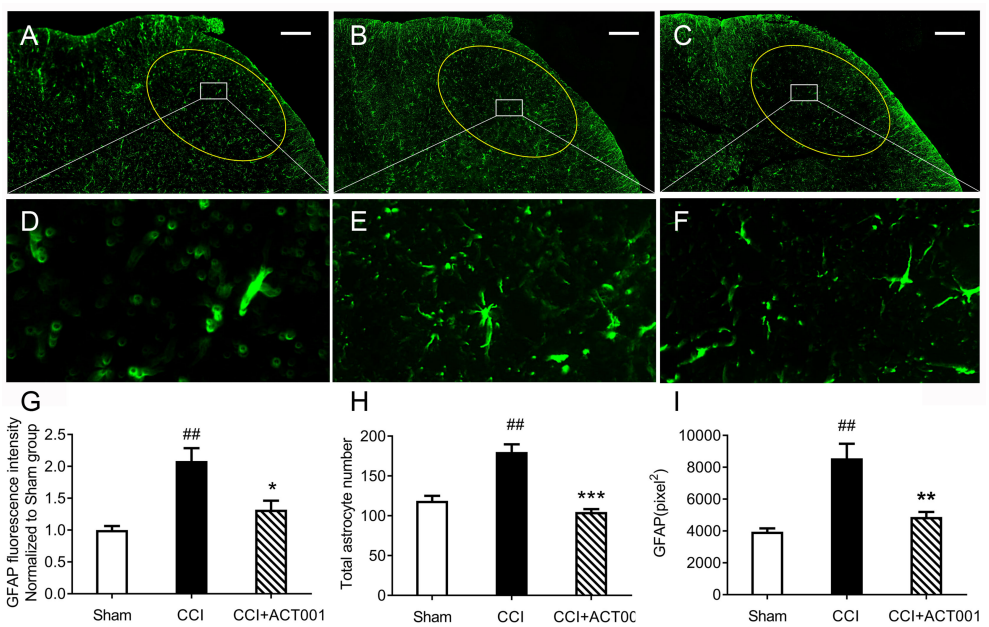

FIGURE 8 | ACT001 inhibits astrocyte activation markers expression induced by CCI. The lumbar spinal cords (L4-L6) were collected following the final behavioral testing shown in **Figure 6**. These tissues were stained for astrocyte activation markers. **(A-C)** Representative immunofluorescence GFAP images for the sham group **(A)**, CCI group **(B),** and CCI + ACT001 group **(C)**. **(D-F)** Representative images for sham group **(D)**, CCI group **(E),** and CCI + ACT001 group **(F)** with high magnification (×60).**(G-I)** The quantification of GFAP expression was shown as normalized fluorescence intensity **(G)**, number **(H)** and size of **(I)** astrocyte. Scale bar = 200 μm. All the data represented mean ± SEM. $^{\#\#}$P< 0.01 *versus* the sham group; *P< 0.05, **P< 0.01, *** P< 0.001 versus the CCI group.

urgent need for the development of therapeutic agent for treating neuropathic pain. Extensive studies have demonstrated that the contribution of activated glia and their pro-inflammatory products to allodynia and that TLR4/MD-2 could be a novel drug target for treating neuropathic pain (7, 8, 56). Consequently, several TLR4 antagonists have been developed (6, 57, 58). However, few of these could cross BBB. Herein, ACT001, which can diffuse through BBB after oral administration (9), was repositioned as a TLR4 antagonist to attenuate allodynia in a preclinical model of neuropathic pain. The systemic administration of ACT001 resulted in antagonism of TLR4-expressing glial cells in the lumbar spinal dorsal horn. The *in vivo* studies provide support for ACT001 as a novel therapeutic drug for chronic pain, which would expand the clinical application of ACT001. It should be acknowledged that the *in vivo* behavioral testing in this study lacked dose-dependent investigation and was performed only in male rats. Further studies should be considered to evaluate the effect of ACT001 with different doses *in vivo* and also evaluate the sex differences of ACT001 as a TLR4 antagonist for treating neuropathic pain.

In summary, this study provides the first evidence that ACT001 binds to MD2, therefore blocking the TLR4 signaling. Furthermore, ACT001 attenuates allodynia induced by CCI and glial activation in dorsal horn of lumbar spinal cord. The results indicate that ACT001 could be a potential therapeutic intervention for chronic neuropathic pain. Our results add that MD2 is one of the important targets of ACT001and can partially explain its interference of innate immune function in CNS diseases.

DATA AVAILABILITY STATEMENT

The original contributions presented in the study are included in the article/**Supplementary Material**. Further inquiries can be directed to the corresponding authors.

ETHICS STATEMENT

All the animal-handling procedures were approved by the Institutional Animal Care and Use Committee (IACUC) of Changchun Institute of Applied Chemistry, Chinese Academy of Sciences (CIAC2021-0026).

AUTHOR CONTRIBUTIONS

XW and YP designed the experiments; SW, SJ, CL, and TZ performed the experiments, acquired and analyzed data; TZ and CL wrote the manuscript; XL and XW edited the manuscript. All authors contributed to the article and approved the submitted version.

FUNDING

This work was supported by the National Natural Science Foundation of China (91956121, 21877106); the Chinese Academy of Sciences (CAS) Pioneer Hundred Talents Program; the State Key Laboratory of Natural and Biomimetic Drugs (K202115); Beijing National Laboratory for Molecular Sciences (BNLMS202108).

ACKNOWLEDGMENTS

Computing time was supported by the Advanced Computing East China Sub-center. The numerical calculations in this paper have also been done on CAS Xiandao-1 computing environment.

SUPPLEMENTARY MATERIAL

The Supplementary Material for this article can be found online at: https://www.frontiersin.org/articles/10.3389/fimmu.2022.873054/full#supplementary-material

REFERENCES

1. Finnerup NB, Kuner R, Jensen TS. Neuropathic Pain: From Mechanisms to Treatment. *Physiol Rev* (2021) 101(1):259–301. doi: 10.1152/physrev.00045.2019
2. Colloca L, Ludman T, Bouhassira D, Baron R, Dickenson AH, Yarnitsky D, et al. Neuropathic Pain. *Nat Rev Dis Primers* (2017) 3:17002. doi: 10.1038/nrdp.2017.2
3. Inoue K, Tsuda M. Microglia in Neuropathic Pain: Cellular and Molecular Mechanisms and Therapeutic Potential. *Nat Rev Neurosci* (2018) 19(3):138–52. doi: 10.1038/nrn.2018.2
4. Chen G, Zhang YQ, Qadri YJ, Serhan CN, Ji RR. Microglia in Pain: Detrimental and Protective Roles in Pathogenesis and Resolution of Pain. *Neuron* (2018) 100(6):1292–311. doi: 10.1016/j.neuron.2018.11.009
5. Sommer C, Leinders M, Üçeyler N. Inflammation in the Pathophysiology of Neuropathic Pain. *Pain* (2018) 159(3):595–602. doi: 10.1097/j.pain.0000000000001122
6. Lin C, Wang H, Zhang M, Mustafa S, Wang Y, Li H, et al. TLR4 Biased Small Molecule Modulators. *Pharmacol Ther* (2021) 228:107918. doi: 10.1016/j.pharmthera.2021.107918
7. Bruno K, Woller SA, Miller YI, Yaksh TL, Wallace M, Beaton G, et al. Targeting Toll-Like Receptor-4 (TLR4)-An Emerging Therapeutic Target for Persistent Pain States. *Pain* (2018) 159(10):1908–15. doi: 10.1097/j.pain.0000000000001306
8. Lacagnina MJ, Watkins LR, Grace PM. Toll-Like Receptors and Their Role in Persistent Pain. *Pharmacol Ther* (2018) 184:145–58. doi: 10.1016/j.pharmthera.2017.10.006
9. Xi XN, Liu N, Wang QQ, Wu HT, He HB, Wang LL, et al. Pharmacokinetics, Tissue Distribution and Excretion of ACT001 in Sprague-Dawley Rats and Metabolism of ACT001. *J Chromatogr B Analyt Technol BioMed Life Sci* (2019) 1104:29–39. doi: 10.1016/j.jchromb.2018.11.004
10. Jin XH, Jia YS, Shi YH, Li QY, Bao SQ, Lu WP, et al. ACT001 can Prevent and Reverse Tamoxifen Resistance in Human Breast Cancer Cell Lines by Inhibiting NF-κb Activation. *J Cell Biochem* (2018) 120:1386–97. doi: 10.1002/jcb.27146
11. Li Q, Sun Y, Liu B, Li J, Hao X, Ge W, et al. ACT001 Modulates the NF-κb/MnSOD/ROS Axis by Targeting Ikkβ to Inhibit Glioblastoma Cell Growth. *J Mol Med (Berl)* (2020) 98(2):263–77. doi: 10.1007/s00109-019-01839-0
12. Tong L, Li J, Li Q, Wang X, Medikonda R, Zhao T, et al. ACT001 Reduces the Expression of PD-L1 by Inhibiting the Phosphorylation of STAT3 in Glioblastoma. *Theranostics* (2020) 10(13):5943–56. doi: 10.7150/thno.41498
13. Yao S, Ye J, Yin M, Yu R. DMAMCL Exerts Antitumor Effects on Hepatocellular Carcinoma Both *In Vitro* and *In Vivo*. *Cancer Lett* (2020) 483:87–97. doi: 10.1016/j.canlet.2020.04.003

14. Li J, Li S, Guo J, Li Q, Long J, Ma C. Natural Product Micheliolide (MCL) Irreversibly Activates Pyruvate Kinase M2 and Suppresses Leukemia. *J Med Chem* (2018) 61(9):4155–64. doi: 10.1021/acs.jmedchem.8b00241
15. Xi X, Liu N, Wang Q, Chu Y, Yin Z, Ding Y, et al. ACT001, a Novel PAI-1 Inhibitor, Exerts Synergistic Effects in Combination With Cisplatin by Inhibiting PI3K/AKT Pathway in Glioma. *Cell Death Dis* (2019) 10(10):757. doi: 10.1038/s41419-019-1986-2
16. Liu Q, Guo X, Huang Z, He Q, Zhu D, Zhang S, et al. Anti-Neuroinflammatory Effects of Dimethylaminomylide (DMAMCL, I.E., ACT001) Are Associated With Attenuating the NLRP3 Inflammasome in MPTP-Induced Parkinson Disease in Mice. *Behav Brain Res* (2020) 383:112539. doi: 10.1016/j.bbr.2020.112539
17. Liu Q, Zhang S, Zhu D, Tang X, Che Y, Feng X. The Parthenolide Derivative ACT001 Synergizes With Low Doses of L-DOPA to Improve MPTP-Induced Parkinson's Disease in Mice. *Behav Brain Res*. (2020) 379:112337. doi: 10.1016/j.bbr.2019.112337
18. Cook DN, Pisetsky DS, Schwartz DA. Toll-Like Receptors in the Pathogenesis of Human Disease. *Nat Immunol* (2004) 5(10):975–9. doi: 10.1038/ni1116
19. Yang H, Wang H, Andersson U. Targeting Inflammation Driven by HMGB1. *Front Immunol* (2020) 11:484. doi: 10.3389/fimmu.2020.00484
20. Li H, Peng Y, Lin C, Zhang X, Zhang T, Wang Y, et al. Nicotine and its Metabolite Cotinine Target MD2 and Inhibit TLR4 Signaling. *Innovation (N Y)* (2021) 2(2):100111. doi: 10.1016/j.xinn.2021.100111
21. Zhang X, Wang Y. Exploring Methamphetamine Nonenantioselectively Targeting Toll-Like Receptor 4/Myeloid Differentiation Protein 2 by in Silico Simulations and Wet-Lab Techniques. *J Chem Inf Model* (2020) 60 (3):1607–13. doi: 10.1021/acs.jcim.9b01040
22. Northcutt AL, Hutchinson MR, Wang X, Baratta MV, Hiranita T, Cochran TA, et al. DAT Isn't All That: Cocaine Reward and Reinforcement Require Toll-Like Receptor 4 Signaling. *Mol Psychiatry* (2015) 20(12):1525–37. doi: 10.1038/mp.2014.177
23. Zhang T, Zhang X, Lin C, Wu S, Wang F, Wang H, et al. Artemisinin Inhibits TLR4 Signaling by Targeting Co-Receptor MD2 in Microglial BV-2 Cells and Prevents Lipopolysaccharide-Induced Blood-Brain Barrier Leakage in Mice. *J Neurochem* (2021) 157(3):611–23. doi: 10.1111/jnc.15302
24. GaussView V, Dennington R, Keith TA, Millam JM. (2016). Semichem Inc., Shawnee Mission, KS.
25. Gaussian 09 RB, Frisch MJ, Trucks GW, Schlegel HB, Scuseria GE, Robb MA, et al. (2016). Gaussian, Inc., Wallingford CT.
26. S Maestro ed. *Schrödinger Release 2021-2*. New York, NY: LLC (2021).
27. Trott OOA. AutoDock Vina: Improving the Speed and Accuracy of Docking With a New Scoring Function, Efficient Optimization and Multithreading. *J Comput Chem* (2010) 31:455–61. doi: 10.1002/jcc.21334
28. Baxter J. Local Optima Avoidance in Depot Location. *J Oper Res Soc* (1981) 32 (9):815–9. doi: 10.1057/jors.1981.159
29. Blum CA MJB, Roli A, Sampels M. : Hybrid Metaheuristics, An Emerging Approach to Optimization. *Springer-Verlag Berlin Heidelberg* (2008) 114:31-290. doi: 10.1007/978-3-540-78295-7
30. Phillips JC, Braun R, Wang W, Gumbart J, Tajkhorshid E, Villa E, et al. Scalable Molecular Dynamics With NAMD. *J Comput Chem* (2005) 26 (16):1781–802. doi: 10.1002/jcc.20289
31. Duan Y, Wu C, Chowdhury S, Lee MC, Xiong G, Zhang W, et al. A Point-Charge Force Field for Molecular Mechanics Simulations of Proteins Based on Condensed-Phase Quantum Mechanical Calculations. *J Comput Chem* (2003) 24(16):1999–2012. doi: 10.1002/jcc.10349
32. Wang J, Wolf RM, Caldwell JW, Kollman PA, Case DA. Development and Testing of a General Amber Force Field. *J Comput Chem* (2004) 25(9):1157–74. doi: 10.1002/jcc.20035
33. Dupradeau FY, Pigache A, Zaffran T, Savineau C, Lelong R, Grivel N, et al. The R.E.D. Tools: Advances in RESP and ESP Charge Derivation and Force Field Library Building. *Phys Chem Chem Phys* (2010) 12(28):7821–39. doi: 10.1039/c0cp00111b
34. Darden T, York D, Pedersen L. Particle Mesh Ewald: AnN·log(N) Method for Ewald Sums in Large Systems. *J Chem Phys* (1993) 98(12):10089–92. doi: 10.1063/1.464397
35. Feller SE, Zhang Y, Pastor RW, Brooks BR. Constant Pressure Molecular Dynamics Simulation: The Langevin Piston Method. *J Chem Phys* (1995) 103 (11):4613–21. doi: 10.1063/1.470648
36. Humphrey W, Dalke A, Schulten K. VMD: Visual Molecular Dynamics. *J Mol Graph* (1996) 14(1):33–8. doi: 10.1016/0263-7855(96)00018-5
37. Grant BJ, Rodrigues AP, ElSawy KM, McCammon JA, Caves LS. Bio3d: An R Package for the Comparative Analysis of Protein Structures. *Bioinformatics* (2006) 22(21):2695–6. doi: 10.1093/bioinformatics/btl461
38. Laskowski RA, Swindells MB. LigPlot+: Multiple Ligand-Protein Interaction Diagrams for Drug Discovery. *J Chem Inf Model* (2011) 51(10):2778–86. doi: 10.1021/ci200227u
39. PyMol. *The PyMOL Molecular Graphics System*. LLC: Schrödinger. (2015).
40. Wang X, Loram LC, Ramos K, de Jesus AJ, Thomas J, Cheng K, et al. Morphine Activates Neuroinflammation in a Manner Parallel to Endotoxin. *Proc Natl Acad Sci USA* (2012) 109(16):6325–30. doi: 10.1073/pnas.1200130109
41. Peng Y, Zhang X, Zhang T, Grace PM, Li H, Wang Y, et al. Lovastatin Inhibits Toll-Like Receptor 4 Signaling in Microglia by Targeting its Co-Receptor Myeloid Differentiation Protein 2 and Attenuates Neuropathic Pain. *Brain Behav Immun* (2019) 82:432–44. doi: 10.1016/j.bbi.2019.09.013
42. Chaplan SR, Bach FW, Pogrel JW, Chung JM and Yaksh TL. Quantitative Assessment of Tactile Allodynia in the Rat Paw. *J Neurosci Methods* (1994) 53 (1):55–63. doi: 10.1016/0165-0270(94)90144-9
43. Georgieva M, Wei Y, Dumitrascuta M, Pertwee R, Finnerup NB, Huang W. Fatty Acid Suppression of Glial Activation Prevents Central Neuropathic Pain After Spinal Cord Injury. *Pain* (2019) 160(12):2724–42. doi: 10.1097/j.pain.0000000000001670
44. Yosten GL, Harada CM, Haddock C, Giancotti LA, Kolar GR, Patel R, et al. GPR160 De-Orphanization Reveals Critical Roles in Neuropathic Pain in Rodents. *J Clin Invest* (2020) 130(5):2587–92. doi: 10.1172/jci133270
45. Park BS, Song DH, Kim HM, Choi BS, Lee H, Lee JO. The Structural Basis of Lipopolysaccharide Recognition by the TLR4-MD-2 Complex. *Nature* (2009) 458(7242):1191–5. doi: 10.1038/nature07830
46. Angulo J, Nieto PM. STD-NMR: Application to Transient Interactions Between Biomolecules-a Quantitative Approach. *Eur Biophys J* (2011) 40 (12):1357–69. doi: 10.1007/s00249-011-0749-5
47. Viegas A, Manso J, Nobrega FL, Cabrita EJ. Saturation-Transfer Difference (STD) NMR: A Simple and Fast Method for Ligand Screening and Characterization of Protein Binding. *J Chem Educ* (2011) 88(7):990–4. doi: 10.1021/ed101169t
48. Tych KM, Batchelor M, Hoffmann T, Wilson MC, Hughes ML, Paci E, et al. Differential Effects of Hydrophobic Core Packing Residues for Thermodynamic and Mechanical Stability of a Hyperthermophilic Protein. *Langmuir* (2016) 32(29):7392–402. doi: 10.1021/acs.langmuir.6b01550
49. Henn A, Lund S, Hedtjärn M, Schrattenholz A, Pörzgen P, Leist M. The Suitability of BV2 Cells as Alternative Model System for Primary Microglia Cultures or for Animal Experiments Examining Brain Inflammation. *Altex* (2009) 26(2):83–94. doi: 10.14573/altex.2009.2.83
50. Hou Y, Sun B, Liu W, Yu B, Shi Q, Luo F, et al. Targeting of Glioma Stem-Like Cells With a Parthenolide Derivative ACT001 Through Inhibition of AEBP1/PI3K/AKT Signaling. *Theranostics* (2021) 11(2):555–66. doi: 10.7150/thno.49250
51. Xu N, Hua Z, Ba G, Zhang S, Liu Z, Thiele CJ, et al. The Anti-Tumor Growth Effect of a Novel Agent DMAMCL in Rhabdomyosarcoma*In Vitro* and *In Vivo*. *J Exp Clin Cancer Res* (2019) 38(1):118. doi: 10.1186/s13046-019-1107-1
52. Ba G, Hua Z, Xu N, Zhang S, Liu Z, Thiele CJ, et al. Novel Agent DMAMCL Suppresses Osteosarcoma Growth and Decreases the Stemness of Osteosarcoma Stem Cell. *Cell Cycle* (2020) 19(12):1530–44. doi: 10.1080/15384101.2020.1762041
53. van Hecke O, Austin SK, Khan RA, Smith BH, Torrance N. Neuropathic Pain in the General Population: A Systematic Review of Epidemiological Studies. *Pain* (2014) 155(4):654–62. doi: 10.1016/j.pain.2013.11.013
54. Neuman MD, Bateman BT, Wunsch H. Inappropriate Opioid Prescription After Surgery. *Lancet* (2019) 393(10180):1547–57. doi: 10.1016/s0140-6736(19)30428-3
55. Patel R, Montagut-Bordas C, Dickenson AH. Calcium Channel Modulation as a Target in Chronic Pain Control. *Br J Pharmacol* (2018) 175(12):2173–84. doi: 10.1111/bph.13789

56. Inoue K, Tsuda M. Purinergic Systems, Neuropathic Pain and the Role of Microglia. *Exp Neurol* (2012) 234(2):293–301. doi: 10.1016/j.expneurol.2011.09.016
57. Wang Y, Zhang S, Li H, Wang H, Zhang T, Hutchinson MR, et al. Small-Molecule Modulators of Toll-Like Receptors. *Acc Chem Res* (2020) 53 (5):1046–55. doi: 10.1021/acs.accounts.9b00631
58. Fengchao C, Yunqi L, Yinghua P, Xiaohui W, Tianshu Z, Xiaozheng Z. Toll-Like Receptor 4 Small Molecule Modulators. *Chin J Appl Chem* (2016) 33 (8):876–86. doi: 10.11944/j.issn.1000-0518.2016.08.160206

Conflict of Interest: The authors declare that the research was conducted in the absence of any commercial or financial relationships that could be construed as a potential conflict of interest.

Publisher's Note: All claims expressed in this article are solely those of the authors and do not necessarily represent those of their affiliated organizations, or those of the publisher, the editors and the reviewers. Any product that may be evaluated in this article, or claim that may be made by its manufacturer, is not guaranteed or endorsed by the publisher.

frontiers | Frontiers in Immunology

MINI REVIEW
published: 23 June 2022
doi: 10.3389/fimmu.2022.941931

Nucleic Acid Sensing by Toll-Like Receptors in the Endosomal Compartment

Kensuke Miyake[1*], *Takuma Shibata*[1], *Ryutaro Fukui*[1], *Ryota Sato*[1], *Shin-Ichiroh Saitoh*[1] *and Yusuke Murakami*[2]

[1] Division of Innate Immunity, Department of Microbiology and Immunology, The Institute of Medical Science, The University of Tokyo, Minato-ku, Japan, [2] Faculty of Pharmacy, Department of Pharmaceutical Sciences and Research Institute of Pharmaceutical Sciences, Musashino University, Tokyo, Japan

Toll-like receptors (TLRs) respond to pathogen constituents, such as microbial lipids and nucleic acids (NAs). TLRs recognize NAs in endosomal compartments. Structural and functional studies have shown that recognition of NAs by TLRs depends on NA processing by RNases and DNases. DNase II-dependent DNA degradation is required for TLR9 responses to single-stranded DNAs, whereas RNase T2-dependent RNA degradation enables TLR7 and TLR8 to respond to nucleosides and oligoribonucleotides. In contrast, RNases and DNases negatively regulate TLR responses by degrading their ligands. RNase T2 negatively regulates TLR3 responses to degrading the TLR3 ligand double-stranded RNAs. Therefore, NA metabolism in the endosomal compartments affects the endosomal TLR responses. Dysregulation of NA metabolism in the endosomal compartment drives the TLR-dependent pathologies in human diseases.

Keywords: nuclease, nucleoside, autoimmune disease, endosome, toll-like receptor

OPEN ACCESS

Edited by:
Hang Yin,
Tsinghua University, China

Reviewed by:
Yoshinori Hirano,
The University of Tokyo, Japan

****Correspondence:***
Kensuke Miyake
kmiyake@ims.u-tokyo.ac.jp

Specialty section:
This article was submitted to Molecular Innate Immunity, a section of the journal Frontiers in Immunology

Received: *12 May 2022*
Accepted: *27 May 2022*
Published: *23 June 2022*

Citation:
Miyake K, Shibata T, Fukui R, Sato R, Saitoh S-I and Murakami Y (2022) Nucleic Acid Sensing by Toll-Like Receptors in the Endosomal Compartment. Front. Immunol. 13:941931. doi: 10.3389/fimmu.2022.941931

1 INTRODUCTION

The Toll family of receptors are expressed in innate immune cells, such as macrophages and dendritic cells (DCs), and respond to pathogen components to activate defense responses during bacterial and viral infections. Nucleic acids (NAs) are sensed by a subfamily of toll-like receptors (TLRs) including TLR3, TLR7, TLR8, TLR9, and TLR13. These NA-sensing TLRs are localized in the endosomal compartment to prevent hazardous autoimmune responses (1). NA degradation in the endosomal compartment negatively regulates TLR responses to self-derived NAs. However, evidence for another reason of TLR localization to the endosomal compartment is emerging. Structural and functional studies have shown that NA-sensing TLRs sense NA-degradation products, such as oligonucleotides and nucleosides (2–4), demonstrating that NA degradation generates TLR ligands. NA metabolism in the endosomal compartment is considered a positive and negative regulator of NA-sensing TLRs.

The endosomal compartment affects downstream signaling as well as NA sensing. TLRs activate two signaling pathways: proinflammatory signals activating NF-κB transcription factors and type I interferon signals activating transcription factors called interferon regulatory factors (IRFs) (5, 6). Both signals are activated in a mutually exclusive manner with the former preceding the latter

pathway. Delayed activation of IRFs is ascribed to the requirement of endosomal trafficking for IRF activation by TLRs. Therefore, endosomal trafficking serves as a switch to change TLR responses from proinflammatory to type I interferon (IFN) responses.

Constitutive activation of NA-sensing TLRs causes inflammatory diseases. Constitutive TLR activation is caused by alteration in NA metabolism, the endosomal compartment, or downstream signaling. These inflammatory diseases reveal molecular and cellular mechanisms by which endosomal TLRs are controlled by the endosomal compartment (1, 7).

Here, we provide an overview of recent progress in our understanding of the mechanisms by which endosomal TLR responses are controlled and the diseases caused by dysregulation of these controlling mechanisms.

1.1 Nucleic Acid Recognition by TLRs in the Endosomal Compartment

1.1.1 TLR3

TLR3 responds to double-stranded RNAs (dsRNAs) longer than 40–50 bp (8); this length is required to interact with a pair of TLR3 molecules and induce their dimerization. However, it remains unclear whether longer dsRNAs induce stronger TLR3 responses. TLR3 is expressed not only in the innate immune cells, such as macrophages and dendritic cells, but also in non-immune cells, such as neurons and keratinocytes. Broad expression enables TLR3 to serve as a sentinel protein in non-immune cells. For example, loss-of-function mutations in the genes required for TLR3-dependent type I IFN responses increase susceptibility to herpes encephalitis (9). Because neurons express only a limited set of pathogen sensors, TLR3 expressed in neurons plays an indispensable role in the control of herpes virus infection. TLR3 is probably activated by dsRNAs of virus origin, of which expression increase during viral infection. TLR3 also responds to self-derived RNAs during tissue damage. In keratinocytes, TLR3 responds to self-derived U1 RNA released from UV-irradiated cells to promote tissue repair (10). In contrast, TLR3 plays a pathologic role in radiation-induced gastrointestinal syndrome (11). TLR3 expressed in intestinal crypt cells responds to dsRNAs released p53-dependently from irradiated cells. Expression of TLR3 in crypt cells causes cell death and exacerbates radiation-induced gastrointestinal syndromes. Broad expression and responses to self-derived dsRNAs allow TLR3 to serve as a sensor not only for viruses but also for various tissue damage.

1.1.2 TLR7, TLR8, and TLR13

TLR7 and TLR8 are known to respond to single-stranded RNAs (ssRNAs), but their structural and functional analyses have shown that these TLRs bind to nucleosides and oligoribonucleotides (2–4). TLR7 is activated by guanosine or deoxyguanosine along with oligoribonucleotides, whereas TLR8 responds to uridine and oligoribonucleotides. Nucleosides and oligonucleotides synergistically activate both TLRs because oligoribonucleotides enhance TLR7/8 affinity to nucleosides. TLR7 and TLR8, therefore, respond to RNA degradation products generated in the endosomal compartment. This is a strong reason for the localization of TLR7 and TLR8 in the endosomal compartment. In mice, TLR8 is not active, but TLR13 serves as a *bona fide* ssRNA sensor. TLR13 binds directly to bacterial 23S ribosomal RNA in a sequence-specific manner (12, 13).

1.1.3 TLR9

TLR9 responds to single-stranded DNAs (ssDNAs). Because TLR9 has two binding sites, ssDNA fragment binds to a pair of TLR9 molecules, leading to the formation of a TLR9 dimer with two ssDNA fragments (14). Because cell surface expression of TLR9 drives systemic inflammation (15), ssDNA fragments may be present in the extracellular space as well as in the endosomal compartment.

1.2 Effect of Nucleic Acid Metabolism on Endosomal TLR Responses

1.2.1 DNase I and DNase I-Like 3

NAs released from dead cells are internalized into the endosomal compartment of the macrophages. Extracellular DNA is degraded by members of the DNASE1 family, such as DNase I and DNase I-like 3 (**Figure 1**). Because these enzymes require an optimal pH of 7.0, they degrade DNA before internalization into the endosomal compartment. DNase I is expressed in the kidney and lacrimal gland, whereas DNase I-like 3 is expressed in the innate immune cells, such as DCs. Despite their restricted expression, DNases are secreted and can degrade DNA in the circulation (16). Lupus-like diseases develop in patients harboring loss-of-function mutations in *DNASE1* or *DNASE1L3* genes (17, 18). Consistent with this, *Dnse1l3* deficiency in mice causes TLR7 and TLR9-dependent systemic autoimmune response (19). TLR7 activation in *Dnse1l3*$^{-/-}$ mice may be explained by TLR7 response to DNA-derived deoxyribonucleosides (2). Although DNase I is thought to negatively regulates TLR responses to self-DNA, TLR-dependency of lupus nephritis in *Dnase1*$^{-/-}$ mice has not been shown yet.

1.2.2 DNase II

DNase II is expressed in various cell types and exhibits optimal activity at pH 5.0. It plays an indispensable role in DNA degradation in the endosomal compartment. Loss-of-function mutations in the *DNASE2* gene cause type I interferonopathy characterized by anemia, thrombocytopenia, hepatosplenomegaly, glomerulonephritis, and liver fibrosis (20). Consistent with this, *Dnase2a*$^{-/-}$ mice are embryonically lethal owing to type I IFN-dependent anemia (21). Type I IFN production is driven by the cGAS-STING axis, because *Dnase2a*$^{-/-}$ *Sting*$^{-/-}$ mice are born normal (22). Although DNA accumulates in the endosomal compartment, TLR9 is not involved in type II IFN-dependent lethality (23) because DNase II is required for generation of a TLR9 ligand in DCs (24). *Dnase2a*$^{-/-}$ mice rescued by type I IFN receptor deficiency suffer from arthritis due to the constitutive activation of cGAS-STING and another cytoplasmic dsDNA sensor absent in melanoma 2 (AIM2) (25). The activation of cytoplasmic dsDNA sensors in *Dnase2a*$^{-/-}$ mice raises the question

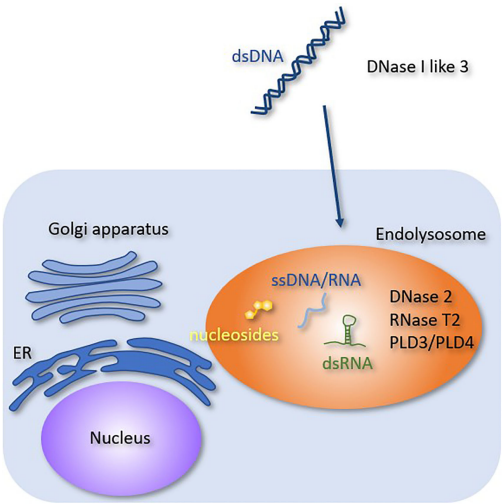

	Processing (ligand generation)	Degradation (negative regulation)
TLR3	?	RNase T2
TLR7/TLR8	RNase T2	PLD3/PLD4 DNase I like 3
TLR9	DNase 2	PLD3/PLD4 DNase I like 3

FIGURE 1 | Processing or degradation of TLR ligands by DNases and RNases. The extracellular and lysosomal enzymes involved in NA metabolism are shown. The Table summarizes the role of each enzyme in TLR responses. RNase T2 negatively regulates TLR3 responses but is required for TLR7 and TLR8 responses. PLD3, PLD4, and DNase I-like 3 negatively regulate TLR7, TLR8, and TLR9 responses. DNase 2 is required for TLR9 response.

of how lysosomal DNA enters the cytoplasm. dsDNAs are released from the nucleus to the cytoplasm under various stresses, and cytoplasmic dsDNAs are degraded by endosomal DNase II (26). cGAS-STING and AIM2 may be activated by nuclear DNA, which escapes lysosomal degradation in *Dnase2a*$^{-/-}$ mice.

1.2.3 RNase T2

RNase T2, the member of the T2 family of RNases with optimal activity at pH 4–5, is broadly expressed in various cell types. RNase T2 degrades RNA in the endosomal compartment, such as ribosomal RNA (27, 28). Loss-of-function mutations in the *RNASET2* gene cause cystic leukoencephalopathy (29), and RNase T2-deficient mice show type I interferonopathy; however, the responsible RNA sensor remains unclear (30). RNase T2 negatively regulates TLR3 responses by degrading dsRNAs, whereas it is required for TLR7/8 responses *via* the generation of ligands (31–33). These RNA-sensing TLRs might play a role in cystic leukoencephalopathy.

1.2.4 Phospholipase D3 and Phospholipase D4

Phospholipase D3 (PLD3) and Phospholipase D4 (PLD4) belong to the phospholipase D family. Macrophages express both PLD3 and PLD4, whereas B cells and DCs express only PLD4. Genome-wide association studies have shown that the *PLD4* gene is linked to autoimmune diseases, such as systemic sclerosis, systemic lupus erythematosus (SLE), and rheumatoid arthritis (34–36). In contrast, the *PLD3* gene is linked to neurodegenerative diseases, such as Alzheimer's disease and spinocerebellar ataxia (37, 38). *Pld3*$^{-/-}$ *Pld4*$^{-/-}$ mice exhibit macrophage activation syndrome (39, 40). PLD3 and PLD4 exonucleases degrade both DNA and RNA and negatively regulate TLR7 and TLR9 responses. The constitutive activation of TLR7 and TLR9 contributes to the pathology in *Pld3*$^{-/-}$ *Pld4*$^{-/-}$ mice (39).

1.3 Endosomal Compartment as the Platform Controlling Endosomal TLRs

1.3.1 Unc93B1

Unc93B1 is a multi-transmembrane endoplasmic reticulum (ER) molecule that is directly associated with the endosomal TLRs, including TLR3, TLR5, TLR7, TLR8, TLR9, and TLR13 (**Figure 2**). Without Unc93B1, these TLRs remain in the ER and fail to respond to their cognate ligands (41). In addition to its

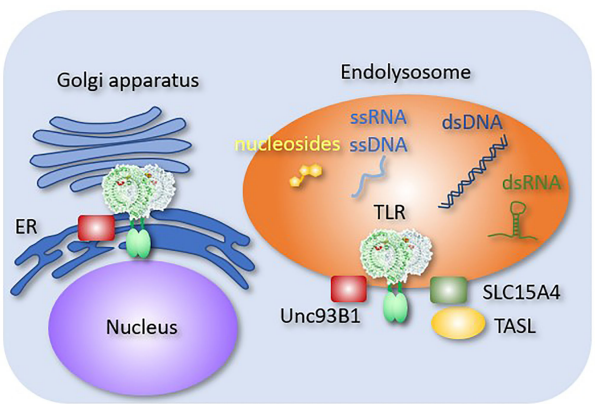

FIGURE 2 | Endosomal molecules controlling TLR responses. Endosomal molecules that control TLR responses are shown. Unc93B1 negatively regulates TLR9 dimerization. A complex consisting of SLC15A4 and TASL mediates TLR-dependent type I IFN production.

role as a TLR-specific chaperone, Unc93B1 directly affects TLR response. For example, Unc93B1 dissociates from TLR9 and TLR3 upon ligand stimulation. If Unc93B1 stays with TLR9 and TLR3, these TLRs fail to dimerize and activate downstream signals (42, 43). In TLR7, Unc93B1 remains associated with ligated TLR7, but the complex is degraded after being transported into intralumenal vesicles (44). These results demonstrated the role of Unc93B1 as a negative regulator of endosomal TLR response by inhibiting dimerization or degradation. The D34A mutation of Un93B1 in mice causes systemic inflammation due to constitutive TLR7 activation (45), suggesting that Unc93B1 serves as a negative regulator of TLR7 at the steady state. However, little is known about the mechanism by which Unc93B1 dissociates from TLR9 or TLR3 upon ligand stimulation.

1.3.2 Mechanisms of Type I IFN Production

TLR-dependent type I IFN production is controlled by the endosomal compartment in multiple ways. For instance, the endosomal compartment is the site where metabolic information is gathered. It is not surprising that metabolic sensors, such as mammalian target of rapamycin complex 1 (mTORC1), are localized in the endosomal compartment. Type I IFN production by TLR7 or TLR9 in pDCs is dependent on mTORC1 activation. Interestingly, proinflammatory cytokine production does not depend on mTORC1. Because mTORC1 activation drives anabolic processes in immune cells, type I IFN response might be more dependent on the anabolic activity than on proinflammatory responses.

TLR-dependent type I IFN induction is preceded by the stimulation of proinflammatory cytokines (46). This delayed type I IFN induction is ascribed to the requirement of endosomal trafficking for type I IFN production (47). Endosomal trafficking depends on small GTPases such as ADP ribosylation factors like 8b (Arl8b) and Rab7a. Interestingly, these proteins are differentially activated by TLRs. For example, TLR7 trafficking in pDCs depends on Arl8b, whereas TLR3 trafficking is regulated by Rab7a (46, 48). These GTPases mediate anterograde trafficking of TLR-containing endosomes from perinuclear regions to the cell periphery. Endosomal trafficking enables TLRs to interact with mTORC1 (49), suggesting that such trafficking connects the metabolic status with type I IFN responses.

TLR7 activation in pDCs initiates inside-out signaling of $\alpha_L\beta_2$ integrin, the adhesion of which is required to induce endosomal trafficking (46). Consistent with this, cell-cell interactions enhance type I IFN production by pDCs (50). The initiation of type I IFN responses is likely to depend on the optimal environment, such as the anabolic process and cell adhesion. TLRs sense these environmental conditions through endosomal trafficking. In other words, environmental cues affect TLR-dependent type I IFN responses *via* endosomal positioning.

SLC15A3 and SLC15A4 are peptide transporters in endosomal compartments. These molecules transport endosomal muramyl dipeptides (MDPs), which are sensed by NOD2 in the cytoplasm (51). SLC15A4 is required for TLR7 and TLR9 responses in pDCs (52). It also mediates AP3-dependent endosomal trafficking required for TLR7 and TLR9 responses (53). Moreover, SLC15A4 serves as a scaffold protein by associating with TLR adaptor interacting with SLC15A4 on the lysosome (TASL) (54), which recruits IRFs to transmit signals from TLR7, TLR8, and TLR9. These molecules mediate the production of TLR-dependent type-I IFN. Interestingly, *SLC15A4*, *IRF5* and *TASL* are all lupus-associated genes (55), which strongly suggest that type I IFN production by endosomal TLRs is activated in SLE.

1.4 Inflammatory Diseases Associated With Dysregulated Responses of Endosomal TLRs

1.4.1 Monogenic Diseases

Gain-of-function mutations in the *TLR8* gene such as P432L, F494L, and G527D, cause neutropenia, infections, lymphoproliferation, and B cell deficiency (56). Although TLR8 is expressed in myeloid cells, T cell activation and B cell deficiency develop, probably because of the cell non-autonomous mechanisms. These clinical manifestations are not necessarily consistent with the phenotypes of TLR8 transgenic mice, in which TLR8 expression is driven by a human endogenous promoter (57). TLR8 transgenic mice exhibit severe inflammation in the pancreas, salivary glands, and joints. In contrast to human patients harboring gain-of-function mutations in the *TLR8* gene, neither neutropenia nor B cell deficiency was observed. The TLR8 responses in TLR8 transgenic mice are distinct from those in humans.

Constitutive activation of TLR7 due to its gain-of-function mutation causes monogenic SLE in humans (58). The increase in B cell number depends on TLR7 expression. Because TLR7 is expressed not only in myeloid cells, but also in B cells, mutated TLR7 drives cell-autonomous B cell activation. A lupus-prone mouse strain, the Y-linked autoimmune accelerator strain, has an additional copy of the TLR7 gene that results in TLR7 hyperactivation, leading to lupus-like state (59, 60). Clinical manifestations in patients harboring gain-of-function mutations in *TLR7* genes differ from those with *TLR8* mutations and are ascribed to different expression in different immune cells. TLR7 is highly expressed in B cells and pDCs, whereas TLR8 is highly expressed in monocytes and macrophages.

The *ACP5* gene encodes lysosomal acid phosphatase expressed in osteoclasts, macrophages, and DCs. Loss-of-function mutations in the *ACP5* gene cause spondyloenchondrodysplasia with immune dysregulation, a disease characterized by skeletal dysplasia and neurologic and autoimmune manifestations (61). The detailed mechanisms underlying autoimmune manifestations remain unclear. ACP5 deficiency increases the level of hyperphosphorylated osteopontin, which is suggested to promote TLR9 responses in osteoclasts and macrophages.

1.4.2 Polygenic Diseases

SLE is an autoimmune disease characterized by autoantibody production and clinical manifestations affecting the skin, joints, kidneys, and the central nervous system (62). Causative autoimmune responses are driven by autoreactive B cells that

produce autoantibodies against NA-associated autoantigens and cDCs and pDCs that produce proinflammatory cytokines and type I IFN, respectively (63, 64). In addition to these cells, monocytes/macrophages infiltrate the glomeruli and play pathologic roles in glomerular damage associated with SLE, independent of immune complex (IC) deposition (65–67). The TLR7 agonist imiquimod drives lupus nephritis in mice (68, 69), whereas the pathologies in the lupus-prone strain, New Zealand Black/New Zealand White F1 (NZBWF1) mice, is ameliorated by TLR7 chemical inhibitor or by anti-TLR7 monoclonal antibody (70, 71). The number of Ly6C^{low} patrolling monocytes TLR7-dependently increases in NZBWF1 mice (39). Interestingly, during monocyte maturation from Ly6C^{hi} to Ly6C^{low} cells, TLR9 expression decreases with TLR7 expression unchanged (72). The IC-independent glomerular accumulation of Ly6C^{low} patrolling monocytes causes lupus nephritis in another lupus-prone mouse strain lacking the human SLE susceptibility gene, *Tnip1* (67).

The TLR7-dependent increase in Ly6C^{low} monocytes/macrophages might be driven by self-derived RNAs. The 60 kDa Ro60 ribonucleoprotein, also known as the SSA/Ro antigen, is one of the most studied autoantigens associated with SLE or primary Sjögren syndrome. Because Alu retroelements, repetitive transposons, bind to Ro60 and activate TLR7 and TLR8 (73), the IC consisting of Ro60, Alu retroelements, and autoantibodies is formed in lupus-prone mice and internalized by autoreactive B cells or DCs *via* the BCR or FcR, respectively. Alu retroelements in the IC activate endosomal TLR7 or TLR8 to drive autoimmunity (74). TLR7 may also be activated by RNA from bacteria, which enter the circulation through the leaky gut (75). Notably, commensal orthologs of Ro60 might play a pathologic role in SLE (76).

Systemic sclerosis (SSc) is a multisystem life-threatening fibrosing disorder (77). Aberrant TLR8 expression in pDCs has been reported in patients with SSc (78). pDCs normally express only TLR7. Additional expression of TLR8 may promote autoimmune responses in SSc.

AUTHOR CONTRIBUTIONS

KM wrote the manuscript. TS, RF, RS, SS, and YM made comments on the manuscript. All authors contributed to the article and approved the submitted version.

FUNDING

This work was supported in part by: Grant-in-Aid for Scientific Research (S and A) to KM (16H06388, 21H04800), (B) to S-IS (26293083), and (C) (16K08827) to TS; JST CREST (JPMJCR13M5, JPMJCR21E4) to TS and KM, respectively; Joint Research Project of the Institute of Medical Science at the University of Tokyo; and JSPS KAKENHI Grant Number JP 16H06276 (AdAMS).

REFERENCES

1. Barton GM, Kagan JC. A Cell Biological View of Toll-Like Receptor Function: Regulation Through Compartmentalization. *Nat Rev Immunol* (2009) 9 (8):535–42. doi: 10.1038/nri2587
2. Shibata T, Ohto U, Nomura S, Kibata K, Motoi Y, Zhang Y, et al. Guanosine and its Modified Derivatives are Endogenous Ligands for TLR7. *Int Immunol* (2016) 28(5):211–22. doi: 10.1093/intimm/dxv062
3. Zhang Z, Ohto U, Shibata T, Krayukhina E, Taoka M, Yamauchi Y, et al. Structural Analysis Reveals That Toll-Like Receptor 7 Is a Dual Receptor for Guanosine and Single-Stranded RNA. *Immunity* (2016) 45(4):737–48. doi: 10.1016/j.immuni.2016.09.011
4. Tanji H, Ohto U, Shibata T, Taoka M, Yamauchi Y, Isobe T, et al. Toll-Like Receptor 8 Senses Degradation Products of Single-Stranded RNA. *Nat Struct Mol Biol* (2015) 22(2):109–15. doi: 10.1038/nsmb.2943
5. Miyake K, Shibata T, Ohto U, Shimizu T, Saitoh SI, Fukui R, et al. Mechanisms Controlling Nucleic Acid-Sensing Toll-Like Receptors. *Int Immunol* (2018) 30(2):43–51. doi: 10.1093/intimm/dxy016
6. Kaisho T, Akira S. Toll-Like Receptor Function and Signaling. *J Allergy Clin Immunol* (2006) 117(5):979–87. doi: 10.1016/j.jaci.2006.02.023
7. Miyake K, Saitoh SI, Sato R, Shibata T, Fukui R, Murakami Y. Endolysosomal Compartments as Platforms for Orchestrating Innate Immune and Metabolic Sensors. *J Leukoc Biol* (2019) 106(4):853–62. doi: 10.1002/JLB.MR0119-020R
8. Bell JK, Botos I, Hall PR, Askins J, Shiloach J, Segal DM, et al. The Molecular Structure of the Toll-Like Receptor 3 Ligand-Binding Domain. *Proc Natl Acad Sci U S A* (2005) 102(31):10976–80. doi: 10.1073/pnas.0505077102
9. Zhang S-Y, Casanova J-L. Inborn Errors Underlying Herpes Simplex Encephalitis: From TLR3 to IRF3. *J Exp Med* (2015) 212(9):1342. doi: 10.1084/jem.2129insight4
10. Bernard JJ, Cowing-Zitron C, Nakatsuji T, Muehleisen B, Muto J, Borkowski AW, et al. Ultraviolet Radiation Damages Self Noncoding RNA and Is Detected by TLR3. *Nat Med* (2012) 18:1286–90. doi: 10.1038/nm.2861.
11. Takemura N, Kawasaki T, Kunisawa J, Sato S, Lamichhane A, Kobiyama K, et al. Blockade of TLR3 Protects Mice From Lethal Radiation-Induced Gastrointestinal Syndrome. *Nat Commun* (2014) 5:3492. doi: 10.1038/ncomms4492
12. Song W, Wang J, Han Z, Zhang Y, Zhang H, Wang W, et al. Structural Basis for Specific Recognition of Single-Stranded RNA by Toll-Like Receptor 13. *Nat Struct Mol Biol* (2015) 22(10):782–7. doi: 10.1038/nsmb.3080
13. Oldenburg M, Krüger A, Ferstl R, Kaufmann A, Nees G, Sigmund A, et al. TLR13 Recognizes Bacterial 23S rRNA Devoid of Erythromycin Resistance-Forming Modification. *Science* (2012) 337(6098):1111–5. doi: 10.1126/science.1220363
14. Ohto U, Shibata T, Tanji H, Ishida H, Krayukhina E, Uchiyama S, et al. Structural Basis of CpG and Inhibitory DNA Recognition by Toll-Like Receptor 9. *Nature* (2015) 520(7549):702–5. doi: 10.1038/nature14138
15. Mouchess ML, Arpaia N, Souza G, Barbalat R, Ewald SE, Lau L, et al. Transmembrane Mutations in Toll-Like Receptor 9 Bypass the Requirement for Ectodomain Proteolysis and Induce Fatal Inflammation. *Immunity* (2011) 35(5):721–32. doi: 10.1016/j.immuni.2011.10.009
16. Jiménez-Alcázar M, Rangaswamy C, Panda R, Bitterling J, Simsek YJ, Long AT, et al. Host DNases Prevent Vascular Occlusion by Neutrophil Extracellular Traps. *Science* (2017) 358(6367):1202–6. doi: 10.1126/science.aam8897
17. Yasutomo K, Horiuchi T, Kagami S, Tsukamoto H, Hashimura C, Urushihara M, et al. Mutation of DNASE1 in People With Systemic Lupus Erythematosus. *Nat Genet* (2001) 28(4):313–4. doi: 10.1038/91070
18. Al-Mayouf SM, Sunker A, Abdwani R, Abrawi SA, Almurshedi F, Alhashmi N, et al. Loss-Of-Function Variant in DNASE1L3 Causes a Familial Form of

Systemic Lupus Erythematosus. *Nat Genet* (2011) 43(12):1186–8. doi: 10.1038/ng.975
19. Soni C, Perez OA, Voss WN, Pucella JN, Serpas L, Mehl J, et al. Plasmacytoid Dendritic Cells and Type I Interferon Promote Extrafollicular B Cell Responses to Extracellular Self-DNA. *Immunity* (2020) 52(6):1022–38.e7. doi: 10.1016/j.immuni.2020.04.015
20. Rodero MP, Tesser A, Bartok E, Rice GI, Della Mina E, Depp M, et al. Type I Interferon-Mediated Autoinflammation Due to DNase II Deficiency. *Nat Commun* (2017) 8(1):2176. doi: 10.1038/s41467-017-01932-3
21. Yoshida H, Okabe Y, Kawane K, Fukuyama H, Nagata S. Lethal Anemia Caused by Interferon-Beta Produced in Mouse Embryos Carrying Undigested DNA. *Nat Immunol* (2005) 6(1):49–56. doi: 10.1038/ni1146
22. Ahn J, Gutman D, Saijo S, Barber GN. STING Manifests Self DNA-Dependent Inflammatory Disease. *Proc Natl Acad Sci U S A* (2012) 109(47):19386–91. doi: 10.1073/pnas.1215006109
23. Okabe Y, Kawane K, Akira S, Taniguchi T, Nagata S. Toll-Like Receptor-Independent Gene Induction Program Activated by Mammalian DNA Escaped From Apoptotic DNA Degradation. *J Exp Med* (2005) 202 (10):1333–9. doi: 10.1084/jem.20051654
24. Chan MP, Onji M, Fukui R, Kawane K, Shibata T, Saitoh S, et al. DNase II-Dependent DNA Digestion Is Required for DNA Sensing by TLR9. *Nat Commun* (2015) 6:5853. doi: 10.1038/ncomms6853
25. Baum R, Sharma S, Carpenter S, Li Q-Z, Busto P, Fitzgerald KA, et al. Cutting Edge: AIM2 and Endosomal TLRs Differentially Regulate Arthritis and Autoantibody Production in DNase II–Deficient Mice. *J Immunol* (2015) 194(3):873–7. doi: 10.4049/jimmunol.1402573
26. Lan Yuk Y, Londoño D, Bouley R, Rooney Michael S, Hacohen N. Dnase2a Deficiency Uncovers Lysosomal Clearance of Damaged Nuclear DNA *via* Autophagy. *Cell Rep* (2014) 9(1):180–92. doi: 10.1016/j.celrep.2014.08.074
27. Huang H, Kawamata T, Horie T, Tsugawa H, Nakayama Y, Ohsumi Y, et al. Bulk RNA Degradation by Nitrogen Starvation-Induced Autophagy in Yeast. *EMBO J* (2015) 34(2):154–68. doi: 10.15252/embj.201489083
28. Haud N, Kara F, Diekmann S, Henneke M, Willer JR, Hillwig MS, et al. Rnaset2 Mutant Zebrafish Model Familial Cystic Leukoencephalopathy and Reveal a Role for RNase T2 in Degrading Ribosomal RNA. *Proc Natl Acad Sci U S A* (2011) 108(3):1099–103. doi: 10.1073/pnas.1009811107
29. Henneke M, Diekmann S, Ohlenbusch A, Kaiser J, Engelbrecht V, Kohlschutter A, et al. RNASET2-Deficient Cystic Leukoencephalopathy Resembles Congenital Cytomegalovirus Brain Infection. *Nat Genet* (2009) 41(7):773–5. doi: 10.1038/ng.398
30. Kettwig M, Ternka K, Wendland K, Krüger DM, Zampar S, Schob C, et al. Interferon-Driven Brain Phenotype in a Mouse Model of RNaseT2 Deficient Leukoencephalopathy. *Nat Commun* (2021) 12(1):6530. doi: 10.1038/s41467-021-26880-x
31. Ostendorf T, Zillinger T, Andryka K, Schlee-Guimaraes TM, Schmitz S, Marx S, et al. Immune Sensing of Synthetic, Bacterial, and Protozoan RNA by Toll-Like Receptor 8 Requires Coordinated Processing by RNase T2 and RNase 2. *Immunity* (2020) 52(4):591–605. doi: 10.1016/j.immuni.2020.03.009
32. Greulich W, Wagner M, Gaidt MM, Stafford C, Cheng Y, Linder A, et al. TLR8 Is a Sensor of RNase T2 Degradation Products. *Cell* (2019) 179(6):1264–75.e13. doi: 10.1016/j.cell.2019.11.001
33. Liu K, Sato R, Shibata T, Hiranuma R, Reuter T, Fukui R, et al. Skewed Endosomal RNA Responses From TLR7 to TLR3 in RNase T2-Deficient Macrophages. *Int Immunol* (2021) 33(9):479–90. doi: 10.1093/intimm/dxab033
34. Akizuki S, Ishigaki K, Kochi Y, Law SM, Matsuo K, Ohmura K, et al. PLD4 is a Genetic Determinant to Systemic Lupus Erythematosus and Involved in Murine Autoimmune Phenotypes. *Ann Rheum Dis* (2019) 78(4):509–18. doi: 10.1136/annrheumdis-2018-214116
35. Terao C, Ohmura K, Kawaguchi Y, Nishimoto T, Kawasaki A, Takehara K, et al. PLD4 as a Novel Susceptibility Gene for Systemic Sclerosis in a Japanese Population. *Arthritis Rheumatol* (2013) 65(2):472–80. doi: 10.1002/art.37777
36. Okada Y, Terao C, Ikari K, Kochi Y, Ohmura K, Suzuki A, et al. Meta-Analysis Identifies Nine New Loci Associated With Rheumatoid Arthritis in the Japanese Population. *Nat Genet* (2012) 44(5):511–6. doi: 10.1038/ng.2231
37. Cruchaga C, Karch CM, Jin SC, Benitez BA, Cai Y, Guerreiro R, et al. Rare Coding Variants in the Phospholipase D3 Gene Confer Risk for Alzheimer's Disease. *Nature* (2014) 505(7484):550–4. doi: 10.1038/nature12825
38. Nibbeling EAR, Duarri A, Verschuuren-Bemelmans CC, Fokkens MR, Karjalainen JM, Smeets CJLM, et al. Exome Sequencing and Network Analysis Identifies Shared Mechanisms Underlying Spinocerebellar Ataxia. *Brain* (2017) 140(11):2860–78. doi: 10.1093/brain/awx251
39. Gavin AL, Huang D, Blane TR, Thinnes TC, Murakami Y, Fukui R, et al. Cleavage of DNA and RNA by PLD3 and PLD4 Limits Autoinflammatory Triggering by Multiple Sensors. *Nat Commun* (2021) 12(1):5874. doi: 10.1038/s41467-021-26150-w
40. Gavin AL, Huang D, Huber C, Mårtensson A, Tardif V, Skog PD, et al. PLD3 and PLD4 are Single-Stranded Acid Exonucleases That Regulate Endosomal Nucleic-Acid Sensing. *Nat Immunol* (2018) 19(9):942–53. doi: 10.1038/s41590-018-0179-y
41. Kim YM, Brinkmann MM, Paquet ME, Ploegh HL. UNC93B1 Delivers Nucleotide-Sensing Toll-Like Receptors to Endolysosomes. *Nature* (2008) 452(7184):234–8. doi: 10.1038/nature06726
42. Majer O, Liu B, Woo BJ, Kreuk LSM, Van Dis E, Barton GM. Release From UNC93B1 Reinforces the Compartmentalized Activation of Select TLRs. *Nature* (2019) 575(7782):371–4. doi: 10.1038/s41586-019-1611-7
43. Ishida H, Asami J, Zhang Z, Nishizawa T, Shigematsu H, Ohto U, et al. Cryo-EM Structures of Toll-Like Receptors in Complex With UNC93B1. *Nat Struct Mol Biol* (2021) 28(2):173–80. doi: 10.1038/s41594-020-00542-w
44. Majer O, Liu B, Kreuk LSM, Krogan N, Barton GM. UNC93B1 Recruits Syntenin-1 to Dampen TLR7 Signalling and Prevent Autoimmunity. *Nature* (2019) 575(7782):366–70. doi: 10.1038/s41586-019-1612-6
45. Fukui R, Saitoh S, Kanno A, Onji M, Shibata T, Ito A, et al. Unc93B1 Restricts Systemic Lethal Inflammation by Orchestrating Toll-Like Receptor 7 and 9 Trafficking. *Immunity* (2011) 35(1):69–81. doi: 10.1016/j.immuni.2011.05.010
46. Saitoh SI, Abe F, Kanno A, Tanimura N, Mori Saitoh Y, Fukui R, et al. TLR7 Mediated Viral Recognition Results in Focal Type I Interferon Secretion by Dendritic Cells. *Nat Commun* (2017) 8(1):1592. doi: 10.1038/s41467-017-01687-x
47. Cao W, Manicassamy S, Tang H, Kasturi SP, Pirani A, Murthy N, et al. Toll-Like Receptor-Mediated Induction of Type I Interferon in Plasmacytoid Dendritic Cells Requires the Rapamycin-Sensitive PI(3)K-mTOR-P70s6k Pathway. *Nat Immunol* (2008) 9(10):1157–64. doi: 10.1038/ni.1645
48. Sato R, Kato A, Chimura T, Saitoh SI, Shibata T, Murakami Y, et al. Combating Herpesvirus Encephalitis by Potentiating a TLR3-Mtorc2 Axis. *Nat Immunol* (2018) 19(10):1071–82. doi: 10.1038/s41590-018-0203-2
49. Korolchuk VI, Saiki S, Lichtenberg M, Siddiqi FH, Roberts EA, Imarisio S, et al. Lysosomal Positioning Coordinates Cellular Nutrient Responses. *Nat Cell Biol* (2011) 13(4):453–60. doi: 10.1038/ncb2204
50. Kim S, Kaiser V, Beier E, Bechheim M, Guenthner-Biller M, Ablasser A, et al. Self-Priming Determines High Type I IFN Production by Plasmacytoid Dendritic Cells. *Eur J Immunol* (2014) 44(3):807–18. doi: 10.1002/eji.201343806
51. Nakamura N, Lill JR, Phung Q, Jiang Z, Bakalarski C, de Mazière A, et al. Endosomes are Specialized Platforms for Bacterial Sensing and NOD2 Signalling. *Nature* (2014) 509(7499):240–4. doi: 10.1038/nature13133
52. Kobayashi T, Shimabukuro-Demoto S, Yoshida-Sugitani R, Furuyama-Tanaka K, Karyu H, Sugiura Y, et al. The Histidine Transporter SLC15A4 Coordinates mTOR-Dependent Inflammatory Responses and Pathogenic Antibody Production. *Immunity* (2014) 41(3):375–88. doi: 10.1016/j.immuni.2014.08.011
53. Rimann I, Gonzalez-Quintial R, Baccala R, Kiosses WB, Teijaro JR, Parker CG, et al. The Solute Carrier SLC15A4 Is Required for Optimal Trafficking of Nucleic Acid-Sensing TLRs and Ligands to Endolysosomes. *Proc Natl Acad Sci U S A* (2022) 119(14):e2200544119. doi: 10.1073/pnas.2200544119
54. Heinz LX, Lee J, Kapoor U, Kartnig F, Sedlyarov V, Papakostas K, et al. TASL is the SLC15A4-Associated Adaptor for IRF5 Activation by TLR7-9. *Nature* (2020) 581(7808):316–22. doi: 10.1038/s41586-020-2282-0
55. Bentham J, Morris DL, Graham DSC, Pinder CL, Tombleson P, Behrens TW, et al. Genetic Association Analyses Implicate Aberrant Regulation of Innate and Adaptive Immunity Genes in the Pathogenesis of Systemic Lupus Erythematosus. *Nat Genet* (2015) 47(12):1457–64. doi: 10.1038/ng.3434
56. Aluri J, Bach A, Kaviany S, Chiquetto Paracatu L, Kitcharoensakkul M, Walkiewicz MA, et al. Immunodeficiency and Bone Marrow Failure With Mosaic and Germline TLR8 Gain of Function. *Blood* (2021) 137(18):2450–62. doi: 10.1182/blood.2020009620

57. Guiducci C, Gong M, Cepika AM, Xu Z, Tripodo C, Bennett L, et al. RNA Recognition by Human TLR8 can Lead to Autoimmune Inflammation. *J Exp Med* (2013) 210(13):2903–19. doi: 10.1084/jem.20131044
58. Brown GJ, Cañete PF, Wang H, Medhavy A, Bones J, Roco JA, et al. TLR7 Gain-of-Function Genetic Variation Causes Human Lupus. *Nature* (2022) 605:349–56. doi: 10.1038/s41586-022-04642-z
59. Pisitkun P, Deane JA, Difilippantonio MJ, Tarasenko T, Satterthwaite AB, Bolland S. Autoreactive B Cell Responses to RNA-Related Antigens Due to TLR7 Gene Duplication. *Science* (2006) 312(5780):1669. doi: 10.1126/science.1124978
60. Subramanian S, Tus K, Li Q-Z, Wang A, Tian X-H, Zhou J, et al. A Tlr7 Translocation Accelerates Systemic Autoimmunity in Murine Lupus. *Proc Natl Acad Sci USA* (2006) 103(26):9970–5. doi: 10.1073/pnas.0603912103
61. Briggs TA, Rice GI, Daly S, Urquhart J, Gornall H, Bader-Meunier B, et al. Tartrate-Resistant Acid Phosphatase Deficiency Causes a Bone Dysplasia With Autoimmunity and a Type I Interferon Expression Signature. *Nat Genet* (2011) 43(2):127–31. doi: 10.1038/ng.748
62. Yu F, Haas M, Glassock R, Zhao MH. Redefining Lupus Nephritis: Clinical Implications of Pathophysiologic Subtypes. *Nat Rev Nephrol* (2017) 13 (8):483–95. doi: 10.1038/nrneph.2017.85
63. Smith CK, Kaplan MJ. The Role of Neutrophils in the Pathogenesis of Systemic Lupus Erythematosus. *Curr Opin Rheumatol* (2015) 27(5):448–53. doi: 10.1097/BOR.0000000000000197
64. Tsokos GC, Lo MS, Reis PC, Sullivan KE. New Insights Into the Immunopathogenesis of Systemic Lupus Erythematosus [Review]. *Nat Rev Rheumatol* (2016) 12(12):716–30. doi: 10.1038/nrrheum.2016.186
65. Clynes R, Dumitru C, Ravetch JV. Uncoupling of Immune Complex Formation and Kidney Damage in Autoimmune Glomerulonephritis. *Science* (1998) 279(5353):1052–4. doi: 10.1126/science.279.5353.1052
66. Bergtold A, Gavhane A, D'Agati V, Madaio M, Clynes R. FcR-Bearing Myeloid Cells are Responsible for Triggering Murine Lupus Nephritis. *J Immunol* (2006) 177(10):7287–95. doi: 10.4049/jimmunol.177.10.7287
67. Kuriakose J, Redecke V, Guy C, Zhou J, Wu R, Ippagunta SK, et al. Patrolling Monocytes Promote the Pathogenesis of Early Lupus-Like Glomerulonephritis. *J Clin Invest* (2019) 129(6):2251–65. doi: 10.1172/JCI125116
68. Goel RR, Wang X, O'Neil LJ, Nakabo S, Hasneen K, Gupta S, et al. Interferon Lambda Promotes Immune Dysregulation and Tissue Inflammation in TLR7-Induced Lupus. *Proc Natl Acad Sci U S A* (2020) 117(10):5409–19. doi: 10.1073/pnas.1916897117
69. Yokogawa M, Takaishi M, Nakajima K, Kamijima R, Fujimoto C, Kataoka S, et al. Epicutaneous Application of Toll-Like Receptor 7 Agonists Leads to Systemic Autoimmunity in Wild-Type Mice: A New Model of Systemic Lupus Erythematosus. *Arthritis Rheumatol* (2014) 66(3):694–706. doi: 10.1002/art.38298
70. Tojo S, Zhang Z, Matsui H, Tahara M, Ikeguchi M, Kochi M, et al. Structural Analysis Reveals TLR7 Dynamics Underlying Antagonism. *Nat Commun* (2020) 11(1):5204. doi: 10.1038/s41467-020-19025-z
71. Murakami Y, Fukui R, Tanaka R, Motoi Y, Kanno A, Sato R, et al. Anti-TLR7 Antibody Protects Against Lupus Nephritis in NZBWF1 Mice by Targeting B Cells and Patrolling Monocytes. *Front Immunol* (2021) 12:777197. doi: 10.3389/fimmu.2021.777197
72. Sato R, Reuter T, Hiranuma R, Shibata T, Fukui R, Motoi Y, et al. The Impact of Cell Maturation and Tissue Microenvironments on the Expression of Endosomal Toll-Like Receptors in Monocytes and Macrophages. *Int Immunol* (2020) 32(12):785–98. doi: 10.1093/intimm/dxaa055
73. Hung T, Pratt GA, Sundararaman B, Townsend MJ, Chaivorapol C, Bhangale T, et al. The Ro60 Autoantigen Binds Endogenous Retroelements and Regulates Inflammatory Gene Expression. *Science* (2015) 350(6259):455. doi: 10.1126/science.aac7442
74. Marshak-Rothstein A, Rifkin IR. Immunologically Active Autoantigens: The Role of Toll-Like Receptors in the Development of Chronic Inflammatory Disease. *Annu Rev Immunol* (2007) 25:419–41. doi: 10.1146/annurev.immunol.22.012703.104514
75. Manfredo Vieira S, Hiltensperger M, Kumar V, Zegarra-Ruiz D, Dehner C, Khan N, et al. Translocation of a Gut Pathobiont Drives Autoimmunity in Mice and Humans. *Science* (2018) 359(6380):1156–61. doi: 10.1126/science.aar7201
76. Greiling TM, Dehner C, Chen X, Hughes K, Iñiguez AJ, Boccitto M, et al. Commensal Orthologs of the Human Autoantigen Ro60 as Triggers of Autoimmunity in Lupus. *Sci Transl Med* (2018) 10(434):eaan2306. doi: 10.1126/scitranslmed.aan2306
77. Varga J, Abraham D. Systemic Sclerosis: A Prototypic Multisystem Fibrotic Disorder. *J Clin Invest* (2007) 117(3):557–67. doi: 10.1172/JCI31139
78. Ah Kioon MD, Tripodo C, Fernandez D, Kirou KA, Spiera RF, Crow MK, et al. Plasmacytoid Dendritic Cells Promote Systemic Sclerosis With a Key Role for TLR8. *Sci Transl Med* (2018) 10(423):01. doi: 10.1126/scitranslmed.aam8458

Conflict of Interest: The authors declare that the research was conducted in the absence of any commercial or financial relationships that could be construed as potential conflicts of interest.

frontiers | Frontiers in Immunology

ORIGINAL RESEARCH
published: 29 June 2022
doi: 10.3389/fimmu.2022.913955

The Non-Receptor Protein Tyrosine Phosphatase PTPN6 Mediates a Positive Regulatory Approach From the Interferon Regulatory Factor to the JAK/STAT Pathway in *Litopenaeus vannamei*

Mengting Luo[1†], *Xiaopeng Xu*[1,2,3†], *Xinxin Liu*[1], *Wenjie Shen*[1], *Linwei Yang*[1,2,3], *Zhiming Zhu*[2], *Shaoping Weng*[1,2,3], *Jianguo He*[1,2,3*] and *Hongliang Zuo*[1,2,3*]

[1] State Key Laboratory of Biocontrol, School of Life Sciences, Sun Yat-sen University, Guangzhou, China, [2] Southern Marine Science and Engineering Guangdong Laboratory (Zhuhai), Zhuhai, China, [3] China-Association of Southeast Asian Nations (ASEAN) Belt and Road Joint Laboratory on Marine Aquaculture Technology, Sun Yat-sen University, Guangzhou, China

OPEN ACCESS

Edited by:
Ying Zhang,
Tsinghua University, China

Reviewed by:
Yueling Zhang,
Shantou University, China
Haijun Tu,
Hunan University, China

***Correspondence:**
Hongliang Zuo
zuohliang@mail.sysu.edu.cn
Jianguo He
lsshjg@mail.sysu.edu.cn

[†]These authors have contributed equally to this work

Specialty section:
This article was submitted to Molecular Innate Immunity, a section of the journal Frontiers in Immunology

Received: 06 April 2022
Accepted: 25 May 2022
Published: 29 June 2022

Citation:
Luo M, Xu X, Liu X, Shen W, Yang L, Zhu Z, Weng S, He J and Zuo H (2022) The Non-Receptor Protein Tyrosine Phosphatase PTPN6 Mediates a Positive Regulatory Approach From the Interferon Regulatory Factor to the JAK/STAT Pathway in Litopenaeus vannamei. Front. Immunol. 13:913955. doi: 10.3389/fimmu.2022.913955

SH2-domain-containing protein tyrosine phosphatases (PTPs), belonging to the class I PTP superfamily, are responsible for the dephosphorylation on the phosphorylated tyrosine residues in some proteins that are involved in multiple biological processes in eukaryotes. The Janus kinase/signal transducers and activators of transcription (JAK/STAT) pathway transduce signaling responding to interferons and initiate cellular antiviral responses. The activity of the JAK/STAT pathway is generally orchestrated by the de-/phosphorylation of the tyrosine and serine residues of JAKs and STATs, in which the dephosphorylation processes are mainly controlled by PTPs. In the present study, an SH2-domian-contianing PTP, temporally named as LvPTPN6, was identified in *Litopenaeus vannamei*. LvPTPN6 shares high similarity with PTPN6s from other organisms and was phylogenetically categorized into the clade of arthropods that differs from those of fishes and mammals. LvPTPN6 was constitutively expressed in all detected tissues, located mainly in the cytoplasm, and differentially induced in hemocyte and gill after the challenge of stimulants, indicating its complicated regulatory roles in shrimp immune responses. Intriguingly, the expression of LvPTPN6 was regulated by interferon regulatory factor (IRF), which could directly bind to the LvPTPN6 promoter. Surprisingly, unlike other PTPN6s, LvPTPN6 could promote the dimerization of STAT and facilitate its nuclear localization, which further elevated the expression of STAT-targeting immune effector genes and enhanced the antiviral immunity of shrimp. Therefore, this study suggests a PTPN6-mediated regulatory approach from IRF to the JAK/STAT signaling pathway in shrimp, which provides new insights into the regulatory roles of PTPs in the JAK/STAT signaling pathway and contributes to the further understanding of the mechanisms of antiviral immunity in invertebrates.

Keywords: non-receptor protein tyrosine phosphatase, antiviral immunity, IFN regulatory factor, JAK/STAT signaling pathway, *Litopenaeus vannamei*

INTRODUCTION

Protein tyrosine phosphatases (PTPs) are a sort of fundamental phosphatases responsible for the dephosphorylation of phosphorylated tyrosines in proteins that are involved in various biological processes including embryogenesis, organ development, tissue homeostasis, and the immune defenses in multicellular eukaryotes (1, 2). To date, more than 100 PTPs have been identified in the human genome and most of them possess non-redundant functions verified by the unique phenotypes of many reported gene deletions in mice (3, 4). According to the features of catalytic domains, PTPs can be classified into four subfamilies, among which classes I, II, and III are independently evolved PTPs that possess similar catalytic mechanisms and active targets, while class IV performs the catalytic function with a key aspartic acid and dependence on a cation (5–8). Class I PTPs are cysteine-based and strictly tyrosine-specific PTPs that possess the largest number of subfamily members, including the classical PTPs, vaccinia virus *H1*-like (VH1-like) enzymes, and "dual-specific" protein phosphatases (DSPs), constituting the most diverse group in terms of substrate specificity (9, 10). The classical PTPs can be further divided into receptor-like enzymes (RPTPs) and non-receptor PTPs (NRPTPs), which are distinguished by the containing of the transmembrane domain, while both of them are essential for the dephosphorylation of the tyrosine residues in their specific targets (5, 11).

The interferon (IFN) system plays a critical role in immunity, establishing a cellular antiviral state in cells of vertebrates and invertebrates (12, 13). The IFN regulatory factor (IRF) family is a kind of transcriptional factors, responsible for the transcriptional regulation of IFNs that can bind to IFN receptors and activate the Janus kinase (JAK)/signal transducers and activators of transcription (STAT) signaling pathway to promote the transcription of STAT-targeted genes (14, 15). The JAK/STAT pathway has been proved to mediate the transcription of numerous genes that participate in many cellular processes, such as cell proliferation, differentiation, apoptosis, and immunity, *via* a series of intracellular signaling cascades (16, 17). Briefly, after the binding of INFs, the transmembrane receptors are dimerized and trigger the auto- and trans-phosphorylation of JAKs to generate docking sites for the Src homology 2 (SH2) domains of latent STATs (18, 19). STATs are recruited and reversible phosphorylated by JAKs on a crucial tyrosine residue in their C-terminal region and then homo- or heterodimerized through the SH2-domain-phospho-tyrosine interactions. The activated STAT dimers are translocated into the nucleus for establishing the cellular transcriptional landscape (20, 21).

Since phosphorylation of tyrosine residues is a reversible process, activated STATs can be negatively regulated by PTP-mediated dephosphorylation. In mammals, seven PTPs had been proved to negatively regulate the JAK-STAT signaling pathway by dephosphorylating STATs, including PTP receptor-type D (PTPRD), PTP receptor-type T (PTPRT), PTP receptor-type K (PTPRK), Src homology region 2 (SH-2) domain-containing phosphatase 1 (SHP1, also named as PTPN6), SH-2 domain-containing phosphatase 2 (SHP2, also named as PTPN11), MEG2/PTP non-receptor type 9 (PTPN9), and T-cell PTP (TC-PTP)/PTP noc-receptor type 2 (PTPN2). However, some PTPs have been known to positively regulate the JAK/STAT signaling pathway through direct or indirect manners (22). For example, SHP-1 is positively involved in epidermal growth factor (EGF) and IFN-γ-induced STAT activation in non-hematopoietic Hela cells (23). SHP-2 could enhance the stability of JAK2 and facilitate prolactin/STAT5-mediated signaling by dephosphorylating tyrosine (Tyr-1007) of JAK2, a critical recruitment site for the ubiquitin ligase-associated inhibitory protein suppressor of cytokine signaling-1 (SOCS-1) (24).

Pacific white shrimp *Litopenaeus vannamei* is the major cultured shrimp species around the world, which has considerable nutritional and economic values (25). With the rapid development of the shrimp farming industry and the popularization of intensive farming systems, shrimp aquaculture has been threatened by various pathogens that cause huge economic losses (26, 27). Numerous studies had confirmed that *L. vannamei* possesses an IRF-Vago-JAK/STAT regulatory axis that is similar to the IRF-IFN-JAK/STAT axis of vertebrates, which establishes the important role of the JAK/STAT signaling pathway in shrimp anti-viral immunity (12, 28, 29). However, the detailed regulatory mechanism of the shrimp JAK/STAT signaling pathway remains unclear. In this study, the non-receptor protein tyrosine phosphatases 6 gene, temporarily named as LvPTPN6, was identified in *L. vannamei*. Results intriguingly revealed that LvPTPN6 mediated an intracellular IRF-JAK/STAT positive regulatory axis. These findings may provide new insights into the regulatory mechanism of the IRF-JAK/STAT signaling pathway in shrimp and give a better understanding of PTP evolution.

MATERIALS AND METHODS

Shrimps

L. vannamei (~10 g) were obtained from an aquaculture farm in Zhuhai, acclimated in a recirculating water tank system filled with air-pumped seawater (2.0% salinity), fed with 3% body weight artificial diet for two times each day, and detected by PCR to ensure they are free of WSSV, *Vibrio parahaemolyticus*, and *Staphylococcus aureus* with 5% random sampling.

Cloning of LvPTPN6

Total RNA was extracted from mixed tissues including gill, hepatopancreas, intestine, and stomach sampled from healthy *L. vannamei* using an RNeasy Plus Mini Kit (QIAGEN, Hilden, Germany). The first-strand cDNA was synthesized using the PrimeScript™ II 1st-strand cDNA synthesis kit (Takara, Shiga, Japan) with DNase-treated total RNA as template and Oligo d(T) 18 as a reverse transcript primer, and the open reading frame (ORF) of LvPTPN6 was amplified by primers of PTPN6-KpnIF and PTPN6-HA-PmeIR (**Table 1**). The 3′ and 5′ ends of LvPTPN6 mRNA were amplified by rapid amplification of cDNA ends (RACE) using a SMARTer RACE cDNA

TABLE 1 | Primers and probes used in this study.

Name	Sequence (5′–3′)
RACE	
PTPN6-3′F1	ATGAGAACTCACAGTAGAAAAGATGATC
PTPN6-3′F2	TCGATTCTGTTGGTTTCTGTCTTCAG
PTPN6-5′R1	GATCATGGATTTGGGAAGATCTGTG
PTPN6-5′R2	AATTCACCTTTCTTGAGGCCTCATG
Eukaryotic and prokaryotic expression vector	
PTPN6-KpnIF	CGGGGTACCATGAGCTCGAGGAGATGGTTCCACCCG
PTPN6-HA-PmeIR	GGGTTTAAACTTAAGCGTAGTCTGGGACGTCGTATGGGTAGGTGGCACGGGGCGGCACAGATG
Dorsal-EcoRIF	TATGAATTCATCAAAATGTTTGTTGCCCAGCGTACTTCC
Dorsal-PmeIR	GGCGTTTAAACTTACATATCAGAAAATATCCAAAAC
Relish-EcoRIF	CAGGAATTCATCAAAATGGTGAGAGGTGACAGAGGTGG
Relish-XhoIR	ATACTCGAGCGCCTGGTCCAGTACAGCTACAC
STAT-XhoIF	ACTCTCGAGATCAAA ATGTCGTTGTGGAACAGAGC
STAT-V5-BstBIR	ACTTTCGAACTGAGGCTTCATGAAGTTGGTC
IRF-KpnIF	CATGGTACCATCAAA ATGCCGCCATCTTTCACCAATG
IRF-PmeIR	CATGTTTAAACTTACGGCAACGTCCTCTCGCCG
JAK-XbaIF	GTCTCTAGAATCAAA ATGCTGACAATCAGCTTCTACG
JAK-V5-BstBIR	GTCTTCGAACATGTACTCCTCTTGCAGTTCC
GFP-KpnIF	TGAGGTACCATCAAAATGGTGAGCAAGGGCGAGGAG
GFP-HA-PmeIR	CGAGTTTAAACTTAAGCGTAGTCTGGGACGTCGTATGGGTACTTGTACAGCTCGTCCAT
IRF-32a-EcoRIF	CCGGAATTCATGCCGCCATCTTTCACC
IRF-32a-NotIR	AAGGAAAAAAGCGGCCGCCTACGGCAACGTCCTCTCG
EMSA	
PTPN6 probe	/5Bio/ATAATGGTGATGATAGGTTGCTGGGGGAAAGGGGAAGGATCAAGGAGCAAGCGGAAGTGT
Dual-luciferase reporter assays	
PTPN6-pro-KpnIF	CGGGGTACCTGCATGTCAATGTATGAGTGTGTG
PTPN6-pro-HindIIIR	CCCAAGCTTCTCCAAACAAAATATCGACAATGA
PTPN6-p1-3′-KpnIF	CGGGGTACCGAGAAAATGTTGAGTGTGTGTG
PTPN6-p2-3′-KpnIF	CGGGGTACCAAAGATCTATTTAACTAGGTTAATG
PTPN6-p3-3′-KpnIF	CGGGGTACCTCACTTTCCCCGCCTTCGTG
PTPN6-p4-3'-KpnIF	CGGGGTACCTAAAATTATTATTATTTTTAAATTTAACC
ALF2-Pro-AscIF	AATGGCGCGCCGTGTACGTATGTATGTGTGTATGTG
ALF2-Pro-FseIR	ATTGGCCGGCCATGTGTTATGAATTGAAGTTCCTGAAG
ALF5-Pro-AscIF	AATGGCGCGCCCGCATATGTATGTATTCATGTATGTACAC
ALF5-Pro-FseIR	ATTGGCCGGCCGGAAGACGTGTTGTTGCTGTC
CTL4-Pro-SacIF	AATGGCGCGCCCTCTGAACAATGGCGGTTGAG
CTL4-Pro-FseIR	ATTGGCCGGCCGTTATCTGGTGAGAATGTGTCATG
Lys-IT2-SacIF	AATGGCGCGCCCAATTAAATTCTCCTTTGTATTGCACG
Lys-IT2-FseIR	ATTGGCCGGCCCCATGTGATGGGAGATCTACCTG
dsRNA synthesis	
PTPN6-dsT7F	GGATCCTAATACGACTCACTATAGGAGAAGTATGGTCGCATCACTGTCAG
PTPN6-dsR	CTGCTGCCTCACTGCTGTATTTG
PTPN6-dsF	AGTATGGTCGCATCACTGTCAG
PTPN6-dsT7R	GGATCCTAATACGACTCACTATAGGCTGCTGCCTCACTGCTGTATTTG
IRF-dsT7F	GGATCCTAATACGACTCACTATAGGGCCTTCAGTAGAACGCATAGAG
IRF-dsR	CCGTGCAGGTAGAGGTGGT
IRF-dsF	GCCTTCAGTAGAACGCATAGAG
IRF-dsT7R	GGATCCTAATACGACTCACTATAGGCCGTGCAGGTAGAGGTGGT
GFP-dsT7F	GGATCCTAATACGACTCACTATAGGATGGTGAGCAAGGGCGAGGAG
GFP-dsR	TTACTTGTACAGCTCGTCCATGCC
GFP-dsF	ATGGTGAGCAAGGGCGAGGAG
GFP-dsT7R	GGATCCTAATACGACTCACTATAGGTTACTTGTACAGCTCGTCCATGCC
qRT-PCR	
PTPN6-qRTF	GAGCATCAGGGTCCCACTATG
PTPN6-qRTR	GGCCTTCCTTGCGTGAGTAG
IRF-qRTF	GCATCTTCAGGATTCTGTGGAC
IRF-qRTR	AGAGCCCAGTAGCGAAAGAG
ie1-qRTF	GCCATGAAATGGATGGCTAGG
ie1-qRTR	ACCTTTGCACCAATTGCTAGTAG
ALF2-qRTF	TAGCGTGACACCGAAATTCAAG
ALF2-qRTR	CGAAGTCTTGCGTAGTTCTGC
ALF5-qRTF	TGGTGAAGGCTTCCTACAAGAG
ALF5-qRTR	CATCAGCAGTAGCAGTGTCAG

(Continued)

TABLE 1 | Continued

Name	Sequence (5′–3′)
CTL4-qRTF	AACAAGCGGAGCAGTTCTG
CTL4-qRTR	CACAGCCAGTCACCTTCATAAG
Lys-IT2-qRTF	ACGCAGATAAGCCAATCATTGAG
Lys-IT2-qRTR	CAATCGTTCAGGAATTTAGCCATG
EF-1α-qRTF	TATGCTCCTTTTGGACGTTTTGC
EF-1α-qRTR	CCTTTTCTGCGGCCTTGGTAG

amplification kit (Clontech, Shiga, Japan) according to the manufacturer's instructions as previously described (30).

Quantitative Real-Time PCR

For the transcriptional-level analysis of specific genes in *L. vannamei*, cDNAs were synthesized from total RNAs using PrimeScript RT reagent kit with gDNA eraser (Takara, Japan) according to the manufacturer's instructions. Quantitative real-time PCRs (qRT-PCRs) were performed at a final volume of 10 μl containing 1 μl cDNA, 5 μl 2 × SYBR Premix Ex Taq II (Takara, Japan), and 0.5 μl each primer (10 μM) (**Table 1**) on a LightCycler 480 System (Roche, Germany). The optimized thermal cycling parameters were 95°C for 2 min to activate the polymerase, followed by 40 cycles of 95°C for 15 s, 60°C for 15 s, and 72°C for 15 s. Melting curves were generated by increasing the temperature from 72°C to 95°C (0.5°C/s) to denature the annealed DNA. The expression level of detected genes was determined using the $2^{-\Delta\Delta Ct}$ method after normalization to the internal control gene elongation factor 1 alpha (EF-1α, GenBank accession no:. GU136229) (31).

Immune Challenge

For immune challenge, *V. parahaemolyticus* and *S. aureus* were cultured to the logarithmic phase and diluted to 10^5 colony-forming units (CFUs) in 50 ml PBS after centrifugal collection, respectively. WSSV was prepared freshly from moribund shrimps infected with preserved WSSV stored at −80°C in our lab. Virus stock was quantified using absolute qRT-PCR and diluted to 10^6 copes in 50 μl PBS as described previously (30).

For expression pattern analysis of LvPTPN6, healthy shrimps were divided into six experimental groups in independent recirculating water tank systems. After acclimation for 1 week, shrimps of six groups were injected with 10^6 copies of WSSV, 10^5 CFU of *V. parahaemolyticus* 10^5 CFU of *S. aureus*, 5 μg of LPS, 5 μg of Poly(I:C), and PBS at the second abdominal segment, respectively. Hemocyte and gill were sampled from six randomly selected shrimps in each group at 0, 4, 12, 24, 48, 72, and 96 h post stimulant injection. After then, total RNAs were isolated and cDNAs were synthesized for qRT-PCR. For cumulative mortality analysis, shrimps (n = 40) were challenged with 10^6 copies of WSSV at 48 h after the injection of LvPTPN6 or green fluorescent protein (GFP, as negative control) dsRNA. The cumulative mortality was recorded every 6 h after WSSV challenge. The WSSV copy number in muscle was detected at 3 and 5 days after WSSV challenge in parallel experiments. In each group, six living shrimps were randomly selected and the total DNA of muscle was extracted using DNeasy Blood and Tissue Kit (QIAGEN, USA), then the *ie1* (wsv069) DNA sequence (GenBank accession No. AY422228) was detected using relative qRT-PCR with shrimp EF-1α as internal control.

Immunofluorescence

For subcellular localization analysis, the LvPTPN6 coding sequence was cloned into the pAc5.1 vector to express the HA-tagged LvPTPN6 protein. Drosophila Schneider 2 (S2) cells were plated on a siliconized coverslip with approximately 80% confluence, transfected with the pAc5.1-PTPN6-HA vector using FuGENE HD transfection reagent (Promega, Madison, WI, USA), and fixed with 4% paraformaldehyde for 5 min at 48 h post transfection. For nuclear translocation of *L. vannamei* STAT, shrimps were challenged with Poly(I:C) for 12 h as mentioned above, then hemolymph smear samples were made on siliconized slides and fixed with 4% paraformaldehyde for 10 min. For immunofluorescence assay, 4% paraformaldehyde fixed cells were infiltrated with 1% Triton X-100 for 20 min then successively incubated with rabbit Ab against HA (CST, Danvers, MA, USA) or shrimp STAT (GL Biochem, Shanghai, China) together with mouse Ab against β-actin (MBL, Tokyo, Japan) and Alexa Fluor 488-conjugated goat anti-rabbit Ab (CST, USA) together with Alexa Fluor 594-conjugated goat anti-mouse Ab (CST, USA). After staining with Hoechst 33342 (Invitrogen, Carlsbad, CA, USA) for the nuclei, sliders were observed using a TCS SP8 STED 3X Confocal Microscope (Leica, Munich, Germany). The immunofluorescence intensities of the cytoplasm- and nuclear-localized STAT were quantified and calculated using JACoP with an ImageJ plugin from four randomly selected microscopic vision fields in each group (32).

RNA Interference *In Vivo*

To investigate the transcription and function of LvPTPN6, the selected transcription factors as well as LvPTPN6 were knocked down through RNA interference (RNAi). The templates of shrimp genes or GFP for dsRNA synthesis were cloned from the *L. vannamei* cDNA or pAc5.1-GFP plasmid and incorporated with T7 RNA polymerase promoter at the 5′ end using specific primes listed in **Table 1**, respectively. The dsRNAs were synthesized *in vitro* using the T7 RiboMAX™ Express RNAi system (Promega, USA), annealed from two independently transcribed single-strand RNAs, and then purified according to the manufacturer's instruction. Acclimated healthy shrimps were divided into several groups (n = 40) and intramuscularly injected with 10 μg specific dsRNAs. Hemocytes and gills were sampled from nine shrimps

in each group for the following mRNA and protein analysis at 48 h post-dsRNA injection as described above.

Protein Preparation for Nuclear Localization Analysis of STAT

For nuclear localization analysis of STAT regulated by LvPTPN6 at the cellular level, S2 cells were co-transfected with pAc5.1-STAT and pAc5.1-PTPN6 or pAc5.1-STAT and pAc5.1-GFP (as control). Cells were collected at 48 h post-transfection followed by protein analysis as follows. For the analysis of nuclear localization of STAT, LvPTPN6 in *L. vannamei* were knocked down through RNAi as mentioned above. At 36 h post dsRNA injection, shrimps were challenged with Poly(I:C) for 12 h as mentioned above, then hemocytes were sampled from 30 randomly selected shrimps in each group followed by protein analysis. After preprocessing, the nuclear and cytoplasmic protein of S2 cells or hemocytes were isolated using NE-PER Nuclear and Cytoplasmic Extraction Reagents (Thermo, Waltham, MA, USA), respectively.

Western Blot

For analysis of STAT localization, protein extractions were directly treated with SDS loading buffer to obtain protein samples, which were separated using 12% sodium dodecyl sulfate polyacrylamide gel electrophoresis (SDS-PAGE) and transferred to polyvinylidene difluoride (PVDF) membranes using the Trans-Blot Transfer system (Bio-Rad, Hercules, CA, USA) for the determination of the STAT level. For analysis of the STAT dimer level, S2 cells were lysed using Pierce IP Lysis buffer (Thermo, USA) at 48 h post-transfection to obtain the native proteins, which were separated with 10% native polyacrylamide gel electrophoresis and transferred to PVDF membranes in native transfer buffer. Western blot was performed using rabbit antibodies against shrimp STAT (GL Biochem, China), HistoneH3 (CST, USA), and β-actin (MBL, Japan), as previously described (33). HistoneH3 or β-actin was detected as an internal control of cytoplasmic or nuclear protein to rule out the possible contamination of nuclear or cytoplasmic protein, respectively. The protein levels were determined by analyzing the gray values of specific protein bands using Quantity One 4.6.2 software (Bio-Rad, USA) by the Gauss model and normalized to those of internal control.

Co-Immunoprecipitation

The interactions between LvPTPN6 and *L. vannamei* JAK or STAT were analyzed using co-immunoprecipitation (Co-IP). The ORFs of STAT and *L. vannamei* JAK (JAK) were cloned into the pAc5.1/V5-His A plasmid (Invitrogen, USA) to generate V5-tagged STAT and JAK expression vectors, respectively. An HA-tagged GFP expression vector was used as control. HA-tagged LvPTPN6 or GFP and V5-tagged STAT or JAK were co-transfected into S2 cells. After 48 h, cells were harvested and lysed in IP Lysis Buffer (Thermo, USA) with a protease inhibitor cocktail (Sigma, St. Louis, MO, USA). Co-IPs were performed using anti-HA affinity agarose (Sigma, USA), and Western blot was performed with a rabbit anti-V5 primary antibody (Merck, Burlington, MA, USA) and a horseradish peroxidase (HRP)-conjugated goat anti-rabbit secondary antibody (Promega, USA).

Dual-Luciferase Reporter Assay

For transcriptional regulation analysis of LvPTPN6, the promoter sequence of LvPTPN6 was retrieved from the genome data of *L. vannamei* (34) and completely or partly cloned into the firefly luciferase plasmid pGL3-Basic (Promega, USA) using primers listed in **Table 1** to generate pLG3-PTPN6, pGL3-PTPN6-p1, pGL3-PTPN6-p2, pGL3-PTPN6-p3, and pGL3-PTPN6-p4 recombinant plasmids. The ORF of transcription factors of *L. vannamei* including Dorsal, Relish, STAT, and IRF, as well as green fluorescent protein (GFP, set as negative control), was cloned into the pAc5.1-V5 plasmid (Invitrogen, USA) using specific primers listed in **Table 1** to obtain eukaryotic expression vectors, respectively. To verify the transcriptional activation of STAT on the anti-lipopolysaccharide factor (ALF), C-type lectin (CTL), and lysozymes (Lys), promoter sequences of ALF2, ALF5, CTL4, and Lys-IT2 were cloned into pGL3-Basic using primers listed in **Table 1** to generate pGL3-ALF2, pGL3-ALF5, pGL3-CTL4, and pGL3-Lys-IT2 recombinant plasmids. S2 cells were plated in a 96-well plate with 70% confluence and transfected with 50 ng pGL3 firefly luciferase plasmid, 30 ng pRL-TK Renilla luciferase plasmid (as an internal control) (Promega, USA), and 100 ng pAc5.1 expression vector mentioned, respectively. At 48 h post transfection, cells were lysed for examination of firefly and Renilla luciferase activities using a dual-luciferase reporter assay system (Promega, USA).

Electrophoretic Mobility Shift Assay

To verify the regulatory role of LvIRF on LvPTPN6 transcription, the interaction between the LvIRF protein and LvPTPN6 promoter was detected through electrophoretic mobility shift assay (EMSA) *in vitro*.

LvIRF ORF was amplified using primers of IRF-32a-EcoRIF/NotIR, then cloned into the pET32a (Invitrogen, USA) prokaryotic expression vector; the original pET32a plasmid which expresses the thioredoxin (TRX) protein was set as negative control. The recombinant plasmids were transformed into *Escherichia coli* Rosetta (DE3) cells and induced with 1 mM isopropyl-beta-D-thiogalactoside (IPTG) in the logarithmic phase after enlarged cultivation. The His-tagged LvIRF or TRX protein was purified using Ni-NTA Agarose (QIAGEN, USA) and quantified using BCA Protein Assay Kit (Beyotime, Shanghai, China) according to the manufacturer's instruction.

The 5′ biotin-labeled probe that contains the predicted IRF-binding motif sequence (GGAAAGGGGAAGGATCAA) was synthesized by Invitrogen (Shanghai, China) (**Table 1**). EMSA was performed using a LightShift Chemiluminescent EMSA Kit (Thermo, USA) as described previously (35). In general, the purified proteins (10 μg) were incubated with 20-fmol probes for the binding reactions between probes and proteins, separated by 5% native PAGE, transferred to positively charged nylon membranes, and cross-linked by UV light (256 nm). Then the biotin-labeled DNAs on the membrane were detected by chemiluminescence and captured by Amersham Imager 600 (GE, USA).

Bioinformatics and Statistical Analysis

The IRF-binding motif in the LvPTPN6 promoter was predicted using JASPAR 2016 (http://jaspar2016.genereg.net/cgi-bin/jaspar_db.pl). The multiple-sequence alignment of PTPN6 homologs was performed using ClustalX 2.1, and the phylogenetic tree was constructed using MEGA 5.0. All data were presented mean ± SD. The significance of difference between groups of numerical data was calculated using Student's *t*-test. The cumulative mortalities were analyzed using GraphPad Prism 5.01 to generate the Kaplan–Meier plot (log-rank χ^2 test).

RESULTS

Cloning and Bioinformatics Analysis of LvPTPN6

The full length of LvPTPN6 mRNA is 2,746 bp with a 5′ untranslated region (UTR) of 140 bp, an ORF of 2,010 bp encoding a protein of 669 amino acids, and a 3′ UTR of 596 bp (GenBank accession no.: OL652660). The LvPTPN6 protein has a calculated molecular weight of 75.62 kDa and a theoretical isoelectric point of 8.60 (**Supplemental figure 1A**). LvPTPN6 was predicted to contain two Src homology 2 (SH2) domains and a protein tyrosine phosphatase catalytic (PTPc) domain covering residues of 4–87, 110–193, and 248–519 (**Supplemental figure 1B**), which share the identical domain character as human PTPN6. Multiple-sequence alignment showed that LvPTPN6 shared high homology to the PTPN6s from Crustacea, Insect, and Arachnoidea, especially in the SH2 and PTPc domains, which shared higher identities of 98.2%, 96.15 and 92.2% with those of PTPN6s from *Penaeus japonicus*, *Penaeus monodon*, and *Homarus americanus*, and lower identities of 68.1%, 68.1%, 68.5%, and 69.9% from *Stegodyphus dumicola*, *Trichonephila clavata*, *Nephila pilipes*, and *Nymphon striatum*, respectively (**Figure 1**). In the constructed phylogenetic tree, the analyzed PTPN6s could be categorized into three clades of arthropods, fishes, and mammals (**Figure 2**), and LvPTPN6 was most closely clustered with the *Armadillidium vulgare* PTPN6 in the arthropod clade.

Tissue Distribution and Subcellular Localization of LvPTPN6

The expression level of LvPTPN6 in 12 tissues of *L. vannamei* was detected by qRT-PCR (**Figure 3A**). Results showed that LvPTPN6 could be detected in all selected tissues, and the lowest expression level was revealed in pyloric cecum. The expression level of LvPTPN6 was gradually increased in the epithelium, heart, eyestalk, hepatopancreas, scape, gill, hemocyte, and stomach, which was 1.22-, 1.39-, 1.53-, 1.62-, 1.71-, 1.85-, 1.87-, and 2.01-fold compared with it in pyloric cecum, respectively, and was roughly increased in the intestine, muscle, and the highest of nerve, which was 3.74-, 4.69-, and 9.80-fold compared with it in pyloric cecum. The subcellular localization of LvPTPN6 was detected using immunofluorescence assay in S2 cells which expressed the HA-tagged LvPTPN6 protein (**Figure 3B**). Results showed that LvPTPN6 was mainly located in the cytoplasm.

Expression Profiles of LvPTPN6 After Immune Stimulation

The expression profiles of LvPTPN6 were investigated through qRT-PCR in hemocyte and gill from immune stimulated *L. vannamei* (**Figure 4**). In hemocyte, the expression levels of LvPTPN6 were generally upregulated after the stimulation of all stimulants. It was gradually increased from 1.18-fold at 4 h to 16.30-fold at 96 h after the stimulation of WSSV. However, it was roughly up-regulated of 3.2-, 2.05-, 1.71-, and 1.71-fold at 4 h, then gradually calmed down at the following time points, and up-regulated again of 1.43-, 1.90-, 2.29-, and 1.82-fold at 96 h after the stimulation of *V. parahaemolyticus*, *S. aureus*, LPS, and poly(I:C), respectively. Notably, the expression pattern of LvPTPN6 in gill was totally different from that in hemocyte, which was generally suppressed after the stimulation of WSSV, *V. parahaemolyticus*, *S. aureus*, and poly(I:C), while it did not significantly change, except being up-regulated of 1.57-fold at 4 h, after the stimulation of LPS.

Regulation of LvPTPN6 Expression by IRF

A 1,609-bp promoter sequence (**Supplemental Figure 2A**) of LvPTPN6 was cloned into the pLG3-Basic vector and the transcriptional activity regulated by *L. vannamei* immune-related transcriptional factors, including Dorsal, Relish, STAT, and IRF, were analyzed through dual-luciferase assay. Results demonstrated that IRF could significantly up-regulate the transcription of the LvPTPN6 promoter of 2.03-fold compared with the GFP control (**Figure 5A**). To search the IRF-binding motif, the LvPTPN6 promoter was cleaved to -13,60, -737, -517, and -297 bp upstream of the transcriptional initiation site (**Figure 5B**) and cloned into the pGL3-Basic promoter. Results of dual-luciferase assay unveiled that the IRF-mediated transcriptional activation was vanished after the deletion of the -1,609 to -1,360 regions of the LvPTPN6 promoter (**Figure 5C**). In this region, a potential IRF-binding motif (GGAAAGGGGAAGGATCAA) was predicted through bioinformatics analysis (**Supplemental Figure 2B**), and its combination with IRF was verified *in vitro*. EMSA results showed that the IRF protein bound the biotin-labeled probe of the LvPTPN6 promoter to form a retarded shift band, which was gradually eliminated when 200 × and 400 × unlabeled probes were added to competitively bind IRF. In contrast, there was no shift band in the incubation between TRX protein and the biotin-labeled probe (**Figure 5D**). This suggested that LvPTPN6 could be directly regulated by IRF. To further verify the regulatory mechanism of LvPTPN6, IRF was silenced using the RNAi strategy *in vivo* (**Figure 5E**). Consistent with our expectation, silencing of IRF significantly inhibited the transcription of LvPTPN6 in both hemocyte and gill (**Figure 5F**), confirming that LvPTPN6 was transcriptionally regulated by IRF in *L. vannamei*.

Interaction Between LvPTPN6 and JAK/STAT

To explore the mechanisms of LvPTPN6 promoting nuclear translocation of STAT, the interaction between LvPTPN6 and JAK/STAT was analyzed using Co-IP (**Figure 6**). Results showed

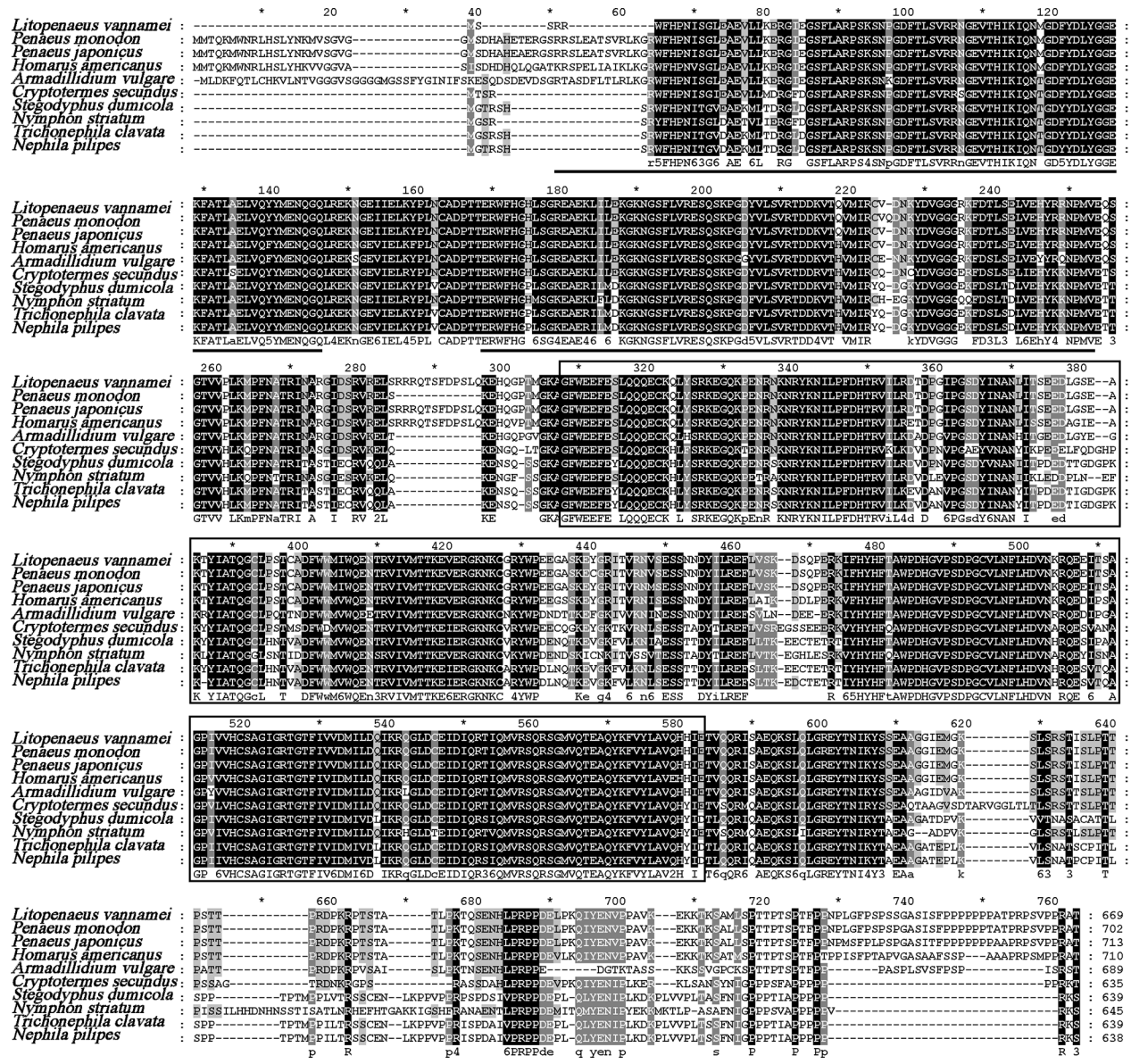

FIGURE 1 | Multiple-sequence alignment of PTPN6 homologs. The two predicted SH2 domains were underlined, and the PTPc domain was framed. The amino acid sequence of PTPN6s was obtained from NCBI with GenBank accession numbers of *Penaeus monodon* (XP_037785856.1), *Penaeus japonicas* (XP_042879519.1), *Homarus americanus* (XP_042242946.1), *Armadillidium vulgare* (RXG72814.1), *Cryptotermes secundus* (XP_023713602.1), *Stegodyphus dumicola* (XP_035233634.1), *Nymphon striatum* (KAG1683061.1), *Trichonephila clavata* (GFR09275.1), and *Nephila pilipes* (GFS80663.1). The five tines star "*" means the middle position of the two Numbers beside it.

that both V5-tagged JAK and STAT could co-precipitate with HA-tagged LvPTPN6 but not GFP protein, confirming the interaction between LvPTPN6 and JAK, and LvPTPN6 and STAT, respectively.

Nuclear Localization of STAT Regulated by LvPTPN6

To reveal the regulatory role of LvPTPN6 on the JAK/STAT signaling pathway, nuclear localization of STAT was investigated after the down- or up-regulation of LvPTPN6 in *in vivo* or S2 cells, respectively. Western blot analysis showed that, after knockdown of LvPTPN6 and stimulation of Poly(I:C) *in vivo* (**Figure 7A**), cytoplasm-localized STAT was increased by 59.9%, and nuclear-localized STAT was decreased by 38.4% compared with the negative control in hemocyte, respectively (**Figure 7B**). This result was confirmed by immunofluorescence assay, which demonstrated that silencing of LvPTPN6 suppressed the nuclear translocation of STAT by 29.3% compared with the GFP control in hemocytes (**Figures 7C, D**). The facilitated role of LvPTPN6 on STAT nuclear localization was further verified through

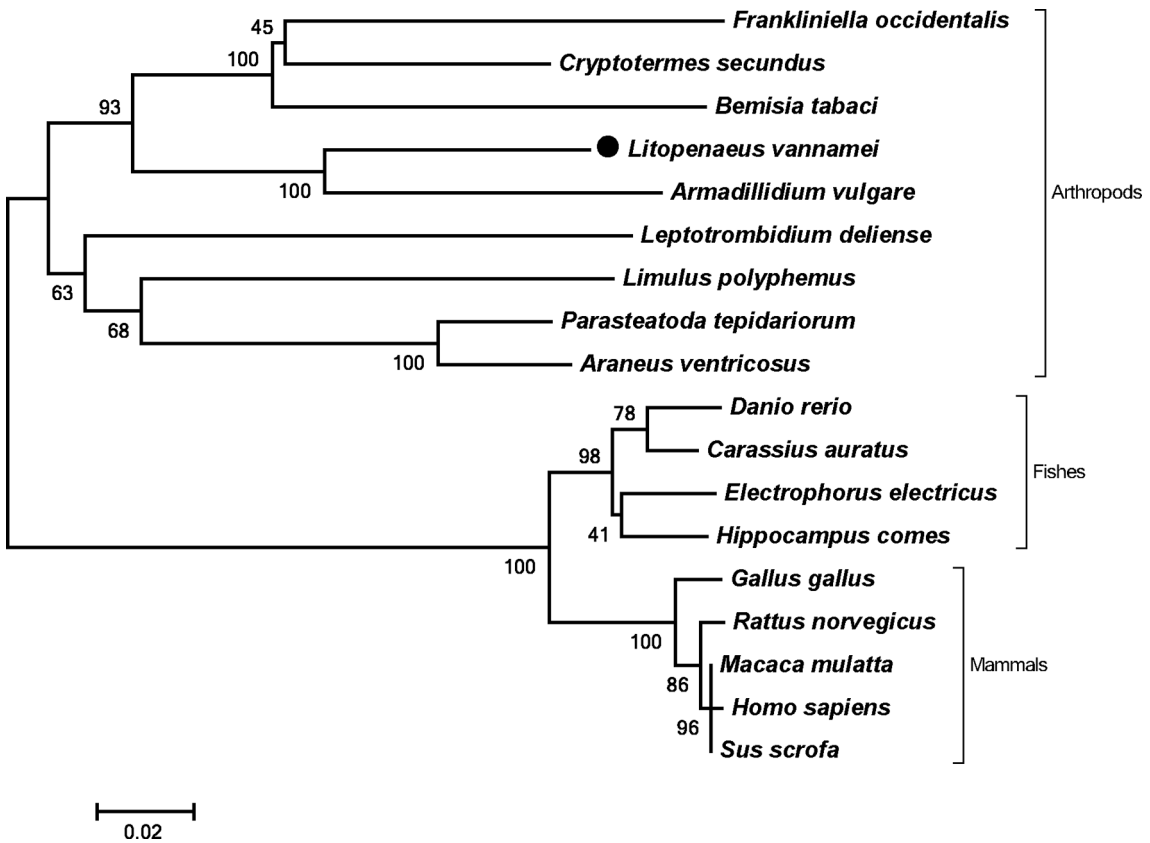

FIGURE 2 | Phylogenetic tree of PTPN6s. Amino acid sequences of PTPN6s were obtained from NCBI with GenBank accession numbers of *Frankliniella occidentalis* (XP_026279043.1), *Cryptotermes secundus* (XP_023713602.1), *Bemisia tabaci* (XP_018912318.1), *Armadillidium vulgare* (RXG72814.1), *Leptotrombidium deliense* (RWS28580.1), *Limulus polyphemus* (XP_022245683.1), *Parasteatoda tepidariorum* (XP_015930014.1), *Araneus ventricosus* (GBM95823.1), *Danio rerio* (NP_956140.1), *Carassius auratus* (XP_026121403.1), *Electrophorus electricus* (XP_026888060.1), *Hippocampus comes* (XP_019712005.1), *Gallus gallus* (NP_990299.1), *Rattus norvegicus* (NP_001171064.1), *Macaca mulatta* (NP_001248038.1), *Homo sapiens* (NP_002822), and *Sus scrofa* (XP_013845818.1).

overexpression LvPTPN6 in S2 cells. Western blot analysis showed that overexpressed LvPTPN6 decreased the cytoplasm-localized shrimp STAT by 38.2% and increased the nuclear-localized shrimp STAT by 59.1% compared with the control, respectively (**Figure 7E**). Besides, overexpression of LvPTPN6 significantly promoted the dimerization of STAT, the essential procedure of STAT activation (**Figure 7F**). These data indicated that LvPTPN6 could facilitate the activation of the JAK/STAT signaling pathway.

Involvement of LvPTPN6 in Antiviral Immunity

Before investigating the regulatory effects on the expression of immune effector genes mediated by LvPTPN6, the transcriptional activation of STAT on the promoters of *L. vannamei* immune effector genes was investigated by dual-luciferase assays. Results revealed that STAT could significantly activate the transcription of ALF2, ALF5, CTL4, and Lys-IT2 (**Figure 8A**). Correspondingly, the expressions of ALF2, ALF5, CTL4, and Lys-IT2 were generally suppressed in hemocyte and gill after knockdown of LvPTPN6 *in vivo* (**Figure 8B**). The antiviral role of LvPTPN6 was further investigated in shrimp. After knockdown of LvPTPN6, the cumulative mortality of shrimps after 3 days of WSSV infection was significantly increased compared with the control (**Figure 8C**), and the difference between the two treatments reached a peak of 33.5% at 4 days post WSSV infection. Consistently, the virus load of WSSV in muscles was significantly increased in the LvPTPN6-silenced group at 3 and 5 days post WSSV infection (**Figure 8D**). These data indicate that LvPTPN6 could facilitate antiviral immunity through the JAK/STAT singling pathway in shrimp.

DISCUSSION

Tyrosyl phosphorylation plays a critical role in multiple signaling pathways regulating innate and acquired immunity, which is mainly regulated by the dynamic equilibrium between protein-tyrosine kinases (PTKs) and protein-tyrosine phosphatases (PTPs) (3). Non-receptor PTPs are a classical type of PTPs, which consist of

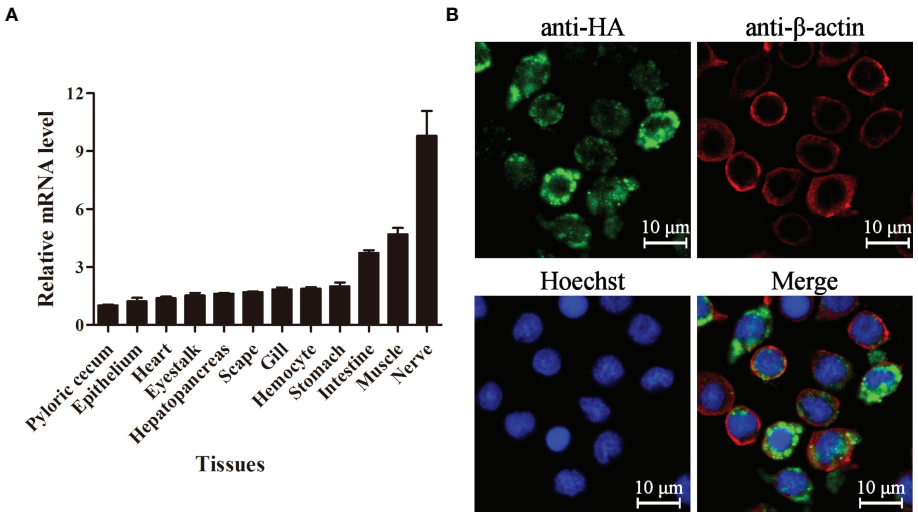

FIGURE 3 | Tissue distribution and subcellular localization of LvPTPN6. **(A)** Expression of LvPTPN6 in *L. vannamei* tissues detected by qRT-PCR with EF-1α as internal control. The expression level of LvPTPN6 in pyloric cecum was set as the baseline (1.0). Each bar represents the mean ± SD (n = 4). **(B)** Subcellular localization of HA-tagged LvPTPN6 was detected by confocal laser scanning microscopy analysis in S2 cells. LvPTPN6 was stained with Alexa Fluor 488 (green), the cytomembranes were visualized by β-actin stain with Alexa Flour 594 (red), and the nuclei were stained with Hoechst 33342 (blue).

several subtypes distinguished with different domain features (11). SH2-domain-containing PTPs (SHPs) are characterized by composition of an N-terminal SH-2 domain, a C-terminal SH-2 domain, a classical PTP domain, and a C-terminal tail that contains two tyrosyl phosphorylation sites (36). In mammals, there are two kinds of SHPs, SHP1 (PTPN6) and SHP2 (PTPN11), which possess similar overall structures and regulatory mechanisms but differ in detailed structure, expression pattern, and, most importantly, physiological functions (3). In this study, an SH2 domain-containing PTP (LvPTPN6) sharing a higher homology with PTPN6 from other animals was identified in *L. vannamei*, which contains the classical domain features of SHPs.

Different from the distribution characters of human PTPN6 which is most abundantly expressed in hematopoietic cells and low in some epithelial, endothelial, and central nervous system cells (37), LvPTPN6 exits in all detected tissues. Besides, human PTPN6 is most abundantly expressed in the nucleus of epithelial cells and the cytoplasm of hematopoietic cells (38), while the subcellular localization analysis in S2 cells showed that LvPTPN6 was mainly located in the cytoplasm. These features corroborate the assertion that LvPTPN6 may have specific functions that differ from those of mammalian PTPN6s.

In addition to the posttranscriptional approaches, such as truncation, phospholipid binding, or tyrosine phosphorylation of the C-terminal tail, the activity of mammalian PTPN6 can also be regulated from transcriptional levels (39, 40). In the current study, LvPTPN6 was transcriptionally regulated after the challenge of stimulants, which share different expression patterns in hemocyte and gill, implying its complicated regulatory role in the shrimp immune responses.

In the canonical IFN systems, IRF activates the JAK/STAT signaling pathway to establish the cellular antiviral state through regulating the secretion of IFNs recognized by INF receptors and initiating the phosphorylation cascade of JAK and STAT (12, 28, 41). The IRF/Vago/JAK-STAT axis in shrimp is known to be similar to the interferon system of mammals and also plays an essential role in antiviral response (26, 42). Except the extracellular signal axis mediated by IFNs, very few studies revealed the intracellular activation of the JAK/STAT pathway regulated by IRF. For instance, in children with autosomal recessive homozygous IRF9 deficiency, IFN-stimulated response element (ISRE)-regulated transcription was attenuated for the disruption of the STAT1/STAT2/IRF9 heterotrimer; this finding presented an instance of IRF that could directly facilitate the transcriptional activation function of STAT (43). In this study, we found that IRF could activate the expression of LvPTPN6, further facilitating the nuclear localization of STAT and promoting the antiviral immunity of shrimp. Our results revealed that in addition to the canonical IRF/Vago/STAT axis, LvPTPN6 mediated an alternative regulatory approach from IRF to STAT. This novel regulatory strategy between IRF and STAT may provide a basis for further research on the IFN systems.

The JAK/STAT pathway is one of the important immune signaling pathways and exists wildly from vertebrates to invertebrates, which is regulated by different posttranscriptional mechanisms including acetylation, demethylation, and serine or tyrosine de-/phosphorylation (21). One of the major mechanisms that attenuate JAK/STAT pathway activation is dephosphorylation of the tyrosine residues by PTPs (22). In mammals, most of the PTP members, such as PTP receptor-type D (PTPRD), PTP receptor-type T (PTPRT), PTP receptor-type K (PTPRK), PTPN2, PTPN6, PTPN9 and PTPN11, had been proved to suppress the signal transduction of the JAK/STAT pathway by dephosphorylating on JAKs or STATs (44–50).

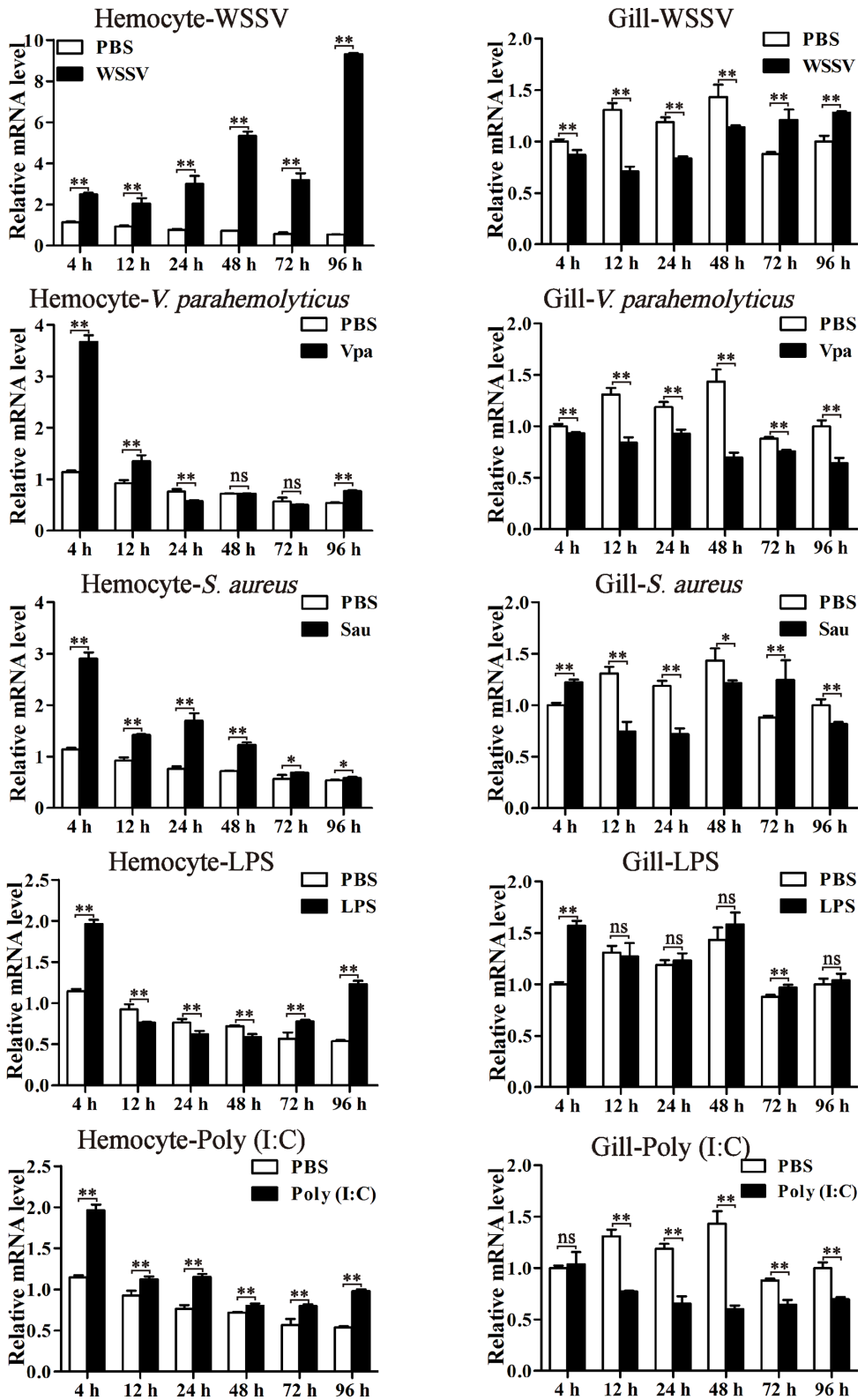

FIGURE 4 | The expression profiles of LvPTPN6 after immune stimulation. The expression of LvPTPN6 in hemocyte and gill of WSSV-, *V. parahaemolyticus*- (Vpa), *S. aureus*- (Sau), LPS-, and Poly(I:C)-challenged shrimps were detected using qRT-PCR. In each panel, the value of PBS group at 4 h was set as the baseline (1.0). Each bar represents the mean ± SD ($n = 4$), $^{**}p < 0.01$, $^{*}p < 0.05$, and *ns* > 0.05 by two-tailed unpaired Student's *t*-test.

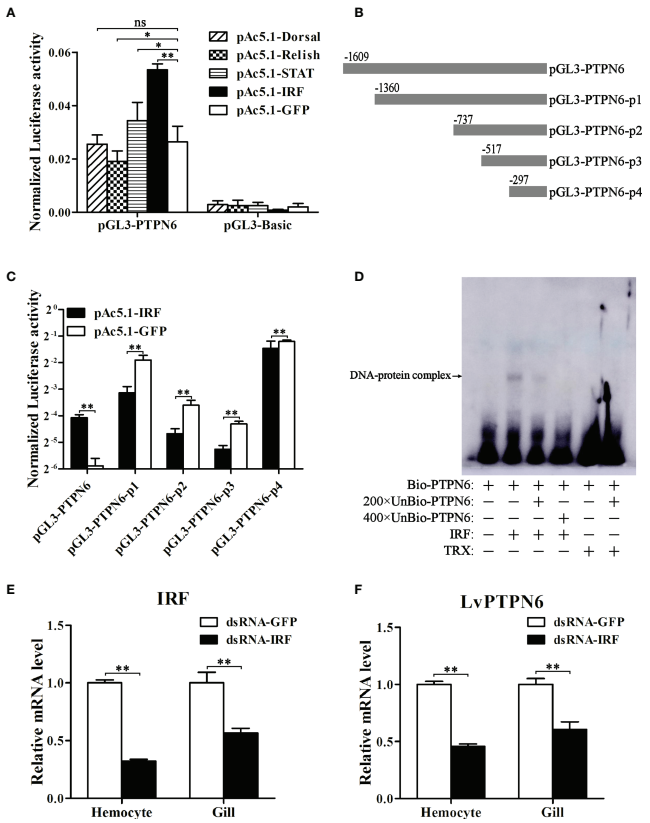

FIGURE 5 | Regulation of LvPTPN6 expression by IRF. **(A)** Regulatory effects of Dorsal, Relish, STAT, IRF, and GFP (as control) on the LvPTPN6 promoter. Each bar represents the mean ± SD (n = 8), $^{**}p < 0.01$, $^{*}p < 0.05$, and *ns*: P > 0.05 by two-tailed unpaired Student's *t*-test. **(B)** Scheme of the cleaved promoters of LvPTPN6. **(C)** Regulatory effects of IRF and GFP on the cleaved promoters of LvPTPN6. Each bar represents the mean ± SD (n = 8), $^{**}p < 0.01$ by two-tailed unpaired Student's *t*-test. **(D)** Interaction of IRF with the LvPTPN6 promoter analyzed by EMSA. The biotin-labeled (Bio-) or unlabeled (Unbio-) probes and purified prokaryotic protein of LvPTPN6 or TRX (as control) are used. **(E, F)** qRT-PCR analysis of IRF and LvPTPN6 mRNA levels in hemocyte and gill at 48 h post dsRNA injection. Values in the dsRNA-GFP control group were set as the baseline (1.0). Each bar represents the mean ± SD (n = 4), $^{**}p < 0.01$ by two-tailed unpaired Student's *t*-test.

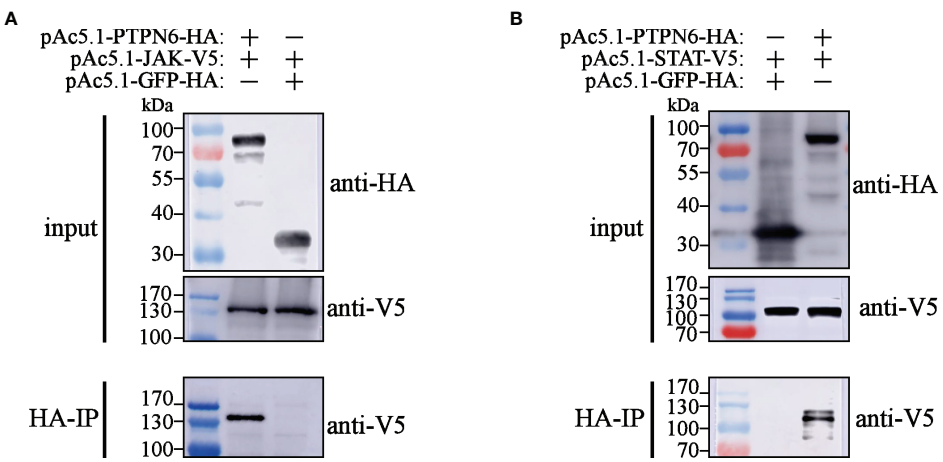

FIGURE 6 | Co-IP analysis of the interaction between LvPTPN6 and JAK/STAT. Interaction between HA-tagged LvPTPN6 and V5-tagged JAK **(A)** or STAT **(B)**, HA-tagged GFP was set as internal control. Interacted proteins were precipitated by anti-HA affinity agarose.

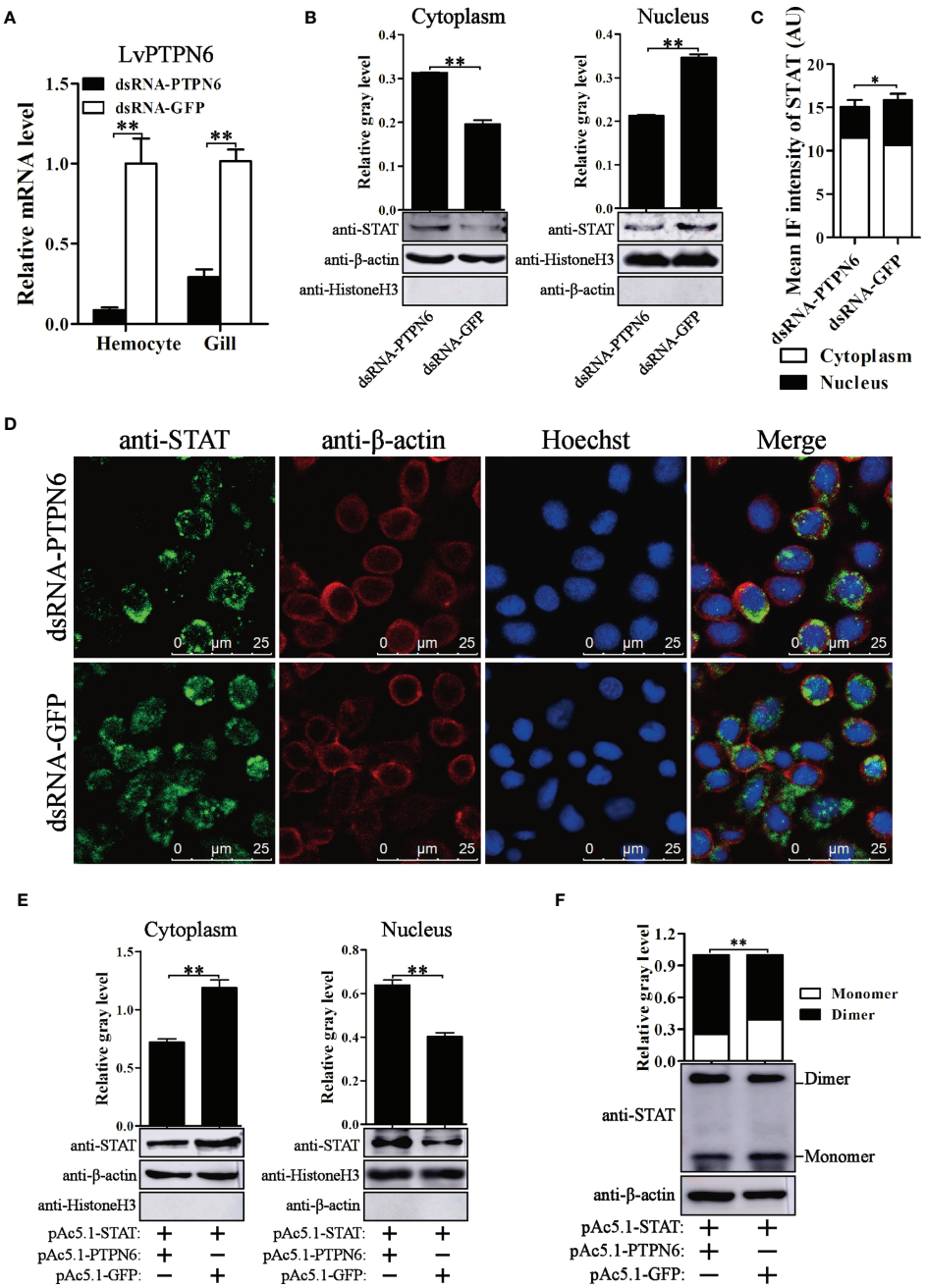

FIGURE 7 | Nuclear localization of STAT regulated by LvPTPN6. **(A)** qRT-PCR analysis of the LvPTPN6 mRNA level in hemocyte and gill at 48 h post dsRNA injection. Values in the dsRNA-GFP control group were set as the baseline (1.0). Each bar represents the mean ± SD ($n = 4$), $^{**}p < 0.01$ by two-tailed unpaired Student's *t*-test. **(B)** Western blot analysis of the protein level of STAT located in the cytoplasm and nucleus of hemocytes after dsRNA injection. **(C)** Immunofluorescence intensities (arbitrary units, AU) of cytoplasm- and nuclear-localized STAT in dsNRA-GFP- and dsRNA-PTPN6-treated hemocytes. Immunofluorescence intensities were calculated using JACoP with an ImageJ plugin from four randomly selected microscopic vision fields (**Supplemental Figure 3**). $^{*}p < 0.05$ by two-tailed unpaired Student's *t*-test. **(D)** Immunofluorescent analysis of STAT in hemocytes after dsRNA injection. STAT was stained with Alexa Fluor 488 (green), the cytomembranes were visualized by β-actin stain with Alexa Flour 594 (red), and the nuclei were stained with Hoechst 33342 (blue). **(E)** Western blot analysis of the protein level of shrimp STAT located in the cytoplasm and nucleus of S2 cells overexpressed with LvPTPN6 or GFP (negative control). **(B, E)** In cytoplasm, the gray values of STAT bands were normalized to those of the cytoplasmic internal control of β-actin, and Histone H3 was detected to verify no contamination of nuclear protein. In nucleus, the gray values of STAT bans were normalized to those of the nuclear internal control of Histone H3, and β-actin was detected to verify no contamination of cytoplasmic protein. **(F)** Western blot analysis of the dimer and monomer levels of STAT through native PAGE after overexpressing LvPTPN6 in S2 cells. The gray values of STAT bans were normalized to those of the internal control of β-actin. **(B–F)** Each bar is mean ± SD of three independent quantification of the electrophoretic bands, $^{**}p < 0.01$ by two-tailed unpaired Student's *t*-test.

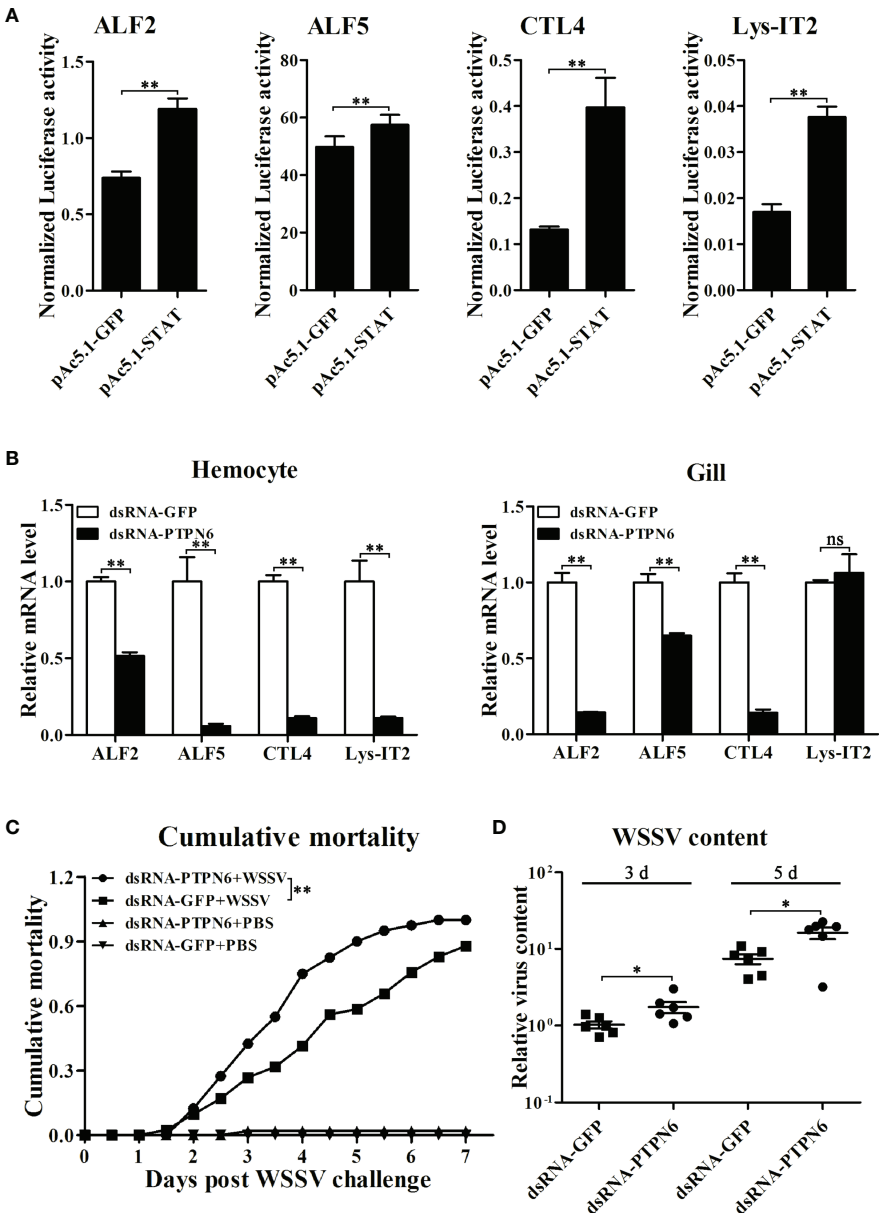

FIGURE 8 | Role of LvPTPN6 in shrimp antiviral immunity. **(A)** Regulatory effects of shrimp STAT on the promoter of immune effector genes. Each bar represents the mean ± SD (n = 8), $^{**}p < 0.01$ by two-tailed unpaired Student's t-test. **(B)** qRT-PCR analysis of the mRNA level of STAT-regulated immune effector genes in hemocyte and gill at 48 h after dsRNA injection. Values in the dsRNA-GFP control group were set as the baseline (1.0). Each bar represents the mean ± SD (n = 4), $^{**}p < 0.01$ and *ns*: $P > 0.05$ by two-tailed unpaired Student's t-test. **(C)** Cumulative mortality of dsRNA-injected shrimps (n = 40) after WSSV infection. Data were recorded every 6 h and statistically analyzed by Kaplan–Meier log-rank χ^2 test, $^{**}p < 0.01$. **(D)** The relative viral load in muscle was analyzed by detecting the DNA of the WSSV *ie1* gene in six randomly selected shrimps using qRT-PCR with three repetitions, and the shrimp EF-1α gene was used as the internal control. The level in dsRNA-GFP group at 3 days post WSSV infection was set as baseline (1.0). $^{*}p < 0.05$ by two-tailed unpaired Student's t-test.

Accumulating evidence has established the important role of PTPN6 in the regulation of the JAK/STAT signaling pathway in different organisms (51). The absence of SPH1 (PTPN6) activates JAK/STAT signaling pathways *via* the enhanced phosphorylation of JAK1, JAK2, JAK3, STAT3, STAT5, or STAT 6 (52), while its induction by chemical compounds could reduce the phosphorylation of STAT3, STAT5, or STAT 6 to block its signal transduction (22). Interestingly, our present finding demonstrated that LvPTPN6 could promote the unclear localization of STAT, activate the expression of STAT-regulated genes, and ultimately initiate the antiviral status of shrimp. Although most of the PTPs exhibit negative regulatory roles through their dephosphorylation activity in the JAK/STAT signaling pathway, some exceptions can promote it in specific

circumstances. For example, the EGF- and IFN-γ-induced STAT activation was suppressed by expressing a catalytically inactive form of SHP1 (PTPN6) in HeLa cells, while overexpression of the native SHP1 had no effect on EGF-induced STAT activation but showed a positive effect on IFN-γ-induced STAT activation. This suggests that SHP-1 can function as a positive regulator in the activation of STAT (23). Inhibition of SHP2 expression initially enhanced and later inhibited STAT5 phosphorylation and reduced the expression of the antiapoptotic genes of MCL1 and BCLXL (53). In mouse mammary gland cells, SHP2 plays a positive role in the prolactin-induced JAK2 activation pathway. JAK2 tends to associate with suppressor of cytokine signaling 1 (SOCS1), which targets JAK2 through a ubiquitin-dependent degradation pathway and serves as a negative regulator for the JAK2/STAT5 pathway. The interaction between JAK2 and SOCS1 is mediated by phosphorylation of Tyr1007 in JAK2. *In vitro* studies demonstrated that SHP2 was able to dephosphorylate this Tyr site and prevent the formation of the JAK2-SOCS1 complex and subsequent degradation of JAK2. Upon being released from the inhibitory effects of SOCS1, JAK2 is recruited to the prolactin receptor (PrlR) and phosphorylates STAT5 (24). However, the precise mechanism of how these molecules achieve positive functions in different systems remains to be clarified. In this study, LvPTPN6 can both combine with JAK and STAT and elevate the dimerization of STAT, providing us with clues that LvPTPN6 may belong to catalytically inactive PTPs, which could enhance the stability of the JAK and STAT dimers by blocking their tyrosyl phosphorylation sites from other PTPs. To the best of our knowledge, it is the first report of a PTP positively regulating JAK/STAT pathway in invertebrates. These findings indicated that the structures and functions of PTPs vary from different organisms that required further excavation to reveal their non-negligible regulatory roles in invertebrates and vertebrates.

DATA AVAILABILITY STATEMENT

The original contributions presented in the study are included in the article/**Supplementary Material**. Further inquiries can be directed to the corresponding authors.

AUTHOR CONTRIBUTIONS

HZ and JH supervised the overall project and designed the experiments. HZ wrote the manuscript. ML and XX performed the experiments and analyzed the data with the help from XL, LY, WS, and SW. ZZ offered the assistance to revise the manuscript. All authors contributed to the article and approved the submitted version.

FUNDING

This work was funded by the Natural Science Foundation of Guangdong Province, China, 2020A1515011152 and 2021A1515010798; National Natural Science Foundation of China under grant nos. 31972823, 32073004, and 31772881; National Key Research and Development Program of China, 2018YFD0900505; China Agriculture Research System CARS48; and Key-Area Research and Development Program of Guangdong Province, China, 2019B020217001.

SUPPLEMENTARY MATERIAL

The Supplementary Material for this article can be found online at: https://www.frontiersin.org/articles/10.3389/fimmu.2022.913955/full#supplementary-material

Supplementary Figure 1 | Sequence and domain analysis of LvPTPN6. **(A)** Nucleotide and deduced amino acid sequences of LvPTPN6. The nucleotide (lower case) and deduced amino acid (upper case) sequences were shown and numbered on the left. The putative SH2 domains were framed and the PTPc domain was shadowed. **(B)** Structural domains of LvPTPN6 predicted by SMART (http://smart.embl-heidelberg.de/).

Supplementary Figure 2 | Sequence and the predicted IRF binding motif of LvPTPN6 promoter. **(A)** Nucleotide sequence of LvPTPN6 promoter. The predicted IRF binding motif was framed, and the cleave site of the cleaved promoters mentioned in FIGURE 5 B were marked by black bars. **(B)** Results of *Homo sapiens* IRF2 binding motif in LvPTPN6 promoter predicted by JASPAR (http://jaspar2016.genereg.net/cgi-bin/jaspar_db.pl).

Supplementary Figure 3 | Microscopic vision fields for the immunofluorescent intensities analysis of **Figure 7C**.

REFERENCES

1. Mustelin T, Feng GS, Bottini N, Alonso A, Kholod N, Birle D, et al. Protein Tyrosine Phosphatases. *Front Biosci* (2002) 7:d85–142. doi: 10.2741/mustelin
2. Fischer EH, Charbonneau H, Tonks NK. Protein Tyrosine Phosphatases: A Diverse Family of Intracellular and Transmembrane Enzymes. *Science* (1991) 253:401–06. doi: 10.1126/science.1650499
3. Alonso A, Sasin J, Bottini N, Friedberg I, Friedberg I, Osterman A, et al. Protein Tyrosine Phosphatases in the Human Genome. *Cell* (2004) 117:699–711. doi: 10.1016/j.cell.2004.05.018
4. Hasegawa K, Martin F, Huang G, Tumas D, Diehl L, Chan AC. Pest Domain-Enriched Tyrosine Phosphatase (PEP) Regulation of Effector/Memory T Cells. *Science* (2004) 303:685–89. doi: 10.1126/science.1092138
5. Andersen JN, Jansen PG, Echwald SM, Mortensen OH, Fukada T, Del VR, et al. A Genomic Perspective on Protein Tyrosine Phosphatases: Gene Structure, Pseudogenes, and Genetic Disease Linkage. *FASEB J* (2004) 18:8–30. doi: 10.1096/fj.02-1212rev
6. Guan KL, Dixon JE. Evidence for Protein-Tyrosine-Phosphatase Catalysis Proceeding via a Cysteine-Phosphate Intermediate. *J Biol Chem* (1991) 266:17026–30. doi: 10.1016/S0021-9258(19)47335-3
7. Tootle TL, Silver SJ, Davies EL, Newman V, Latek RR, Mills IA, et al. The Transcription Factor Eyes Absent is a Protein Tyrosine Phosphatase. *Nature* (2003) 426:299–302. doi: 10.1038/nature02097
8. Rayapureddi JP, Kattamuri C, Steinmetz BD, Frankfort BJ, Ostrin EJ, Mardon G, et al. Eyes Absent Represents a Class of Protein Tyrosine Phosphatases. *Nature* (2003) 426:295–98. doi: 10.1038/nature02093
9. Martell KJ, Angelotti T, Ullrich A. The "VH1-Like" Dual-Specificity Protein Tyrosine Phosphatases. *Mol Cells* (1998) 8:2–11.
10. Chen HF, Chuang HC, Tan TH. Regulation of Dual-Specificity Phosphatase (DUSP) Ubiquitination and Protein Stability. *Int J Mol Sci* (2019) 20:2668. doi: 10.3390/ijms20112668
11. Pao LI, Badour K, Siminovitch KA, Neel BG. Nonreceptor Protein-Tyrosine Phosphatases in Immune Cell Signaling. *Annu Rev Immunol* (2007) 25:473–523. doi: 10.1146/annurev.immunol.23.021704.115647

12. Li C, Li H, Chen Y, Chen Y, Wang S, Weng SP, et al. Activation of Vago by Interferon Regulatory Factor (IRF) Suggests an Interferon System-Like Antiviral Mechanism in Shrimp. *Sci Rep* (2015) 5:15078. doi: 10.1038/srep15078
13. Gao J, Zhao BR, Zhang H, You YL, Li F, Wang XW. Interferon Functional Analog Activates Antiviral Jak/Stat Signaling Through Integrin in an Arthropod. *Cell Rep* (2021) 36:109761. doi: 10.1016/j.celrep.2021.109761
14. Taniguchi T, Ogasawara K, Takaoka A, Tanaka N. IRF Family of Transcription Factors as Regulators of Host Defense. *Annu Rev Immunol* (2001) 19:623–55. doi: 10.1146/annurev.immunol.19.1.623
15. Ikushima H, Negishi H, Taniguchi T. The IRF Family Transcription Factors at the Interface of Innate and Adaptive Immune Responses. *Cold Spring Harb Symp Quant Biol* (2013) 78:105–16. doi: 10.1101/sqb.2013.78.020321
16. Ivashkiv LB. Jak-STAT Signaling Pathways in Cells of the Immune System. *Rev Immunogenet* (2000) 2:220–30. doi: 10.1038/npg.els.0004002
17. Shuai K, Liu B. Regulation of JAK-STAT Signalling in the Immune System. *Nat Rev Immunol* (2003) 3:900–11. doi: 10.1038/nri1226
18. Li WX. Canonical and non-Canonical JAK-STAT Signaling. *Trends Cell Biol* (2008) 18:545–51. doi: 10.1016/j.tcb.2008.08.008
19. Stark GR, Darnell JJ. The JAK-STAT Pathway at Twenty. *Immunity* (2012) 36:503–14. doi: 10.1016/j.immuni.2012.03.013
20. Rawlings JS, Rosler KM, Harrison DA. The JAK/STAT Signaling Pathway. *J Cell Sci* (2004) 117:1281–83. doi: 10.1242/jcs.00963
21. Murray PJ. The JAK-STAT Signaling Pathway: Input and Output Integration. *J Immunol* (2007) 178:2623–29. doi: 10.4049/jimmunol.178.5.2623
22. Kim M, Morales LD, Jang IS, Cho YY, Kim DJ. Protein Tyrosine Phosphatases as Potential Regulators of STAT3 Signaling. *Int J Mol Sci* (2018) 19:2708. doi: 10.3390/ijms19092708
23. You M, Zhao Z. Positive Effects of SH2 Domain-Containing Tyrosine Phosphatase SHP-1 on Epidermal Growth Factor- and Interferon-Gamma-Stimulated Activation of STAT Transcription Factors in HeLa Cells. *J Biol Chem* (1997) 272:23376–81. doi: 10.1074/jbc.272.37.23376
24. Ali S, Nouhi Z, Chughtai N, Ali S. SHP-2 Regulates SOCS-1-Mediated Janus Kinase-2 Ubiquitination/Degradation Downstream of the Prolactin Receptor. *J Biol Chem* (2003) 278:52021–31. doi: 10.1074/jbc.M306758200
25. Wang M, Chen Y, Zhao Z, Weng S, Yang J, Liu S, et al. A Convenient Polyculture System That Controls a Shrimp Viral Disease With a High Transmission Rate. *Commun Biol* (2021) 4:1276. doi: 10.1038/s42003-021-02800-z
26. Li C, Weng S, He J. WSSV-Host Interaction: Host Response and Immune Evasion. *Fish Shellfish Immunol* (2019) 84:558–71. doi: 10.1016/j.fsi.2018.10.043
27. Li C, Wang S, He J. The Two NF-kappaB Pathways Regulating Bacterial and WSSV Infection of Shrimp. *Front Immunol* (2019) 10:1785. doi: 10.3389/fimmu.2019.01785
28. Song X, Zhang Z, Wang S, Li H, Zuo H, Xu X, et al. A Janus Kinase in the JAK/STAT Signaling Pathway From Litopenaeus Vannamei is Involved in Antiviral Immune Response. *Fish Shellfish Immunol* (2015) 44:662–73. doi: 10.1016/j.fsi.2015.03.031
29. Wen R, Li F, Li S, Xiang J. Function of Shrimp STAT During WSSV Infection. *Fish Shellfish Immunol* (2014) 38:354–60. doi: 10.1016/j.fsi.2014.04.002
30. Zuo H, Li H, Wei E, Su Z, Zheng J, Li C, et al. Identification and Functional Analysis of a Hemolin Like Protein From Litopenaeus Vannamei. *Fish Shellfish Immunol* (2015) 43:51–9. doi: 10.1016/j.fsi.2014.12.004
31. Livak KJ, Schmittgen TD. Analysis of Relative Gene Expression Data Using Real-Time Quantitative PCR and the 2(-Delta Delta C(T)) Method. *Methods* (2001) 25:402–08. doi: 10.1006/meth.2001.1262
32. Bolte S, Cordelieres FP. A Guided Tour Into Subcellular Colocalization Analysis in Light Microscopy. *J Microsc* (2006) 224:213–32. doi: 10.1111/j.1365-2818.2006.01706.x
33. Zuo H, Liu X, Luo M, Yang L, Zhu Z, Weng S, et al. miR-10c Facilitates White Spot Syndrome Virus Infection by Targeting Toll3 in Litopenaeus Vannemei. *Front Immunol* (2021) 12:733730. doi: 10.3389/fimmu.2021.733730
34. Zhang X, Yuan J, Sun Y, Li S, Gao Y, Yu Y, et al. Penaeid Shrimp Genome Provides Insights Into Benthic Adaptation and Frequent Molting. *Nat Commun* (2019) 10:356. doi: 10.1038/s41467-018-08197-4
35. Zuo H, Yuan J, Chen Y, Li S, Su Z, Wei E, et al. A MicroRNA-Mediated Positive Feedback Regulatory Loop of the NF-kappaB Pathway in Litopenaeus Vannamei. *J Immunol* (2016) 196:3842–53. doi: 10.4049/jimmunol.1502358
36. Frank C, Keilhack H, Opitz F, Zschornig O, Bohmer FD. Binding of Phosphatidic Acid to the Protein-Tyrosine Phosphatase SHP-1 as a Basis for Activity Modulation. *Biochemistry-Us* (1999) 38:11993–2002. doi: 10.1021/bi982586w
37. Massa PT, Saha S, Wu C, Jarosinski KW. Expression and Function of the Protein Tyrosine Phosphatase SHP-1 in Oligodendrocytes. *Glia* (2000) 29:376–85. doi: 10.1002/(SICI)1098-1136(20000215)29:4<376::AID-GLIA8>3.0.CO;2-S
38. Lu W, Gong D, Bar-Sagi D, Cole PA. Site-Specific Incorporation of a Phosphotyrosine Mimetic Reveals a Role for Tyrosine Phosphorylation of SHP-2 in Cell Signaling. *Mol Cell* (2001) 8:759–69. doi: 10.1016/S1097-2765(01)00369-0
39. Koyama M, Oka T, Ouchida M, Nakatani Y, Nishiuchi R, Yoshino T, Hayashi K, Akagi T, Seino Y. Activated Proliferation of B-Cell Lymphomas/Leukemias with the SHP1 Gene Silencing by Aberrant CpG Methylation. *Lab Invest* (2003) 83(12):1849–58. doi: 10.1097/01.lab.0000106503.65258.2b
40. Frank C, Burkhardt C, Imhof D, Ringel J, Zschornig O, Wieligmann K, et al. Effective Dephosphorylation of Src Substrates by SHP-1. *J Biol Chem* (2004) 279:11375–83. doi: 10.1074/jbc.M309096200
41. Yan M, Li C, Su Z, Liang Q, Li H, Liang S, et al. Identification of a JAK/STAT Pathway Receptor Domeless From Pacific White Shrimp Litopenaeus Vannamei. *Fish Shellfish Immunol* (2015) 44:26–32. doi: 10.1016/j.fsi.2015.01.023
42. Barnes B, Lubyova B, Pitha PM. On the Role of IRF in Host Defense. *J Interferon Cytokine Res* (2002) 22:59–71. doi: 10.1089/107999002753452665
43. Hernandez N, Melki I, Jing H, Habib T, Huang S, Danielson J, et al. Life-Threatening Influenza Pneumonitis in a Child With Inherited IRF9 Deficiency. *J Exp Med* (2018) 215:2567–85. doi: 10.1084/jem.20180628
44. Funato K, Yamazumi Y, Oda T, Akiyama T. Tyrosine Phosphatase PTPRD Suppresses Colon Cancer Cell Migration in Coordination With CD44. *Exp Ther Med* (2011) 2:457–63. doi: 10.3892/etm.2011.231
45. Ku M, MacKinnon RN, Wall M, Narayan N, Walkley C, Cheng HC, et al. Hemopoietic Cell Kinase Amplification With Protein Tyrosine Phosphatase Receptor T Depletion Leads to Polycythemia, Aberrant Marrow Erythoid Maturation, and Splenomegaly. *Sci Rep* (2019) 9:7050. doi: 10.1038/s41598-019-43373-6
46. Zhang X, Guo A, Yu J, Possemato A, Chen Y, Zheng W, et al. Identification of STAT3 as a Substrate of Receptor Protein Tyrosine Phosphatase T. *Proc Natl Acad Sci U.S.A.* (2007) 104:4060–64. doi: 10.1073/pnas.0611665104
47. Sun PH, Ye L, Mason MD, Jiang WG. Protein Tyrosine Phosphatase Kappa (PTPRK) is a Negative Regulator of Adhesion and Invasion of Breast Cancer Cells, and Associates With Poor Prognosis of Breast Cancer. *J Cancer Res Clin Oncol* (2013) 139:1129–39. doi: 10.1007/s00432-013-1421-5
48. Wang W, Liu L, Song X, Mo Y, Komma C, Bellamy HD, et al. Crystal Structure of Human Protein Tyrosine Phosphatase SHP-1 in the Open Conformation. *J Cell Biochem* (2011) 112:2062–71. doi: 10.1002/jcb.23125
49. Bentires-Alj M, Paez JG, David FS, Keilhack H, Halmos B, Naoki K, et al. Activating Mutations of the Noonan Syndrome-Associated SHP2/PTPN11 Gene in Human Solid Tumors and Adult Acute Myelogenous Leukemia. *Cancer Res* (2004) 64:8816–20. doi: 10.1158/0008-5472.CAN-04-1923
50. Zhang D, Marlin MC, Liang Z, Ahmad M, Ashpole NM, Sonntag WE, et al. The Protein Tyrosine Phosphatase MEG2 Regulates the Transport and Signal Transduction of Tropomyosin Receptor Kinase A. *J Biol Chem* (2016) 291:23895–905. doi: 10.1074/jbc.M116.728550
51. Xu D, Qu CK. Protein Tyrosine Phosphatases in the JAK/STAT Pathway. *Front Biosci* (2008) 13:4925–32. doi: 10.2741/3051
52. Han Y, Amin HM, Franko B, Frantz C, Shi X, Lai R. Loss of SHP1 Enhances JAK3/STAT3 Signaling and Decreases Proteosome Degradation of JAK3 and NPM-ALK in ALK+ Anaplastic Large-Cell Lymphoma. *Blood* (2006) 108:2796–803. doi: 10.1182/blood-2006-04-017434
53. Li L, Modi H, McDonald T, Rossi J, Yee JK, Bhatia R. A Critical Role for SHP2 in STAT5 Activation and Growth Factor-Mediated Proliferation, Survival, and Differentiation of Human CD34+ Cells. *Blood* (2011) 118:1504–15. doi: 10.1182/blood-2010-06-288910

Conflict of Interest: The authors declare that the research was conducted in the absence of any commercial or financial relationships that could be construed as a potential conflict of interest.

this article, or claim that may be made by its manufacturer, is not guaranteed or endorsed by the publisher.

frontiers | Frontiers in Immunology

REVIEW
published: 05 July 2022
doi: 10.3389/fimmu.2022.899890

Pathogen-Derived Nucleases: An Effective Weapon for Escaping Extracellular Traps

Chengshui Liao[1*], *Fuchao Mao*[1,2], *Man Qian*[1] *and Xiaoli Wang*[3*]

[1] College of Animal Science and Technology/Luoyang Key Laboratory of Live Carrier Biomaterial and Animal Disease Prevention and Control, Henan University of Science and Technology, Luoyang, China, [2] Animal Diseases and Public Health Engineering Research Center of Henan Province, Luoyang Vocational and Technical College, Luoyang, China, [3] School of Basic Medical Sciences, Henan University of Science and Technology, Luoyang, China

Since the 2004 publication of the first study describing extracellular traps (ETs) from human neutrophils, several reports have shown the presence of ETs in a variety of different animals and plants. ETs perform two important functions of immobilizing and killing invading microbes and are considered a novel part of the phagocytosis-independent, innate immune extracellular defense system. However, several pathogens can release nucleases that degrade the DNA backbone of ETs, reducing their effectiveness and resulting in increased pathogenicity. In this review, we examined the relevant literature and summarized the results on bacterial and fungal pathogens and parasites that produce nucleases to evade the ET-mediated host antimicrobial mechanism.

Keywords: immune evasion, innate immune cells, extracellular traps, pathogens, nucleases

OPEN ACCESS

Edited by:
Hang Yin,
Tsinghua University, China

Reviewed by:
Werner Solbach,
University of Lübeck, Germany
Andrea Kaminski,
National Institute of Environmental Health Sciences (NIH), United States
Sebastián A. Riquelme,
Columbia University Irving Medical Center, United States

***Correspondence:**
Chengshui Liao
liaochengshui33@163.com
Xiaoli Wang
6516757@163.com

Specialty section:
This article was submitted to Molecular Innate Immunity, a section of the journal Frontiers in Immunology

Received: *19 March 2022*
Accepted: *08 June 2022*
Published: *05 July 2022*

Citation:
Liao C, Mao F, Qian M and Wang X (2022) Pathogen-Derived Nucleases: An Effective Weapon for Escaping Extracellular Traps. Front. Immunol. 13:899890. doi: 10.3389/fimmu.2022.899890

INTRODUCTION

Pathogens have evolved various strategies to overcome the killing mechanisms of the host immune system and establish a productive infection. The secreted proteins of pathogens, which include proteases, lipases, collagenases, hyaluronidases, chitinases, and nucleases, have been found to be essential for evading the host defense system (1). Nucleases are a diverse group of enzymes that degrade both DNA and RNA, and there are several ways to classify them (2). According to Linn formulated the criteria, the most acceptable system for classification of nucleases is to divided them into sugar specific and sugar non-specific nucleases (3). Based on their activity on ester bonds, nucleases are considered a subgroup of hydrolases and can be subdivided into exonucleases (EC 3.1.11.X to EC 3.1.16.X) and endonucleases (EC 3.1.21.X to EC 3.1.31.X). For the ability to hydrolyze DNA, sugar specific nucleases are DNases including exodeoxyribonucleases and endodeoxyribonucleases, while sugar non-specific nucleases comprise endonucleases and exonucleases (2). According to their biochemical and biological properties as well as tissue-specific production, DNases can be further divided into the DNase I and DNase II families (4). Pathogen nucleases are mainly involved in physiological processes such as genetic transformation and nutrient scavenging, DNA replication, recombination and DNA repair mechanisms (5); but, they can also act as virulence factors (5), regulate of biofilm formation, enhance fitness and bacterial shedding (6), and allow microbes to enter non-phagocytic cells or survive and replicate in phagocytic cells.

Neutrophils are the most abundant type of white blood cell, and they play an important role in inflammation and host defense through the respiratory burst, degranulation, and phagocytosis (7). In 2014, Brinkmann et al. reported that when attacked by pathogens, human neutrophils released DNA-based network structures called neutrophil extracellular traps (NETs), which immobilized and/or killed pathogens (8). This phenomenon has also been observed in different mammalian species, birds, fish, invertebrates, and plants (9). However, it is also known that certain pathogens have developed strategies to avoid the killing effects of extracellular traps (ETs) by secreting a polysaccharide capsule, forming biofilms, undergoing cell surface modifications, and inhibiting ET formation (10). The main components of ETs are granule proteins and DNA, therefore it was predicted that extracellular nucleases could directly degrade the ETs' scaffold DNA, providing an effective way for pathogens to escape the ET defensive network structures (**Figure 1**). In this article, we review the latest research on the role of extracellular nucleases of bacteria, fungi, parasites, and mycoplasmas in degrading the backbone DNA of ETs, especially NETs (**Table 1**).

BACTERIA

Vibrio cholerae

Vibrio cholerae is a Gram-negative comma-shaped bacterium that is the causative agent of the secretory diarrheal disease cholera. Extracellular DNA is a major component of the *Vibrio* biofilm matrix. The two nucleases secreted by *V. cholerae*, Xds and Dns, are able to degrade extracellular DNA. Dns exhibits endonuclease activity, while Xds has been characterized as an exonuclease (11). Extracellular DNA degradation by the two nucleases results in accumulation of high levels of nucleotides outside the cell. OmpK was used to transport nucleotides to the outer membrane, where they were dephosphorylated by periplasmic phosphatases. Free phosphate was absorbed by the Pst/PhoU system and nucleosides were transported into cells *via* NupC (61). *V. cholerae* exposure caused human neutrophils to form NETs, while secreted Dns and Xds rapidly degraded the NETs' DNA and released the bacteria from the network structures, thus promoting cell colonization by *V. cholerae* (12). Infection with a *Dns/Xds* deletion mutant of *V. cholerae* resulted in prolonged stability of the NET. The C-terminus of Xds has an exonuclease domain, and residues D787 and H837 within the exonuclease domain are the key sites of the catalytic center (13).

Streptococcus spp.

Streptococcus pneumoniae

The endonuclease, EndA, of *S. pneumoniae* is localized on the membrane surface and is a key factor in DNA replication and bacterial virulence. EndA is required for the genetic transformation of *S. pneumoniae* and contributes to gene transfer and genetic diversification (14–16). EndA cannot bind to external DNA or degrade it when *S. pneumoniae* does not undergo gene conversion (17). However, in another study, it was reported that degradation of extracellular DNA by EndA did not require components of the competence regulon (18). EndA was secreted extracellularly during *S. pneumoniae* growth, which helped the pathogen establish an infection in the lung by degrading the DNA backbone of NETs and overcoming the host immune system (18). EndA possesses a DRGH (Asp-Arg-Gly-His) motif containing a ββα metal-finger catalytic core, and the amino acids, His160, Asn191, and Asn182 that are essential for catalytic activity. Expression of the wild-type *EndA* gene in *E.*

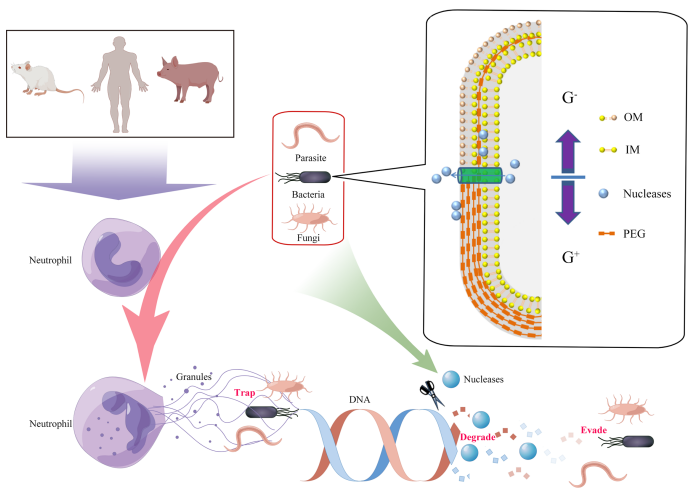

FIGURE 1 | Degradation of extracellular traps (ETs) by the production of pathogen-derived nucleases. Innate immune cells were activated by pathogens, and DNA from nuclei or mitochondria mixed with histones, granular, and cytoplasmic proteins was released to the cellular environment (termed ETs). ETs could immobilize and/or kill the pathogens. However, secreted or cell wallanchored extracellular nucleases of pathogens were capable of destroying DNA backbones of ETs and contributing to evasion of the immune response and development of persistent infections. G^+, Gram-positive bacteria; G^-, Gram-negative bacteria; OM, outer membrane; IM, inner membrane; PEG, peptidoglycan.

TABLE 1 | Pathogen-derived nucleases that degrade ETs.

Pathogene	Nuclease	Nuclease activity	Cellular localization	ET degradation*	Conserved motifs	Reference
Vibrio cholerae	Xds	Exonuclease	Membrane anchored	Deletion mutant increased PMA-inducted NETs in human neutrophils.	LTD, OBD, EEPD	(11–13)
	Dns	Endonuclease	Extracellular secreted	Deletion mutant increased PMA-inducted NETs in human neutrophils.	ND	(11, 12)
Streptococcus pneumoniae	EndA	Endonuclease	Membrane anchored	Deletion mutant failed to degrade NETs induced by PMA or H_2O_2 in human neutrophils *In vivo*: NETs localized to alveoli in deletion mutant-infected lungs of C57BL/6 mice.	DRGH, HNH(N)	(14–20)
	TatD	Exo/ endonuclease	Cell-wall surface anchored	rTatD expressed in E. coli degraded PMA-inducted NETs in human neutrophils, but little degrading activity in deletion mutant.	ND	(21)
Group A Streptococcus	Sda1	DNase	Cell-wall anchored	Significant quantities of NETs persisted in human neutrophils infected with deletion mutant; Sda1-expressing L. lactis eliminated NETs in human neutrophils. *In vivo*: NETs were clearly visualized in murine skin abscess model injected with deletion mutant.	LPXTG, DRSH	(22)
Streptococcus pyogenes	SpnA	Exo/ endonuclease	Cell-wall anchored	Deletion mutant increased PMA-inducted NETs in human neutrophils; rSpnA expressed in E. coli and SpnA-expressing L. lactis cleaved PMA-inducted NETs in human neutrophils.	LPXTG, EEPD, OBD	(23, 24)
Streptococcus suis	SsnA	DNase	Cell-wall anchored	Deletion mutant attenuated NET degradation in PMA-stimulated human neutrophils, but not porcine.	LPXTG	(25)
	EndAsuis	Endonuclease	Membrane anchored	Deletion mutant attenuated NET degradation in PMA-stimulated human neutrophils during exponential growth, but not in stationary phase.	DRGH	(26)
Streptococcus equi subsp. zooepidemicus	ENuc	Sugar non-specific nuclease	Cell-wall anchored	rENuc expressed in E. coli degraded PMA-inducted NETs in neutrophils of ICR mice.	LPXTG, sugar-nonspecific nuclease domain, EEPD	(27)
	5Nuc	5'-nucleotidase	Cell-wall anchored	r5Nuc expressed in E. coli degraded PMA-inducted NETs in neutrophils of ICR mice.	LPXTG, 5'-nucleotidase domain	
Streptococcus agalactiae	NucA	Exo/ endonuclease	Extracellular secreted	The nucA H148A mutant had no effect on NET response in PMA-activated mice neutrophils.	DKGH, HNN	(28, 29)
Streptococcus mutans	DeoC	Nuclease	ND	Deletion mutant stimulated NET production in human neutrophils.	ND	(30)
Streptococcus sanguis	SWAN	Sugar non-specific nuclease	Cell-wall anchored	rSWAN expressed in E. coli digested PMA-inducted NETs in human neutrophils	LPKTG, EEPD, OBD	(31)
Streptococcus iniae	SpnAi	ND	ND	rSpnAi expressed in E. coli degraded PMA-inducted NETs in neutrophils from adult zebrafish kidney.	ND	(32)
Staphylococcus aureus	Nuc1/SNase	Sugar non-specific nuclease	Extracellular secreted	Deletion mutant showed impaired degradation of PMA-inducted NETs in human neutrophils; Snase-expressing L. lactis cleaved PMA-induced NETs in neutrophils of NOD mice.	ND	(33–39)
Mycobacterium tuberculosis	Rv0888	Exo/ endonuclease, Phosphatase, Smase	Extracellular secreted/ Membrane anchored	The Smase activity of Rv0888 efficiently induced NET formation in human neutrophils, but not nuclease activity.	ND	(40–42)
Pseudomonas aeruginosa	EddB	DNase, PDE	Extracellular secreted	The EddAB double mutant with plasmid-encoded pEddB restored the NET degradation capacity in human neutrophils.	ND	(43)
Neisseria gonorrhoeae	Nuc	Sugar non-specific nuclease	Extracellular secreted	rNuc expressed in E. coli decreased the integrity of PMA-induced NETs in human neutrophils, as well as NETs elicited by the deletion mutant.	ND	(44)
Prevotella intermedius	nucA	Sugar non-specific nuclease	Extracellular secreted	rNucA expressed in E. coli was capable of cleaving PMA-induced NETs in human neutrophils.	EEPD	(45)
	nucD	Sugar non-specific nuclease	Extracellular secreted	rNucD expressed in E. coli was capable of cleaving PMA-induced NETs in human neutrophils.	Endonuclease_NS domain	

(Continued)

TABLE 1 | Continued

Pathogene	Nuclease	Nuclease activity	Cellular localization	ET degradation*	Conserved motifs	Reference
Ralstonia solanacearum	NucA/NucB	Endonuclease	Membrane anchored	The nucA/B deletion mutant was immobilized by the DNA of plant border cell traps, and reversed by rNucA and rNucB expressed in E. coli.	ND	(46)
Leishmania spp.	3'NT/NU	Sugar non-specific nuclease	Cell surface membrane-anchored	LP parasites with higher 3'NT/NU activity cleaved more NETs in buffy coat neutrophils.	Class I nucleases domain	(47–49)
Nippostrongylus brasiliensis	Nb-DNase	DNase II	ND	The extracellular DNA fibers formed in human neutrophils induced by PMA were hydrolyzed by rNb-DNase II expressed in E. coli.	DNase II	(50)
Plasmodium spp.	PbTatD	DNase	Parasitophorous vacuole membrane	The deletion mutant induced METs and NETs in J774A.1 macrophages and mouse neutrophils, but fewer in WT parasites; rPbTatD expressed in E. coli hydrolyzed METs.	DNase	(51, 52)
Trypanosoma spp.	TryTatD05/ TryTatD15	Endonuclease	Cytoplasm, flagella	rTryTatD05 and rTryTatD15 expressed in E. coli degraded NETs in murine neutrophils.	HPEDHRHFGEDP	(53)
Mycoplasma hominis	MHO_0730	Sugar non-specific nuclease	Membrane anchored	Viable Mycoplasma hominis degraded PMA-induced NETs in human neutrophils.	TNASE_3 domain	(54, 55)
Mycoplasma hyopneumoniae	Mhp597	Sugar non-specific nuclease	Extracellular secreted	PMA-induced NETs in porcine were completely destroyed by rMhp597 expressed in E. coli.	ND	(56)
Mycoplasma bovis	MBOV_RS02825	Sugar non-specific nuclease	Membrane anchored	rMBOV_RS02825 expressed in E. coli reduced PMA-induced NETs in bovine neutrophils.	TNASE_3 domain	(57)
	MnuA	ND	Membrane anchored	NETs were evident in cow neutrophils stimulated with the deletion mutant.	ND	(58)
Mycoplasma pneumoniae	Mpn491	Nuclease	Extracellular secreted	The ability of the deletion mutant to degrade PMA-induced NETs in human PMNs was markedly impaired. *In vivo*: LPS-induced NETs in mice lungs were apparently released by the infection with the deletion mutant.	EEPD	(59)
Leptospira spp.	LigA	Exo/ endonuclease	Surface Protein	rLigA expressed in E. coli degraded the PMA-induced NETs in neutrophils of C57BL/6J mice.	ND	(60)

**Conditions under which pathogen-derived nucleases degrade ETs in vitro and in vivo.*

ND, not determined; ETs, extracellular traps; NETs, neutrophil extracellular traps; PMA, phorbol myristate acetate; Smase, sphingomyelinase; PDE, phosphodiesterase; LTD, lamin-tail domain; OBD, oligonucleotide/oligosaccharide-binding fold domain; EEPD, endonuclease/exonuclease/phosphatase domain.

coli was difficult due to its extreme cytotoxicity, but an *EndA* gene with the H160A mutation was successfully expressed. Asn182 was required for the stability of EndA (19), while Arg127/Lys128 and Arg209/Lys210 helped the enzyme bind to the substrate (20). In addition, the three mutant strains, H154A, Q186A, and Q192A, exhibited significantly decreased nuclease activities.

The twin-arginine translocase D (TatD) is a soluble cytoplasmic protein that was obtained from the extracellular secreted proteins of *S. pneumoniae*, but has been described in most prokaryotic and eukaryotic species (21). Although TatD functions primarily in the operation of the Tat transport system, it also exhibits endonuclease and exonuclease activity. TatD has been associated with the formation of extracellular vesicles of *S. pneumoniae*, and recombinant TatD (rTatD) had DNase activity. A *TatD* deletion mutant showed little NET degradation activity, while the addition of rTatD reduced the formation of NETs. The deletion mutant greatly reduced the bacterial load in the lung, blood, and spleen in a murine sepsis model (21). In our study, the recombinant TatD-like DNase from *Listeria monocytogenes* 10403s was associated with the degradation of macrophage ETs and its Mg^{2+}-dependent nuclease activity had an optimum reaction temperature of 37°C and pH of 6.0 (62).

Streptococcus pyogenes (GAS, group A streptococci)

Group A streptococci (GAS) produce 26-30 extracellular nucleases, including Sda1, SdaD2, Spd, and Spd3. Sda1 exhibits cell wall-anchored DNase activity and highly expressed by the serotype M1 GAS strain. Sda1 contributed to enhancing the tolerance and virulence of GAS toward neutrophils in a murine model of necrotizing fasciitis. Inhibition of GAS nuclease activity with G-actin enhanced the clearance of pathogens by neutrophils *in vitro* and reduced virulence *in vivo* (63). Sda1 from invasive M1T1 GAS degraded the DNA backbone of NETs in human neutrophils. DNA degradation by Sda1 prevented GAS from inducing murine macrophages to secrete IFN-α and TNF-α, while the levels of IFN-α and TNF-α in mice were significantly decreased by *Sda1*-expressing GAS (64). Degradation of PMA-induced NETs by Sda1 and other phage-encoded DNases in mouse neutrophils was neutralized by antibodies from mice immunized with Sda1 (22). The prophage-encoded SdaD2 enzyme was the major DNase that contributes to GAS virulence (65). Extracellular killing of the *spd3*/*sdaD2*/*spd* deletion mutant of M1 GAS strain MGAS5005 in human PMNs was significantly enhanced. In addition, the virulence of the triple-mutant strain in mice was significantly reduced and bacteria were easily removed from the skin injection site (65).

The *Streptococcus pyogenes* nuclease A (SpnA) is an exo/endonuclease with an LPXTG motif located on the cell surface in *S. pyogenes* and also GAS. Two catalytic domain structures were predicted for the mature SpnA. Multiple oligonucleotide and oligosaccharide binding-fold motifs were found in the N-terminal domain at position 99-395. The C-terminal domain contained a putative endo/exonuclease domain at position 549-851. Glu592, Arg696, His716, Asp767, Asn769, Asp810, and Asp842 were necessary for SpnA activity and contributed to binding of the substrate (23). Both the full-length (99-877) and the truncated (217-877) versions of the recombinant SpnA expressed in *E. coli* exhibited nuclease activity. The rSpnA was capable of dismantling the NET-like structures produced by human neutrophils after stimulation with phorbol myristate acetate (PMA) (24). The nuclease activity of the *spnA* deletion mutant was decreased by about 70%, and antibodies against SpnA in human serum significantly inhibited nuclease activity. Although SpnA promoted bacterial survival and neutrophil killing in whole human blood, the *spnA* deletion mutant showed only a partial reduction in virulence in a *Galleria mellonella* infection model (23).

5′-nucleotidases catalyze the hydrolysis of phosphate esterified at carbon 5′ of ribonucleotides, deoxyribonucleotides, and complexnucleotides (66). 5′-nucleotidases are allocated to the enzyme commission numbers EC 3.1.3.5, and are found in all kingdoms, including plants, animals, bacteria, fungi, and parasites. The biological function of microbial 5′-nucleotidases is related to the location of the enzyme in the cell (66). Membrane-bound or cell wall-anchored 5′-nucleotidases has the ability to convert AMP into the immunomodulator adenosine, thus contributing to the evasion of the bacteria from the host immune response during infection (67). *Streptococcal* 5'-nucleotidase A (S5nA) is a cell wall-anchored 5′-nucleotidases and also a virulence factor of *S. pyogenes* N99A. Recombinant S5nA (rS5nA) produced in *E. coli* showed 5′-nucleotidase activity that hydrolyzed AMP, ADP, and dAMP, but not ATP, to generate adenosine and deoxyadenosine. Expression of rS5nA increased the survival of non-pathogenic *Lactococcus lactis* in human whole blood (68). However, the current data are still not sufficient to prove the role of S5nA in immune evasion by degrading the DNA backbone of ETs.

Streptococcal phage-encoded DNase (Spd1) is a type I extracellular DNase with 28 kDa encoded by a prophage (SF370.1) in *S. pyogenes* strain SF370. Spd1 existed as a monomer in solution and His121, Asn145, and Glu164 were the important conserved residues for nuclease activity (69). Although phage-encoded DNases are capable of promoting bacterial and phage particle dissemination by liquefying pus and cellular material and enhanced the survival of the phage, the crucial role of Spd1 in *S. pyogenes* in evading the host immune response is not fully understood.

Streptococcus suis

SsnA is a secreted DNase that is anchored in the cell wall of *S. suis* and released into the culture medium. SsnA had strong DNase activity during exponential growth. The *ssnA* deletion mutant significantly reduced bacterial adherence and invasion of human laryngeal epithelial Hep-2 cells, and the virulence of the *S. suis* deletion mutant in CD1 mice was significantly decreased (70). SsnA was not necessary for *S. suis* type 2 growth and survival in human and porcine blood *in vitro*, but it did contribute to degradation of NETs stimulated by PMA in human and porcine neutrophils and weakened the antibacterial activity of human NETs (25).

EndAsuis is an endonuclease of *S. suis* with high homology and structural similarity to the membrane anchor of EndA in *S. pneumoniae*, but EndAsuis could not be successfully expressed in *E. coli* (26). The nuclease activity of a recombinant EndAsuis with a point-mutation at H165 in the DRGH motif was confirmed in the presence of Mg^{2+}, but not Ca^{2+}. EndAsuis was not released from *S. suis* into the culture medium; however, the *EndAsuis* deletion mutant significantly attenuated the degradation of human NETs, but had no significant effect on the NET-mediated bactericidal activity (26). High DNase activity of SsnA was found in the cerebrospinal fluid (CSF) of *S. suis*-infected piglets with severe suppurative meningitis. However, neither SsnA nor EndAsuis efficiently degraded NETs, and NET fibers with entrapped streptococci were observed in neutrophils from CSF (71). The up-regulated cathelicidin PR-39 in choroid plexus epithelial cells inhibited the degradation of NETs. In contrast to SsnA, host DNase 1 contributed to the enhancement of neutrophil antimicrobial activity in the CSF of *S. suis*-infected piglets (72).

Streptococcus equi subsp. *zooepidemicus*

ENuc and 5Nuc, encoded by the *SESEC_RS04165* and *SESEC_RS05720* genes, respectively, are two extracellular nucleases from *S. equi* subsp. *zooepidemicus*. ENuc and 5Nuc were a cell-wall anchored nucleotidase with LPXTG motif. The degradation of NETs by these nucleases reduced phagocytosis and the bactericidal capacity of macrophages, but not the intracellular killing process. An *Enuc*/*5Nuc* deletion mutant lost the ability to degrade NETs into deoxyadenosine, but it induced fewer NETs and showed greater survival in the NETs that were produced (27).

Streptococcus agalactiae

Seven genes encoding secreted nucleases from *S. agalactiae* have been found. NucA encoded by the *gbs0661* gene displays a high degree of sequence identity with *S. pneumoniae* EndA and *S. pyogenes* Sda1. NucA contains a putative N-terminal transmembrane domain and is a major extra-cytoplasmic nuclease that required divalent cations, a stable pH, and heat stability. The nuclease activity of the H148A, R111A/H148G, K127A/H148G, K146A/H148G, and Q180A/H148G point-mutated strain was significantly decreased, while the K146R and Q183A mutant strain exhibited significantly increased activity (28). NucA was required to avoid *S. agalactiae* clearance from lung tissue at an early step of infection by degrading the DNA skeleton of NETs induced by PMA in mice, and contributed to dissemination in the bloodstream and persistent infection (29).

Streptococcus mutans

The *S. mutans* culture medium at 48-60 h exhibited a high level of DNase activity, which changed with the same tendency as the

biofilm-released bacterial cells. The *deoxyribose aldolase* gene (*deoC*)-encoded product catalyzed the reversible aldol reaction of acetaldehyde and glyceraldehyde 3-P from the sugar phosphate, deoxyribose 5-phosphate (73) and also catabolized extracellular DNA. The nuclease DeoC was a regulator of the biofilm dispersal of *S. mutans*. *S. mutans* induced the formation of NETs in human neutrophils, and the NETs in turn enhanced the expression of the *deoC* gene of *S. mutans*. The DeoC activity of *S. mutans* was critical for evading killing by neutrophils through degrading NETs (30).

Streptococcus sanguis

Morita et al. reported that oral streptococci showed extracellular DNase activity. Thirty-three cell wall-anchored proteins containing the LPXTG motif were predicted in *S. sanguis*. SWAN is a cell surface protein with a cell wall-sorting signal and a putative nuclease domain. The nuclease activity of a *Swan* deletion mutant was significantly reduced, while a strain over-expressing recombinant SWAN degraded a variety of DNAs including the DNA backbone in NETs, allowing *S. sanguis* to survive NETs from human neutrophils stimulated with PMA. In addition, *L. lactis* heterologously expressing *Swan* showed enhanced resistance to NET-mediated bactericidal activity (31).

Streptococcus iniae

The genes encoding SpnAi and S5nAi in *S. iniae* were similar to those for SpnA and S5nA of GAS, respectively, in terms of amino acid sequence, protein length, domain structures, and biochemical properties, as well as similar virulence mechanisms (74). The *spnAi* and *s5nAi* deletion mutants showed significant loss of DNase and nucleotidase activity, respectively. SpnAi and S5nAi supported the growth, proliferation, and dissemination of *S. iniae* and contributed to *S. iniae* virulence in zebrafish larvae. The *SpnAi* and *S5nAi* deletion mutants were still able to recruit neutrophils and macrophages to infected sites (32). NETs induced by PMA were degraded in the presence of *S. iniae* and also the recombinant SpnAi in neutrophils from the kidneys of adult zebrafish, but not in the presence of the s*pnAi* deletion mutant (32).

Staphylococcus aureus

Staphylococcal nuclease (SNase) is a nonspecific phosphodiesterase that has a strong ability to degrade a DNA scaffold to ssDNA or dsDNA, and we found that the secreted proteins of *S. aureus* possess DNA degradation activity (75). Similarly, Herzog et al. reported significant nuclease activity of clinical *S. aureus* isolates from cystic fibrosis (CF) patients (33). The nuclease activity of sequential isogenic isolates was increased in a time- and phenotype-dependent manner. Strong DNA degradation capability was observed in sputum samples from one CF patient during a long-term chronic *S. aureus* infection. The isolates with high nuclease activity facilitated *S. aureus* survival from NET-mediated killing by human neutrophils (33).

Nuc1, a thermostable nuclease, catalyzes the hydrolysis of both DNA and RNA. *S. aureus* eDNA maintains the structural stability of the biofilm during bacterial colonization. During the early stage of *S. aureus* biofilm formation, Nuc1 is expressed, which was responsible for infection persistence in a mouse subcutaneous implant model (76). Nuc1 can degrade the DNA scaffold in neutrophil NETs, thereby evading the host immune response (34). The breakdown of NET DNA by *S. aureus* nuclease Nuc1 contributed to the survival and dissemination of biofilm bacteria trapped in NETs and caused persistent infections (35). The ability of the *nuc1* deletion mutant to degrade NETs was significantly impaired, and it was more sensitive to extracellular killing by activated neutrophils (36). Nuc2, another thermostable nuclease of *S. aureus*, was considered to be a cell surface-binding protein with nuclease activity. However, Nuc2 had no significant impact on NETs and was not involved in virulence and immune evasion (37).

S. aureus degrades NET DNA into deoxyadenosine to avoid its killing effect. The process triggered the caspase 3-mediated death of immune cells (38). Excessive formation of NETs contributed to the early pathological injury to the pancreas, resulting in the onset of diabetes. Lang et al. showed that a *L. lactis* strain expressing recombinant *SNase* effectively degraded PMA-induced NETs *in vitro* and significantly decreased circulating free DNA in the serum in non-obese diabetic (NOD) mice (39). Moreover, early treatment with SNase ameliorated the gut immune microenvironment of NOD mice by regulating the level of NETs in the intestinal mucosa (77).

Other Bacterial Species

Three different *Yersinia enterocolitica* serotypes (O:8, O:9, and O:3) were able to induce NET formation. The culture supernatants of the three serotypes also showed the capacity to degrade plasmid DNA in the presence of Ca^{2+}/Mg^{2+}, and NETs induced by PMA treatment of human neutrophils were degraded by the bacterial supernatants (78). Although the endonuclease-1 proteins, EndA and NucM, of *Y. enterocolitica* are similar to the NET-degrading *V. cholerae* extracellular deoxyribonuclease, their role in degrading the DNA of NETs to evade the host immune response remains unclear.

Three extracellular nucleases, EndA, ExeS, and ExeM were found in *Shewanella oneidensis* MR-1. ExeM was localized to the cytoplasmic membrane fraction. The activity of ExeM expressed in *E. coli* revealed that it was a nonspecific endonuclease requiring Ca^{2+} and Mg^{2+} or Ca^{2+} and Mn^{2+} as cofactors. ExeM was beneficial for biofilm formation under static conditions, however, externally added recombinant ExeM inhibited biofilm formation but not biofilm removal (79). Although the author hypothesized that ExeM may be related to NETs degradation, not detected in culture supernatants of *S. oneidensis*. Thus, the role of ExeM in NET-mediated extracellular killing is still unclear.

Sphingomyelinase catalyzes the hydrolysis of sphingomyelin into ceramide and phosphorylcholine, and is allocated to the enzyme commission numbers, EC 3.1.4.12 and EC 3.1.4.41 (80). More than six categories of sphingomyelinase have been found in a wide variety of bacteria (80, 81). The important physiological functions of sphingomyelinase are related to membrane permeability, membrane aggregation, and fusion (80). Sphingomyelinase as a virulence factor contributes to bacterial

colonization, dissemination, and evasion of immune response for the establishment of persistent infection (81). Rv0888 obtained from *Mycobacterium tuberculosis* culture filtrate is an outer membrane protein with sphingomyelinase activity. Rv0888 increased intracellular survival, and replication of *M. tuberculosis* in THP-1 macrophages, but was not required for virulence of *M. tuberculosis* in mice (40). The C-terminal sequence of Rv0888 was highly conserved with an endonuclease-exonuclease-phosphatase domain (40). Dang et al. demonstrated that the recombinant Rv0888 expressed in *E. coli* required divalent metal cations (Ca^{2+} and Mn^{2+}) to degrade different types of nucleic acids (41). The optimum temperature and pH for the nuclease activity were 41°C and 6.5, respectively. The activity of Rv0888 was inhibited by four traditional Chinese medicinal compounds, oleuropein, 6-gingerol, corylifolinin, and acteoside. The residues, H353, D387, D438, and H481, were essential for catalysis of Rv0888 (41). Although *M. tuberculosis* induced the formation of NETs and could be captured by them, the bacteria were not killed by NETs *in vitro*. Interestingly, the sphingomyelinase activity of recombinant Rv0888NS/MS stimulated the release of NETs from human neutrophils *in vitro* and in the lung tissues of mice (42).

Phosphodiesterases (EC 3.1.4.1) are a superfamily of enzymes that cleave the cyclic phosphodiester bond of cyclic adenosine and cyclic guanosine monophosphate (82). There are a total of 11 different phosphodiesterase family members (phosphodiesterase 1-11) with 21 isoforms. Phosphodiesterases are involved in diverse physiological functions and play a pivotal role in mediating the cyclic nucleotide signaling (82). In pathogens, phosphodiesterases are essential for controlling the kinetics of biofilm formation, swarming motility, survival, and dissemination (83). *Pseudomonas aeruginosa* has two secreted nucleases, EddA and EddB. EddA has alkaline phosphatase and phosphodiesterase activity, which can restrict the antibacterial activity of NETs (43). EddB can degrade eDNA, and the products can be taken up and used as source of nutrition by cells. The eDNA and NETs were effective inducers of the nuclease-phosphatase operon. The nucleases helped to degrade the DNA backbone of NETs and protected *P. aeruginosa* from NET-mediated killing. Although phosphatase did not the ability of the DNases to degrade DNA, it prevented cations from chelating phosphate from the eDNA phosphodiester backbone. Therefore, both DNase and phosphodiesterase contributed to the resistance to killing of *P. aeruginosa* by NETs (43).

Neisseria gonorrhoeae stimulated human neutrophils to release NETs, and the NETs showed antibacterial activity against *N. gonorrhoeae*. A thermostable nuclease homologue, Nuc, from *N. gonorrhoeae* influenced biofilm formation. Recombinant Nuc expressed in *E. coli* degraded DNA in PMA-induced NETs, and enhanced the survival of extracellular bacteria in human neutrophils (44).

Several studies have demonstrated that the NET-like defense structure as a mechanism is analogous to the situation in periodontitis, where bacteria colonize the periodontal region by avoiding the immune response of the host. Doke *et al.* reported that the periodontal pathogenic bacteria, *Porphyromonas gingivalis*, *Prevotella intermedia*, and *Fusobacterium nucleatum* exhibited extracellular DNA degradation activity (84). The genes, *nucA* and *nucD*, and the encoded secreted nucleases were characterized in *P. intermedia* (ATCC 25611). Recombinant NucA and NucD required Mg^{2+} and Ca^{2+} for optimal digestion of DNA and RNA, and their ability to degrade the DNA framework of NETs was confirmed (45). In our present study, the extracellular secreted proteins from *Salmonella typhimurium*, *S. choleraesuis*, *Klebsiella pneumoniae*, and *Pasteurella multocida* showed nuclease activity in degradation of phage λ DNA. Four proteins with nuclease activity were identified as extracellular proteins secreted from *S. Typhimurium* using the SDS-PAGE nuclease zymography technique combined with LC-ESI/MS/MS (85). METs -induced by *Candida albicans* were degraded by secreted proteins from *S. choleraesuis* (86). However, detailed studies are needed to assess the roles of the extracellular secreted proteins in allowing the bacteria to escape from the ETs.

In peas, corn, and cotton, extracellular DNA with histone is a component of the extracellular matrix secreted from the root cap. This structure was found to function like animal NETs to allow root border cells to capture pathogenic bacteria and fungi in the soil and immobilize them (46). Plant root border cells release DNA-containing ETs in response to the high-impact pathogenic plant bacterium, *Ralstonia solanacearum*. Two functional extracellular DNases, NucA and NucB, were identified in *R. solanacearum* strain GMI1000. The *nucA/B* deletion mutant was immobilized by the DNA of plant border cell traps, while the bacterial trapping was reversed by treatment with recombinant NucA and NucB (46).

FUNGI

Candida spp.

3'-nucleotidase/nuclease (3′-NT/NU, EC 3.1.3.6) is a bifunctional enzyme capable of hydrolyzing 3′-monophosphorylated nucleotides and nucleic acids to generate nucleosides and inorganic phosphate. 3′-NT/NU is about 40 kDa and has five highly conserved regions. The activity of 3′-NT/NU was found in a wide variety of species, including fungi, protozoan, plants, and bacteria (87). The nuclease exhibits diverse functions in different species; however, the process of sulfate assimilation is a remarkably conserved property of the core machinery (88). The yeast nucleotide phosphatase, MET22, is closely associated with the incorporation of inorganic sulfates into amino acids, and also plays an important role in cell growth under high concentrations of Na^{+} and Li^{+}. Numerous studies have reported that ETs were induced by yeast and hyphal forms of *Candida* spp (89). We have previously shown that METs induced by *C. albicans* showed the ability to trap the microbes, but with limited microbicidal activity (90). It was reported that 20% of *Candida* spp. showed *in vitro* DNase activity (91). *C. albicans* escape NETs through extracellular secretion of DNases that degrade the DNA backbone (92). Over recent years, several extracellular nucleotidases from fungi have

been identified (93). 3′NT and 5′NT activities were determined in *C. albicans* and *C. glabrata*, and there was higher 3′NT activity at pH 4 (94). The activity was inhibited by ammonium tetrathiomolybdate (TTM), a 3′NT/NU inhibitor. NET formation and release were prevented through the 3′NT/NU activity of *C. albicans* and *C. glabrata*, and a more pronounced phagocytosis by neutrophils was observed. This feature was restored in the presence of TTM and resulted in better control and elimination of *C. albicans* (94).

Paracoccidioides spp.

Paracoccidioidomycosis is a fungal disease with systemic, progressive, chronic, and endemic infection. The members of *Paracoccidioides* spp. are the etiological agents of mycosis. *P. brasiliensis* induced NET formation by human PMNs *in vitro*, which was involved in extracellular fungicidal action (95). Recently, it was demonstrated that *P. brasiliensis* Pb265 and Pb18 were able to induce different patterns of NET formation (96). Pb265 is a harmless strain while Pb18 is virulent. The Pb18 strain had the ability to produce and release extracellular DNase, which degraded the DNA of NETs induced by the Pb18 strain causing them to be looser and more dispersed. Interestingly, the Pb265 strain did not consistently show DNase activity compared to the virulent strain, and its ability to induce neutrophils to form NETs was greater than that of the Pb18 strain (97).

Cochliobolus heterostrophus

The ET mechanism against fungal infections is also present in plants. This defensive function was abolished by the addition of DNase I, resulting in 100% incidence of root rot. The maize pathogen, *C. heterostrophus*, has many DNase-encoding genes and DNase activity was found in fungal culture filtrates. The deletion of the gene for secreted DNase, *nuc1*, significantly reduced fungal infection of leaves and roots, but virulence was restored by the addition of exogenous DNase I (98). The DNase activity of recombinant Nuc1 was dependent on Mg^{2+}. However, the study did not directly demonstrate that *C. heterostrophus* used extracellular DNases as a counter mechanism against extracellular DNA in ETs from plant cells.

PARASITES

Leishmania spp.

The class I nuclease family has been considered an important factor for several *Leishmania* spp. to inhibit NET-mediated killing through extracellular DNA hydrolysis (99). *Leishmania* spp. have a 3'-NT/NU gene with high homology to the S1 nuclease of *Aspergillus oryzae* and P1 of *Penicillium citrinum*. The 3'-NT/NU belongs to the class I nuclease family (100), and is anchored in the parasite's cell surface membrane (101). Although the C-terminus contains the key site for the membrane anchor domain, it was not necessary for the development of enzymatic activity. The 3'-NT/NU activity did not require N-linked glycosylation, but this modification may be important for proper folding and transport of the protein to the parasite's surface membrane (102). The 3'-NT/NU was highly constitutively expressed and helped *Leishmania* to infect vertebrates during the life cycle (103, 104). The 3'-NT/NU had the ability to produce extracellular adenosine through 3'-AMP hydrolysis, thus contributing to the establishment of *Leishmania* infection (105, 106). Inhibition of 3'-NT/NU by 3'-AMP, 5'-GMP, or the 3'-NT/NU inhibitor, TTM, decreased the survival of promastigotes in neutrophils (47). The exonuclease activity of 3'-NT/NU was directly proportional to the number of parasites, and was more efficient at alkaline pH (48). Both low phosphate (LP) and high phosphate (HP) promastigotes induced the release of NETs from human neutrophils (47), and the NET histones killed *L. infantum*. The *L. infantum* cultured in LP medium possessed higher 3'-NT/NU nuclease activity, and LP parasites showed greater resistance to neutrophil killing. The destruction of NETs can be prevented by TTM. The hydrolysis of extracellular nucleic acids by 3'-NT/NU clearly contributed to the escape and survival of parasites exposed to NETs and promoted the establishment of infection (47, 49).

Nippostrongylus brasiliensis

DNase II belongs to a family of highly homologous DNases that can degrade DNA to produce 3′-phosphorylated and 5′-hydroxyl products. DNase II and homologs were identified in mammals, invertebrates, and non-metazoans (107). DNase II was thought to be involved in the development and homeostasis of nematodes (108). *N. brasiliensis*, a murine hookworm, strongly stimulated neutrophils to release NETs, but the larvae secreted Nb-DNase II which degraded the nucleic acid skeleton of NETs and reduced the neutrophil killing effect. Nb-DNase II was highly expressed at the L3 stage during early infection. The extracellular DNA fibers formed *in vitro* by neutrophils induced by PMA could be hydrolyzed by the recombinant Nb-DNase II, and the degradation of NETs was neutralized by antiserum against rNb-DNase II (50). DNase II activity has also been identified in the excretory/secretory products from helminths. It is noteworthy that in comparison to other nematodes, *Trichinella spiralis* had a more extensive expansion of the DNase II protein family with an estimated 125 genes, and almost half of those were classified as encoding secretory proteins (109). Twenty-seven developmental stage-specific genes putatively encoding DNase II homologs were isolated from a *T. spiralis* cDNA library by immunological screening. In our previous work, we speculated that they may play a role in digestion of host DNA to facilitate tissue migration and escape from host immune responses (110).

Plasmodium spp.

The TatD DNase was identified as one of the multifunctional factors in the development and transmission of malaria parasites. Chang et al. reported that a TatD-like DNase was present in every *Plasmodium* spp. and was highly expressed in the most virulent strains (51). The *PbTatD* deletion mutant of *P. berghei* induced J774A.1 macrophages and mouse neutrophils to generate METs and NETs *in vitro*, respectively; but, less ET network formation was observed in the presence of WT parasites. A recombinant PbTatD was able to restore hydrolysis of the DNA component of METs by a *PbTatD*

deletion mutant. Interestingly, the TatD DNase activity of *P. falciparum* was inhibited by Mg^{2+}, but strongly enhanced in *P. knowlesi* (52).

Trypanosoma spp.

Two TatD-like DNases, TryTatD05 and TryTatD15, were identified in the supernatants of cultures of Africana trypanosome parasites, *T. evansi* and *T. brucei*, but were not released from dead parasites. *T. evansi* and T. *brucei* have been shown to induce NETs in murine neutrophils and to also be captured by NETs. However, NETs could be degraded by recombinant TryTatD05 and TryTatD15, or parasite culture supernatants (53). The degradation of NETs was significantly prevented by treatment with the DNase inhibitor, aurintricarboxylic acid. The 3'-NT/NU is a bifunctional trypanosomal enzyme, which acts as a phosphodiesterase cleaving the bond between the 3'-hydroxy and 5'-phosphoryl groups of adjacent nucleotides, or as a phosphomonoesterase to remove the 3'-terminal phosphate group of 3'-monophosphorylated nucleotides (111, 112).

MYCOPLASMA SPP.

Mycoplasma spp. nucleases have the ability of degradation of nucleotide substrates from host or microbial nucleic acids released in a variety of cellular processes, and several nucleases are regarded as a source of nucleotides for biosynthetic and survival purposes important and a cytotoxic factors contributing to pathogenicity (113). Intracellular, extracellularly secreted, and membrane-associated nuclease activities have been detected in most *Mycoplasma* spp. studied so far, and Ca^{2+}/Mg^{2+} -dependent endonuclease activity has also been found in a comparatively large number of *Mycoplasma* spp (114). Nucleases include MGA_0676 of *M. gallisepticum*, MHO_0730 of *M. hominis*, Mhp379 and Mhp597 of *M. hyopneumoniae*, *Mbov_rs02825 and* MnuA of *M. bovis*, Mpn133 and Mpn491 of *M. pneumoniae*.

Mycoplasma hominis

MHO_0730 is a cell-surface lipoprotein localized on the membrane of *M. hominis.* MHO_0730 shares significant homology with the Snase and acts as a Ca^{2+}-dependent, sugar-nonspecific nuclease. A recombinant MHO_0730 expressed in *E. coli* was able to digest different nucleic acid substrates. PMA-stimulated NETs from human neutrophils were disassembled by *M. hominis* (54). MHO_0730 was also a potent inducer of NET formation and release through the action of the *M. hominis* liposoluble fraction and MHO_0730-based synthetic lipopeptides (55).

Mycoplasma hyopneumoniae

Mhp597 is a secreted nuclease of *M. hyopneumoniae*. The recombinant Mhp597 (rMhp597) expressed in *E. coli* exhibited a heat stable Ca^{2+}- or Mg^{2+}-dependent nuclease activity. The recombinant rMhp597 induced apoptosis and caused cytotoxicity in PK15 cells. NETs induced by PMA or *M. hyopneumoniae* were completely destroyed by rMhp597, as well as culture supernatants of *M. hyopneumoniae* (56).

Mycoplasma bovis

MbovNase is localized in the cell membrane and a recombinant MbovNase (rMbovNase) exhibited nuclease activity at 22-65°C in the presence of Ca^{2+} (115). The rMbovNase Δ181-342 without the TNASE 3 domain was deficient in all biological functions. NETs were not detected in bovine neutrophils stimulated by *M. bovis*, and NETs induced by PMA disappeared after the addition of rMbovNase. However, the degradation of NETs and *M. bovis* survival were greatly reduced by the addition of EDTA (57). MnuA was the major membrane nuclease of *M. bovis* PG45, and NET degradation was observed in WT *M. bovis*. The *MnuA* deletion mutant lacked significant nuclease activity but still stimulated bovine neutrophils to release NETs. The generation of ROS in neutrophils was not affected by the presence or absence of mycoplasma nuclease (58).

Mycoplasma pneumoniae

Mpn491 is the main extracellular nuclease of *M. pneumoniae* and contains domains responsible for endonuclease, exonuclease, and phosphatase activities. Yamamoto et al. reported that the culture supernatants of *M. pneumoniae* had strong DNase activity and Mpn491 (approx. 55 kDa) was identified by zymographic analysis of the culture supernatant. The ability of the *Mpn491* deletion mutant to degrade NETs from PMNs was markedly abolished (59), demonstrating that Mpn491 was essential for *M. pneumoniae* to evade the NET-mediated killing *in vitro* and *in vivo*.

Mycoplasma spp. have certain defects in their survival process, such as a lack of ability for *de novo* synthesis of nucleotides. *Mycoplasma* spp. secrete nucleases to obtain nucleotides from host genomic DNA to compensate for this defect. MET production induced by PMA could be observed in THP-1 cells, and was degraded by the membrane nucleases from *M. hyopneumoniaea*. MET degradation was inhibited by deficiency in *M. hyopneumoniae* nucleases. The nucleotides from MET degradation can be used for DNA synthesis (116). Therefore, nucleases are widely considered to be essential proteins for *Mycoplasma*, and also have been proven to be important virulence factors during infection.

LEPTOSPIRA SPP.

It has been shown that pathogenicity and viability of *Leptospira* spp. were relevant factors for induction of NETs, but not for motility. A pathogenic *Leptospira*, *L. interrogans* serovar Copenhageni strain Fiocruz L1-130, induced human neutrophils to release NETs, which were capable of killing *L. interrogans* (60). The pathogenic *Leptospira* showed DNA degradation activity, but not the saprophytic *Leptospira*. *Leptospira* immunoglobulin-like proteins (Lig) are surface proteins expressed in pathogenic strains of *Leptospira*, including LigA, LigB, and LigC. The Lig proteins were involved in leptospiral adhesion, complement resistance, and modulation of hemostasis and play a vital role in invasion and immune evasion (117).The recombinant variable region of LigA was able to degrade DNA with both endonuclease and exonuclease activities, and could degrade PMA-induced NETs (118).

CONCLUSIONS AND PERSPECTIVES

Since their discovery in 2004, ETs have been described from a wide variety of innate immune cells and are now widely regarded as an ancient and evolutionarily conserved host defense mechanism in the plant and animal kingdoms (119, 120). Several pathogens can produce one or more nucleases to directly act on the DNA skeleton of ETs (6). In this review, we summarized the current study results on nucleases expressed by pathogens to evade the ETs produced by the host immune system. The main concerns are 1) only certain pathogen-derived nucleases degrade ETs. Pathogens included *V. cholerae*, *Streptococcus* spp., *S. aureus*, *M. tuberculosis*, *P. aeruginosa*, *N. gonorrhoeae*, *P. intermedius*, *R. solanacearum*, *Leishmania* spp., *N. brasiliensis*, *Plasmodium* spp., *Trypanosoma* spp., *Mycoplasma* spp., and *Leptospira* spp. 2) types of nucleases. Thirty-four nucleases have been reported to be associated with ET degradation, and among them, eleven were exonuclease/endonuclease and twenty-three were categorized as DNase, sugar nonspecific nuclease, or nucleotidase. 3) with regard to the cellular localization of nucleases in pathogens. The formation of ETs occurs in the extracellular space of immune cells, and secreted extracellular nucleases from pathogens are the most direct way of degradating the extracellular networks. The nucleases may be anchored on the cell wall, the cell-wall surface, the membrane, or the cell-surface membrane; and parasitophorous vacuole membranes and surface proteins also have the ability to degrade ETs. 4) only ETs from certain species and cell types were used to investigate to the degradation of ETs by pathogen-derived nucleases. Neutrophils were initially used as the cells for producing and studying ETs, and considering the similar network structures of NETs and ETs from other immune cells, current research has mostly focused on the nucleases that hydrolyze the DNA of NETs. Therefore, for a number of other ETs, the role of nucleases still needs to be evaluated.

Future research will most likely focus on designing drugs to neutralize the nuclease activity of pathogens to preserve the integrity of host NETs and combat invading organisms. The protein synthesis inhibitor clindamycin and the immunoglobulins efficiently inhibited the nuclease activity of *S. aureus* by reducing the transcription of *nuc1*, resulting in enhanced NET-mediated extracellular clearance in human blood-derived neutrophils (121). The antimicrobial peptide (AMP), LL-37, a member of the cathelicidin family, facilitated the formation of NETs by human blood-derived neutrophils (122). Interestingly, LL-37 effectively prevented the nucleases of *S. aureus*, *S. pneumoniae* and GAS from degrading NETs (123), as well as the cationic AMPs, human β-defensin-3 and human neutrophil peptide-1.

ETs are thought to be dismantled by the secreted nucleases, DNase I and DNase1-like three protein (DNase1L3, also known as DNase γ) in host (124). The fragments or remnants are removed by macrophages and dendritic cells, and the process was dependent on the cytosolic exonuclease TREX1 (also known as DNaseIII) and extracellular DNase1L3, respectively (125). It is worth noting that uncontrolled NET formation or insufficient NET removal can cause highly detrimental effects to host cells *in vivo* such as cell damage, delay in tissue repair, inflammation, vaso-occlusion, autoantibody production, tumor capture, tumor growth, cytokine, and chemokine degradation (126). The crucial role of NETs in the pathogenesis of metabolic diseases, sepsis, thrombosis, autoimmune and autoinflammatory diseases, cancer, and other human diseases has been extensively studied and reviewed (127). The administration of DNase to dismantle ET structures can ameliorate disease progression in mouse models of breast cancer, lung injury, and systemic lupus erythematosus (128–130). Dornase alfa (Pulmozyme®, recombinant human DNase) is currently used in the clinic to treat pulmonary disease in CF (131). Dornase alfa treatment reduced the amount of NETs in the respiratory tract, leading to less airway obstruction in severe bovine RSV infection (132). Therefore, pathogen-derived nucleases should be considered as the treatment of choice for ET-mediated diseases in the future.

On the one hand, the massive amounts of ETs degraded by nucleases *in vivo* are helpful for preventing the occurrence of cardiovascular, immunological, and metabolic diseases, and cancer (133). On the other hand, some pathogens such as *V. cholerae*, *S. aureus*, *P. intermedia*,and *Actinobacillus pleuropneumoniae* (*A. pp*) may benefit from circulating cell-free DNA, adenosine, and NAD from degraded NETs as a source of nutrients. For example, *A. pp* did not produce extracellular DNases, whereas porcine NETs were efficiently degraded by nucleases from *S. suis* and the products could be used as an external NAD source for *A. pp* growth when co-infecting *S. suis* (134). Therefore, more studies are needed in the future to unambiguously determine the relationship between ET formation and degradation by pathogen nucleases or host DNases (135, 136).

AUTHOR CONTRIBUTIONS

CL conceived the idea and guided the whole work, and wrote the draft. FM and MQ searched the literature and wrote the draft. MQ and XW revised the manuscript. All authors read and approved the final manuscript.

FUNDING

The review was supported by the National Natural Science Foundation of China (32102705 and 31802159) and the youth backbone teachers training program of Henan University of Science and Technology (13450009).

ACKNOWLEDGMENTS

We thank Pivot Sciedit for editing the manuscript. Special thanks to Figdraw (www.figdraw.com) for providing the resources and platform to draw the figure.

REFERENCES

1. Tam K, Torres VJ. Staphylococcus Aureus Secreted Toxins and Extracellular Enzymes. *Microbiol Spectr* (2019) 7(2):10.1128/microbiolspec.GPP3-0039-2018. doi: 10.1128/microbiolspec.GPP3-0039-2018.
2. Yang W. Nucleases: Diversity of Structure, Function and Mechanism. *Q Rev Biophys* (2011) 44(1):1–93. doi: 10.1017/S0033583510000181
3. Joshi AP, Deshmukh SS. Streptomyces Nucleases. *Crit Rev Microbiol* (2011) 37(3):227–36. doi: 10.3109/1040841X.2011.562173
4. Lauková L, Konečná B, Janovičová Ľ, Vlková B, Celec P. Deoxyribonucleases and Their Applications in Biomedicine. *Biomolecules* (2020) 10(7):1036. doi: 10.3390/biom10071036
5. Sharma P, Garg N, Sharma A, Capalash N, Singh R. Nucleases of Bacterial Pathogens as Virulence Factors, Therapeutic Targets and Diagnostic Markers. *Int J Med Microbiol* (2019) 309(8):151354. doi: 10.1016/j.ijmm.2019.151354
6. Garcia Gonzalez J, Hernandez FJ. Nuclease Activity: An Exploitable Biomarker in Bacterial Infections. *Expert Rev Mol Diagn* (2022) 22 (3):265–94. doi: 10.1080/14737159.2022.2049249
7. Fine N, Tasevski N, McCulloch CA, Tenenbaum HC, Glogauer M. The Neutrophil: Constant Defender and First Responder. *Front Immunol* (2020) 11:571085. doi: 10.3389/fimmu.2020.571085
8. Brinkmann V, Reichard U, Goosmann C, Fauler B, Uhlemann Y, Weiss DS, et al. Neutrophil Extracellular Traps Kill Bacteria. *Science* (2004) 303 (5663):1532–5. doi: 10.1126/science.1092385
9. Cubillo-Martínez AA, Pereyra MA, Garfias Y, Guluarte C, Zenteno E, Sánchez-Salgado JL. Extracellular Traps Involved in Invertebrate Immune Mechanisms. *Fish Shellfish Immunol* (2022) 121:380–6. doi: 10.1016/j.fsi.2022.01.024
10. Ríos-López AL, González GM, Hernández-Bello R, Sánchez-González A. Avoiding the Trap: Mechanisms Developed by Pathogens to Escape Neutrophil Extracellular Traps. *Microbiol Res* (2021) 243:126644. doi: 10.1016/j.micres.2020.126644
11. Seper A, Fengler VH, Roier S, Wolinski H, Kohlwein SD, Bishop AL, et al. Extracellular Nucleases and Extracellular DNA Play Important Roles in Vibrio Cholerae Biofilm Formation. *Mol Microbiol* (2011) 82(4):1015–37. doi: 10.1111/j.1365-2958.2011.07867.x
12. Seper A, Hosseinzadeh A, Gorkiewicz G, Lichtenegger S, Roier S, Leitner DR, et al. Vibrio Cholerae Evades Neutrophil Extracellular Traps by the Activity of Two Extracellular Nucleases. *PLoS Pathog* (2013) 9(9):e1003614. doi: 10.1371/journal.ppat.1003614
13. Pressler K, Mitterer F, Vorkapic D, Reidl J, Oberer M, Schild S. Characterization of Vibrio Cholerae's Extracellular Nuclease Xds. *Front Microbiol* (2019) 10:2057. doi: 10.3389/fmicb.2019.02057
14. Lacks S, Greenberg B, Neuberger M. Role of a Deoxyribonuclease in the Genetic Transformation of Diplococcus Pneumoniae. *Proc Natl Acad Sci USA* (1974) 71(6):2305–9. doi: 10.1073/pnas.71.6.2305
15. Lacks S, Greenberg B, Neuberger M. Identification of a Deoxyribonuclease Implicated in Genetic Transformation of Diplococcus Pneumoniae. *J Bacteriol* (1975) 123(1):222–32. doi: 10.1128/jb.123.1.222-232.1975
16. Puyet A, Greenberg B, Lacks SA. Genetic and Structural Characterization of endA. A Membrane-Bound Nuclease Required for Transformation of Streptococcus Pneumoniae. *J Mol Biol* (1990) 213(4):727–38. doi: 10.1016/S0022-2836(05)80259-1
17. Bergé M, Moscoso M, Prudhomme M, Martin B, Claverys JP. Uptake of Transforming DNA in Gram-Positive Bacteria: A View From Streptococcus PNeumoniae. *Mol Microbiol* (2002) 45(2):411–21. doi: 10.1046/j.1365-2958.2002.03013
18. Zhu L, Kuang Z, Wilson BA, Lau GW. Competence-Independent Activity of Pneumococcal EndA [Corrected] Mediates Degradation of Extracellular Dna and Nets and is Important for Virulence. *PLoS One* (2013) 8(7): e70363. doi: 10.1371/journal.pone.0070363
19. Midon M, Schäfer P, Pingoud A, Ghosh M, Moon AF, Cuneo MJ, et al. Mutational and Biochemical Analysis of the DNA-Entry Nuclease EndA From Streptococcus Pneumoniae. *Nucleic Acids Res* (2011) 39(2):623–34. doi: 10.1093/nar/gkq802
20. Moon AF, Midon M, Meiss G, Pingoud A, London RE, Pedersen LC. Structural Insights Into Catalytic and Substrate Binding Mechanisms of the Strategic EndA Nuclease From Streptococcus Pneumoniae. *Nucleic Acids Res* (2011) 39(7):2943–53. doi: 10.1093/nar/gkq1152
21. Jhelum H, Sori H, Sehgal D. A Novel Extracellular Vesicle-Associated Endodeoxyribonuclease Helps Streptococcus Pneumoniae Evade Neutrophil Extracellular Traps and Is Required for Full Virulence. *Sci Rep* (2018) 8(1):7985. doi: 10.1038/s41598-018-25865-z
22. Bi S, Wang J, Xu M, Li N, Wang B. Immunity to Sda1 Protects Against Infection by Sda1+ and Sda1- Serotypes of Group A Streptococcus. *Vaccines (Basel)* (2022) 10(1):102. doi: 10.3390/vaccines10010102
23. Chalmers C, Khemlani AHJ, Sohn CR, Loh JMS, Tsai CJ, Proft T. Streptococcus Pyogenes Nuclease A (SpnA) Mediated Virulence Does Not Exclusively Depend on Nuclease Activity. *J Microbiol Immunol Infect* (2020) 53(1):42–8. doi: 10.1016/j.jmii.2017.09.006
24. Chang A, Khemlani A, Kang H, Proft T. Functional Analysis of Streptococcus Pyogenes Nuclease A (SpnA), a Novel Group A Streptococcal Virulence Factor. *Mol Microbiol* (2011) 79(6):1629–42. doi: 10.1111/j.1365-2958.2011.07550.x
25. de Buhr N, Neumann A, Jerjomiceva N, von Köckritz-Blickwede M, Baums CG. Streptococcus Suis DNase SsnA Contributes to Degradation of Neutrophil Extracellular Traps (NETs) and Evasion of NET-Mediated Antimicrobial Activity. *Microbiol (Reading)* (2014) 160(Pt 2):385–95. doi: 10.1099/mic.0.072199-0
26. de Buhr N, Stehr M, Neumann A, Naim HY, Valentin-Weigand P, von Köckritz-Blickwede M, et al. Identification of a Novel DNase of Streptococcus Suis (EndAsuis) Important for Neutrophil Extracellular Trap Degradation During Exponential Growth. *Microbiol (Reading)* (2015) 161(Pt 4):838–50. doi: 10.1099/mic.0.000040
27. Ma F, Guo X, Fan H. Extracellular Nucleases of Streptococcus Equi Subsp. Zooepidemicus Degrade Neutrophil Extracellular Traps and Impair Macrophage Activity of the Host. *Appl Environ Microbiol* (2016) 83(2): e02468–16. doi: 10.1128/AEM.02468-16
28. Moon AF, Gaudu P, Pedersen LC. Structural Characterization of the Virulence Factor Nuclease A From Streptococcus Agalactiae. *Acta Crystallogr D Biol Crystallogr* (2014) 70(Pt 11):2937–49. doi: 10.1107/S1399004714019725
29. Derré-Bobillot A, Cortes-Perez NG, Yamamoto Y, Kharrat P, Couvé E, Da Cunha V, et al. (Gbs0661), an Extracellular Nuclease of Streptococcus Agalactiae, Attacks the Neutrophil Extracellular Traps and Is Needed for Full Virulence. *Mol Microbiol* (2013) 89(3):518–31. doi: 10.1111/mmi.12295
30. Liu J, Sun L, Liu W, Guo L, Liu Z, Wei X, et al. A Nuclease From Streptococcus Mutans Facilitates Biofilm Dispersal and Escape From Killing by Neutrophil Extracellular Traps. *Front Cell Infect Microbiol* (2017) 7:97. doi: 10.3389/fcimb.2017.00097
31. Morita C, Sumioka R, Nakata M, Okahashi N, Wada S, Yamashiro T, et al. Cell Wall-Anchored Nuclease of Streptococcus Sanguinis Contributes to Escape From Neutrophil Extracellular Trap-Mediated Bacteriocidal Activity. *PLoS One* (2014) 9(8):e103125. doi: 10.1371/journal.pone.0103125
32. Soh KY, Loh JMS, Hall C, Proft T. Functional Analysis of Two Novel Streptococcus INIAE Virulence Factors Using a Zebrafish Infection Model. *Microorganisms* (2020) 8(9):1361. doi: 10.3390/microorganisms8091361
33. Herzog S, Dach F, de Buhr N, Niemann S, Schlagowski J, Chaves-Moreno D, et al. High Nuclease Activity of Long Persisting Staphylococcus Aureus Isolates Within the Airways of Cystic Fibrosis Patients Protects Against NET-Mediated Killing. *Front Immunol* (2019) 10:2552. doi: 10.3389/fimmu.2019.02552
34. Sultan AR, Hoppenbrouwers T, Lemmens-den Toom NA, Snijders SV, van Neck JW, Verbon A, et al. During the Early Stages of Staphylococcus Aureus Biofilm Formation, Induced Neutrophil Extracellular Traps Are Degraded by Autologous Thermonuclease. *Infect Immun* (2019) 87(12):e00605–19. doi: 10.1128/IAI.00605-19
35. Bhattacharya M, Berends ETM, Zheng X, Hill PJ, Chan R, Torres VJ, et al. Leukocidins and the Nuclease Nuc Prevent Neutrophil-Mediated Killing of Staphylococcus Aureus Biofilms. *Infect Immun* (2020) 88(10):e00372–20. doi: 10.1128/IAI.00372-20
36. Berends ET, Horswill AR, Haste NM, Monestier M, Nizet V, von Köckritz-Blickwede M. Nuclease Expression by Staphylococcus Aureus Facilitates Escape From Neutrophil Extracellular Traps. *J Innate Immun* (2010) 2 (6):576–86. doi: 10.1159/000319909

37. Yu J, Jiang F, Zhang F, Hamushan M, Du J, Mao Y, et al. Thermonucleases Contribute to Staphylococcus Aureus Biofilm Formation in Implant-Associated Infections- A Redundant and Complementary Story. *Front Microbiol* (2021) 12:687888. doi: 10.3389/fmicb.2021.687888
38. Thammavongsa V, Missiakas DM, Schneewind O. Staphylococcus Aureus Degrades Neutrophil Extracellular Traps to Promote Immune Cell Death. *Science* (2013) 342(6160):863–6. doi: 10.1126/science.1242255
39. Lang J, Wang X, Liu K, He D, Niu P, Cao R, et al. Oral Delivery of Staphylococcal Nuclease by Lactococcus Lactis Prevents Type 1 Diabetes Mellitus in NOD Mice. *Appl Microbiol Biotechnol* (2017) 101(20):7653–62. doi: 10.1007/s00253-017-8480-5
40. Speer A, Sun J, Danilchanka O, Meikle V, Rowland JL, Walter K, et al. Surface Hydrolysis of Sphingomyelin by the Outer Membrane Protein Rv0888 Supports Replication of Mycobacterium Tuberculosis in Macrophages. *Mol Microbiol* (2015) 97(5):881–97. doi: 10.1111/mmi.13073
41. Dang G, Cao J, Cui Y, Song N, Chen L, Pang H, et al. Characterization of Rv0888, a Novel Extracellular Nuclease From Mycobacterium Tuberculosis. *Sci Rep* (2016) 6:19033. doi: 10.1038/srep19033
42. Ramos-Kichik V, Mondragón-Flores R, Mondragón-Castelán M, Gonzalez-Pozos S, Muñiz-Hernandez S, Rojas-Espinosa O, et al. Neutrophil Extracellular Traps Are Induced by Mycobacterium Tuberculosis. *Tuberculosis (Edinb)* (2009) 89(1):29–37. doi: 10.1016/j.tube.2008.09.009
43. Wilton M, Halverson TWR, Charron-Mazenod L, Parkins MD, Lewenza S. Secreted Phosphatase and Deoxyribonuclease Are Required by Pseudomonas Aeruginosa to Defend Against Neutrophil Extracellular Traps. *Infect Immun* (2018) 86(9):e00403–18. doi: 10.1128/IAI.00403-18
44. Juneau RA, Stevens JS, Apicella MA, Criss AK. A Thermonuclease of Neisseria Gonorrhoeae Enhances Bacterial Escape From Killing by Neutrophil Extracellular Traps. *J Infect Dis* (2015) 212(2):316–24. doi: 10.1093/infdis/jiv031
45. Doke M, Fukamachi H, Morisaki H, Arimoto T, Kataoka H, Kuwata H. Nucleases From Prevotella Intermedia can Degrade Neutrophil Extracellular Traps. *Mol Oral Microbiol* (2017) 32(4):288–300. doi: 10.1111/omi.12171
46. Tran TM, MacIntyre A, Hawes M, Allen C. Escaping Underground Nets: Extracellular DNases Degrade Plant Extracellular Traps and Contribute to Virulence of the Plant Pathogenic Bacterium Ralstonia Solanacearum. *PLoS Pathog* (2016) 12(6):e1005686. doi: 10.1371/journal.ppat.1005686
47. Guimarães-Costa AB, DeSouza-Vieira TS, Paletta-Silva R, Freitas-Mesquita AL, Meyer-Fernandes JR, Saraiva EM. 3'-Nucleotidase/Nuclease Activity Allows Leishmania Parasites to Escape Killing by Neutrophil Extracellular Traps. *Infect Immun* (2014) 82(4):1732–40. doi: 10.1128/IAI.01232-13
48. Freitas-Mesquita AL, Dick CF, Dos-Santos ALA, Nascimento MTC, Rochael NC, Saraiva EM, et al. Cloning, Expression and Purification of 3'-Nucleotidase/Nuclease, an Enzyme Responsible for the Leishmania Escape From Neutrophil Extracellular Traps. *Mol Biochem Parasitol* (2019) 229:6–14. doi: 10.1016/j.molbiopara.2019.02.004
49. Freitas-Mesquita AL, Meyer-Fernandes JR. 3'Nucleotidase/Nuclease in Protozoan Parasites: Molecular and Biochemical Properties and Physiological Roles. *Exp Parasitol* (2017) 179:1–6. doi: 10.1016/j.exppara.2017.06.001
50. Bouchery T, Moyat M, Sotillo J, Silverstein S, Volpe B, Coakley G, et al. Hookworms Evade Host Immunity by Secreting a Deoxyribonuclease to Degrade Neutrophil Extracellular Traps. *Cell Host Microbe* (2020) 27 (2):277–89.e6. doi: 10.1016/j.chom.2020.01.011
51. Chang Z, Jiang N, Zhang Y, Lu H, Yin J, Wahlgren M, et al. The TatD-Like DNase of Plasmodium Is a Virulence Factor and a Potential Malaria Vaccine Candidate. *Nat Commun* (2016) 7:11537. doi: 10.1038/ncomms11537
52. Zhou Y, Xiao B, Jiang N, Sang X, Yang N, Feng Y, et al. Expression and Functional Analysis of the TatD-Like DNase of Plasmodium Knowlesi. *Parasit Vectors* (2018) 11(1):629. doi: 10.1186/s13071-018-3251-4
53. Zhang K, Jiang N, Chen H, Zhang N, Sang X, Feng Y, et al. TatD DNases of African Trypanosomes Confer Resistance to Host Neutrophil Extracellular Traps. *Sci China Life Sci* (2021) 64(4):621–32. doi: 10.1007/s11427-020-1854-2
54. Cacciotto C, Dessì D, Cubeddu T, Cocco AR, Pisano A, Tore G, et al. MHO_0730 as a Surface-Exposed Calcium-Dependent Nuclease of Mycoplasma Hominis Promoting Neutrophil Extracellular Trap Formation and Escape. *J Infect Dis* (2019) 220(12):1999–2008. doi: 10.1093/infdis/jiz406
55. Cacciotto C, Cubeddu T, Addis MF, Anfossi AG, Tedde V, Tore G, et al. Mycoplasma Lipoproteins Are Major Determinants of Neutrophil Extracellular Trap Formation. *Cell Microbiol* (2016) 18(12):1751–62. doi: 10.1111/cmi.12613
56. Li P, Zhang Y, Li X, Zhou W, Li X, Jiang F, et al. Mycoplasma Hyopneumoniae Mhp597 Is a Cytotoxicity, Inflammation and Immunosuppression Associated Nuclease. *Vet Microbiol* (2019) 235:53–62. doi: 10.1016/j.vetmic.2019.05.011
57. Gondaira S, Higuchi H, Nishi K, Iwano H, Nagahata H. Mycoplasma Bovis Escapes Bovine Neutrophil Extracellular Traps. *Vet Microbiol* (2017) 199:68–73. doi: 10.1016/j.vetmic.2016.12.022
58. Mitiku F, Hartley CA, Sansom FM, Coombe JE, Mansell PD, Beggs DS, et al. The Major Membrane Nuclease MnuA Degrades Neutrophil Extracellular Traps Induced by Mycoplasma Bovis. *Vet Microbiol* (2018) 218:13–9. doi: 10.1016/j.vetmic.2018.03.002
59. Yamamoto T, Kida Y, Sakamoto Y, Kuwano K. Mpn491, a Secreted Nuclease of Mycoplasma Pneumoniae, Plays a Critical Role in Evading Killing by Neutrophil Extracellular Traps. *Cell Microbiol* (2017) 19(3):e12666. doi: 10.1111/cmi.12666
60. Scharrig E, Carestia A, Ferrer MF, Cédola M, Pretre G, Drut R, et al. Neutrophil Extracellular Traps Are Involved in the Innate Immune Response to Infection With Leptospira. *PLoS Negl Trop Dis* (2015) 9(7): e0003927. doi: 10.1371/journal.pntd.0003927
61. McDonough E, Kamp H, Camilli A. Vibrio Cholerae Phosphatases Required for the Utilization of Nucleotides and Extracellular DNA as Phosphate Sources. *Mol Microbiol* (2016) 99(3):453–69. doi: 10.1111/mmi.13128
62. Mao FC, Zhang MK, Liao CS, Jia YY, Wang XL, Yu C, et al. Structural Characterization, Expression Purification and Activity of Recombinant Protein of Listeria Monocytogenes TatD-Like DNase. *Chin Vet Sci* (2020) 50(1):84–92. doi: 10.16656/j.issn.1673-4696.2020.0003
63. Buchanan JT, Simpson AJ, Aziz RK, Liu GY, Kristian SA, Kotb M, et al. DNase Expression Allows the Pathogen Group A Streptococcus to Escape Killing in Neutrophil Extracellular Traps. *Curr Biol* (2006) 16(4):396–400. doi: 10.1016/j.cub.2005.12.039
64. Uchiyama S, Andreoni F, Schuepbach RA, Nizet V, Zinkernagel AS. DNase Sda1 Allows Invasive M1T1 Group A Streptococcus to Prevent TLR9-Dependent Recognition. *PLoS Pathog* (2012) 8(6):e1002736. doi: 10.1371/journal.ppat.1002736
65. Sumby P, Barbian KD, Gardner DJ, Whitney AR, Welty DM, Long RD, et al. Extracellular Deoxyribonuclease Made by Group A Streptococcus Assists Pathogenesis by Enhancing Evasion of the Innate Immune Response. *Proc Natl Acad Sci USA* (2005) 102(5):1679–84. doi: 10.1073/pnas.0406641102
66. Zimmermann H. 5'-Nucleotidase: Molecular Structure and Functional Aspects. *Biochem J* (1992) 285(Pt 2):345–65. doi: 10.1042/bj2850345
67. Zakataeva NP. Microbial 5'-Nucleotidases: Their Characteristics, Roles in Cellular Metabolism, and Possible Practical Applications. *Appl Microbiol Biotechnol* (2021) 105(20):7661–81. doi: 10.1007/s00253-021-11547-w
68. Zheng L, Khemlani A, Lorenz N, Loh JM, Langley RJ, Proft T. Streptococcal 5'-Nucleotidase A (S5nA), a Novel Streptococcus Pyogenes Virulence Factor That Facilitates Immune Evasion. *J Biol Chem* (2015) 290(52):31126–37. doi: 10.1074/jbc.M115.677443
69. Korczynska JE, Turkenburg JP, Taylor EJ. The Structural Characterization of a Prophage-Encoded Extracellular DNase From Streptococcus Pyogenes. *Nucleic Acids Res* (2012) 40(2):928–38. doi: 10.1093/nar/gkr789
70. Li M, Cai RJ, Li CL, Song S, Li Y, Jiang ZY, et al. Deletion of ssnA Attenuates the Pathogenicity of Streptococcus Suis and Confers Protection Against Serovar 2 Strain Challenge. *PLoS One* (2017) 12(1):e0169791. doi: 10.1371/journal.pone.0169791
71. de Buhr N, Reuner F, Neumann A, Stump-Guthier C, Tenenbaum T, Schroten H, et al. Neutrophil Extracellular Trap Formation in the Streptococcus Suis-Infected Cerebrospinal Fluid Compartment. *Cell Microbiol* (2017) 19(2):e12649. doi: 10.1111/cmi.12649
72. Meurer M, Öhlmann S, Bonilla MC, Valentin-Weigand P, Beineke A, Hennig-Pauka I, et al. Role of Bacterial and Host DNases on Host-Pathogen Interaction During Streptococcus Suis Meningitis. *Int J Mol Sci* (2020) 21(15):5289. doi: 10.3390/ijms21155289

73. Han TK, Zhu Z, Dao ML. Identification, Molecular Cloning, and Sequence Analysis of a Deoxyribose Aldolase in Streptococcus Mutans GS-5. *Curr Microbiol* (2004) 48(3):230–6. doi: 10.1007/s00284-003-4159-5
74. Soh KY, Loh JMS, Proft T. Orthologues of Streptococcus Pyogenes Nuclease A (SpnA) and Streptococcal 5'-Nucleotidase A (S5nA) Found in Streptococcus Iniae. *J Biochem* (2018) 164(2):165–71. doi: 10.1093/jb/mvy039
75. Li Q, Liao CS, Mao FC, Wang XL, Zhang MK, Zhang XJ, et al. Characterization of the Nuclease Activity of Extracellular Proteins From Staphylococcus Aureus. *Chin J Prev Vet Med* (2020) 42(2):175–81. doi: 10.3969/j.issn.1008-0589.201905030
76. Forson AM, Rosman CWK, van Kooten TG, van der Mei HC, Sjollema J. Micrococcal Nuclease Stimulates Staphylococcus Aureus Biofilm Formation in a Murine Implant Infection Model. *Front Cell Infect Microbiol* (2022) 11:799845. doi: 10.3389/fcimb.2021.799845
77. Liang Y, Wang X, He D, You Q, Zhang T, Dong W, et al. Ameliorating Gut Microenvironment Through Staphylococcal Nuclease-Mediated Intestinal NETs Degradation for Prevention of Type 1 Diabetes in NOD Mice. *Life Sci* (2019) 221:301–10. doi: 10.1016/j.lfs.2019.02.034
78. Möllerherm H, Neumann A, Schilcher K, Blodkamp S, Zeitouni NE, Dersch P, et al. Yersinia Enterocolitica-Mediated Degradation of Neutrophil Extracellular Traps (NETs). *FEMS Microbiol Lett* (2015) 362(23):fnv192. doi: 10.1093/femsle/fnv192
79. Binnenkade L, Kreienbaum M, Thormann KM. Characterization of ExeM, an Extracellular Nuclease of Shewanella Oneidensis MR-1. *Front Microbiol* (2018) 9:1761. doi: 10.3389/fmicb.2018.01761
80. Goñi FM, Alonso A. Sphingomyelinases: Enzymology and Membrane Activity. *FEBS Lett* (2002) 531(1):38–46. doi: 10.1016/s0014-5793(02)03482-8
81. Flores-Díaz M, Monturiol-Gross L, Naylor C, Alape-Girón A, Flieger A. Bacterial Sphingomyelinases and Phospholipases as Virulence Factors. *Microbiol Mol Biol Rev* (2016) 80(3):597–628. doi: 10.1128/MMBR.00082-15
82. Maurice DH, Ke H, Ahmad F, Wang Y, Chung J, Manganiello VC. Advances in Targeting Cyclic Nucleotide Phosphodiesterases. *Nat Rev Drug Discov* (2014) 13(4):290–314. doi: 10.1038/nrd4228
83. Martínez-Méndez R, Camacho-Hernández DA, Sulvarán-Guel E, Zamorano-Sánchez D. A Trigger Phosphodiesterase Modulates the Global C-Di-GMP Pool, Motility, and Biofilm Formation in Vibrio Parahaemolyticus. *J Bacteriol* (2021) 203(13):e0004621. doi: 10.1128/JB.00046-21
84. Palmer LJ, Chapple IL, Wright HJ, Roberts A, Cooper PR. Extracellular Deoxyribonuclease Production by Periodontal Bacteria. *J Periodontal Res* (2012) 47(4):439–45. doi: 10.1111/j.1600-0765.2011.01451.x
85. Liao C, Zhang M, Cheng X, Li Q, Mao F, Wang X, et al. Identification and Characterization of the Nuclease Activity of the Extracellular Proteins From Salmonella Enterica Serovar Typhimurium. *Curr Microbiol* (2020) 77(11):3651–60. doi: 10.1007/s00284-020-02201-1
86. Li Q, Niu JH, Wang XL, Mao J, Quan YY, Liu GK, et al. The Nuclease Activity of Extracellular Products From Salmonella Choleraesuis and Its Effect on the Formation of Macrophages Extracellular Traps. *Acta Veterinaria Zootechnica Sin* (2021) 52(3):733–41. doi: 10.11843/j.issn.0366-6964.2021.03.017
87. Koval T, Dohnálek J. Characteristics and Application of S1-P1 Nucleases in Biotechnology and Medicine. *Biotechnol Adv* (2018) 36(3):603–12. doi: 10.1016/j.biotechadv.2017.12.007
88. Hudson BH, York JD. Roles for Nucleotide Phosphatases in Sulfate Assimilation and Skeletal Disease. *Adv Biol Regul* (2012) 52(1):229–38. doi: 10.1016/j.advenzreg.2011.11.002
89. Urban CF, Nett JE. Neutrophil Extracellular Traps in Fungal Infection. *Semin Cell Dev Biol* (2019) 89:47–57. doi: 10.1016/j.semcdb.2018.03.020
90. Liu P, Wu X, Liao C, Liu X, Du J, Shi H, et al. Escherichia Coli and Candida Albicans Induced Macrophage Extracellular Trap-Like Structures With Limited Microbicidal Activity. *PLoS One* (2014) 9(2):e90042. doi: 10.1371/journal.pone.0090042
91. Riceto ÉB, Menezes Rde P, Penatti MP, Pedroso Rdos S. Enzymatic and Hemolytic Activity in Different Candida Species. *Rev Iberoam Micol* (2015) 32(2):79–82. doi: 10.1016/j.riam.2013.11.003
92. Zhang X, Zhao S, Sun L, Li W, Wei Q, Ashman RB, et al. Different Virulence of Candida Albicans Is Attributed to the Ability of Escape From Neutrophil Extracellular Traps by Secretion of DNase. *Am J Transl Res* (2017) 9(1):50–62.
93. Rodrigues L, Russo-Abrahão T, Cunha RA, Gonçalves T, Meyer-Fernandes JR. Characterization of Extracellular Nucleotide Metabolism in Candida Albicans. *FEMS Microbiol Lett* (2016) 363(1):fnv212. doi: 10.1093/femsle/fnv212
94. Afonso M, Mestre AR, Silva G, Almeida AC, Cunha RA, Meyer-Fernandes JR, et al. Candida Extracellular Nucleotide Metabolism Promotes Neutrophils Extracellular Traps Escape. *Front Cell Infect Microbiol* (2021) 11:678568. doi: 10.3389/fcimb.2021.678568
95. Bachiega TF, Dias-Melicio LA, Fernandes RK, de Almeida Balderramas H, Rodrigues DR, Ximenes VF, et al. Participation of Dectin-1 Receptor on NETs Release Against Paracoccidioides Brasiliensis: Role on Extracellular Killing. *Immunobiology* (2016) 221(2):228–35. doi: 10.1016/j.imbio.2015.09.003
96. Della Coletta AM, Bachiega TF, de Quaglia e Silva JC, Soares ÂM, De Faveri J, Marques SA, et al. Neutrophil Extracellular Traps Identification in Tegumentary Lesions of Patients With Paracoccidioidomycosis and Different Patterns of NETs Generation *In Vitro*. *PLoS Negl Trop Dis* (2015) 9(9):e0004037. doi: 10.1371/journal.pntd.0004037
97. Zonta YR, Dezen ALO, Della Coletta AM, Yu KST, Carvalho L, Dos Santos LA, et al. Paracoccidioides Brasiliensis Releases a DNase-Like Protein That Degrades NETs and Allows for Fungal Escape. *Front Cell Infect Microbiol* (2021) 10:592022. doi: 10.3389/fcimb.2020.592022
98. Park HJ, Wang W, Curlango-Rivera G, Xiong Z, Lin Z, Huskey DA, et al. A DNase From a Fungal Phytopathogen Is a Virulence Factor Likely Deployed as Counter Defense Against Host-Secreted Extracellular DNA. *mBio* (2019) 10(2):e02805–18. doi: 10.1128/mBio.02805-18
99. Freitas-Mesquita AL, Meyer-Fernandes JR. Stage-Specific Class I Nucleases of Leishmania Play Important Roles in Parasite Infection and Survival. *Front Cell Infect Microbiol* (2021) 11:769933. doi: 10.3389/fcimb.2021.769933
100. Debrabant A, Gottlieb M, Dwyer DM. Isolation and Characterization of the Gene Encoding the Surface Membrane 3'-Nucleotidase/Nuclease of Leishmania Donovani. *Mol Biochem Parasitol* (1995) 71(1):51–63. doi: 10.1016/0166-6851(95)00035-y
101. Debrabant A, Ghedin E, Dwyer DM. Dissection of the Functional Domains of the Leishmania Surface Membrane 3'-Nucleotidase/Nuclease, a Unique Member of the Class I Nuclease Family. *J Biol Chem* (2000) 275(21):16366–72. doi: 10.1074/jbc.M908725199
102. Yamage M, Debrabant A, Dwyer DM. Molecular Characterization of a Hyperinducible, Surface Membrane-Anchored, Class I Nuclease of a Trypanosomatid Parasite. *J Biol Chem* (2000) 275(46):36369–79. doi: 10.1074/jbc.M004036200
103. Gottlieb M, Dwyer DM. Evidence for Distinct 5'- and 3'-Nucleotidase Activities in the Surface Membrane Fraction of Leishmania Donovani Promastigotes. *Mol Biochem Parasitol* (1983) 7(4):303–17. doi: 10.1016/0166-6851(83)90013-0
104. Kaye P, Scott P. Leishmaniasis: Complexity at the Host-Pathogen Interface. *Nat Rev Microbiol* (2011) 9(8):604–15. doi: 10.1038/nrmicro2608
105. Paletta-Silva R, Vieira DP, Vieira-Bernardo R, Majerowicz D, Gondim KC, Vannier-Santos MA, et al. Leishmania Amazonensis: Characterization of an Ecto-3'-Nucleotidase Activity and Its Possible Role in Virulence. *Exp Parasitol* (2011) 129(3):277–83. doi: 10.1016/j.exppara.2011.07.014
106. Vieira DP, Paletta-Silva R, Saraiva EM, Lopes AH, Meyer-Fernandes JR. Leishmania Chagasi: An Ecto-3'-Nucleotidase Activity Modulated by Inorganic Phosphate and Its Possible Involvement in Parasite-Macrophage Interaction. *Exp Parasitol* (2011) 127(3):702–7. doi: 10.1016/j.exppara.2010.11.003
107. Evans CJ, Aguilera RJ. DNase II: Genes, Enzymes and Function. *Gene* (2003) 322:1–15. doi: 10.1016/j.gene.2003.08.022
108. Liu MF, Wu XP, Wang XL, Yu YL, Wang WF, Chen QJ, et al. The Functions of Deoxyribonuclease II in Immunity and Development. *DNA Cell Biol* (2008) 27(5):223–8. doi: 10.1089/dna.2007.0691
109. Mitreva M, Jasmer DP, Zarlenga DS, Wang Z, Abubucker S, Martin J, et al. The Draft Genome of the Parasitic Nematode Trichinella Spiralis. *Nat Genet* (2011) 43(3):228–35. doi: 10.1038/ng.769

110. Liao C, Liu M, Bai X, Liu P, Wang X, Li T, et al. Characterisation of a Plancitoxin-1-Like DNase II Gene in Trichinella Spiralis. *PLoS Negl Trop Dis* (2014) 8(8):e3097. doi: 10.1371/journal.pntd.0003097
111. Gottlieb M. The Surface Membrane 3'-Nucleotidase/Nuclease of Trypanosomatid Protozoa. *Parasitol Today* (1989) 5(8):257–60. doi: 10.1016/0169-4758(89)90259-7
112. Volbeda A, Lahm A, Sakiyama F, Suck D. Crystal Structure of Penicillium Citrinum P1 Nuclease at 2.8 A Resolution. *EMBO J* (1991) 10(7):1607–18. doi: 0.1002/j.1460-2075.1991.tb07683.x
113. Bendjennat M, Blanchard A, Loutfi M, Montagnier L, Bahraoui E. Purification and Characterization of Mycoplasma Penetrans Ca^{2+}/Mg^{2+}-Dependent Endonuclease. *J Bacteriol* (1997) 179(7):2210–20. doi: 10.1128/jb.179.7.2210-2220.1997
114. Li L, Krishnan M, Baseman JB, Kannan TR. Molecular Cloning, Expression, and Characterization of a Ca^{2+}-Dependent, Membrane-Associated Nuclease of Mycoplasma Genitalium. *J Bacteriol* (2010) 192(19):4876–84. doi: 10.1128/JB.00401-10
115. Zhang H, Zhao G, Guo Y, Menghwar H, Chen Y, Chen H, et al. Mycoplasma Bovis MBOV_RS02825 Encodes a Secretory Nuclease Associated With Cytotoxicity. *Int J Mol Sci* (2016) 17(5):628. doi: 10.3390/ijms17050628
116. Henthorn CR, Chris Minion F, Sahin O. Utilization of Macrophage Extracellular Trap Nucleotides by Mycoplasma Hyopneumoniae. *Microbiol (Reading)* (2018) 164(11):1394–404. doi: 10.1099/mic.0.000717
117. Haake DA, Matsunaga J. Leptospiral Immunoglobulin-Like Domain Proteins: Roles in Virulence and Immunity. *Front Immunol* (2021) 11:579907. doi: 10.3389/fimmu.2020.579907
118. Kumar A, Varma VP, Sridhar K, Abdullah M, Vyas P, Ashiq Thalappil M, et al. Deciphering the Role of Leptospira Surface Protein LigA in Modulating the Host Innate Immune Response. *Front Immunol* (2021) 12:807775. doi: 10.3389/fimmu.2021.807775
119. Neumann A, Brogden G, von Köckritz-Blickwede M. Extracellular Traps: An Ancient Weapon of Multiple Kingdoms. *Biol (Basel)* (2020) 9(2):34. doi: 10.3390/biology9020034
120. Schultz BM, Acevedo OA, Kalergis AM, Bueno SM. Role of Extracellular Trap Release During Bacterial and Viral Infection. *Front Microbiol* (2022) 13:798853. doi: 10.3389/fmicb.2022.798853
121. Schilcher K, Andreoni F, Uchiyama S, Ogawa T, Schuepbach RA, Zinkernagel AS. Increased Neutrophil Extracellular Trap-Mediated Staphylococcus Aureus Clearance Through Inhibition of Nuclease Activity by Clindamycin and Immunoglobulin. *J Infect Dis* (2014) 210(3):473–82. doi: 10.1093/infdis/jiu091
122. Neumann A, Berends ET, Nerlich A, Molhoek EM, Gallo RL, Meerloo T, et al. The Antimicrobial Peptide LL-37 Facilitates the Formation of Neutrophil Extracellular Traps. *Biochem J* (2014) 464(1):3–11. doi: 10.1042/BJ20140778
123. Neumann A, Völlger L, Berends ET, Molhoek EM, Stapels DA, Midon M, et al. Novel Role of the Antimicrobial Peptide LL-37 in the Protection of Neutrophil Extracellular Traps Against Degradation by Bacterial Nucleases. *J Innate Immun* (2014) 6(6):860–8. doi: 10.1159/000363699
124. Jiménez-Alcázar M, Rangaswamy C, Panda R, Bitterling J, Simsek YJ, Long AT, et al. Host DNases Prevent Vascular Occlusion by Neutrophil Extracellular Traps. *Science* (2017) 358(6367):1202–6. doi: 10.1126/science.aam8897
125. Lazzaretto B, Fadeel B. Intra- and Extracellular Degradation of Neutrophil Extracellular Traps by Macrophages and Dendritic Cells. *J Immunol* (2019) 203(8):2276–90. doi: 10.4049/jimmunol.1800159
126. Papayannopoulos V. Neutrophil Extracellular Traps in Immunity and Disease. *Nat Rev Immunol* (2018) 18(2):134–47. doi: 10.1038/nri.2017.105
127. Daniel C, Leppkes M, Muñoz LE, Schley G, Schett G, Herrmann M. Extracellular DNA Traps in Inflammation, Injury and Healing. *Nat Rev Nephrol* (2019) 15(9):559–75. doi: 10.1038/s41581-019-0163-2
128. Macanovic M, Sinicropi D, Shak S, Baughman S, Thiru S, Lachmann PJ. The Treatment of Systemic Lupus Erythematosus (SLE) in NZB/W F1 Hybrid Mice; Studies With Recombinant Murine DNase and With Dexamethasone. *Clin Exp Immunol* (1996) 106(2):243–52. doi: 10.1046/j.1365-2249.1996.d01-839.x
129. Meng W, Paunel-Görgülü A, Flohé S, Witte I, Schädel-Höpfner M, Windolf J, et al. Deoxyribonuclease is a Potential Counter Regulator of Aberrant Neutrophil Extracellular Traps Formation After Major Trauma. *Mediators Inflammation* (2012) 2012:149560. doi: 10.1155/2012/149560
130. Jorch SK, Kubes P. An Emerging Role for Neutrophil Extracellular Traps in Noninfectious Disease. *Nat Med* (2017) 23(3):279–87. doi: 10.1038/nm.4294
131. Yang C, Montgomery M. Dornase Alfa for Cystic Fibrosis. *Cochrane Database Syst Rev* (2021) 3(3):CD001127. doi: 10.1002/14651858.CD001127.pub5
132. Cortjens B, de Jong R, Bonsing JG, van Woensel JBM, Antonis AFG, Bem RA. Local Dornase Alfa Treatment Reduces NETs-Induced Airway Obstruction During Severe RSV Infection. *Thorax* (2018) 73(6):578–80. doi: 10.1136/thoraxjnl-2017-210289
133. Brinkmann V. Neutrophil Extracellular Traps in the Second Decade. *J Innate Immun* (2018) 10(5-6):414–21. doi: 10.1159/000489829
134. de Buhr N, Bonilla MC, Pfeiffer J, Akhdar S, Schwennen C, Kahl BC, et al. Degraded Neutrophil Extracellular Traps Promote the Growth of Actinobacillus Pleuropneumoniae. *Cell Death Dis* (2019) 10(9):657. doi: 10.1038/s41419-019-1895-4
135. de Buhr N, von Köckritz-Blickwede M. The Balance of Neutrophil Extracellular Trap Formation and Nuclease Degradation: An Unknown Role of Bacterial Coinfections in COVID-19 Patients? *mBio* (2021) 12(1):e03304–20. doi: 10.1128/mBio.03304-20
136. Angeletti A, Volpi S, Bruschi M, Lugani F, Vaglio A, Prunotto M, et al. Neutrophil Extracellular Traps-DNase Balance and Autoimmunity. *Cells* (2021) 10(10):2667. doi: 10.3390/cells10102667

Conflict of Interest: The authors declare that the research was conducted in the absence of any commercial or financial relationships that could be construed as a potential conflict of interest.

Publisher's Note: All claims expressed in this article are solely those of the authors and do not necessarily represent those of their affiliated organizations, or those of the publisher, the editors and the reviewers. Any product that may be evaluated in this article, or claim that may be made by its manufacturer, is not guaranteed or endorsed by the publisher.

frontiers | Frontiers in Immunology

REVIEW
published: 15 July 2022
doi: 10.3389/fimmu.2022.882706

Cross-Activation of Hemichannels/Gap Junctions and Immunoglobulin-Like Domains in Innate–Adaptive Immune Responses

Jiang-Hui Meng[1,2†], *Chang-Xu Chen*[1,2†], *Mohammad R. Ahmadian*[3], *Hong Zan*[4], *Kai-Jun Luo*[1,2*] *and Jean X. Jiang*[5*]

[1] School of Life Sciences, Yunnan University, Kunming, China, [2] Key Laboratory of the University in Yunnan Province for International Cooperation in Intercellular Communications and Regulations, Yunnan University, Kunming, China, [3] Institute of Biochemistry and Molecular Biology II, Medical Faculty and University Hospital Düsseldorf, Heinrich Heine University Düsseldorf, Düsseldorf, Germany, [4] Department of Microbiology, Immunology and Molecular Genetics, University of Texas Health Science Center, San Antonio, TX, United States, [5] Department of Biochemistry and Structural Biology, University of Texas Health Science Center, San Antonio, TX, United States

Hemichannels (HCs)/gap junctions (GJs) and immunoglobulin (Ig)-like domain-containing proteins (IGLDCPs) are involved in the innate–adaptive immune response independently. Despite of available evidence demonstrating the importance of HCs/GJs and IGLDCPs in initiating, implementing, and terminating the entire immune response, our understanding of their mutual interactions in immunological function remains rudimentary. IGLDCPs include immune checkpoint molecules of the immunoglobulin family expressed in T and B lymphocytes, most of which are cluster of differentiation (CD) antigens. They also constitute the principal components of the immunological synapse (IS), which is formed on the cell surface, including the phagocytic synapse, T cell synapse, B cell synapse, and astrocytes–neuronal synapse. During the three stages of the immune response, namely innate immunity, innate–adaptive immunity, and adaptive immunity, HCs/GJs and IGLDCPs are cross-activated during the entire process. The present review summarizes the current understanding of HC-released immune signaling factors that influence IGLDCPs in regulating innate–adaptive immunity. ATP-induced “eat me” signals released by HCs, as well as CD31, CD47, and CD46 “don’t eat me” signaling molecules, trigger initiation of innate immunity, which serves to regulate phagocytosis. Additionally, HC-mediated trogocytosis promotes antigen presentation and amplification. Importantly, HC-mediated $CD4^+$ T lymphocyte activation is critical in the transition of the innate immune response to adaptive immunity. HCs also mediate non-specific transcytosis of

OPEN ACCESS

Edited by:
Hang Hubert Yin,
Tsinghua University, China

Reviewed by:
Carola J. Maturana,
Princeton University, United States
Chenju Yi,
Sun Yat-Sen University, China
Anaclet Ngezahayo,
Leibniz University Hannover, Germany

***Correspondence:**
Kai-Jun Luo
kaijun_luo@ynu.edu.cn
Jean X. Jiang
jiangj@uthscsa.edu

[†]These authors have contributed equally to this work

Specialty section:
This article was submitted to Molecular Innate Immunity, a section of the journal Frontiers in Immunology

Received: *24 February 2022*
Accepted: *23 June 2022*
Published: *15 July 2022*

Citation:
Meng J-H, Chen C-X, Ahmadian MR, Zan H, Luo K-J and Jiang JX (2022) Cross-Activation of Hemichannels/Gap Junctions and Immunoglobulin-Like Domains in Innate–Adaptive Immune Responses. Front. Immunol. 13:882706. doi: 10.3389/fimmu.2022.882706

antibodies produced by mature B lymphocytes, for instance, IgA transcytosis in ovarian cancer cells, which triggers innate immunity. Further understanding of the interplay between HCs/GJs and IGLDCPs would aid in identifying therapeutic targets that regulate the HC–Ig-like domain immune response, thereby providing a viable treatment strategy for immunological diseases. The present review delineates the clinical immunology-related applications of HC–Ig-like domain cross-activation, which would greatly benefit medical professionals and immunological researchers alike. HCs/GJs and IGLDCPs mediate phagocytosis *via* ATP; "eat me and don't eat me" signals trigger innate immunity; HC-mediated trogocytosis promotes antigen presentation and amplification in innate–adaptive immunity; HCs also mediate non-specific transcytosis of antibodies produced by mature B lymphocytes in adaptive immunity.

Keywords: connexin, pannexin, immunological synapse, T and B lymphocytes, cluster of differentiation antigens, phagocytosis, trogocytosis, transcytosis

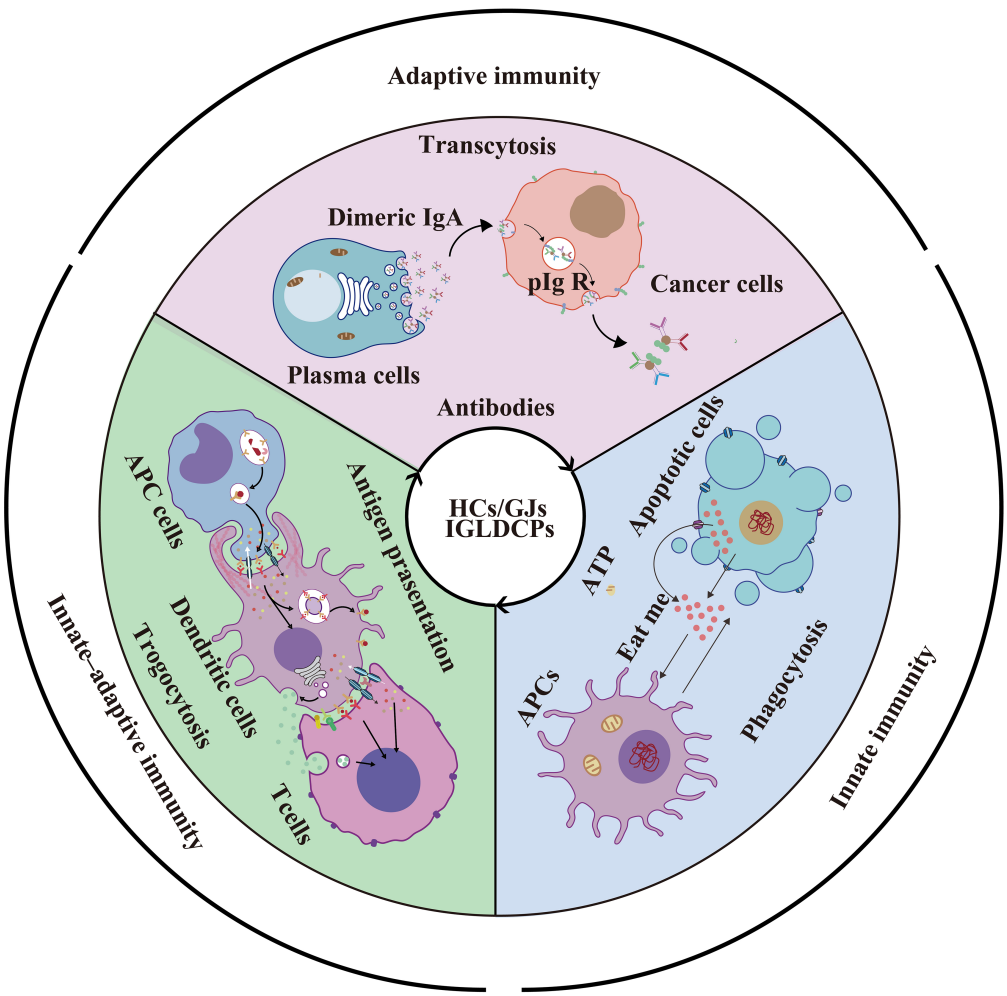

GRAPHICAL ABSTRACT | HCs/GJs and IGLDCPs mediate phagocytosis via ATP; "eat me and don't eat me" signals trigger innate immunity; HC-mediated trogocytosis promotes antigen presentation and amplification in innate–adaptive immunity; HCs also mediate non-specific transcytosis of antibodies produced by mature B lymphocytes in adaptive immunity.

HIGHLIGHTS

- Cx43 directly or indirectly interact with at least 20 IGLDCPs
- HCs/Panx release ATP to regulate APCs for initiating innate immunity
- Cx43-GJs between T cells and B cells activate adaptive immunity
- IgA induces APCs to transit adaptive immunity to innate immunity

INTRODUCTION

Both types of immune responses, namely innate and adaptive, are linked to immune signal transduction. Hemichannel (HC)/gap junction (GJ)-mediated immune signal transduction in cells triggers an immune response. A similar immunological response is triggered by Ig-like domain-containing proteins (IGLDCPs). Both HCs/GJs and IGLDCPs localize on the immune cell surface to manipulate innate and adaptive immune responses. Previous studies have shown that the cross-activation of HCs/GJs and IGLDCPs is essential in mediating phagocyte migration, inflammation, and fever, among other successive stages of the innate immune response (1–6). In particular, in antigen-presenting cells (APCs), as well as T and B lymphocytes, HCs/GJs and IGLDCPs regulate the adaptive immune response (3, 7–11). However, numerous contentious issues persist, highlighting a potentially important goal: to elucidate the link between HCs/GJs and IGLDCPs in innate–adaptive immunity and provide available evidence on this potentially important topic.

Cell–cell communication during the immune responses confirms that HCs/GJs are closely involved in numerous cellular physiological processes. It is likely that antigen presentation, encompassing the T and B lymphocyte responses, involves in the regulation of cell migration and phagocytosis by pannexins (Panx) and GJ proteins, namely, connexins (Cxs) (12). Cxs form HCs on the cell surface; they can form both independent HCs and two HCs from two neighboring cells dock with each other to form intercellular gap junction channel. Conversely, Panxs form a structure, which is a single plasma membrane channel mediating extracellular communication. Cxs and Panxs are topologically similar with four transmembrane domains, two extracellular loops, one intracellular loop, and one N-terminal and one C-terminal. However, their potential interaction with IGLDCPs remains unclear.

The Ig-like domains are among the most widespread domains. Both sequence and structure of these domains can be found in diverse protein families. Proteins containing an Ig-like domain vary in their tissue distribution, amino acid composition, and biological function. IGLDCPs include immune checkpoint molecules of the immunoglobulin family expressed in T and B lymphocytes, most of which are cluster of differentiation (CD) antigens. The function of immune checkpoint modulators is to regulate immunological responses to infectious agents, foreign tissues, and cancerous cells; furthermore, they act to balance the immune response through either enhancement or inhibition (13–16). However, there are relatively few studies on the regulation of HCs/GJs by IGLDCPs

Although there is limited understanding of the interactive mechanisms between HCs/GJs and IGLDCPs, we have attempted to present a rational and balanced evaluation to bridge this gap. In the present review, several important questions have been raised on the seminal findings. HCs/GJs, which mediate intracellular and extracellular communication, are involved in immune response regulation. The following pertinent questions arise. Do HCs/GJs directly interact with IGLDCPs, including immune checkpoint molecules such as CD antigens, to regulate innate–adaptive immunity? Do HCs/GJs regulate IGLDCPs in T and B lymphocytes? Although both HCs/GJs and IGLDCPs regulate phagocytosis, what is the physical and function relationship between them? How do HCs/GJs and IGLDCPs trigger trogocytosis and transcytosis?

MUTUAL CROSS-ACTIVATION OF HCS AND IGLDCPS

Cxs and Panx1 on the Immunological Cell Surface

Cxs are localized on the cell membrane of at least nine subtypes of APCs, namely, monocytes, macrophages, dendritic cells (DCs), including follicular dendritic cells (FDCs), Kupffer cells, B cells, astrocytes, microglia, neutrophils, and natural killer (NK) cells. Panx1 is also found on the eight subtypes of APCs (**Figure 1A**). As shown in **Figure 1A**, Cx43 is expressed in the aforementioned nine APC subtypes. Moreover, Cx37 is expressed on macrophages and neutrophils; Cx45 is present on the surface of DCs and microglial cells; Cx40 on the membrane of B cells and neutrophil cells; and Cx26 on astrocytes. In addition to those listed above, Cx36 and Cx32 are expressed on the microglial cell surface. Seven Cxs, namely, Cx30.3, Cx31.1, Cx32, Cx40, Cx43, Cx45, and Cx46, are present in T cells (4, 17, 18, 27–31). Unexpectedly, 8 of the 21 Cxs in the human gap junction protein family serve as components of synapses or participate in them. There are probably more Cx subtypes that remain to be identified in future research, as most previous studies focused on immune checkpoint molecules without conclusively evaluating Cxs in innate–adaptive immunity. Therefore, elucidating the interaction between HCs and IGLDCPs will offer mechanistic insights into the innate–adaptive immune response. In the following section, we have further detailed the mutual interaction between Cxs and IGLDCPs.

Mutual Interaction of Cxs and IGLDCPs

Cx43 interacts extensively with at least 20 IGLDCPS, either directly or indirectly, namely, CLMP, BCR, HepaCAM, CD4, CD8, CD19, CD25, CD3/CD28, CD31, CD39, CD40, CD46, CD47, CD60, CD69, CD73, CD80, CD86, IgG, and IgA (**Figure 1B**). Cx43 regulates T lymphocytes and DCs *via* IGLDCPs. Cx43/Cx40 maintains lymphocyte homeostasis and

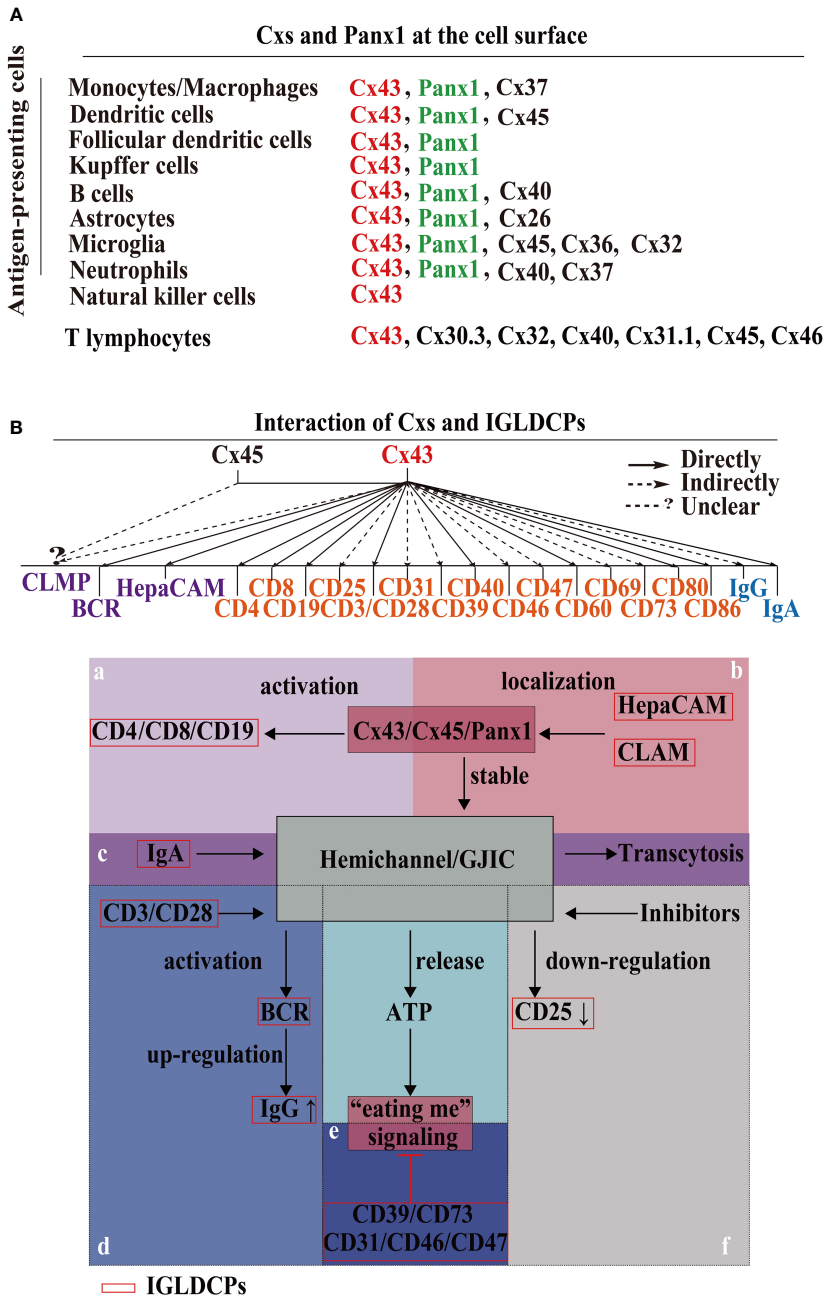

FIGURE 1 | Cxs and Panx1 on the immunological cell surface and their mutual interaction with IGLDCPs. **(A)** Cxs and Panx1 localize at the cell surface. Cxs and Panx1 HCs have been identified in nine types of APCs and T lymphocytes, primarily for the signaling role of HCs with IGLDCPs in the innate–adaptive immune response (17, 18). **(B)** The mutual interaction of HCs and IGLDCPs. Cx43, which interacts with at least 20 IGLDCPs: a The activation of CD4/CD8/CD19 requires Cx43/HC (19–21). b HepaCAM and CLAM facilitates Cx43 membrane localization and GJIC establishment (22–24). c GJIC mediates the transcytosis of IgA in $CD19^+$ B cells (21). d CD3/CD28/CD40 activate BCR signaling and upregulate IgG expression by Cx43/HC opening (25). e The "eating me" signaling pathway is inhibited by CD39/CD73/CD31/CD46/CD47 (14, 26). f CD25/69 are downregulated by the inhibition of Cx43/HC (3). Cxs, connexins; Panx, pannexin; IGLDCP, Ig-like domain-containing protein; HC, hemichannel; APC, antigen-presenting cell.

cytokine production, such as in the case of Cx43 HC inhibition, which suppresses IL-2 and IL-6 mRNA expression (32). Furthermore, the use of mimic peptides as an inhibitor of Cx43 HCs downregulated CD69 and CD25 activation in T cells, and led to IFN-γ by release by DC-stimulated NK cells (3). Similarly, CD3/CD28 induced ATP release by γδT cells, aided by HCs, resulting in cell activation (33, 34). Furthermore, Cx43 HCs in the plasma membrane of $CD4^+$ T lymphocytes

establish gap junction intracellular communication (GJIC) with macrophages to synthesize and secrete Igs and cytokines in immune regulation (19). Similarly, in DC–DC interaction, CD80, CD 86, and MHC class II are expressed (33, 35). Directly, Cx43 activates spleen cells and facilitates IgG production. Targeting *Cx43* is a potential strategy to treat diseases associated with the antibody response (14). Cx43 regulates B lymphocyte activation directly, through BCR signaling, which involves migration and motility (7, 36).

The IGLDCPs regulate Cx43 HCs/GJs. The Ig-like domain in hepatocyte cell adhesion molecule (hepaCAM) stabilizes the Cx43 HCs on the cell surface. The hepaCAM gene was first described in hepatocellular carcinoma and was also discovered in the central nervous system (CNS); it is named GlialCAM, based on the site of its identification (37). HepaCAM is reportedly a member of the immunoglobulin superfamily (IgSF); it consists of an extracellular domain with two Ig loops, a transmembrane region, and a cytoplasmic tail, and functions in conjunction with Cx43 (38). In previous studies in U373 MG glioblastoma cells studies, it was found that hepaCAM expression redistributes Cx43, especially to the site of cell–cell contact, where co-localization of the two molecules is detected (38). Furthermore, altering the Ig-like domain of hepaCAM, especially the first extracellular IGLDCP reduces the co-localization of intercellular Cx43. Cx43 is shuttled back to the cytoplasm from the cell membrane, consequently decreasing its membrane-bound expression. In summary, the presence of IGLDCPs stabilizes Cx43 expression and promotes transport of a protein localized in the cytoplasm to the cell surface (22, 23). Additionally, CAR-like membrane protein (CLMP) regulates Cx43 and Cx45, and the absence of CLMP causes functional obstruction due to a lack of GJIC (24). Cxs and IGLDCPs are co-localized and interact at the immunological synapses (ISs). An increased intracellular Ca^{2+} level, which induces T cell activation and signal amplification, is facilitated by IS Cx43 HCs. Therefore, the formation of ISs is an important function structure, which allows us to understand how HCs/GJs and IGLDCP collaboratively modulate the precise roles in innate–adaptive immune responses.

HCS/GJS AND IGLDCPS INTERACT TO FORM THE SYNAPSE

Importantly, HCs/GJs are complex signaling components of the ISs (39, 40)—phagocytic synapse, T cell synapse, B cell synapse and astrocyte–neuronal synapses. First, HCs are involved in phagocytic synapse formation between APCs and pathogens (41) (**Figure 2A**). Cx HC-linked "pathologic pores" are involved in spreading injury and perpetuating chronic disease. Opening HCs are involved in spinal cord injury progression and the spread of cellular edema. They also control important aspects of the innate–adaptive immune response, particularly under chronic disease conditions, as well as the initiation and perpetuation of the inflammasome pathway in astrocytes (45). It has been reported that Cx43 also regulates FDC development (46), implying Cx43 may form a phagocytic synapse and perform important functions, which warrant further research. Second, the T cell synapse contains GJs. GJIC established by Cx43 is an important functional component of the T cell synapse (41) (**Figure 2B**); it also activates T cells by sustaining the communication between T cells and APCs (11, 19, 47–49). Furthermore, in melanoma cancer cells, Cx43 GJIC plaques localized at the IS are required for augmenting granzyme B activity, to enable cytotoxic T lymphocytes (CTLs) to kill B16F19 melanoma cells (50). It has been reported that Cx43 GJIC between DCs and also activated T cells (51). These findings confirmed that Cx43 plays a vital role in the T cell synapse. Additionally, Cx43-forming HCs/GJs activate the T cell IS (25). Third, the B cell synapse is formed between B cells and APCs (42) (**Figure 2C**). However, compared with phagocytosis and T cell synapses, data on B cell synapse are rather limited. These findings demonstrated that the HCs/GJs are an intrinsic part of the ISs and are essential to mediate IS intracellular communication in regulating the delivery of immune factors.

The astrocyte–neuronal synapse is established between neurons and astrocytes, which release diffusible factors to activate microglia *via* NF-κB signaling (41, 52–54). Astrocytes interact with neuronal synapses to establish astrocyte–neuronal communication (55). Research has shown that astrocyte-derived extracellular vesicles promote synaptic formation through fibrin 2-mediated TGF-β signaling. Consequently, microglia MHC-II protein, CD44, and other molecules recruit T cells for effective antigen delivery (43, 44) (**Figure 2D**). Investigating the interaction between HCs/GJs and IGLDCPs in the astrocyte–neuronal synapse presents a worthwhile research opportunity. Interactions of HCs/GJs and IGLDCPs with IS provide direct evidence suggesting that both may play an important role in immune responses.

CX/PANX AND IGLDCPS DISPLAY DUAL FUNCTIONS IN INNATE IMMUNITY

ATP "Eat Me" Signaling, as Well as CD31, CD46, CD47 "Don't Eat Me" Signal Molecules, Triggers Phagocytosis

Panx1 releases ATP from apoptotic cells to trigger an "eat me" signal (56) (**Figures 3A–C**). Key phagocytic inducers, ATP and UTP, have been confirmed to recruit apoptotic cells *in vitro* and *in vivo*. In contrast, "don't eat-me" signals comprise CD31, CD46, and CD47 expression. These signals on healthy viable cells, which are capable of phosphatidylserine (PtdSer) exposure under physiological conditions, may positively inhibit phagocytic uptake (26). These findings elucidate the mechanism governing HC–IGLDCP interaction in phagocytosis.

In the macrophage cell line J774, Cx43 RNAi showed impaired phagocytosis of the polystyrene-covered beads, and sheep erythrocytes opsonized by IgG (47); in contrast, in sheep erythrocytes with heterozygously or homozygously deleted *Cx43*, no changes were observed in phagocytosis (12, 57). Recently, Dosch *et al.* assessed Cx43 function in phagocytosis using *Cx43* deletion and inhibition. It was determined that the inhibition of autocrine communication of Cx43-dependent ATP in macrophages improved sepsis outcome (33, 48, 49). Therefore,

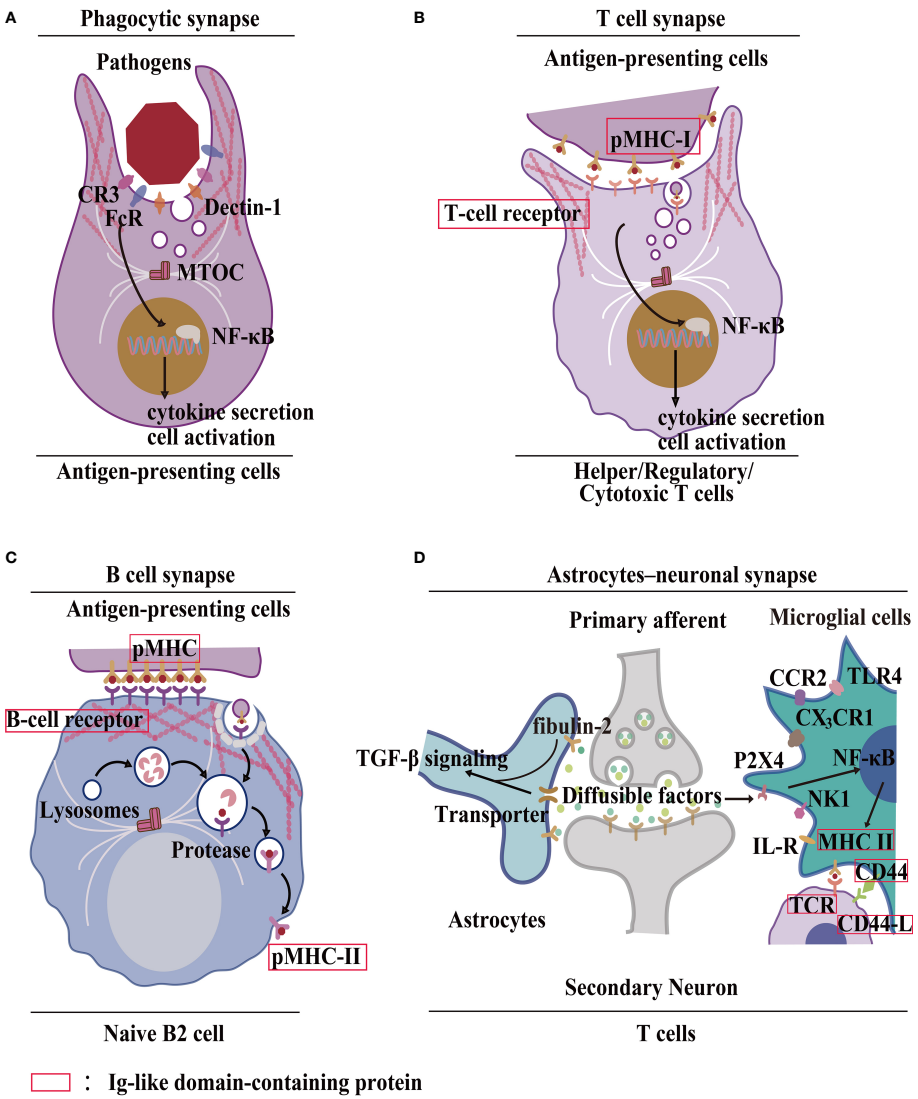

FIGURE 2 | Formation of the IS by HC–IGLDCP interaction. **(A)** A phagocytic synapse formed by APCs. Phagocytes possess specific molecules on the synaptic surface that trigger phagocytosis. For example, recognition of Fcy receptor (FcR) sites, CR3 envelope site, Dectin-1 receptor trigger site (41). MTOC: Center for Microtubule Organization. **(B)** T-cell immunological synapse. A specific cellular contact between T cells and APCs. Major histocompatibility complex (pMHC-I) molecules on the surface of APCs bind to the T-cell receptor (TCR) and deliver the antigen, leading to the polarization of APCs by T cells and the coordinated recombination of various components of T cells, including signaling molecules and adhesion molecules, actin and microtubule cytoskeleton (41). **(C)** B-cell immunological synapse. A specific cellular contact between B cells and APCs. The pMHC-I molecules are phagocytosed in a clathrin-dependent manner. The antigens are transported to lysosomal vesicles for digestion, and the resulting peptides are loaded onto MHC-II molecules and transported back to the cell surface for presentation to T cells (42). **(D)** Neuronal Synapse. It consists of neurons, astrocytes, microglia, and T cells. Astrocyte-derived extracellular vesicles promote synapse formation through fibrin 2-mediated TGF-β signaling. Microglia MHC-II protein, CD40, and other stimulating molecules recruit T cells to deliver antigens. Different receptors bind to different ligands (43, 44). HC, hemichannel; IGLDCP, Ig-like domain-containing protein; Cx, connexin; Panx, pannexin; APC, antigen-presenting cell.

full expression of intact Cx43 is essential in regulating of the immune response through the directionality and rate of DC migration (58). Different cytokines regulate intercellular communication, facilitated by HCs/GJs in APCs, to execute purinergic signaling (3). This presents an interesting research opportunity for further investigation of Cx43-macrophage-phagocytosis. Apoptotic cells attract phagocytes by releasing chemotactic factors known as "find-me" signals (26).

Cx/Panx and IGLDCPs Regulate the Inflammatory Response

Cumulative evidence shows that ATP triggers the inflammatory response. Cx HCs serve as a major pathway for the release of cytoplasmic ATP into the extracellular space. In granulocytes, Cxs enhance the inflammatory responses and promote cellular activation (33) (**Figure 4B**). For example, ATP released by Panx1 promotes the opening of Cx43 HCs (62) and is also involved in the

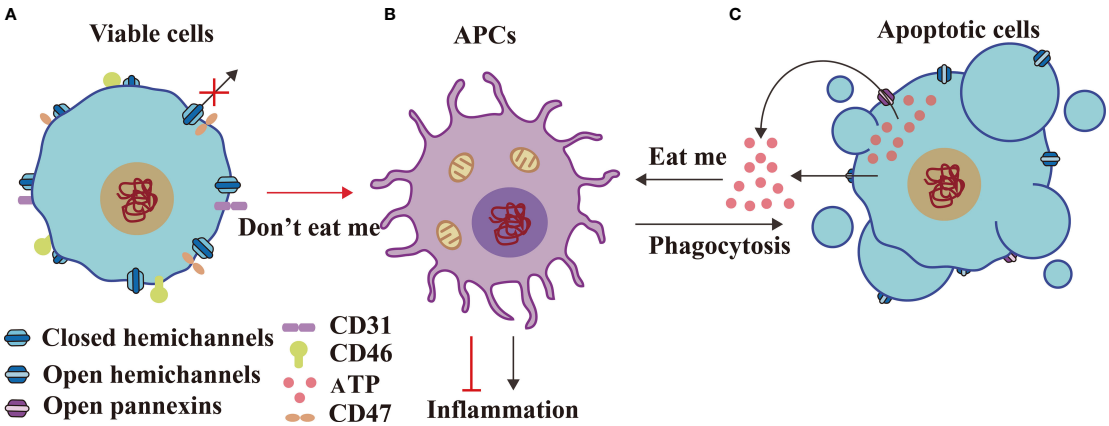

FIGURE 3 | HCs and IGLDCPs display dual functions in innate immunity. Viable cells form closed HCs **(A)** with APCs **(B)** transmitting "don't eat me" signals, including CD31, CD47, and CD46, to suppress inflammation. In contrast, apoptotic cells **(C)** send an "eat me" signal to APCs by opening the HCs and releasing ATP, which engulfs apoptotic cells and causes inflammation (56). HC, hemichannel; IGLDCP, Ig-like domain-containing protein; APC, antigen-presenting cell.

innate immune response and inflammation (26, 63–70). In contrast, the blockage of Cx43 isoform HCs alleviates inflammation and enhances healing (2). In other inflammatory pathologies, Cx43 expression regulates monocyte–endothelial adhesion, with criteria for baseline adhesion set by Cx43-expressing monocytes (71). Similarly, elevated macrophage Cx43 HC activation and *Panx1* expression inhibit pathogenesis (1, 49). Cx43 GJs transfer hypoxia-induced miR-192-5p, allowing cancer cells to acquire immune-resistant phenotypes (25). During inflammation in response to spinal cord injury, a decrease in the expression of Cx43 proteins shortens animal recovery time (33). ATP release has been inhibited using several Cx43 mimic peptides, thereby influencing the inflammatory process (72). Therefore, ATP integrated with the HC function promotes inflammation.

Open Cxs HCs in macrophages facilitate an effective immune response. GJs and HCs help spread toxicity into neighboring areas to augment viral/bacterial replication, and promote the spread of the inflammatory response by infectious agents, such as HIV (33),. Ig-like domains presenting T cell immunoglobulin molecules regulate inflammation and immune responses (16, 73). Single immunoglobulin IL-1R-related molecule (SIGIRR) is a specific inhibitor of IL-1R and toll-like receptor signals (74, 75).

In summary, Cxs HCs and Panx1 release ATP, which serves as an "eat me" signal; conversely, CD31, CD47, and CD46 function as "don't eat-me" signals, which regulate phagocytosis in innate immunity.

CX43 AND IGLDCPS ACTIVATE INNATE–ADAPTIVE IMMUNITY

Cx43-Dependent Trogocytosis of Macrophages and Dendritic Cells in Antigen Presentation

The interaction between innate and adaptive immune response is defined as innate–adaptive immunity, which is important for antigen presentation. Cx43 contributes to trogocytosis (**Figures 4A, B**). The mechanism of innate control of adaptive immune responses involves multiple signaling pathways (16). We focused on how macrophages detect pathogens or injured cells. Trogocytosis is a process whereby lymphocytes extract surface molecules of APCs and express them on their own membranes (59, 60) (**Figure 4B**). However, the role of HCs and IGLDCPs in trogocytosis has not been examined adequately. *Cx43*-deleted macrophages are more proficient in T cell priming, implying an increased accumulation of antigens as these macrophages cannot transfer them to neighboring DCs, resulting in efficient presentation (57, 76–80). These findings delineate a potential mechanism by which HCs and IGLDCPs regulate antigen presentation.

GJs also have a pivotal function in DC activation and the amplification of antigen presentation, such as antigen transport, dendritic activation, and antigen cross-presentation (10, 33, 81–83). GJs-mediated antigen transfer between monocytes and $CD8^+$DCs may serve as a simple and efficacious immunotherapy strategy for cancers, such as in the case of undifferentiated monocytes loaded with tumor antigen (20). Molecules containing Ig-like domains, such as pMHC-I and II, are involved in Cx43-dependent trogocytosis on the surface of acceptor cells (78). This is a valuable research direction to explore the underlying mechanism by which Cxs and IGLDCPs regulate antigen presentation *via* trogocytosis.

Cx43/Panx-Mediated Activation of $CD4^+$ T Lymphocytes

In addition to the roles of Cx43 in regulating macrophages and dendritic cells. HCs also mediate $CD4^+$ T lymphocyte activation is critical in the transition of the innate immune response to adaptive immunity (**Figure 4C**). In a previous study, it was found that Cx43 in the IS delivers microRNAs from hypoxic melanoma cells to CTLs (25). Therefore, Cx43 stimulates T lymphocytes by the delivery of immune factors. Cx43 is involved in the formation

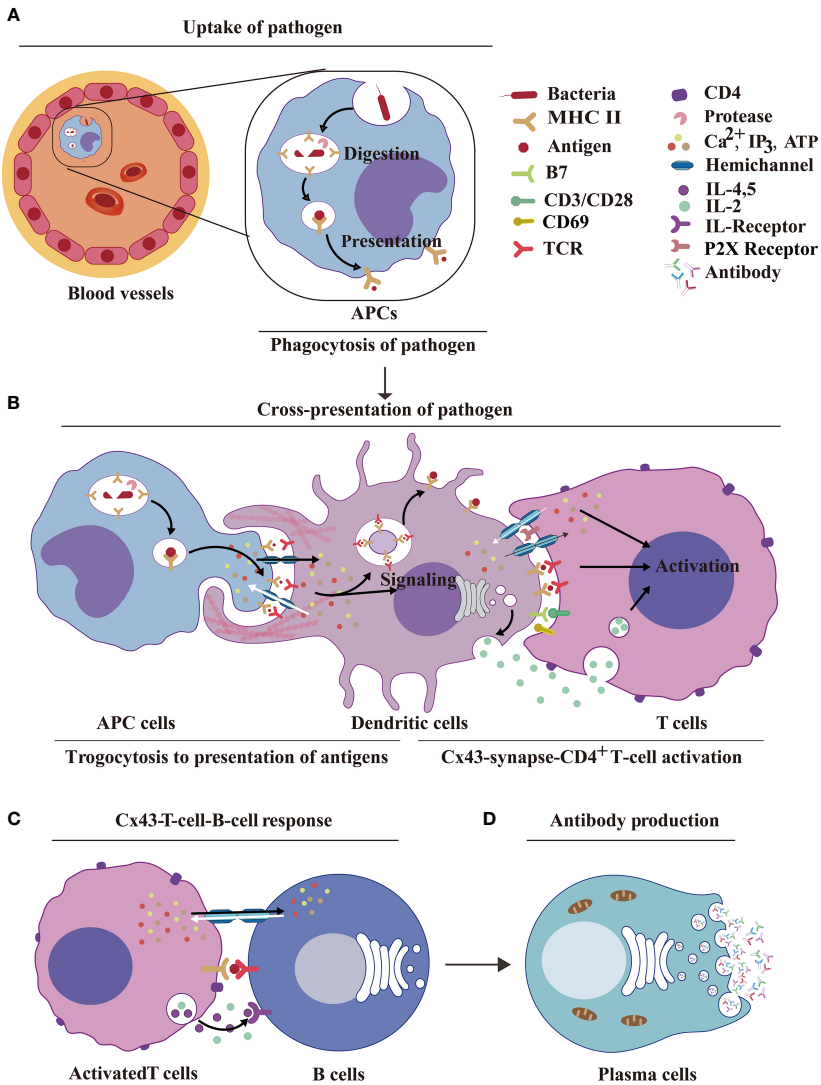

FIGURE 4 | HCs and IGLDCPs activate innate–adaptive immunity. **(A)** Uptake of pathogens by APCs. The pathogenic antigens are phagocytosed by APCs and digested by proteases to form peptides, which are then transmitted by MHC molecules to the cell surface by phagocytosis. **(B)** Dendritic cell Cx43s are dependent on trogocytosis for antigen delivery to T cells. The antigen is processed by APCs and binds to MHC receptors on the APC membrane. The HCs and IGLDCPs in innate–adaptive immunity recognize and remember specific pathogens to trigger immunity. The former facilitates ATP release and autocrine feedback mechanisms that control Ca^{2+} entry. GJs between monocytes and $CD8^+$ DCs transfer antigens *via* Cx43-synapse-$CD4^+$ T cells (59, 60). **(C)** Cx43-T-cell–B-cell response. The activated T cells facilitate the opening of HCs, which liberally release ATP into B cells. This results in the simultaneous release of IL-2, IL-4, and IL-5, which act on the IL-R receptor and further stimulate B cells to produce antibodies. **(D)** Antibody production. Activated B cells form plasma cells, which produce antibodies (61). HC, hemichannel; IGLDCP, Ig-like domain-containing protein; APC, antigen-presenting cell; MHC, major histocompatibility complex; DC, dendritic cell.

of GJs in $CD4^+$ T lymphocytes, Th0, Th1, and Th2, and macrophages; this pathway was found to be especially prominent in Cx43-Th1–macrophage interaction (19). This, in turn, suggests the potential capability of HCs in controlling IGLDCP activation. Cx43-GJs at the IS between DCs and $CD4^+$ T cells promote T cell activation during antigen presentation (11), whereas the inhibition of GJs hindered DC-mediated T cell activation, reflected by lower T cell proliferation, CD69 expression, and IL-2 secretion.

Interestingly, in the absence of DCs, Cx43 GJ blockers did not affect the activation of $CD4^+$ T cells triggered by anti-CD3/anti-CD28. Therefore, it was inferred that suppression of Cx43 inhibits Cx43 GJ assembly between DCs and T cells, resulting in T cell inactivation (84). In the DC–T cell IS, the blocking of Cx43 HCs/GJs (on either DCs or T cells) inhibited IFN-γ secretion and decreased the intracellular Ca^{2+} concentration, upon interaction of T cells with antigen-loaded DCs. These results strongly suggested that Cx43 HCs act in signaling amplification and T cell activation, by either releasing ATP or taking up of inositol triphosphate (IP_3) from DCs (25).

Cx43-GJs amplify antigens to activate T lymphocytes *via* the antigen cross-presentation pathway. In the immune synapse,

Panx1, which releases ATP, controls Ca^{2+} entry to activate T cells; this happens by stimulating autocrine/paracrine receptors, such as P2X1 and P2X4 (85). Cx43-GJs between monocytes and $CD8^+$ DCs transfer antigens (20), whereas Cx43 HCs activate $CD4^+$ T cells (86). Together, Cx43-dependent trogocytosis of macrophages and dendritic cells promote antigen uptake, transfer, and presentation to activate innate–adaptive immunity. The GJ protein Cx43 induces B lymphocytes (8) to produce antibodies in plasma cells (61) (**Figure 4D**).

CXS AND IGLDCPS MEDIATE ADAPTIVE IMMUNITY AND IGA TRANSITS ADAPTIVE IMMUNITY TO INNATE IMMUNITY

Cx43-CD39/CD73-Treg-Mediated Immunosuppression

In cellular suppression mechanisms, naturally occurring Treg cells and helper T cells communicate *via* GJs to deliver cAMP to responder T cells, thereby inhibiting T cell proliferation and IL-2 synthesis (87–89) (**Figures 5A–C**). In a recent review, it has been reported how the cross-talk between Cxs and cAMP regulates cell-cycle progression, particularly in cancer cell populations (90). Furthermore, Cx43 expressed by thymic Treg cell progenitors supports Treg cell development. Conversely, *Cx43* deletion decreased the number of functional Tregs and increased non-functional $CD4^+CD25^+GITR^+FOXp3^-$ T cells, which are incapable of producing inflammatory cytokines and inhibiting cancer cell progression (91). In human Treg cells, it has been shown that CD4-mediated activation involves elevation in the intracellular cAMP concentration. In contrast, the decrease in the cAMP level, caused by the application of adenylate cyclase (AC) inhibitor MDL12, resulted in the proliferation of Treg cells, *in vitro* and *in vivo* (87, 89) (**Figure 5B**). Consequently, it is inferred that Cx43 HCs may release cAMP; however, this needs to be studied further.

Cx43-GJs accumulate at the cytotoxic IS, enabling CTL-mediated melanoma cell killing (50). Additionally, Cx43 regulates the proliferation of $CD4^+CD25^+$ T lymphocytes and production of cytokines (92). Cx43-GJs regulate $CD4^+CD25^+$ Treg lymphocyte activation and inflammatory cytokine (IL-2 and IL-6) production in hypertensive inflammation in the spleen of rats (32, 92).

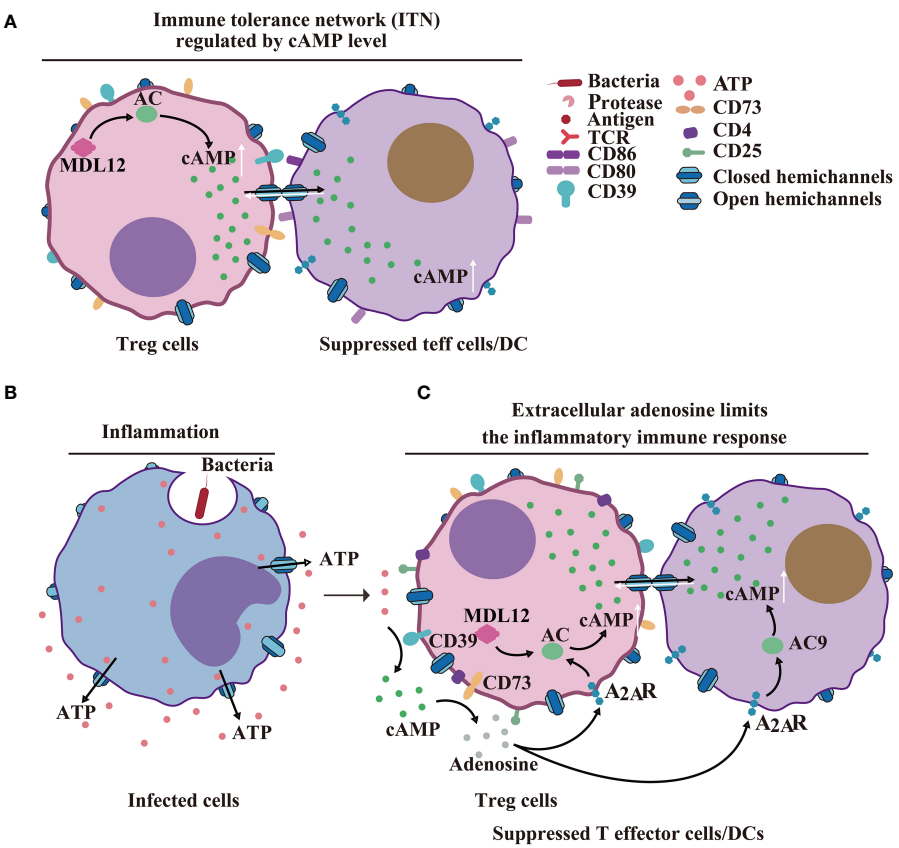

FIGURE 5 | HCs/GJs and IGLDCPs mediate adaptive immunity. **(A)** Cx43-cAMP cell-mediated immune response. Regulatory T cell-mediated inhibition of naturally occurring Treg cells and conventional T cells delivers cAMP to responder T cells *via* GJs to inhibit T-cell proliferation and IL-22 synthesis (89). **(B)** HCs in infected inflammatory cells release ATP. **(C)** Extracellular adenosine limits the extent of the inflammatory immune response. Activated $CD4^+$ T cells. The activated $CD39^+$ cells release cAMP *via* paracrine signaling, to suppress T effector (Teff) cell and dendritic cell (DC) functions (89). HC, hemichannel; IGLDCP, Ig-like domain-containing protein.

CD19$^+$ B Cell IgA Transcytosis Transits Adaptive Immunity to Innate Immunity

Recently, it was determined that tumor antigen-specific and tumor antigen-independent IgA transcytosis and antigen regulate ovarian cancer immunity. Tumor B cell-derived IgA binds to the polymeric immunoglobulin IgA receptors (pIgR) on ovarian cancer cells and reprograms myeloid cells against extracellular oncogenic drivers, such as EGFR and KRAS, which causes cell death. In particular, innate immunity triggered by antigen-independent IgA transcytosis is a novel strategy. IgA transcytosis through malignant epithelial cells causes tumor cells to encounter cytotoxic T cells, thereby hampering malignant progression; furthermore, the associated transcription changes result in suppression of the RAS pathway (21). In the ovarian cancer immunological response, IgA, B cells, and atypical B cells are observed (93). Transcytosis is a process in which molecules cross cellular barriers, which includes pinocytosis, endocytosis, and trafficking of vesicles to the opposite membrane (94).

In summary, Cx43-CD39/CD73-Treg-immunosuppression mediates adaptive immunity, specifically, IgA transcytosis, with tumor antigen-dependent and -independent mechanisms. It also regulates the establishment of immunity in ovarian cancer.

CONCLUDING REMARKS AND FUTURE PERSPECTIVES

In conclusion, GJs between two APCs interact with pMHC-1 of phagocytic APCs and TCR of trogocytic APCs to execute antigen delivery (14, 50) during innate immunity (**Figure 6A**). GJs interact with pMHC-I, B7 from APCs and TCR, CD28 from T cells to facilitate Ca^{2+}-mediated T cell activation (**Figure 6B**); GJs interact with CD40, pMHC-II from activated T cells and with BCR, CD40-L from activated B cells to stimulate B cell response during innate–adaptive immunity (95) (**Figure 6C**). The adaptive immunological response involves the generation of antibodies by plasma cells; innate immunity is regulated by IgA transcytosis in ovarian cancer (96) (**Figure 6D**). The transition from the innate immune response to adaptive immune response involves antigen presentation, followed by T

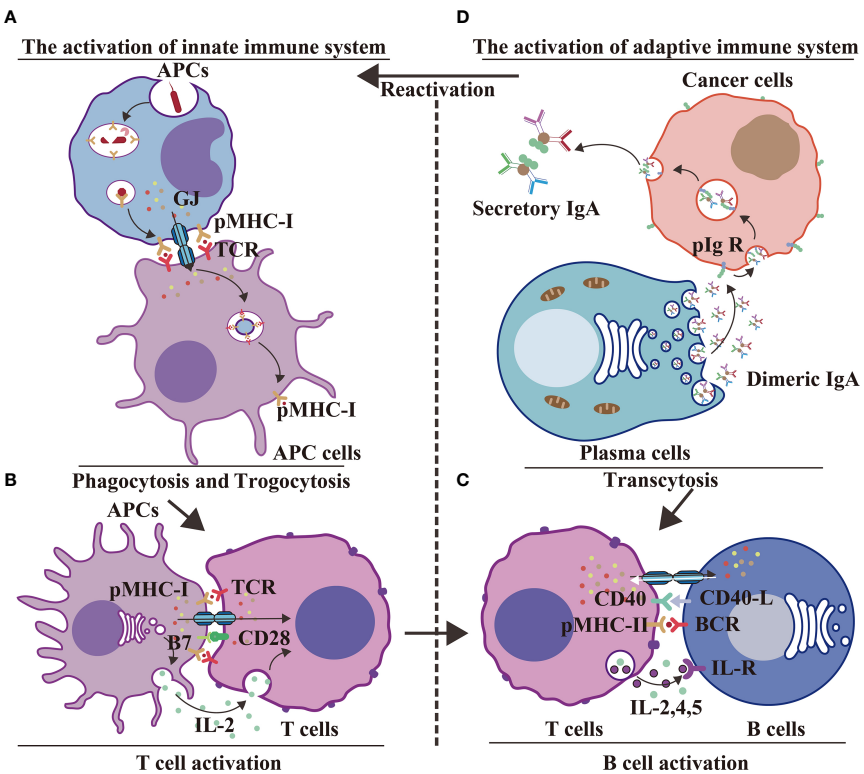

FIGURE 6 | GJs and IGLDCPs regulate phagocytosis, trogocytosis, and transcytosis during innate–adaptive immunity. **(A)** Innate immunity – antigen production. APCs receive pathogens and form epitopes on the membrane surface through digestion and processing of antigens. Interaction of GJs with IGLDCPs triggers phagocytosis and trogocytosis, thereby resulting in T-cell activation (14, 50). **(B)** Innate immunity – T-cell activation. Interaction of GJs with IGLDCPs: the former delivers Ca^{2+} and ATP to T cells, whereas the latter, in contact with CD28 and facilitated by paracrine IL-2 signal transmission, activates T cells. **(C)** Adaptive immunity – B-cell activation. After CD4$^+$ T-cell activation, pMHC-II establishes contact with the B-cell receptor (BCR). The resultant release of IL-2, IL-4, and IL-5 leads to B-cell activation. The adaptive immune response is jointly mediated by GJs and IGLDCPs (95). **(D)** Adaptive immunity – Antibodies affect pathogens. GJs activate the adaptive immune response to generate antibodies **(D)**. Conversely, IgA can induce APCs to activate the innate immune response *via* transcytosis **(A)** IgA can also promote B-cell activation **(C)** (96). HC, hemichannel; IGLDCP, Ig-like domain-containing protein; APC, antigen-presenting cell; GJ, gap junction.

cell activation, and, finally, B cell activation. The immune system is an unitary entity, and its regulation is dependent on a range of complex and diverse factors. HCs and IGLDCPs play an essential role in the three stages of the immune response, namely, innate immunity, innate–adaptive immunity, and adaptive immunity.

In the present review, we have discussed the interactive roles of HCs and IGLDCPs. Our goal is to provide novel insights based on existing concepts, and we believe that this will serve as a foundation for future research. The questions raised in the introductory section of the manuscript have been addressed and the knowledge gaps in the existing literature have been acknowledged. Along this line of investigation, potential clinical and research-related applications would greatly benefit immunological researchers and medical professionals.

AUTHOR CONTRIBUTIONS

K-JL, J-HM, C-XC, and JXJ structured the manuscript. K-JL, J-HM, C-XC, JXJ, HZ, and MRA wrote the manuscript. C-XC constructed the figures. K-JL, J-HM, and C-XC collected and compiled the references. K-JL, MRA, JXJ, and HZ proofread the manuscript. All authors contributed to the article and approved the submitted version.

FUNDING

K-JL was supported by the National Natural Science Foundation of China (NSFC) (32160662, 31772225, 31471823, 31260448, 31060251) and the Science and Technology Planning Project in Key Areas of Yunnan Province (202001BB050002). K-JL was also supported by the Donglu Scholar Program of Yunnan University. JXJ was supported by the Welch Foundation (AQ-1507). MRA was supported by the German Federal Ministry of Education and Research (BMBF)—German Network of RASopathy Research (GeNeRARe; grant number: 01GM1902C) and the European Network on Noonan Syndrome and Related Disorders (NSEuroNet; grant number: 01GM1621B).

REFERENCES

1. Chen W, Zhu S, Wang Y, Li J, Qiang X, Zhao X, et al. Enhanced Macrophage Pannexin 1 Expression and Hemichannel Activation Exacerbates Lethal Experimental Sepsis. *Sci Rep* (2019) 9(1):160. doi: 10.1038/s41598-018-37232-z
2. Calder BW, Matthew Rhett J, Bainbridge H, Fann SA, Gourdie RG, Yost MJ. Inhibition of Connexin 43 Hemichannel-Mediated Atp Release Attenuates Early Inflammation During the Foreign Body Response. *Tissue Eng Part A* (2015) 21(11-12):1752–62. doi: 10.1089/ten.TEA.2014.0651
3. Saez PJ, Shoji KF, Aguirre A, Saez JC. Regulation of Hemichannels and Gap Junction Channels by Cytokines in Antigen-Presenting Cells. *Mediators Inflammation* (2014) 2014:742734. doi: 10.1155/2014/742734
4. Orellana JA, Velasquez S, Williams DW, Sáez JC, Berman JW, Eugenin EA. Pannexin1 Hemichannels Are Critical for Hiv Infection of Human Primary Cd4+ T Lymphocytes. *J Leukoc Biol* (2013) 94(3):399–407. doi: 10.1189/jlb.0512249
5. Burra S, Nicolella DP, Francis WL, Freitas CJ, Mueschke NJ, Poole K, et al. Dendritic Processes of Osteocytes Are Mechanotransducers That Induce the Opening of Hemichannels. *Proc Natl Acad Sci USA* (2010) 107(31):13648–53. doi: 10.1073/pnas.1009382107
6. Ni X, Wang A, Zhang L, Shan LY, Zhang HC, Li L, et al. Up-Regulation of Gap Junction in Peripheral Blood T Lymphocytes Contributes to the Inflammatory Response in Essential Hypertension. *PloS One* (2017) 12(9):e0184773. doi: 10.1371/journal.pone.0184773
7. Machtaler S, Choi K, Dang-Lawson M, Falk L, Pournia F, Naus CC, et al. The Role of the Gap Junction Protein Connexin43 in B Lymphocyte Motility and Migration. *FEBS Lett* (2014) 588(8):1249–58. doi: 10.1016/j.febslet.2014.01.027
8. Machtaler S, Dang-Lawson M, Choi K, Jang C, Naus CC, Matsuuchi L. The Gap Junction Protein Cx43 Regulates B-Lymphocyte Spreading and Adhesion. *J Cell Sci* (2011) 124(Pt 15):2611–21. doi: 10.1242/jcs.089532
9. Ring S, Karakhanova S, Johnson T, Enk AH, Mahnke K. Gap Junctions Between Regulatory T Cells and Dendritic Cells Prevent Sensitization of Cd8 (+) T Cells. *J Allergy Clin Immun* (2010) 125(1):237–46. doi: 10.1016/j.jaci.2009.10.025
10. Pang B, Neijssen J, Qiao X, Janssen L, Janssen H, Lippuner C, et al. Direct Antigen Presentation and Gap Junction Mediated Cross-Presentation During Apoptosis. *J Immunol* (2009) 183(2):1083–90. doi: 10.4049/jimmunol.0900861
11. Elgueta R, Tobar JA, Shoji KF, De Calisto J, Kalergis AM, Bono MR, et al. Gap Junctions at the Dendritic Cell-T Cell Interface Are Key Elements for Antigen-Dependent T Cell Activation. *J Immunol* (2009) 183(1):277–84. doi: 10.4049/jimmunol.0801854
12. Glass AM, Snyder EG, Taffet SM. Connexins and Pannexins in the Immune System and Lymphatic Organs. *Cell Mol Life Sci* (2015) 72(15):2899–910. doi: 10.1007/s00018-015-1966-3
13. Flies AS, Blackburn NB, Lyons AB, Hayball JD, Woods GM. Comparative Analysis of Immune Checkpoint Molecules and Their Potential Role in the Transmissible Tasmanian Devil Facial Tumor Disease. *Front Immunol* (2017) 8:513(513). doi: 10.3389/fimmu.2017.00513
14. Huang Y, Mao Z, Zhang X, Yang X, Sawada N, Takeda M, et al. Connexin43 Is Required for the Effective Activation of Spleen Cells and Immunoglobulin Production. *Int J Mol Sci* (2019) 20(22):1–15. doi: 10.3390/ijms20225789
15. Köhler N, Ruess DA, Kesselring R, Zeiser R. The Role of Immune Checkpoint Molecules for Relapse After Allogeneic Hematopoietic Cell Transplantation. *Front Immunol* (2021) 12:634435(535). doi: 10.3389/fimmu.2021.634435
16. Sun L, Wang X, Saredy J, Yuan Z, Yang X, Wang H. Innate-Adaptive Immunity Interplay and Redox Regulation in Immune Response. *Redox Biol* (2020) 37:101759. doi: 10.1016/j.redox.2020.101759
17. Willebrords J, Crespo Yanguas S, Maes M, Decrock E, Wang N, Leybaert L, et al. Connexins and Their Channels in Inflammation. *Crit Rev Biochem Mol Biol* (2016) 51(6):413–39. doi: 10.1080/10409238.2016.1204980
18. Takeuchi H, Suzumura A. Gap Junctions and Hemichannels Composed of Connexins: Potential Therapeutic Targets for Neurodegenerative Diseases. *Front Cell Neurosci* (2014) 8:189. doi: 10.3389/fncel.2014.00189
19. Bermudez-Fajardo A, Ylihärsilä M, Evans WH, Newby AC, Oviedo-Orta E. Cd4+ T Lymphocyte Subsets Express Connexin 43 and Establish Gap Junction Channel Communication With Macrophages in Vitro. *J Leukoc Biol* (2007) 82(3):608–12. doi: 10.1189/jlb.0307134
20. Huang MN, Nicholson LT, Batich KA, Swartz AM, Kopin D, Wellford S, et al. Antigen-Loaded Monocyte Administration Induces Potent Therapeutic Antitumor T Cell Responses. *J Clin Invest* (2020) 130(2):774–88. doi: 10.1172/JCI128267
21. Biswas S, Mandal G, Payne KK, Anadon CM, Gatenbee CD, Chaurio RA, et al. Iga Transcytosis and Antigen Recognition Govern Ovarian Cancer Immunity. *Nature* (2021) 591(7850):464–70. doi: 10.1038/s41586-020-03144-0
22. Wu M, Moh MC, Schwarz H. Hepacam Associates With Connexin 43 and Enhances Its Localization in Cellular Junctions. *Sci Rep* (2016) 6(1):36218. doi: 10.1038/srep36218

23. Ai XL, Chi Q, Qiu Y, Li HY, Li DJ, Wang JX, et al. Gap Junction Protein Connexin43 Deregulation Contributes to Bladder Carcinogenesis Via Targeting Mapk Pathway. *Mol Cell Biochem* (2017) 428(1-2):109–18. doi: 10.1007/s11010-016-2921-9
24. Langhorst H, Juttner R, Groneberg D, Mohtashamdolatshahi A, Pelz L, Purfurst B, et al. The Igcam Clmp Regulates Expression of Connexin43 and Connexin45 in Intestinal and Ureteral Smooth Muscle Contraction in Mice. *Dis Model Mech* (2018) 11(2):1–14. doi: 10.1242/dmm.032128
25. Tittarelli A, Navarrete M, Gleisner MA, Gebicke-Haerter P, Salazar-Onfray F. Connexin-Mediated Signaling at the Immunological Synapse. *Int J Mol Med* (2020) 21(10):1–16. doi: 10.3390/ijms21103736
26. Poon IK, Lucas CD, Rossi AG, Ravichandran KS. Apoptotic Cell Clearance: Basic Biology and Therapeutic Potential. *Nat Rev Immunol* (2014) 14(3):166–80. doi: 10.1038/nri3607
27. Araya R, Eckardt D, Maxeiner S, Kruger O, Theis M, Willecke K, et al. Expression of Connexins During Differentiation and Regeneration of Skeletal Muscle: Functional Relevance of Connexin43. *J Cell Sci* (2005) 118(1):27–37. doi: 10.1242/jcs.01553
28. Gonzalez HE, Eugenin EA, Garces G, Solis N, Pizarro M, Accatino L, et al. Regulation of Hepatic Connexins in Cholestasis: Possible Involvement of Kupffer Cells and Inflammatory Mediators. *Am J Physiol-Gastroint Liver Physiol* (2002) 282(6):G991–G1001. doi: 10.1152/ajpgi.00298.2001
29. Kielian T. Glial Connexins and Gap Junctions in Cns Inflammation and Disease. *J Neurochem* (2008) 106(3):1000–16. doi: 10.1111/j.1471-4159.2008.05405.x
30. Altevogt BM, Kleopa KA, Postma FR, Scherer SS, Paul DL. Connexin29 Is Uniquely Distributed Within Myelinating Glial Cells of the Central and Peripheral Nervous Systems. *J Neurosci* (2002) 22(15):6458–70. doi: 10.1523/jneurosci.22-15-06458.2002
31. Odermatt B, Wellershaus K, Wallraff A, Seifert G, Degen J, Euwens C, et al. Connexin 47 (Cx47)-Deficient Mice With Enhanced Green Fluorescent Protein Reporter Gene Reveal Predominant Oligodendrocytic Expression of Cx47 and Display Vacuolized Myelin in the Cns. *J Neurosci* (2003) 23 (11):4549–59. doi: 10.1523/jneurosci.23-11-04549.2003
32. Ni X, Li XZ, Fan ZR, Wang A, Zhang HC, Zhang L, et al. Increased Expression and Functionality of the Gap Junction in Peripheral Blood Lymphocytes Is Associated With Hypertension-Mediated Inflammation in Spontaneously Hypertensive Rats. *Cell Mol Biol Lett* (2018) 23:1–18. doi: 10.1186/s11658-018-0106-0
33. Valdebenito S, Barreto A, Eugenin EA. The Role of Connexin and Pannexin Containing Channels in the Innate and Acquired Immune Response. *Biochim Biophys Acta Biomembr* (2018) 1860(1):154–65. doi: 10.1016/j.bbamem.2017.05.015
34. Cerny J, Striz I. Adaptive Innate Immunity or Innate Adaptive Immunity? *Clin Sci (Lond)* (2019) 133(14):1549–65. doi: 10.1042/CS20180548
35. Matsue H, Yao J, Matsue K, Nagasaka A, Sugiyama H, Aoki R, et al. Gap Junction-Mediated Intercellular Communication Between Dendritic Cells (Dcs) Is Required for Effective Activation of Dcs. *J Immunol* (2006) 176 (1):181–90. doi: 10.4049/jimmunol.176.1.181
36. Falk L, Dang-Lawson M, Vega JL, Pournia F, Choi K, Jang C, et al. Mutations of Cx43 That Affect B Cell Spreading in Response to Bcr Signaling. *Biol Open* (2014) 3(3):185–91. doi: 10.1242/bio.20147328
37. Favre-Kontula L, Rolland A, Bernasconi L, Karmirantzou M, Power C, Antonsson B, et al. Glialcam, an Immunoglobulin-Like Cell Adhesion Molecule Is Expressed in Glial Cells of the Central Nervous System. *Glia* (2008) 56(6):633–45. doi: 10.1002/glia.20640
38. Tan B, Tan JX, Du HF, Quan Z, Xu XD, Jiang XL, et al. Hepacam Inhibits Clear Cell Renal Carcinoma 786-0 Cell Proliferation Via Blocking Pkc Epsilon Translocation From Cytoplasm to Plasma Membrane. *Mol Cell Biochem* (2014) 391(1-2):95–102. doi: 10.1007/s11010-014-1991-9
39. Tittarelli A, Navarrete M, Lizana M, Hofmann-Vega F, Salazar-Onfray F. Hypoxic Melanoma Cells Deliver Micrornas to Dendritic Cells and Cytotoxic T Lymphocytes Through Connexin-43 Channels. *Int J Mol Sci* (2020) 21 (20):7567. doi: 10.3390/ijms21207567
40. Oviedo-Orta E, Evans WH. Gap Junctions and Connexins: Potential Contributors to the Immunological Synapse. *J Leukoc Biol* (2002) 72 (4):636–42. doi: 10.1189/jlb.72.4.636
41. Niedergang F, Di Bartolo V, Alcover A. Comparative Anatomy of Phagocytic and Immunological Synapses. *Front Immunol* (2016) 7:18. doi: 10.3389/fimmu.2016.00018
42. Kuokkanen E, Sustar V, Mattila PK. Molecular Control of B Cell Activation and Immunological Synapse Formation. *Traffic* (2015) 16(4):311–26. doi: 10.1111/tra.12257
43. Lakatos A. State-Of-Art Modelling of Inflammatory Astrocyte-Synapse Interactions in Injury and Amyotrophic Lateral Sclerosis. *Neural Regener Res* (2017) 12(1):75–6. doi: 10.4103/1673-5374.198977
44. Sikandar S, Patel R, Patel S, Sikander S, Bennett DL, Dickenson AH. Genes, Molecules and Patients–Emerging Topics to Guide Clinical Pain Research. *Eur J Pharmacol* (2013) 716(1-3):188–202. doi: 10.1016/j.ejphar.2013.01.069
45. Leybaert L, Lampe PD, Dhein S, Kwak BR, Ferdinandy P, Beyer EC, et al. Connexins in Cardiovascular and Neurovascular Health and Disease: Pharmacological Implications. *Pharmacol Rev* (2017) 69(4):396–478. doi: 10.1124/pr.115.012062
46. Rajnai H, Teleki I, Kiszner G, Meggyeshazi N, Balla P, Vancsik T, et al. Connexin 43 Communication Channels in Follicular Dendritic Cell Development and in Follicular Lymphomas. *J Immunol Res* (2015) 2015:528098. doi: 10.1155/2015/528098
47. Anand RJ, Dai S, Gribar SC, Richardson W, Kohler JW, Hoffman RA, et al. A Role for Connexin43 in Macrophage Phagocytosis and Host Survival After Bacterial Peritoneal Infection. *J Immunol* (2008) 181(12):8534–43. doi: 10.4049/jimmunol.181.12.8534
48. Dosch M, Zindel J, Jebbawi F, Melin N, Sanchez-Taltavull D, Stroka D, et al. Connexin-43-Dependent Atp Release Mediates Macrophage Activation During Sepsis. *Elife* (2019) 8:1–24. doi: 10.7554/eLife.42670
49. Rodjakovic D, Salm L, Beldi G. Function of Connexin-43 in Macrophages. *Int J Mol Sci* (2021) 22(3):1–11. doi: 10.3390/ijms22031412
50. Hofmann F, Navarrete M, Alvarez J, Guerrero I, Gleisner MA, Tittarelli A, et al. Cx43-Gap Junctions Accumulate at the Cytotoxic Immunological Synapse Enabling Cytotoxic T Lymphocyte Melanoma Cell Killing. *Int J Mol Sci* (2019) 20(18):1–16. doi: 10.3390/ijms20184509
51. Mendoza-Naranjo A, Bouma G, Pereda C, Ramírez M, Webb KF, Tittarelli A, et al. Functional Gap Junctions Accumulate at the Immunological Synapse and Contribute to T Cell Activation. *J Immunol* (2011) 187(6):3121–32. doi: 10.4049/jimmunol.1100378
52. Moretto G, Xu RY, Kim SU. Cd44 Expression in Human Astrocytes and Oligodendrocytes in Culture. *J Neuropathol Exp Neurol* (1993) 52(4):419–23. doi: 10.1097/00005072-199307000-00009
53. Zhang Y, Sloan SA, Clarke LE, Caneda C, Plaza CA, Blumenthal PD, et al. Purification and Characterization of Progenitor and Mature Human Astrocytes Reveals Transcriptional and Functional Differences With Mouse. *Neuron* (2016) 89(1):37–53. doi: 10.1016/j.neuron.2015.11.013
54. Liu X, Bates R, Yin D-M, Shen C, Wang F, Su N, et al. Specific Regulation of Nrg1 Isoform Expression by Neuronal Activity. *J Neurosci* (2011) 31 (23):8491–501. doi: 10.1523/jneurosci.5317-10.2011
55. Allen NJ, Eroglu C. Cell Biology of Astrocyte-Synapse Interactions. *Neuron* (2017) 96(3):697–708. doi: 10.1016/j.neuron.2017.09.056
56. Westman J, Grinstein S, Marques PE. Phagocytosis of Necrotic Debris at Sites of Injury and Inflammation. *Front Immunol* (2020) 10:3030. doi: 10.3389/fimmu.2019.03030
57. Glass AM, Wolf BJ, Schneider KM, Princiotta MF, Taffet SM. Connexin43 Is Dispensable for Phagocytosis. *J Immunol* (2013) 190(9):4830–5. doi: 10.4049/jimmunol.1202884
58. Ruez R, Dubrot J, Zoso A, Bacchetta M, Molica F, Hugues S, et al. Dendritic Cell Migration Toward Ccl21 Gradient Requires Functional Cx43. *Front Physiol* (2018) 9:288. doi: 10.3389/fphys.2018.00288
59. Martinez-Martin N, Fernandez-Arenas E, Cemerski S, Delgado P, Turner M, Heuser J, et al. T Cell Receptor Internalization From the Immunological Synapse Is Mediated by Tc21 and Rhog Gtpase-Dependent Phagocytosis. *Immunity* (2011) 35(2):208–22. doi: 10.1016/j.immuni.2011.06.003
60. Thaiss CA, Semmling V, Franken L, Wagner H, Kurts C. Chemokines: A New Dendritic Cell Signal for T Cell Activation. *Front Immunol* (2011) 2:31. doi: 10.3389/fimmu.2011.00031
61. Kwek SS, Cha E, Fong L. Unmasking the Immune Recognition of Prostate Cancer With Ctla4 Blockade. *Nat Rev Cancer* (2012) 12(4):289–97. doi: 10.1038/nrc3223

62. Garre JM, Yang G, Bukauskas FF, Bennett MVL. Fgf-1 Triggers Pannexin-1 Hemichannel Opening in Spinal Astrocytes of Rodents and Promotes Inflammatory Responses in Acute Spinal Cord Slices. *J Neurosci* (2016) 36 (17):4785–801. doi: 10.1523/jneurosci.4195-15.2016
63. Alves LA, de Carvalho AC, Savino W. Gap Junctions: A Novel Route for Direct Cell-Cell Communication in the Immune System? *Immunol Today* (1998) 19(6):269–75. doi: 10.1016/s0167-5699(98)01256-0
64. Chekeni FB, Elliott MR, Sandilos JK, Walk SF, Kinchen JM, Lazarowski ER, et al. Pannexin 1 Channels Mediate 'Find-Me' Signal Release and Membrane Permeability During Apoptosis. *Nature* (2010) 467(7317):863–7. doi: 10.1038/nature09413
65. Elliott MR, Chekeni FB, Trampont PC, Lazarowski ER, Kadl A, Walk SF, et al. Nucleotides Released by Apoptotic Cells Act as a Find-Me Signal for Phagocytic Clearance. *Nature* (2009) 461(7261):282–6. doi: 10.1038/nature08296
66. Hochreiter-Hufford A, Ravichandran KS. Clearing the Dead: Apoptotic Cell Sensing, Recognition, Engulfment, and Digestion. *Cold Spring Harbor Perspect Biol* (2013) 5(1):a008748. doi: 10.1101/cshperspect.a008748
67. Jankowski J, Perry HM, Medina CB, Huang L, Yao J, Bajwa A, et al. Epithelial and Endothelial Pannexin1 Channels Mediate Aki. *J Am Soc Nephrol* (2018) 29(7):1887–99. doi: 10.1681/ASN.2017121306
68. Oviedo-Orta E, Howard Evans W. Gap Junctions and Connexin-Mediated Communication in the Immune System. *Biochim Biophys Acta* (2004) 1662(1-2):102–12. doi: 10.1016/j.bbamem.2003.10.021
69. Poon IK, Hulett MD, Parish CR. Molecular Mechanisms of Late Apoptotic/Necrotic Cell Clearance. *Cell Death Differ* (2010) 17(3):381–97. doi: 10.1038/cdd.2009.195
70. Saez JC, Branes MC, Corvalan LA, Eugenin EA, Gonzalez H, Martinez AD, et al. Gap Junctions in Cells of the Immune System: Structure, Regulation and Possible Functional Roles. *Braz J Med Biol Res* (2000) 33(4):447–55. doi: 10.1590/s0100-879x2000000400011
71. Yuan D, Sun G, Zhang R, Luo C, Ge M, Luo G, et al. Connexin 43 Expressed in Endothelial Cells Modulates Monocyteendothelial Adhesion by Regulating Cell Adhesion Proteins. *Mol Med Rep* (2015) 12(5):7146–52. doi: 10.3892/mmr.2015.4273
72. Xu C-Y, Zhang W-S, Zhang H, Cao Y, Zhou H-Y. The Role of Connexin-43 in the Inflammatory Process: A New Potential Therapy to Influence Keratitis. *J Ophthalmol* (2019) 2019:9312827. doi: 10.1155/2019/9312827
73. Song L, Sun J, Soderholm M, Melander O, Orho-Melander M, Nilsson J, et al. Association of Tim-1 (T-Cell Immunoglobulin and Mucin Domain 1) With Incidence of Stroke. *Arterioscler Thromb Vasc Biol* (2020) 40(7):1777–86. doi: 10.1161/ATVBAHA.120.314269
74. Zhao R, Song C, Liu L, Liu Q, Zhou N, Zhou X, et al. Single Immunoglobulin and Tollinterleukin1 Receptor Domain Containing Molecule Protects Against Severe Acute Pancreatitis in Vitro by Negatively Regulating the Tolllike Receptor4 Signaling Pathway: A Clinical and Experimental Study. *Mol Med Rep* (2020) 22(4):2851–9. doi: 10.3892/mmr.2020.11379
75. Zhang J, Hou C, Dou S, Li G, Wang Z, Liu Y, et al. T Cell Immunoglobulin and Mucin Domain Protein 3 Inhibits Glycolysis in Raw 264.7 Macrophages Through Hexokinase 2. *Scand J Immunol* (2020) 93(2):e12981. doi: 10.1111/sji.12981
76. Hamieh M, Dobrin A, Cabriolu A, van der Stegen SJC, Giavridis T, Mansilla-Soto J, et al. Car T Cell Trogocytosis and Cooperative Killing Regulate Tumour Antigen Escape. *Nature* (2019) 568(7750):112–6. doi: 10.1038/s41586-019-1054-1
77. Joly E, Hudrisier D. What Is Trogocytosis and What Is Its Purpose? *Nat Immunol* (2003) 4(9):815–. doi: 10.1038/ni0903-815
78. Mazzini E, Massimiliano L, Penna G, Rescigno M. Oral Tolerance Can Be Established *Via* Gap Junction Transfer of Fed Antigens From Cx3cr1(+) Macrophages to Cd103(+) Dendritic Cells. *Immunity* (2014) 40(2):248–61. doi: 10.1016/j.immuni.2013.12.012
79. Smyth LA, Hervouet C, Hayday T, Becker PD, Ellis R, Lechler RI, et al. Acquisition of Mhc:Peptide Complexes by Dendritic Cells Contributes to the Generation of Antiviral Cd8+ T Cell Immunity in Vivo. *J Immunol* (2012) 189 (5):2274–82. doi: 10.4049/jimmunol.1200664
80. Wakim LM, Bevan MJ. Cross-Dressed Dendritic Cells Drive Memory Cd8+ T-Cell Activation After Viral Infection. *Nature* (2011) 471(7340):629–32. doi: 10.1038/nature09863
81. Handel A, Yates A, Pilyugin SS, Antia R. Gap Junction-Mediated Antigen Transport in Immune Responses. *Trends Immunol* (2007) 28(11):463–6. doi: 10.1016/j.it.2007.08.006
82. Mendoza-Naranjo A, Saez PJ, Johansson CC, Ramirez M, Mandakovic D, Pereda C, et al. Functional Gap Junctions Facilitate Melanoma Antigen Transfer and Cross-Presentation Between Human Dendritic Cells. *J Immunol* (2007) 178(11):6949–57. doi: 10.4049/jimmunol.178.11.6949
83. Neijssen J, Herberts C, Drijfhout JW, Reits E, Janssen L, Neefjes J. Cross-Presentation by Intercellular Peptide Transfer Through Gap Junctions. *Nature* (2005) 434(7029):83–8. doi: 10.1038/nature03290
84. Eugenin EA. Role of Connexin/Pannexin Containing Channels in Infectious Diseases. *FEBS Lett* (2014) 588(8):1389–95. doi: 10.1016/j.febslet.2014.01.030
85. Woehrle T, Yip L, Elkhal A, Sumi Y, Chen Y, Yao Y, et al. Pannexin-1 Hemichannel-Mediated Atp Release Together With P2x1 and P2x4 Receptors Regulate T-Cell Activation at the Immune Synapse. *Blood* (2010) 116 (18):3475–84. doi: 10.1182/blood-2010-04-277707
86. Oviedo-Orta E, Perreau M, Evans WH, Potolicchio I. Control of the Proliferation of Activated Cd4+ T Cells by Connexins. *J Leukoc Biol* (2010) 88(1):79–86. doi: 10.1189/jlb.0909613
87. Klein M, Bopp T. Cyclic Amp Represents a Crucial Component of Treg Cell-Mediated Immune Regulation. *Front Immunol* (2016) 7:315(315). doi: 10.3389/fimmu.2016.00315
88. Bopp T, Becker C, Klein M, Klein-Hessling S, Palmetshofer A, Serfling E, et al. Cyclic Adenosine Monophosphate Is a Key Component of Regulatory T Cell-Mediated Suppression. *J Exp Med* (2007) 204(6):1303–10. doi: 10.1084/jem.20062129
89. Zhao H, Liao X, Kang Y. Tregs: Where We Are and What Comes Next? *Front Immunol* (2017) 8:1578. doi: 10.3389/fimmu.2017.01578
90. Chen CX, He HJ, Cai QC, Zhang W, Kou TC, Zhang XW, et al. Bracovirus-Mediated Innexin Hemichannel Closure in Cell Disassembly. *iScience* (2021) 24(4):102281. doi: 10.1016/j.isci.2021.102281
91. Kuczma M, Lee JR, Kraj P. Connexin 43 Signaling Enhances the Generation of Foxp3+ Regulatory T Cells. *J Immunol* (2011) 187(1):248–57. doi: 10.4049/jimmunol.1003785
92. Zhang HC, Zhang ZS, Zhang L, Wang A, Zhu H, Li L, et al. Connexin 43 in Splenic Lymphocytes Is Involved in the Regulation of Cd4(+)Cd25(+) T Lymphocyte Proliferation and Cytokine Production in Hypertensive Inflammation. *Int J Mol Med* (2018) 41(1):13–24. doi: 10.3892/ijmm.2017.3201
93. Lichtman A. The Abcs of Ovarian Cancer Immunology: Iga, B Cells, and Ctls. *Sci Immunol* (2021) 6(57):1–5. doi: 10.1126/sciimmunol.abh3184
94. Tuma PL, Hubbard AL. Transcytosis: Crossing Cellular Barriers. *Physiol Rev* (2003) 83(3):871–932. doi: 10.1152/physrev.00001.2003
95. Kreer C, Rauen J, Zehner M, Burgdorf S. Cross-Presentation: How to Get There - or How to Get the Er. *Front Immunol* (2011) 2:87. doi: 10.3389/fimmu.2011.00087
96. Fung KYY, Fairn GD, Lee WL. Transcellular Vesicular Transport in Epithelial and Endothelial Cells: Challenges and Opportunities. *Traffic* (2018) 19(1):5–18. doi: 10.1111/tra.12533

Conflict of Interest: The authors declare that the research was conducted in the absence of any commercial or financial relationships that could be construed as a potential conflict of interest.

frontiers | Frontiers in Immunology

TYPE Review
PUBLISHED 28 July 2022
DOI 10.3389/fimmu.2022.891220

OPEN ACCESS

EDITED BY
Hang Yin,
Tsinghua University, China

REVIEWED BY
Tara Sutherland,
The University of Manchester, United Kingdom
Yukihiro Yamaguchi,
University of North Carolina at Chapel Hill, United States

*CORRESPONDENCE
Wenhua Zhu
zhuwenhua@xjtu.edu.cn
Liesu Meng
mengliesu@xjtu.edu.cn

†These authors have contributed equally to this work

SPECIALTY SECTION
This article was submitted to Molecular Innate Immunity, a section of the journal Frontiers in Immunology

RECEIVED 07 March 2022
ACCEPTED 06 July 2022
PUBLISHED 28 July 2022

CITATION
Kang Q, Li L, Pang Y, Zhu W and Meng L (2022) An update on Ym1 and its immunoregulatory role in diseases.
Front. Immunol. 13:891220.
doi: 10.3389/fimmu.2022.891220

An update on Ym1 and its immunoregulatory role in diseases

Qi Kang[1,2,3†], Luyao Li[1,2,3†], Yucheng Pang[1,2,3†], Wenhua Zhu[1,2*] and Liesu Meng[1,2,4*]

[1]Institute of Molecular and Translational Medicine, and Department of Biochemistry and Molecular Biology, School of Basic Medical Sciences, Xi'an Jiaotong University Health Science Center, Xi'an, China, [2]Key Laboratory of Environment and Genes Related to Diseases, Xi'an Jiaotong University, Ministry of Education, Xi'an, China, [3]Department of Clinical Medicine, Xi'an Jiaotong University Health Science Center, Xi'an, China, [4]National Joint Engineering Research Center of Biodiagnostics and Biotherapy, Second Affiliated Hospital, Xi'an Jiaotong University, Xi'an, China

Ym1 is a rodent-specific chitinase-like protein (CLP) lacking catalytic activity, whose cellular origins are mainly macrophages, neutrophils and other cells. Although the detailed function of Ym1 remains poorly understood, Ym1 has been generally recognized as a fundamental feature of alternative activation of macrophages in mice and hence one of the prevalent detecting targets in macrophage phenotype distinguishment. Studies have pointed out that Ym1 may have regulatory effects, which are multifaceted and even contradictory, far more than just a mere marker. Allergic lung inflammation, parasite infection, autoimmune diseases, and central nervous system diseases have been found associations with Ym1 to varying degrees. Thus, insights into Ym1's role in diseases would help us understand the pathogenesis of different diseases and clarify the genuine roles of CLPs in mammals. This review summarizes the information on Ym1 from the gene to its expression and regulation and focuses on the association between Ym1 and diseases.

KEYWORDS

Ym1/Chil3, chitinase like protein, innate immunity, immunoregulatory roles, inflammation related diseases

Introduction

Ym1, known as chitinase-like protein 3 (Chil3), is a member of chitinase-like proteins (CLPs) specifically produced by rodents, which is also referred to as eosinophil chemotactic factor (ECF-L) since it was originally purified as eosinophilic crystals in mice with pulmonary inflammation. Chitinases refer to a class of chitin-degrading enzymes produced in the host, which have been proven to play a protective role in innate immunity against the chitin-containing pathogens, including parasites, fungi, and arthropods (1). CLPs lose their activity on chitin degradation due to mutations of key

sites in the enzyme domain, but still participate in various inflammatory responses in mammals. Among the three CLPs in mice (Ym1, Ym2 and BRP-39), and two in humans (YKL-39 and YKL-40), YKL-40 retains the chitin-binding property, while Ym1 has a specific binding affinity for chitin-like saccharides such as glucosamine (GlcN) oligosaccharides, heparin and heparan sulfate (HS), which is presumed to belong to a new lectin family (2).

The producing cells of Ym1 are alternatively activated macrophages (Mφ) denoted as M2 or M2a (3), and neutrophils (4). It is expressed under the physiological state, and is induced by type 2 cytokines in the pathological condition, which often leads to a significant upregulation in the acute stage of inflammation. The enriched Ym1 even forms crystals in specific pathological environments (5). Ym1 has been used as a marker of M2 and is involved in the modulation of Mφ activation, the expression of Th2 cytokines and IL-17, the chemotaxis of neutrophils (and probably eosinophils) and other inflammatory responses (6, 7).

Ym1 has been confirmed to contribute to the immunopathology of certain diseases in the lung, brain, skin, joint, etc (6–8). However, the influencing factors of these diseases are complicated and diverse, and the existence of Ym1-highly-similar homologs becomes a constraint in its research techniques. Therefore, the role of Ym1 in disease pathogenesis remains unclear.

Basics of *Chil3* gene

As a rodent-specific gene, *Chil3* is situated in the F2.2 region of mouse chromosome 3. As early as 1998, *Chil3* was reported to locate in the center of mouse chromosome 3, which is also an equivalent region to human chromosome 1 p13 (9). The same conclusion was also obtained by Southern blotting in 2001, indicating that *Chil3* is a single copy gene (2). What people first learned about *Chil3* was its cDNA sequence out of the mouse peritoneal exudate cDNA library, which was deposited in the GenBank database (GenBank M94584) in 1992. Subsequently, the second full-length cDNA sequence *ECF-L* was deposited in the database (GenBank D87757) in 1996. Now people know the *Chil3* gene is composed of 20,011 pairs of bases, containing 11 exon sequences, and the position of exon-intron splice site is consistent with that of human *CHI3L1* gene, but there is no splice site corresponding to the last *Chil3* splice site in human genes (9). For the transcriptional start site, 20 nucleotides upstream of the translation start codon ATG in exon 1 were determined by primer extension analysis, and now it's generally believed that there are 43 nucleotides upstream of ATG in exon 1. Meanwhile, there are four signal transducer and activator of transcription (STAT)-binding sites TTCNxGAA near the upstream of exon 1, in which only the first and the third one could bind STAT6-containing complexes with high affinity in the EMSA experiments (10). In addition, for Ym1 protein, it was found to be a single peptide chain containing 373 residues, excluding the first 21 leading peptide and the last 4 carboxyl terminal residues, clearly divided into a large β/α barrel (TIM barrel) domain and a small α+β domain (11, 12). The information on *Chil3* gene, RNA and protein are summarized in Figure 1.

All gene sequences of CLPs are highly similar, in the same or different species, but there are still differences among them. Since *Chil3* gene are similar to all the known human chitinase-like genes (~ 50% nucleotide similarity), the exact human ortholog of *Chil3* cannot be clearly defined by now (9). At the same time, there is a high degree of homology between *Chil3* and *Chil4* genes in mice (9). Although the basic expression patterns of *Chil3* and *Chil4* do not overlap substantially, the first 1,200 nucleotides upstream of exon 1 of *Chil3* are 92% identical to those of *Chil4* and contain a STAT-binding site, while the first 1,700 nucleotides downstream of exon 1 of *Chil3* are 93% the same as those of *Chil4*. This high genomic similarity indicates that *Chil3* and *Chil4* are generated by relatively recent gene duplication events (10). At the evolutionary level, the research on GH18 family proteins showed that mouse CLP genes (*Chil3, Chil4, etc.*) evolved from the rodent *Chia* gene. A replication event produced CLPs, which lost its catalytic motif before further branching and expanding, may lead to the birth of *Chil3, Chil4*, and their predicted homologous pseudogenes GM6522 (previously assumed *Ym3*, *Ym4* were parsed into single predicted pseudogenes by the database) (13). The similarity of Ym1 and Ym2 once hindered the determination of the research object. At the RNA level, reverse transcription-polymerase chain reaction with specific primer pairs targeting the differences of *Chil3* and *Chil4* sequences allows the identification of the two genes (10, 14). At the protein level, Ym1 and Ym2 share a considerable number of sequences (91.7% of the amino acid sequences are the same, 33 different amino acids). In early years studies, monoclonal antibodies against Ym1 had the same effect on Ym2 (15), so immunological detection had to work in conjunction with mRNA *in situ* hybridization to make a distinction (16). However, in a recent study, specific antibodies targeting Ym1 and Ym2 respectively have been developed, and the two proteins now can be distinguished successfully (17). For early studies where Ym1 and Ym2 were not clearly distinguished, in this review we collectively refer to the relevant research objects as Ym protein.

Ym1 expression and its regulation

The expression patterns of C/CLPs including Ym1 have obvious tissue specificity, thus here we try to summarize Ym1 expression accordingly under both physiological and pathophysiological conditions (as shown in Figure 2).

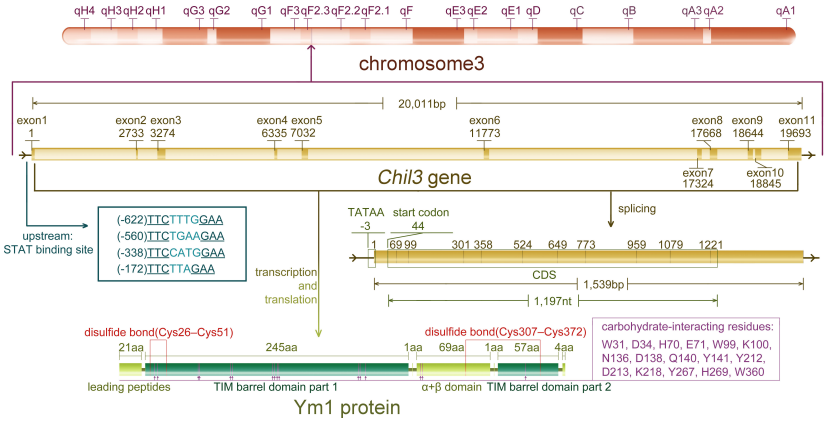

FIGURE 1
The information of *Chil3* gene, RNA and protein. *Chil3* gene is situated in the F2.2 region of mouse chromosome 3, it is composed of 20,011 pairs of bases, containing 11 exon sequences, which are 1,539bp in length. Four STAT binding sites are located near exon 1. The 1,197nt CDS sequence encodes the Ym1 protein containing 398 residues. Ym1 protein, excluding the first 21 leading peptides and the last 4 carboxyl terminal residues, can be divided into a large β/α barrel (TIM barrel) domain and a small α+β domain. Ym1 also has several carbohydrate-interacting residues though it has no chitinase activity, and these residues are marked on the diagram.

Physiological condition

In healthy adult mice, Ym1, with different cellular origins, is constitutively expressed in the spleen, bone marrow and notably in lungs (16). Ym1 was originally purified from the supernatant of mouse splenocyte culture as an eosinophil chemokine (18), and the expressing cells were identified as immature neutrophils in red pulp (16). In the lung, alveolar macrophages (AMs) (16, 17, 19, 20) and neutrophils (4) constitutively contain Ym1. In the bone marrow, Ym1 was reported to be expressed in myeloid cells (20), and subsequent studies have further located the expressing cells as myeloid progenitor cells (destined to be monocytes or neutrophils) (19) and immature neutrophils and large mononuclear cells (16). And as neutrophil progenitors mature,

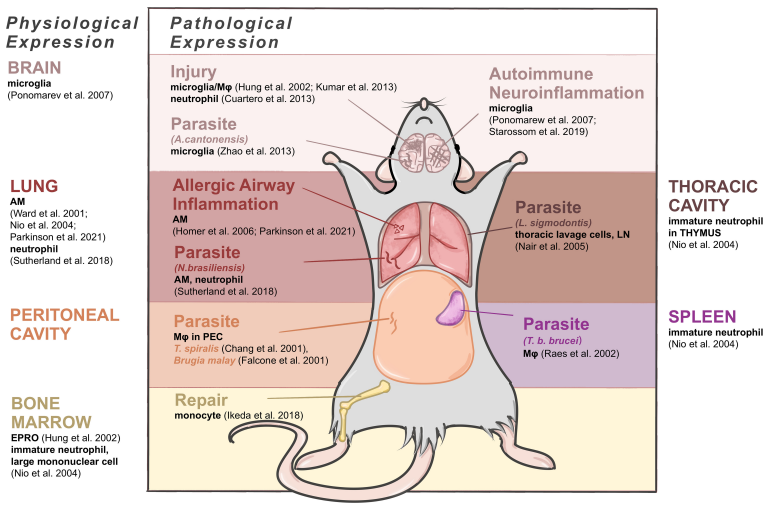

FIGURE 2
Expressing cells of Ym1 in mice under physiological and pathophysiological conditions. Brain produces Ym1 by M2-typed microglia normally, by microglia in the parasitic infection and autoimmune neuroinflammation, and by microglia, Mφ and neutrophils in injuries. Lungs express Ym1 by alveolar macrophages (AMs) and/or neutrophils in normal, allergic lung inflammation and parasitic conditions. Thoracic cavity and peritoneal cavity express Ym1 in parasite infection respectively by thoracic lavage cells and Mφ in peritoneal exudative cells. Spleen and bone marrow are also main normal origins of Ym1 performed by immature neutrophils. The former also produces increased Ym1 in Mφ during parasite infection, and the latter does it by monocytes when repairing tissue injuries.

their Ym1 expression will decrease to undetectable (16). Some bone marrow-derived cells, like osteoclast precursors (early immature proliferative mononuclear phagocytes) and mature osteoclasts (OCs) (21) and connective tissue type-like mast cells (22), were also detected to produce Ym1. Subsequent studies related to central and peripheral nervous system pointed out that alternatively activated microglia could also produce Ym1 in physiological condition, though at a relatively low level (23). And the accumulation of Ym1 protein in olfactory epithelia was observed during normal aging process (24).

For fetal mice, it might be noteworthy that during the development, the trace of Ym1 expression coincides with the migration of tissue resident Mφ. Ym1 is initially expressed in the yolk sac and then in the liver, spleen and bone marrow where early myeloid precursor cells in hematopoietic tissues undertake Ym1 expression, and later the expression of Ym1 in newborn mice reaches its peak in the liver and spleen (19). Similarly, the vast majority of tissue resident Mφ are derived from erythromyeloid progenitor cells (EMPs) in the yolk sac, including microglia in brain and AMs in lung, and EMPs then migrate and colonize in the newborn fetal liver as well (25). For newborn mice, Ym1 in the lung becomes detectable only about two weeks after birth, while their liver and spleen gradually decrease Ym1 production, and finally, the expression status becomes consistent with that of adult mice (19). In general, AMs and lung have a close link with Ym1 in terms of the development and physiological expression, also in terms of pathology and diseases actually, thus considerable research has been devoted to relevant fields.

Pathophysiological condition

Ym1 can be transiently induced according to various inflammatory stimuli. Allergic airway inflammation is one of the major causes of increased Ym expression. Ym1 is produced by AM (26) and contained in bronchoalveolar lavage fluid (BALF) (15, 27). Besides, parasite response enhances pulmonary Ym1 production as a universal feature (28). A quintessential example of Ym1 response to parasites was provided by the gastrointestinal nematode *Nippostrongylus brasiliensis (N. brasiliensis)*, in which Ym1 was detected in Mφ and neutrophils of lungs mainly, accompanied by a rising secretion but a reduced cell ratio (4).

In peritoneal cavity, the expression of Ym1 mainly appears in parasite infection, related to activated Mφ in peritoneal exudative cells, such as acute-phase response caused by *T. spiralis* (2) and *Brugia malay* (29). Similarly, the infection of parasite *L. sigmodontis* in thoracic cavity could also cause thoracic lavage cells to upregulate Ym1 expression (28).

In central nervous system (CNS), its expression level is upregulated during certain phases of neurotraumatic and neurodegenerative diseases, drug-induced epilepsy, autoimmune neuroinflammation as well as parasite infection (19, 24, 30), for which it has been regarded as a significant marker of the alternatively activated microglia/Mφ. Nevertheless, the specific cellular origins and time course concerning Ym1 expression under these circumstances remain elusive. Mice infected with *Angiostrongylus cantonensis* (*A. cantonensis*) were found to synthesize Ym1 primarily *via* microglia, while the infiltrating macrophages contributed more to producing Ym1 in the stroke-injured mice (31). It is also noteworthy that neutrophils can express Ym1 in the focal cerebral ischemia mice (32). In marked contrast to the CNS, Ym1 can be secreted by the supporting cells in the olfactory epithelium, and its distribution is less confined, ranging from the injured olfactory mucosa to the dorsolateral turbinates of the nasal cavity (24).

In other tissues and organs Ym1 expression in specific situations can be found as well. After *Trypanosoma brucei brucei* (*T. b. brucei*) infection, significant expression of Ym protein was detected in splenic Mφ (3). In the draining lymph nodes after parasitic infection, antigen-presenting cells were reported as the only cell group producing Ym1, most highly in B cells and Mφ (28). In traumatic wounds, Ym1 expression was restricted to granulation tissue, closely related to neutrophils rather than Mφ (33). Most of the pathological upregulation of Ym1 mentioned above emerged in the acute stage of inflammatory injury. Bone marrow, however, was observed an augment in Ym1 expression in the repairing period of tissue injury as well, explained by the fact that precursor cells of $Ly6C^{hi}$ monocytes differentiate and proliferate into Ym1-expressing monocytes ($Ym1^{+}Ly6C^{hi}$), which would infiltrate into corresponding injury sites (34).

In sum, under the stimulation of different pathogenic factors or in different phases of the same pathological process, the specific synthesis sites of Ym1 are different. These differences are gradually becoming crucial components of a proliferation of studies. What can be applied to various parts is that Mφ (including microglia) and neutrophils constitute the dominant Ym1 expressing cells in the pathological state.

Regulation of Ym1 expression

Previous studies have found that multiple inflammatory factors or stimulating drugs are able to induce or regulate the expression of Ym1 (as shown in Figure 3). It has been confirmed that Ym1 expression is mediated by STAT6 and induced by IL-4/IL-13 in Mφ, dendritic cells (DCs) (3, 10, 35–38) and microglia (39, 40), and Ym1 is the reigning Ym protein subtype induced by IL-4 (41). The effects of IL-4 and IL-13 are different to some extent, and IL-13 might offer a more powerful inducement on Ym1 expression *in vivo* (38). Intraperitoneal injection of anti-IL-4 antibody can block the expression of Ym1, but only the concomitant blocking on IL-4 and IL-13 can eliminate the induced Ym protein expression in BAL (10).

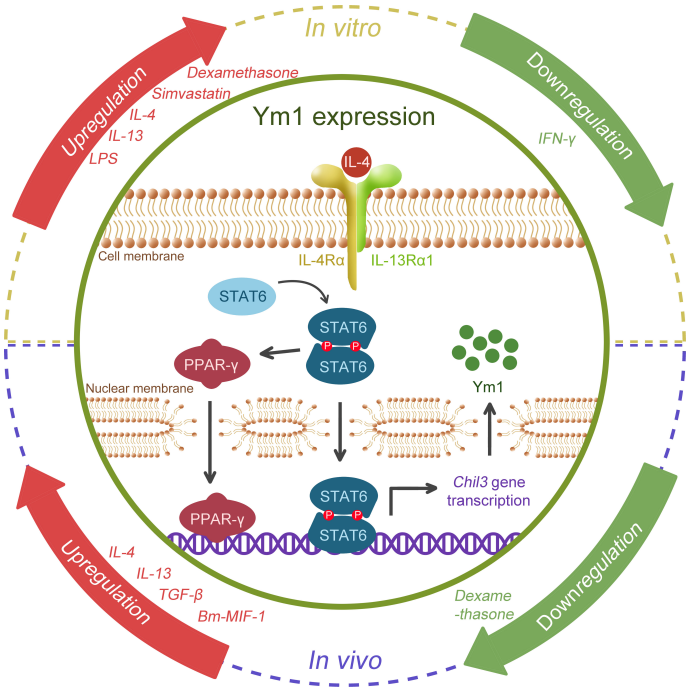

FIGURE 3
Schematic regulation of Ym1 expression. Various cytokines, drugs, microbial antigens are possible regulators. IL-4 and IL-13, the popular M2 drivers, were confirmed to promote Ym1 expression in both the *in vitro* and *in vivo* studies. TGF-β, Bm-MIF-1, LPS and Simvastatin were also found to be associated with Ym1 upregulation, and IFN-γ might correlate with its downregulation, while divergent views of dexamethasone remain in place. However, how Ym1 expression is fine-tuned by these signals remains elusive. The figure particularly illustrates the well-studied IL-4/STAT6 pathway. When stimulated by IL-4, STAT6 is phosphorylated, forming a homodimer and translocating to the nucleus, activating the gene transcription of *Chil3*. STAT6 can further activate PPAR-γ, which enhances *Chil3* expression cooperatively.

In addition, lipopolysaccharide (LPS) could boost the Ym protein expression induced by IL-4 *in vitro*, while IFN-γ could diminish the influence of IL-4, even causing Ym protein undetectable (3, 37). Glucocorticoids like dexamethasone were reported to induce Ym1 through STAT6, which have a co-enhancement effect with IL-4 on Ym1 (35). Simvastatin, a lipid-lowering drug, was also found to intensify Ym1 expression dependent on IL-4R (co-receptor of IL-4 and IL-13) (42). *In vivo*, endogenous TGF-β was reported to upregulate IL-4Rα, giving rise to a significant enhancement to the M2 activation of microglia caused by IL-4, thus increasing the synthesis and secretion of Ym1 (39, 40). Interestingly, opposite to its effects *in vitro*, dexamethasone was found to counteract the influence of IL-4 and reduce Ym1 expression in the ovalbumin (OVA)-induced asthma model (43). A cytokine homolog *Bm* macrophage migration inhibitory factor (MIF)-1 generated by the helminth parasite *Brugia malayi* showed an upregulating effect on Ym1 expression, in which case, IL-4 or IL-5 was not necessary for the induction of Ym1, but it remained unclear whether type 2 cytokines like IL-13 were required (29).

Moreover, accumulating evidence has suggested that the activation of immuno-metabolic regulatory peroxisome proliferator-activated receptor (PPAR)γ facilitates Ym1 expression in a STAT6-dependent manner. 15dPGJ2 (a natural PPARγ ligand) (44) and rosiglitazone (a PPARγ agonist) (32, 45) were reported to contribute to the Ym1 upregulation, while GW9662 (a selective antagonist) significantly blunted IL-4-induced Ym1 expression (46). Further, ChIP analysis proved Ym1 as one of the direct target genes of PPARγ (47), and the integrin $\alpha_V\beta_5$ may play a crucial role in PPARγ-induced Ym1 upregulation (48).

In general, it is prevalent to use Ym1 as one of the detecting markers of M2 Mφ (3), especially for M2a activation induced by IL-4/13 (49). Ym1 has also been proposed as a marker of alternative neutrophil (N2) polarization (32, 50). However, a recent study has found that the M2 phenotype was enhanced in *Chil3*-deficient mice, demonstrating that Ym1 may control or limit the M2 activation of Mφ (6). Ym1 protein was also found to be absorbed by wound healing Mφ in Stat6-deficient mice (33), which might suggest that there could be some loopholes in the application of Ym1 as a Mφ phenotype marker, and it is recommended to define the Mφ phenotype together with other markers. Besides, Ym1 was observed as a unique one with increased expression among STAT6-associated M2 markers

when STAT6 expression was augmented by the inhibitor of heat shock protein B1 (HSPB1) (51). These facts indicate that Ym1 serves as a function performer rather than a marker and zoom in the question that what the exact role of Ym1 is in M2 and relevant progress.

Role of Ym1 in diseases

Allergic lung inflammation

Allergic asthma is a chronic inflammatory disease of the lower respiratory tract, clinically leading to manifestations as recurrent wheezing, dyspnea, chest tightness and paroxysmal cough. Its pathophysiological features are inflammatory responses such as increased IgE synthesis, airway hyperresponsiveness, mucus hypersecretion and airway remodeling. The similar airway inflammation in lung can be modeled in mice challenged by some typical protein antigens like OVA or certain allergens like house dust mite (52). Recent studies have shown that the mechanisms driving the development of mild and severe asthma are different (53). Patients with mild and moderate asthma present a typical response, that is, helper T cell type 2 (Th2) inflammation, mediated by cytokines such as IL-4, IL-5 and IL-13, and eosinophilia (54). In contrast, patients with severe asthma could present a low Th2 and a high Th17 response, accompanied by neutrophil inflammation in airway (55). It was also found in mouse model that hyperresponsiveness could be induced without Th2 response but with increased IL-17 expression (56). Importantly, Ym1 has been found to be involved in the airway inflammation model in mice, and may lay effects on both types of mechanisms as shown in Figure 4.

On the one hand, Ym1 can intensify Th2 inflammatory response. The study on *Chil3*-deficient mice supports the effect of Ym1 on Th2 cytokines conclusively, as a fall was detected in the expression of IL-4 and IL-5 in *Chil3*-deficient mice during OVA induced pulmonary inflammation (6). This immunoregulatory effect of Ym1 was realized by M2 Mφ in disease. In human body, although the role of M2 Mφ has not been determined in asthma, it has been confirmed that the function of AMs in asthmatic patients is different from that of normal people (57). In the mouse model of allergic lung inflammation, Mφ tend to the M2 phenotype, which is considered unnecessary and should be inhibited by the body (58). Some studies, however, believe that the immune molecules on the M2 surface can mediate the uptake and clearance of allergens and control the development and severity of allergic inflammation, thus serving as protectors (59). Additionally, Ym1 or M2 could be unnecessary in the development of allergic airway disease, as IL-

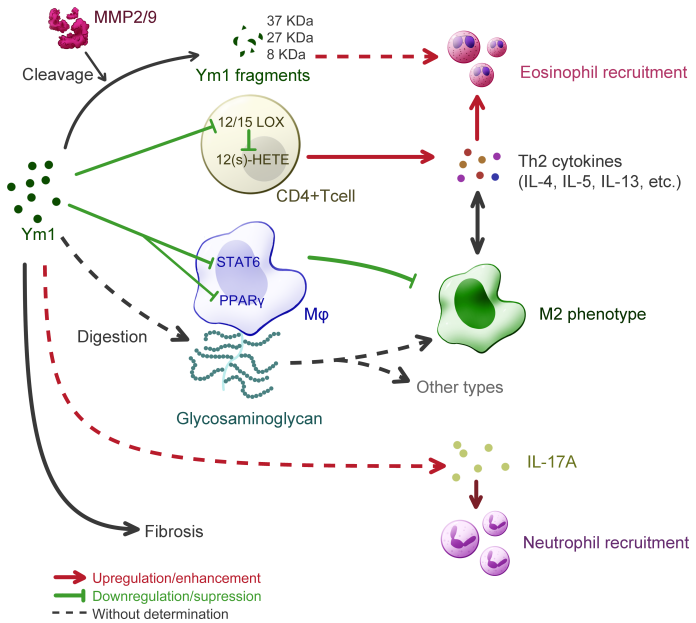

FIGURE 4
Understanding of Ym1 behavior in allergic lung inflammation in mice. The overall effect of Ym1 in Th2 allergic lung inflammation is intensifying eosinophil recruitment. Ym1 plays that in a combinatorial manner. Ym1 depresses 12/15(S)-lipoxygenase (12/15-LOX) in $CD4^+$ T cells and its catalysate 12-hydroxyeicosatetraenoic acid (12(S)-HETE), leading to the rise of Th2 cytokines. And Ym1 limits M2 polarization by downregulating the activation of STAT6 and PPAR-γ in macrophages. It might also regulate phenotypes directly by digesting glycosaminoglycan on macrophage surface. Matrix metalloproteinase (MMP) 2/9 engage in this system as Ym1 catalytic crackers, whose products may help to eosinophil recruitment. Ym1 recruits neutrophils as well, which may depend on IL-17 responses and contribute to lung inflammation. At the end of allergic lung inflammation, Ym1 may affect fibrosis to some extent.

4Rα-impaired mice were still found classic airway inflammation in histologic pathology with decreased level of Ym1 and other M2 markers (60). Considerable research has been devoted to exploring the role of M2 Mφ in allergic lung inflammation with the detection of Ym1 as a marker, rather less attention has been paid to that whether Ym1 itself influenced these models. It was found that *Chil3*-deficiency could enhance the alternative activation of Mφ by regulating the activation of STAT6 and PPARγ pathways to alleviate pulmonary inflammation (6). Besides, Ym1 might also influence Mφ more directly due to its weak β-*N*-acetylglucosaminidase activity, which means a possibility to contribute to the digestion of glycosaminoglycans (5). Ym1 was presumed to involve in fine-tuning at the level of HS in Mφ, thereby affecting the activation of Mφ (49). DCs have also been demonstrated to generate Ym protein in response to IL-13 in the OVA-induced respiratory allergy, in which case Ym protein downregulated the activity of 12/15(S)-lipoxygenase (12/15-LOX) and the following products, 12-hydroxyeicosatetraenoic acid (12(S)-HETE), thereby enhancing the ability of $CD4^+$ T cells to produce Th2 cytokines such as IL-5, IL-13, etc (61).

In addition, Ym1 may recruit eosinophils with the participation of matrix metalloproteinase (MMP) family. It was proposed that Ym1 protein might be modified or cleaved by MMPs to participate in the chemotaxis of eosinophils (62). In the complete *Aspergillus* allergen (CAA)-induced mouse model, multiple cleavage fragments of Ym1 protein were observed in BALF of wild-type mice, while more complete Ym1 protein in that of MMP2 and MMP9 double null ($MMP2/9^{-/-}$) mice, and the number of eosinophils was also reduced. Ym1 was also proven to be the substrate of MMP2/9 and products would be 37 kDa, ~27 kDa and ~8 kDa peptide fragments. As MMPs are reported to clear allergic inflammatory cells in the lung by hydrolyzing protein, and MMP2 and MMP9 could also regulate the activity of Th2 chemokine, Ym1 may play a role in linking MMPs and eosinophils and participate in regulating the migration of allergic inflammatory cells to the pulmonary vesicle. By far, however, this view still lacks direct evidence.

On the other hand, in recent years, considerable literature has grown up around the role of IL-17 and neutrophils in allergic lung inflammation, and the influence of Ym1 is worthy of more attention. Ym1 may influence the recruitment of neutrophils by regulating IL-17 produced by γδT cells, which plays a key role in neutrophil-mediated defensive immunity (7, 63). And after anti-Ym1 antibody treatment, the number and proportion of neutrophils in the lung were decreased, and the expression of IL-17A and IL-17A target genes were also reduced (7). But in this case, eosinophilia, goblet cell proliferation and apnea enhancement did not show significant difference, so that further investigation is needed to prove the role of Ym1 in IL-17 related allergic inflammation in lung. In addition, in most models of airway inflammation for Ym1 study, mice were sensitized by OVA. LPS challenge, however, was suggested to realize the pathological state with strong Th17 response and modest Th2 response (64), thus might be a worth tool for studying the relationship between IL-17 and Ym1 in allergic inflammation, which has not gained enough attention.

Fibrosis is subject to Th2 and Th17 responses at the end stage of chronic inflammation like asthma, where M2 plays a vital role (65). Although no evidence has showed direct connection between Ym1 and fibrosis, J2, a pulmonary fibrosis suppressor, was found to upregulate Ym1 expression of M2 in the anti-fibrosis progress (51), which elucidated a possibility that Ym1 alleviates pulmonary fibrosis.

Parasitic infection

Anti-parasitic immunity is characterized by eosinophilia and Th2 cytokines. In most anti-parasitic response studies in mice, Ym1 is regarded as a bridge between M2a cells and eosinophils, that is, Ym1 is secreted by Mφ activated by parasite antigens, and then participates in the recruitment of eosinophils to the injury site. For example, Bm-MIF-1 secreted by *Brugia malayi* was found involved in activating Mφ, inducing the upregulation of Ym1 expression, and cooperating with IL-5 to recruit eosinophils in a manner that is partially dependent on IL-4 (29). In another case, the larvae of *A.cantonensis* breaking into brain, was reported to induce M2 polarization of microglia and infiltrating Mφ within the CNS which then synthesized and secreted Ym1 in large quantities, accompanied by an increase in eosinophils (30). This idea was reinforced by an earlier study which confirmed the direct chemotactic effect of Ym on eosinophils *in vitro* (18). In this study recombinant Ym protein was applied to the back of mice subcutaneously in parasitic settings, and the result was consistent as Ym protein caused an abundant local recruitment of eosinophils. Nevertheless, people have not yet clarified the specific mechanism by which Ym1 protein "recruits" eosinophils. In the peritonitis, the expression of Ym1 was not proposed as a precondition for the recruitment of eosinophils, which means a possible substitutability of Ym1 in mice (10). In addition, an overexpression model through plasmid transfection showed that the exogenous expression of Ym1 protein in the lungs led to a decrease in the number of eosinophils but an increase in neutrophils (7). The differences among above studies might resulted from different situation (overexpression and different inflammatory models), but it at least indicates that inflammatory microenvironment could convert Ym1's chemoattractant state.

Interestingly, in terms of Th2 cytokine response, Ym1 can play diametrically opposite roles in different stages of parasite response. After injecting anti-Ym1 antibodies into the peritoneal cavity, mice infected with *N. brasiliensis* were found that blocking Ym1 in the early innate immune stage could reduce the amount of Th2 cytokines in mice; after the establishment of an adaptive type 2 response, blocking Ym1 did not inhibit their expression, but significantly increased the number of cells expressing these factors (4). Although the

reason why the effect of Ym1 changes with the course of the immune response has not yet been discovered, it again supports the multifaceted function of Ym1 in different inflammatory microenvironment.

In recent years, the role of neutrophils in the immune response against parasitic infection as well as its relationship with Ym1 has drawn researchers' attention. Similar to eosinophils, as the "forerunner" of innate immunity, neutrophils also play a dual role in anti-parasitic immunity besides phagocytosis and initiation of Th2 response, and need to be contained in the later stage for inflammation resolution and tissue repair (66). In *N. brasiliensis*-infected mice, it was found that IL-17 and neutrophilic inflammation induced by Ym1 could impair parasite survival but at the cost of enhanced lung injury (7). This result suggested that Ym1 could be cursed blessing as well, and showed a possibility of Ym1 in the recruitment of neutrophils through regulating IL-17 production.

Autoimmune diseases

Autoimmune diseases are a pathophysiological state, wherein the immune responses are directed against and damage the body's own tissues, such as rheumatoid arthritis (RA) and psoriasis (Ps). Ym1 had been positionally identified to be associated with autoimmune arthritis, using collagen-induced arthritis (CIA) mouse model (67, 68). Later, a protective effect due to Ym1 deficiency using Ym1 congenic mice absent in Ym1 expression (6), was confirmed in collagen antibody induced arthritis (CAIA) model and mannan induced Ps model, both of which are Mφ dependent, and adaptive immune independent (69–71). The study also discovered that Ym1 protein i.n. supplement could reverse this effect in mannan induced Ps model of Ym1-low-expression mice, while AM depletion attenuated the disease. These results proved that Ym1 is one of the factors responsible for the development of skin and joint inflammation, and strongly suggested that Ym1 may participate in the diseases through regulating Mφ and innate immunity. However, how the M2 regulation from Ym1 in lung can ripple through the systemic autoimmunity remains unclear.

As for autoimmune neuroinflammatory diseases, the experimental autoimmune encephalomyelitis (EAE), which models the pathology of multiple sclerosis (MS) in mice, is often used to study the corresponding molecular mechanisms and treatment strategies. It was clarified that Ym1 was able to activate epidermal growth factor receptor (EGFR) and affected the directional differentiation of endogenous neural stem cells (NSCs) through the CLPs-EGFR-Pyk2 pathway by using EAE model mice (8). Therefore, drugs targeting the CLPs-EGFR-Pyk2 signaling axis may be used to treat acute demyelinating diseases such as neuromyelitis optica and relapsing multiple sclerosis. However, whether there is a direct interaction between Ym1 and EGFR as well as the proteins involved in the subsequent cascade needs to be further confirmed at the molecular level.

Nervous system diseases

In the context of nervous system diseases, most studies related to Ym1 fail to uncover its detailed function, where Ym1 usually takes the supporting role for marking M2. This is because the immune response compared with diseases occurring in other tissues and organs is more sophisticated, considering the difficulty of distinguishing resident microglia from recruited macrophages and outlining the temporal change in their polarization change under various stimuli (72). Meanwhile, it is still debatable whether Ym1 is a bona fide marker of M2-like cells or not, since Ym1 was observed to be upregulated with LPS exposure (a kind of M1 stimulation) alone (73). By far, Ym1 and its expression in traumatic injury and ischemic stroke is more recognizable. Therefore, the following section will focus primarily on these two types of diseases. Figure 5 helped summarize the proposed functions of Ym1 from some key findings, which also included the aforementioned demyelinating diseases and bacterial infection.

Ischemic stroke is the primary type of cerebrovascular insult with high mortality risk. To unravel the mechanism of its immune response, Ym1 has greatly aided in the identification of microglia/Mφ polarization and a novel subpopulation of neutrophils (32). Researchers using the upregulated Ym1 expression to represent the neuroprotective cell phenotype, generally agreed on an increased M2-like state in the acute phase followed by an M1-like one in the subacute and chronic phase, though they didn't specify the cellular origin of Ym1 until they started to analyze the cell specificity of each phenotype. Some pieces of research consistently suggested that recruited Mφ contributed remarkably to the gene expression of Ym1 at the early stage of ischemic stroke (74–76), whereas microglia was more pro-inflammatory and suppressive until about one week after stroke induction (76), with its *Chil3* promoter activity elevated for at least 14 days (31). In terms of Ym1's function, the correlation between the upregulated *Chil3* mRNA and better post-stroke recovery was observed, including more neurovascular units (31), reduced infarct volume (75, 76), improved sensorimotor ability (74, 76), which could justify the protective role of Ym1. Besides, several intriguing findings of Ym1 are worth digging into, like its distribution was spatiotemporal (77) and its maximal expression and the time to peak didn't seem to correlate with the lesion size (31). Hence, further investigations should monitor the actions of Ym1 protein over different regions and with different severity of stroke.

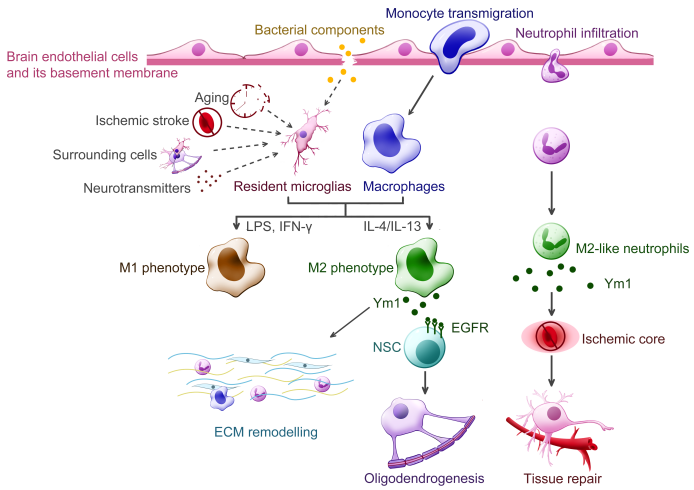

FIGURE 5
Putative functions of Ym1 in the central nervous system diseases. Various inflammatory stimuli promote the expression of Ym1, including bacterial infection, traumatic injury, ischemic stroke, aging and certain cytokines released from the surrounding cells. In the CNS, Ym1 is expressed and secreted by alternatively activated myeloid cells, including resident microglia, recruited macrophages, and even a subpopulation of neutrophils. Ym1 is proposed to facilitate extracellular matrix (ECM) remodeling for its binding specificity to particular components like heparan sulfate. In demyelinating diseases, Ym1 may bind to epidermal growth factor receptor (EGFR) of the neural stem cells (NSCs) and activate the Ym1-EGFR-Pyk2 pathway, leading to oligodendrogenesis. The Ym1-expressing neutrophils display increased ability to infiltrate the ischemic core and undergo phagocytosis, thereby contributing to inflammation resolution and neuroprotection.

In response to traumatic injury, a series of orchestrated events occur in the peripheral nervous system (PNS) and CNS, where the activation and polarization of microglia/Mφ play a crucial role. Early studies found that Ym1 was heterogeneously expressed in penetrating brain injury and epileptic seizures (19), and it has been gradually used to mark M2-like microglia/Mφ, guiding us to learn the actions of immune cells in turn (78). Indeed, an increasing body of research has centered on the temporal profile of microglia/Mφ polarization, enabling us to determine which phenotype to enhance or suppress. Ym1, although typically represented the M2 phenotype (specifically the M2a (79) and M2c (72) marker) and upregulated both in the early inflammation stage and the later remodeling stage, has not been adequately studied yet. Ym1's putative function in neuroinflammation and tissue repair is essentially based on its binding specificity to N-unsubstituted GlcN polymers and HS (2). Hence Ym1 is likely to antagonize inflammation by slowing down leukocyte adhesion and promote tissue repair by preventing HS from damage. In addition to its help in remyelination (8), only a few studies focused on its involvement in post-injury reactions. For instance, it was found that the accumulation of Ym1 protein within the injured olfactory epithelia was closely related to the inflammatory and healing process, with its level decreasing once tissue regeneration was achieved (24). In sum, to define Ym1's function as neuroprotective still requires closer observations in its protein interactions with surrounding cells and tissues during the progression of neurotrauma.

Crystallization of Ym1 *in vivo*

Crystals rarely spontaneously form in animals, but some proteins do spontaneously crystallize in animals under certain conditions. The typical example in the human body is Charcot-Leyden Crystals (CLCs), found by Ernst Viktor von Leyden in the sputum of patients with asthma in 1872. Subsequent studies found that the blood separated from patients with bronchial asthma was easy to form CLCs after lysis (80). Besides, eosinophilic crystals with similar morphology were observed in mice with lung cancer and mutant mice infected with *Pneumocystis carinii*. These crystals were finally confirmed to be Ym1, with similar morphology but different biochemical properties to CLCs (81).

In vivo crystallization of Ym1 was observed in many mouse models (see Table 1). In 1999, transgenic mice with over-expression of IL-13 had crystals similar to that of Charcot-Leyden crystals in the lungs, which were later confirmed as Ym1 (86, 90). In the same year, eosinophilic crystals with different shapes and sizes were observed in alveolar macrophages and multinucleated giant cells of a variety of immunodeficient mice, including Moth-eaten mice (viable motheaten mice, me^v/me^v), SPCTNFRIIFc transgenic mice, and CD40L-deficient mice spontaneously infected with *Pneumocystis carinii*. These crystals were distributed in the activated alveolar macrophages and dispersed in the lungs of young mice, while crystals located both intracellular and extracellular in the dying me^v/me^v mice and SPCTNFRIIFc transgenic mice (81). It is worth noting that

TABLE 1 Crystals formed in mice.

Mouse Models	Model Characters					Crystals		Reference
	Strain of Origin	Type of Gene Editing	Gene	Primary Effects	Diseases/Abnormal Effects	Location	Morphology	
***me*^{v}/*me*^{v} mice (viable motheaten mice)**	C57BL/6J	Spontaneous mutation (recessive, single point)	*Ptpn6* gene, *motheaten (me)* locus on Chr6	SHP-1 protein tyrosine phosphatase activity deficiency	Severe autoimmune disease, premature death of pneumonitis, hematopoietic disorders, immune cell abnormality (hyperactivity of AM, lymphocytes, granulocytes in the lungs)	M2 and matrix in lungs	Long, rectangular crystals in tissues, flat crystals (10-μm^2) and multifaceted crystals (20-120 μm) in BAL fluid of *me*^{v}/*me*^{v} mice	(81–83)
CD40L-deficient mice infected with *P. carinii*	C57BL/6C57BL/6NTac × Sv/129	Gene knockout	*CD40L* gene	CD40 ligand of activated T-cells deficiency (immunoglobulin isotype switching failure)	X-linked hyper-IgM syndrome, severe respiratory infection (cannot defend against *P. carinii*)	M2 in lungs		(81, 84)
SPCTNFRIIFc transgenic mice	C57BL/6NTac × Sv/129	Transgenic	Surfactant apoprotein C promotor/soluble TNF receptor p75 (type II)-Fc fusion protein	lung-specific protein sTNFRIIFc expression (a soluble TNF inhibitor)	Depression on TNF-α responses in lungs	M2 and occasionally matrix in lungs		(81, 85)
mice with over-expression of IL-13	CBA × C57BL/6	Transgenic	Clara cell 10-kDa protein (CC10) promoter/IL-13	IL-13 over-expression in airway	Asthma-like inflammatory responses in lungs	Eosinophils and AM in alveoli and occasionally in airways	Needle-like crystals	(86)
C57BL/6 infected with *C. neoformans*	C57BL/6	–	–	–	Eosinophilic pneumonia (immune responses to microorganisms containing chitin)	Mφ-originated large multinucleated cells in lungs	Needle-like crystals (protruded through the membrane of some cells)*without strict determination of Ym1	(87)
p47$^{phox\ -/-}$ mice	129	Gene knockout	*p47^{phox}* gene	p47phox subunit defect of NADPH oxidase in phagocytes	Chronic granulomatous disease	Lung matrix in aged mice (related to giant cells and Mφ)Bile ductsSpontaneous skin abscesses	Multifaceted crystals (10-100 μm)	(5)
***Hpse*$^{-/-}$ transgenic mice**	C57BL/6J	Gene knockout	*Heparanase* gene	Heparanase-deficient	Normally no major abnormalities	AM	Needle-like crystals	(88)
ddY mice	ddY	–	-	–	Spontaneous IgA nephropathy	Mφ in bone morrow (frequently with several erythroblasts)	Needle-like crystals*without strict determination of Ym1	(16, 89)

AM, alveolar macrophages; M2, alternatively activated macrophages.

14 days after C57BL/6 mice are infected with *Cryptococcus neoformans*, the crystal structure was also visible in the lungs, which is similar to that of Ym1. Studies also found some crystals, whose composition was not strictly analyzed, formed at the edge of the polysaccharide membrane, and the progress was closely related to the deposition of intracellular polysaccharide CNPS, suggesting that bacterial capsular polysaccharides contributed to the protein enrichment of this crystal (87). Given that *Cryptococcus neoformans* also contain chitin and that Ym1 may be part of the host's response to microorganisms containing chitin, this crystal is likely to be Ym1. Shortly afterward, Ym1 crystal was also found in p47phox $^{-/-}$ (p47phox subunit defect of NADPH oxidase) mice. This multifaceted crystal appeared outside the lung of mice older than two months and increased with age (5). Also, p47phox deficiency will cause macrophage dysfunction and eventually

lead to progressive crystalline macrophage pneumonia (91). In tissue sections, the morphology of these Ym1 crystals has been described as intracellular fine needle-like crystals and flat, faceted crystals in BALF (5, 16, 81), thus providing new clues when similar crystals arise under some cases. In 2010, needle-like crystals were observed in the lung macrophages of the constructed heparanase-deficient mice ($Hpse^{-/-}$), which were surrounded by membranes, suggesting that they are developed in capsule organelles such as lysosomes, endoplasmic reticulum or Golgi bodies. It is conclusively demonstrated that Ym1 is the crystal formation unit of $Hpse^{-/-}$ alveolar macrophages, and heparanase regulates the accumulation and crystal formation of Ym1 in the airway (88). At the same time, in addition to various models or mice under specific conditions, several studies pointed out that Ym1 crystals or Ym1 protein accumulation existed in normal mouse lung macrophages (81, 88).

In line with the tissue expression of Ym1 protein, Ym1 crystals were primarily found in the lungs, while they could also present outside the lungs. Membrane-encapsulated needle Ym1-immunoreactive crystals have been detected in macrophages in the bone marrow of ddY mice with spontaneous IgA nephropathy. The study also found that Ym1 was produced mainly by immature neutrophils and Ym1 may be phagocytosed by macrophages after forming crystals outside the cells, or directly absorbed by macrophages and crystallized in the cytoplasm (16).

In the above studies, there seems to be no clear relationship between the crystallization of Ym1 protein, but when crystals appear, Ym1 tends to show a state of high expression or abnormal protein degradation, resulting in the accumulation of Ym1 protein. At the same time, environmental factors are conducive to the formation of crystals. The high expression of Ym1 may be related to the function of Ym1 or the function of its ancestral genes (such as interaction with heparin, chitin and other substances). The pathological changes of tissues under different diseases may also provide similar environments for Ym1 crystallization (such as pH), which may be a new idea to study the causes of crystals.

Ym1 crystallization is a strong signal of lung inflammation and injury. As mentioned above, after purifying and identifying the Ym1 protein crystal in the BALF of me^{v}/me^{v} mice, plenty of eosinophils were also observed in lungs (81). Collectively, Ym1 crystal was considered to be a reflection of the response to severe parasitic eosinophilic pneumonia. Besides, the formation of Ym1 crystal itself could also damage cell membrane mechanically and lead to cell death (87). Bronchial epithelial rupture directly leads to lung injury, and macrophage rupture death interferes with host defense mechanisms and causes persistent infection. Some studies suggested that Ym1 crystal might directly activate inflammatory bodies *in vivo*, resulting in lung injury (7). However, similar to CLCs in human body, relevant studies usually only observed the presence of Ym1 crystals in severe inflammatory environments. The role of crystals remains to be dug out.

Discussion

In sum, Ym1 is expressed or upregulated under various pathological conditions, particularly the lung diseases. As a traditional M2 marker, Ym1 itself has not received adequate attention, given that most relevant studies focused on the Ym1-producing cells, including macrophages and microglia. However, we could comb out some intriguing clues to Ym1's functions from previous literature resources. Current models demonstrate that the role of Ym1, albeit pleiotropic and dynamic, lays parallels between allergic lung inflammation and pulmonary parasite infection. Ym1 participates in these inflammatory responses generally in two ways, the modulation of Mφ polarization and the recruitment of eosinophils and neutrophils. And in both diseases, Ym1 generally shows association with two trends, the enhancement of Th2 response and IL-17 production, and the latter is gathering more attention. However, it is worth-noting that Ym1 displays time-dependent function in tissue repair and inflammation resolution. Ym1 not only promotes reparative Th2 response in the early phase of inflammation (34), but can reduce IL-5/IL-13 expression and regulate Th2 balance once the repair initiate (4). For skin and joint autoimmune inflammation, Ym1 contributes to its development through innate immunity, especially M2. In respect to the nervous system diseases, although existing research hardly distinguishes the cellular origins of Ym1, it generally agrees that Ym1s upregulation correlates with improved prognosis in most cases. A few Ym1-centered studies attempted to map the possible signal pathways for oligodendrogenesis, and to understand the relationships of Ym1 protein accumulation with olfactory epithelium injury, but the follow-up research is still lacking.

Considering that abundant C/CLPs exist in human bodies, despite no real homologous gene for Ym1, research on Ym1 has significance in facilitating the understanding of human C/CLPs in diseases. In addition, Ym1 is one of the only proteins that can form crystals in mice. Ym1 crystals are still poorly unraveled, but further explorations may help decipher the confusing eosinophilic crystals in human bodies, like CLCs in lungs. Previous work has not furnished details on how Ym1 exerts influence on other immune mediators like Th2 and Th17 cytokines or on the hierarchy of their actions in inflammatory responses. Thus, figuring out the position of Ym1 on these interactive networks is beneficial for revealing disease pathogenesis and finding optimal treatment targets and strategies. Besides, the kinetics of Ym1 expression is rather

complex, depending on the site, mode and severity of injury. And recent research has cast doubt on whether Ym1 is a bona fide M2 marker. Hence future work should give the expression patterns of Ym1 upon different stimuli sufficient consideration.

Author contributions

QK, LL and YP drafted the original manuscript, and WZ and LM advised on the outline and revised the manuscript. All authors contributed to the article and approved the submitted version.

Funding

This work is supported by the National Natural Science Foundation of China (82171724, 82171784 and 81970029), and College Students' Innovative Entrepreneurial Training Plan Program, Ministry of Education, China (S202110698612).

Acknowledgement

We thank Huaizhi Jing from Xi'an Jiaotong University for collecting part of the literatures.

Conflict of interest

The authors declare that the research was conducted in the absence of any commercial or financial relationships that could be construed as a potential conflict of interest.

Publisher's note

References

1. Elieh-Ali-Komi D, Hamblin MR. Chitin and chitosan: Production and application of versatile biomedical nanomaterials. *Int J advanced Res* (2016) 4 (3):411–27.

2. Chang NC, Hung SI, Hwa KY, Kato I, Chen JE, Liu CH, et al. A macrophage protein, Ym1, transiently expressed during inflammation is a novel mammalian lectin. *J Biol Chem* (2001) 276(20):17497–506. doi: 10.1074/jbc.M010417200

3. Raes G, Noel W, Beschin A, Brys L, de Baetselier P, Hassanzadeh GH. FIZZ1 and ym as tools to discriminate between differentially activated macrophages. *Dev Immunol* (2002) 9(3):151–9. doi: 10.1080/1044667031000137629

4. Sutherland TE, Ruckerl D, Logan N, Duncan S, Wynn TA, Allen JE, et al. Ym1 induces RELMalpha and rescues IL-4Ralpha deficiency in lung repair during nematode infection. *PloS Pathog* (2018) 14(11):e1007423. doi: 10.1371/journal.ppat.1007423

5. Harbord M, Novelli M, Canas B, Power D, Davis C, Godovac-Zimmermann J, et al. Ym1 is a neutrophil granule protein that crystallizes in p47phox-deficient mice. *J Biol Chem* (2002) 277(7):5468–75. doi: 10.1074/jbc.M110635200

6. Zhu WH, Lonnblom E, Forster M, Johannesson M, Tao P, Meng LS, et al. Natural polymorphism of Ym1 regulates pneumonitis through alternative activation of macrophages. *Sci Adv* (2020) 6(43):eaba9337. doi: 10.1126/sciadv.aba9337

7. Sutherland TE, Logan N, Ruckerl D, Humbles AA, Allan SM, Papayannopoulos V, et al. Chitinase-like proteins promote IL-17-mediated neutrophilia in a tradeoff between nematode killing and host damage. *Nat Immunol* (2014) 15(12):1116–25. doi: 10.1038/ni.3023

8. Starossom SC, Campo Garcia J, Woelfle T, Romero-Suarez S, Olah M, Watanabe F, et al. Chi3l3 induces oligodendrogenesis in an experimental model of autoimmune neuroinflammation. *Nat Commun* (2019) 10(1):217. doi: 10.1038/s41467-018-08140-7

9. Jin HM, Copeland NG, Gilbert DJ, Jenkins NA, Kirkpatrick RB, Rosenberg M. Genetic characterization of the murine Ym1 gene and identification of a cluster of highly homologous genes. *Genomics* (1998) 54(2):316–22. doi: 10.1006/geno.1998.5593

10. Welch JS, Escoubet-Lozach L, Sykes DB, Liddiard K, Greaves DR, Glass CK, et al. TH2 cytokines and allergic challenge induce Ym1 expression in macrophages by a STAT6-dependent mechanism. *J Biol Chem* (2002) 277(45):42821–9. doi: 10.1074/jbc.M205873200

11. Sun YJ, Chang NC, Hung SI, Chang AC, Chou CC, Hsiao CD. The crystal structure of a novel mammalian lectin, Ym1, suggests a saccharide binding site. *J Biol Chem* (2001) 276(20):17507–14. doi: 10.1074/jbc.M010416200

12. Tsai ML, Liaw SH, Chang NC. The crystal structure of Ym1 at 1.31 a resolution. *J Struct Biol* (2004) 148(3):290–6. doi: 10.1016/j.jsb.2004.07.002

13. Hussain M, Wilson JB. New paralogues and revised time line in the expansion of the vertebrate GH18 family. *J Mol Evol* (2013) 76(4):240–60. doi: 10.1007/s00239-013-9553-4

14. Ohno M, Kida Y, Sakaguchi M, Sugahara Y, Oyama F. Establishment of a quantitative PCR system for discriminating chitinase-like proteins: catalytically inactive breast regression protein-39 and Ym1 are constitutive genes in mouse lung. *BMC Mol Biol* (2014) 15:23. doi: 10.1186/1471-2199-15-23

15. Webb DC, McKenzie AN, Foster PS. Expression of the Ym2 lectin-binding protein is dependent on interleukin (IL)-4 and IL-13 signal transduction: identification of a novel allergy-associated protein. *J Biol Chem* (2001) 276 (45):41969–76. doi: 10.1074/jbc.M106223200

16. Nio J, Fujimoto W, Konno A, Kon Y, Owhashi M, Iwanaga T. Cellular expression of murine Ym1 and Ym2, chitinase family proteins, as revealed by *in situ* hybridization and immunohistochemistry. *Histochem Cell Biol* (2004) 121 (6):473–82. doi: 10.1007/s00418-004-0654-4

17. Parkinson JE, Pearson S, Ruckerl D, Allen JE, Sutherland TE. The magnitude of airway remodeling is not altered by distinct allergic inflammatory responses in BALB/c versus C57BL/6 mice but matrix composition differs. *Immunol Cell Biol* (2021) 99(6):640–55. doi: 10.1111/imcb.12448

18. Owhashi M, Arita H, Hayai N. Identification of a novel eosinophil chemotactic cytokine (ECF-l) as a chitinase family protein. *J Biol Chem* (2000) 275(2):1279–86. doi: 10.1074/jbc.275.2.1279

19. Hung SI, Chang AC, Kato I, Chang NC. Transient expression of Ym1, a heparin-binding lectin, during developmental hematopoiesis and inflammation. *J Leukoc Biol* (2002) 72(1):72–82. doi: 10.1189/jlb.72.1.72

20. Ward JM, Yoon M, Anver MR, Haines DC, Kudo G, Gonzalez FJ, et al. Hyalinosis and Ym1/Ym2 gene expression in the stomach and respiratory tract of 129S4/SvJae and wild-type and CYP1A2-null B6, 129 mice. *Am J Pathol* (2001) 158 (1):323–32. doi: 10.1016/S0002-9440(10)63972-7

21. Oba Y, Chung HY, Choi SJ, Roodman GD. Eosinophil chemotactic factor-l (ECF-l): a novel osteoclast stimulating factor. *J Bone Miner Res* (2003) 18(7):1332–41. doi: 10.1359/jbmr.2003.18.7.1332

22. Lee E, Yook J, Haa K, Chang HW. Induction of Ym1/2 in mouse bone marrow-derived mast cells by IL-4 and identification of Ym1/2 in connective tissue type-like mast cells derived from bone marrow cells cultured with IL-4 and stem cell factor. *Immunol Cell Biol* (2005) 83(5):468–74. doi: 10.1111/j.1440-1711.2005.01352.x

23. Ponomarev ED, Maresz K, Tan Y, Dittel BN. CNS-derived interleukin-4 is essential for the regulation of autoimmune inflammation and induces a state of alternative activation in microglial cells. *J Neurosci* (2007) 27(40):10714–21. doi: 10.1523/JNEUROSCI.1922-07.2007

24. Giannetti N, Moyse E, Ducray A, Bondier JR, Jourdan F, Propper A, et al. Accumulation of Ym1/2 protein in the mouse olfactory epithelium during regeneration and aging. *Neuroscience* (2004) 123(4):907–17. doi: 10.1016/j.neuroscience.2003.09.024

25. Gomez Perdiguero E, Klapproth K, Schulz C, Busch K, Azzoni E, Crozet L, et al. Tissue-resident macrophages originate from yolk-sac-derived erythro-myeloid progenitors. *Nature* (2015) 518(7540):547–51. doi: 10.1038/nature13989

26. Homer RJ, Zhu Z, Cohn L, Lee CG, White WI, Chen S, et al. Differential expression of chitinases identify subsets of murine airway epithelial cells in allergic inflammation. *Am J Physiol Lung Cell Mol Physiol* (2006) 291(3):L502–11. doi: 10.1152/ajplung.00364.2005

27. Zhang L, Wang M, Kang X, Boontheung P, Li N, Nel AE, et al. Oxidative stress and asthma: proteome analysis of chitinase-like proteins and FIZZ1 in lung tissue and bronchoalveolar lavage fluid. *J Proteome Res* (2009) 8(4):1631–8. doi: 10.1021/pr800685h

28. Nair MG, Gallagher IJ, Taylor MD, Loke P, Coulson PS, Wilson RA, et al. Chitinase and fizz family members are a generalized feature of nematode infection with selective upregulation of Ym1 and Fizz1 by antigen-presenting cells. *Infect Immun* (2005) 73(1):385–94. doi: 10.1128/IAI.73.1.385-394.2005

29. Falcone FH, Loke P, Zang X, MacDonald AS, Maizels RM, Allen JE, et al. A brugia malayi homolog of macrophage migration inhibitory factor reveals an important link between macrophages and eosinophil recruitment during nematode infection. *J Immunol* (2001) 167(9):5348–54. doi: 10.4049/jimmunol.167.9.5348

30. Zhao J, Lv Z, Wang F, Wei J, Zhang Q, Li S, et al. Ym1, an eosinophilic chemotactic factor, participates in the brain inflammation induced by angiostrongylus cantonensis in mice. *Parasitol Res* (2013) 112(7):2689–95. doi: 10.1007/s00436-013-3436-x

31. Collmann FM, Pijnenburg R, Hamzei-Taj S, Minassian A, Folz-Donahue K, Kukat C, et al. Individual in vivo profiles of microglia polarization after stroke, represented by the genes iNOS and Ym1. *Front Immunol* (2019) 10:. doi: 10.3389/fimmu.2019.01236

32. Cuartero MI, Ballesteros I, Moraga A, Nombela F, Vivancos J, Hamilton JA, et al. N2 neutrophils, novel players in brain inflammation after stroke: modulation by the PPARgamma agonist rosiglitazone. *Stroke* (2013) 44(12):3498–508. doi: 10.1161/STROKEAHA.113.002470

33. Goren I, Pfeilschifter J, Frank S. Uptake of neutrophil-derived Ym1 protein distinguishes wound macrophages in the absence of interleukin-4 signaling in murine wound healing. *Am J Pathol* (2014) 184(12):3249–61. doi: 10.1016/j.ajpath.2014.08.011

34. Ikeda N, Asano K, Kikuchi K, Uchida Y, Ikegami H, Takagi R, et al. Emergence of immunoregulatory Ym1(+)Ly6C(hi) monocytes during recovery phase of tissue injury. *Sci Immunol* (2018) 3(28):eaat0207. doi: 10.1126/sciimmunol.aat0207

35. Ng Kuet Leong N, Leong N, Brombacher F, Dalpke AH, Weitnauer M. Crosstalk between glucocorticoids and IL-4 modulates Ym1 expression in alternatively activated myeloid cells. *Immunobiology* (2017) 222(5):759–67. doi: 10.1016/j.imbio.2017.02.003

36. Dasgupta P, Chapoval SP, Smith EP, Keegan AD. Transfer of *in vivo* primed transgenic T cells supports allergic lung inflammation and FIZZ1 and Ym1 production in an IL-4Rα and STAT6 dependent manner. *BMC Immunol* (2011) 12:60. doi: 10.1186/1471-2172-12-60

37. Raes G, De Baetselier P, Noël W, Beschin A, Brombacher F, Hassanzadeh Gh G, et al. Differential expression of FIZZ1 and Ym1 in alternatively versus classically activated macrophages. *J Leukoc Biol* (2002) 71(4):597–602. doi: 10.1189/jlb.71.4.597

38. Wu F, Wei J, Liu Z, Zeng X, Yu Z, Lv Z, et al. Soluble antigen derived from IV larva of angiostrongylus cantonensis promotes chitinase-like protein 3 (Chil3) expression induced by interleukin-13. *Parasitol Res* (2016) 115(10):3737–46. doi: 10.1007/s00436-016-5135-x

39. Zhou X, Spittau B, Krieglstein K. TGFβ signalling plays an important role in IL4-induced alternative activation of microglia. *J Neuroinflamm* (2012) 9(1):210. doi: 10.1186/1742-2094-9-210

40. Spittau B, Wullkopf L, Zhou X, Rilka J, Pfeifer D, Krieglstein K. Endogenous transforming growth factor-beta promotes quiescence of primary microglia in vitro. *Glia* (2013) 61(2):287–300. doi: 10.1002/glia.22435

41. Loke P, Nair MG, Parkinson J, Guiliano D, Blaxter M, Allen JE, et al. IL-4 dependent alternatively-activated macrophages have a distinctive in vivo gene expression phenotype. *BMC Immunol* (2002) 3:7. doi: 10.1186/1471-2172-3-7

42. Arora M, Chen L, Paglia M, Gallagher I, Allen JE, Vyas YM, et al. Simvastatin promotes Th2-type responses through the induction of the chitinase family member Ym1 in dendritic cells. *Proc Natl Acad Sci U.S.A.* (2006) 103(20):7777–82. doi: 10.1073/pnas.0508492103

43. Lee E, Jin M, Quan Z, Hwang NK, Lin CX, Kang S, et al. Effect of dexamethasone on STAT6-dependent Ym1/2 expression *in vivo* and *in vitro*. *Biol Pharm Bull* (2008) 31(9):1663–6. doi: 10.1248/bpb.31.1663

44. Penas F, Mirkin GA, Vera M, Cevey Á, González CD, Gómez MI, et al. Treatment in vitro with PPARα and PPARγ ligands drives M1-to-M2 polarization of macrophages from t. cruzi-infected mice. *Biochim Biophys Acta (BBA) - Mol Basis Dis* (2015) 1852(5):893–904. doi: 10.1016/j.bbadis.2014.12.019

45. Nelson VL, Nguyen HCB, Garcìa-Cañaveras JC, Briggs ER, Ho WY, DiSpirito JR, et al. PPARγ is a nexus controlling alternative activation of macrophages via glutamine metabolism. *Genes Dev* (2018) 32(15-16):1035–44. doi: 10.1101/gad.312355.118

46. Li L, Wu Y, Wang Y, Wu J, Song L, Xian W, et al. Resolvin D1 promotes the interleukin-4-induced alternative activation in BV-2 microglial cells. *J Neuroinflamm* (2014) 11:72. doi: 10.1186/1742-2094-11-72

47. Pan J, Jin J-l, Ge H-M, Yin K-l, Chen X, Han L-J, et al. Malibatol a regulates microglia M1/M2 polarization in experimental stroke in a PPARγ-dependent manner. *J Neuroinflamm* (2015) 12(1):51. doi: 10.1186/s12974-015-0270-3

48. Yao Q, Liu J, Zhang Z, Li F, Zhang C, Lai B, et al. Peroxisome proliferator-activated receptor γ (PPARγ) induces the gene expression of integrin α(V)β(5) to promote macrophage M2 polarization. *J Biol Chem* (2018) 293(43):16572–82. doi: 10.1074/jbc.RA118.003161

49. Rőszer T. Understanding the mysterious M2 macrophage through activation markers and effector mechanisms. *Mediators Inflammation* (2015) 2015:816460. doi: 10.1155/2015/816460

50. García-Culebras A, Durán-Laforet V, Peña-Martínez C, Moraga A, Ballesteros I, Cuartero MI, et al. Role of TLR4 (Toll-like receptor 4) in N1/N2 neutrophil programming after stroke. *Stroke* (2019) 50(10):2922–32. doi: 10.1161/STROKEAHA.119.025085

51. Oh A, Jeon S, Jeong MG, Kim HK, Kang J, Lee YS, et al. HSPB1 inhibitor J2 attenuates lung inflammation through direct modulation of Ym1 production and paracrine signaling. *BioMed Pharmacother* (2021) 143:112225. doi: 10.1016/j.biopha.2021.112225

52. Kim DI, Song MK, Lee K. Comparison of asthma phenotypes in OVA-induced mice challenged via inhaled and intranasal routes. *BMC Pulm Med* (2019) 19(1):241. doi: 10.1186/s12890-019-1001-9

53. Al-Ramli W, Préfontaine D, Chouiali F, Martin JG, Olivenstein R, Lemière C, et al. T(H)17-associated cytokines (IL-17A and IL-17F) in severe asthma. *J Allergy Clin Immunol* (2009) 123(5):1185–7. doi: 10.1016/j.jaci.2009.02.024

54. Mims JW. Asthma: definitions and pathophysiology. *Int Forum Allergy Rhinol* (2015) 5 Suppl 1:S2–6. doi: 10.1002/alr.21609

55. Ramakrishnan RK, Al Heialy S, Hamid Q. Role of IL-17 in asthma pathogenesis and its implications for the clinic. *Expert Rev Respir Med* (2019) 13(11):1057–68. doi: 10.1080/17476348.2019.1666002

56. He R, Kim HY, Yoon J, Oyoshi MK, MacGinnitie A, Goya S, et al. Exaggerated IL-17 response to epicutaneous sensitization mediates airway inflammation in the absence of IL-4 and IL-13. *J Allergy Clin Immunol* (2009) 124(4):761–70.e1. doi: 10.1016/j.jaci.2009.07.040

57. Fitzpatrick AM, Holguin F, Teague WG, Brown LA. Alveolar macrophage phagocytosis is impaired in children with poorly controlled asthma. *J Allergy Clin Immunol* (2008) 121(6):1372–8,1378.e1-3. doi: 10.1016/j.jaci.2008.03.008

58. Martinez FO, Helming L, Gordon S. Alternative activation of macrophages: an immunologic functional perspective. *Annu Rev Immunol* (2009) 27:451–83. doi: 10.1146/annurev.immunol.021908.132532

59. Zhou Y, Do DC, Ishmael FT, Squadrito ML, Tang HM, Tang HL, et al. Mannose receptor modulates macrophage polarization and allergic inflammation through miR-511-3p. *J Allergy Clin Immunol* (2018) 141(1):350–364.e8. doi: 10.1016/j.jaci.2017.04.049

60. Nieuwenhuizen NE, Kirstein F, Jayakumar J, Emedi B, Hurdayal R, Horsnell WG, et al. Allergic airway disease is unaffected by the absence of IL-4Rα-dependent alternatively activated macrophages. *J Allergy Clin Immunol* (2012) 130(3):743–750.e8. doi: 10.1016/j.jaci.2012.03.011

61. Cai Y, Kumar RK, Zhou J, Foster PS, Webb DC. Ym1/2 promotes Th2 cytokine expression by inhibiting 12/15(S)-lipoxygenase: identification of a novel pathway for regulating allergic inflammation. *J Immunol* (2009) 182(9):5393–9. doi: 10.4049/jimmunol.0803874

62. Greenlee KJ, Corry DB, Engler DA, Matsunami RK, Tessier P, Cook RG, et al. Proteomic identification of in vivo substrates for matrix metalloproteinases 2 and 9 reveals a mechanism for resolution of inflammation. *J Immunol* (2006) 177(10):7312–21. doi: 10.4049/jimmunol.177.10.7312

63. Liu R, Lauridsen HM, Amezquita RA, Pierce RW, Jane-Wit D, Fang C, et al. IL-17 promotes neutrophil-mediated immunity by activating microvascular pericytes and not endothelium. *J Immunol* (2016) 197(6):2400–8. doi: 10.4049/jimmunol.1600138

64. Wilson RH, Whitehead GS, Nakano H, Free ME, Kolls JK, Cook DN. Allergic sensitization through the airway primes Th17-dependent neutrophilia and airway hyperresponsiveness. *Am J Respir Crit Care Med* (2009) 180(8):720–30. doi: 10.1164/rccm.200904-0573OC

65. Barron L, Wynn TA. Fibrosis is regulated by Th2 and Th17 responses and by dynamic interactions between fibroblasts and macrophages. *Am J Physiol Gastrointest Liver Physiol* (2011) 300(5):G723–8. doi: 10.1152/ajpgi.00414.2010

66. Egholm C, Heeb LEM, Impellizzieri D, Boyman O. The regulatory effects of interleukin-4 receptor signaling on neutrophils in type 2 immune responses. *Front Immunol* (2019) 10:2507. doi: 10.3389/fimmu.2019.02507

67. Johannesson M, Karlsson J, Wernhoff P, Nandakumar KS, Lindqvist AK, Olsson L, et al. Identification of epistasis through a partial advanced intercross reveals three arthritis loci within the Cia5 QTL in mice. *Genes Immun* (2005) 6 (3):175–85. doi: 10.1038/sj.gene.6364155

68. Johannesson M, Olsson LM, Lindqvist AK, Möller S, Koczan D, Wester-Rosenlöf L, et al. Gene expression profiling of arthritis using a QTL chip reveals a complex gene regulation of the Cia5 region in mice. *Genes Immun* (2005) 6(7):575–83. doi: 10.1038/sj.gene.6364242

69. Khmaladze I, Kelkka T, Guerard S, Wing K, Pizzolla A, Saxena A, et al. Mannan induces ROS-regulated, IL-17A-dependent psoriasis arthritis-like disease in mice. *Proc Natl Acad Sci U.S.A.* (2014) 111(35):E3669–78. doi: 10.1073/pnas.1405798111

70. Nandakumar KS, Bäcklund J, Vestberg M, Holmdahl R. Collagen type II (CII)-specific antibodies induce arthritis in the absence of T or b cells but the arthritis progression is enhanced by CII-reactive T cells. *Arthritis Res Ther* (2004) 6 (6):R544–50. doi: 10.1186/ar1217

71. Hagert C, Sareila O, Kelkka T, Nandakumar KS, Collin M, Xu B, et al. Chronic active arthritis driven by macrophages without involvement of T cells: A novel experimental model of rheumatoid arthritis. *Arthritis Rheumatol* (2018) 70 (8):1343–53. doi: 10.1002/art.40482

72. Dervan A, Franchi A, Almeida-Gonzalez FR, Dowling JK, Kwakyi OB, McCoy CE, et al. Biomaterial and therapeutic approaches for the manipulation of macrophage phenotype in peripheral and central nerve repair. *Pharmaceutics* (2021) 13(12):2161. doi: 10.3390/pharmaceutics13122161

73. Kolosowska N, Keuters MH, Wojciechowski S, Keksa-Goldsteine V, Laine M, Malm T, et al. Peripheral administration of IL-13 induces anti-inflammatory Microglial/Macrophage responses and provides neuroprotection in ischemic stroke. *Neurotherapeutics* (2019) 16(4):1304–19. doi: 10.1007/s13311-019-00761-0

74. Wattananit S, Tornero D, Graubardt N, Memanishvili T, Monni E, Tatarishvili J, et al. Monocyte-derived macrophages contribute to spontaneous long-term functional recovery after stroke in mice. *J Of Neurosci* (2016) 36 (15):4182–95. doi: 10.1523/JNEUROSCI.4317-15.2016

75. Perego C, Fumagalli S, Zanier ER, Carlino E, Panini N, Erba E, et al. Macrophages are essential for maintaining a M2 protective response early after ischemic brain injury. *Neurobiol Dis* (2016) 96:284–93. doi: 10.1016/j.nbd.2016.09.017

76. Li T, Zhao J, Xie WG, Yuan WR, Guo J, Pang SR, et al. Specific depletion of resident microglia in the early stage of stroke reduces cerebral ischemic damage. *J Of Neuroinflamm* (2021) 18(1):81. doi: 10.1186/s12974-021-02127-w

77. Yang Y, Salayandia VM, Thompson JF, Yang LY, Estrada EY, Yang Y. Attenuation of acute stroke injury in rat brain by minocycline promotes blood-brain barrier remodeling and alternative microglia/macrophage activation during recovery. *J Neuroinflamm* (2015) 12:26–6. doi: 10.1186/s12974-015-0245-4

78. Kumar A, Stoica BA, Sabirzhanov B, Burns MP, Faden AI, Loane DJ. Traumatic brain injury in aged animals increases lesion size and chronically alters microglial/macrophage classical and alternative activation states. *Neurobiol Aging* (2013) 34(5):1397–411. doi: 10.1016/j.neurobiolaging.2012.11.013

79. Gensel JC, Zhang B. Macrophage activation and its role in repair and pathology after spinal cord injury. *Brain Res* (2015) 1619:1–11. doi: 10.1016/j.brainres.2014.12.045

80. Su J. A brief history of charcot-Leyden crystal Protein/Galectin-10 research. *Molecules* (2018) 23(11):2931. doi: 10.3390/molecules23112931

81. Guo L, Johnson RS, Schuh JC. Biochemical characterization of endogenously formed eosinophilic crystals in the lungs of mice. *J Biol Chem* (2000) 275(11):8032–7. doi: 10.1074/jbc.275.11.8032

82. Shultz LD, Coman DR, Bailey CL, Beamer WG, Sidman CL. "Viable motheaten," a new allele at the motheaten locus. i. pathology. *Am J Pathol* (1984) 116(2):179–92.

83. Tsui FW, Martin A, Wang J, Tsui HW. Investigations into the regulation and function of the SH2 domain-containing protein-tyrosine phosphatase, SHP-1. *Immunol Res* (2006) 35(1-2):127–36. doi: 10.1385/IR:35:1:127

84. Opata MM, Hollifield ML, Lund FE, Randall TD, Dunn R, Garvy BA, et al. B lymphocytes are required during the early priming of CD4+ T cells for clearance of pneumocystis infection in mice. *J Immunol* (2015) 195(2):611–20. doi: 10.4049/jimmunol.1500112

85. Smith S, Skerrett SJ, Chi EY, Jonas M, Mohler K, Wilson CB, et al. The locus of tumor necrosis factor-alpha action in lung inflammation. *Am J Respir Cell Mol Biol* (1998) 19(6):881–91. doi: 10.1165/ajrcmb.19.6.3146

86. Zhu Z, Homer RJ, Wang Z, Chen Q, Geba GP, Wang J, et al. Pulmonary expression of interleukin-13 causes inflammation, mucus hypersecretion, subepithelial fibrosis, physiologic abnormalities, and eotaxin production. *J Clin Invest* (1999) 103(6):779–88. doi: 10.1172/JCI5909

87. Feldmesser M, Kress Y, Casadevall A. Intracellular crystal formation as a mechanism of cytotoxicity in murine pulmonary cryptococcus neoformans infection. *Infect Immun* (2001) 69(4):2723–7. doi: 10.1128/IAI.69.4.2723-2727.2001

88. Waern I, Jia J, Pejler G, Zcharia E, Vlodavsky I, Li JP, et al. Accumulation of Ym1 and formation of intracellular crystalline bodies in alveolar macrophages lacking heparanase. *Mol Immunol* (2010) 47(7-8):1467–75. doi: 10.1016/j.molimm.2010.02.004

89. Imai H, Nakamoto Y, Asakura K, Miki K, Yasuda T, Miura AB. Spontaneous glomerular IgA deposition in ddY mice: an animal model of IgA nephritis. *Kidney Int* (1985) 27(5):756–61. doi: 10.1038/ki.1985.76

90. Lee CG, Da Silva CA, Dela Cruz CS, Ahangari F, Ma B, Kang M-J, et al. Role of chitin and Chitinase/Chitinase-like proteins in inflammation, tissue remodeling, and injury. *Annu Rev Physiol* (2011) 73(1):479–501. doi: 10.1146/annurev-physiol-012110-142250

91. Liu Q, Cheng LI, Yi L, Zhu N, Wood A, Changpriroa CM, et al. p47phox deficiency induces macrophage dysfunction resulting in progressive crystalline macrophage pneumonia. *Am J Pathol* (2009) 174(1):153–63. doi: 10.2353/ajpath.2009.080555

frontiers | Frontiers in Immunology

TYPE Original Research
PUBLISHED 10 August 2022
DOI 10.3389/fimmu.2022.929222

OPEN ACCESS

EDITED BY
Toshiyuki Shimizu,
The University of Tokyo, Japan

REVIEWED BY
Yam Nath Paudel,
Sydney, Australia
Matthew Gerald Frank,
University of Colorado Boulder,
United States
Sun Young Park,
Pusan National University, South Korea

*CORRESPONDENCE
Cong Lin
cong.lin@ciac.ac.cn
Yanfang Jiang
yanfangjiang@hotmail.com
Xiaohui Wang
xiaohui.wang@ciac.ac.cn

SPECIALTY SECTION
This article was submitted to Molecular Innate Immunity, a section of the journal Frontiers in Immunology

RECEIVED 26 April 2022
ACCEPTED 22 July 2022
PUBLISHED 10 August 2022

CITATION
Wang X, Lin C, Wu S, Zhang T, Wang Y, Jiang Y and Wang X (2022) Cannabidivarin alleviates neuroinflammation by targeting TLR4 co-receptor MD2 and improves morphine-mediated analgesia. *Front. Immunol.* 13:929222. doi: 10.3389/fimmu.2022.929222

Cannabidivarin alleviates neuroinflammation by targeting TLR4 co-receptor MD2 and improves morphine-mediated analgesia

Xue Wang[1], Cong Lin[2]*, Siru Wu[2,3], Tianshu Zhang[2,3], Yibo Wang[2], Yanfang Jiang[4]* and Xiaohui Wang[2,3,5]*

[1]Department of Anesthesiology, The First Hospital of Jilin University, Changchun, China, [2]Laboratory of Chemical Biology, Changchun Institute of Applied Chemistry, Chinese Academy of Sciences, Changchun, China, [3]School of Applied Chemistry and Engineering, University of Science and Technology of China, Hefei, China, [4]Key Laboratory of Organ Regeneration and Transplantation of the Ministry of Education, Genetic Diagnosis Centre, The First Hospital of Jilin University, Changchun, China, [5]Beijing National Laboratory for Molecular Sciences, Beijing, China

Toll-like receptor 4 (TLR4) is a pattern-recognition receptor (PRR) that regulates the activation of immune cells, which is a target for treating inflammation. In this study, Cannabidivarin (CBDV), an active component of Cannabis, was identified as an antagonist of TLR4. *In vitro*, intrinsic protein fluorescence titrations revealed that CBDV directly bound to TLR4 co-receptor myeloid differentiation protein 2 (MD2). Cellular thermal shift assay (CETSA) showed that CBDV binding decreased MD2 stability, which is consistent with *in silico* simulations that CBDV binding increased the flexibility of the internal loop of MD2. Moreover, CBDV was found to restrain LPS-induced activation of TLR4 signaling axes of NF-κB and MAPKs, therefore blocking LPS-induced pro-inflammatory factors NO, IL-1β, IL-6 and TNF-α. Hot plate test showed that CBDV potentiated morphine-induced antinociception. Furthermore, CBDV attenuated morphine analgesic tolerance as measured by the formalin test by specifically inhibiting chronic morphine-induced glial activation and pro-inflammatory factors expression in the nucleus accumbent. This study confirms that MD2 is a direct binding target of CBDV for the anti-neuroinflammatory effect and implies that CBDV has great translational potential in pain management.

KEYWORDS

Toll-like receptor 4, myeloid differentiation protein 2, cannabidivarin, neuroinflammation, analgesia, pain

Introduction

The innate immune is the first line of defense against bacterial infections of the immune system (1). Innate immune responses, such as inflammation, are mediated by pattern-recognition receptors (PRRs) that recognize pathogen-associated molecular patterns (PAMPs). Toll-like receptors (TLRs) are the first identified PRRs to trigger innate immune responses (2, 3). TLR4 is a key member of the TLRs family, which forms a complex on the cell surface with myeloid differentiation protein 2 (MD2) (4). Lipopolysaccharide (LPS), a significant component of the outer wall of Gram-negative bacteria, is the natural ligand of TLR4 as PAMPs (5). Besides for PAMPs, TLR4 also recognizes damages-associated molecular patterns (DAMPs) and xenobiotic-associated molecular patterns (XAMPs) (5). The high mobility group box 1 (HMGB1), heat shock protein 70 (HSP70) and the myeloid-related protein 8 (MRP8) are the endogenous ligands of TLR4 as DAMPs (6). Some psychoactive compounds, such as morphine, act as XAMPs to activate the TLR4 signaling pathway and create neuroinflammation (7–11). Morphine induces glia activation (12) and creates a neuroinflammatory response within the central nervous system (CNS), compromising morphine-induced analgesia as well as contributing to morphine-induced analgesic tolerance (7, 13, 14). Therefore, TLR4 antagonists could be potential agents for enhancing morphine analgesic efficacy and preventing morphine tolerance (9, 15). Numerous TLR4 small-molecule inhibitors have been developed (16). However, no TLR4 antagonists have been approved for clinical use.

Cannabidivarin (CBDV) is a safe, non-psychoactive phytocannabinoid isolated from *Cannabis Sativa* (17). Although CBDV is usually a minor constituent of naturally-occurring cannabinoids found in cannabis, CBDV has been attracting great interest owing to its potential benefits to clinical conditions that cannabidiol (CBD) cannot effectively treat (18, 19). Owing to its lipophilicity and blood-brain barrier (BBB) penetrability (20, 21), CBDV has recently gained much attention as for its ability to modulate neurological diseases (17, 22, 23). Considering TLR4 is a XAMPs receptor for surveiling foreign substances in CNS, it would be interesting to explore whether CBDV acts as a XAMP and can be sensed by MD2, an accessory protein of TLR4 responsible for the recognition of ligand. Herein, MD2 was found as a direct target of CDBV. CBDV inhibited TLR4 signaling NF-κB and MAPK signaling axes and the downstream pro-inflammatory factors. Moreover, CBDV improved morphine-induced analgesia by specifically inhibiting chronic morphine-induced glial activation and pro-inflammatory factors expression in the nucleus accumbent (NAc). This study implies that CBDV has great translational potential in pain management.

Manuscript formatting

Materials and methods

Materials

Microglial BV-2 cells were obtained from the China Center for Type Culture Collection. CBDV, crystal violet, 2, 3-diaminonaphthalene and paraformaldehyde were purchased from Sigma-Aldrich. Morphine was obtained from China National Institutes for Food and Drug Control. Ultrapure LPS, HEK Blue hTLR4 cells, and HEK-Blue Selection were purchased from *In vivo*gen. The Phospha-Light™ SEAP Reporter Gene Assay System was purchased from Applied Biosystems. The Dual-Glo Luciferase Assay System was purchased from Promega. Hifair III 1st Strand cDNA Synthesis SuperMix for qPCR and HieffqPCR SYBR Master Mix were obtained from Yeasen Biotech Co., Ltd. PCR primers were purchased from Comate Bioscience Co., Ltd. Cell lysis buffer for western blotting was purchased from Beyotime Biotechnology. Primary antibodies targeting GFAP, p38 MAPK, NF-κB p65, ERK (1/2), IKKβ, SAPK/JNK, phospho-NF-κB p65, phospho-ERK (1/2), phospho-SAPK/JNK, phospho-IKKα/β, phospho-p38 MAPK, goat anti-rabbit HRP-linked antibody and goat anti-mouse HRP-linked antibody were purchased from Cell Signaling Technology. The anti-Iba-1 antibody was purchased from Affinity Bioscience. 4', 6-diamidino-2-phenylindole (DAPI) was purchased from Absin Bioscience Inc.

Fluorescence titrations of MD2 with CBDV

The method of fluorescence titrations of MD2 with CBDV was performed as described (24).

Cellular thermal shift assay (CETSA)

CETSA assay was performed as described (24).

In silico simulation

The crystal structure of MD2 was extracted from the mouse TLR4/MD2 complex (PDB ID: 2Z64) (25). Autodock Vina 1.1.2 was used for molecular docking in a box of $46 \times 58 \times 53$ Å^3 with default settings (26). MD2 was considered rigid and CBDV was treated as semi-flexible during the docking process. Twenty docking poses were generated and the best docking pose was selected for further simulations.

Apo-MD2 and MD2-CBDV were further investigated through molecular dynamics (MD) simulations performed

by the Gromacs 2021.2 program (27, 28). The CHARMM36m force field was used for proteins (29, 30). The ligand parameters were generated by the Antechamber tool (31). All solutes were solvated in a TIP3P water box with 0.15 M NaCl to mimic the physiological condition. The systems were equilibrated in the isothermal-isobaric (NPT) ensemble at a temperature of 310 K for 100 ns. The SHAKE algorithm was applied to restrain all bonds involving hydrogen (32). The particle-mesh Ewald (PME) summation method was applied to treat long-range electrostatic interactions (33). The pressure was set at 1 atm with the Nosé-Hoover Langevin piston method (34).

The RMSD (root-mean-square deviation) and RMSF (root-mean-square fluctuation) analyses were performed through MD Analysis (35). The binding energy (enthalpy) and per-residue energy contributions were calculated by the molecular mechanics/Poisson-Boltzmann (generalized-Born) surface area method with the gmx_MMPBSA tool (36, 37). Each system was repeated three times independently. The interactions between MD2 and CBDV were shown by PyMol (38).

Immunoblotting

Immunoblotting was performed as described (24). BV-2 cells were seeded at 5 × 10^5 cells/well in 6-well plates. After 24 h incubation, cells were treated with 200 ng/mL LPS and indicated concentrations of CBDV for 1 h. The cells were lysed in RIPA buffer with complete protease inhibitor cocktail and phosphatase inhibitors. Equal amounts of protein (20-40 μg) were separated by SDS-PAGE and transferred to PVDF membranes. After blocking with 5% non-fat dry milk for 1 h, membranes were incubated with corresponding primary antibodies (All primary antibodies were diluted at 1: 1000) overnight at 4°C. After washing three times in Tris-buffered saline with 0.1% Tween 20 (TBST) for 5 min each time, membranes were incubated with secondary antibody-HRP conjugate (1: 3000) for 1 h at room temperature. After washing three times in TBST, the membranes were detected using Tanon-5200 Multi. Image J was used for later densitometric analysis.

Nitric oxide (NO) assay

BV-2 cells were seeded in 96-well plates at a density of 4 ×10^4 cells per well and cultured in Dulbecco's modified Eagle's medium (DMEM) with 10% fetal bovine serum (FBS), 50 U/mL penicillin, and 50 μg/mL streptomycin for 24 hours at 37°C in a 5% CO_2 incubator. After 24 hours, the media was replaced with DMEM alone and treated with LPS (200 ng/mL) and the indicated concentrations of CBDV. The supernatant was transferred to another 96-well plate and determined by the 2, 3-diaminonaphthalene-based fluorescent method as described (24).

Secreted embryonic alkaline phosphatase (SEAP) assay

SEAP assay was performed as described (7). Briefly, HEK Blue hTLR4 cells were cultured in DMEM supplemented with 10% FBS, 50 unit/mL penicillin, 50 μg/mL streptomycin and 1 × HEK-Blue selection. Cells were seeded in 96-well plates at a density of 4 ×10^4 cells per well. After 24 h incubation, the medium was replaced with Opti-MEM supplemented with 0.5% FBS, 50 unit/mL penicillin, 50 μg/mL streptomycin and 1 × non-essential amino acid. Cells were treated with 20 ng/mL LPS and indicated concentrations of CBDV. After 24 h incubation, NF-κB activity was measured through the Phospha-Light SEAP Reporter Gene Assay System according to the manufacturer's instructions.

Dual-luciferase NF-κB reporter assay

Dual-luciferase NF-κB reporter assay was performed as described (7). Briefly, BV-2 NF-κB luciferase reporter cells were cultured in DMEM supplemented with 10% FBS, 50 unit/mL penicillin, 50 μg/mL streptomycin and 2 μg/mL puromycin. Cells were seeded in 96-well plates at a density of 1 ×10^4 cells per well. After 24 h incubation, the medium was replaced with Opti-MEM supplemented with 0.5% FBS, 50 unit/mL penicillin, 50 μg/mL streptomycin and 1 × non-essential amino acid). Cells were treated with 200 ng/mL LPS and indicated concentrations of CBDV. After 24 h incubation, NF-κB activity was measured through Dual-Glo Luciferase Assay System according to the manufacturer's instructions.

Cell viability assays

Cellular viability was determined by the crystal violet staining method and Cell Counting Kit-8 (CCK-8) assay. Crystal violet staining was performed as described in the following. BV-2 NF-κB luciferase reporter cells were cultured and treated as indicated in the dual-luciferase NF-κB reporter assay. After 24 h treatment, cells were fixed with 100 μL 4% paraformaldehyde for 5 minutes and then stained with 100 μL 0.05% crystal violet for 15 minutes. After washing three times with water, 200 μL ethanol was added for each well and incubated for 20 min at room temperature. Absorbance at 540 nm was measured using a SYNERGY H1 Microplate Reader.

For CCK-8 assay, HEK Blue hTLR4 cells were cultured and treated as indicated in the SEAP assay. HEK Blue hTLR4 cells were treated in 96-well plates. After 24 h treatment, 20 μL CCK-8 assay solution was added for each well and cells were incubated in a 5% CO2, 37°C incubator for 2 h. Absorbance was detected at 450 nm with 650 nm as the reference wavelength.

qRT-PCR

BV-2 cells were counted and plated in 6-well plates at a density of 4 ×10^4 cells per well. After overnight incubation, LPS (200 ng/mL) and indicated concentrations of CBDV were added. After 24 h incubation, TRIzol was used to isolate total RNA from BV-2 cells. RNA was reverse-transcribed into cDNA. qPCR was performed subsequently using the SYBR Green method. Rpl27 was set as a reference gene. The primers sequence for TNF-α, IL-1β, and Rpl27 were shown in Table 1. The data were analyzed by the $^{\Delta\Delta}$Ct method.

For qRT-PCR of brain tissue, nucleus accumbent (NAc) region was firstly collected as following. Animals were deeply anesthetized by intraperitoneal injection of pentobarbital (100 mg/kg) and perfused with saline. The brain was removed and NAc region was dissected. The tissues were immediately kept in liquid nitrogen. After solubilizing the tissue in Trizol using homogenizer, total RNA from the NAc was isolated. RNA was reverse-transcribed into cDNA and qPCR was performed as described above.

In vivo studies

Animal

Adult male BALB/c mice (weight: 20-25 g) purchased from the Liaoning Changsheng Biotech Company were employed in this study. Mice were housed 3-5 per cage at standard conditions (22-25°C, 12h: 12h light: dark cycle, free access to standard food and water). All experiments were approved by the Institutional Animal Care and Use Committee (IACUC) of Changchun Institute of Applied Chemistry, Chinese Academy of Sciences (2022–0090).

Hot plate assay

The temperature of the hot plate was set at 55°C. The latency period was measured by the pain threshold when the mouse lifted or licked a hind paw, jumping or vocalizing. One day before the experiment, the baseline pain threshold was measured by averaging the values of two 1 h interval measures. The pain threshold was calculated as described (7), and the cut-off duration was 30 s. Animals were randomly divided into four groups (n = 5), including the control group, CBDV group, morphine group, and morphine + CBDV group. Before the test, mice were intraperitoneally injected with CBDV (8 mg/kg or 50 mg/kg) 30 min before morphine (5 mg/kg, *i.p.*). Following morphine administration, the pain threshold was recorded at different time points. Data were expressed as percent maximum potential effect (% MPE): %MPE = (post-drug latency - baseline latency)/(cut-off time - baseline latency) × 100.

TABLE 1 Primer sequences of IL-1β, IL-6, TNF-α and Rpl27.

Gene		Sequence (5' - 3')
IL-1β	Forward	CCACCTTTTGACAGTGATGA
	Reverse	GAGATTTGAAGCTGGATGCT
IL-6	Forward	TAGTCCTTCCTACCCCAATTTCC
	Reverse	TTGGTCCTTAGCCACTCCTTC
TNF-α	Forward	CCCTCCAGAAAAGACACCATG
	Reverse	GCCACAAGCAGGAATGAGAAG
Rpl27	Forward	AAGCCGTCATCGTGAAGAACA
	Reverse	CTTGATCTTGGATCGCTTGGC

Formalin test

Animals were randomly divided into each group (n = 5-6). The mice had 30 min to get used to the plastic chamber with black sides and transparent bottom (12 cm ×12 cm ×15 cm). 20 μL of 2% formalin was injected into the hind paw with a 27-gauge needle described previously for the formalin test (39). CBDV (50 mg/kg) was intraperitoneally injected 1 h before the administration of formalin. Morphine (1 mg/kg, *i.p.*) was given 30 min before the injection of formalin. Once formalin had been injected, the mice returned to the chamber, and the video was recorded for 40 min. There were two phases in the formalin test: the first (acute phase) ranged from 0-10 min and the second phase (tonic phase) ranged from 10-40 min. The seconds of licking and biting of the injected paw was calculated and analyzed in each phase.

Immunofluorescence

The procedure for immunofluorescence staining follows the steps described previously (40). Animals were deeply anesthetized by intraperitoneal injection of pentobarbital (100 mg/kg) and perfused with phosphate-buffered solution (PBS, pH 7.4) followed by 4% paraformaldehyde. After dissection, the brain was removed and soaked in 4% paraformaldehyde overnight. Then, the brain was cryoprotected in 20% sucrose in PBS at 4°C overnight. Brain sections (40 μm thick) containing the medial prefrontal cortex (mPFC), nucleus accumbens (NAc), and ventral tegmental area (VTA) regions were obtained by a cryostat microtome. The slides were washed with 0.1 M PBS buffer three times and then incubated in primary antibodies Iba-1 (Affinity, DF6442) and GFAP (Cell Signaling Technology, 3670) at 4°C for two days. After three washes with PBS, the sections were exposed to a secondary antibody for overnight incubation. After a thorough wash in PBS, 4', 6- diamidino-2-phenylindole (DAPI) staining was performed. Olympus VS120 microscope was used to take the fluorescent images.

Statistical analysis

Data were expressed as the mean ± S.E.M, and analysis of variance was carried out using one-way analysis of variance (ANOVA). All statistical analyses were performed with GraphPad Prism 8.0 and Origin 8. The statistical significance was marked above the bar for each figure. $P < 0.05$ was considered statistically significant in all analyses.

Results

Biophysical binding of CBDV with MD2

MD2 is the TLR4 co-receptor that is responsible for the recognition of ligands (41). In order to explore whether CBDV could be sensed by TLR4, the direct interaction of MD2 and CBDV (Figure 1A) was investigated. *In vitro* MD2 intrinsic fluorescence quenching titration with CBDV was performed (Figure 1B). A dissociation constant K_d of 3.9 ± 0.3 μM was derived by the nonlinear least-square fitting of the titration curve of MD2-CBDV interaction. To verify that MD2 is indeed the endogenous target of CBDV, cellular thermal shift assay (CETSA) was carried out (Figure 1C). The folding fraction of MD2 decreased with the increasing of temperature and CBDV binding decreased the melting temperature (T_m) of MD2 by 4.3 ± 0.1°C (Figure 1D), indicating that CBDV decreased MD2 thermal stability. Taken together, these biophysical binding characterizations show that MD2 is a direct target of CDBV.

In silico simulation of CBDV interacting with MD2

To investigate atomic details of the interactions between CBDV and MD2, MD simulations were performed. As shown in Figure 2A, the root-mean-square deviation (RMSD) values of backbone atoms of apo-MD2 and MD2 complexed with CBDV showed that both systems reached stable states in 100 ns simulations. The RMSD value of apo-MD2 stabilized at around 4.0 Å, and the RMSD value of MD2 complexed with CBDV stabilized at around 5.5 Å. Root-mean-square fluctuation (RMSF) analysis was performed (Figure 2B). The binding of CBDV rendered an internal loop (residues 100 - 108) of MD2 flipped out and much more flexible, indicating that CBDV destabilizes MD2. This result is consistent with the experimental CETSA data. The binding energy of CBDV to MD2 was decomposed (Figure 2C) and CBDV was stabilized by the interactions with Ile32, Cys51, Ile52, Val61, Phe76, Leu78, Phe119, Cys133, Ala135, and Ile153 (Figure 2D).

CBDV inhibits TLR4 signaling and LPS-induced pro-inflammatory factors

NF-κB and MAPKs are the two main TLR4 signaling axes. Immunoblotting was employed to measure the effect of CBDV on TLR4 signaling. As shown in Figure 3, CBDV inhibited LPS-induced phosphorylation of IKKβ and p65 as well as LPS-induced phosphorylation of JNK, ERK and p38 in a concentration-dependent manner. These results indicate that CBDV inhibits TLR4 signaling NF-κB and MAPK signaling axes.

To further quantitatively investigate the effect of CBDV on TLR4 signaling NF-κB activity, SEAP assay based on the HEK

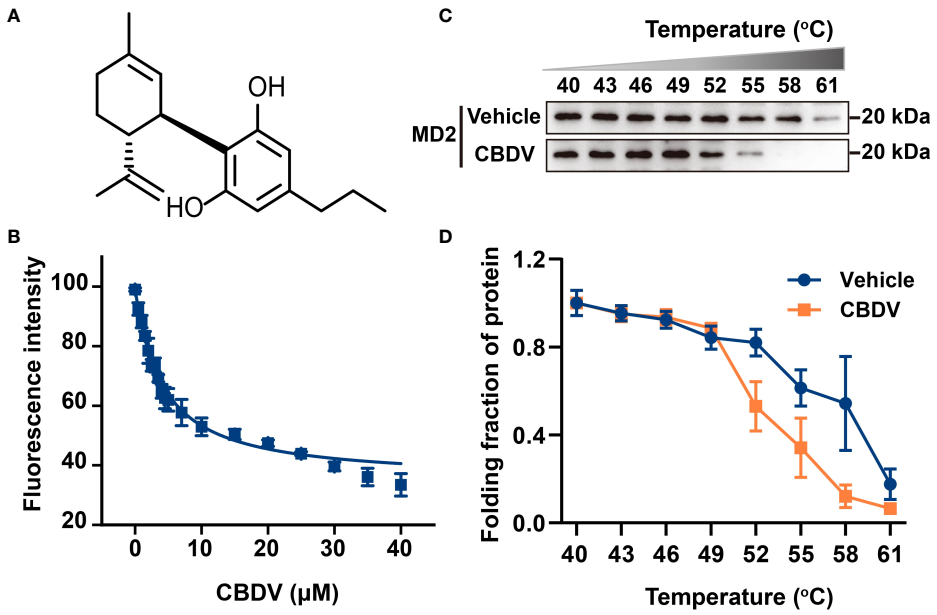

FIGURE 1
Biophysical binding of CBDV with MD2. **(A)** The chemical structure of CBDV. **(B)** Titration curve of MD2 intrinsic fluorescence with the increasing concentrations of CBDV. Emission at 337 nm (excitation at 280 nm) was plotted against the titrated CBDV concentration. K_d value of 3.9 ± 0.3 μM was derived by nonlinear least-squares fitting of a one-site binding model for CBDV interacting with MD2. **(C, D)** Cellular thermal shift assay (CETSA) of MD2 with CBDV. CBDV binding decreased MD2 thermal stability (ΔT_m = -4.3 ± 0.1 °C). All experiments were performed three times independently, and data were given as the mean ± S.E.M.

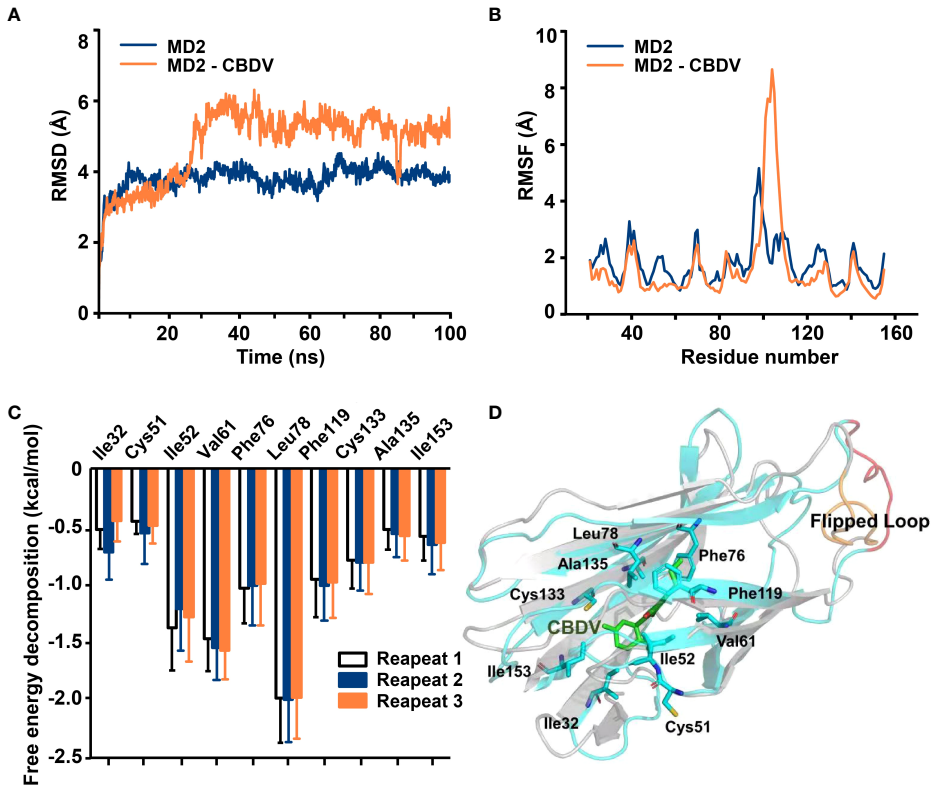

FIGURE 2
In silico simulation of CBDV interacting with MD2. **(A)** Time evolution of RMSDs for apo-MD2 and CBDV-bound MD2 (MD2-CBDV) during the MD simulations at 310 K. **(B)** Time evolution of RMSFs of MD2 and CBDV bound MD2 during the MD simulations at 310 K. **(C)** Per-residue energy decomposition for key residues. **(D)** The representative binding mode of CBDV with MD2 at 310 K after MD simulation. CBDV was shown as ball-stick model. MD2 in the MD2-CBDV system was shown as cartoon model (cyan) aligned to apo-MD2. Key residues of MD2 in interacting with ligands were shown as sticks. The flipped loops were labeled with orange and red in apo-MD2 and MD2-CBDV, respectively.

Blue hTLR4 cells was performed. As shown in Figure 4A, CBDV inhibited LPS-induced NF-κB activation in a dose-dependent manner, with an IC_{50} of 1.4 ± 0.2 μM, while the cellular toxicity of CBDV on HEK Blue hTLR4 cells (IC_{50} = 23.3 ± 2.5 μM) was low. In addition to HEK-based NF-κB reporter cells, the effect of CBDV on NF-κB activity in BV-2 microglial cells was also examined. CBDV inhibited LPS-induced NF-κB activation in BV-2 cells in a dose-dependent manner with an IC_{50} of 1.7 ± 0.2 μM without apparent cellular toxicity within 10 μM (Figure 4B). These data clearly show that CBDV inhibits TLR4 signaling NF-κB activation.

The activation of TLR4 signaling promotes the over-production of pro-inflammatory factors, including NO, IL-1β, IL-6, and TNF-α. To validate the effect of CBDV on downstream inflammatory factors, NO assay and qPCR were performed. CBDV inhibited LPS-induced NO elevation with an IC_{50} of 0.5 ± 0.3 μM (Figure 5A). Moreover, CBDV suppressed LPS-induced IL-1β (Figure 5B), IL-6 (Figure 5C), and TNF-α (Figure 5D) mRNA expression in a dose-dependent manner. Together, these cellular data show that CBDV restrains LPS-induced activation of TLR4 signaling, therefore inhibiting the over-production of TLR4 downstream pro-inflammatory factors.

CBDV improves morphine-mediated analgesia

Morphine induces glia activation and neuroinflammation *via* TLR4 (7, 14), and TLR4 antagonists have been found to enhance the morphine analgesic effect and attenuate morphine tolerance (42, 43). Hot plate assay was performed to test whether CBDV could potentiate morphine analgesia (Figure 6A). Morphine produced significant analgesia to the hot plate, compared to baseline. TLR4 antagonist CBDV was found to increase and prolong morphine analgesia in a dose-dependent manner (Figure 6B). However, CBDV had no effect on heat pain responsivity in the absence of co-administered morphine.

In addition to hot plate assay, formalin test was also performed to evaluate the analgesic activity of CBDV and to assess the combinational effect of CBDV and morphine. The formalin test is a popular model of clinical pain, which includes both acute pain (0-10 min) and tonic pain (10-40 min). The first phase is attributed to C-fiber activation due to the peripheral

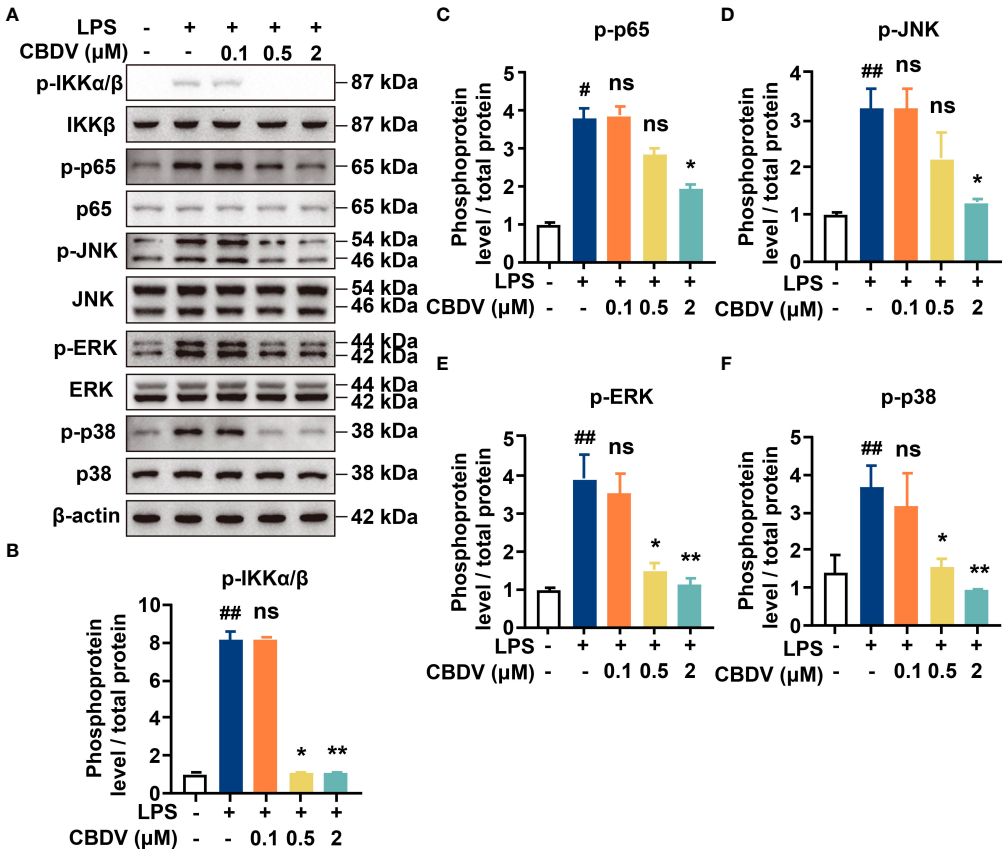

FIGURE 3
Cellular characterizations of CBDV on TLR4 signaling. **(A)** The effect of CBDV on LPS-induced TLR4 signaling as measured by western blotting. **(B-F)** The quantification of the phosphorylation of IKKβ **(B)**, p65 **(C)**, JNK **(D)**, ERK **(D)** and p38 **(F)** shown in **(A)**. All experiments were performed three times independently, and data were given as the mean ± S.E.M. The P-value was set at # $P < 0.05$, ## $P < 0.01$ versus the control group; *$P < 0.05$, **$P < 0.01$ versus the LPS group; ns, not significant versus the LPS group.

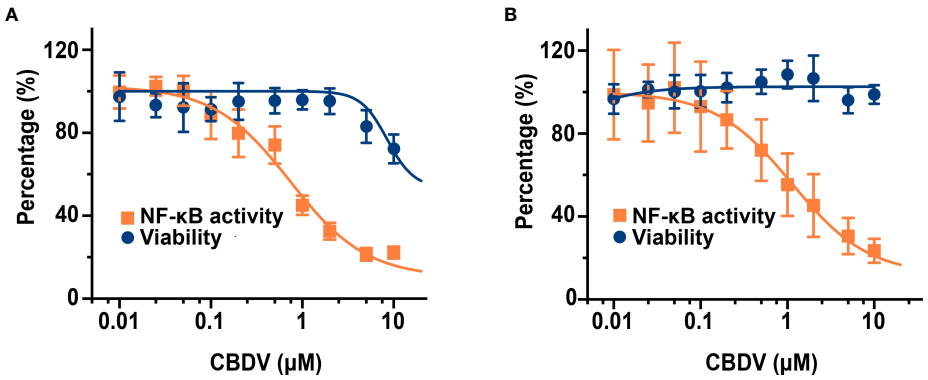

FIGURE 4
CBDV inhibits LPS-induced NF-κB activation in HEK Blue hTLR4 cells **(A)** and immunocompetent microglial BV-2 cells **(B)**. **(A)** HEK Blue hTLR4 cells, which overexpress human CD14, TLR4, and MD-2, were stimulated with LPS and indicated concentrations of CBDV. The NF-κB activity was determined by SEAP assay and the cellular viability was measured by CCK-8 Kit. **(B)** BV-2 NF-κB luciferase reporter cells were treated with LPS and indicated concentrations of CBDV. The NF-κB activity was determined by the Steady-Glo luciferase assay and the cellular viability was measured by crystal violet staining. All experiments were performed three times independently, and data were given as the mean ± S.E.M.

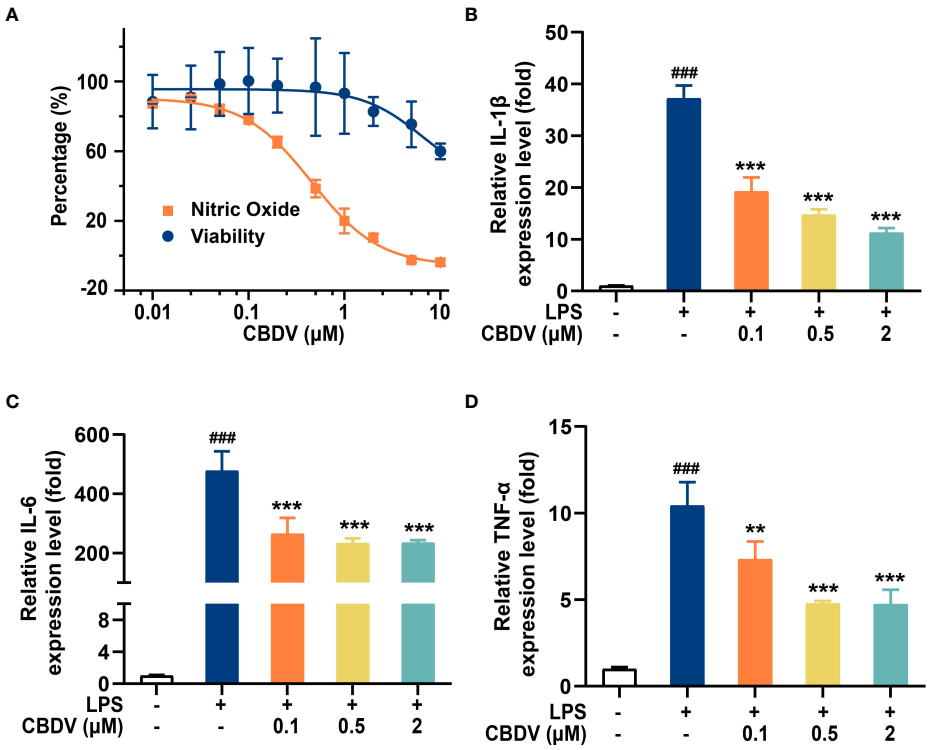

FIGURE 5
CBDV inhibits LPS-induced NO overproduction **(A)** as well as the pro-inflammatory factors IL-1β **(B)**, IL-6 **(C)**, and TNF-α **(D)** mRNAs expression. All the data represented the mean ± S.E.M.; the number of independent cell culture preparations = 3. The P-value was set at ### P < 0.001 versus the control group; **P < 0.01, ***P < 0.001 versus the LPS group.

stimulus by formalin, while the second phase appears to be associated with the inflammation response. CBDV showed analgesic effects in both the acute phase and tonic phase (Figure 7A). Compared to single administration, chronic morphine treatment induced analgesia tolerance as reflected in both phases of the formalin test. Moreover, co-administration of CBDV was found to attenuate tolerance to morphine analgesia (Figure 7B). To further analyze whether the attenuation of

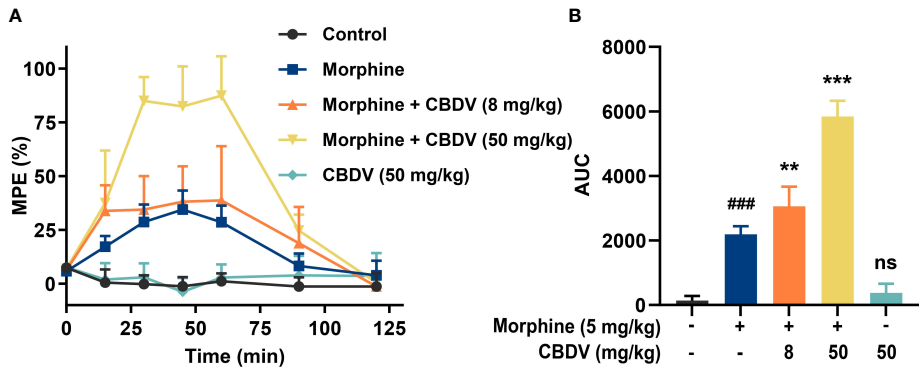

FIGURE 6
CBDV potentiates morphine-induced antinociception. **(A)** Intraperitoneal co-administration of morphine (5 mg/kg) and CBDV produced a significant potentiation of morphine hot plate analgesia. **(B)** The area under the curve (AUC) curves shown in panel **(A)**. Data were presented as the mean ± S.E.M. n = 5/group; The P-value was set at ### P < 0.001 versus the control group; **P < 0.01, ***P < 0.001 versus the morphine group; ns, not significant versus the control group.

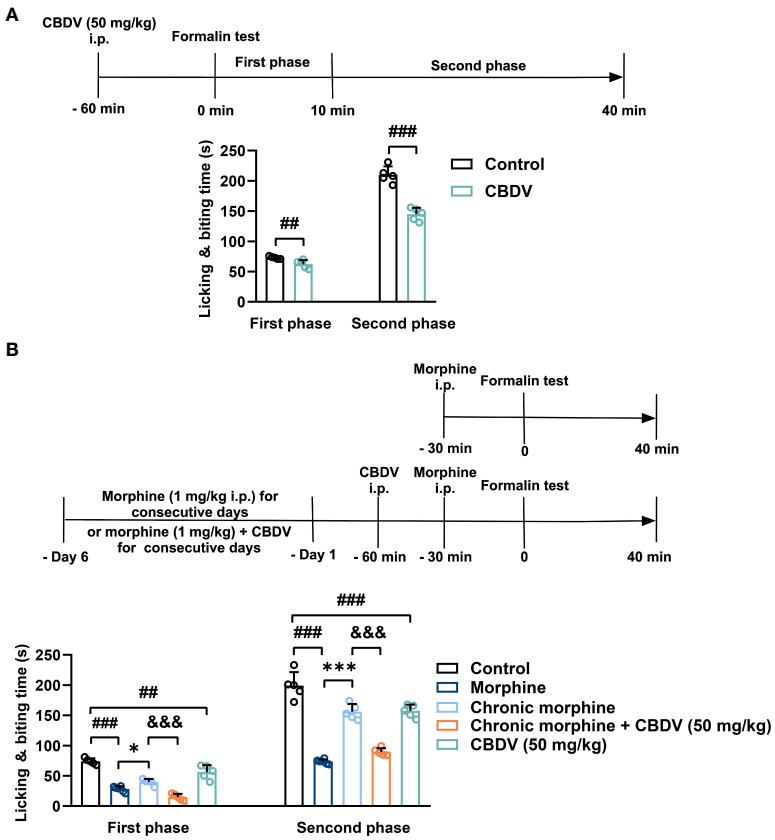

FIGURE 7
CBDV shows analgesic effect and attenuates morphine analgesic tolerance as measured by formalin test. **(A)** The analgesic effect of single administration of CBDV as assessed by formalin test. **(B)** The effect of CBDV on the analgesic activity of chronic morphine as measured by the formalin test. Data were presented as the mean ± S.E.M. n = 5/group; The P-value was set at ## P < 0.01, ### P < 0.001 versus the control group; *P < 0.05, ***P < 0.001 versus the morphine group; &&& P < 0.001 versus the chronic morphine group.

morphine tolerance by CBDV was associated with its inhibition of glial activation, nucleus accumbens (NAc) that is a key neural substrate for opioid-mediated pain modulation (44, 45), was dissected following the behavioral testing. The tissues were stained for microglia and astrocyte markers Iba-1 and GFAP, respectively (Figures 8A–C). Compared to the control, the number and size of microglia, as well as astrocyte in the NAc were elevated in the chronic morphine treated group. CBDV inhibited the activation of microglia (Figures 8D, E) and astrocytes (Figures 8F, G). Meanwhile, the tissue RNA extraction and qPCR were performed to examine the expression of pro-inflammatory factors. Chronic morphine treatment was found to increase pro-inflammatory factors TNF-α (Figure 8H) and IL-6 (Figure 8I) mRNAs expression in the NAc, which clearly shows that morphine induces a neuroinflammatory milieu. CBDV was found to inhibit morphine-induced TNF-α (Figure 8H) and IL-6 (Figure 8I) mRNAs expression in the NAc. In contrast, chronic morphine failed to activate glia in mPFC (Supplementary Figure 1) and VTA (Supplementary Figure 2) regions and CBDV did not affect TNF-α and IL-6 mRNAs expression in these regions. These results imply that CBDV improves morphine-mediated analgesia by specifically inhibiting morphine-induced glial activation and pro-inflammatory factors expression in NAc.

Discussion

Since being isolated in 1969 (46), the underlying mechanisms of CBDV actions are little known. It should be noted that cannabinoid receptors are not the primary targets of CBDV owing to the low binding affinity (47, 48). Considering that CBDV has good BBB permeability (20, 21), it would be interesting to investigate how CBDV regulates central immunity, which is mainly mediated by CNS resident innate immune cells microglia and astrocytes. TLR4 is abundantly expressed in glia and is the key PRR of the innate immune system, which detects PAMPs, DAMPs and XMAPs (5). Therefore, the interaction of

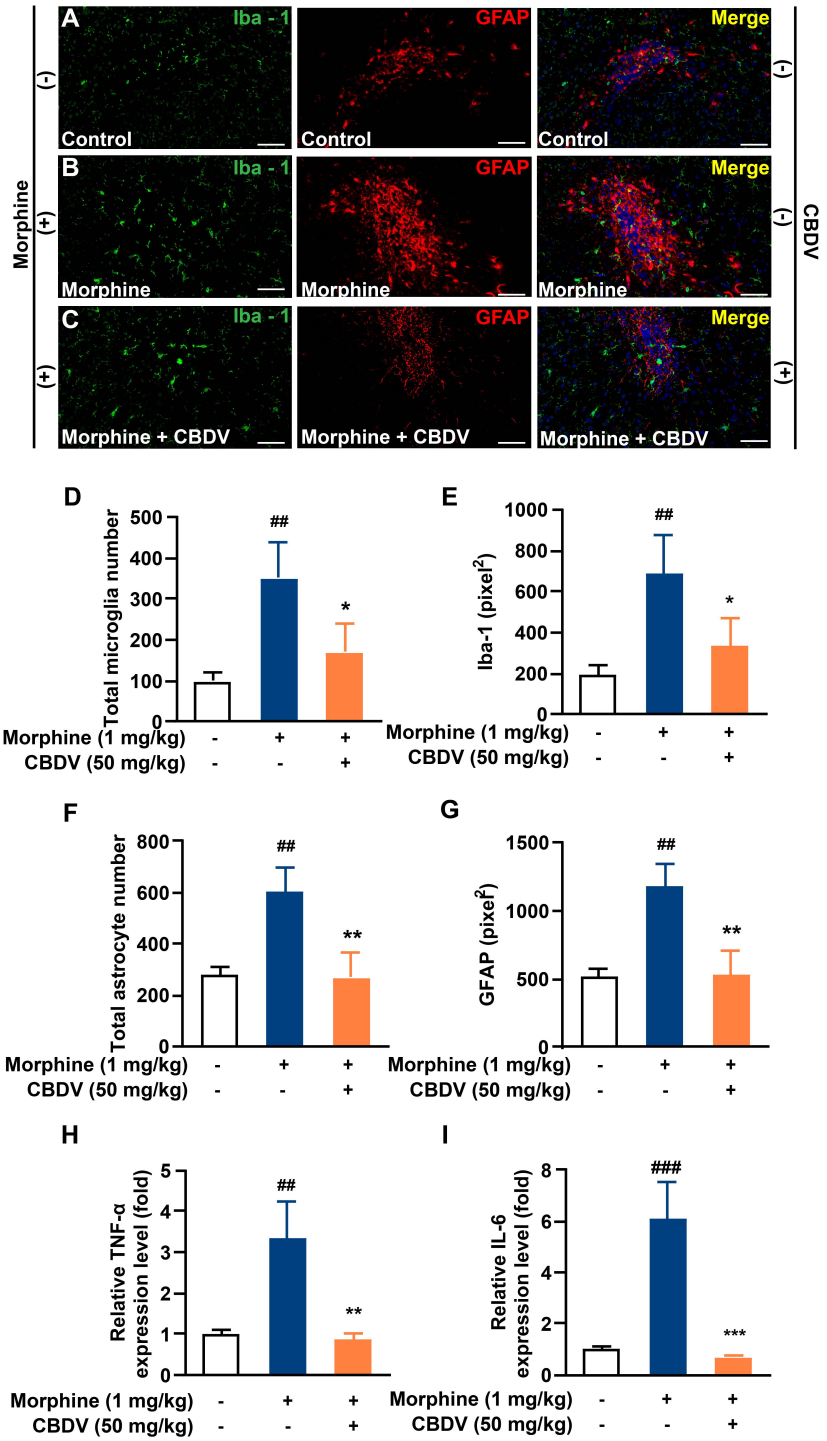

FIGURE 8
CBDV inhibits chronic morphine treatment-induced glial activation and pro-inflammatory factors IL-6 and TNF-α mRNA expression in NAc. **(A–C)** Representative double immunofluorescent staining images of Iba1 and GFAP for the control group **(A)**, morphine group **(B)**, and morphine + CBDV group **(C)**. NAc regions were collected following the final behavioral testing shown in Figure 7B. **(D, F)** The quantification of microglia **(D)** and astrocytes **(F)**. **(E, G)** The size of the microglia **(E)** and astrocytes **(G)**. **(H, I)** Total RNAs were extracted and qRT-PCR was performed to measure the expression of TNF-α **(H)** and IL-6 **(I)** in NAc. Scale bar: 200 μm. All the data represented mean ± S.E.M. ## $P < 0.01$, ### $P < 0.001$ versus the control group; *$P < 0.05$, **$P < 0.01$, ***$P < 0.001$ versus the morphine group.

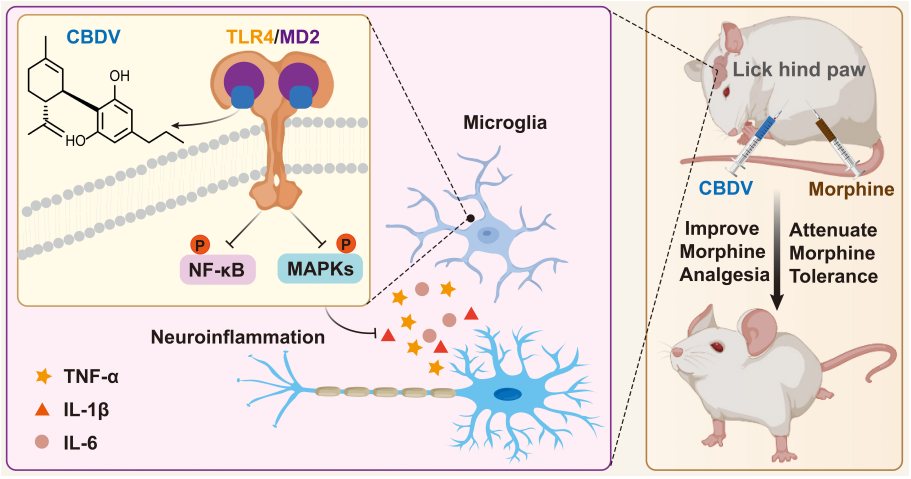

FIGURE 9
A schematic illustration of the role of CBDV in modulating TLR4 signaling *via* targeting MD2. CBDV binds to TLR4 co-receptor MD2, inhibits TLR4 signaling NF-κB and MAPKs, and suppresses downstream pro-inflammatory cytokines TNF-α, IL-1β and IL-6. By inhibiting microglial-induced neuroinflammation, CBDV improves morphine-mediated analgesia.

CBDV with TLR4 co-receptor MD2, which is responsible for the recognition of TLR4 ligand, was investigated. Herein, *in vitro* quenching titrations of MD2 intrinsic fluorescence showed the direct binding of CBDV to MD2. CETSA confirmed that MD2 was the endogenous target of CBDV. The RMSF analysis indicated that CBDV destabilized MD2, which is consistent with CETSA data. Cellular characterizations found that CBDV inhibited TLR4 signaling NF-κB and MAPKs axes, therefore suppressing neuroinflammation. This study identified MD2 as a direct target of CBDV, which at least in part accounts for its anti-neuroinflammatory activity. It should be acknowledged that there may be other unknown targets, which are worth further investigation.

Our previous work demonstrated that morphine bound to MD-2, induced TLR4 oligomerization, and activated TLR4 signaling (7). Morphine induces glial activation and neuroinflammation, which compromises morphine analgesia and contributes to morphine tolerance (42, 43). Therefore, TLR4 would be a novel target for therapeutic development to improve the current opioid-based pain management therapies. In this study, TLR4 antagonist CBDV was found to increase and prolong morphine analgesia in a dose-dependent manner. Moreover, CBDV attenuated morphine tolerance. Furthermore, the *in vivo* results show that CBDV improved morphine-mediated analgesia by specifically inhibiting chronic morphine-induced glial activation and pro-inflammatory factors expression in the NAc. It should be noted that CBDV alone showed no analgesic activity as tested by the hot plate assay while CBDV showed analgesic effects in both the acute phase and tonic phase as measured by the formalin test. This is not surprising considering that these two behavioral models of nociception show contrast different cellular and molecular mechanisms of pain (49, 50). Further elucidation is needed for a better understanding of these different behavioral responses of CBDV.

Considering the facts that morphine is the most commonly used opioid analgesic in the clinic (51) and the opioid crisis has been a significant public health burden (52), there is an urgent need to boost the analgesic activity, reduce the used dose and prevent the tolerance side effect of morphine. Previous proof-of-concept studies have demonstrated that TLR4 small-molecule antagonists would provide a nonconventional avenue to improve the clinical efficacy of opioids and possibly improve safety (7, 53). Consequently, numerous TLR4 antagonists have been developed (54, 55). However, few of them could cross BBB (16). This study adds CBDV, which has good BBB penetrability, as a potent TLR4 antagonist. Although CBDV is safe (18), the solubility of CBDV is poor, which may limit the therapeutic applications of CBDV by its low bioavailability (56). Incorporating CBDV into a novel drug delivery system is hopefully to boost its bioavailability, prolong its half-life, and enhance the therapeutic efficacy.

In summary, this study clearly confirms that MD2 is a direct binding target of CBDV for the anti-neuroinflammatory effect and implies that CBDV is a TLR4 antagonist, which can partially explain its interference of innate immune function in CNS. Furthermore, CBDV improves morphine-mediated analgesia by inhibiting morphine-induced glial activation and pro-inflammatory factors expression (Figure 9). The results imply that CBDV could be a potential therapeutic agent for improving morphine-mediated analgesia.

Data availability statement

The original contributions presented in the study are included in the article/Supplementary Material. Further inquiries can be directed to the corresponding authors.

Ethics statement

The animal study was reviewed and approved by The Institutional Animal Care and Use Committee (IACUC) of Changchun Institute of Applied Chemistry, Chinese Academy of Sciences (2022-0090).

Author contributions

XiW designed the experiments. XuW, CL, YW, TZ and SW performed the experiments, acquired and analyzed data. XuW, CL and XiW wrote the manuscript. YJ and XiW edited the manuscript. All authors read and approved the final manuscript.

Funding

This work was supported by Brain Science and Brain-Like Intelligence Technology Program (2021ZD0203003), Beijing National Laboratory for Molecular Sciences (BNLMS202108), and the Chinese Academy of Sciences (CAS) Pioneer Hundred Talents Program.

Acknowledgments

Computing time was supported by National Supercomputer Center in Tianjin.

Conflict of interest

The authors declare that the research was conducted in the absence of any commercial or financial relationships that could be construed as a potential conflict of interest.

Publisher's note

Supplementary material

The Supplementary Material for this article can be found online at: https://www.frontiersin.org/articles/10.3389/fimmu.2022.929222/full#supplementary-material

References

1. Albiger B, Dahlberg S, Henriques-Normark B, Normark S. Role of the innate immune system in host defence against bacterial infections: focus on the toll-like receptors. *J Intern Med* (2007) 261(6):511–28. doi: 10.1111/j.1365-2796.2007.01821.x

2. Kawai T, Akira S. The role of pattern-recognition receptors in innate immunity: update on toll-like receptors. *Nat Immunol* (2010) 11(5):373–84. doi: 10.1038/ni.1863

3. Fitzgerald KA, Kagan JC. Toll-like receptors and the control of immunity. *Cell* (2020) 180(6):1044–66. doi: 10.1016/j.cell.2020.02.041

4. Takeuchi O, Akira S. Pattern recognition receptors and inflammation. *Cell* (2010) 140(6):805–20. doi: 10.1016/j.cell.2010.01.022

5. Lin C, Wang H, Zhang M, Mustafa S, Wang Y, Li H, et al. TLR4 biased small molecule modulators. *Pharmacol Ther* (2021) 228:107918. doi: 10.1016/j.pharmthera.2021.107918

6. Paudel YN, Angelopoulou E, Akyuz E, Piperi C, Othman I and Shaikh MF. Role of innate immune receptor TLR4 and its endogenous ligands in epileptogenesis. *Pharmacol Res* (2020) 160:105172. doi: 10.1016/j.phrs.2020.105172

7. Wang X, Loram LC, Ramos K, de Jesus AJ, Thomas J, Cheng K, et al. Morphine activates neuroinflammation in a manner parallel to endotoxin. *Proc Natl Acad Sci U.S.A.* (2012) 109(16):6325–30. doi: 10.1073/pnas.1200130109

8. Northcutt AL, Hutchinson MR, Wang X, Baratta MV, Hiranita T, Cochran TA, et al. DAT Isn't all that: cocaine reward and reinforcement require toll-like receptor 4 signaling. *Mol Psychiatry* (2015) 20(12):1525–37. doi: 10.1038/mp.2014.177

9. Bachtell R, Hutchinson MR, Wang X, Rice KC, Maier SF and Watkins LR. Targeting the toll of drug abuse: The translational potential of toll-like receptor 4. *CNS Neurol Disord Drug Targets* (2015) 14(6):692–9. doi: 10.2174/1871527314666150529132503

10. Wang X, Northcutt AL, Cochran TA, Zhang X, Fabisiak TJ, Haas ME, et al. Methamphetamine activates toll-like receptor 4 to induce central immune signaling within the ventral tegmental area and contributes to extracellular dopamine increase in the nucleus accumbens shell. *ACS Chem Neurosci* (2019) 10(8):3622–34. doi: 10.1021/acschemneuro.9b00225

11. Zhang X, Wang Y, Wang H, Li H, Zhang T, Peng Y, et al. Exploring methamphetamine nonenantioselectively targeting toll-like receptor 4/Myeloid differentiation protein 2 by in silico simulations and wet-Lab techniques. *J Chem Inf Model* (2020) 60(3):1607–13. doi: 10.1021/acs.jcim.9b01040

12. Bachtell RK, Jones JD, Heinzerling KG, Beardsley PM and Comer SD. Glial and neuroinflammatory targets for treating substance use disorders. *Drug Alcohol Depend* (2017) 180:156–70. doi: 10.1016/j.drugalcdep.2017.08.003

13. Wang H, Zhang Y, Ma X, Wang W, Xu X, Huang M, et al. Spinal TLR4/P2X7 receptor-dependent NLRP3 inflammasome activation contributes to the development of tolerance to morphine-induced antinociception. *J Inflammation Res* (2020) 13:571–82. doi: 10.2147/jir.S266995

14. Wang H, Huang M, Wang W, Zhang Y, Ma X, Luo L, et al. Microglial TLR4-induced TAK1 phosphorylation and NLRP3 activation mediates neuroinflammation and contributes to chronic morphine-induced antinociceptive tolerance. *Pharmacol Res* (2021) 165:105482. doi: 10.1016/j.phrs.2021.105482

15. Eidson LN, Murphy AZ. Blockade of toll-like receptor 4 attenuates morphine tolerance and facilitates the pain relieving properties of morphine. *J Neurosci* (2013) 33(40):15952–63. doi: 10.1523/jneurosci.1609-13.2013

16. Wang Y, Zhang S, Li H, Wang H, Zhang T, Hutchinson MR, et al. Small-molecule modulators of toll-like receptors. *Acc Chem Res* (2020) 53(5):1046–55. doi: 10.1021/acs.accounts.9b00631

17. Alves P, Amaral C, Teixeira N, Correia-da-Silva G. Cannabis sativa: Much more beyond Δ(9)-tetrahydrocannabinol. *Pharmacol Res* (2020) 157:104822. doi: 10.1016/j.phrs.2020.104822

18. Huizenga MN, Sepulveda-Rodriguez A, Forcelli PA. Preclinical safety and efficacy of cannabidivarin for early life seizures. *Neuropharmacology* (2019) 148:189–98. doi: 10.1016/j.neuropharm.2019.01.002

19. Hill TD, Cascio MG, Romano B, Duncan M, Pertwee RG, Williams CM, et al. Cannabidivarin-rich cannabis extracts are anticonvulsant in mouse and rat *via* a CB1 receptor-independent mechanism. *Br J Pharmacol* (2013) 170(3):679–92. doi: 10.1111/bph.12321

20. Calapai F, Cardia L, Sorbara EE, Navarra M, Gangemi S, Calapai G, et al. Cannabinoids, blood-brain barrier, and brain disposition. *Pharmaceutics* (2020) 12 (3):265. doi: 10.3390/pharmaceutics12030265

21. Stone NL, England TJ, O'Sullivan SE. Protective effects of cannabidivarin and cannabigerol on cells of the blood-brain barrier under ischemic conditions. *Cannabis Cannabinoid Res* (2021) 6(4):315–26. doi: 10.1089/can.2020.0159

22. Zamberletti E, Rubino T and Parolaro D. Therapeutic potential of cannabidivarin for epilepsy and autism spectrum disorder. *Pharmacol Ther* (2021) 226:107878. doi: 10.1016/j.pharmthera.2021.107878

23. Pretzsch CM, Floris DL, Voinescu B, Elsahib M, Mendez MA, Wichers R, et al. Modulation of striatal functional connectivity differences in adults with and without autism spectrum disorder in a single-dose randomized trial of cannabidivarin. *Mol Autism* (2021) 12(1):49. doi: 10.1186/s13229-021-00454-6

24. Zhang T, Zhang X, Lin C, Wu S, Wang F, Wang H, et al. Artemisinin inhibits TLR4 signaling by targeting co-receptor MD2 in microglial BV-2 cells and prevents lipopolysaccharide-induced blood-brain barrier leakage in mice. *J Neurochem* (2021) 157(3):611–23. doi: 10.1111/jnc.15302

25. Kim HM, Park BS, Kim JI, Kim SE, Lee J, Oh SC, et al. Crystal structure of the TLR4-MD-2 complex with bound endotoxin antagonist eritoran. *Cell* (2007) 130(5):906–17. doi: 10.1016/j.cell.2007.08.002

26. Trott O OA. AutoDock vina: improving the speed and accuracy of docking with a new scoring function, efficient optimization and multithreading. *J Comput Chem* (2010) 31:455–61. doi: doi:10.1002/jcc.21334

27. Van Der Spoel D, Lindahl E, Hess B, Groenhof G, Mark AE and Berendsen HJ. GROMACS: fast, flexible, and free. *J Comput Chem* (2005) 26(16):1701–18. doi: 10.1002/jcc.20291

28. Abraham MJ, Murtola T, Schulz R, Páll S, Smith JC, Hess B, et al. GROMACS: High performance molecular simulations through multi-level parallelism from laptops to supercomputers. *SoftwareX* (2015) 1-2:19–25. doi: 10.1016/j.softx.2015.06.001

29. Best RB, Zhu X, Shim J, Lopes PE, Mittal J, Feig M, et al. Optimization of the additive CHARMM all-atom protein force field targeting improved sampling of the backbone phi, psi and side-chain chi(1) and chi(2) dihedral angles. *J Chem Theory Comput* (2012) 8(9):3257–73. doi: 10.1021/ct300400x

30. Huang J, Rauscher S, Nawrocki G, Ran T, Feig M, de Groot BL, et al. CHARMM36m: an improved force field for folded and intrinsically disordered proteins. *Nat Methods* (2017) 14(1):71–3. doi: 10.1038/nmeth.4067

31. Wang J, Wang W, Kollman PA and Case DA. Automatic atom type and bond type perception in molecular mechanical calculations. *J Mol Graph Model* (2006) 25(2):247–60. doi: 10.1016/j.jmgm.2005.12.005

32. Blum CA MJB, Roli A. *Sampels, m: Hybrid metaheuristics, an emerging approach to optimization*. Berlin Heidelberg: Springer-Verlag (2008).

33. Darden T, York D. And pedersen l. particle mesh ewald: AnN·log(N) method for ewald sums in large systems. *J Chem Phys* (1993) 98(12):10089–92. doi: 10.1063/1.464397

34. Feller SE, Zhang Y, Pastor RW and Brooks BR. Constant pressure molecular dynamics simulation: The langevin piston method. *J Chem Phys* (1995) 103 (11):4613–21. doi: 10.1063/1.470648

35. Michaud-Agrawal N, Denning EJ, Woolf TB and Beckstein O. MDAnalysis: a toolkit for the analysis of molecular dynamics simulations. *J Comput Chem* (2011) 32(10):2319–27. doi: 10.1002/jcc.21787

36. Valdes-Tresanco MS, Valdes-Tresanco ME, Valiente PA and Moreno E. gmx_MMPBSA: A new tool to perform end-state free energy calculations with GROMACS. *J Chem Theory Comput* (2021) 17(10):6281–91. doi: 10.1021/acs.jctc.1c00645

37. Massova I, Kollman PA. Combined molecular mechanical and continuum solvent approach (MM-PBSA/GBSA) to predict ligand binding. *Perspect Drug Discovery Design* (2000) 18:113–35. doi: 10.1023/A:1008763014207

38. PyMol. *The PyMOL molecular graphics system*. Schrödinger LLC (2015).

39. Chen C, Zhang J, Sun L, Zhang Y, Gan WB, Tang P, et al. Long-term imaging of dorsal root ganglia in awake behaving mice. *Nat Commun* (2019) 10 (1):3087. doi: 10.1038/s41467-019-11158-0

40. Baltan S. Histone deacetylase inhibitors preserve function in aging axons. *J Neurochem* (2012) 123 Suppl 2(Suppl 2):108–15. doi: 10.1111/j.1471-4159.2012.07949.x

41. Park BS, Song DH, Kim HM, Choi BS, Lee H and Lee JO. The structural basis of lipopolysaccharide recognition by the TLR4-MD-2 complex. *Nature* (2009) 458(7242):1191–5. doi: 10.1038/nature07830

42. Ellis A, Grace PM, Wieseler J, Favret J, Springer K, Skarda B, et al. Morphine amplifies mechanical allodynia *via* TLR4 in a rat model of spinal cord injury. *Brain Behav Immun* (2016) 58:348–56. doi: 10.1016/j.bbi.2016.08.004

43. Hutchinson MR, Northcutt AL, Hiranita T, Wang X, Lewis SS, Thomas J, et al. Opioid activation of toll-like receptor 4 contributes to drug reinforcement. *J Neurosci* (2012) 32(33):11187–200. doi: 10.1523/jneurosci.0684-12.2012

44. Christie MJ. Cellular neuroadaptations to chronic opioids: tolerance, withdrawal and addiction. *Br J Pharmacol* (2008) 154(2):384–96. doi: 10.1038/bjp.2008.100

45. Schmidt BL, Tambeli CH, Barletta J, Luo L, Green P, Levine JD, et al. Altered nucleus accumbens circuitry mediates pain-induced antinociception in morphine-tolerant rats. *J Neurosci* (2002) 22(15):6773–80. doi: 10.1523/jneurosci.22-15-06773.2002

46. Vollner L, Bieniek D and Korte F. [Hashish. XX. cannabidivarin, a new hashish constituent]. *Tetrahedron Lett* (1969) (3):145–7. doi: 10.1016/s0040-4039(01)87494-3

47. Rosenthaler S, Pöhn B, Kolmanz C, Huu CN, Krewenka C, Huber A, et al. Differences in receptor binding affinity of several phytocannabinoids do not explain their effects on neural cell cultures. *Neurotoxicol Teratol* (2014) 46:49–56. doi: 10.1016/j.ntt.2014.09.003

48. Navarro G, Varani K, Lillo A, Vincenzi F, Rivas-Santisteban R, Raïch I, et al. Pharmacological data of cannabidiol- and cannabigerol-type phytocannabinoids acting on cannabinoid CB(1), CB(2) and CB(1)/CB(2) heteromer receptors. *Pharmacol Res* (2020) 159:104940. doi: 10.1016/j.phrs.2020.104940

49. Basbaum AI, Bautista DM, Scherrer G and Julius D. Cellular and molecular mechanisms of pain. *Cell* (2009) 139(2):267–84. doi: 10.1016/j.cell.2009.09.028

50. Swieboda P, Filip R, Prystupa A and Drozd M. Assessment of pain: types, mechanism and treatment. *Ann Agric Environ Med* (2013) Spec no. 1:2–7.

51. Kalso E, Edwards JE, Moore AR and McQuay HJ. Opioids in chronic non-cancer pain: systematic review of efficacy and safety. *Pain* (2004) 112(3):372–80. doi: 10.1016/j.pain.2004.09.019

52. Institute of Medicine Committee on Advancing Pain Research C and Education. The national academies collection: Reports funded by national institutes of health. In: *Relieving pain in America: A blueprint for transforming prevention, care, education, and research*. US: National Academies Press (2011). doi: 10.17226/13172

53. Lewis SS, Loram LC, Hutchinson MR, Li CM, Zhang Y, Maier SF, et al. (+)-naloxone, an opioid-inactive toll-like receptor 4 signaling inhibitor, reverses multiple models of chronic neuropathic pain in rats. *J Pain* (2012) 13(5):498–506. doi: 10.1016/j.jpain.2012.02.005

54. Bettoni I, Comelli F, Rossini C, Granucci F, Giagnoni G, Peri F, et al. Glial TLR4 receptor as new target to treat neuropathic pain: efficacy of a new receptor antagonist in a model of peripheral nerve injury in mice. *Glia* (2008) 56(12):1312–9. doi: 10.1002/glia.20699

55. Kwilasz AJ, Green Fulgham SM, Duran-Malle JC, Schrama AEW, Mitten EH, Todd LS, et al. Toll-like receptor 2 and 4 antagonism for the treatment of experimental autoimmune encephalomyelitis (EAE)-related pain. *Brain Behav Immun* (2021) 93:80–95. doi: 10.1016/j.bbi.2020.12.016

56. Gaston TE, Friedman D. Pharmacology of cannabinoids in the treatment of epilepsy. *Epilepsy Behav* (2017) 70(Pt B):313–8. doi: 10.1016/j.yebeh.2016.11.016

frontiers | Frontiers in Immunology

TYPE Original Research
PUBLISHED 12 August 2022
DOI 10.3389/fimmu.2022.930510

OPEN ACCESS

EDITED BY
Toshiyuki Shimizu,
The University of Tokyo, Japan

REVIEWED BY
Takuma Shibata,
The University of Tokyo, Japan
Cristina Corina Clement,
Cornell University, United States

*CORRESPONDENCE
Wanli Xing
wlxing@tsinghua.edu.cn

SPECIALTY SECTION
This article was submitted to Molecular Innate Immunity, a section of the journal Frontiers in Immunology

RECEIVED 28 April 2022
ACCEPTED 21 July 2022
PUBLISHED 12 August 2022

CITATION
Wei S, Jiao D and Xing W (2022) A rapid method for isolation of bacterial extracellular vesicles from culture media using epsilon-poly-L–lysine that enables immunological function research.
Front. Immunol. 13:930510.
doi: 10.3389/fimmu.2022.930510

A rapid method for isolation of bacterial extracellular vesicles from culture media using epsilon-poly-L–lysine that enables immunological function research

Shujin Wei[1], Dian Jiao[2] and Wanli Xing[1]*

[1]School of Medicine, Tsinghua University, Beijing, China, [2]School of Life Sciences, Tsinghua University, Beijing, China

Both Gram-negative and Gram-positive bacteria can release vesicle-like structures referred to as bacterial extracellular vesicles (BEVs), which contain various bioactive compounds. BEVs play important roles in the microbial community interactions and host-microbe interactions. Markedly, BEVs can be delivered to host cells, thus modulating the development and function of the innate immune system. To clarify the compositions and biological functions of BEVs, we need to collect these vesicles with high purity and bioactivity. Here we propose an isolation strategy based on a broad-spectrum antimicrobial epsilon-poly-L-lysine (ϵ-PL) to precipitate BEVs at a relatively low centrifugal speed (10,000 × g). Compared to the standard ultracentrifugation strategy, our method can enrich BEVs from large volumes of media inexpensively and rapidly. The precipitated BEVs can be recovered by adjusting the pH and ionic strength of the media, followed by an ultrafiltration step to remove ϵ-PL and achieve buffer exchange. The morphology, size, and protein composition of the ϵ-PL-precipitated BEVs are comparable to those purified by ultracentrifugation. Moreover, ϵ-PL-precipitated BEVs retained the biological activity as observed by confocal microscopy studies. And THP-1 cells stimulated with these BEVs undergo marked reprogramming of their transcriptome. KEGG analysis of the differentially expressed genes showed that the signal pathways of cellular inflammatory response were significantly activated. Taken together, we provide a new method to rapidly enrich BEVs with high purity and bioactivity, which has the potential to be applied to BEVs-related immune response studies.

KEYWORDS

bacterial extracellular vesicles, epsilon-poly-L–lysine, bacterial culture medium, isolation, precipitation, innate immunity, cytokine

Introduction

One of the functions of the innate immune system is to surveil the microbes in our bodies. Innate immune cells can recognize conserved bacterial molecular structures known as pathogen-associated molecular patterns (PAMPs) through pattern-recognition receptors (PRRs), which are crucial for the development of appropriate immune responses (1, 2). Even though the access of microbes to the immune cells is restricted physically in most situations, recent evidence have shown that the microbiota can communicate with the host through various effector molecules (3), such as short-chain fatty acids (SCFAs), lipopolysaccharide (LPS), proteins, and bacterial extracellular vesicles (BEVs) (4). Among these microbiota-secreted factors, BEV is likely to have a more important role in interkingdom interactions (5–7) for the release of vesicle-like structures is a universally conserved cellular process that occurs in all domains of life (8). BEVs harbor various components derived from bacterial cells, like genetic materials, proteins, lipids, and virulence factors. By interacting with innate immune cells, BEV can regulate immune reactions in the host (9, 10). Evaluation of the interaction between BEV and the innate immune system can provide a better understanding of the molecular mechanisms underlying innate immune responses, and has the potential to develop a new avenue of therapies on the basis of BEVs.

Unfortunately, the isolation of BEVs is still facing some challenges. Similar to exosomes secreted by mammal cells, BEVs are heterogeneous vesicles and have quite small diameters in the range from 20 to 200 nm (11, 12). Until now, the most commonly used BEV enrichment method is ultracentrifugation (> 100,000 × g) (13, 14), which requires expensive instrumentation, long processing times, and cumbersome operation. Other available enrichment methods include ultrafiltration (UF), precipitation by addition of a high concentration of salt, and gel filtration (15). However, each of these methods suffers from its disadvantages (16). In UF techniques, the membrane is easily clogged, retarding the process of isolation. In precipitation techniques, the concentration of salt should be raised to more than 40%, and the non-specific binding of free proteins to BEV is highly probable. As to gel filtration technique, many factors, including column packing, flow rate, media types, and pore size should be considered to achieve high efficiency. There is an urgent need to develop more convenient methods for BEV isolation.

Some features of BEVs can be used to develop new isolation methods. It has been shown that BEVs derived from Gram-negative bacteria harbor abundant amounts of LPS on the membrane (17, 18), while lipoteichoic acid is often considered a component of Gram-positive bacterial extracellular vesicles (19). Hence the BEVs often have a concentrated negative charge. ϵ-Poly- L -lysine (ϵ -PL) is a natural antimicrobial substance and consists of 25 to30 L-lysine residues which possess positively charged amine groups (20). ϵ-PL has broad-spectrum antimicrobial activity and low toxicity; hence it is utilized as a food additive for various products. The interaction of bacteria and ϵ-PL relies on negative charges on the bacterial membrane (21, 22). Nanoparticles functionalized with ϵ-PL have been used for broad-spectrum bacterial capture (23). Yet there's no report applying this substance in BEVs enrichment.

In this work, we established an ϵ-PL-based technique to enrich BEVs from bacterial culture media at a relatively low centrifugal speed (10,000 × g). The extracted materials isolated by our new method have similar protein profiles as the BEVs isolated by ultracentrifugation. Subsequently, by adjusting the pH and ionic strength of the buffer, the pellets could become dispersed in suspension without visible aggregation. We then conducted ultrafiltration to remove ϵ-PL and achieve buffer exchange. The morphology and size of the harvested BEVs were found to be comparable to those purified by ultracentrifugation. Finally, we validated that the ϵ-PL-precipitated BEVs can be internalized by THP-1 cells and induce activation of inflammation-related signaling pathways. Overall, it suggested that our method could potentially contribute to studies on BEVs and their immunoregulatory effect on innate immunity.

Materials and methods

Microbial culture and preparation of culture medium

Escherichia coli laboratory strain DH5a (*E. coli*) and *Staphylococcus aureus* (*S. aureus*, CICC 10384) were grown overnight in LB broth (1% tryptone, 0.5% yeast extract, 1% NaCl) at 37°C with shaking (200 rpm). The supernatant fraction was collected by centrifugation (6,000 g, 15 min, 4°C, and 10,000 g, 15 min, 4°C). Then the supernatant was filtered through a PVDF 0.45-μm filter (HYCX, China) to remove any remaining cells. The resultant filtrate could be used for subsequent BEV isolation.

Isolation of BEVs by ultracentrifugation

The bacterial culture medium preprocessed by centrifugation and filtration was loaded into ultracentrifuge tubes and centrifuged at 160,000 × g for 2h at 4°C (rotor 70Ti, L-80XP, Beckman Coulter, Germany) to obtain vesicle-rich pellets. Then the pellets were resuspended in phosphate buffer saline (PBS) and centrifuged at 160,000 × g for 2h at 4°C. Finally, the pellets were resuspended in a minimal volume of PBS and stored at −80°C until use.

Isolation of BEVs by ϵ-PL-based method

3 M 4-Morpholineethanesulfonic acid (Aladdin, China) was combined with sodium chloride (0.15 M) to make a ten-fold concentrated (10× MES) stock solution. The 10x MES solution

was added to a tenfold volume of bacterial culture medium preprocessed by centrifugation and filtration to adjust the pH value of the bacterial culture medium to near neutrality. The ε-PL (Shanghai yuanye, China) stock solution was prepared by dissolving ε-PL in PBS at a concentration of 10 mg/mL. Then the ε-PL stock solution was added to the bacterial culture medium to achieve a final concentration of 100 μg/mL. After rocking on a shaker for 45 min at room temperature, the mixture was subjected to centrifugation at 10,000 × g for 15 min. Then the pellet was washed in PBS buffer twice and resuspended by re-suspension buffer (50 mM Tris-HCl, 0.5 M NaCl, pH 8.5). Finally, the sample was subjected to four rounds of ultrafiltration using 1.5-mL 100 kDa ultrafiltration tubes (Merck Millipore, Germany). The buffer was replaced by PBS and stored at −80°C until use.

Transmission electron microscopy

BEVs isolated by UC or ε-PL were diluted to an appropriate concentration. Then, 7 μL of the BEVs were dropped onto carbon-coated grids and incubated for 2 min at room temperature. Next, BEVs were negatively stained with uranyl acetate for 1 min. Finally, BEVs were observed using an electron microscope (FEI Tecnai Spirit TEM D1266, FEI, USA) operating at 110 kV.

Nanoparticle tracking analysis

BEVs isolated by UC or ε-PL were diluted 3000-fold with distilled water. The particle size distribution of BEVs was determined using nanoparticle tracking analysis (Particle Metrix, Germany). All particle-size analyses used the same set of parameters to ensure comparable results.

Bicinchoninic acid assay

The BEV protein concentration was quantified using the BCA protein assay kit (Solarbio, China) following the manufacturer's instructions.

Proteomic analysis of BEVs by LC-MS/MS

BEVs isolated by UC or ε-PL were used for proteomic analysis. BEVs (10 μg) were separated by SDS-PAGE (10%). Then the gel bands were excised and subjected to in-gel digestion. The peptides were extracted redissolved in 0.1% TFA solution and analyzed by LC-MS/MS.

For LC-MS/MS analysis, the peptides were separated by a 120 min gradient elution at a flow rate of 0.30 μL/min with a Thermo-Dionex Ultimate 3000 HPLC system, which was directly interfaced with a Thermo Scientific Q Exactive™ HF-X mass spectrometer. The mass spectrometer was operated in the data-dependent acquisition mode using Xcalibur 2.2 software and there was a single full-scan mass spectrum in the orbitrap (300-1800 m/z, 60,000 resolution) followed by data-dependent MS/MS scans at NCE 27%.

The MS/MS spectra from each LC-MS/MS run were searched against datasets from UniProt using an in-house Proteome Discoverer (Version PD1.4, Thermo-Fisher Scientific, USA). The peptide false discovery rate (FDR) was calculated using Percolator provided by PD. The peptide spectrum match (PSM) was considered to be correct only when the q-value was smaller than 1%. FDR was determined based on PSMs when searched against the reverse, decoy database. Peptides only assigned to a given protein group were considered unique. The false discovery rate (FDR) was set to 0.01 for protein identification.

Analysis of proteins was performed as previously described (24, 25). Spectral counts of each protein are normalized for quantification. Statistical testing was performed using R software 4.0.2 (R Foundation for Statistical Computing, Austria) (26).

Cytotoxicity assessment

THP-1 monocytes were seeded in 96-well plates (4×10^4 cells per well) and let grow for 24h under 5% CO_2 at 37°C. The cells were then treated with different protein concentrations (5, 10, and 15μg/ml) of BEVs for 6 h. PBS-treated cells were considered a negative control with 100% viability. The viability assay was conducted using the Cell Counting Kit-8 (CCK-8) assay kit (Lablead, China) following the manufacturer's instructions.

Assessment of uptake of BEVs

Analysis of the internalization of BEVs was performed as previously described (27). Briefly, BEVs were diluted in 500 μL PBS, and 2 μL DiI dye (Thermo Fisher Scientific, USA) was added and incubated for 30 min at 37°C. After incubation, the samples were transferred to 1.5-mL 100-kDa ultrafiltration tubes and washed four times with PBS at 14,000 × g. The filters were inverted and centrifuged at 1000 × g for 2 min to collect the labeled BEVs. PBS labeled with DiI using the same protocol performed with BEVs was used as the control for uptake study.

THP-1 cells were seeded in 96-well plates (2×10^5 cells per well). Then labeled BEVs were added onto cells at protein concentrations of 5, 10, and 20 μg/mL and incubated for 4h under 5% CO_2 at 37°C. The cells were washed three times with PBS to remove residual BEVs. The cellular suspensions were collected and measured with flow cytometry. DiI-positive cells (PE-A channel) after successful uptake of DiI-labeled BEVs were

determined, as compared with PBS-treated cells (negative control), using FlowJo 7.6 software (FlowJo LLC, USA).

To conduct confocal imaging of cells, THP-1 cells incubated with BEVs at a protein concentration of 20 μg/mL were fixed with 4% paraformaldehyde for 15 min and stained with 4', 6-diamidino-2-phenylindole (DAPI, Thermo Fisher Scientific, USA) for 3 min. The cells were analyzed with a confocal laser scanning microscope (Zeiss, Germany).

Transcriptional analysis of THP-1 cells stimulated with BEVs

THP-1 monocytes were seeded at a density of 0.75×10^6 cells per mL in 6-well plates in 2 mL RPMI 1640 medium (Thermo Fisher Scientific, USA) supplemented with 10% fetal bovine serum (Gibco, USA) and antibiotics. Then *E. coli* BEVs at a protein concentration of 1μg/mL and *S.aureus* BEVs at a concentration of 10 μg/mL were added to each well followed by incubation for 6 h. Cells stimulated with PBS served as the negative control. The experiments were performed in triplicate for each group.

Total RNA was extracted with Trizol (Invitrogen) and assessed with Agilent 2100 BioAnalyzer (Agilent Technologies, Santa Clara, CA, USA) and Qubit Fluorometer (Invitrogen). The NEB Next Ultra RNA Library Prep Kit for Illumina (NEB) was used to construct the libraries. Then libraries were subjected to paired-end sequencing with pair-end 150-base pair reading length on an Illumina NovaSeq sequencer (Illumina).

For data analysis, the genome of human genome version of hg38 was used as a reference. The sequencing quality was assessed with FastQC (28) and the clean reads were aligned to the reference genome using HISAT2 (29) with default parameters. DESeq2 (30) was used to analyze the DEGs (differently expressed genes) between samples. Parameters for classifying significantly DEGs are ≥2-fold differences (|log2FC|≥1, FC: the fold change of expressions) in the transcript abundance and adjusted $p \leq 0.01$. Kyoto Encyclopedia of Genes and Genomes (KEGG) pathway analysis was performed using the Clusterprofile package (26).

Detection of cytokine production

THP-1 monocytes were seeded at a density of 1×10^6 cells per mL in 12-well plates. Then *E. coli* BEVs at a protein concentration of 1μg/mL and *S.aureus* BEVs at a concentration of 10 μg/mL were added to each well followed by incubation for 6 h. Cells stimulated with PBS served as the negative control.

To measure gene expression of IL-6, IL-8, and IL-1β, total RNA was isolated with an RNA Extraction kit (Tiangen, China) according to the manufacturer's instructions. 1 μg of isolated RNA was reverse transcribed into cDNA using the 1st Strand cDNA Synthesis SuperMix Kit (Novoprotein, China). Then, 0.5 μl of cDNA was used as the template for each real-time PCR. Real-time PCR was performed using a SYBR qPCR SuperMix (Novoprotein, China) on ABI7500 real-time PCR system (Thermo Fisher Scientific, USA). Primers for target genes are presented in Supplementary Table 1. Gene expression was normalized to GAPDH production in each sample, and the fold induction was determined by using the $\triangle\triangle C_T$ method. Each experiment was performed with triplicate samples and repeated three times.

To determine the production of cytokines, cell culture supernatants were collected. The levels of IL-8 and IL-1β were measured by enzyme-linked immunosorbent assay kits (ELISA, solarbio, China) according to the manufacturer's instructions. Each experiment was performed with triplicate samples and repeated three times.

Statistical analysis

Analysis of cell viability, BEV internalization and cytokine production was performed at least three times independently, and the data are shown as means ± SEM. One-way analysis of variance (ANOVA) using Tukey's multiple-comparison test was applied to differentiate between groups. Statistical analyses were performed using R software 4.0.2 (R Foundation for Statistical Computing, Austria).

Results

Treatment of bacterial culture medium using ϵ-PL could enrich membrane-bound structures

The zeta potentials of BEVs derived from Gram-negative and Gram-positive bacteria are negative owing to a high percentage of negatively charged phospholipids in bacterial membranes. We isolated BEVs from the culture supernatant of *Escherichia coli* (*E. coli*) and *Staphylococcus aureus* (*S. aureus*) by ultracentrifugation. And we confirmed the surface zeta potential values were highly negative (Supplementary Figure 1). Epsilon-poly-L–lysine (ϵ-PL) is a hydrophilic linear homo-poly-amino acid, which typically consists of 25 to 35 L–lysine residues. Because of its amino groups, ϵ-PL contains a strong positive charge and can interact with both gram-positive and gram-negative bacteria through electrostatic adsorption.

The scheme of the whole isolation process is presented in Figure 1. Negatively charged BEVs can bind to positively charged ϵ-PL, which leads to aggregation of BEVs and makes isolation by centrifugation easier. Pellets are re-suspended in a buffer with a high pH value and high concentration of salt. The resulting mixtures are loaded into the assembled ultrafiltration

column to remove ϵ-PL and achieve buffer exchange. The recovered BEVs could be used for subsequent analyses directly. In this work, we chose *E. coli* and *S. aureus* grown in LB broth to evaluate the ϵ-PL-based isolation method.

BEVs isolated by the ϵ-PL-based precipitation method (PL) were examined for morphology and size distribution. The results were compared with those of the commonly used ultracentrifugation method (UC). In transmission electron microscopy (TEM) analysis, round particles with typical cup-shaped morphology were identified in all samples (Figures 2A–D). We then conducted a Nanoparticle tracking analysis (NTA) to compare the size distributions of the BEVs obtained using the two methods. The majority of vesicles isolated by UC are in the size range of 50–150 nm (Figures 2E, G), with a major peak size of around 100 nm. The size distributions of BEVs isolated by PL were comparable to the results of UC, though the average particle size is slightly larger (Figures 2F, H).

Proteomic analysis shows enrichment of vesicle-related proteins for both isolation methods

SDS-PAGE was carried out to evaluate the protein profiles of BEVs isolated by UC or PL. The motion pattern of BEVs in a gel presented similar protein profiles between the two methods (Figures 3A, B), although there were several differently represented protein bands (Figure 3A). To reveal differences in the protein content in BEVs isolated by different methods, proteomic analysis was performed using liquid chromatography-tandem mass spectroscopy (Data are available *via* ProteomeXchange with identifier PXD034259). As summarized in the Venn diagrams, there were substantial overlaps between the identified proteins in BEVs isolated by the two methods for both *E. coli* and *S. aureus* (Figures 3C, D). And the correlations of protein levels between fractions isolated using UC and PL were also high (Figures 3E, F). However, some proteins indeed showed differences between the two methods. A representative protein is 60 kDa chaperonin GroEL derived from *E. coli*, which was enriched in the fraction isolated by UC, and may be the reason for the high intensity of the 60-kDa band in the UC group. Although GroEL has been detected in many BEV studies, one study using BEVs purified by density gradient centrifugation and size exclusion chromatography described the protein as a potential contamination marker (31). The implication of GroEL in vesicle biosynthesis requires further in-depth study.

To determine what type of proteins each method isolates, we employed k-means clustering and visualized the clustering results by heatmap (Figure 4A, Supplementary Figure 2A, Supplementary Table 2). In general, proteins showing similar protein profiles across the two methods were highly abundant (Figure 4A, Supplementary Figure 2 cluster D, cluster E), while the proteins showing differences between the UC and PL groups were frequently low abundant (Figure 4A, Supplementary Figure 2A cluster A-C). For proteins derived from *E. coli*, we then performed functional enrichment analysis to identify enriched cellular components of the common proteins. The GO annotation of cluster D and E showed enrichment of terms such as "outer membrane" and "ribosome", supporting the outer membrane vesicle origin of these proteins. And several potential BEV-related proteins (32, 33) were among the most abundant proteins, such as outer membrane porin C (OmpC), outer membrane protein A (OmpA) and elongation factor Tu (EF-

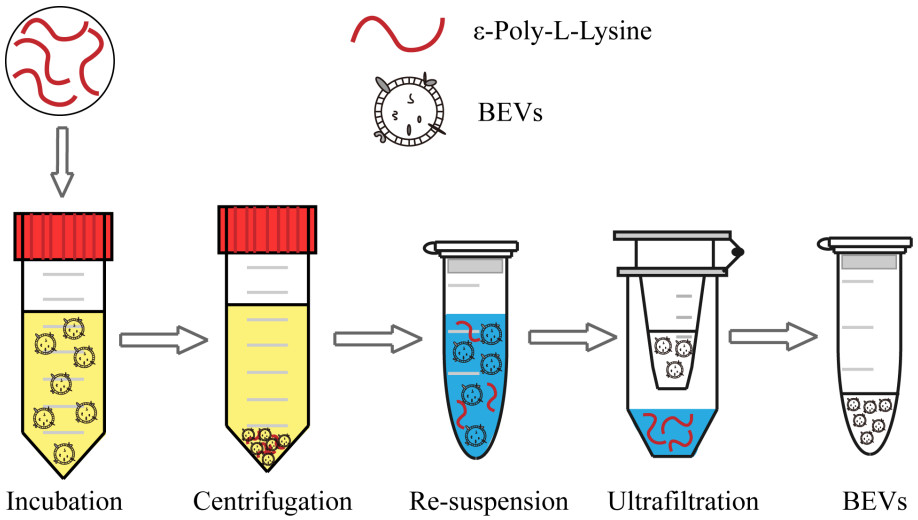

FIGURE 1
Schematic of the BEV isolation from the bacterial culture medium using the ϵ-PL-based method.

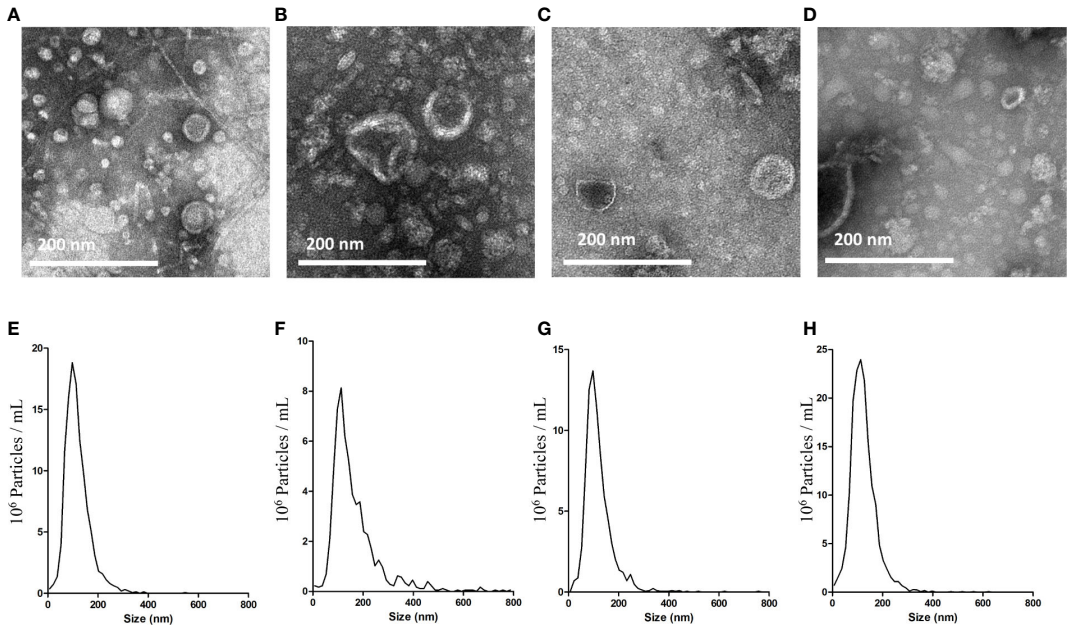

FIGURE 2
Characterization of BEVs using TEM and NTA. TEM images of BEVs derived from *E. coli* isolated by UC **(A)** or PL **(B)**. TEM images of BEVs derived from *S. aureus* isolated by UC **(C)** or PL **(D)**. Representative particle size-distribution curve of BEVs derived from *E. coli* isolated by UC **(E)** or PL **(F)**. Representative particle size-distribution curve of BEVs derived from *S. aureus* isolated by UC **(G)** or PL **(H)**.

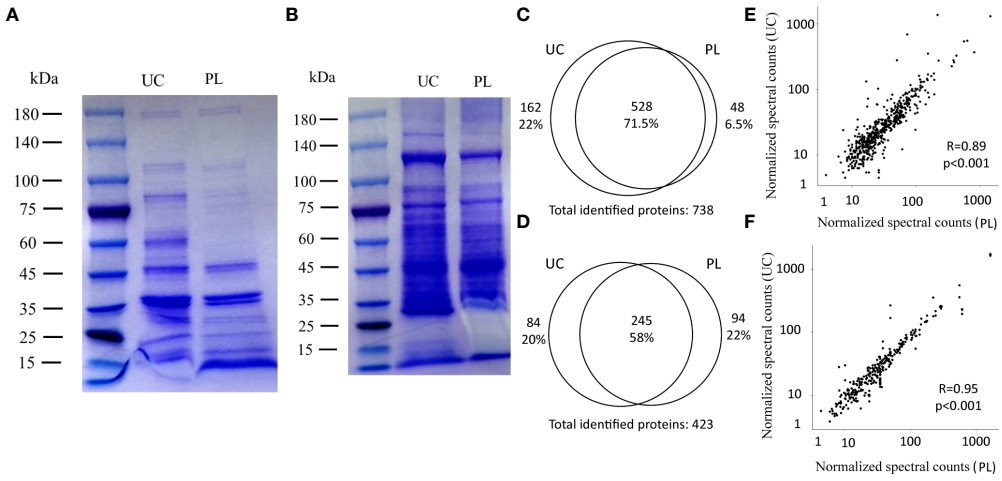

FIGURE 3
Comparison of identified proteins between UC and PL. SDS-PAGE of BEVs derived from *E. coli* **(A)** and *S. aureus* **(B)** isolated by UC and PL. Venn diagrams showing the identified proteins in *E. coli* **(C)** and *S. aureus* **(D)** BEVs isolated by UC or PL. Correlation analysis of proteins identified in *E. coli* **(E)** and *S. aureus* **(F)** BEVs isolated by UC compared to PL. Shown proteins were identified in at least 2 of the 4 patients in each species.

Tu) (Figure 4B). We also compared the identified proteins with a public dataset (top 50 proteins that are most frequently identified in Gram-negative bacterial outer membrane proteins, Supplementary Table 3). Of the top 50 most reported proteins (32), 43 were found in our dataset. Among them, 33 proteins were included in cluster E and 8 were included in cluster D. In contrast, the proteins showing differences between the UC and PL groups (cluster A-C) revealed no significant enrichment in any GO cellular component category,

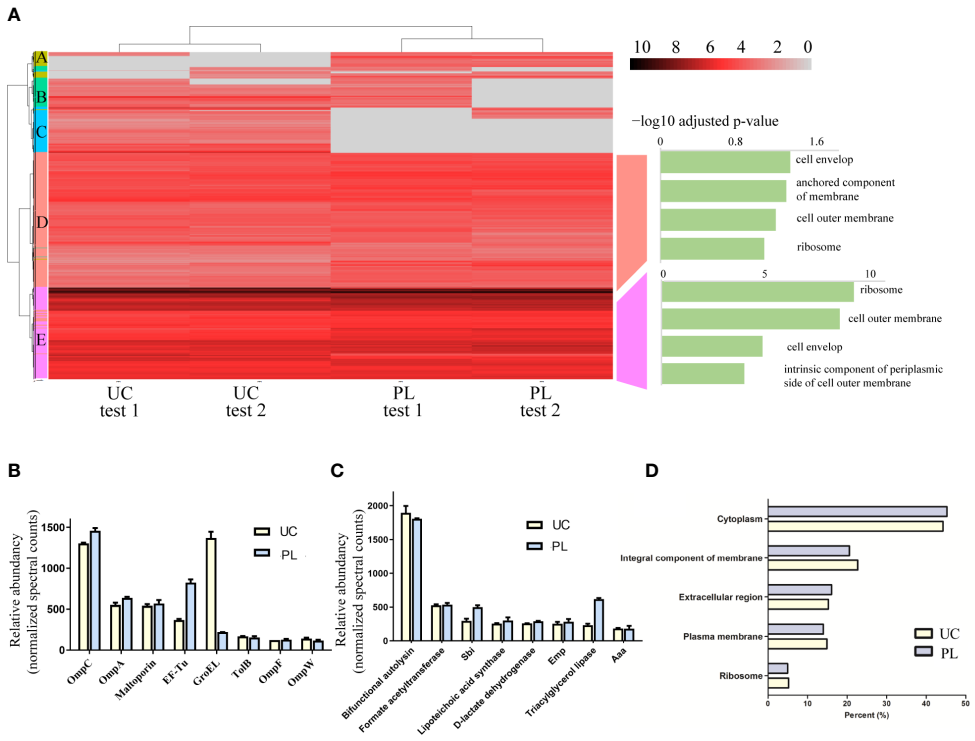

FIGURE 4
Identification of proteins isolated by the two methods. **(A)** Clustering analysis and subsequent GO enrichment for Cellular Components on the identified common clusters was performed for isolated samples from *E. coli*. The scale of the heatmap shows log2 transformed intensities of the proteins. Absent proteins are displayed in grey. **(B)** The abundance of representative proteins BEVs derived from *E. coli* isolated by UC and PL. **(C)** The abundance of representative proteins BEVs derived from *S. aureus* isolated by UC and PL. **(D)** Distribution of vesicular proteins derived from *S. aureus* based on their subcellular locations.

though many of them are categorized as cytosolic protein. Whether these proteins are exported inside BEVs or co-precipitated with the vesicle remains to be validated. For proteins derived from *S. aureus* (Figure 4C), the high abundant cluster D consists of proteins involved in cell wall biosynthesis/degradation (bifunctional autolysin, lipoteichoic acid synthase), adhesins (extracellular matrix protein-binding adhesin Emp, and autolysin/adhesin Aaa), metabolic enzymes (triacylglycerol lipase, D-lactate dehydrogenase, and Formate acetyltransferase), and immune evasion factors (immunoglobulin-binding protein Sbi). Most proteins were located in the cytoplasm and membrane (Figure 4D), which agreed with what was described earlier (31). Overall, these data indicate that PL isolates a similar vesicle-rich fraction as the commonly used UC method.

BEVs isolated by PL can be internalized by human monocytic THP-1 cells

To find out whether the ϵ-PL-based method impacts the biological activity of BEVs, we verified the ability of BEVs collected by UC or PL to be taken up by recipient cells. It has been reported that BEVs isolated by UC can be internalized by mammalian cells after 4 h of incubation. So, THP-1, a human monocytic cell line, was incubated with DiI-stained BEVs at protein concentrations of 5, 10, and 20 μg/mL. After 4 h of incubation, THP-1 exhibited uptake of BEVs isolated by both UC and PL, as indicated by a shift of fluorescence intensity of cell populations in flow cytometry (Figure 5A). A dose-dependent increase in uptake rate was detected for both UC and PL BEVs. (Figure 5B) BEVs enriched using ϵ-PL were taken up as well as, or better than those enriched using UC. We validated the flow cytometry results by confocal laser scanning microscopy (Figure 5C). Both types of BEVs were uptake by the THP-1 cells, which were confirmed by the appearance of numerous red dots of DiI-stained BEVs. No DiI staining was observed in the negative control group.

Transcriptional analysis shows triggered immune response in THP-1 cell by PL isolated BEVs

Examination of whether the BEVs isolated by UC or PL have any cytotoxic effects was performed on THP-1 cells. Various

concentrations (0, 5, 10, and 15 μg/mL) of BEVs were applied to THP-1 cells, and the cell line exhibited tolerance to the BEV from all samples during the incubation time (Figure 6A). The cells incubated with BEVs showed comparable viability to the positive control group (PBS treated), indicating the BEVs isolated by both methods have compatibility with immune cells and do not show obvious cytotoxic effects.

To address whether BEVs isolated by different methods lead to different host responses, we stimulated THP-1 cells with 1 μg/mL *E. coli* BEV or 10 μg/mL *S. aureus* BEVs. The global transcript profiles were evaluated 6 hours after incubation by the RNA-seq technique, and this time period was reasonably selected to collect the transcription profiles at the early stage of stimulation. The heatmap visualized the pairwise correlations between samples and the correlation values were hierarchically clustered. In comparison to non-stimulated THP-1 cells, BEV stimulated cells triggered a striking alteration in the gene expression patterns, as indicated by the clear separation of clusters of unstimulated groups from the BEVs stimulated groups (Figure 6B). Hierarchical clustering also segregated the cells stimulated with *E. coli* BEVs from those of stimulated with *S.aureus* BEVs.

Then differential expression analysis was conducted in BEV-stimulated cells compared with non-stimulated cells by DESeq2 package. Genes with adjusted p-value < 0.01 were considered differentially expressed and we then identified differentially expressed genes (DEGs) based on the values of log2 fold-change (|log2 foldchange| > 1). Compared with non-stimulated cells, *E. coli* UC BEV stimulated cells showed 1337 up-regulated genes and 780 down-regulated genes (Supplementary Figure 3A). While *E. coli* PL BEV stimulated cells showed 1341 up-regulated genes and 690 down-regulated gene (Supplementary Figure 3B). We found a substantial overlap (≈80%) between the DEGs in the two groups (Figure 6C) and the correlations of gene expression fold change were also high (Figure 6D). In order to understand how the BEV-stimulation translates into physiological functions, we performed pathway analysis on the overlapping DEGs using the KEGG database. The results showed that the DEGs were mainly related to innate immunity response (Figure 6E), such as NF-kappa B signaling pathway, Toll-like receptor signaling pathway NOD-like receptor signaling pathway, and C-type lectin receptors signaling pathway (Supplementary Figures 3C-F). For BEVs derived from *S.aureus*, the two methods also showed similar effects (Supplementary Figures 4A-D), and the common DEGs enriched in KEGG terms related to innate immunity as well (Supplementary Figures 4E)

To verify the transcriptome analysis data and determine the immunostimulatory activity of the isolated BEVs in host cells, we further investigated the effects of BEVs on the mRNA levels of IL-1β, IL-6, and IL-8 by qRT-PCR. Results showed that the expressions of these pro-inflammatory cytokines were significantly higher (100- to 1000-fold) in all BEV-stimulated groups than in the negative control group (Figures 7A-C). THP-

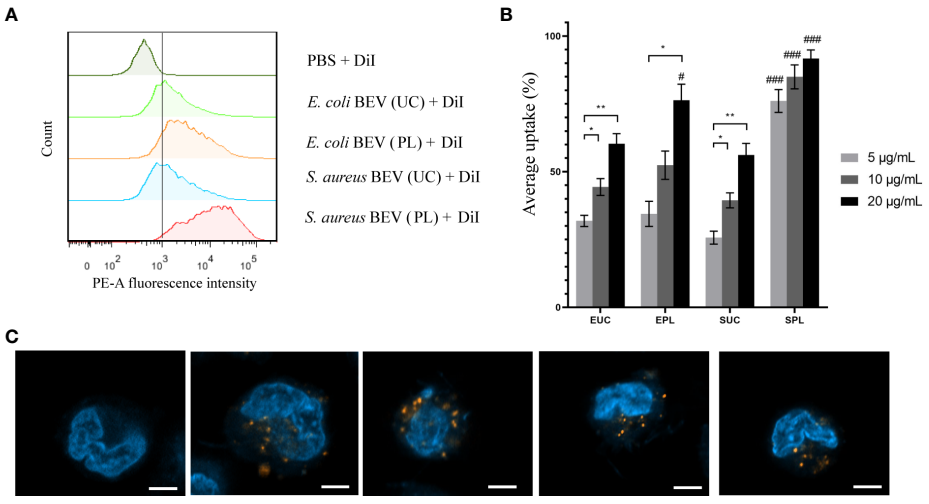

FIGURE 5
BEVs show successful uptake within THP-1 cells. **(A)** The phycoerythrin (PE-A) channel fluorescence intensity after incubation of cells with DiI-labeled BEVs in a flow cytometry measurement. The dashed line separates PE-A channel positive and negative cells. **(B)** Average percentage uptake of fluorescently labeled BEVs at different concentrations (5, 10 and 20 μg/mL) inside THP-1 cells. EUC, *E. coli* BEV isolated by UC; EPL, *E. coli* BEV isolated by PL; SUC, *S. aureus* BEV isolated by UC; SPL, *S. aureus* BEV isolated by PL. Significant differences between different BEV concentrations are indicated by asterisks: *p < 0.05; **<0.01. Significant differences compared BEVs isolated by different method among the same concentrations are indicated by hash sign: # p < 0.05; ### p < 0.001. **(C)** Confocal microscopy images of internalization of BEVs into THP-1 cells. PBS-treated THP-1 cells served as the negative control. (Left to right: negative control, BEVs derived from *E. coli* isolated by UC and PL, and BEVs derived from *S.aureus* isolated by UC and PL.) Red, DiI-stained BEVs; blue, DAPI-stained nucleus of THP-1 cells. Scale bar: 5 μm.

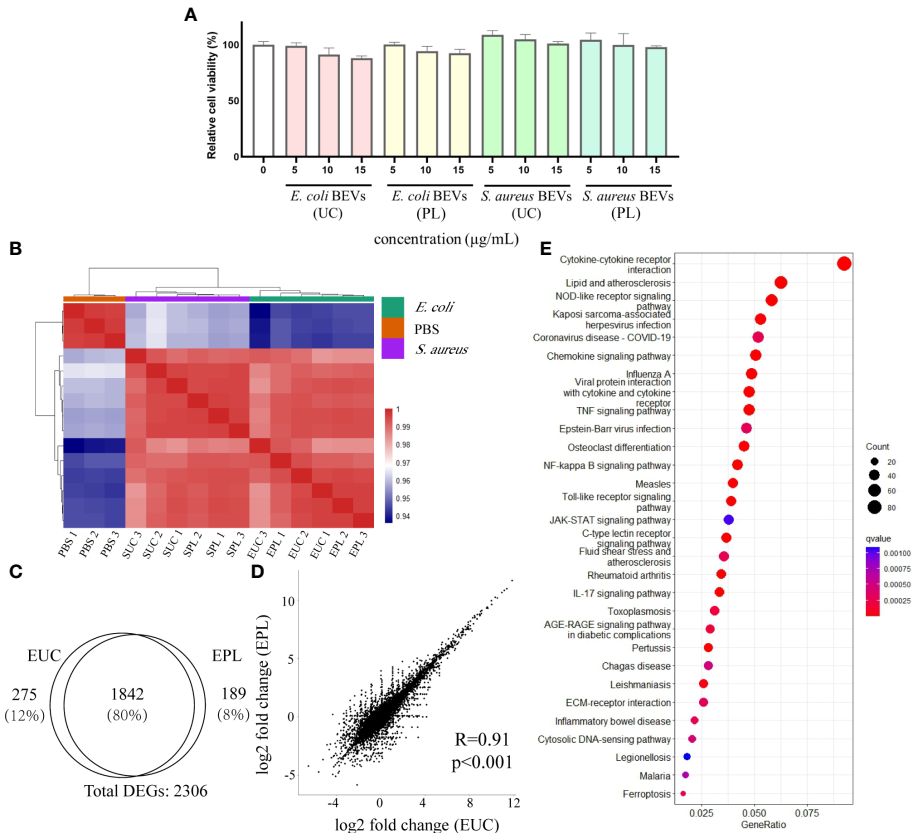

FIGURE 6
Transcriptional analysis of THP-1 cells stimulated with BEVs. **(A)** Calculated percentage cytotoxicity of cells (EUC, 1 μg/mL *E. coli* BEV isolated by UC; EPL, 1 μg/mL *E. coli* BEV isolated by PL; SUC, 10 μg/mL *S. aureus* BEV isolated by UC; SPL, 10 μg/mL *S. aureus* BEV isolated by PL). **(B)** The heat map was performed by using the Euclidean distance method with complete linkage for all samples (PBS1, PBS2, PBS3 are triplicates of non-stimulated THP-1 cells; EUC1-3 and EPL 1-3 are triplicates of cells stimulated with 1 μg/mL *E. coli* BEV isolated by UC and PL, respectively; SUC1-3 and SPL 1-3 are triplicates of cells stimulated with 10 μg/mL *S. aureus* BEV isolated by UC and PL, respectively). **(C)** Venn diagram of genes that are differentially expressed compared to non-stimulated cells in EUC and EPL group. **(D)** Correlation analysis of DEGs identified in EUC and EPL group. **(E)** Enrichment analysis of KEGG pathways enriched for overlapping DEGs in EUC and EPL group. Top 30 enriched KEGG pathways were selected for visualization.

1 cells treated with ϵ-PL-only didn't show significant differences from the PBS group (Supplementary Figure 5). Then the overall amounts of secreted IL-1β and IL-8 were analyzed in the culture media of the different experimental groups. BEVs derived from both species promoted the secretion of cytokines in THP-1 cells Figures 7D, E). Taken together, these results demonstrated that BEVs enriched by PL have the potential to activate host cells to the same degree as the BEVs isolated by UC.

Discussion

The production of BEVs is ubiquitously present in Gram-negative and Gram-positive bacteria (34). Recently, BEVs have been considered key players in the exchange of biological signals between microbe and host (5, 35–37). BEVs released by commensal microorganisms have the potential to contribute to host physiology including interaction with immune cells to induce host immunological tolerance or diseases (10, 38), which is an active area of research. However, the isolation processes have been a bottleneck for BEV research due to technical difficulties. There is an urgent need to develop inexpensive, rapid and adaptable methods to enrich BEVs.

Due to the composition characteristics of the phospholipid head groups, the surfaces of bacteria usually contain negative charges (39), thus interacting readily with cationic antimicrobial peptide (40, 41). Extracellular vesicles derived from microbial surfaces also contain excessive negative charges. We analyzed the zeta potential of BEVs derived from *E. coli* (a gram-negative bacterium) and *S. aureus* (a gram-positive bacterium), and the results agreed with what was described earlier (42–44). It has been shown that the adsorption of ϵ-PL, a natural antimicrobial, to the bacterial cell surface plays an important role in its antibacterial activity. While ϵ-PL has been used to develop a

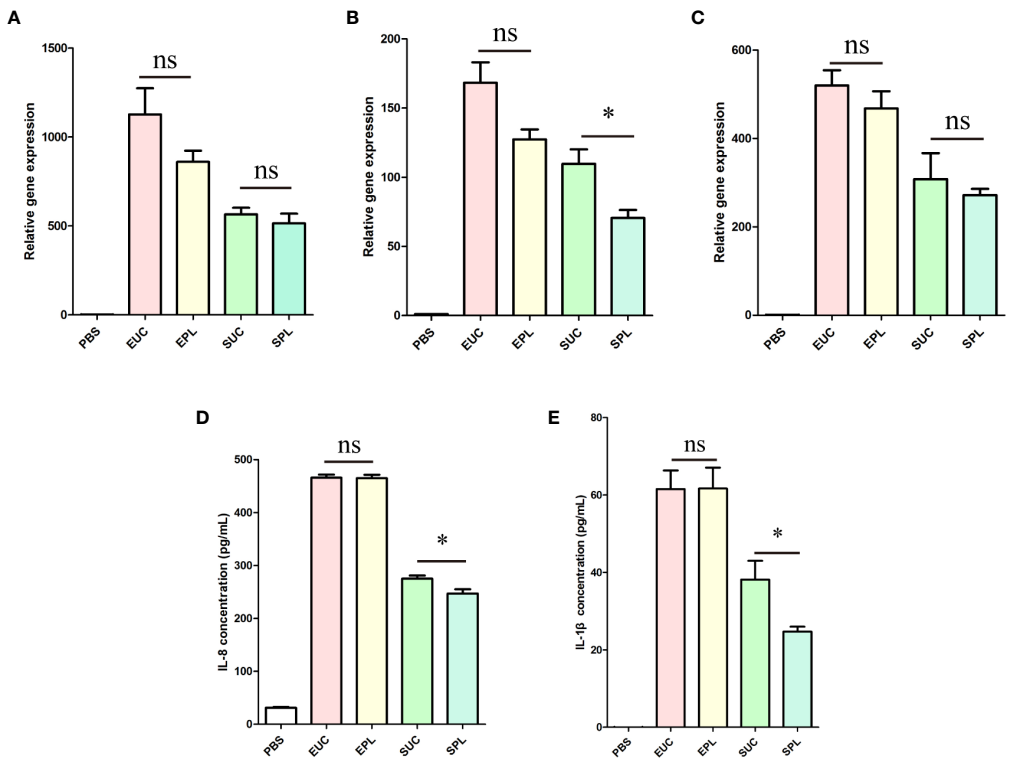

FIGURE 7
The expression of cytokines by THP-1 cells upon stimulation with BEVs. EUC, 1 μg/mL *E. coli* BEV isolated by UC; EPL, 1 μg/mL *E. coli* BEV isolated by PL; SUC, 10 μg/mL *S. aureus* BEV isolated by UC; SPL, 10 μg/mL *S. aureus* BEV isolated by PL. **(A)** The gene expression of IL-1β. **(B)** The gene expression of IL-6. **(C)** The gene expression of IL-8. **(D)** The release of IL-8. **(E)** The release of IL-1β. n = 3 biological replicates, ± s.e.m. Significant differences compared to the PBS groups are indicated by asterisks: *p < 0.05; ns represents no significance.

broad-spectrum bacterial cell capture technique (23), there is no study for the isolation of BEVs using ϵ-PL. Here we developed a novel ϵ-PL-based isolation method (PL) for rapid enrichment of BEVs from bacterial culture medium. We then demonstrated that BEVs isolated by PL are comparable to those isolated by UC in size distribution, morphology, protein profile and biological functions. The current method is simple, cost-effective and scalable, and is expected to be applied to basic research that requires the isolation of BEVs.

The images of the BEVs enriched by UC and PL were obtained by a TEM for physical characterization. The integrity of the vesicles from all samples was demonstrated by the presence of typical membrane-bound structures. However, we detected a broader particle size range of the BEVs isolated by PL measured by NTA. One reason for this difference could be the aggregation of vesicles caused by the ϵ-PL treatment (21). Further optimization of the reagents and the isolation workflows is necessary.

In terms of identified proteins and associated gene ontologies, the proteome of BEVs isolated by PL is largely comparable to that of BEVs isolated by UC. The correlation of protein levels was high and the predicted localization of proteins is similar between the two methods, with a high abundance of outer membrane protein (*E. coli*) or cytoplasmic protein (*S. aureus*). We then examined the overlap between the proteins derived from *E. coli* with a dataset in EVpedia (top 50 proteins that are most frequently identified in Gram-negative bacterial outer membrane vesicles). The majority of overlapping proteins were found in cluster D and E. Therefore, many of the proteins in these two clusters were able to be confirmed in previous studies on the BEV proteome. For example, the most abundant proteins identified in the samples derived from *E. coli* were outer membrane proteins (OmpC, OmpA, OmpF, etc.) (33) In contrast, the abundant of proteins in cluster A-C were relatively low and many were located in cytosol and plasma membrane. The characteristic in common for this set of proteins is their engagement in metabolic processes, such as nucleotide metabolic in PL-enriched group (cluster A) and amino acid and polysaccharide metabolic in UC-enriched groups (cluster B and C). However, these proteins were normally not considered as typical BEV proteins. Whether these proteins are actually co-isolated contaminants or proteins that are specific to certain subtypes of BEVs remains to be elucidated. It is worth noticing that we identified a protein that was consistently under-

represented in *E. coli* BEVs isolated by PL. This protein is GroEL, which is a chaperonin required for protein folding. Interestingly, a previous study (45) showed that GroEL was detected at higher levels in the crude input *E. coli* BEVs than the purified BEVs. The PL method may help to remove a number of contaminating proteins. Future researches are needed to validate the localization of this protein.

The study of the bioactivity of BEVs in cell cultures has gained popularity in an effort to understand their biological functions. The BEVs isolated by UC have been widely used in the studies of interkingdom communication and innate immunity (27, 46–50). As a human monocytic cell line, THP-1 has been extensively used in these BEV exposure studies. For example, a previous study (49) treated THP-1 cells with *Filifactor alocis* BEVs for 24 h and analyzed cytokines in the culture supernatants. They detected various pro-inflammatory cytokines related to inducing immune cell activation and infiltration. Another study (51) stimulated THP-1 cells with BEVs isolated from dust samples for 5 h and found that BEVs increased inflammatory mediators in an NF-κB-dependent manner. THP-1 monocytes have the ability to respond fast to inflammatory activators. The over-expression of inflammation-related cytokines could be detected within several hours of incubation (52). Thus, here we chose the THP-1 monocyte as a model to investigate the immune-modulating effects of the BEVs isolated by different methods.

First of all, we studied the internalization of BEVs into THP-1 cells. After 4 h incubation, THP-1 exhibited uptake of BEVs isolated by both UC and PL. Interestingly, BEVs isolated by PL were taken up better than those enriched by UC. Cationic polymers (i.e., ϵ-PL) and negatively charged molecules can form complexes in aqueous physiological solutions. And it has been widely accepted that these complexes can be internalized by various endocytic routes (53). So, we hypothesized that residual ϵ-PL might improve the internalization of BEVs. The amount of residual ϵ-PL was estimated by SDS-PAGE. For BEVs with a protein content of 20 μg, the residual amount of ϵ-PL was less than 2 μg [< 10%, Supplementary Figure 6A)]. Next, ϵ-PL was added into UC BEVs, and the uptake rate was measured by flow cytometry. At the adding amount of 10%, the difference of fluorescence intensity was not as significant as that between BEVs isolated by UC and PL (Supplementary Figure 6B), and an obvious shift in the fluorescence profile was only observed when the amount of ϵ-PL was high (Supplementary Figures 6C, D). Since the amount of residual ϵ-PL itself was insufficient to enhance endocytosis, the ϵ-PL-based isolation method may affect other biological structures of BEV, and the mechanisms of controlling BEV uptake needs to be further studied.

BEVs display multiple PAMPs and deliver cargos to target host cells. THP-1 cells stimulated with BEVs could undergo substantial reprogramming of their transcriptome. We used RNA sequencing to analyze the changes in gene expression profiles of THP-1 cells by BEV stimulation. The result showed that BEV stimulation triggered a striking alteration in the gene expression patterns. In the meantime, the samples treated with the same species of BEVs grouped together, which indicates the biological functions of PL BEVs are similar to those of UC BEVs. We also found that the response of cells to *E. coli* and *S. aureus* BEVs involved the upregulation of a common set of genes (supp Table), which were enriched in pathways like NF-kappa B signaling pathway, and Toll-like receptor signaling pathway. Similar to what was described in previous studies (46, 47, 54), the common cellular response mainly involved genes related to the immune response, especially those encoding cytokines and chemokines. The results support the concept that BEVs are potent stimulators of innate immune responses. QRT-PCR and ELISA were used to detect the expression of cytokines, and the intact biological function of BEVs isolated by PL was validated. In a word, these results demonstrated that BEVs isolated by our method still retained the *in vitro* biological activity.

In comparison with the isolation method based on UC, the ϵ-PL-based method has the merits of operational simplicity, accessibility and low cost. However, our study still has some limitations. Firstly, the current study was limited to BEVs derived from *E. coli* and *S. aureus*. Evaluation of the isolation results using other bacterial species would lend further support to the efficiency of the ϵ-PL-based technique. Secondly, the components of some nutrient-rich broths may show interference effects against the isolation method (20). Here we mainly tested bacteria grown in the commonly used LB broth, further optimizations of the workflows for different broths are necessary. Thirdly, we only assessed the protein profiles of the isolated fractions. A comprehensive analysis of proteins, nuclear acids, lipids and other metabolites harbored by BEVs could provide more information. Finally, the ultrafiltration step requires a lot of manual operation and can reduce the recovery rate due to the clogging and trapping of BEVs in the filters (55). The use of microfluidics in combination with ϵ-PL is promising in the development of more adaptable separation techniques (56, 57).

In conclusion, we have established an ϵ-PL-based isolation method and demonstrated that it could be used for efficient isolation of BEVs from bacterial culture medium. The new method could contribute to studies on BEVs, including research on the composition of BEVs and interkingdom communication between microbiota and the host.

Data availability statement

The datasets presented in this study can be found in online repositories. The names of the repository/repositories and accession number(s) can be found below: The proteomics data have been deposited in the ProteomeXchange *via* the PRIDE repository with the data set identifier PXD034259. RNA-seq data

were deposited in the Gene Expression Omnibus (GEO) database under the accession number GSE207009.

Author contributions

SW and DJ conceived and designed the experiments. SW and DJ performed the experiments. SW wrote the paper. SW, DJ and WX revised the manuscript. All authors contributed to the article and approved the submitted version.

Funding

This work was supported by the National Key R&D Program of China (Grant No. 2021YFE0109300).

Acknowledgments

The authors would like to thank Dr. Junge Chen for using the DLS device and thank Fengqiang Cao for using the NTA device. We also thank Xun Xu for her support in capturing confocal microscopy images.

Conflict of interest

The authors declare that the research was conducted in the absence of any commercial or financial relationships that could be construed as a potential conflict of interest.

Publisher's note

Supplementary material

The Supplementary Material for this article can be found online at: https://www.frontiersin.org/articles/10.3389/fimmu.2022.930510/full#supplementary-material

References

1. Brubaker SW, Bonham KS, Zanoni I, Kagan JC. Innate immune pattern recognition: A cell biological perspective. *Annu Rev Immunol* (2015) 33:257–90. doi: 10.1146/annurev-immunol-032414-112240

2. Cao X. Self-regulation and cross-regulation of pattern-recognition receptor signalling in health and disease. *Nat Rev Immunol* (2016) 16(1):35–50. doi: 10.1038/nri.2015.8

3. Thaiss CA, Zmora N, Levy M, Elinav E. The microbiome and innate immunity. *Nature* (2016) 535(7610):65–74. doi: 10.1038/nature18847

4. Zlatkov N, Nadeem A, Uhlin BE, Wai SN. Eco-evolutionary feedbacks mediated by bacterial membrane vesicles. *FEMS Microbiol Rev* (2021) 45(2): fuaa047. doi: 10.1093/femsre/fuaa047

5. Díaz-Garrido N, Badia J, Baldomà L. Microbiota-derived extracellular vesicles in interkingdom communication in the gut. *J Extracellular Vesicles* (2021) 10(13):e12161. doi: 10.1002/jev2.12161

6. Ñahui Palomino RA, Vanpouille C, Costantini PE, Margolis L. Microbiota–host communications: Bacterial extracellular vesicles as a common language. *PloS Pathog* (2021) 17(5):e1009508. doi: 10.1371/journal.ppat.1009508

7. Caruana JC, Walper SA. Bacterial membrane vesicles as mediators of microbe–microbe and microbe–host community interactions. *Front Microbiol* (2020) 11:432. doi: 10.3389/fmicb.2020.00432

8. Gill S, Catchpole R, Forterre P. Extracellular membrane vesicles in the three domains of life and beyond. *FEMS Microbiol Rev* (2019) 43(3):273–303. doi: 10.1093/femsre/fuy042

9. Villard A, Boursier J, Andriantsitohaina R. Microbiota-derived extracellular vesicles and metabolic syndrome. *Acta Physiolog* (2021) 231(4):e13600. doi: 10.1111/apha.13600

10. Díaz-Garrido N, Badia J, Baldomà L. Modulation of dendritic cells by microbiota extracellular vesicles influences the cytokine profile and exosome cargo. *Nutrients* (2022) 14(2):344. doi: 10.3390/nu14020344

11. Çelik PA, Derkuş B, Erdoğan K, Barut D, Manga EB, Yıldırım Y, et al. Bacterial membrane vesicle functions, laboratory methods, and applications. *Biotechnol Adv* (2022) 54:107869. doi: 10.1016/j.biotechadv.2021.107869

12. Tulkens J, De Wever O, Hendrix A. Analyzing bacterial extracellular vesicles in human body fluids by orthogonal biophysical separation and biochemical characterization. *Nat Protoc* (2020) 15(1):40–67. doi: 10.1038/s41596-019-0236-5

13. Lee EY, Bang JY, Park GW, Choi DS, Kang JS, Kim HJ, et al. Global proteomic profiling of native outer membrane vesicles derived from escherichia coli. *Proteomics* (2007) 7(17):3143–53. doi: 10.1002/pmic.200700196

14. Brown L, Wolf JM, Prados-Rosales R, Casadevall A. Through the wall: Extracellular vesicles in gram-positive bacteria, mycobacteria and fungi. *Nat Rev Microbiol* (2015) 13(10):620–30. doi: 10.1038/nrmicro3480

15. Klimentová J, Stulík J. Methods of isolation and purification of outer membrane vesicles from gram-negative bacteria. *Microbiol Res* (2015) 170:1–9. doi: 10.1016/j.micres.2014.09.006

16. Shao H, Im H, Castro CM, Breakefield X, Weissleder R, Lee H. New technologies for analysis of extracellular vesicles. *Chem Rev* (2018) 118(4):1917–50. doi: 10.1021/acs.chemrev.7b00534

17. Tulkens J, Vergauwen G, Van Deun J, Geeurickx E, Dhondt B, Lippens L, et al. Increased levels of systemic lps-positive bacterial extracellular vesicles in patients with intestinal barrier dysfunction. *Gut* (2020) 69(1):191–3. doi: 10.1136/gutjnl-2018-317726

18. Kuipers ME, Hokke CH, Smits HH, Nolte-'t Hoen EN. Pathogen-derived extracellular vesicle-associated molecules that affect the host immune system: An overview. *Front Microbiol* (2018) 9:2182. doi: 10.3389/fmicb.2018.02182

19. Kim JH, Lee J, Park J, Gho YS. Gram-negative and gram-positive bacterial extracellular vesicles. *Semin Cell Dev Biol* (2015) 40:97–104. doi: 10.1016/j.semcdb

20. Liu J-N, Chang S-L, Xu P-W, Tan M-H, Zhao B, Wang X-D, et al. Structural changes and antibacterial activity of epsilon-Poly-L-Lysine in response to ph and phase transition and their mechanisms. *J Agric Food Chem* (2020) 68(4):1101–9. doi: 10.1021/acs.jafc.9b07524

21. Hyldgaard M, Mygind T, Vad BS, Stenvang M, Otzen DE, Meyer RL. The antimicrobial mechanism of action of epsilon-Poly-L-Lysine. *Appl Environ Microbiol* (2014) 80(24):7758–70. doi: 10.1128/AEM.02204-14

22. Ye R, Xu H, Wan C, Peng S, Wang L, Xu H, et al. Antibacterial activity and mechanism of action of E-Poly-L-Lysine. *Biochem Biophys Res Commun* (2013) 439(1):148–53. doi: 10.1016/j.bbrc.2013.08.001

23. Wu X, Lai T, Jiang J, Ma Y, Tao G, Liu F, et al. An on-site bacterial detection strategy based on broad-spectrum antibacterial E-polylysine functionalized magnetic nanoparticles combined with a portable fluorometer. *Microchim Acta* (2019) 186(8):1–8. doi: 10.1007/s00604-019-3632-1

24. Pham TV, Jimenez CR. An accurate paired sample test for count data. *Bioinformatics* (2012) 28(18):i596–602. doi: 10.1093/bioinformatics/bts394

25. Bijnsdorp IV, Maxouri O, Kardar A, Schelfhorst T, Piersma SR, Pham TV, et al. Feasibility of urinary extracellular vesicle proteome profiling using a robust and simple, clinically applicable isolation method. *J Extracellular Vesicles* (2017) 6 (1):1313091. doi: 10.1080/20013078.2017.1313091

26. Yu G, Wang L-G, Han Y, He Q-Y. Clusterprofiler: An r package for comparing biological themes among gene clusters. *Omics: A J Integr Biol* (2012) 16(5):284–7. doi: 10.1089/omi.2011.0118

27. Mehanny M, Koch M, Lehr C-M, Fuhrmann G. Streptococcal extracellular membrane vesicles are rapidly internalized by immune cells and alter their cytokine release. *Front Immunol* (2020) 80. doi: 10.3389/fimmu.2020.00080

28. Andrews S. *Fastqc: A quality control tool for high throughput sequence data*. Cambridge, United Kingdom: Babraham Bioinformatics, Babraham Institute (2010).

29. Pertea M, Kim D, Pertea GM, Leek JT, Salzberg SL. Transcript-Level Expression Analysis of RNA-Seq Experiments With HISAT, StringTie and Ballgown. *Nat Protoc* (2016) 11:1650–67. doi: 10.1038/nprot.2016.095

30. Love MI, Huber W, Anders S. Moderated estimation of fold change and dispersion for rna-seq data with Deseq2. *Genome Biol* (2014) 15(12):1–21. doi: 10.1186/s13059-014-0550-8

31. Hong J, Dauros-Singorenko P, Whitcombe A, Payne L, Blenkiron C, Phillips A, et al. Analysis of the escherichia coli extracellular vesicle proteome identifies markers of purity and culture conditions. *J Extracellular Vesicles* (2019) 8 (1):1632099. doi: 10.1080/20013078.2019.1632099

32. Lee J, Kim OY, Gho YS. Proteomic profiling of gram-negative bacterial outer membrane vesicles: Current perspectives. *PROTEOMICS–Clinical Appl* (2016) 10 (9-10):897–909. doi: 10.1002/prca.201600032

33. McBroom AJ, Johnson AP, Vemulapalli S, Kuehn MJ. Outer membrane vesicle production by escherichia coli is independent of membrane instability. *J Bacteriol* (2006) 188(15):5385–92. doi: 10.1128/JB.00498-06

34. McMillan HM, Kuehn MJ. The extracellular vesicle generation paradox: A bacterial point of view. *EMBO J* (2021) 40(21):e108174. doi: 10.15252/embj.2021108174

35. Liu JH, Chen CY, Liu ZZ, Luo ZW, Rao SS, Jin L, et al. Extracellular vesicles from child gut microbiota enter into bone to preserve bone mass and strength. *Advanced Sci* (2021) 8(9):2004831. doi: 10.1002/advs.202004831

36. Villard A, Boursier J, Andriantsitohaina R. Bacterial and eukaryotic extracellular vesicles and nonalcoholic fatty liver disease: New players in the gut-liver axis? *Am J Physiol-Gastrointest Liver Physiol* (2021) 320(4):G485–G95. doi: 10.1152/ajpgi.00362.2020

37. Hendrix A, De Wever O. Systemically circulating bacterial extracellular vesicles: Origin, fate, and function. *Trends Microbiol* (2022) 30(3):213–6. doi: 10.1016/j.tim.2021.12.012

38. Gul L, Modos D, Fonseca S, Madgwick M, Thomas JP, Sudhakar P, et al. Extracellular vesicles produced by the human commensal gut bacterium bacteroides thetaiotaomicron affect host immune pathways in a cell-type specific manner that are altered in inflammatory bowel disease. *J Extracellular Vesicles* (2022) 11(1):e12189. doi: 10.1002/jev2.12189

39. Li Z, Ma J, Ruan J, Zhuang X. Using positively charged magnetic nanoparticles to capture bacteria at ultralow concentration. *Nanoscale Res Lett* (2019) 14(1):1–8. doi: 10.1186/s11671-019-3005-z

40. Teixeira V, Feio MJ, Bastos M. Role of lipids in the interaction of antimicrobial peptides with membranes. *Prog Lipid Res* (2012) 51(2):149–77. doi: 10.1016/j.plipres.2011.12.005

41. Schwartz O, Bercovici M. Microfluidic assay for continuous bacteria detection using antimicrobial peptides and isotachophoresis. *Analytical Chem* (2014) 86(20):10106–13. doi: 10.1021/ac5017776

42. Mohamed Z, Shin J-H, Ghosh S, Sharma AK, Pinnock F, Bint E Naser Farnush S, et al. Clinically relevant bacterial outer membrane models for antibiotic screening applications. *ACS Infect Dis* (2021) 7(9):2707–22. doi: 10.1021/acsinfecdis.1c00217

43. Marchant P, Carreño A, Vivanco E, Silva A, Nevermann J, Otero C, et al. "One for all": Functional transfer of omv-mediated polymyxin b resistance from salmonella enterica sv. typhi Δtolr and Δdegs to susceptible bacteria. *Front Microbiol* (2021) 12:1068. doi: 10.3389/fmicb.2021.672467

44. Echeverría-Bugueño M, Balada C, Irgang R, Avendaño-Herrera R. Evidence for the existence of extracellular vesicles in renibacterium salmoninarum and related cytotoxic effects on shk-1 cells. *J Fish Dis* (2021) 44(7):1015–24. doi: 10.1111/jfd.13362

45. Lee EY, Choi DY, Kim DK, Kim JW, Park JO, Kim S, et al. Gram-positive bacteria produce membrane vesicles: Proteomics-based characterization of Staphylococcus aureus-derived membrane vesicles. *Proteomics* (2009) 9 (24):5425–36. doi: 10.1002/pmic.200900338

46. Ellis TN, Leiman SA, Kuehn MJ. Naturally produced outer membrane vesicles from pseudomonas aeruginosa elicit a potent innate immune response *via* combined sensing of both lipopolysaccharide and protein components. *Infection Immun* (2010) 78(9):3822–31. doi: 10.1128/IAI.00433-10

47. Zaborowska M, Vazirisani F, Shah FA, Firdaus R, Omar O, Ekström K, et al. Immunomodulatory effects exerted by extracellular vesicles from staphylococcus epidermidis and staphylococcus aureus isolated from bone-anchored prostheses. *Biomaterials* (2021) 278:121158. doi: 10.1016/j.biomaterials.2021.121158

48. Bitto NJ, Baker PJ, Dowling JK, Wray-McCann G, De Paoli A, Tran LS, et al. Membrane vesicles from pseudomonas aeruginosa activate the noncanonical inflammasome through caspase-5 in human monocytes. *Immunol Cell Biol* (2018) 96(10):1120–30. doi: 10.1111/imcb.12190

49. Kim HY, Lim Y, An SJ, Choi BK. Characterization and immunostimulatory activity of extracellular vesicles from filifactor alocis. *Mol Oral Microbiol* (2020) 35 (1):1–9. doi: 10.1111/omi.12272

50. Martin-Gallausiaux C, Malabirade A, Habier J, Wilmes P. Fusobacterium nucleatum extracellular vesicles modulate gut epithelial cell innate immunity *via* foma and Tlr2. *Front Immunol* (2020) 11:583644. doi: 10.3389/fimmu.2020.583644

51. Meganathan V, Moyana R, Natarajan K, Kujur W, Kusampudi S, Mulik S, et al. Bacterial extracellular vesicles isolated from organic dust induce neutrophilic inflammation in the lung. *Am J Physiology-Lung Cell Mol Physiol* (2020) 319(6): L893–907. doi: 10.1152/ajplung.00107.2020

52. Chanput W, Mes JJ, Wichers HJ. Thp-1 cell line: An *in vitro* cell model for immune modulation approach. *Int Immunopharmacol* (2014) 23(1):37–45. doi: 10.1016/j.intimp.2014.08.002

53. Boddu SH, Bhagav P, Karla PK, Jacob S, Adatiya MD, Dhameliya TM, et al. Polyamide/Poly (Amino acid) polymers for drug delivery. *J Appl Biomat Funct Materials* (2021) 12(4):58. doi: 10.3390/jfb12040058

54. Jenner RG, Young RA. Insights into host responses against pathogens from transcriptional profiling. *Nat Rev Microbiol* (2005) 3(4):281–94. doi: 10.1038/nrmicro1126

55. Shirejini SZ, Inci F. The yin and yang of exosome isolation methods: Conventional practice, microfluidics, and commercial kits. *Biotechnol Adv* (2021) 54:107814. doi: 10.1016/j.biotechadv.2021.107814

56. Bathini S, Pakkiriswami S, Ouellette RJ, Ghosh A, Packirisamy M. Magnetic particle based liquid biopsy chip for isolation of extracellular vesicles and characterization by gene amplification. *Biosensors Bioelectr* (2021) 194:113585. doi: 10.1016/j.bios.2021.113585

57. Chiriacò MS, Bianco M, Nigro A, Primiceri E, Ferrara F, Romano A, et al. Lab-on-Chip for exosomes and microvesicles detection and characterization. *Sensors* (2018) 18(10):3175. doi: 10.3390/s18103175

frontiers | Frontiers in Immunology

TYPE Original Research
PUBLISHED 31 August 2022
DOI 10.3389/fimmu.2022.955175

OPEN ACCESS

EDITED BY
Zhichao Fan,
UCONN Health, United States

REVIEWED BY
Yueyang Wang,
Harvard Medical School, United States
Juan Antonio Fafian Labora,
University of A Coruña, Spain

*CORRESPONDENCE
Hang Yin
yin_hang@tsinghua.edu.cn
Qian Wang
wangqian@smu.edu.cn

SPECIALTY SECTION
This article was submitted to Molecular Innate Immunity, a section of the journal Frontiers in Immunology

RECEIVED 28 May 2022
ACCEPTED 29 July 2022
PUBLISHED 31 August 2022

CITATION
Xiao Y, Liang J, Witwer KW, Zhang Y, Wang Q and Yin H (2022) Extracellular vesicle-associated microRNA-30b-5p activates macrophages through the SIRT1/ NF-κB pathway in cell senescence. *Front. Immunol.* 13:955175. doi: 10.3389/fimmu.2022.955175

Extracellular vesicle-associated microRNA-30b-5p activates macrophages through the SIRT1/ NF-κB pathway in cell senescence

Yu Xiao[1], Jiaqi Liang[2,3,4], Kenneth W. Witwer[5,6], Ying Zhang[2,3,4], Qian Wang[1]* and Hang Yin[2,3,4]*

[1]Department of Laboratory Medicine, Zhujiang Hospital, Southern Medical University, Guangzhou, China, [2]School of Pharmaceutical Sciences, Tsinghua University, Beijing, China, [3]Tsinghua University-Peking University Joint Center for Life Sciences, Tsinghua University, Beijing, China, [4]Beijing Advanced Innovation Center for Structural Biology, Tsinghua University, Beijing, China, [5]Department of Molecular and Comparative Pathobiology, Baltimore, MD, United States, [6]Department of Neurology, The Johns Hopkins University School of Medicine, Baltimore, MD, United States

Chronic inflammation is widely observed in aging, but it is unclear whether extracellular vesicles (EVs) play a role in chronic disease-associated senescence. In our study, LC/MS profiling revealed that senescent cell derived EVs (SEN EVs) activate the immune response pathways of macrophages. Significantly more EVs were found in the supernatant of SEN than of control (CON) cell cultures, and SEN EVs were enriched in miR-30b-5p, which directly target sirtuin1 (SIRT1). *In vitro*, we found that SEN EV treatment resulted in increased cellular levels of interleukin-1β (IL-1β) and IL-6 and decreased levels of SIRT1. Increased cytokine levels could be reversed by SIRT1 activation and miR-30b-5p inhibition. Furthermore, miR-30b-5p significantly increased with age in both mouse liver tissue and EVs harvested from the tissue, with differences in EVs observed both earlier and in the later magnitude of aging. Western blot and qPCR proved that miR-30b-5p downregulated the level of SIRT1 in mouse macrophages. Collectively, we propose that EVs carrying miR-30b-5p from SEN cells can induce chronic inflammation through macrophage activation. This occurs through the downregulation of SIRT1 and the corresponding activation of NF-κB pathways that enhance pro-inflammatory cytokine production. Collectively, these results demonstrate that EVs carrying pro-inflammatory signals are released by SEN cells and then activate immune cells in the SEN microenvironment, changing the inflammatory balance. Our results also explain why inflammation increases with age even though SEN cells can be immediately eliminated under rigorous immune surveillance.

KEYWORDS

extracellular vesicles, miRNA, SIRT1, cell senescence, NF-κB

Introduction

The control and balance of cell senescence can regulate the occurrence and development of chronic diseases (1). During the process of aging, cells at different stages of cellular senescence (2) accumulate in tissues and secrete a large number of biologically active molecules, particularly pro-inflammatory cytokines, chemokines, and matrix remodeling enzymes that collectively contribute to the senescence-associated secretory phenotype (SASP) (3). Factors involved in SASP drive the systemic, low-grade, chronic inflammation that accompanies human aging (4). Short-term exposure to SASP stimulates the recruitment of immune cells to eliminate precancerous and senescent (SEN) cells, thereby preventing tumorigenesis; however, long-term exposure to SASP produces chronic inflammation and promotes tumorigenesis (5). In aging microenvironment, with the increasing investigation of the significant role of Extracellular vesicles (EVs), aging-associated EVs are now believed to play multiple complex roles in disease progression.

EVs can be released by a variety of cells and are believed to play a pivotal role in cell-cell communication both locally and remotely (6–13). These particles are thought to be effective circulating factors that regulate immune responses including inflammatory responses (14–16). Due to their lipid bilayers, EVs are readily phagocytosed by many different cell types (17, 18), especially immune cells, which makes it particularly important to study the influence of EVs and their contents on recipient cells. Recent studies have also revealed the functions of SEN cell-derived EVs (SEN EVs) (19). Specifically, EVs are widely reported in the aging, extracellular microenvironment and may transmit senescence signals in autocrine, paracrine, and endocrine ways like SASP (20).

Y RNA and tRNA fragments from EVs can trigger immune responses (16), and EVs microRNAs (miRNAs) have several reported roles in immune regulation. EV-miR-155 enhances the expression of pro-inflammatory cytokines, while EV-miR-146a attenuates inflammatory responses *via* dendritic cells, and macrophages uptake circulating EVs (17). Also, EV-miR-192, an immunomodulatory aging-associated microRNA, attenuated the hyperinflammatory state and improved vaccine efficacy in geriatric mice (21). Although major contributions to organismal aging have been demonstrated for EVs and their miRNA cargo, there is limited knowledge of the effect of cellular senescence on EVs contents and, in turn, on how EV-shuttled miRNAs might influence immune cells. However, circulating EVs concentrations seem to decline with age, possibly as a consequence of increased internalization by immune cells (22). Downregulated, inhibited, or defective activity of SIRT1 has been investigated in various cardiovascular (23, 24), renal (25), and aging-associated diseases (26, 27). SIRT1, as a type III histone/protein deacetylase, has many non-histone targets, such as p53 (28), FOXO (29), PGC1-α (30), NF-κB (31), which are involved in inflammation, cellular senescence, oxidative stress, energy metabolism, and DNA damage response (32). Among downstream targets of SIRT1, NF-κB is thought to be a major regulator of inflammation because it regulates the transcription of genes involved in establishing immune and inflammatory responses (24, 33, 34). Recent studies show that SIRT1 could be a regulatory element in the immune system, whose altered functions influence immune disorder disease development (35). Also, in a mouse lupus model, a SIRT1 activator effectively protected against disease progression (36). In the clinic, SIRT1 is well known to have anti-inflammatory properties (37–39).

In this study, we report that SEN EVs can induce transcription of pro-inflammatory cytokine genes in macrophages *via* downregulating SIRT1. We then evaluate several miRNAs that target the mRNA of SIRT1. Our results suggest that EV-associated miR-30b-5p reduces the levels of SIRT1 in recipient cells. In mouse aging and cell senescence processes, miR-30b-5p in EVs increases in a senescence degree-dependent fashion. Taken together, our study demonstrates that EV-carried miR-30b-5p regulates inflammatory responses of macrophages by downregulating SIRT1. A key challenge is to understand more precisely how EVs function in truly physiological settings. Our findings have revealed an EV-mediated delivery mechanism for miR-30b-5p, which reduces SIRT1 levels and counteracts NF-κB signaling, suggesting a potential avenue for anti-inflammatory intervention in humans.

Materials and methods

Cell lines and cell culture

An *in vitro* SEN EV functional assay was established using L929 cell lines that were cultured for 45 to 50 generations, and hyper SEN (h-SEN) cell lines were used etoposide-induced SEN cells. Non-senescent (control, CON) cells were used for comparison representing young cells. Raw 264.7 cells were used as the macrophage model. All cells were purchased from ATCC and cultured in Dulbecco's Modified Eagle's Medium (Gibco™, USA) supplemented with 10% (V/V) fetal bovine serum (FBS) (10099-141, Gibco™, USA) or EV-free FBS, 2 mM L-glutamine, 100 U/ml penicillin and 100 mg/ml streptomycin (Gibco™, USA). EV-free FBS was prepared by ultracentrifugation (Beckman Coulter, Optima XPN-100) at 120,000 × *g* for 12 h at 4 °C and filtration of the FBS supernatant with a 0.22 μm PVDF filter (Merck Millipore ltd). Cells were cultured at 37°C in a humidified incubator containing 5% CO_2 and tested negative for mycoplasma infection every week.

Senescence was confirmed in the SEN and h-SEN models using the ratio of phospho-H2A.X to β-Actin, a DNA damage marker, (40, 41) and SASP levels.

Peripheral blood mononuclear cell (PBMC) were isolated from murine whole blood with Ficoll reagent following the previously established protocols (42).

Cell transfection was performed with Lipofectamine™ 3000 Transfection Reagent (L3000150, Invitrogen™, USA) according to the manufacturer's protocols.

Drug administration

The stock solution of SRT1720 (Sigma-Aldrich, St. Louis, MO, USA), a previously reported selective SIRT1 agonist (43), was prepared in dimethyl sulfoxide (DMSO) (D2438, Sigma-Aldrich) at storage concentration. The stock solutions were diluted by cell culture medium to the indicated concentrations prior to cell treatment.

EVs isolation and characterization

The supernatant was collected from different groups of cells after 24-48 h culture and stored at 4 °C before EVs isolation within 72 h of harvest by differential ultracentrifugation (14, 44). Briefly, cell supernatants were firstly centrifuged at 2,000 × *g* for 15 min at 4 °C to remove floating dead cells and cell debris. Supernatants were gently transferred to a new tube and centrifuged at 12,000 × *g* for 45 min at 4 °C to pellet larger microvesicles and subcellular organelles. The medium was filtered through a 0.22 μm PVDF filter (Merck Millipore ltd) (44) before ultracentrifugation at 120,000 × *g* for 1 h. Then, the supernatant was discarded, followed by a washing step in PBS. Finally, the EVs were resuspended in 100 μL PBS or ddH2O.

To further characterize EVs, we used transmission electron microscopy (TEM), nanoparticle tracking analysis (NTA), and Western blots (WB) as recommended by the Minimal Information For Studies of Extracellular Vesicles (MISEV) guidelines developed by the International Society for Extracellular Vesicles in 2018 (45).

EVs (20 μL, ~10^7 particles) suspended in ddH_2O were loaded onto a copper grid and negatively stained with uranyl acetate solution for 30 seconds. The grid was then examined with an H7650B transmission electron microscope.

The particle size distribution and concentration of EVs samples were measured by a light-scattering-based NTA device (Malvern Instruments, United Kingdom) (46). To maximize the reliability of quantifications and size-distribution results, we diluted each EVs samples into the proper concentration range before measurement (47) and tracked the Brownian motion of laser-illuminated individual particles using cameral level 16 and detection threshold 7. Each sample was measured using three 60 s videos and analyzed by NanoSight NTA 3.1 software, which calculates particle diameter using the Stokes-Einstein equation and also analyzes concentration.

Immunoblot analysis

For whole-cell and EVs proteins extraction, cells and EVs were firstly washed three times in ice-cold pH=7.4 PBS (10010094, Gibco™, USA) and solubilized in RIPA lysis buffer (P0013B, Beyotime, China) supplemented with protease inhibitor cocktails (78434, Thermo Scientific™, USA) on ice for 10 min. Samples were centrifuged at 12,000 × *g* at 4°C to remove cell debris. Sample lysates were quantified by Pierce BCA protein assay according to the manufacturer's protocols (23235, Thermo Scientific™, USA). Protein samples were added with a proper volume of 6X protein loading buffer (DL101-02, TransGen Biotech, China) before protein denaturing. Proteins were separated by 8%-12% SDS–PAGE, electrotransferred to 0.45um PVDF membranes (Millipore, MA, USA) by SDS-PAGE gel transfer system (Bio-Rad, USA), and blocked with TBST containing 5% (w/v) skimmed milk powder (D8340, Solarbio, China) before incubation with primary antibodies at room temperature (RT) for 2 h or 4°C overnight and with 1:5000 diluted secondary antibodies for 1 h at RT. Protein immunoblots were detected by horseradish peroxidase-based ECL agent (34580, Thermo Scientific™, USA) for 5 min, and images were acquired with an iBright™ 1500 imaging system. Target protein levels were normalized by β-Actin level of the same samples.

Primary antibodies used in this study are listed below:

CD63 (1:1000) (rabbit monoclonal, ab59479, Abcam, Cambridge, UK), Alix (1:1000) (Proteintech, 12422-1-AP, USA), Calnexin (1:1000) (rabbit monoclonal, ab133615, Abcam, Cambridge, UK), SIRT1 (D1D7) (1:1000) (Rabbit mAb #9475, Cell Signaling Technology, Danvers, MA), Phospho-Histone H2A.X (Ser139) (20E3) (1:1000) (Rabbit mAb #9718, Cell Signaling Technology, Danvers, MA), β-Actin (13E5) (1:1000) (Rabbit mAb #4970, Cell Signaling Technology, Danvers, MA)

Immunofluorescence staining

Cells were seeded on coverslips in 12-well plates and treated as indicated. After the supernatants were removed, the cells were washed with PBS for three times, then fixed with 4% paraformaldehyde (P1110, Solarbio, China) for 10 min, and permeabilized with 0.2% (v/v) Triton X-100 (T8200, Solarbio, China) after three times of washing, and blocked with 3% (w/v) BSA for 1 h. Then, the cells were incubated with 3% [w/v] BSA diluted anti-NF-κB p65 antibody (1:200) (recombinant antibody, 80979-1-RR, proteintech, USA) overnight at 4°C and incubated with 3% [w/v] BSA diluted Alexa Fluor 488-labeled goat anti-rabbit IgG (H+L) (1:2000) (A11034, Invitrogen™, USA) and DAPI for 1 h at RT after three washes. Finally, the coverslips were fixed on slides using a fluorescent mounting medium (HC08, Sigma-Aldrich, USA), and images were acquired with a Nikon A1RMP confocal microscope.

Proteomics

Protein samples were separated by SDS-PAGE. In-gel digestion was carried out with sequencing-grade modified trypsin in 50 mM ammonium bicarbonate at 37°C overnight. The peptides were extracted twice with 0.1% trifluoroacetic acid in a 50% acetonitrile aqueous solution. Extracts were centrifuged in a speedvac to reduce the volume. Tryptic peptides were dissolved in 20 µl 0.1% TFA.

For LC-MS/MS analysis, the peptides were separated by Thermo-Dionex Ultimate 3000 HPLC system, which was directly interfaced with a Thermo Scientific Q Exactive mass spectrometer. The Q Exactive mass spectrometer was operated in the data-dependent acquisition mode using Xcalibur 2.1.2 software, and there was a single full-scan mass spectrum in the orbitrap (300-1800 m/z, 70,000 resolution) followed by 20 data-dependent MS/MS scans at 27% normalized collision energy (HCD).

Perseus software was used to analyze the data (48).

Quantitative reverse-transcription PCR of mRNA and miRNAs

For qRT-PCR of mRNA, cells were seeded in 6-well plates and treated as indicated. Total RNA was collected with TRIzol reagent (15596018, Invitrogen ™, USA). The DEPC H_2O diluted RNA was reverse transcribed using an iScript cDNA synthesis kit and analyzed by qPCR using iTaq Universal SYBR Green Supermix (in a Bio-Rad T100 thermal cycler). All reagents were used according to the manufacturer's instructions. β-Actin was used as the internal control of mRNA and U6 was used as an internal normalization control of miRNAs.

The primers are listed below:

Mouse-*Il-1β*-F: GCAACTGTTCCTGAACTCAACT
Mouse-*Il-1β*-R: ATCTTTTGGGGTCCGTCAACT
Mouse-*Il-6*-F: TAGTCCTTCCTACCCCAATTTCC
Mouse-*Il-6*-R: TTGGTCCTTAGCCACTCCTTC
Mouse-*Sirt1*-F: ATGACGCTGTGGCAGATTGTT
Mouse-*Sirt1*-R: CCGCAAGGCGAGCATAGAT
Mouse-*β-Actin*-F: TGACGTTGACATCCGTAAAGACC
Mouse-*β-Actin*-R: AAGGGTGTAAAACGCAGCTCA
Mouse- *Il-8*-F: CAAGGCTGGTCCATGCTCC
Mouse- *Il-8*-R: TGCTATCACTTCCTTTCTGTTGC
Mouse-p16-F: CGCAGGTTCTTGGTCACTGT
Mouse-p16-R: TGTTCACGAAAGCCAGAGCG
Mouse-p21-F: CCTGGTGATGTCCGACCTG
Mouse-p21-R: CCATGAGCGCATCGCAATC
Mouse-TP53-F: CCATGAGCGCATCGCAATC
Mouse-TP53-R: CGGAACATCTCGAAGCGTTTA

For qRT-PCR of miRNA, total RNA of cells or EVs was extracted with TRIzol reagent (15596018, Invitrogen ™, USA). The DEPC H_2O diluted RNA was reverse transcribed using an iScript cDNA synthesis kit supplemented with stem-loop RT primers. qPCR analysis was conducted using iTaq Universal SYBR Green Supermix in a Bio-Rad T100 thermal cycler. ADD normalization strategy.

The primers are listed below:

mmu-miR-30b-5p-RT(stem): GTCGTATCCAGTGCAGG GTCCGAGGTATTCGCACTGGATACGACAGCTGA
mmu-miR-30b-5p-F(stem): GCGCTGTAAACATCCTACAC
U6-F: CTCGCTTCGGCAGCACA
U6-R: AACGCTTCACGAATTTGCGT
Universal-R: GCGATCACATTGCCAGGG

The sequences used for miRNA mimics and antagonists are listed below:

mmu-miR-30b-5p mimics:
sense: 5'-UGUAAACAUCCUACACUCAGCU-3'
anti-sense 5'-CUGAGUGUAGGAUGUUUACAUU-3'
mmu-miR-30b-5p antagonist: 5'-AGCUGAGUGUAGG AUGUUUACA-3'

Dual-luciferase reporter assay

pGLO vector-SIRT1-wild type and pGLO-SIRT1-mutant reporter plasmid vectors were constructed by integrating target fragments of miR-30b-5p. SIRT1-WT or SIRT1-MUT was co-transfected with miR-30b-5p mimics for 48 h. And then measured the luciferase activity with the Dual-Lumi™ Luciferase Reporter Assay Kit (RG088S, Beyotime, China).

Statistical analyses

The data are presented as group mean ± SD. Unpaired Student's t-tests were used to analyze two-group comparisons, and one-way ANOVA for more than two groups, followed by Bonferroni's *post-hoc* test, using GraphPad Prism 6.0. Group differences at the level of $p < 0.05$ were considered to be statistically significant. "*" represents $p < 0.05$; "**" represents $p < 0.01$, and "***" represents $p < 0.001$. "ns" denotes not significant versus control.

Results

SEN EVs induce macrophage immune responses

Since EVs mediate crucial cell-cell communication (49, 50), we aimed to assess the function of EVs at an early stage of

senescence. Raw 264.7 cells were co-cultured for 24 h with EVs from SEN and CON cells (Figure 1A). Cellular protein content extracted from co-cultured cells was then assessed with liquid chromatography-tandem mass spectrometry (LC-MS/MS). In total, 2939 unique proteins were identified (Figure S1C). These are shown by hierarchical clustering (Figure S1A). In addition, a volcano plot was prepared to visualize differentially expressed proteins (Figure 1B). Based on false discovery rate cutoffs of 0.025, 157 protein were identified as differentially expressed between Raw 264.7 cells treated with CON EVs and SEN EVs, including 48 up-regulated proteins (see heatmap, Figure S1D). We were interested to observe that SIRT1 decreased in SEN EV-treated cells (Figure S1D). By protein categorization by Metascape (51), we first identified all statistically enriched terms, including Gene

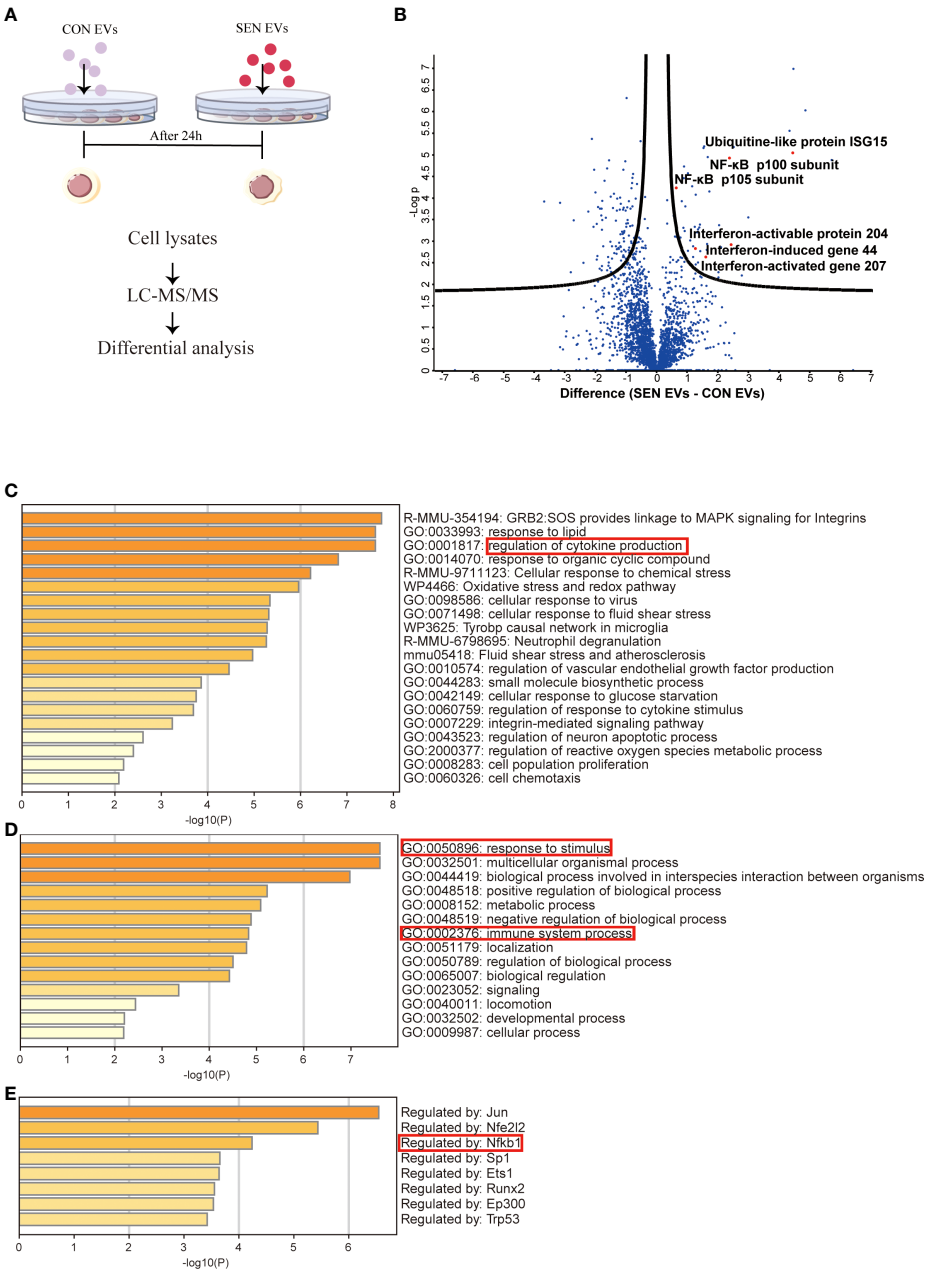

FIGURE 1
Proteomics study of Raw 264.7 cells treated with CON and SEN EVs. **(A)** Workflow used for proteomic analysis. **(B)** Volcano plot of differentially expressed proteins; dots above the black curves represent proteins with differences with False Discovery Rate (FDR) < 0.025. Bar graphs of enriched terms **(C)** across input gene lists; **(D)** with GO terms only; and **(E)** by TRRUST. Data were from four independent repeats.

Ontology (GO), Kyoto Encyclopedia of Genes and Genomes (KEGG), canonical pathways, and hallmark gene sets. Accumulative hypergeometric *p*-values and enrichment factors were calculated and used for filtering (Figure 1C). Next, we did GO analysis for the biological process subclass and found enriched proteins related to the immune system (Figure 1D). Finally, Transcriptional Regulatory Relationships Unraveled by Sentence-based Text mining (TRRUST) (Figure 1E) revealed that, among others, inflammation-related proteins and the NF-κB signaling pathway were enriched in the cellular proteome after SEN EVs treatment. The network of these enriched proteins is shown in Figures S1A, B. Taken together, our proteomics results and knowledge of pathways involved in senescence prompted us to further investigate the possible role of SEN EVs in influencing the NF-κB mediated inflammation pathway.

SEN EVs regulate SIRT1 and induce canonical NF-κB activation

SIRT1 is a histone and non-histone deacetylase that is widely present in the nucleus and cytoplasm and can regulate the NF-κB signaling pathway (31). To test the hypothesis that SEN EVs may regulate SIRT1/NF-κB signaling, we constructed an EV co-culture system (Figure 2A). Having identified the NF-κB signaling pathway in our proteomics study, we found that the level of SIRT1 decreased after being co-cultured with SEN EVs in a time-dependent manner (Figure 2B). We hypothesized that it might be the upstream protein SIRT1, which can deacetylate NF-κB and thus inhibits activation of the NF-κB signaling pathway (52) and related inflammation. We further hypothesized that the decrease in SIRT1 is due to EV-associated miRNAs that target SIRT1 in Raw 264.7 macrophage cells allowing NF-κB-related inflammatory responses to tip the balance between pro-inflammatory and anti-inflammatory cytokines. We attempted to test ourthe hypotheses in the cell system shown in Figure 2A. Through fluorescence microscopy, the RelA/p65 subunit of NF-κB which is involved in canonical signaling was found to enter the nucleus of cells exposed to SEN EVs. In contrast, treating cells with a SIRT1 agonist decreased the amount of p65 nuclear entry (Figures 2C, D). We also tested the pro-inflammatory functions of SEN EVs by measuring cytokines. mRNA levels of pro-inflammatory cytokines IL-1β and IL-6 were increased by the addition of SEN EVs, but this increase was abrogated by treatment with a miRNA antagonist of miR-30b-5p and a SIRT1 agonist (Figures 2E, F).

miR-30b-5p can target SIRT1 in cells

To investigate EV cargo that might regulate the activation of macrophages, we utilized the TargetScan and ENCORI prediction tools to identify possible miRNA regulators of *Sirt1* mRNA. Among the candidate miRNAs, miR-30b-5p target the 3'UTR region of the *Sirt1* mRNA in both humans and mice (Figure 3A) and have relatively high prediction scores (Figure S2A). Also, miR-30 (53, 54) have been widely reported to be detected in EVs and are closely related to the progression of diverse diseases (54–56). To further investigate the role of miR-30b-5p in NF-κB mediated inflammation, we sought to verify *Sirt1* as a predicted target mRNA of this miRNA. Therefore, we set out to verify this target *in vitro*. We transfected Raw 264.7 cells with the miR-30b-5p anti-sense antagonist and found a significant upregulation of the mRNA level of *Sirt1* in cells (Figure 3C). Meanwhile, transfecting Raw 264.7 cells with miR-30b-5p mimics downregulated the mRNA level of *Sirt1* in cells (Figure 3D). These effects were also dose-dependent. In addition, the immunoblot assay showed that transfection of the antagonist and mimics of miR-30b-5p regulated the protein level of *SIRT1* in Raw 264.7 cells (Figure 3E). In conclusion, the mRNA of *Sirt1* may be an important target of miR-30b-5p in cells. Co-culturing macrophages with the antisense sequence of miR-30b-5p as the antagonist (Figures 2C-F) can reverse the pro-inflammatory function of SEN EVs, and the transfection of 10 nM miR-30b-5p caused a remarkable inhibition of cell inflammatory compared with that of the control group (Figures 2E, F). Together, these results indicate that the functions of SEN EVs may include SIRT1-downregulating effects of EV miR-30b-5p.

miR-30b-5p level in cells and EVs are correlated with aging

Hypothesizing that these miRNAs play a role in SEN EV-induced inflammation, we accordingly measured miRNA levels in cells and their EVs at several stages of senescence. Cell senescence was quantitated in CON, SEN, and h-SEN cells using the phospho-HA.X/β-Actin ratio (40, 41) (Figure 4A). The morphology and SASP level of CON, SEN, and h-SEN cells is shown in Figures S3A-B. NTA and TEM results for EVs secreted from CON, SEN, and h-SEN cells indicated that particle count in EVs preparations was positively correlated with senescence degree (Figures 4B, C). Also, h-SEN EVs have more EVs in a small, 60-nm subcluster, which might be more easily internalized by cells. Although EVs are rich in miRNAs and RNA binding proteins such as hnRNPA2B1 have been reported to sort miRNAs into EVs (57, 58), it is as yet unclear if or how miR-30b-5p is sorted. However, RT-qPCR of miR-30b-5p shows increased levels in cells and EVs, and that miRNA levels are positively correlated with senescence degree (Figures 4E, F).

10.3389/fimmu.2022.955175

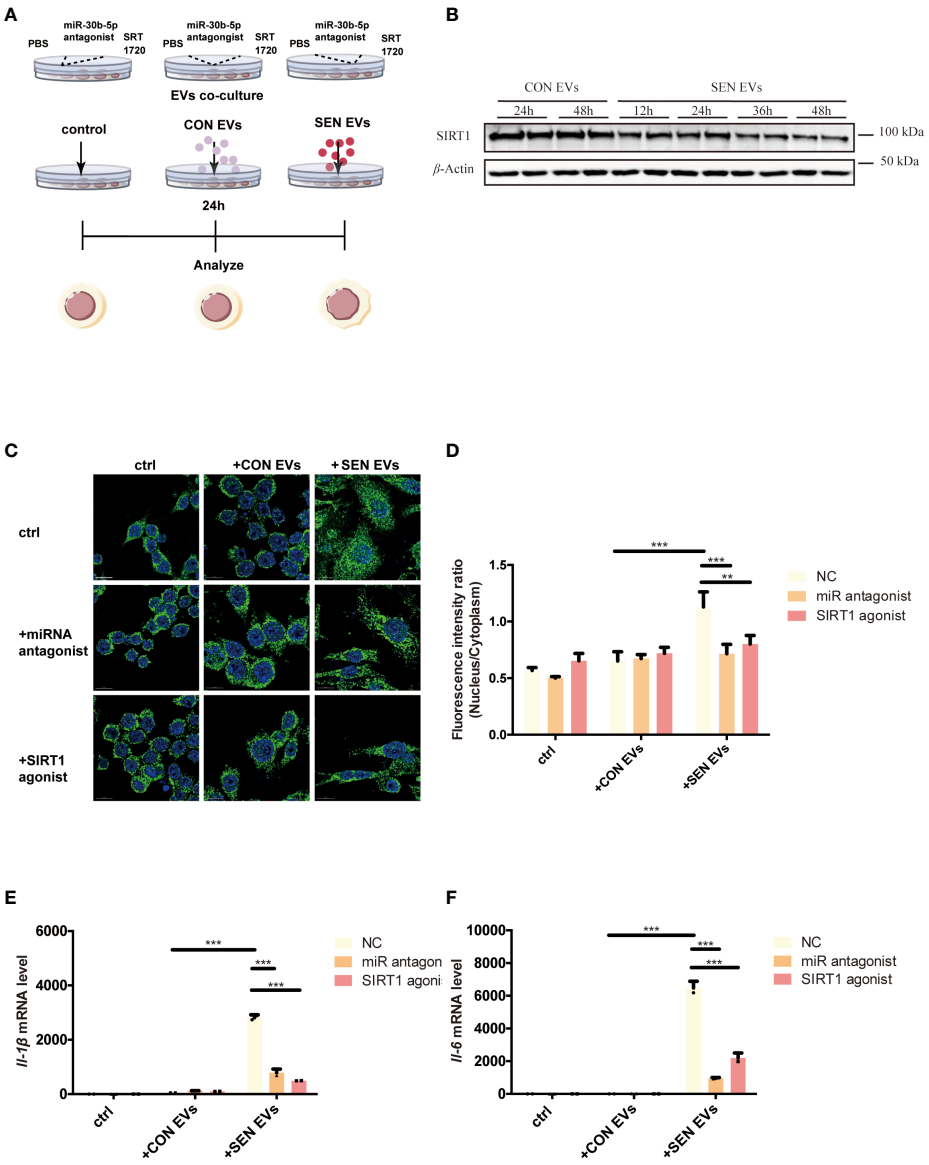

FIGURE 2
SIRT1 regulates NF-κB activation induced by SEN EVs. **(A)** Workflow of the experimental design. Cells were treated with PBS (Control, ctrl), CON, or SEN EVs after being pretreated with PBS, miR-30b-5p antagonist, or SRT1720. **(B)** Immunoblot analysis of SIRT1 protein level of cells treated with CON or SEN EVs for a time course. **(C)** Immunofluorescence analysis of DAPI (blue) and p65 (green) in Raw 264.7 cells. Scale bars: 5 μm. **(D)** Quantification of immunofluorescence ratio of p65 (Nucleus/cytoplasm). RT-qPCR analysis of **(E)** *Il-1β* and **(F)** *Il-6* mRNA levels of Raw 264.7 cells treated with PBS, CON, or SEN EVs and the indicated inhibitors. Data are from at least three independent experiments and are presented as the mean ± SD. $^{**}p<0.01$; and $^{***}p<0.001$.

Morphology of adult and aging mouse liver EVs

Livers were harvested from mice of different ages and used to prepare tissue and isolate tissue EVs. The latter were characterized by following established guidelines (45) (Figure 5). We used electron microscopy to reveal the morphology of isolated EVs, specifically definition by a lipid bilayer and a size of 30–150 nm (Figure 5A). Size-based EVs subclusters were measured and displayed (Figures 5B-D), and size profiles and concentrations of EVs from the liver were measured by NTA. By NTA, particle mode diameters ranged mostly from 120-160 nm, both in adult and different aging liver EVs samples (Figure 5E). It has been reported that SEN cells generally secrete more EVs than CON cells (59). Interestingly, we observed that particle counts in the liver tissue did not increase. By contrast, the EV levels decreased while the mice

10.3389/fimmu.2022.955175

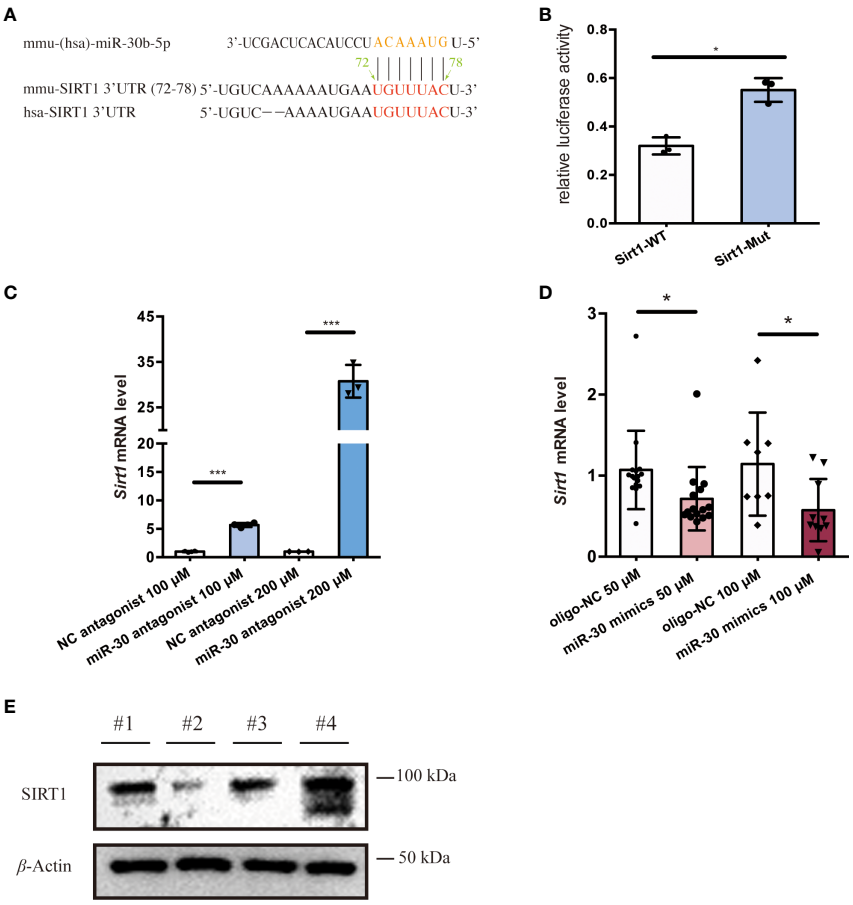

FIGURE 3
miR-30b-5p directly targets SIRT1 in macrophages. **(A)** miR-30b-5p target sequence in the 3'UTR of Sirt1. **(B)** Relative activity of firefly luciferase and *Renilla* luciferase after co-transfection with mimics and plasmids expressing wild-type or mutated target sites. **(C)** RT-qPCR analysis of *Sirt1* mRNA level of cells treated with the miR-30b-5p antagonist. **(D)** RT-qPCR analysis of *Sirt1* mRNA level of cells treated with miR-30b-5p mimics. **(E)** Immunoblot analysis of SIRT1 protein level of cells treated with miR-30b-5p mimics and antagonists. #1:mimics control group; #2: miR-30b-5p mimics group; #3: antagonists control group; #4: miR-30b-5p antagonists group. The data represent at least three independent experiments and are presented as mean ± SD. *$p<0.05$; and ***$p<0.001$.

aged (Figure 5F), which contradicted with the previous reports, opening up new possibilities for the study of tissue-derived EVs. As reported, EVs of different sizes have different architectural features and uptake rates, and EVs of small sizes are more easily taken up by target cells (60). A larger subcluster of 60-nm EVs was observed in the 18-week (18W) group, while almost no 60-nm EVs were observed in the 6-week (6W) group. There is a speculation that these smaller EVs (60nm) produced during aging might contain more pro-inflammatory miRNAs, but this hypothesis cannot be confirmed at present due to technical limitations. Finally, several EVs marker proteins (CD63 and Alix) were detected from isolated EVs from different groups of mouse livers (Figure 5G) by immunoblotting, while calnexin, a cellular marker, was undetected or greatly depleted in EVs preparations.

Levels of EV miR-30b-5p increased significantly with age in mice

To find the source tissues of elevated miR-30b-5p, we measured heart, lung, spleen, along with liver tissue-derived EVs. We found that this miRNA increased with age in the liver. Next, we turned to the RNA extracted from different groups of mouse liver EVs and liver tissue and investigated the relationship between senescence and levels of EVs miRNA in the mouse model. The level of miR-30b-5p in mouse liver and liver tissue-derived EVs were measured (Figures 6A-C). The results showed that EV-derived miR-30b-5p increased with aging (Figure 6A). EV-associated miRNAs were increased already at 3 months, while in liver

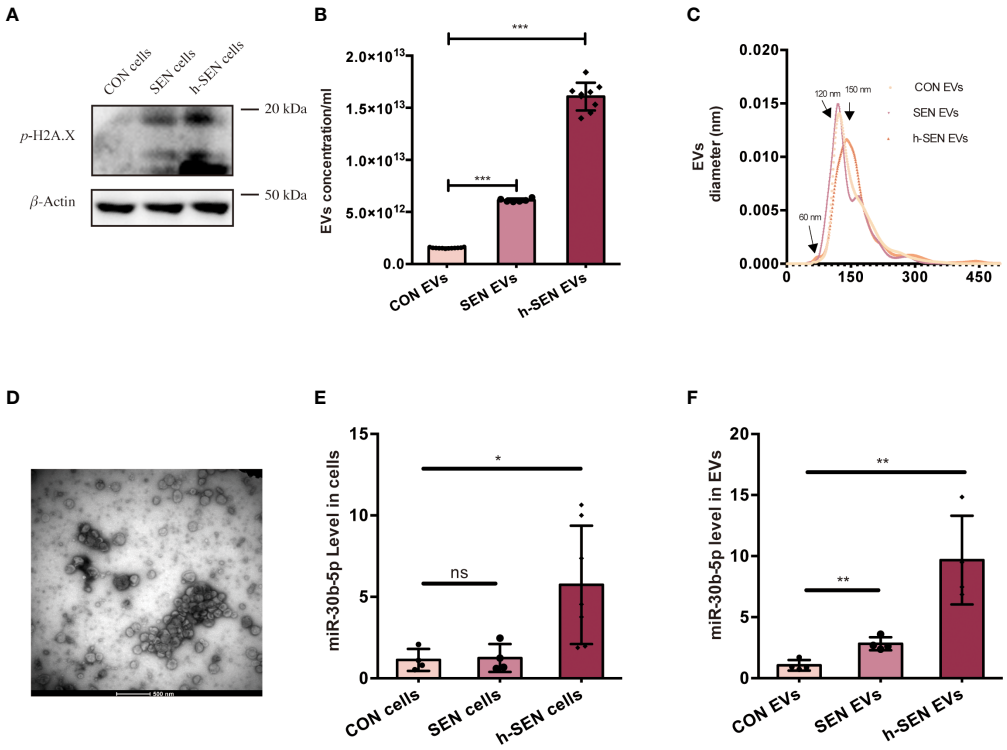

FIGURE 4
Characterization of CON and SEN cells and derived EVs. **(A)** Immunoblot of *p*-H2A.X/*β*-actin of CON, SEN, and h-SEN cell models. 10 μg proteins were loaded in each gel lane. **(B)** Particle concentrations and **(C)** particle size distributions of EVs preparations were determined by nanoparticle tracking analysis (NTA). **(D)** Transmission electron microscopy (TEM) micrograph of representative isolated SEN EVs. RT-qPCR result of miR-30b-5p levels of CON, SEN, and h-SEN cells **(E)** and EVs **(F)**. The data are from at least three independent experiments and are presented as mean ± SD. **p*<0.05; ***p*<0.01; and ****p*<0.001; ns denotes not significant versus control..

tissue, increases in miR-30b-5p were not discernible until 16 months, respectively (Figure 6B). We directly compared the miRNA levels between indicated EVs and cells, and the magnitude of the difference was also greater in EV preparations than in liver tissue (Figure 6C). To better observe the relationship between miR-30b-5p and SIRT1 in mouse liver, we assessed SIRT1 levels of liver tissues and PBMC in young and aging mouse populations (Figures 6D, E).

Discussion

In natural senescence, previously reported evidence supports a major contribution of secreted EVs to the effects of SEN cells on their micro-environment (20, 61). In our study, we confirmed and extended these findings, showing that SEN EVs transport pro-inflammatory signals, but not pro-senescence signals directly, to recipient macrophages. A model of the mechanism is shown in Figure 7. SEN cells indeed released a significantly higher level of small (60-nm) EVs compared with normal cells. Importantly, these EVs were released relatively early in the process. Our data agree with the results of previous studies, including a mouse model of oncogene-induced senescence and human lung fibrotic lesions enriched in SEN cells (50) and bone marrow stromal cells (62).

Our findings support the hypothesis that SEN EVs are enriched in a group of "pre-aging" microRNAs that are transferred to recipient macrophages and influence important biological pathways. , although it remains to be shown what level of transported miRNA is necessary to induce changes in recipient cells. Analyzing the candidate miRNAs of EVs that could be involved in these effects, we found that miR-30b-5p directly targets the mRNA of Sirt1 and is more abundant in SEN EVs in vivo and in vitro. This miRNA is closely related to tumor and inflammation. Our results reveal that the early function of SEN EVs is mainly pro-inflammatory via the SIRT1/NF-κB signaling pathway, different from other reports that emphasize the pro-senescence function of SEN EVs. Indeed, also supporting a role for EV miRNAs, SEN EVs are reportedly enriched in miR-21-5p and miR-217, which were over-expressed in SEN cells and were capable of targeting not just SIRT1, but also DNMT1, another key enzyme in methylation pattern maintenance (63, 64).

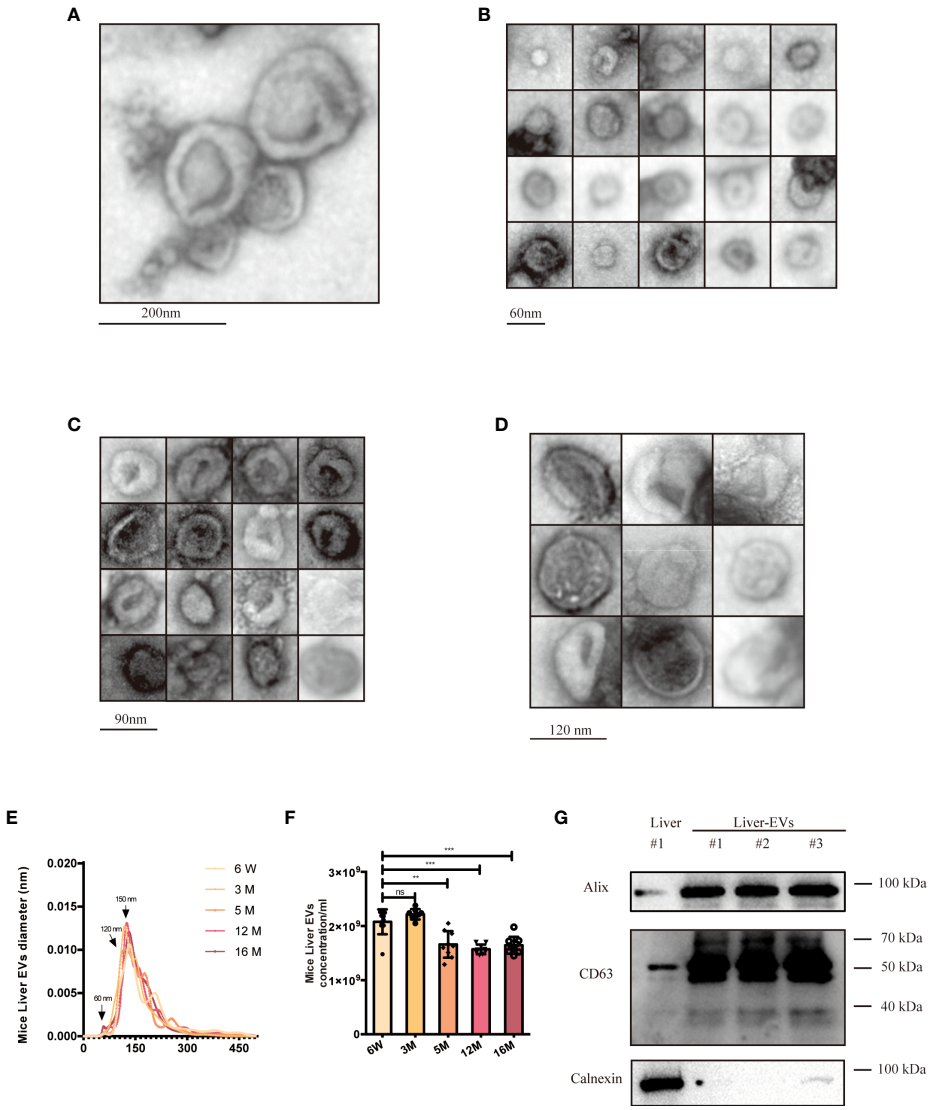

FIGURE 5
Characterization of young (6-week old) and aged (16-month old) mice liver EVs. **(A)** TEM analysis of EV clusters; scale bars: 200 nm. **(B)** TEM analysis of small EVs (60 nm). scale bars: 60 nm. **(C)** TEM analysis of EVs with diameter of ~80-90 nm; scale bars: 90 nm. **(D)** TEM analysis of EVs at a diameter of ~120 nm. scale bars; 120 nm. NTA size distributions **(E)** and particle concentrations **(F)** of liver EV preparations from mice at six ages as indicated. **(G)** Western blot of Alix, CD63, and Calnexin from liver EVs and liver tissues. The data represent at least three independent experiments and are presented as mean ± SD. $^{**}p<0.01$; and $^{***}p<0.001$; ns denotes not significant versus control..

To further elucidate the function of SEN EVs and understand if we could potentially manipulate them to change biological processes, we employed multiple regulators to treat recipient cells. Both SIRT1 agonist and miR-30b-5p anti-sense antagonist ameliorated processes associated with the pro-inflammatory function of SEN EVs. Encouragingly, these findings suggest that interventions against miRNAs in SEN cells and/or SEN EVs may be feasible.

In aged humans, levels of extracellular miR-30b-5p have been reported to be related with aging processes, albeit with apparently opposite results in different studies (41–43). In our study, we first addressed the EVs miR-30b-5p level and raise several questions that may be addressed in future studies. For example, we observed differences in the size distribution of EVs released from SEN cells, but whether miR-30b-5p are enriched in specific size classes of EVs is still unknown. It would also be interesting to investigate whether different size classes of EVs are different not just in content, but also in cell uptake or fusion abilities in this model, much as previously reported elsewhere (50). The topology of miRNAs, in or on EVs, might also be

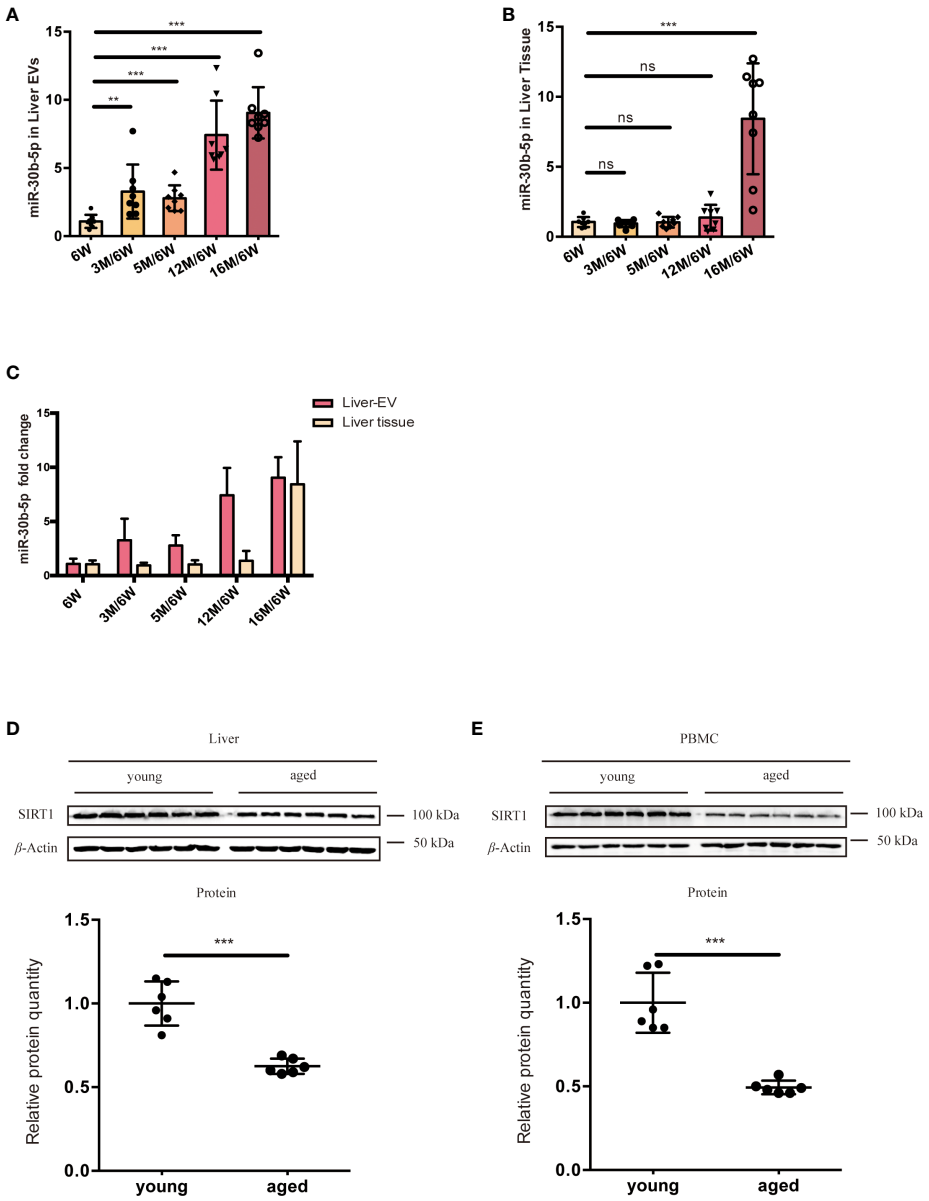

FIGURE 6
miR-30b-5p increase with aging in liver tissue and liver tissue EVs. **(A)** RT-qPCR of miR-30b-5p levels of mouse liver EVs. **(B)** RT-qPCR of miR-30b-5p levels from mouse liver tissue. **(C)** Comparison of miR-30b-5p levels from liver EVs and tissue. **(D)** Immunoblotting analysis of SIRT1 protein level of young (6-week old) and aged (16-month old) group ouse liver. 6 mice were randomly selected from each group. **(E)** Immunoblot analysis of SIRT1 protein level of young (6-week old) and aged (16-month old) group mouse PBMCs. 6 mice were randomly selected from each group. The data represent at least three independent experiments and are presented as mean ± SD. $^{**}p<0.01$; and $^{***}p<0.001$, ns denotes not significant versus control. 6W: 6-week-old mice, 3M, 5M, 12M, and 16M: 3, 5, 12, and 16-month-old mice.

analyzed. Finally, we cannot fully rule out additional contributions of non-EV or non-miRNA effectors to the transferred senescence phenomenon.

Altogether, we provide evidence that during progression from a pre-senescence to a hyper-senescence stage, SEN cells can spread their miRNA signature, thus contributing to the development of a pro-inflammatory environment for immune cells. These microRNAs can be selectively sorted into and delivered through EVs. Also, our results indicate that EV-miR-30b-5p might be used as a pre-aging or early aging biomarkers to track aging trajectories. In conclusion, our finding may lay the foundation for further research, in particular to understanding

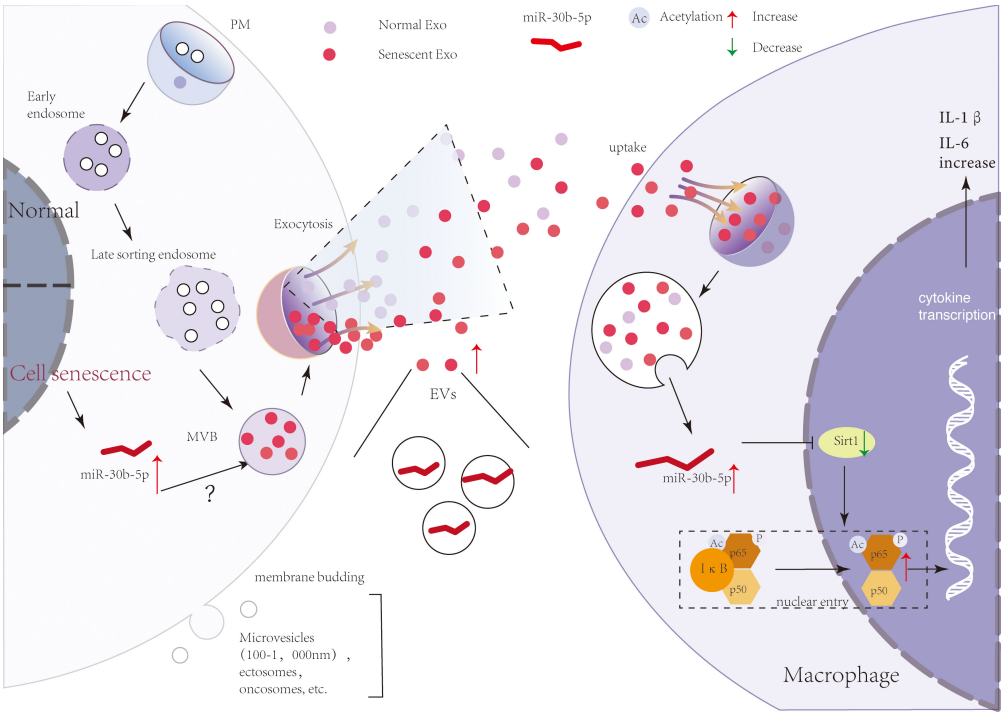

FIGURE 7
A brief model describing a theoretical mechanism whereby SEN cell-derived EVs transport pro-inflammatory signals to macrophages. SEN cells release more EVs that contain miR-30b-5p. With the uptake of SEN EVs by macrophages, miR-30b-5p is released from EVs and reduces the level of SIRT1, thereby mediating the increase of p65 entry into the nucleus, and then increasing the synthesis of cytokines IL-6 and IL-1β.

how pro-inflammatory and pro-senescence signals carried by EVs can become druggable targets that can help modulate the immune-regulating and aging process and delay aging-associated disease development.

In conclusion, cellular senescence is a state of permanent cell-cycle arrest, the causes of which are incompletely understood. Learning more about the cellular and molecular contributors to senescence will facilitate new approaches to treating senescence-related phenomena and diseases. Our work here reveals an unappreciated relationship between innate immune responses and senescence, establishing a link between cells and different cell types that involves cellular EVs transfer of miRNAs. These results give new insights into the inflammatory process in SASP and therefore heighten our understanding of the accurate regulation of senescence. SEN EV-induced inflammatory responses of macrophages may also be persistent: the macrophages will not be cleared by immune cells, since these SEN cells, possibly influenced chronically by released SEN EVs, are in a state of immune escape. The sustained action of SEN EVs may thus assist in transforming the macrophage into a promoter of aging and disease.

Data availability statement

The datasets presented in this study can be found in online repositories. The names of the repository/repositories and accession number(s) can be found in the article/Supplementary Material.

Ethics statement

The animal study was reviewed and approved by Laboratory Animal Resources Center at Tsinghua University.

Author contributions

The corresponding author HY and QW contributed to the conception and design of the study. YX designed all experiments. YX, JL, and YZ performed all experiments. HY, KW, and QW have made great contributions to the manuscript guidance. All authors contributed to the article and approved the submitted version.

Funding

This work was supported by funds from the National Natural Science Foundation of China (Grant No. 21825702, 22137004, 82072334, and 21977061), Beijing Advanced Innovation Center for Structural Biology Funding (Grant No. 20151551402), Beijing Outstanding Young Scientist Program (Grant No. BJJWZYJH01201910003013).

Acknowledgments

We thank all the laboratory secretaries for their support in the operation of the laboratory. We thank the Protein Research Technology Center at Tsinghua University for the LC-MS/MS instruments utilization and data analysis guidance. We thank the State Key Laboratory of Membrane Biology at Tsinghua University for permission to utilize ultracentrifuges and other instruments. We thank the Laboratory Animal Resources Center at Tsinghua University for the experimental animal breed. We thank the Central Laboratory at Southern Medical University for instrument use training and instruction. We thank the funding from the National Natural Science Foundation of China and other affiliations.

Conflict of interest

The authors declare that the research was conducted in the absence of any commercial or financial relationships that could be construed as a potential conflict of interest.

Publisher's note

Supplementary material

The Supplementary Material for this article can be found online at: https://www.frontiersin.org/articles/10.3389/fimmu.2022.955175/full#supplementary-material

References

1. Bussian TJ, Aziz A, Meyer CF, Swenson BL, van Deursen JM, Baker DJ. Clearance of senescent glial cells prevents tau-dependent pathology and cognitive decline. *Nature* (2018) 562(7728):578–82. doi: 10.1038/s41586-018-0543-y

2. Ogrodnik M. Cellular aging beyond cellular senescence: Markers of senescence prior to cell cycle arrest *in vitro* and *in vivo*. *Aging Cell* (2021) 20(4): e13338. doi: 10.1111/acel.13338

3. Coppe JP, Patil CK, Rodier F, Sun Y, Munoz DP, Goldstein J, et al. Senescence-associated secretory phenotypes reveal cell-nonautonomous functions of oncogenic RAS and the p53 tumor suppressor. *PloS Biol* (2008) 6 (12):2853–68. doi: 10.1371/journal.pbio.0060301

4. Franceschi C, Bonafe M, Valensin S, Olivieri F, De Luca M, Ottaviani E, et al. Inflamm-aging. an evolutionary perspective on immunosenescence. *Ann N Y Acad Sci* (2000) 908:244–54. doi: 10.1111/j.1749-6632.2000.tb06651.x

5. Loo TM, Miyata K, Tanaka Y, Takahashi A. Cellular senescence and senescence-associated secretory phenotype *via* the cGAS-STING signaling pathway in cancer. *Cancer Sci* (2020) 111(2):304–11. doi: 10.1111/cas.14266

6. Thery C, Zitvogel L, Amigorena S. Exosomes: composition, biogenesis and function. *Nat Rev Immunol* (2002) 2(8):569–79. doi: 10.1038/nri855

7. Thery C, Ostrowski M, Segura E. Membrane vesicles as conveyors of immune responses. *Nat Rev Immunol* (2009) 9(8):581–93. doi: 10.1038/nri2567

8. Gurunathan S, Kang MH, Jeyaraj M, Qasim M, Kim JH. Review of the isolation, characterization, biological function, and multifarious therapeutic approaches of exosomes. *Cells* (2019) 8(4). doi: 10.3390/cells8040307

9. Raposo G, Stoorvogel W. Extracellular vesicles: exosomes, microvesicles, and friends. *J Cell Biol* (2013) 200(4):373–83. doi: 10.1083/jcb.201211138

10. Holme PA, Solum NO, Brosstad F, Roger M, Abdelnoor M. Demonstration of platelet-derived microvesicles in blood from patients with activated coagulation and fibrinolysis using a filtration technique and western blotting. *Thromb Haemost* (1994) 72(5):666–71.

11. Hess C, Sadallah S, Hefti A, Landmann R, Schifferli JA. Ectosomes released by human neutrophils are specialized functional units. *J Immunol* (1999) 163 (8):4564–73.

12. Cocucci E, Racchetti G, Meldolesi J. Shedding microvesicles: artefacts no more. *Trends Cell Biol* (2009) 19(2):43–51. doi: 10.1016/j.tcb.2008.11.003

13. Gyorgy B, Modos K, Pallinger E, Paloczi K, Pasztoi M, Misjak P, et al. Detection and isolation of cell-derived microparticles are compromised by protein complexes resulting from shared biophysical parameters. *Blood* (2011) 117(4):e39–48. doi: 10.1182/blood-2010-09-307595

14. Colombo M, Raposo G, Thery C. Biogenesis, secretion, and intercellular interactions of exosomes and other extracellular vesicles. *Annu Rev Cell Dev Biol* (2014) 30:255–89. doi: 10.1146/annurev-cellbio-101512-122326

15. Robbins PD, Morelli AE. Regulation of immune responses by extracellular vesicles. *Nat Rev Immunol* (2014) 14(3):195–208. doi: 10.1038/nri3622

16. Xiao Y, Driedonks T, Witwer KW, Wang Q, Yin H. How does an RNA selfie work? EV-associated RNA in innate immunity as self or danger. *J Extracell Vesicles* (2020) 9(1):1793515. doi: 10.1080/20013078.2020.1793515

17. Alexander M, Hu R, Runtsch MC, Kagele DA, Mosbruger TL, Tolmachova T, et al. Exosome-delivered microRNAs modulate the inflammatory response to endotoxin. *Nat Commun* (2015) 6:7321. doi: 10.1038/ncomms8321

18. Valadi H, Ekstrom K, Bossios A, Sjostrand M, Lee JJ, Lotvall JO. Exosome-mediated transfer of mRNAs and microRNAs is a novel mechanism of genetic exchange between cells. *Nat Cell Biol* (2007) 9(6):654–9. doi: 10.1038/ncb1596

19. Horowitz AM, Fan X, Bieri G, Smith LK, Sanchez-Diaz CI, Schroer AB, et al. Blood factors transfer beneficial effects of exercise on neurogenesis and cognition to the aged brain. *Science* (2020) 369(6500):167–73. doi: 10.1126/science.aaw2622

20. Yin Y, Chen H, Wang Y, Zhang L, Wang X. Roles of extracellular vesicles in the aging microenvironment and age-related diseases. *J Extracell Vesicles* (2021) 10 (12):e12154. doi: 10.1002/jev2.12154

21. Tsukamoto H, Kouwaki T, Oshiumi H. Aging-associated extracellular vesicles contain immune regulatory microRNAs alleviating hyperinflammatory state and immune dysfunction in the elderly. *iScience* (2020) 23(9):101520. doi: 10.1016/j.isci.2020.101520

22. Eitan E, Green J, Bodogai M, Mode NA, Baek R, Jorgensen MM, et al. Age-related changes in plasma extracellular vesicle characteristics and internalization by leukocytes. *Sci Rep* (2017) 7(1):1342. doi: 10.1038/s41598-017-01386-z

23. Karbowska M, Kaminski TW, Znorko B, Domaniewski T, Misztal T, Rusak T, et al. Indoxyl sulfate promotes arterial thrombosis in rat model *via* increased levels of complex TF/VII, PAI-1, platelet activation as well as decreased contents of SIRT1 and SIRT3. *Front Physiol* (2018) 9:1623. doi: 10.3389/fphys.2018.01623

24. Breitenstein A, Stein S, Holy EW, Camici GG, Lohmann C, Akhmedov A, et al. Sirt1 inhibition promotes *in vivo* arterial thrombosis and tissue factor expression in stimulated cells. *Cardiovasc Res* (2011) 89(2):464–72. doi: 10.1093/cvr/cvq339

25. Vasko R, Xavier S, Chen J, Lin CH, Ratliff B, Rabadi M, et al. Endothelial sirtuin 1 deficiency perpetrates nephrosclerosis through downregulation of matrix metalloproteinase-14: relevance to fibrosis of vascular senescence. *J Am Soc Nephrol* (2014) 25(2):276–91. doi: 10.1681/ASN.2013010069

26. Haigis MC, Guarente LP. Mammalian sirtuins–emerging roles in physiology, aging, and calorie restriction. *Genes Dev* (2006) 20(21):2913–21. doi: 10.1101/gad.1467506

27. Potente M, Ghaeni L, Baldessari D, Mostoslavsky R, Rossig L, Dequiedt F, et al. SIRT1 controls endothelial angiogenic functions during vascular growth. *Genes Dev* (2007) 21(20):2644–58. doi: 10.1101/gad.435107

28. Ong ALC, Ramasamy TS. Role of Sirtuin1-p53 regulatory axis in aging, cancer and cellular reprogramming. *Ageing Res Rev* (2018) 43:64–80. doi: 10.1016/j.arr.2018.02.004

29. Kobayashi Y, Furukawa-Hibi Y, Chen C, Horio Y, Isobe K, Ikeda K, et al. SIRT1 is critical regulator of FOXO-mediated transcription in response to oxidative stress. *Int J Mol Med* (2005) 16(2):237–43. doi: 10.3892/ijmm.16.2.237

30. Higashida K, Kim SH, Jung SR, Asaka M, Holloszy JO, Han DH. Effects of resveratrol and SIRT1 on PGC-1alpha activity and mitochondrial biogenesis: a reevaluation. *PloS Biol* (2013) 11(7):e1001603.

31. de Mingo A, de Gregorio E, Moles A, Tarrats N, Tutusaus A, Colell A, et al. Cysteine cathepsins control hepatic NF-kappaB-dependent inflammation *via* sirtuin-1 regulation. *Cell Death Dis* (2016) 7(11):e2464.

32. Finkel T, Deng CX, Mostoslavsky R. Recent progress in the biology and physiology of sirtuins. *Nature* (2009) 460(7255):587–91. doi: 10.1038/nature08197

33. He G, Karin M. NF-kappaB and STAT3 - key players in liver inflammation and cancer. *Cell Res* (2011) 21(1):159–68. doi: 10.1038/cr.2010.183

34. Liu T, Zhang L, Joo D, Sun SC. NF-kappaB signaling in inflammation. *Signal Transduct Target Ther* (2017) 2. doi: 10.1038/sigtrans.2017.23

35. Qiu Y, Zhou X, Liu Y, Tan S, Li Y. The role of sirtuin-1 in immune response and systemic lupus erythematosus. *Front Immunol* (2021) 12:632383. doi: 10.3389/fimmu.2021.632383

36. Wang ZL, Luo XF, Li MT, Xu D, Zhou S, Chen HZ, et al. Resveratrol possesses protective effects in a pristane-induced lupus mouse model. *PloS One* (2014) 9(12):e114792. doi: 10.1371/journal.pone.0114792

37. Singh V, Ubaid S. Role of silent information regulator 1 (SIRT1) in regulating oxidative stress and inflammation. *Inflammation* (2020) 43(5):1589–98. doi: 10.1007/s10753-020-01242-9

38. Yang Y, Liu Y, Wang Y, Chao Y, Zhang J, Jia Y, et al. Regulation of SIRT1 and its roles in inflammation. *Front Immunol* (2022) 13:831168. doi: 10.3389/fimmu.2022.831168

39. Granchi C, Minutolo F. Activators of sirtuin-1 and their involvement in cardioprotection. *Curr Med Chem* (2018) 25(34):4432–56. doi: 10.2174/0929867325666180214115438

40. Sharma A, Singh K, Almasan A. Histone H2AX phosphorylation: a marker for DNA damage. *Methods Mol Biol* (2012) 920:613–26. doi: 10.1007/978-1-61779-998-3_40

41. Plappert-Helbig U, Libertini S, Frieauff W, Theil D, Martus HJ. Gamma-H2AX immunofluorescence for the detection of tissue-specific genotoxicity *in vivo*. *Environ Mol Mutagen* (2019) 60(1):4–16. doi: 10.1002/em.22238

42. Yang Y, Luo S, Huang J, Xiao Y, Fu Y, Liu W, et al. Photoactivation of innate immunity receptor TLR8 in live mammalian cells by genetic encoding of photocaged tyrosine. *Chembiochem* (2022) 23(4):e202100344. doi: 10.1002/cbic.202100344

43. Gano LB, Donato AJ, Pasha HM, Hearon CMJr., Sindler AL, Seals DR. The SIRT1 activator SRT1720 reverses vascular endothelial dysfunction, excessive superoxide production, and inflammation with aging in mice. *Am J Physiol Heart Circ Physiol* (2014) 307(12):H1754–63. doi: 10.1152/ajpheart.00377.2014

44. Thery C, Amigorena S, Raposo G, Clayton A. Isolation and characterization of exosomes from cell culture supernatants and biological fluids. *Curr Protoc Cell Biol* (2006) Chapter 3:Unit 3 22. doi: 10.1002/0471143030.cb0322s30

45. Thery C, Witwer KW, Aikawa E, Alcaraz MJ, Anderson JD, Andriantsitohaina R, et al. Minimal information for studies of extracellular vesicles 2018 (MISEV2018): a position statement of the international society for extracellular vesicles and update of the MISEV2014 guidelines. *J Extracell Vesicles* (2018) 7(1):1535750. doi: 10.1080/20013078.2018.1535750

46. Dragovic RA, Gardiner C, Brooks AS, Tannetta DS, Ferguson DJ, Hole P, et al. Sizing and phenotyping of cellular vesicles using nanoparticle tracking analysis. *Nanomedicine* (2011) 7(6):780–8. doi: 10.1016/j.nano.2011.04.003

47. Gardiner C, Ferreira YJ, Dragovic RA, Redman CW, Sargent IL. Extracellular vesicle sizing and enumeration by nanoparticle tracking analysis. *J Extracell Vesicles* (2013) 2. doi: 10.3402/jev.v2i0.19671

48. Tyanova S, Temu T, Sinitcyn P, Carlson A, Hein MY, Geiger T, et al. The Perseus computational platform for comprehensive analysis of (prote)omics data. *Nat Methods* (2016) 13(9):731–40. doi: 10.1038/nmeth.3901

49. Teng F, Fussenegger M. Shedding light on extracellular vesicle biogenesis and bioengineering. *Adv Sci (Weinh)* (2020) 8(1):2003505.

50. Borghesan M, Fafian-Labora J, Eleftheriadou O, Carpintero-Fernandez P, Paez-Ribes M, Vizcay-Barrena G, et al. Small extracellular vesicles are key regulators of non-cell autonomous intercellular communication in senescence *via* the interferon protein IFITM3. *Cell Rep* (2019) 27(13):3956–71 e6. doi: 10.1016/j.celrep.2019.05.095

51. Zhou Y, Zhou B, Pache L, Chang M, Khodabakhshi AH, Tanaseichuk O, et al. Metascape provides a biologist-oriented resource for the analysis of systems-level datasets. *Nat Commun* (2019) 10(1):1523. doi: 10.1038/s41467-019-09234-6

52. Yeung F, Hoberg JE, Ramsey CS, Keller MD, Jones DR, Frye RA, et al. Modulation of NF-kappaB-dependent transcription and cell survival by the SIRT1 deacetylase. *EMBO J* (2004) 23(12):2369–80. doi: 10.1038/sj.emboj.7600244

53. Ota Y, Takahashi K, Otake S, Tamaki Y, Okada M, Aso K, et al. Extracellular vesicle-encapsulated miR-30e suppresses cholangiocarcinoma cell invasion and migration *via* inhibiting epithelial-mesenchymal transition. *Oncotarget* (2018) 9(23):16400–17. doi: 10.18632/oncotarget.24711

54. Chen K, Wang Q, Liu X, Wang F, Yang Y, Tian X. Hypoxic pancreatic cancer derived exosomal miR-30b-5p promotes tumor angiogenesis by inhibiting GJA1 expression. *Int J Biol Sci* (2022) 18(3):1220–37. doi: 10.7150/ijbs.67675

55. Zang J, Maxwell AP, Simpson DA, McKay GJ. Differential expression of urinary exosomal MicroRNAs miR-21-5p and miR-30b-5p in individuals with diabetic kidney disease. *Sci Rep* (2019) 9(1):10900. doi: 10.1038/s41598-019-47504-x

56. Klein JD, Wang XH. Electrically stimulated acupuncture increases renal blood flow through exosome-carried miR-181. *Am J Physiol Renal Physiol* (2018) 315(6):F1542–F9. doi: 10.1152/ajprenal.00259.2018

57. Groot M, Lee H. Sorting mechanisms for MicroRNAs into extracellular vesicles and their associated diseases. *Cells* (2020) 9(4). doi: 10.3390/cells9041044

58. Fabbiano F, Corsi J, Gurrieri E, Trevisan C, Notarangelo M, D'Agostino VG. RNA Packaging into extracellular vesicles: An orchestra of RNA-binding proteins? *J Extracell Vesicles* (2020) 10(2):e12043. doi: 10.1002/jev2.12043

59. Mensa E, Guescini M, Giuliani A, Bacalini MG, Ramini D, Corleone G, et al. Small extracellular vesicles deliver miR-21 and miR-217 as pro-senescence effectors to endothelial cells. *J Extracell Vesicles* (2020) 9(1):1725285. doi: 10.1080/20013078.2020.1725285

60. Zhang H, Freitas D, Kim HS, Fabijanic K, Li Z, Chen H, et al. Identification of distinct nanoparticles and subsets of extracellular vesicles by asymmetric flow field-flow fractionation. *Nat Cell Biol* (2018) 20(3):332–43. doi: 10.1038/s41556-018-0040-4

61. Terlecki-Zaniewicz L, Pils V, Bobbili MR, Lammermann I, Perrotta I, Grillenberger T, et al. Extracellular vesicles in human skin: Cross-talk from senescent fibroblasts to keratinocytes by miRNAs. *J Invest Dermatol* (2019) 139(12):2425–+. doi: 10.1016/j.jid.2019.05.015

62. Lehmann BD, Paine MS, Brooks AM, McCubrey JA, Renegar RH, Wang R, et al. Senescence-associated exosome release from human prostate cancer cells. *Cancer Res* (2008) 68(19):7864–71. doi: 10.1158/0008-5472.CAN-07-6538

63. Dellago H, Preschitz-Kammerhofer B, Terlecki-Zaniewicz L, Schreiner C, Fortschegger K, Chang MW, et al. High levels of oncomiR-21 contribute to the senescence-induced growth arrest in normal human cells and its knock-down increases the replicative lifespan. *Aging Cell* (2013) 12(3):446–58. doi: 10.1111/acel.12069

64. Zhang G, Esteve PO, Chin HG, Terragni J, Dai N, Correa IRJr., et al. Small RNA-mediated DNA (cytosine-5) methyltransferase 1 inhibition leads to aberrant DNA methylation. *Nucleic Acids Res* (2015) 43(12):6112–24. doi: 10.1093/nar/gkv518

frontiers | Frontiers in Immunology

TYPE Review
PUBLISHED 15 September 2022
DOI 10.3389/fimmu.2022.953530

OPEN ACCESS

EDITED BY
Hang Yin,
Tsinghua University, China

REVIEWED BY
Jijie Chai,
Tsinghua University, China
Bikash Ranjan Sahoo,
Howard Hughes Medical Institute (HHMI), United States
Koichi Fukase,
Osaka University, Japan
Christopher Lupfer,
Missouri State University, United States

*CORRESPONDENCE
Umeharu Ohto
umeji@mol.f.u-tokyo.ac.jp

SPECIALTY SECTION
This article was submitted to Molecular Innate Immunity, a section of the journal Frontiers in Immunology

RECEIVED 26 May 2022
ACCEPTED 29 August 2022
PUBLISHED 15 September 2022

CITATION
Ohto U (2022) Activation and regulation mechanisms of NOD-like receptors based on structural biology. *Front. Immunol.* 13:953530. doi: 10.3389/fimmu.2022.953530

Activation and regulation mechanisms of NOD-like receptors based on structural biology

Umeharu Ohto*

Graduate School of Pharmaceutical Sciences, University of Tokyo, Tokyo, Japan

Innate immunity is a primary defense system against microbial infections. Innate immune pattern recognition receptors (PRRs) play pivotal roles in detection of invading pathogens. When pathogens, such as bacteria and viruses, invade our bodies, their components are recognized by PRRs as pathogen-associated molecular patterns (PAMPs), activating the innate immune system. Cellular components such as DNA and RNA, acting as damage-associated molecular patterns (DAMPs), also activate innate immunity through PRRs under certain conditions. Activation of PRRs triggers inflammatory responses, interferon-mediated antiviral responses, and the activation of acquired immunity. Research on innate immune receptors is progressing rapidly. A variety of these receptors has been identified, and their regulatory mechanisms have been elucidated. Nucleotide-binding and oligomerization domain (NOD)-like receptors (NLRs) constitute a major family of intracellular PRRs and are involved in not only combating pathogen invasion but also maintaining normal homeostasis. Some NLRs are known to form multi-protein complexes called inflammasomes, a process that ultimately leads to the production of inflammatory cytokines and induces pyroptosis through the proteolytic cascade. The aberrant activation of NLRs has been found to be associated with autoimmune diseases. Therefore, NLRs are considered targets for drug discovery, such as for antiviral drugs, immunostimulants, antiallergic drugs, and autoimmune disease drugs. This review summarizes our recent understanding of the activation and regulation mechanisms of NLRs, with a particular focus on their structural biology. These include NOD2, neuronal apoptosis inhibitory protein (NAIP)/NLRC4, NLR family pyrin domain containing 1 (NLRP1), NLRP3, NLRP6, and NLRP9. NLRs are involved in a variety of diseases, and their detailed activation mechanisms based on structural biology can aid in developing therapeutic agents in the future.

KEYWORDS

innate immunity, pathogen-associated molecular patterns, damage-associated molecular patterns, pattern recognition receptors, NOD-like receptors (NLRs), inflammasome

Introduction

Bacteria and viruses invading our bodies are recognized as foreign substrates and, therefore, activate the immune system. Immune responses are classified into innate and acquired immunity. In the early stages of microbial invasion, innate immunity is triggered first (1, 2). Pathogen-associated molecular patterns (PAMPs) are recognized by an innate immune receptor called pattern recognition receptor (PRR) (3). Signals are transmitted downstream, ultimately triggering inflammatory responses, interferon-mediated antiviral responses, and the activation of acquired immunity (4). The discovery of toll-like receptors (TLRs) in the late 1990s led to an explosion of research on innate immune receptors, resulting in the identification of a variety of innate immune receptors (5). Each of these receptors was found to be involved in the recognition of unique PAMPs (6). Previously, innate immunity was considered a nonspecific immune response; however, it has now been recognized as a specific immune response due to PRRs (7). In addition to recognizing PAMPs, innate immune receptors may be activated by self-derived molecular patterns (damage-associated molecular patterns, DAMPs) released from necrotic cells, which are known to cause autoimmune diseases (8). Therefore, innate immune receptors are potential drug targets, such as for antiviral drugs, immunostimulants, antiallergic drugs, and drugs for autoimmune diseases (9).

In addition to the aforementioned TLRs, representative innate immune receptors have been identified as nucleotide-binding and oligomerization domain (NOD)-like receptors (NLRs) (10), retinoic acid-inducible gene I (RIG I)-like receptors (11), absent in melanoma 2 (AIM2)-like receptors (12), and cyclic GMP-AMP synthase (cGAS)/stimulator of interferon genes (STING) (13). TLRs are located on the plasma membrane surface and endosomal membranes, whereas other receptors are located in the cytoplasm. Moreover, TLRs recognize PAMPs and DAMPs that have entered the cell. Recently, a rapid progress in the study of intracellular sensors that exist in the cytoplasm and activate innate immunity by recognizing foreign substances, such as pathogen-derived DNA and RNA, has been observed (14, 15). Structural biology studies using X-ray crystallography and cryo-electron microscopy (EM) have made remarkable progress in recent years. Moreover, these studies have played a major role in elucidating the mechanisms by which innate immune receptors recognize PAMPs and DAMPs and activate innate immunity. This review focuses on NLRs, a family of innate immune receptors that exist primarily in the cytoplasm, and introduces the mechanisms of activity regulation and signal transduction revealed by structural biology studies conducted over the past decade (Table 1).

TABLE 1 Summary of structural studies of NLRs.

	Structural features
NLRC4	Inactive form (monomer) (16) Active form (ring-like oligomer complexed with NAIP/ligand) (17–21)
NLRP3	Inactive form (NEK7-bound monomer) (22) Inactive form (cage-like oligomer) (23–25) Inhibitor bound form (23, 24, 26)
NLRP1	Inactive C-terminal fragment (DPP9-bound form) (27, 28)
NOD2	Inactive form (monomer) (29)
NLRP9	Inactive form (monomer) (30)

NOD-like receptors

To date, 22 NLRs with various functional roles have been identified in humans (31). NLR typically consists of three functional domains, namely N-terminal signaling, central [NAIP, CIITA, HETE, TP1 (NACHT)], and leucine-rich repeat (LRR) domains (32–35) (Figure 1A). The N-terminal signaling domain is responsible for signal transduction through interactions with downstream adaptor proteins. The central NACHT domain has ATPase activity and is assumed to be self-oligomerized through this domain on activation. The NACHT domain is further classified into nucleotide-binding domain (NBD), helical domain 1 (HD1), winged-helix domain (WHD), and HD2 subdomains. The LRR domain on the C-terminal side is believed to be involved in ligand recognition and functional regulation. NLRs are classified into subfamilies according to the type of N-terminal signaling domain: those with pyrin domain (PYD) are called the NLR pyrin domain containing (NLRP) family and those with caspase recruitment domain (CARD) are called the NLR CARD containing (NLRC) family. An NLRP uses its PYD to form a scaffold that interacts with the adaptor, apoptosis-associated, speck-like protein containing a CARD (ASC) through PYD-PYD interactions to recruit procaspase-1. Procaspase-1 is activated to caspase-1, which further cleaves pro-interleukin (IL)-1β and pro-IL-18, resulting in the generation of mature IL-1β and IL-18, respectively, and triggering an inflammatory response. Caspase-1 also induces pyroptosis by cleaving gasdermin D. In addition to the caspase-1-mediated canonical inflammasomes, noncanonical inflammasomes involving caspase-4/5 in human and caspase-11 in mice have been identified and are known to respond to cytosolic LPS (37). An NLRC, however, is thought to activate caspase-1 through direct CARD-CARD interactions in addition to the ASC-mediated activation of caspase-1. Diverse PAMPs and DAMPs have been found to activate NLRs. Some NLRs are known to activate innate immunity by forming high-molecular-weight multi-protein complexes called inflammasomes to signal downstream.

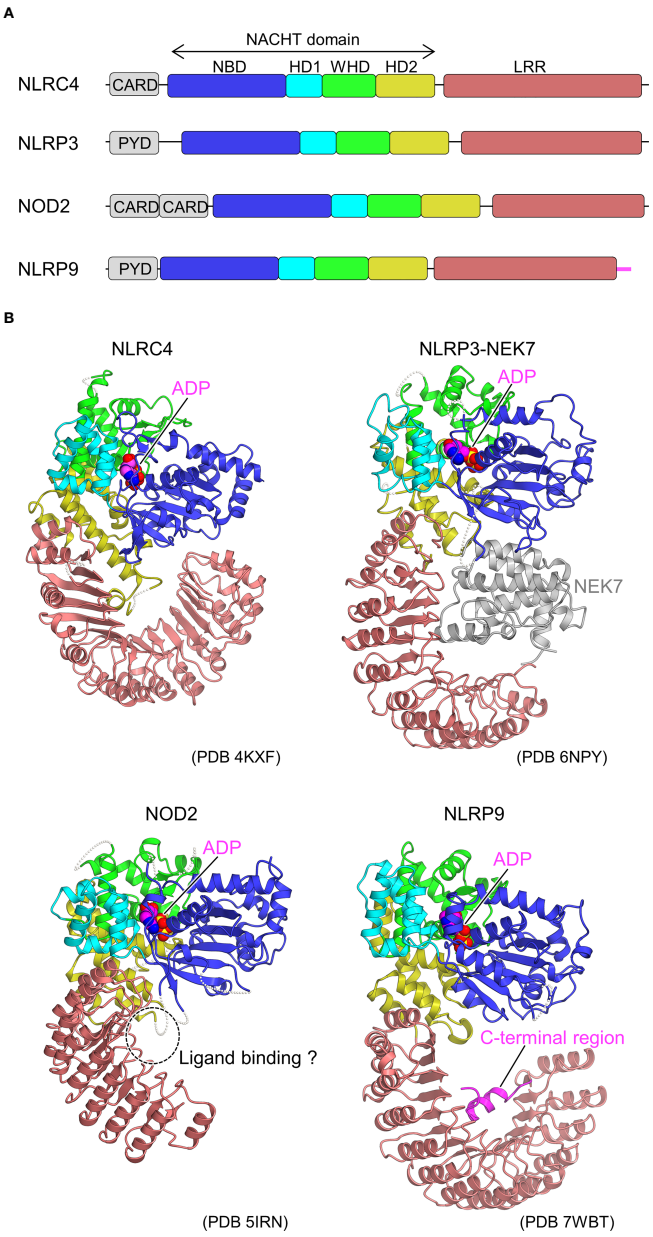

FIGURE 1
Domain organization and structures of inactive NLRs. **(A)** Domain organization of NLRs. Each of the domains and sub domains are indicated by the different colors and are correspondingly indicated in Figure 1B. **(B)**, Structures of inactive NLRs. Structures of inactive NLRC4 (PDB 4KXF) (16), NLRP3-NEK7 complex (PDB 6NPY) (36), NOD2 (PDB 5IRN) (29), and NLRP9 (PDB 7WBT) (30) are shown with the domains colored as per **(A)**. Bound ADP molecules are shown in space filling representations. In the NLRP3-NEK7 complex, bound NEK7 is shown in gray. The potential ligand-binding site in NOD2 and the C-terminal region of NLRP9 are indicated. Structural figures were generated using CueMol throughout this review (http://www.cuemol.org).

NLRC4

In the neuronal apoptosis inhibitory protein (NAIP)/NLRC4 pathway, flagellin, a component of bacterial flagella, and the bacterial rod protein PrgJ bind to NAIPs, whereupon NLRC4 binds as an adapter to form active inflammasome (38–43).

In 2013, the first crystal structure of NLR was reported for the inactive form of NLRC4, lacking the CARD domain (16) (Figure 1B). The inactivated conformation of NLRC4 was a monomeric, autoinhibited conformation, in which the region of the NACHT domain involved in self-association was covered by the LRR domain. Thus, the LRR domain of NLRC4 functions to

sequester NLRC4 in a monomeric state. It was also found that ADP bound to the NACHT domain stabilizes the closed and autoinhibited conformation of NLRC4 by mediating the interactions between the subdomains of the NACHT domain. This was consistent with previous biochemical experiments showing that the deletion of the LRR domain leads to self-activation without NAIP or FliC (39).

Subsequently, cryo-EM analysis revealed that the inflammasome structure of NAIP2-NLRC4 is induced by the bacterial rod protein PrgJ, as reported almost simultaneously by two groups (17, 18) (Figure 2). A low-resolution structure of the NAIP5-NLRC4 helical oligomer induced by flagellin was also reported using cryo-EM tomography (19). Afterwards, cryo-EM structures of the flagellin-NAIP5-NLRC4 were reported, revealing the detailed ligand recognition mechanism of NAIP5 as well as how it leads to the oligomerization of NLRC4 (20, 21). The NAIP2-NLRC4 or NAIP5-NLRC4 oligomer induced by ligand forms a ring-like structure consisting of 10–12 molecules, including one NAIP molecule (Figure 2B). This oligomer is formed by unidirectional chain oligomerization of NLRC4 molecules, starting with the ligand-bound NAIP molecule. In the upper part of the ring, CARD assembly may provide a scaffold for CARD-CARD interactions with downstream caspase-1 (Figure 2B). Upon activation, closed NLRC4 is converted to an open conformation by binding to open NLRC4 *via* the NACHT domain (Figure 2A). During this process, rigid body motion at the linkage between HD1 and WHD of the NACHT domain is observed. This mechanism amplifies the signal by catalytically converting the closed structure to an open structure in a self-propagating manner. Moreover, this mechanism contrasts with the activation mechanism of the apoptotic protease-activating factor-1 (Apaf-1) apoptosome (octameric ring structure), which is related to the NLR. In the case of Apaf-1, each subunit must be activated by its own ligand, that is, a stoichiometric number of ligands is required for all subunits activation (44).

NLRP3

NLRP3 is one of the most well-studied inflammasome-forming NLRs. Moreover, its activators are diverse. For

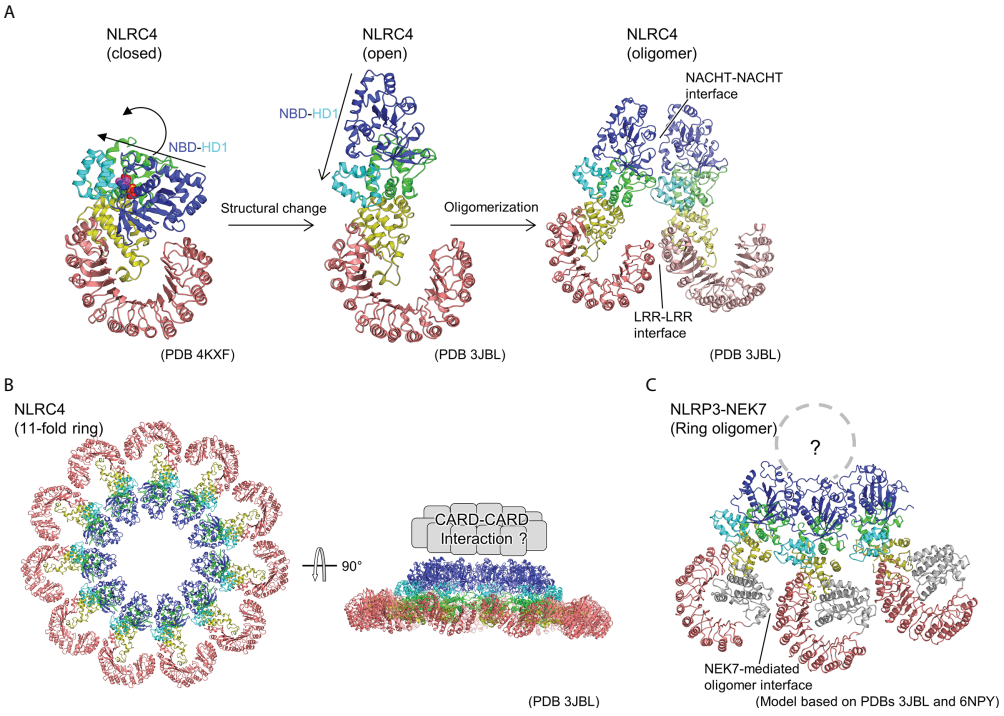

FIGURE 2
Ring-shaped active oligomer of NLRC4. **(A)** Structural changes underlying NLRC4 oligomerization. The NLRC4 monomer undergoes a structural change from a closed (PDB 4KXF) (16) to an open form (PDB 3JBL) (17), causing the NBD-HD1 part to undergo a large rotational movement relative to the other parts. This opens the NACHT domain and the corresponding activated NLRC4 molecules to form a laterally aligned dimer and subsequently form ring-shaped oligomer. **(B)** Structure of 11-fold ring-shaped NLRC4 oligomer (PDB 3JBL) (17). Top (left) and side (right) views are shown. The CARD domains are predicted to be concentrated at the top of the ring as shown schematically in the side view (right). **(C)** Hypothetical structure of NLR3-NEK7 oligomer. The structure of the inactive form of the NLRP3-NEK7 complex (6NPY) (36) was split into the NBD-HD1 and the WHD-HD2-LRR parts, and each was fitted into the corresponding part of the 11-fold ring oligomer of NLRC4 (PDB 3JBL) (17).

instance, nigericin, uric acid, amyloid-beta fibrils, extracellular ATP, and reactive oxygen species are a few activators of NLRP3 (20, 35). Some of these are thought to trigger NLRP3 activation by lowering intracellular K^+ concentrations (45). NLRP3 activation requires two steps of stimulation: "priming" and "activation" (45–47). Priming stimuli include the TLR ligands Pam3CSK4, Poly(I:C), lipopolysaccharide (LPS), and R848, which activate TLRs to upregulate NLRP3 and caspase-1 expression and provide the soil for NLRP3 activation. In addition, priming causes post-translational modifications in NLRP3, such as phosphorylation (48), which are thought to be important for NLRP3 activation. The activating factors include nigericin, extracellular ATP, as well as silica, cholesterol, and uric acid crystals that destabilize lysosomes. As mentioned previously, a wide variety of NLRP3 activators exists, and the direct triggers of NLRP3 activation remain unclear. In addition, it has been reported that NLRP3 activation involves interactions with a variety of proteins. These include SGT1, HSP90 (49), thioredoxin-interacting protein (TXNIP) (50), mitochondrial antiviral-signaling protein (MAVS) (51), never in mitosis A-related kinase 7 (NEK7) (52–54), MAP/microtubule affinity-regulating kinase 4 (MARK4) (55), macrophage migration inhibitory factor (MIF) (56), DEAD box RNA helicase (DDX) 3X (57), and receptor of activated protein C kinase 1 (RACK1) (58). However, the mechanisms by which these factors regulate NLRP3 activation remain unclear.

NLRP3–NEK7 complex

As a starting point for the structural biology studies of NLRP3, the cryo-EM structure of inactivated human NLRP3 (PYD domain deleted) bound to NEK7 was first revealed (36) (Figure 1B). The overall structure was similar to the previously reported structures of NLRC4 (16) and NOD2 (29) in the inactivated form. The kinase C-lobe of NEK7 binds to the concave side of the LRR of NLRP3. Only the C-lobe of NEK7 was visible in the cryo-EM map, but the N-lobe did not clash with NLRP3 even when full-length NEK7 was superimposed. NLRP3 binds to NEK7 at multiple interaction sites (LRR, HD2, and NBD). This binding is suggested to involve electrostatic interactions between the positively charged surface of NEK7 and the negatively charged surface of NLRP3. NEK7 is known to form a complex with NEK9 to participate in mitosis (59); however, the NEK7 surface used for this complexation overlaps in part with the surface used for binding to NLRP3. Therefore, it was expected that once NEK7 binds to NLRP3, it cannot bind to NEK9 and vice versa.

As mentioned previously, upon activation, NLRC4 multimerizes and activates by opening the NACHT domain *via* a large rigid body rotation between HD1 and WHD (Figure 2A) (17, 18). Imitating the oligomeric structure of NLRC4, an oligomeric model of the NLRP3-NEK7 complex was constructed (Figure 2C), where NEK7 was found to be located at the boundary with the neighboring molecule in the oligomer. To investigate the importance of this modeled oligomeric interface, the authors of this paper performed experiments using mutants of NLRP3 and NEK7 and demonstrated that both mutants reduce NLRP3 activation, indicating that this NEK7–NLRP3 interface may be used when NLRP3 is activated (36). In the case of NLRC4, in addition to the contacts at the NACHT site, interactions at the LRR-LRR sites are observed during the formation of ring-shaped oligomers (Figure 2A, B) (17, 18). However, the LRR-LRR interaction in the NLRP3 oligomer is not possible between adjacent monomers because the LRR of NLRP3 is smaller than that of NLRC4. Considering the result of the mutational experiment showing the importance of hypothetical NEK7-NLRP3 interface describe earlier, NEK7-mediated bridging of adjacent LRRs of NLRP3 may reinforce the oligomerization of NLRP3. In other words, in NLRP3, as in the case of NLRC4, the interaction between NACHTs in the inner ring layer and that between LRRs *via* NEK7 in the outer ring layer are thought to contribute to oligomer formation.

Full-length NLRP3 oligomer

Although experimental structural information on the activated oligomer of NLRP3 is not yet available, three groups have reported cryo-EM structures of the full-length NLRP3 oligomer in its inactivated form recently (Figure 3) (23–25). Paradoxically, this inactivated oligomer formation has been shown to be important in the regulation of NLRP3 activation (25). Mouse NLRP3 forms 12-, 14-, and 16-mer (Figure 3A) (23, 25), whereas human NLRP3 forms 10-mer (Figure 3B) (24) hollow, cage-like oligomeric structures with NACHT on the top surface and LRR-LRR interactions on the sides. The density of the PYD domains could not be clearly confirmed, but they were considered to be disordered and located inside or at the top of the cage.

LRR-LRR interactions on the side of the cage are the main contributors to the multimer formation. The interactions at this site are "face-to-face" or "head-to-head," in which neighboring LRRs interact closely with each other (Figure 3). These interactions are mainly due to electrostatic complementarity and hydrophobicity, respectively. In contrast, the NACHTs on the upper and lower surfaces of the cage are proximal to each other, but there is little direct interaction between them. As a result, in all the reported oligomer structures, the density of the LRR portions on the sides of the cage is clear, whereas that of the NACHT portions on the top and bottom surfaces of the cage is relatively obscure.

The structure of the NLRP3 protomer in the oligomer matches well with the previously reported structure of NLRP3 in the inactivated NLRP3-NEK7 structure (36). The LRR-LRR

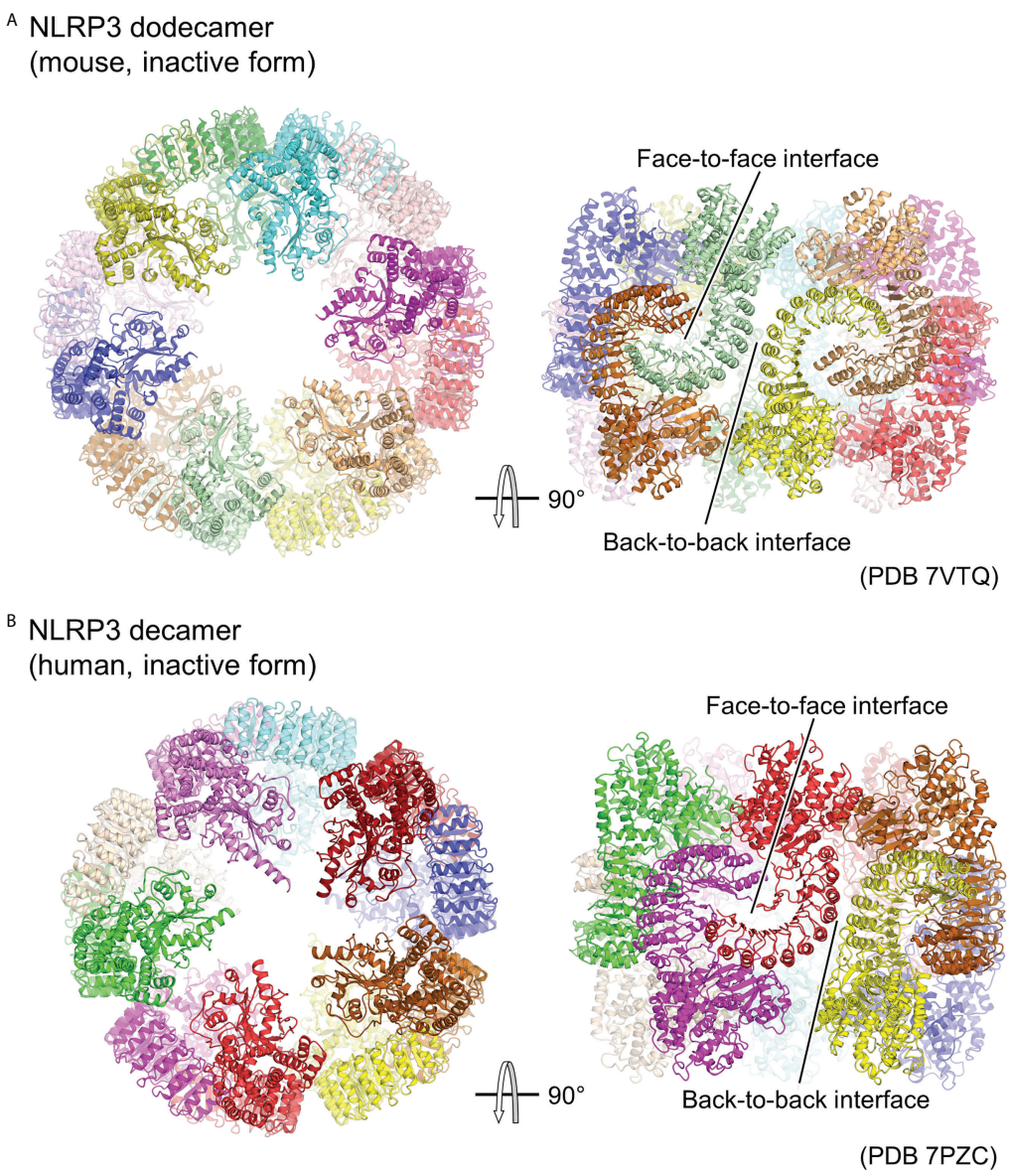

FIGURE 3
Cage-shaped inactive oligomer of NLRP3. Top and side views of the structure of **(A)** full-length mouse NLRP3 dodecamer (PDB 7VTQ) (23) and **(B)** Human NLRP3 decamer (PDB 7PZC) (24). Each protomer is shown in a different color. The LRR-mediated oligomer interfaces are indicated.

and NLRP3-NEK7 interaction interfaces overlap, suggesting that this cage-like NLRP3 oligomer cannot accommodate NEK7. Moreover, this suggests that the cage-like NLRP3 oligomer is reorganized when NEK7 binds to and activates NLRP3. Furthermore, it has been shown that adding NEK7 to the NLRP3 oligomer partially dissociates the oligomer (36). NEK7 is a centrosomal kinase that mainly localizes to the microtubule-organizing center (60, 61), where NLRP3 does not encounter NEK7 in resting cells, suggesting that spatial isolation is one of the mechanisms preventing NLRP3 from being unintentionally activated (25).

Although the density of PYD was not clearly identified in the cage-like oligomeric structure, it is likely that PYD contributes to the formation of this cage-like oligomer, as it does not form when PYD is deleted (23, 25). Moreover, the PYD-deleted form of human NLRP3 forms a hexamer, while intact human NLRP3 forms a cage-like decamer (29, 59). The cage-like NLRP3 oligomers did not induce downstream ASC filament formation (25), suggesting that the PYDs in the oligomers were confined or spatially constrained within the cage, thereby inhibiting filament formation (23–25). This has been proposed as one of the mechanisms limiting NLRP3 activation.

The cage-like NLRP3 oligomer has been shown to have an affinity for membranes (23, 25). Oligomers of NLRP3 have been detected in membrane-extracted fractions from HEK293T cells overexpressing NLRP3 or from immortalized bone marrow-derived macrophages that express NLRP3 endogenously by LPS stimulation (25). Lipid strip assay results have shown that NLRP3 has an affinity for acidic lipids such as phosphatidylinositides, phosphatidic acid, phosphatidyl serine, and cardiolipin (23, 25). This corresponds well with the localization of NLRP3 to acidic lipids in the trans-Golgi network (TGN) (62). Furthermore, thorough functional assay results indicated that the cage-like NLRP3 oligomer is essential for TGN dispersion and NLRP3 activation (25).

In summary, the following mechanism has been proposed (23–25): NLRP3 is localized as a cage-like oligomer on the TGN and mitochondrial membranes in the resting state, where its activation is inhibited by the confinement or structural restriction of PYD. NLRP3 is then activated by activation signals such as due to nigericin, which induces a conformational change to form an activated oligomer.

NLRP3 inhibitor

The cryo-EM structures of the artificial hexamer of human NLRP3 (PYD-deficient), full-length mouse NLRP3 dodecamer (23), and full-length human NLRP3 decamer (24) as well as the crystal structure of the NACHT domain of human NLRP3 (26) have been determined in the presence of the NLRP3 inhibitor MCC950 or its analogs (63–66). This revealed the inhibitor binding mode and the mechanism of inhibition of NLRP3 activation (Figure 4). The inhibitor binds to the bottom of the cavity in the NACHT domain. This cavity is composed of all the domains and subdomains of NLRP3. Although the inhibitor binds spatially close to the ADP binding site, the binding sites are separated by an interaction between NBD, HD1, and WHD, allowing the inhibitor to access NLRP3 from the NBD-HD2-LRR side, whereas ADP accesses NLRP3 from the opposite side. The closed conformation of NACHT domains is generally characterized by tight packing between NACHT subdomains *via* ADP binding (16, 29, 30, 36). Like ADP, the inhibitor binds to NLRP3 and mediates its interaction with its subdomain as well as with LRR. This suggests that inhibitors stabilize the closed conformation of the NACHT domain of NLRP3, thereby preventing the NACHT domain from changing to an open conformation and being activated (23, 24, 26).

NLRP1

Human-NLRP1 is an NLR with an atypical domain configuration with PYD, NACHT, LRR, a function to find domain (FIIND), and CARD domains from the N-terminal to the C-terminal side (Figure 5A) (67, 68). FIIND is further divided into ZU5 (found in ZO-1 and UNC5) and UPA (found in UNC5, PIDD, and ankyrins) subdomains. Autoproteolysis between these two subdomains is important for NLRP1 activation (69, 70). Gain-of-function mutations in NLRP1 are known to cause inflammatory diseases, particularly in the skin (67, 71). NLRs generally signal through their N-terminal PYD or CARD domains, but previous studies have shown that the C-terminal CARD domain is responsible for signaling in NLRP1 (69). The trigger for the activation of NLRP1 has been unknown for many years. However, recently, it was shown that the activation is triggered by the cleavage of human NLRP1 *via* the enteroviral 3C protease at the linker between PYD and NACHT (Q130-G131) (Figure 5A) (72, 73). The resulting N-terminal glycine activates the N-glycine-mediated degradation pathway, which degrades the autoinhibitory NACHT-LRR domain and releases a C-terminal fragment (UPA-CARD) to activate NLRP1 (74–76). The CARD domain of the free C-terminal fragment forms filaments, through which ASC or procaspase-1 is recruited to form the inflammasome (77, 78). Similarly, mouse NLRP1B is cleaved near its N-terminal side by bacterial lethal toxin proteases, resulting in the initiation of N-terminal degradation and release of the C-terminal activating fragment (79–81). In addition, ubiquitination of NLRP1B by bacterial pathogen *Shigella flexneri* IpaH7.8 E3 ubiquitin ligase has shown to activate NLRP1B (75). Dipeptidyl peptidase (DPP) 8 and DPP9 are cytoplasmic dipeptidyl peptidases that bind directly to NLRP1 and inhibit its activation. Inhibition of NLRP1 by DPP8/DPP9 is counteracted by DPP8/DPP9 inhibitors; DPP8/DPP9 inhibitors activate NLRP1 (74, 82–85). Furthermore, human NLRP1 has been shown to be activated by recognition of virus-derived double-stranded RNA (dsRNA) (86).

Regarding the structural biology of NLRP1, the structure of the region containing the central NACHT-LRR domain has not yet been elucidated. However, cryo-EM analysis has recently revealed a mechanism by which the C-terminal fragment released by the N-terminal degradation is repressed by DPP9 (Figure 5B) (27, 28). A ternary complex consisting of one molecule of full-length NLRP1 ($NLRP1^A$) and one molecule of the C-terminal fragment of NLRP1 ($NLRP1^B$) with one molecule of DPP9 was elucidated. The complex contained full-length NLRP1A, but only DPP9, the FIIND domain of $NLRP1^A$ (ZU5 and UPA), and the UPA portion of $NLRP1^B$ were resolved by cryo-EM analysis; other portions were not observed in the cryo-EM map. A peptide of approximately 10 residues on the N-terminal side of $NLRP1^B$, generated by the auto-cleavage of the FIIND domain, was inserted into the substrate recognition pocket of DPP9. Thus, inhibitors of DPP9 that bind to this pocket competitively drive out $NLRP1^B$, allowing the C-terminal fragment to escape capture by DPP9 and become active. In the complex structure, interactions between ZU5 of $NLRP1^A$ and DPP9, UPA of $NLRP1^B$ and DPP9, as well as UPAs of $NLRP1^A$

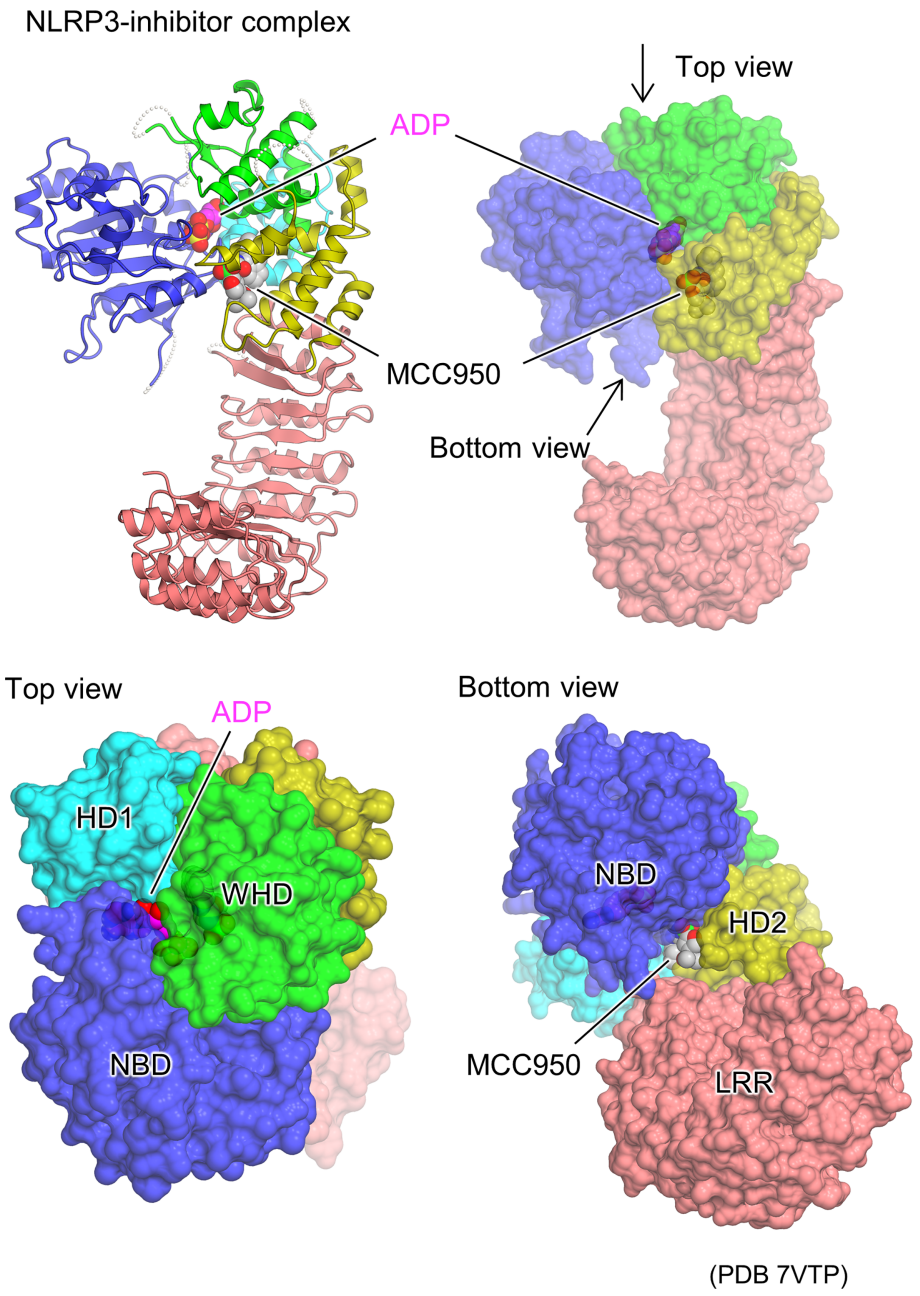

FIGURE 4
Structural basis of NLRP3 inhibitor binding. Protomer structure of the human NLRP3 (PYD deleted) hexamer (PDB 7VTP) (23) with bound molecules of the ADP and NLRP3 inhibitor, MCC950, is illustrated as space filling representations. Ribbon representation (top left) and surface representations from three different views (top right, bottom left, and bottom right) are demonstrated.

and NLRP1^{B} were identified. It has been shown that mutations in the first two parts cause constitutive activation of NLRP1, while mutations in the latter inhibits NLRP1 activation. This suggests that not only the C-terminal fragment of NLRP1^{B}, which binds to the substrate recognition pocket of DPP9, but also the ZU5 domain of full-length NLRP1^{A} is important for the inhibition of activation of the C-terminal fragment of NLRP1^{B} by DPP9. In other words, when a small amount of the C-terminal fragment is unintentionally generated, the presence of intact NLRP1 provides a checkpoint to prevent unintended activation of NLRP1 by the DPP9 inhibitory mechanism (27, 28). However, increased production of the C-terminal fragment of NLRP1, such as during viral infection, is thought to decrease intact NLRP1, rendering this DPP9 checkpoint

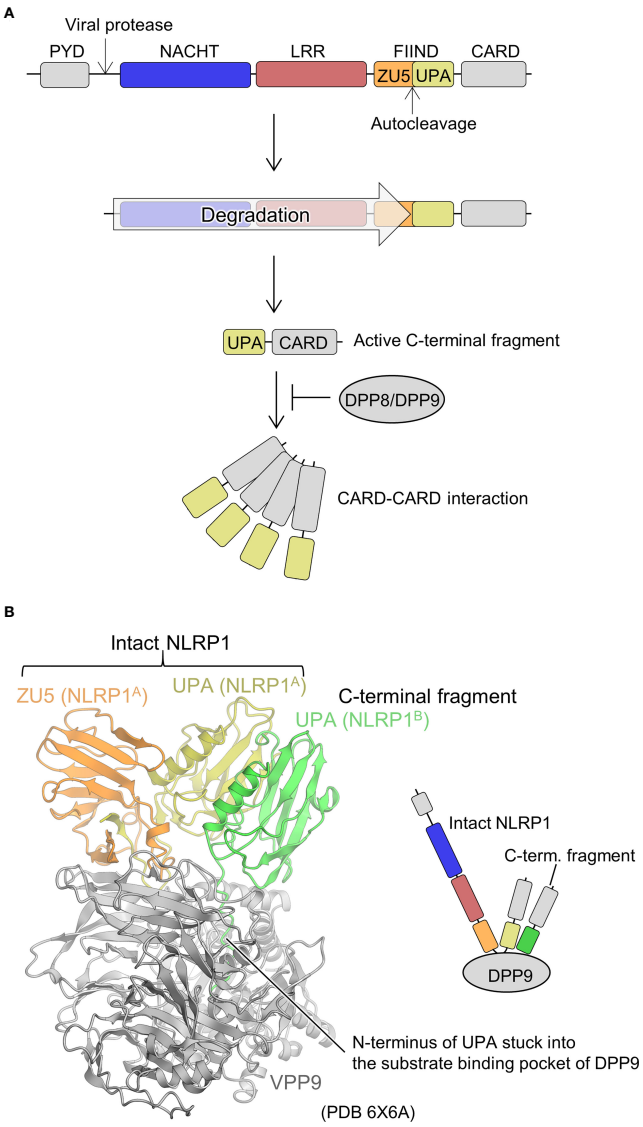

FIGURE 5
Mechanism underlying NLRP1 activation and DPP9-mediated suppression of NLRP1 activation. **(A)** NLRP1 activation mechanism. The domains are indicated in various colors and are correspondingly represented in Figure 5B. **(B)** Structure of the DPP9-NLRP1 complex (PDB 6X6A) (28). In the structure, the ZU5-UPA region from intact NLRP1 (denoted as $NLRP1^{A}$) and UPA portion of the C-terminal fragment of NLRP1 (denoted as $NLRP1^{B}$) bound to a DPP9 molecule are indicated. The schematic of the complex is represented in the right panel.

dysfunctional, resulting in the release of the C-terminal fragment, which in turn leads to NLRP1 activation.

However, the mechanism of NLRP1 activation remains unclear. In other NLRs, oligomerization *via* the NACHT-LRR portion causes spatial proximity between the signaling domains, which is thought to trigger activation (17, 18). The NACHT-LRR portion of NLRP1 acts as a domain that inhibits the release of the C-terminal fragment in the functional degradation mechanism (75, 76) described above. Moreover, the NACHT-LRR portion of NLRP1 is involved in dsRNA recognition during NLRP1 activation by a recently reported virus-derived dsRNA (86). Further studies are required to elucidate the precise role of the NACHT-LRR portion of NLRP1.

NOD2

NOD2 is a member of the NLRC family, and its mutations are closely associated with inflammatory diseases such as Crohn's disease, Blau syndrome, and early-onset sarcoidosis (87, 88), requiring further functional explanation based on its structural biology. It has two CARD domains on its N-terminal side as

signaling domains (Figure 1A). NOD2 is believed to be activated by muramyl dipeptide (MDP) from the bacterial cell wall (89, 90). In addition, diverse stimuli, including *Salmonella typhimurium* effector protein SipA and SopE have been identified to activate NOD2 (91, 92). Upon activation, NOD2 oligomerizes to bring its CARD domains into proximity, recruiting downstream RIPK2 through CARD-CARD interaction, and ultimately activating nuclear factor-κB and inducing an inflammatory response (89, 90).

To date, the crystal structure of the ADP-bound, inactivated form of NOD2 lacking the CARD domain has been determined (Figure 1B) (29). Similar to the inactivated forms of NLRC4 (16) and NLRP3 (36) (Figure 1B), the NACHT domain maintains a closed structure by binding ADP. Mutations that disrupt the interactions between NACHT subdomains increase NOD2 activation, indicating that the interactions between these subdomains are important in maintaining the inactivated conformation (29). The MDP-binding site inferred from previous mutation experiments (93) was located on the concave side of the LRR (29). Mutations in the residues at this site have been shown to decrease the MDP responsiveness of NOD2. It is thought that the binding of MDP to this site induces a conformational change that results in oligomer formation; however, the details have not been yet clarified. Disease-associated mutations are distributed throughout NOD2. Among these, gain-of-function mutations are particularly prevalent at residues located at the interface between the NACHT subdomains. Few studies reported that NOD2 functions by binding to the membrane (94), and some disease-associated mutations are located on positively charged surface residues of HD2, suggesting that NOD2 may bind to the membrane at this site (29).

NLRP9

NLRP9, a member of the NLRP family, together with DExH box RNA helicase (DHX) 9, recognizes rotavirus RNA in intestinal epithelial cells to form inflammasomes and is involved in resistance to rotavirus infection (95). Recently, the crystal and cryo-EM structures of an ADP-bound inactivated form of NLRP9 lacking the PYD domain have been reported (Figure 1B) (30), and both structures are nearly identical. ADP-bound NLRP9, like other inactive forms of NLRs (16, 29, 36), has a closed NACHT domain. Approximately 10 residues on the C-terminal side of NLRP9 have been found to fold back from the tip of LRR to the concave side of LRR, forming an extensive interaction with the concave side of LRR. As discussed, the concave surface of the LRR of each NLR has a distinctive function (23–25, 29, 36, 96). Moreover, it has been speculated that this region of NLRP9 may also play an important role in interactions with other proteins and oligomer formation. However, most mechanisms remain unclear, including the mechanism of inflammasome activation by NLRP9 and the recognition of virus-derived RNA in cooperation with DHX9 (95).

NLRP6

NLRP6 is a member of the NLRP family and, as with NLRP9, plays an important role in immune responses in intestinal epithelial cells (97, 98). Similar to NLRP9, it cooperates with DHX15, an RNA helicase, to bind to the RNA introduced by enteric viruses and induce interferon production through MAVS (98). It is also known to sense microbiota-associated metabolites and form ASC-dependent inflammasomes (97). For NLRP6, the structures of the PYD domain and its filament structure are known (99). However, the structure of the remaining NACHT-LRR portion remains unclear. Recently, it has become clear that liquid-liquid phase separation (LLPS), which has attracted much attention recently because of its involvement in various biological phenomena, plays an important role in the activation of NLRP6 (100). *In vitro* and intracellular experiments indicate that dsRNA induces LLPS formation of NLRP6 and that this LLPS formation is important for the activation of the NLRP6 inflammasome. The adaptor molecule ASC solidifies the LLPS of NLRP6 and activates the inflammasome. The poly-lysine sequence in the NACHT domain of NLRP6 has been shown to be important for LLPS formation. LLPS-mediated NLRP6 activation is a novel NLR inflammasome activation mechanism, and whether similar mechanisms exist for other NLRs must be further investigated in the future.

Concluding remark

The past decade has provided a better understanding of the activation mechanisms of NLRs based on structural biology studies. The mechanism of ring-shaped oligomers as a starting point for downstream adaptor signaling, as evidenced structurally in NLRC4 and postulated in NLRP3, is now clear. However, there is little structural evidence regarding the activation mechanism of NLRs. For instance, how ATPase activities of NLR are involved in the activation, how the conformational change leading to the oligomerization is triggered, and further studies are essential to clarify the activation mechanisms of NLRs. In contrast, the mechanism by which the NACHT-LRR portion of NLRP1 is degraded and that by which the released C-terminal fragment serves as a scaffold for downstream adaptor molecules have been elucidated. Moreover, the mechanism by which NLRP6 condensed by LLPS serves as a scaffold for downstream adaptor molecules has also been revealed. Although these activation mechanisms promote recruitment of downstream adaptor molecules by increasing the local concentration of signaling domains, diverse NLR activation mechanisms are still being uncovered. NLRs are involved in a variety of

diseases, and their detailed activation mechanisms based on structural biology should be further studied to aid in developing therapeutic agents.

Author contributions

The author confirms being the sole contributor of this work and has approved it for publication.

Funding

This work was supported by a Grant-in-Aid from the Japanese Ministry of Education, Culture, Sports, Science, and Technology (Grant Nos. 22H02556 and 19H03164).

Conflict of interest

The author declares that the research was conducted in the absence of any commercial or financial relationships that could be construed as a potential conflict of interest.

Publisher's note

References

1. Beutler B. Innate immunity: an overview. *Mol Immunol* (2004) 40:845–59. doi: 10.1016/j.molimm.2003.10.005

2. Medzhitov R, Janeway CJr. Innate immunity. *N Engl J Med* (2000) 343:338–44. doi: 10.1056/NEJM200008033430506

3. Takeuchi O, Akira S. Pattern recognition receptors and inflammation. *Cell* (2010) 140:805–20. doi: 10.1016/j.cell.2010.01.022

4. Palm NW, Medzhitov R. Pattern recognition receptors and control of adaptive immunity. *Immunol Rev* (2009) 227:221–33. doi: 10.1111/j.1600-065X.2008.00731.x

5. Takeda K, Kaisho T, Akira S. Toll-like receptors. *Annu Rev Immunol* (2003) 21:335–76. doi: 10.1146/annurev.immunol.21.120601.141126

6. Fitzgerald KA, Kagan JC. Toll-like receptors and the control of immunity. *Cell* (2020) 180:1044–66. doi: 10.1016/j.cell.2020.02.041

7. Takeuchi O, Akira S. Innate immunity to virus infection. *Immunol Rev* (2009) 227:75–86. doi: 10.1111/j.1600-065X.2008.00737.x

8. Waldner H. The role of innate immune responses in autoimmune disease development. *Autoimmun. Rev* (2009) 8:400–4. doi: 10.1016/j.autrev.2008.12.019

9. Ulevitch RJ. Therapeutics targeting the innate immune system. *Nat Rev Immunol* (2004) 4:512–20. doi: 10.1038/nri1396

10. Franchi L, Warner N, Viani K, Nunez G. Function of nod-like receptors in microbial recognition and host defense. *Immunol Rev* (2009) 227:106–28. doi: 10.1111/j.1600-065X.2008.00734.x

11. Loo YM, Gale MJr. Immune signaling by RIG-i-like receptors. *Immunity* (2011) 34:680–92. doi: 10.1016/j.immuni.2011.05.003

12. Kumari P, Russo AJ, Shivcharan S, Rathinam VA. AIM2 in health and disease: Inflammasome and beyond. *Immunol Rev* (2020) 297:83–95. doi: 10.1111/imr.12903

13. Hopfner KP, Hornung V. Molecular mechanisms and cellular functions of cGAS-STING signalling. *Nat Rev Mol Cell Biol* (2020) 21:501–21. doi: 10.1038/s41580-020-0244-x

14. Tan XJ, Sun LJ, Chen JQ, Chen ZJJ. Detection of microbial infections through innate immune sensing of nucleic acids. *Annu Rev Microbiol* (2018) 72:447–78. doi: 10.1146/annurev-micro-102215-095605

15. Miyake K, Shibata T, Ohto U, Shimizu T, Saitoh SI, Fukui R, et al. Mechanisms controlling nucleic acid-sensing toll-like receptors. *Int Immunol* (2018) 30:43–51. doi: 10.1093/intimm/dxy016

16. Hu Z, Yan C, Liu P, Huang Z, Ma R, Zhang C, et al. Crystal structure of NLRC4 reveals its autoinhibition mechanism. *Science* (2013) 341:172–5. doi: 10.1126/science.1236381

17. Zhang L, Chen S, Ruan J, Wu J, Tong AB, Yin Q, et al. Cryo-EM structure of the activated NAIP2-NLRC4 inflammasome reveals nucleated polymerization. *Science* (2015) 350:404–9. doi: 10.1126/science.aac5789

18. Hu Z, Zhou Q, Zhang C, Fan S, Cheng W, Zhao Y, et al. Structural and biochemical basis for induced self-propagation of NLRC4. *Science* (2015) 350:399–404. doi: 10.1126/science.aac5489

19. Diebolder CA, Halff EF, Koster AJ, Huizinga EG, Koning RI. Cryoelectron tomography of the NAIP5/NLRC4 inflammasome: Implications for NLR activation. *Structure* (2015) 23:2349–57. doi: 10.1016/j.str.2015.10.001

20. Yang X, Yang F, Wang W, Lin G, Hu Z, Han Z, et al. Structural basis for specific flagellin recognition by the NLR protein NAIP5. *Cell Res* (2018) 28:35–47. doi: 10.1038/cr.2017.148

21. Tenthorey JL, Haloupek N, Lopez-Blanco JR, Grob P, Adamson E, Hartenian E, et al. The structural basis of flagellin detection by NAIP5: A strategy to limit pathogen immune evasion. *Science* (2017) 358:888–93. doi: 10.1126/science.aao1140

22. Shen C, Sharif H, Xia S, Wu H. Structural and mechanistic elucidation of inflammasome signaling by cryo-EM. *Curr Opin Struct Biol* (2019) 58:18–25. doi: 10.1016/j.sbi.2019.03.033

23. Ohto U, Kamitsukasa Y, Ishida H, Zhang Z, Murakami K, Hirama C, et al. Structural basis for the oligomerization-mediated regulation of NLRP3 inflammasome activation. *Proc Natl Acad Sci USA* (2022) 119:e2121353119. doi: 10.1073/pnas.2121353119

24. Hochheiser IV, Pilsl M, Hagelueken G, Moecking J, Marleaux M, Brinkschulte R, et al. Structure of the NLRP3 decamer bound to the cytokine release inhibitor CRID3. *Nature* (2022) 604:184–9. doi: 10.1038/s41586-022-04467-w

25. Andreeva L, David L, Rawson S, Shen C, Pasricha T, Pelegrin P, et al. NLRP3 cages revealed by full-length mouse NLRP3 structure control pathway activation. *Cell* (2021) 184:6299–6312 e6222. doi: 10.1016/j.cell.2021.11.011

26. Dekker C, Mattes H, Wright M, Boettcher A, Hinniger A, Hughes N, et al. Crystal structure of NLRP3 NACHT domain with an inhibitor defines mechanism of inflammasome inhibition. *J Mol Biol* (2021) 433:167309. doi: 10.1016/j.jmb.2021.167309

27. Huang M, Zhang X, Toh GA, Gong Q, Wang J, Han Z, et al. Structural and biochemical mechanisms of NLRP1 inhibition by DPP9. *Nature* (2021) 592:773–7. doi: 10.1038/s41586-021-03320-w

28. Hollingsworth LR, Sharif H, Griswold AR, Fontana P, Mintseris J, Dagbay KB, et al. DPP9 sequesters the c terminus of NLRP1 to repress inflammasome activation. *Nature* (2021) 592:778–83. doi: 10.1038/s41586-021-03350-4

29. Maekawa S, Ohto U, Shibata T, Miyake K, Shimizu T. Crystal structure of NOD2 and its implications in human disease. *Nat Commun* (2016) 7:11813. doi: 10.1038/ncomms11813

30. Kamitsukasa Y, Nakano K, Murakami K, Hirata K, Yamamoto M, Shimizu T, et al. The structure of NLRP9 reveals a unique c-terminal region with putative regulatory function. *FEBS Lett* (2022) 596:876–85. doi: 10.1002/1873-3468.14302

31. Kienes I, Weidl T, Mirza N, Chamaillard M, Kufer TA. Role of NLRs in the regulation of type I interferon signaling, host defense and tolerance to inflammation. *Int J Mol Sci* (2021) 22:1301. doi: 10.3390/ijms22031301

32. Broz P, Dixit VM. Inflammasomes: mechanism of assembly, regulation and signalling. *Nat Rev Immunol* (2016) 16:407–20. doi: 10.1038/nri.2016.58

33. Guo H, Callaway JB, Ting JP. Inflammasomes: mechanism of action, role in disease, and therapeutics. *Nat Med* (2015) 21:677–87. doi: 10.1038/nm.3893

34. Lamkanfi M, Dixit VM. Mechanisms and functions of inflammasomes. *Cell* (2014) 157:1013–22. doi: 10.1016/j.cell.2014.04.007

35. Tschopp J, Schroder K. NLRP3 inflammasome activation: The convergence of multiple signalling pathways on ROS production? *Nat Rev Immunol* (2010) 10:210–5. doi: 10.1038/nri2725

36. Sharif H, Wang L, Wang WL, Magupalli VG, Andreeva L, Qiao Q, et al. Structural mechanism for NEK7-licensed activation of NLRP3 inflammasome. *Nature* (2019) 570:338–43. doi: 10.1038/s41586-019-1295-z

37. Matikainen S, Nyman TA, Cypryk W. Function and regulation of noncanonical caspase-4/5/11 inflammasome. *J Immunol* (2020) 204:3063–9. doi: 10.4049/jimmunol.2000373

38. Zhao Y, Yang J, Shi J, Gong YN, Lu Q, Xu H, et al. The NLRC4 inflammasome receptors for bacterial flagellin and type III secretion apparatus. *Nature* (2011) 477:596–600. doi: 10.1038/nature10510

39. Kofoed EM, Vance RE. Innate immune recognition of bacterial ligands by NAIPs determines inflammasome specificity. *Nature* (2011) 477:592–5. doi: 10.1038/nature10394

40. Miao EA, Mao DP, Yudkovsky N, Bonneau R, Lorang CG, Warren SE, et al. Innate immune detection of the type III secretion apparatus through the NLRC4 inflammasome. *Proc Natl Acad Sci USA* (2010) 107:3076–80. doi: 10.1073/pnas.0913087107

41. Miao EA, Alpuche-Aranda CM, Dors M, Clark AE, Bader MW, Miller SI, et al. Cytoplasmic flagellin activates caspase-1 and secretion of interleukin 1beta. *via Ipaf. Nat Immunol* (2006) 7:569–75. doi: 10.1038/ni1344

42. Franchi L, Amer A, Body-Malapel M, Kanneganti TD, Ozoren N, Jagirdar R, et al. Cytosolic flagellin requires ipaf for activation of caspase-1 and interleukin 1beta in salmonella-infected macrophages. *Nat Immunol* (2006) 7:576–82. doi: 10.1038/ni1346

43. Mariathasan S, Newton K, Monack DM, Vucic D, French DM, Lee WP, et al. Differential activation of the inflammasome by caspase-1 adaptors ASC and ipaf. *Nature* (2004) 430:213–8. doi: 10.1038/nature02664

44. Yuan SJ, Topf M, Reubold TF, Eschenburg S, Akey CW. Changes in apaf-1 conformation that drive apoptosome assembly. *Biochemistry* (2013) 52:2319–27. doi: 10.1021/bi301721g

45. He Y, Hara H, Nunez G. Mechanism and regulation of NLRP3 inflammasome activation. *Trends Biochem Sci* (2016) 41:1012–21. doi: 10.1016/j.tibs.2016.09.002

46. Sutterwala FS, Haasken S, Cassel SL. Mechanism of NLRP3 inflammasome activation. *Ann N Y Acad Sci* (2014) 1319:82–95. doi: 10.1111/nyas.12458

47. Jin C, Flavell RA. Molecular mechanism of NLRP3 inflammasome activation. *J Clin Immunol* (2010) 30:628–31. doi: 10.1007/s10875-010-9440-3

48. Song N, Li T. Regulation of NLRP3 inflammasome by phosphorylation. *Front Immunol* (2018) 9:2305. doi: 10.3389/fimmu.2018.02305

49. Mayor A, Martinon F, De Smedt T, Petrilli V, Tschopp J. A crucial function of SGT1 and HSP90 in inflammasome activity links mammalian and plant innate immune responses. *Nat Immunol* (2007) 8:497–503. doi: 10.1038/ni1459

50. Zhou R, Tardivel A, Thorens B, Choi I, Tschopp J. Thioredoxin-interacting protein links oxidative stress to inflammasome activation. *Nat Immunol* (2010) 11:136–40. doi: 10.1038/ni.1831

51. Subramanian N, Natarajan K, Clatworthy MR, Wang Z, Germain RN. The adaptor MAVS promotes NLRP3 mitochondrial localization and inflammasome activation. *Cell* (2013) 153:348–61. doi: 10.1016/j.cell.2013.02.054

52. Shi H, Wang Y, Li X, Zhan X, Tang M, Fina M, et al. NLRP3 activation and mitosis are mutually exclusive events coordinated by NEK7, a new inflammasome component. *Nat Immunol* (2016) 17:250–8. doi: 10.1038/ni.3333

53. Schmid-Burgk JL, Chauhan D, Schmidt T, Ebert TS, Reinhardt J, Endl E, et al. A genome-wide CRISPR (Clustered regularly interspaced short palindromic repeats) screen identifies NEK7 as an essential component of NLRP3 inflammasome activation. *J Biol Chem* (2016) 291:103–9. doi: 10.1074/jbc.C115.700492

54. He Y, Zeng MY, Yang D, Motro B, Nunez G. NEK7 is an essential mediator of NLRP3 activation downstream of potassium efflux. *Nature* (2016) 530:354–7. doi: 10.1038/nature16959

55. Li X, Thome S, Ma X, Amrute-Nayak M, Finigan A, Kitt L, et al. MARK4 regulates NLRP3 positioning and inflammasome activation through a microtubule-dependent mechanism. *Nat Commun* (2017) 8:15986. doi: 10.1038/ncomms15986

56. Lang T, Lee JPW, Elgass K, Pinar AA, Tate MD, Aitken EH, et al. Macrophage migration inhibitory factor is required for NLRP3 inflammasome activation. *Nat Commun* (2018) 9:2223. doi: 10.1038/s41467-018-04581-2

57. Samir P, Kesavardhana S, Patmore DM, Gingras S, Malireddi RKS, Karki R, et al. DDX3X acts as a live-or-die checkpoint in stressed cells by regulating NLRP3 inflammasome. *Nature* (2019) 573:590. doi: 10.1038/s41586-019-1551-2

58. Duan Y, Zhang L, Angosto-Bazarra D, Pelegrin P, Nunez G, He Y. RACK1 mediates NLRP3 inflammasome activation by promoting NLRP3 active conformation and inflammasome assembly. *Cell Rep* (2020) 33:108405. doi: 10.1016/j.celrep.2020.108405

59. Haq T, Richards MW, Burgess SG, Gallego P, Yeoh S, O'Regan L, et al. Mechanistic basis of Nek7 activation through Nek9 binding and induced dimerization. *Nat Commun* (2015) 6:8771. doi: 10.1038/ncomms9771

60. Magupalli VG, Negro R, Tian Y, Hauenstein AV, Di Caprio G, Skillern W, et al. HDAC6 mediates an aggresome-like mechanism for NLRP3 and pyrin inflammasome activation. *Science* (2020) 369:eaas8995. doi: 10.1126/science.aas8995

61. Kim S, Lee K, Rhee K. NEK7 is a centrosomal kinase critical for microtubule nucleation. *Biochem Bioph Res Co* (2007) 360:56–62. doi: 10.1016/j.bbrc.2007.05.206

62. Chen J, Chen ZJ. PtdIns4P on dispersed trans-golgi network mediates NLRP3 inflammasome activation. *Nature* (2018) 564:71–6. doi: 10.1038/s41586-018-0761-3

63. Tapia-Abellan A, Angosto-Bazarra D, Martinez-Banaclocha H, de Torre-Minguela C, Ceron-Carrasco JP, Perez-Sanchez H, et al. MCC950 closes the active conformation of NLRP3 to an inactive state. *Nat Chem Biol* (2019) 15:560–4. doi: 10.1038/s41589-019-0278-6

64. Coll RC, Hill JR, Day CJ, Zamoshnikova A, Boucher D, Massey NL, et al. MCC950 directly targets the NLRP3 ATP-hydrolysis motif for inflammasome inhibition. *Nat Chem Biol* (2019) 15:556–9. doi: 10.1038/s41589-019-0277-7

65. Primiano MJ, Lefker BA, Bowman MR, Bree AG, Hubeau C, Bonin PD, et al. Efficacy and pharmacology of the NLRP3 inflammasome inhibitor CP-456,773 (CRID3) in murine models of dermal and pulmonary inflammation. *J Immunol* (2016) 197:2421–33. doi: 10.4049/jimmunol.1600035

66. Coll RC, Robertson AA, Chae JJ, Higgins SC, Munoz-Planillo R, Inserra MC, et al. A small-molecule inhibitor of the NLRP3 inflammasome for the treatment of inflammatory diseases. *Nat Med* (2015) 21:248–55. doi: 10.1038/nm.3806

67. Taabazuing CY, Griswold AR, Bachovchin DA. The NLRP1 and CARD8 inflammasomes. *Immunol Rev* (2020) 297:13–25. doi: 10.1111/imr.12884

68. Mitchell PS, Sandstrom A, Vance RE. The NLRP1 inflammasome: new mechanistic insights and unresolved mysteries. *Curr Opin Immunol* (2019) 60:37–45. doi: 10.1016/j.coi.2019.04.015

69. Finger JN, Lich JD, Dare LC, Cook MN, Brown KK, Duraiswami C, et al. Autolytic proteolysis within the function to find domain (FIIND) is required for NLRP1 inflammasome activity. *J Biol Chem* (2012) 287:31456–6. doi: 10.1074/jbc.A112.378323

70. D'Osualdo A, Weichenberger CX, Wagner RN, Godzik A, Wooley J, Reed JC, et al. CARD8 and NLRP1 undergo autoproteolytic processing through a ZU5-like domain. *PloS One* (2011) 6:e27396. doi: 10.1371/journal.pone.0027396

71. Fenini G, Karakaya T, Hennig P, Di Filippo M, Beer HD. The NLRP1 inflammasome in human skin and beyond. *Int J Mol Sci* (2020) 21(13):4788. doi: 10.3390/ijms21134788

72. Tsu BV, Beierschmitt C, Ryan AP, Agarwal R, Mitchell PS, Daugherty MD, et al. Diverse viral proteases activate the NLRP1 inflammasome. *Elife* (2021) 10:e60609. doi: 10.7554/eLife.60609

73. Robinson KS, Teo DET, Tan KS, Toh GA, Ong HH, Lim CK, et al. Enteroviral 3C protease activates the human NLRP1 inflammasome in airway epithelia. *Science* (2020) 370(6521):eaay2002. doi: 10.1126/science.aay2002

74. Xu H, Shi J, Gao H, Liu Y, Yang Z, Shao F, et al. The n-end rule ubiquitin ligase UBR2 mediates NLRP1B inflammasome activation by anthrax lethal toxin. *EMBO J* (2019) 38:e101996. doi: 10.15252/embj.2019101996

75. Sandstrom A, Mitchell PS, Goers L, Mu EW, Lesser CF, Vance RE, et al. Functional degradation: A mechanism of NLRP1 inflammasome activation by diverse pathogen enzymes. *Science* (2019) 364(6435):eaau1330. doi: 10.1126/science.aau1330

76. Chui AJ, Okondo MC, Rao SD, Gai K, Griswold AR, Johnson DC, et al. N-terminal degradation activates the NLRP1B inflammasome. *Science* (2019) 364:82–5. doi: 10.1126/science.aau1208

77. Robert Hollingsworth L, David L, Li Y, Griswold AR, Ruan J, Sharif H, et al. Mechanism of filament formation in UPA-promoted CARD8 and NLRP1 inflammasomes. *Nat Commun* (2021) 12:189. doi: 10.1038/s41467-020-20320-y

78. Gong Q, Robinson K, Xu C, Huynh PT, Chong KHC, Tan EYJ, et al. Structural basis for distinct inflammasome complex assembly by human NLRP1 and CARD8. *Nat Commun* (2021) 12:188. doi: 10.1038/s41467-020-20319-5

79. Levinsohn JL, Newman ZL, Hellmich KA, Fattah R, Getz MA, Liu S, et al. Anthrax lethal factor cleavage of Nlrp1 is required for activation of the inflammasome. *PloS Pathog* (2012) 8:e1002638. doi: 10.1371/journal.ppat.1002638

80. Hellmich KA, Levinsohn JL, Fattah R, Newman ZL, Maier N, Sastalla I, et al. Anthrax lethal factor cleaves mouse nlrp1b in both toxin-sensitive and toxin-resistant macrophages. *PloS One* (2012) 7:e49741. doi: 10.1371/journal.pone.0049741

81. Chavarria-Smith J, Vance RE. Direct proteolytic cleavage of NLRP1B is necessary and sufficient for inflammasome activation by anthrax lethal factor. *PloS Pathog* (2013) 9(6):e1003452. doi: 10.1371/journal.ppat.1003452

82. Zhong FL, Robinson K, Teo DET, Tan KY, Lim C, Harapas CR, et al. Human DPP9 represses NLRP1 inflammasome and protects against autoinflammatory diseases *via* both peptidase activity and FIIND domain binding. *J Biol Chem* (2018) 293:18864–78. doi: 10.1074/jbc.RA118.004350

83. Okondo MC, Rao SD, Taabazuing CY, Chui AJ, Poplawski SE, Johnson DC, et al. Inhibition of Dpp8/9 activates the Nlrp1b inflammasome. *Cell Chem Biol* (2018) 25:262–267 e265. doi: 10.1016/j.chembiol.2017.12.013

84. Johnson DC, Taabazuing CY, Okondo MC, Chui AJ, Rao SD, Brown FC, et al. DPP8/DPP9 inhibitor-induced pyroptosis for treatment of acute myeloid leukemia. *Nat Med* (2018) 24:1151–6. doi: 10.1038/s41591-018-0082-y

85. Okondo MC, Johnson DC, Sridharan R, Go EB, Chui AJ, Wang MS, et al. DPP8 and DPP9 inhibition induces pro-caspase-1-dependent monocyte and macrophage pyroptosis. *Nat Chem Biol* (2017) 13:46–53. doi: 10.1038/nchembio.2229

86. Bauernfried S, Scherr MJ, Pichlmair A, Duderstadt KE, Hornung V. Human NLRP1 is a sensor for double-stranded RNA. *Science* (2021) 371:482. doi: 10.1126/science.abd0811

87. Abraham C, Cho JH. Functional consequences of NOD2 (CARD15) mutations. *Inflammation Bowel Dis* (2006) 12:641–50. doi: 10.1097/01.MIB.0000225332.83861.5f

88. Ogura Y, Bonen DK, Inohara N, Nicolae DL, Chen FF, Ramos R, et al. A frameshift mutation in NOD2 associated with susceptibility to crohn's disease. *Nature* (2001) 411:603–6. doi: 10.1038/35079114

89. Inohara N, Ogura Y, Fontalba A, Gutierrez O, Pons F, Crespo J, et al. Host recognition of bacterial muramyl dipeptide mediated through NOD2. implications for crohn's disease. *J Biol Chem* (2003) 278:5509–12. doi: 10.1074/jbc.C200673200

90. Girardin SE, Boneca IG, Viala J, Chamaillard M, Labigne A, Thomas G, et al. Nod2 is a general sensor of peptidoglycan through muramyl dipeptide (MDP) detection. *J Biol Chem* (2003) 278:8869–72. doi: 10.1074/jbc.C200651200

91. Keestra AM, Winter MG, Klein-Douwel D, Xavier MN, Winter SE, Kim A, et al. A salmonella virulence factor activates the NOD1/NOD2 signaling pathway. *mBio* (2011) 2(6):e00266-11. doi: 10.1128/mBio.00266-11

92. Keestra AM, Winter MG, Auburger JJ, Frassle SP, Xavier MN, Winter SE, et al. Manipulation of small rho GTPases is a pathogen-induced process detected by NOD1. *Nature* (2013) 496:233. doi: 10.1038/nature12025

93. Tanabe T, Chamaillard M, Ogura Y, Zhu L, Qiu S, Masumoto J, et al. Regulatory regions and critical residues of NOD2 involved in muramyl dipeptide recognition. *EMBO J* (2004) 23:1587–97. doi: 10.1038/sj.emboj.7600175

94. Barnich N, Aguirre JE, Reinecker HC, Xavier R, Podolsky DK. Membrane recruitment of NOD2 in intestinal epithelial cells is essential for nuclear factor-kappa b activation in muramyl dipeptide recognition. *J Cell Biol* (2005) 170:21–6. doi: 10.1083/jcb.200502153

95. Zhu S, Ding SY, Wang PH, Wei Z, Pan W, Palm NW, et al. Nlrp9b inflammasome restricts rotavirus infection in intestinal epithelial cells. *Nature* (2017) 546:667. doi: 10.1038/nature22967

96. Reubold TF, Hahne G, Wohlgemuth S, Eschenburg S. Crystal structure of the leucine-rich repeat domain of the NOD-like receptor NLRP1: implications for binding of muramyl dipeptide. *FEBS Lett* (2014) 588:3327–32. doi: 10.1016/j.febslet.2014.07.017

97. Levy M, Thaiss CA, Zeevi D, Dohnalova L, Zilberman-Schapira G, Mahdi JA, et al. Microbiota-modulated metabolites shape the intestinal microenvironment by regulating NLRP6 inflammasome signaling. *Cell* (2015) 163:1428–43. doi: 10.1016/j.cell.2015.10.048

98. Wang P, Zhu S, Yang L, Cui S, Pan W, Jackson R, et al. Nlrp6 regulates intestinal antiviral innate immunity. *Science* (2015) 350:826–30. doi: 10.1126/science.aab3145

99. Shen C, Lu A, Xie WJ, Ruan J, Negro R, Egelman EH, et al. Molecular mechanism for NLRP6 inflammasome assembly and activation. *Proc Natl Acad Sci U.S.A.* (2019) 116:2052–7. doi: 10.1073/pnas.1817221116

100. Shen C, Li R, Negro R, Cheng J, Vora SM, Fu TM, et al. Phase separation drives RNA virus-induced activation of the NLRP6 inflammasome. *Cell* (2021) 184:5759–5774 e5720. doi: 10.1016/j.cell.2021.09.032

frontiers | Frontiers in Immunology

TYPE Original Research
PUBLISHED 05 October 2022
DOI 10.3389/fimmu.2022.930683

OPEN ACCESS

EDITED BY
Toshiyuki Shimizu,
The University of Tokyo, Japan

REVIEWED BY
Saeedeh Ghorbanalipoor,
University of Veterinary Medicine Vienna, Austria
Huina Zhang,
Beijing Anzhen Hospital, Capital Medical University, China

*CORRESPONDENCE
Masahiro Nishibori
mbori@md.okayama-u.ac.jp

SPECIALTY SECTION
This article was submitted to Molecular Innate Immunity, a section of the journal Frontiers in Immunology

RECEIVED 28 April 2022
ACCEPTED 22 September 2022
PUBLISHED 05 October 2022

CITATION
Gao S, Liu K, Ku W, Wang D, Wake H, Qiao H, Teshigawara K and Nishibori M (2022) Histamine induced high mobility group box-1 release from vascular endothelial cells through H_1 receptor.
Front. Immunol. 13:930683.
doi: 10.3389/fimmu.2022.930683

Histamine induced high mobility group box-1 release from vascular endothelial cells through H_1 receptor

Shangze Gao[1,2,3], Keyue Liu[1], Wenhan Ku[1], Dengli Wang[1], Hidenori Wake[1], Handong Qiao[1], Kiyoshi Teshigawara[1] and Masahiro Nishibori[4*]

[1]Department of Pharmacology, Okayama University Graduate School of Medicine, Dentistry and Pharmaceutical Sciences, Okayama, Japan, [2]School of Pharmaceutical Sciences, Tsinghua University, Beijing, China, [3]Tsinghua-Peking Center for Life Sciences, Tsinghua University, Beijing, China, [4]Department of Translational Research and Drug Development, Okayama University Graduate School of Medicine, Dentistry and Pharmaceutical Sciences, Okayama, Japan

Background: Systemic allergic reaction is characterized by vasodilation and vascular leakage, which causes a rapid, precipitous and sustained decrease in arterial blood pressure with a concomitant decrease of cardiac output. Histamine is a major mediator released by mast cells in allergic inflammation and response. It causes a cascade of inflammation and strongly increases vascular permeability within minutes through its four G-protein-coupled receptors (GPCRs) on endothelial cells. High mobility group box-1 (HMGB1), a nonhistone chromatin-binding nuclear protein, can be actively secreted into the extracellular space by endothelial cells. HMGB1 has been reported to exert pro-inflammatory effects on endothelial cells and to increase vascular endothelial permeability. However, the relationship between histamine and HMGB1-mediated signaling in vascular endothelial cells and the role of HMGB1 in anaphylactic-induced hypotension have never been studied.

Methods and results: EA.hy 926 cells were treated with different concentrations of histamine for the indicated periods. The results showed that histamine induced HMGB1 translocation and release from the endothelial cells in a concentration- and time-dependent manner. These effects of histamine were concentration-dependently inhibited by *d*-chlorpheniramine, a specific H_1 receptor antagonist, but not by H_2 or $H_{3/4}$ receptor antagonists. Moreover, an H_1-specific agonist, 2-pyridylethylamine, mimicked the effects of histamine, whereas an H_2-receptor agonist, 4-methylhistamine, did not. Adrenaline and noradrenaline, which are commonly used in the clinical treatment of anaphylactic shock, also inhibited the histamine-induced HMGB1 translocation in endothelial cells. We therefore established a rat model of allergic shock by i.v. injection of compound 48/80, a potent histamine-releasing agent. The plasma HMGB1 levels in compound 48/80-injected rats were higher than those in controls. Moreover, the treatment with anti-HMGB1 antibody successfully facilitated the recovery from compound 48/80-induced hypotension.

Conclusion: Histamine induces HMGB1 release from vascular endothelial cells solely through H_1 receptor stimulation. Anti-HMGB1 therapy may provide a novel treatment for life-threatening systemic anaphylaxis.

KEYWORDS

Histamine, HMGB1, vascular endothelial cell, H_1 receptor, hypotension

Introduction

Histamine, 2-(4-imodazole)-ethylamine, is synthesized from L-histidine exclusively by histidine decarboxylase and can be produced by various cells, including central nervous system neurons, vascular endothelial cells (VECs), gastric mucosa parietal cells, mast cells, basophils and lymphocytes (1). Histamine plays an important role both in normal human physiology as well as in various pathologies, such as allergic inflammation and response (2–4), gastric acid secretion (5), neurotransmission in the central nervous system (6, 7), and the regulation of innate immune response (8, 9). Anaphylactic shock (AS) often results from an immunoglobulin E (IgE)-mediated systemic allergic reaction. AS is characterized by vasodilation and vascular leakage, and causes a rapid decrease in systemic arterial blood pressure that contributes to the onset of hypotension (10–12). Histamine is a major inducer of vascular hyperpermeability, and thus it is a central component of permeability-related human pathologies, such as allergy and anaphylaxis (13). Histamine released from mast cells and basophils triggers acute symptoms due to its very rapid activity on the vascular endothelium and bronchial and smooth muscle cells, which leads to a rapid increase in vascular permeability within minutes. Histamine-induced production of NO through eNOS in the VECs also results in NO diffusion into the smooth muscle cell layer in the vessel wall and dilates smooth muscle cells by activating cytosolic guanylate cyclase (14).

Histamine acts through its four G-protein-coupled receptors (GPCRs), histamine receptors 1 to 4 (H_1R to H_4R) (15, 16). These vascular effects of histamine are in general mediated by histamine H_1-receptor and constitute the main actions of histamine on blood vessels (14), whereas the H_2-receptor modifies gastric acid secretion, airway mucus production, and vascular permeability (16). The H_3-receptor has been shown to be involved in neuron-inflammatory diseases (17). The H_4-receptor plays an important role in allergy and inflammation (18).

High mobility group box-1 (HMGB1) is a ubiquitous nuclear protein that binds to chromatin DNA, thereby regulating transcription activity and maintaining chromatin structure (19, 20). Under injurious stimuli and stress, HMGB1 is translocated from nuclei to the extracellular space through the cytosolic compartment (21). Extracellular HMGB1 is now recognized as a representative damage-associated molecular pattern (DAMP) and has been shown to be involved in many diseases as an inflammation enhancer through the direct stimulation of TLR-4/2 and RAGE as well as through complex formation with IL-1β and CXCL12, with subsequent enhancement of the activation of cognate receptors (22). In addition, HMGB1 may carry LPS to Kupffer cells, leading to the efficient production of inflammatory cytokines in a gasdermin- and caspase-dependent manner (23). Among the diverse range of effects of HMGB1 on cellular responses, the effects on capillary blood vessels are especially notable. In an ischemic/reperfusion model in rats, it was demonstrated that HMGB1 released from neurons and other cells directly affected the BBB-constituting cells, VECs and pericytes, leading to increased permeability and brain edema formation (24, 25). In peripheral capillary endothelial cells in culture, an HMGB1-induced contractile response and subsequent increase in permeability were observed (26). However, whether histamine-induced vascular permeability is related with HMGB1 release from endothelial cells has never been investigated.

VECs should be controlled precisely depending on the micromilieu. Under a resting condition, the luminal surface of VECs is maintained in an anti-coagulation state. At the same time, the interaction between endothelial cells and blood cells is expected to be kept minimal. However, once the disruption of vascular walls occurs or agonistic stimuli reach the endothelial cells, rapid changes in the cellular phenotype should occur, including phenotypic changes related to the direction of coagulation or facilitation of inflammation through the migration of infiltrating leukocytes. To elucidate these phenomena, numerous bioactive factors on VECs that finely tune the state of VECs have been identified. In the previous study (27), we demonstrated that LPS and TNF-α induced the release of HMGB1 from VECs in culture, associated with the production of the inflammatory cytokines and the expression of adhesion molecules on their surface although the signaling pathways leading to the translocation of HMGB1 remain unclear.

In the present study, we found that a classical mediator of inflammation, histamine, concentration-dependently caused HMGB1 release from VECs in culture through the stimulation of specific H_1-receptor. Moreover, our findings suggest that the hypotensive response induced *in vivo* by a liberator of histamine from mast cells may be mediated in part by HMGB1. These findings will provide new insights into our understanding of vascular biology and could lead to therapeutic strategies for histamine-induced vascular reactions in allergy and anaphylaxis.

Materials and methods

Chemicals and reagents

Histamine dihydrochloride was obtained from Nakalai Tesque (Kyoto, Japan). 2-Pyridylethylamine dihydrochloride and 4-methylhistamine dihydrochloride were gifts from Drs. W.A.M. Duncan and G.J. Durant (The Research Institute, Smith Kline & French Laboratories, Welwyn Garden City, Herts). d-Chlorpheniramine maleate and famotidine were obtained from Takeda Pharmaceutical Company (Osaka, Japan) and Yamanouchi Pharmaceuticals (Tokyo), respectively. Compound 48/80 trihydrochloride was obtained from Funakoshi (Tokyo).

Cell cultures

EA.hy 926 endothelial cells (ATCC Cat# CRL-2922, RRID: CVCL_3901), a hybridoma of human umbilical vein endothelial cells (HUVECs) and the human epithelial cell line A549, were cultured using Dulbecco's modified Eagle medium (DMEM, #D6546, Sigma, St. Louis, MO) supplemented with 10% fetal bovine serum (Gibco, Grand Island, NY), 5% L-glutamine (#G7513, Sigma), and 10% penicillin/streptomycin (Gibco) in 5% CO_2 at 37°C. After reaching confluence, the EA.hy 926 cells were detached from culture flasks using 0.25% Trypsin-EDTA (Gibco), washed, and resuspended in DMEM. The cells were used between the third and sixth passage in our experiments.

Immunostaining assay

EA.hy 926 cells were pretreated with FBS-free medium for 1 h before being stimulated with different concentrations of histamine (Nakalai Tesque) for the indicated periods. The cells were then fixed with 4% paraformaldehyde (Wako Pure Chemical Industry, Osaka, Japan) and blocked with 3% bovine serum albumin (BSA), after which the cells were stained by anti-HMGB1 Ab (rabbit, Sigma, RRID:AB_444360) for 1 h at 37°C followed by Alexa Fluor 488-labeled anti-rabbit/mouse IgG. Cell nuclei were stained with DAPI for 5 min, and then observed using a confocal microscope (LSM 780, Carl Zeiss).

Cell viability

EA.hy 926 cells were plated in 96-well plates at 5×10^5 overnight, and then pre-incubated with histamine at the indicated concentrations. The cells were then incubated with MTT at 37 °C for 4 h by adding 10 µl of 5 ng/ml MTT solution to each well. After removal of the cell supernatant, 200 µl of DMSO was added to each well to dissolve the crystals. The absorbance of each well was measured using a microplate reader (model 680; Bio-Rad) at 570 nm wavelength, and the optical density (OD) value was recorded.

Quantitative real-time polymerase chain reaction (qRT-PCR)

EA.hy 926 endothelial cells were harvested and mRNA was extracted using an RNeasy mini kit (Qiagen). Total RNA (1 µg/sample) was incubated with the components of the PrimeScriptR RT reagent kit (Takara Bio, Shiga, Japan; Code No. RR036A) at 37°C for 15 min. The cDNA was then amplified with a SYBRR Premix Ex Taq^{TM} (Tli RNaseH Plus) Kit (Takara Bio, Shiga, Japan; Code No. RR420A) with a Light Cycler (Roche, Basel, Switzerland). All operations followed the manufacturer's protocol. The mRNA expressions of all genes were normalized to the housekeeping gene, β-actin. The fold changes between groups were calculated using the Ct value with the $2^{-\Delta\Delta Ct}$ method ($\Delta Ct = Ct_{\text{target gene}} - Ct_{\beta\text{-actin}}$). Primers were designed according to published sequences (see the Supplementary materials and methods; Table S1).

Enzyme-linked immunosorbent assay (ELISA)

To determine HMGB1 levels in plasma, blood samples were collected through the rat heart under deep anesthesia, then centrifuged for 10 min at 3000 rpm. The cell culture medium was collected after treatment to measure the release of HMGB1 from the cell to the supernatant, and then centrifuged for 10 min at 3000 rpm. HMGB1 was detected by using an ELISA kit (Shino-Test Co., Sagamihara, Japan) according to the manufacturer's instructions.

Effects of histamine receptor subtype-selective agonists and antagonists on HMGB1 mobilization

EA.hy 926 cells were prepared as described above. To determine the effects of receptor subtype-selective antagonists on histamine-induced translocation of HMGB1, EA.hy 926 cells were preincubated with 1 µM *d*-chlorpheniramine (H_1-selective antagonist), famotidine (H_2-selective antagonist) or

thioperamide (H_3/H_4-selective antagonist) for 1 h. The cells were then stimulated with histamine (1 μM) for 12 h. To determine the effects of receptor subtype-selective agonists, 2-pyridylethylamine (H_1-selective agonist) or 4-methylhistamine (H_2-selective agonist) was used instead of histamine. Immunostaining of HMGB1 was performed as described above.

Animals

Experiments were performed using 8-week-old male Wistar rats (body weight: 250 ± 15 g) housed in groups of three in polypropylene cages with a 12-h light-dark cycle at 24–26°C and ad libitum food and water. After a 1-week acclimatization, rats were divided among three groups of six rats each: an experimental group consisting of sensitized rats treated with PBS 1 min after shock induction; an anti-HMGB1 mAb group consisting of sensitized rats treated with α-HMGB1 mAb (2 mg/kg) 1 min after shock induction; and an anti-KLH mAb group consisting of sensitized rats treated with α-KLH mAb (2 mg/kg) 1 min after shock induction.

Anaphylactic shock animal model

Rats were anesthetized with pentobarbital sodium solution (40 mg/kg) administered intraperitoneally. Then, the tissue was bluntly separated, the white ligament of the left leg was found, and the femoral artery was exposed by clamping the hemostatic forceps. Approximately 2 cm of the femoral artery was isolated, a NO. 4-0 surgical suture was passed through the radial and distal ends, and ligation was performed at the distal ends. Arterial puncture was performed with a 24G trocar between the two wires, and then the needle was removed. A blood pressure measuring device was connected to the end of the trocar, and the trocar was fixed to a real-time blood pressure recording system (Shino Test Co.) *via* a pressure transducer to measure the systolic, diastolic, and mean arterial blood pressure (MAP) and heart rate (HR). To prepare the anaphylaxis model, rats were administered a mast cell degranulation agent, compound 48/80, at a dose of 0.5 mg/kg body weight through the tail vein. After AS induction, rats in the three groups were administered with PBS, anti-KLH antibody (2 mg/kg) or anti-HMGB1 antibody (2 mg/kg) through the tail vein, respectively. Measurement of hemodynamic parameters was performed every 5 min for a period of 30 min before the compound 48/80 challenge. The hemodynamic parameters were recorded for 60 min at 1 min intervals after the compound 48/80 challenge.

Statistical analysis

The data were analyzed with GraphPad Prism software ver. 6.01 (GraphPad, San Diego, CA). All values are presented as the means ± SEM and were analyzed by an analysis of variance (ANOVA) followed by Bonferroni's test or *post hoc* Fisher test when the F statistic was significant. Probability (p) values <0.05 were considered significant. At least three independent experiments were performed for all of the assays.

Results

Histamine induced HMGB1 translocation and release from VECs

HMGB1 was exclusively localized in the nuclear compartment in the EA.hy 926 VECs under a resting condition (Figure 1A). Histamine (1 μM) time-dependently induced the translocation of HMGB1 from the nuclei to cytosolic compartment. The translocation of HMGB1 was quantified by the fluorescence intensity of HMGB1 remaining in the cell nuclei of endothelial cells after histamine stimulation (Figure 1B). It appeared that the immunoreactivity of HMGB1 in the nuclei was time-dependently decreased whereas that in the cytosolic compartment was increased (Figure1A). The effects of histamine on HMGB1 translocation at 12 h were concentration-dependent at concentrations from 0.01 μM to 10 μM (Figures 1C, D). To determine whether HMGB1 was further released into the cell culture media, we determined the HMGB1 levels in the supernatant with ELISA. As shown in Figure 1E, HMGB1 was released from VECs into the media after stimulation with histamine in a concentration-dependent manner.

HMGB1 can be actively released from cells in response to various stimuli and also passively released from cells during cell necrosis or apoptosis (27). In order to clarify whether HMGB1 was actively or passively released from the VECs after the stimulation with histamine, we evaluated the cell viability after the histamine stimulation (Figure 1F). The results showed that the stimulation with different concentrations of histamine did not change the cell viability of VECs (Figure 1F), which means that histamine actively induced the translocation and release of HMGB1 from VECs.

Involvement of H_1 receptor in the effects of histamine on HMGB1 translocation and release from VECs

Histamine acts through its four G-protein-coupled receptors (GPCRs), histamine receptors 1 to 4 (H_1R to H_4R) (9). To examine the effects of histamine on HMGB1 translocation and release from VECs, we first used RT-PCR to confirm the expression of histamine receptor subtypes H_1, H_2, and H_3 in EA.hy 926 cells (Figure 2A). The expressions of H_1R and H_2R mRNA were increased 5-fold and 45%, respectively, after the incubation with histamine (1 μM) for 12 h, whereas that of H_3R mRNA was not changed (Figure 2A). To examine which

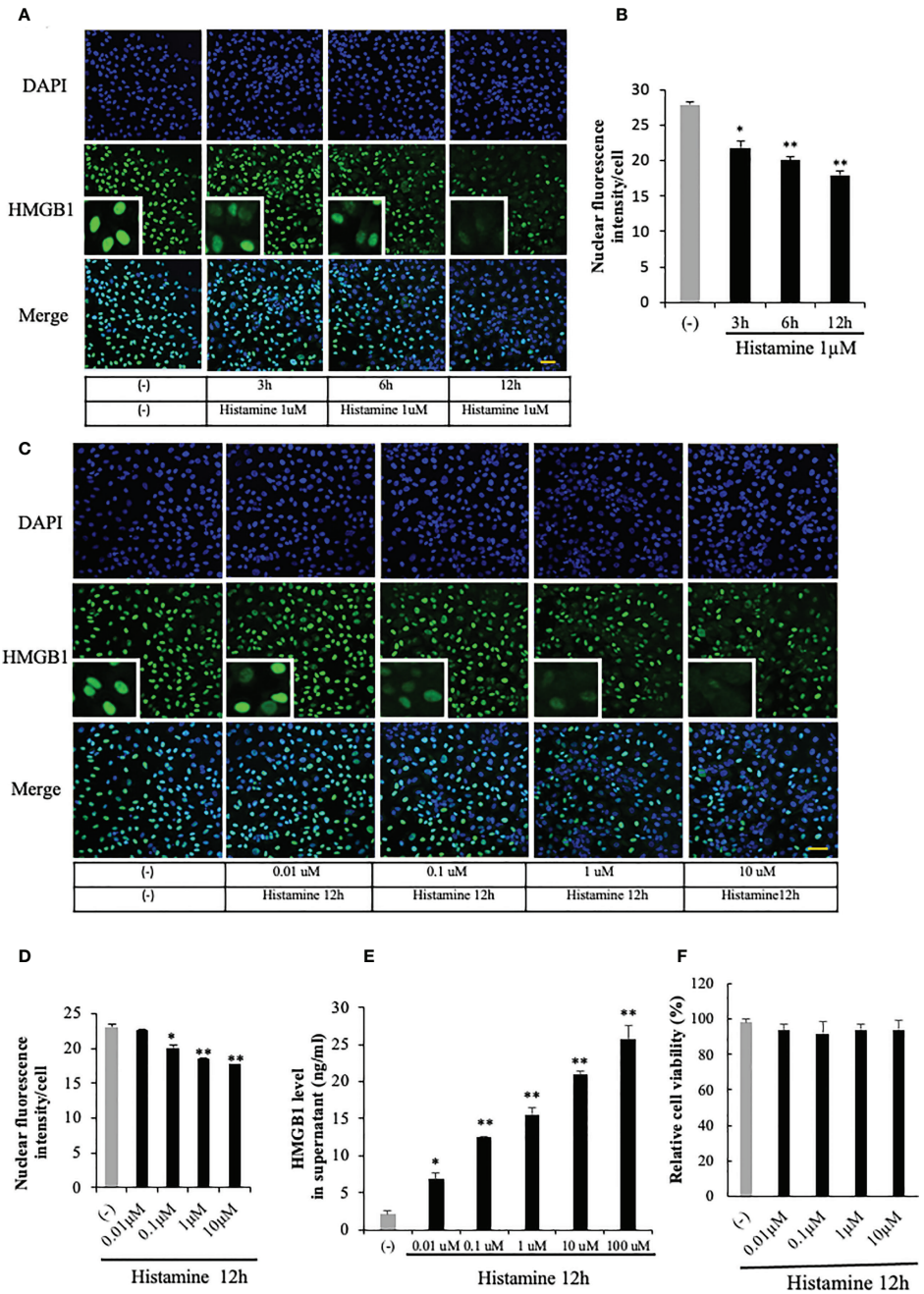

FIGURE 1
HMGB1 translocation and release from VECs after histamine stimulation. **(A)** EA.hy 926 endothelial cells were stimulated with histamine (1 μM) for the periods indicated. HMGB1 was observed by immunostaining with green fluorescence and cell nucleus was observed by blue fluorescence after staining with DAPI. Scale bar = 10 μm, (n=5 per group). **(B)** The translocation of HMGB1 was quantified by the residual presence of the HMGB1 (green fluorescence) in the cell nucleus in each cell. The results were quantified by ImageJ software and are expressed as the ratio of total nuclear HMGB1 intensity/cell numbers. **(C, D)** EA.hy 926 cells were stimulated with the indicated concentrations of histamine for 12 h, and the HMGB1 in the nucleus was determined by the immunostaining (n=5 per group). **(E)** Endothelial cells were cultured for 12 h with different concentrations of histamine. The cell culture medium was collected and analyzed for HMGB1 release by ELISA. All results are the means ± SEM of five different experiments. **(F)** Effects of histamine on the viability of EA.hy 926 cells. EA.hy 926 cells were stimulated with different concentrations of histamine for 12 h. The cells were then incubated with MTT at 37°C for 4 h by adding 10 μl of 5 ng/ml MTT solution to each well. After removal of the cell supernatant, 200 μl of DMSO was added to each well to dissolve the crystals. The OD value was recorded using a microplate reader at 570 nm wavelength. All results are the means ± SEM of three different experiments, (n=5 per group). Statistical analyses were conducted by one-way ANOVA followed by the *post hoc* Fisher test. *p<0.05, **p<0.01 vs. control in the absence of histamine.

receptor was responsible for the histamine-induced translocation and release of HMGB1 from VECs, the receptor subtype-specific antagonists, *d*-chloropheniramine for H_1R, famotidine for H_2R and thioperamide for $H_{3/4}R$, were used. The cells were preincubated with one of the antagonists for 1 h before stimulation with histamine (1 μM). The translocation and release of HMGB1 were evaluated 12 h thereafter (Figures 2B–D). An H_1R-selective antagonist, *d*-chloropheniramine (1 μM), but not either famotidine (1 μM) or thioperamide (1 μM), inhibited the translocation induced by histamine (1 μM) (Figure 2B). The inhibitory effects of *d*-chloropheniramine were concentration-dependent (0.01–1 μM) (Figure 2C). We also confirmed that the secretion of HMGB1 into media induced by histamine (1 μM) was antagonized solely by *d*-chloropheniramine (1 μM). Moreover, an H_1R-selective agonist, 2-pyridylethylamine (28), but not an H_2R-selective agonist, 4-methylhitamine (29), mimicked the effects of histamine in regard to HMGB1 translocation (Figures 3A, B) and release into media (Figure 3C). These results as a whole indicated that the receptor subtypes involved in histamine-induced translocation and release of HMGB1 in VECs was H_1 receptor.

Calcium-dependency of the effects of histamine on HMGB1 translocation and release from VECs

The intracellular signaling systems mediated by H_1R have been well documented (14, 15). H_1R stimulation activates phospholipase Cβ *via* $G_{q/11}$ and the resultant production of IP3 in turn induces calcium mobilization from ER calcium stores. Therefore, if the event of HMGB1 mobilization induced by H_1R stimulation occurs downstream of calcium mobilization, the blocking of calcium signals may lead to the diminution of HMGB1 mobilization. Figure 4 shows that a membrane-permeable calcium chelator, BAPTA-AM (5 μM), significantly inhibited the mobilization as well as the release of HMGB1 induced by histamine (1 μM) (Figures 4A–C), suggesting that free calcium in the cytosolic compartment plays a fundamental role in the mobilization of HMGB1.

Effects of adrenaline and noradrenaline on histamine-induced translocation of HMGB1 in VECs

Because HMGB1 has been reported to induce endothelial contraction and hyperpermeability (25, 26), the results obtained above imply a novel mechanism of histamine-induced anaphylactic shock—namely, histamine could cause the HMGB1 release from VECs through H_1R and lead to the hypotension. In an anaphylactic emergency, adrenaline administration is the first-choice treatment for restoring the blood pressure. Accordingly, we examined the effects of adrenaline and noradrenaline on the histamine-induced HMGB1 in endothelial cells. The results showed that both adrenaline (5 μM) and noradrenaline (5 μM) effectively inhibited the HMGB1 translocation (Figures 5A, B). Adrenomedullin is a potent long-acting vasodilatory peptide which contains 52 amino acids and is produced in vascular endothelial cells. Although adrenomedullin has anti-inflammatory activity, however, adrenomedullin (5 μM) did not show any effects on histamine-induced translocation of HMGB1.

Effects of anti-HMGB1 mAb on compound 48/80-induced anaphylactic shock in rats

Histamine is a major inducer of vascular hyperpermeability, and is thus a central component of permeability-related human pathologies, such as allergy and anaphylaxis. Histamine in the granules of mast cells and basophils is released from preformed stores in an antigen-IgE-dependent manner, leading to a rapid increase in vascular permeability within minutes and causing hypotension. We established an anaphylactic shock model in rats by the intravenous injection of compound 48/80, a mast cell degranulator. We first collected blood samples from rats 10 min after injection with compound 48/80, and found that plasma HMGB1 levels were significantly increased in the compound 48/80-treated rats compared with the non-treated controls (Figure 6A). The post-treatment of rats with the anti-HMGB1 mAb (2 mg/kg, i.v.) reduced the increase in plasma HMGB1 levels compared with the control IgG- and PBS-treated groups (Figure 6A). Then, we measured the mean arterial blood pressure of rats and observed a sharp drop of blood pressure from 120 to 30 mmHg at 10 min after the injection of compound 48/80. This hypotensive state in PBS-treated rats continued until 20 min post-injection and then gradually recovered to the level of 60 mmHg by 60 min post-injection (Figure 6B). The post-treatment of rats with the anti-HMGB1 mAb reduced the maximal decreased level of mean arterial blood pressure and accelerated the recovery of hypotension significantly. At the end of the recording period (at 60 min), the mean arterial blood pressure in the anti-HMGB1 mAb-treated group was above 100 mmHg (Figure 6B). Figure 6C shows the magnitudes of recovery of the mean arterial blood pressure at the indicated time points from the lowest blood pressure. These results demonstrated that the compound 48/80-histamine-induced rapid hypotension was at least partly caused by the HMGB1 release, and that the neutralization of circulating HMGB1 by anti-HMGB1 mAb inhibited the anaphylactic hypotension.

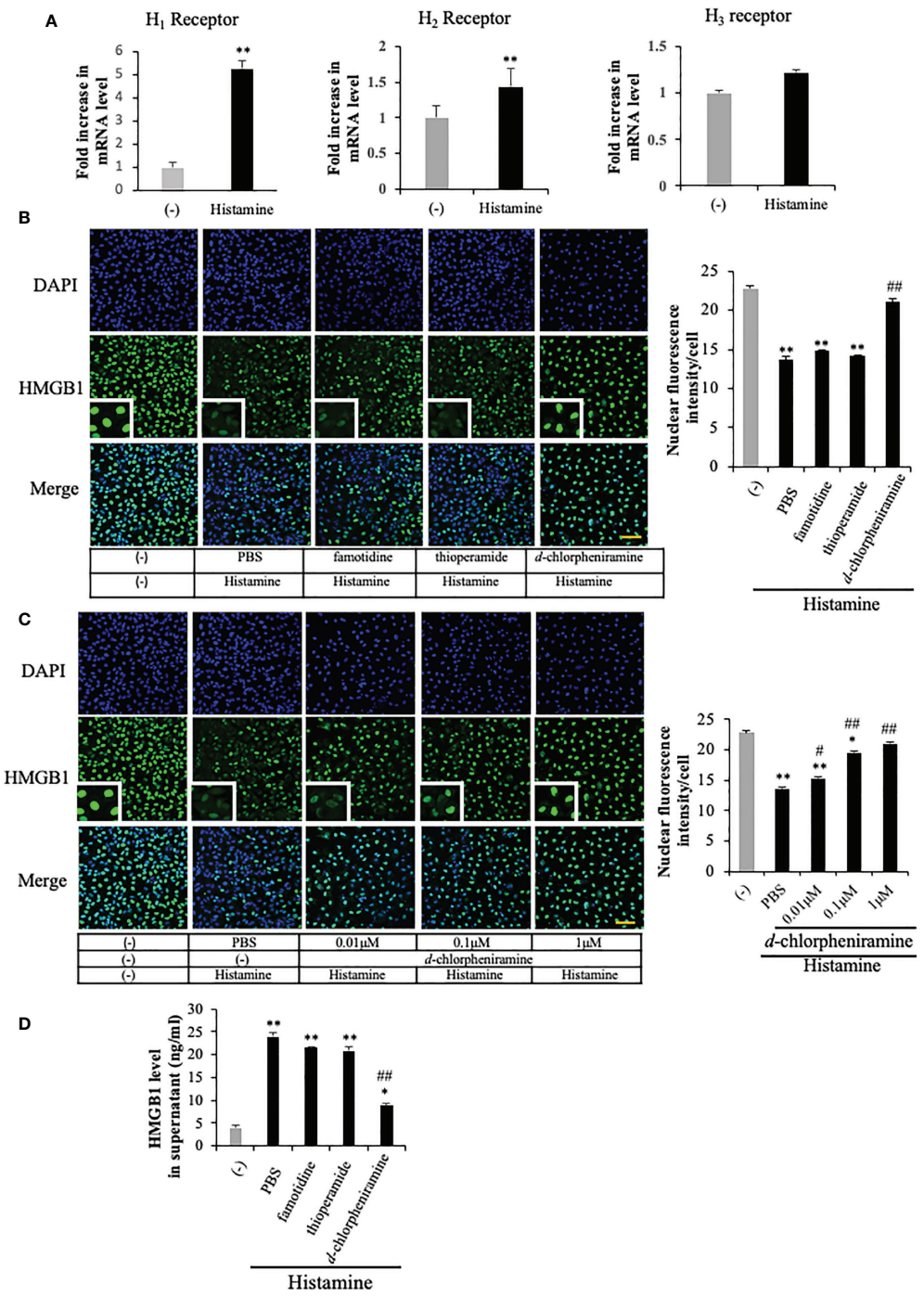

FIGURE 2
The involvement of histamine receptor subtypes in the histamine-induced HMGB1 release in VECs. **(A)** EA.hy 926 cells were cultured with histamine (1 μM) for 12 h. The mRNA expression of each histamine receptor in the presence or absence of histamine in the cells was measured by quantitative RT-PCR. The results were normalized to the expression of β-actin and are expressed as the mean ± SEM (n=5 per group). **(B)** EA.hy 926 cells were preincubated with each antagonist for 1 h before stimulation with histamine (1 μM). HMGB1 translocation was determined by immunostaining at 12 h after histamine stimulation. Scale bar = 10 μm. **(C)** Different concentrations of *d*-chloropheniramine were preincubated with the EA.hy 926 cells for 1 h before stimulation with histamine (1 μM) for 12 h. HMGB1 in the cell nucleus is quantified in the right panel of each group as the means ± SEM (n=5 per group). **(D)** EA.hy 926 cells were preincubated with each antagonist (1 μM) for 1 h. At 12 h after stimulation with histamine (1 μM), the amount of HMGB1 released into the medium was determined. Statistical analyses were conducted by one-way ANOVA followed by the *post hoc* Fisher test. *p<0.05, **p< 0.01 vs. control in the absence of histamine, $^{\#}$p<0.05, $^{\#\#}$p<0.01 vs. histamine-PBS group.

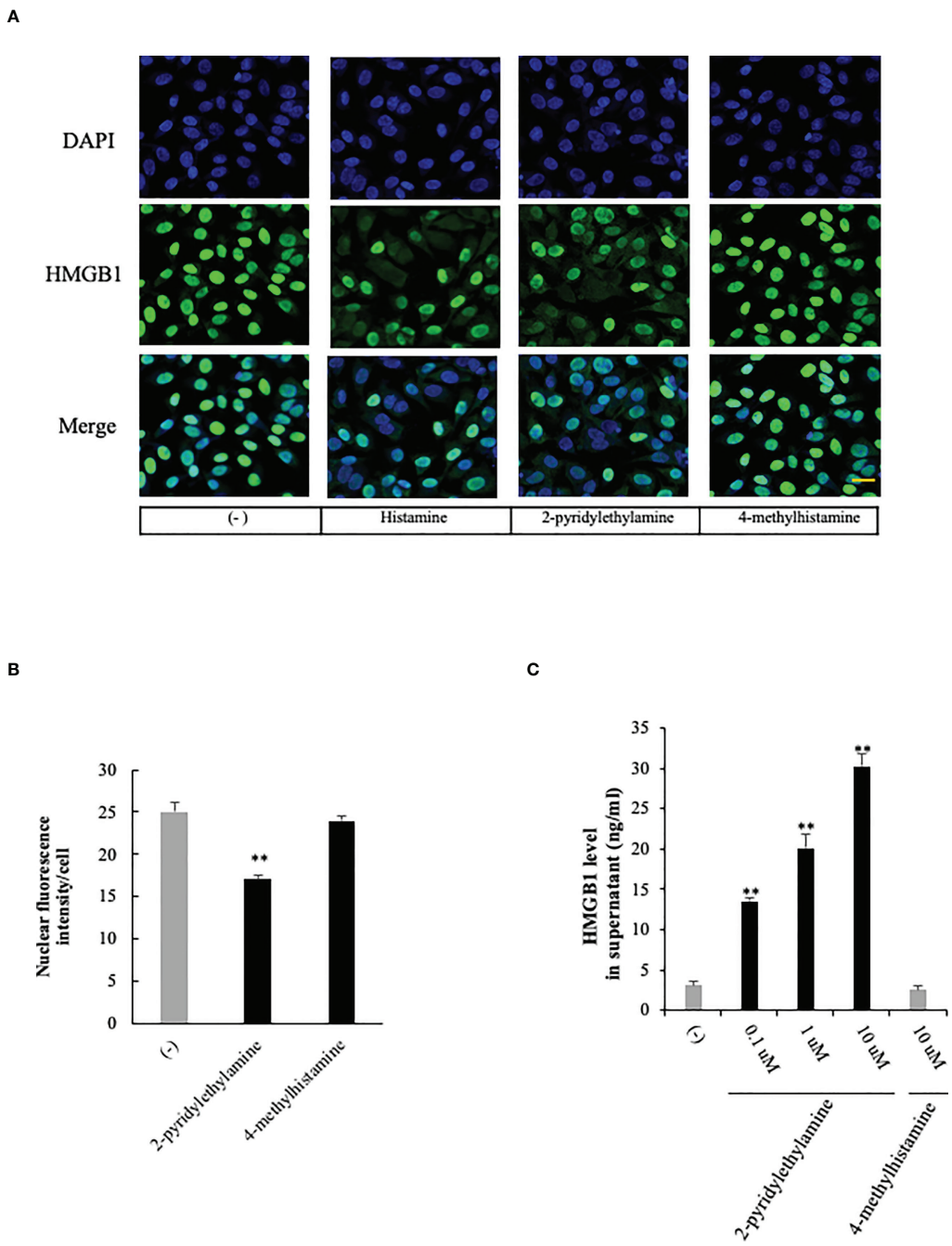

FIGURE 3
Effects of selective histamine receptor agonists on HMGB1 release from VECs. **(A)** EA.hy 926 cells were incubated with 2-pyridylethylamine (H_1R-selective agonist) or 4 methylhitamine (H_2R-selective agonist) for 6 h. HMGB1 translocation was observed with immunostaining as described in Figure 1. Scale bar = 10 µm. **(B)** The results were quantified by ImageJ software and are expressed as the ratio of total nuclear HMGB1 intensity/cell numbers. **(C)** The cell culture medium was collected and the HMGB1 released into media was measured by ELISA. All results are the means ± SEM of five different experiments, (n=5 per group). One-way ANOVA followed by the *post hoc* Fisher test. **p<0.01 vs. control in the absence of agonist.

Discussion

The results of the present study clearly demonstrated that histamine induced the mobilization of HMGB1 from nuclei to the extracellular space through the cytosolic compartment in VECs (Figure 1). The release of HMGB1 induced by histamine was concentration- and time-dependent. The translocation of HMGB1 appeared to proceed in a manner quite similar to those

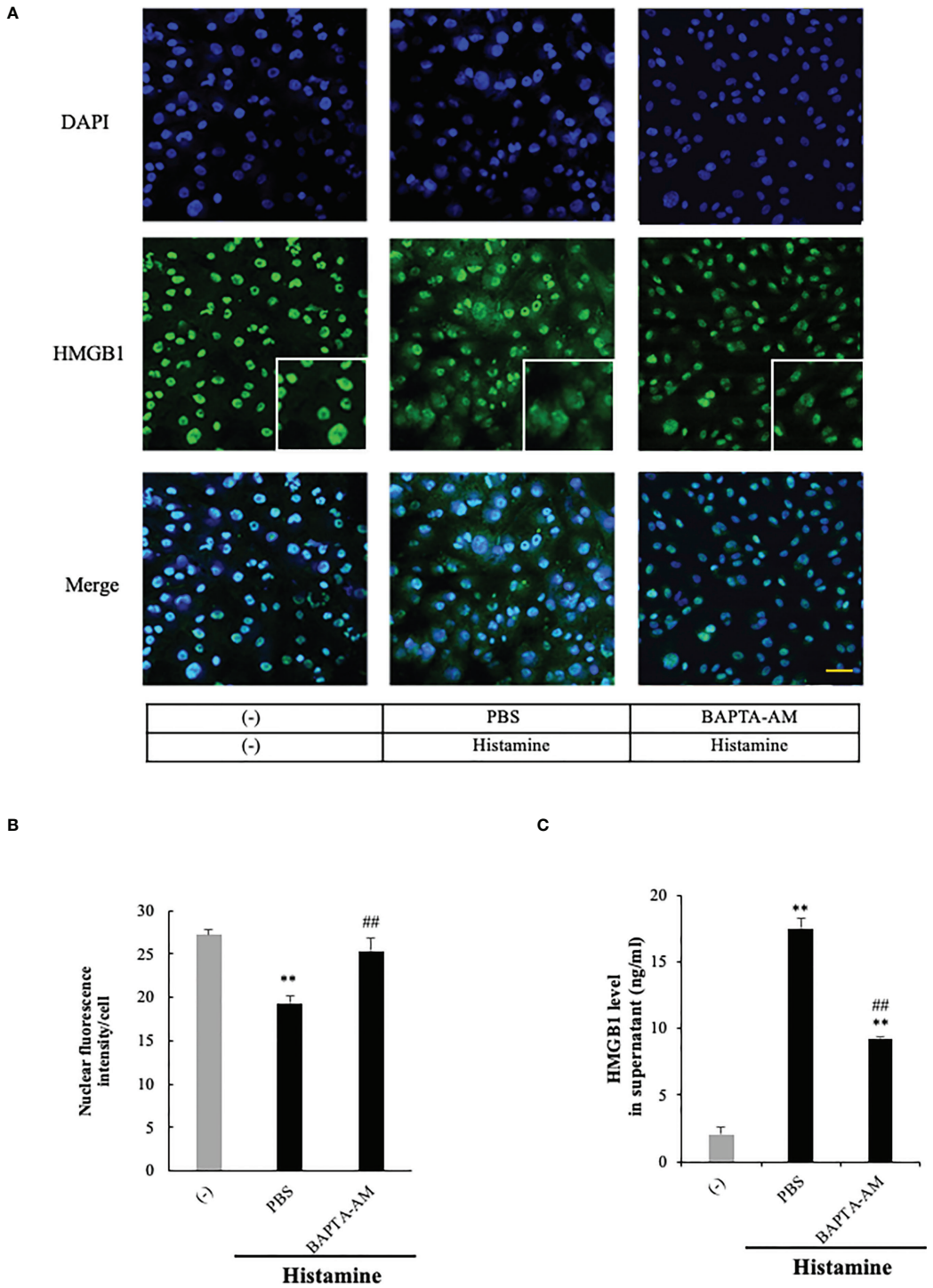

FIGURE 4
Histamine-induced HMGB1 release occurred in a Ca^{2+}- dependent manner. **(A)** Confluent EA.hy 926 cells were preincubated with the Ca^{2+} chelator BAPTA-AM (5 uM) or PBS for 1 h. The cells were then stimulated with histamine (1 μM) for 12 h. HMGB1 translocation in VECs was observed by immunostaining. Scale bar = 10 μm. **(B)** The results were quantified by ImageJ software and are expressed as the ratio of total nuclear HMGB1 intensity/cell numbers. **(C)** The release of HMGB1 into the cell culture medium was measured by ELISA. The results shown are the means ± SEM of three experiments, (n=3 per group). One-way ANOVA followed by the *post hoc* Fisher test. **p<0.01 vs. control in the absence of histamine, $^{\#\#}$p<0.01 vs. histamine-PBS group.

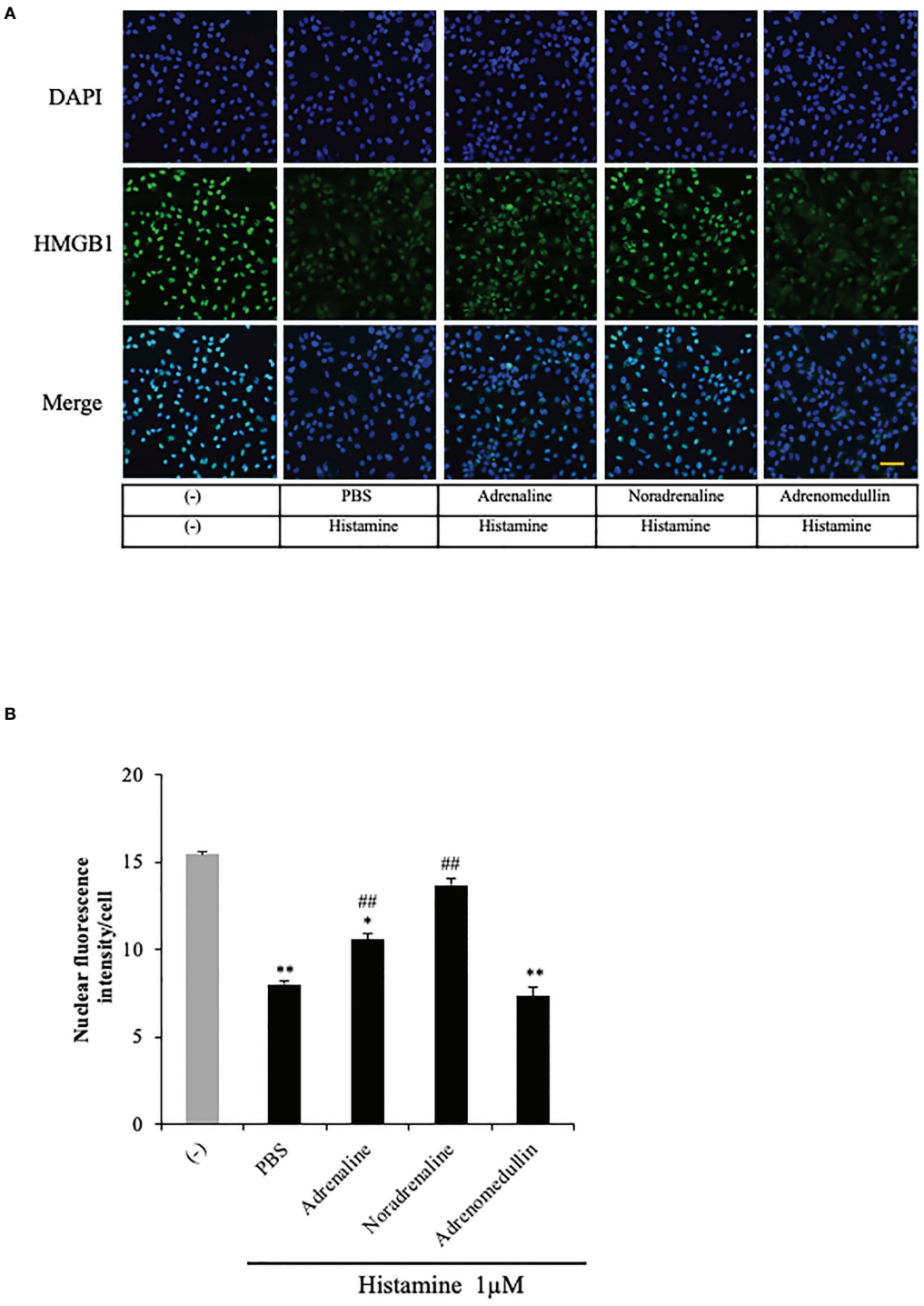

FIGURE 5
Effects of adrenaline and noradrenaline on histamine-induced HMGB1 translocation in VECs. **(A)** EA.hy 926 cells were preincubated with adrenaline, noradrenaline or adrenomedullin (5 μM) for 1 h before stimulation with histamine (1 μM). The translocation of HMGB1 was determined by immunostaining. The results are representative of ≥5 experiments. Scale bar = 10 μm. **(B)** The HMGB1 translocations were quantified by ImageJ software and expressed as the ratio of nuclear HMGB1 intensity against the total cell number. The results shown are the means ± SEM of five different experiments, (n=5 per group). One-way ANOVA followed by the *post hoc* Fisher test. *p<0.05, **p<0.01 vs. control in the absence of histamine, $^{\#\#}$p<0.01 vs. histamine-PBS group.

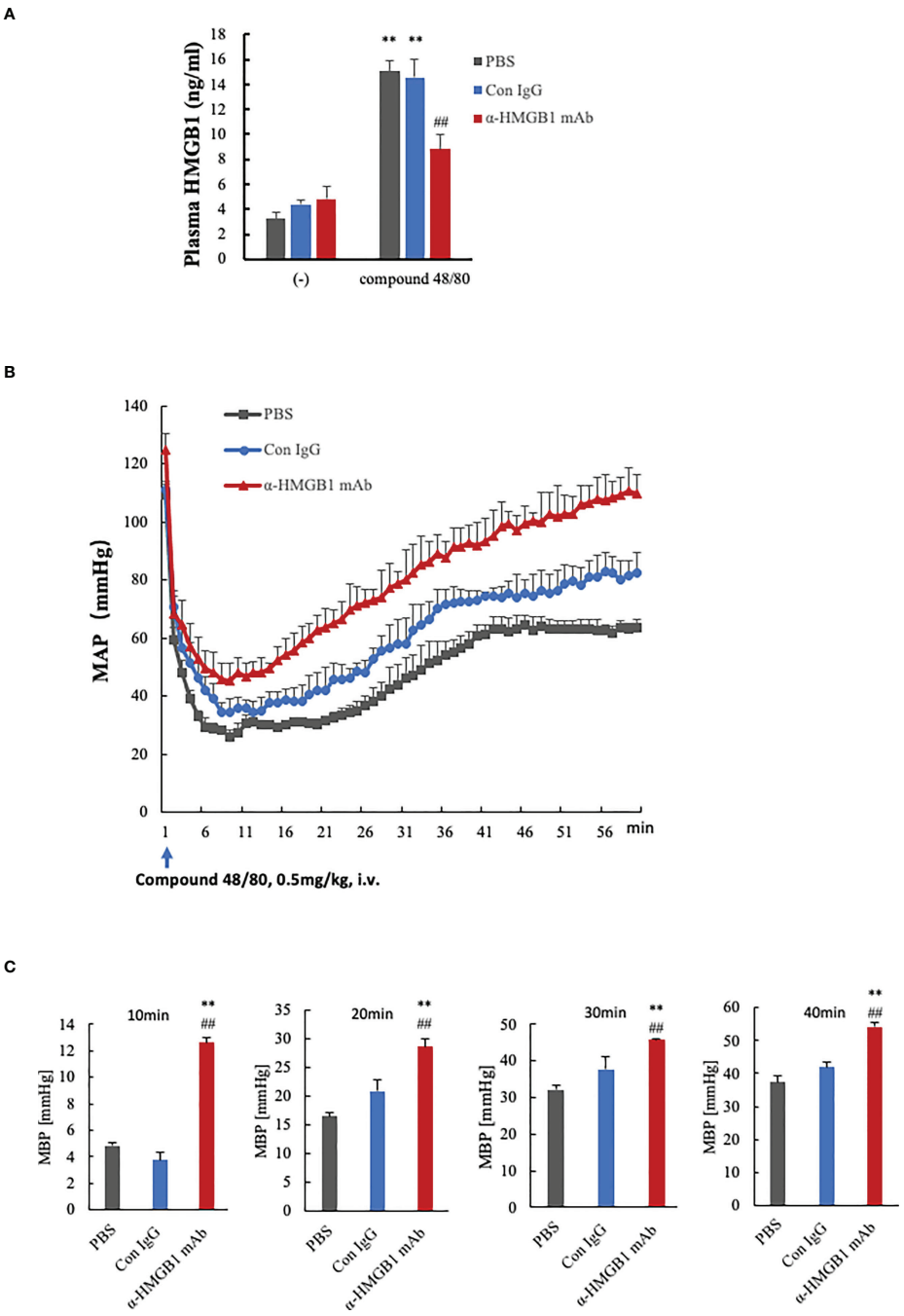

FIGURE 6
Effects of anti-HMGB1 mAb on a compound 48/80-induced rat model of anaphylactic shock. Wistar Rats were given compound 48/80, a mast cell degranulation agent, at a dose of 0.5 mg/kg through the tail vein to induce anaphylactic shock. One minute after compound 48/80 injection, the rats were treated with PBS, anti-KLH mAb (2 mg/kg) or anti-HMGB1 mAb (2 mg/kg) through the tail vein. Measurement of hemodynamic parameters was performed every 5 min for a period of 30 min before the compound 48/80 challenge. The hemodynamic parameters were recorded for 60 min at 1 min intervals after the compound 48/80 challenge. **(A)** Plasma levels of HMGB1 in rats at 10 min after compound 48/80 injection were determined by ELISA. **(B)** Records of mean arterial blood pressure (MAP, mmHg) of rats treated with PBS, control mAb or anti-HMGB1Ab. MAP was recorded every minute until the end of the experiment at 60 min. Each point represents the means ± SEM of six rats, (n=6 per group). All results are the mean ± SEM of five different experiments. One-way ANOVA followed by the *post hoc* Fisher test. **p<0.05 vs. PBS, $^{\#\#}$p<0.05 vs. Control IgG. **(C)** The absolute increase in the value of MBP from the lowest after AS induction to the indicted time was quantified in each group. one-way ANOVA followed by the *post hoc* Fisher test. **p<0.05 vs. control, $^{\#\#}$p<0.05 vs. Con IgG.

induced by LPS and TNF-α (27). The experiments using receptor subtype-specific agonists showed that 2-pyridyl ethylamine was a specific agonist for H_1-receptors, and produced a similar HMGB1 mobilizing activity to histamine, whereas H_2-receptor agonist (4-methylhistamine) (30) did not (Figures 3A, B). Also, *d*-chlorpheniramine, a specific antagonist for H_1-receptor, concentration-dependently inhibited the HMGB1 translocation induced by histamine, while an H_2-receptor antagonist (famotidine) or $H_{3/4}$ antagonist (thioperamide) (31) did not produce any effects (Figures 2B–D). Taken together, these results indicated that the only receptor subtype involved in the action of histamine on HMGB1 mobilization in VECs was the H_1-receptor.

It is well known that H_1 receptor stimulation by histamine causes remarkable functional changes in VECs, including NO production, eNOS induction, upregulation of surface expression of E-selectin, IL-8 secretion and cell contraction (32). The expression of E-selectin induces the rolling of leukocytes on the endothelial cells through the interaction with PSGL-1 (33), which facilitates the inflammatory responses (34). Moreover, NO produced in the endothelial cells diffuses into the smooth muscle cells, leading to the dilatation of vessels (35). The contraction of endothelial cells of postcapillary venules leads to the leakage of plasma proteins and the formation of tissue edema. A previously reported *in vivo* experiment showed that histamine-induced hyperpermeability was dependent predominantly on NO-mediated dilation of vascular smooth muscle and the subsequent blood flow increase, and partially on PKC/ROCK/NO-dependent endothelial barrier disruption (36). HMGB1 can be actively released from the VECs upon exposure to various stimuli, such as LPS or TNF-α (29). The released HMGB1 can further activate endothelial cells, leading to up-regulation of the cell adhesion molecules ICAM-1, VCAM-1, and E-selectin, and is involved in the cytokine secretion in cells (37, 38). The released HMGB1 has also been found to induce early EC barrier disruption, with a potential molecular mechanism being activation of the RhoA/ROCK1 signaling pathway by HMGB1 *via* RAGE (39). These similarities between HMGB1 and histamine in the regulation of cell inflammatory and endothelial cell permeability indicate a possible relationship between them in the vascular system.

Anaphylaxis is triggered by a specific antigen binding to IgE antibody on the surface of mast cells and basophils (40). Histamine is a biogenic amine stored in the granules of mast cells and basophils and a well-known mediator of anaphylaxis (41). The massive release of granule constituents from these cells causes a rapid decrease in arterial blood pressure (42). In the present study, we mimicked the anaphylactic response by intravenous injection of compound 48/80, a mast cell stimulator, in rats. The compound 48/80-induced hypotension was accompanied by an elevation of plasma HMGB1 (Figure 6A). The post-treatment of rats with a neutralizing antibody against HMGB1 significantly accelerated the recovery from the hypotensive response induced by compound 48/80 (Figure 6B). These results strongly suggest that HMGB1 is involved in the hypotensive response to compound 48/80. They also suggest the possibility that histamine released from mast cells in response to compound 48/80 induced the translocation and extracellular release of HMGB1 from VECs.

HMGB1 is expressed ubiquitously in almost all kinds of cells, while not all kinds of cells can actively release HMGB1 after stimulation. Although there is little information about the HMGB1 release from mast cells, one report showed the lack of release of HMGB1 from the murine mast cell line C57 and the human mast cell line HMC-1.2 after stimulation with different cytokines and antigen-IgE (43). In our study, we observed that HMGB1 can be released from vascular endothelial cells after stimulation with histamine *in vitro*. During the anaphylactic response, histamine released from mast cells and basophils gets into blood stream and can easily access to the vascular endothelial cells, therefore, we speculated that the HMGB1 was mainly released from vascular endothelial cells in this process although the release of HMGB1 from other types of cells could not be excluded.

Piao et al. reported that recombinant HMGB1 alone induced a release of β-hexosaminidase associated with the up-regulation of TLR4, Myd88 and NF-kB nuclear translocation in rat basophil leukemic cell line, RBL-2H3, whereas the knockdown of HMGB1 in RBL-2H3 by siRNA of HMGB1 suppressed the expression of TLR4/Myd88-signaling molecules and reduced the secretory response induced by antigen-IgE (44). These results suggested that endogenous HMGB1 may be involved in activation of signaling machinery in basophils and play an important role in the secretory response of basophils. On the other hand, there is little information about the involvement of endogenous HMGB1 in mast activation and secretion. Further works are necessary on this line. Collectively, the results of this study suggest that HMGB1 released from VECs into the blood stream by histamine is at least partly involved in the hypotensive response to compound 48/80 in a paracrine manner. It is noteworthy that the agents currently used for clinical treatment of anaphylaxis, adrenaline and noradrenaline, efficiently inhibited the nuclear translocation of HMGB1 induced by histamine in the present study (Figures 5A, B). Consequently, it is likely that the clinical therapeutic effects of these catecholamines may be ascribed at least in part to the inhibition of HMGB1 release from VECs and the subsequent protection of endothelial cells from the effects of HMGB1.

Zhang et al. (25) observed a direct action of recombinant HMGB1 on a reconstituted blood-brain barrier composed of brain VECs, pericytes and astrocytes. In this system, HMGB1 induced a contractile response in both endothelial cells and pericytes, leading to an increase in BBB permeability. The HMGB1 release from neurons was evident after the brain ischemia/reperfusion or brain trauma in rats (24, 25), indicating that HMGB1 was increased in both plasma and the CNS. The released HMGB1 probably reached the BBB and impaired its structure and function, leading to the brain edema formation and associated brain injury. The treatment with anti-HMGB1 neutralizing antibody used in the present study efficiently inhibited the BBB disruption and the

accompanying inflammatory responses that were mediated by cytokine and inflammation-related molecules in the brain (24, 25). Accordingly, anti-HMGB1 mAb therapy may be very useful to prevent the actions of HMGB1 on VECs. In the case of impairment of BBB integrity in the brain, it has been suggested that both RAGE and TLR4 are involved in the direct effects of HMGB1 on endothelial cells and pericytes (25, 26). Therefore, it might be possible that the HMGB1 released by histamine in turn stimulates endothelial cells in an autocrine and a paracrine fashion. There are several kinds of important factors that induce the contraction of endothelial cells and increase capillary permeability, such as bradykinin, leukotriene C4 and PAF (45–47). However, it remains to be determined whether all of these factors can induce translocation and release of HMGB1 from endothelial cells.

The effects of histamine were thought to be mediated by a rapid and transient increase in cytosolic calcium levels *via* the production of IP3 by activation of phospholipase-Cβ. We also observed that the HMGB1 translocation induced by histamine was Ca^{2+} dependent (Figures 4A–C). The initial intracellular signaling triggered by H_1-receptor stimulation may induce the rapid production of NO, leading to a quick vasodilatory response through diffusion into the smooth muscle cells. However, the mobilization and release of HMGB1 was time-dependent over hours as in the case of eNOS induction, the secretion of IL-8 and von Willebrand factor, and the surface expression of E-selectin. Thus, H_1-receptor stimulation appears to induce rather long-lasting cellular effects by the downstream signaling events, leading to the individual cellular responses. The H_1-receptor upregulation observed in the present study may be one such long-lasting response, which would be consistent with the results reported previously (48).

The intracellular signals triggered by H_1 receptor stimulation include Gq/G_{12} activation, phospholipase C activation and IP3-induced calcium mobilization (49–51). Therefore, it is quite probable that the HMGB1 mobilization occurs downstream of these events. Previously, we observed that an HMGB1 translocation induced by TNF-α or LPS was similar to that induced by histamine in present study. Since the intracellular signalings induced by TNFR1/2 and TLR4/MD2/CD14 are quite different from that induced by histamine H_1 receptor, a G protein-coupled receptor. At present, little is known about the mechanism of HMGB1 mobilization, except for the possible chemical modification of HMGB1 (52). Therefore, the pathway leading to the HMGB1 translocation and release in VECs by histamine stimulation need to be studied in the future.

Data availability statement

The original contributions presented in the study are included in the article/Supplementary Material. Further inquiries can be directed to the corresponding author.

Ethics statement

The animal study was reviewed and approved by Okayama University.

Author contributions

SG conceived the study, designed the experiments, analyzed data, and wrote the manuscript. MN and HW for editing the manuscript. KL, WK, and DW performed the animal experiments. KT and HQ for critically reviewing the manuscript. All authors contributed to the article and approved the submitted version.

Funding

This work was supported by funds from the National Key R&D Program of China (Grant No. 2021YFE0109300). The work was also supported by a MHLW research on chronic pain Program Grant (JPMHLW22FG1003), a Grant-in-Aid for Scientific Research (no.19H03408 to MN), a Grant-in-Aid for Young Scientists (no. 17K15580 to HW) from the Japan Society for the Promotion of Science (JSPS). The author S.G. was supported by a funding from Tsinghua University-Peking University Joint Center for Life Sciences.

Conflict of interest

The authors declare that the research was conducted in the absence of any commercial or financial relationships that could be construed as a potential conflict of interest.

Publisher's note

Supplementary material

The Supplementary Material for this article can be found online at: https://www.frontiersin.org/articles/10.3389/fimmu.2022.930683/full#supplementary-material

References

1. Jutela M, Blaser K, Akdis CA. Histamine in allergic inflammation and immune modulation. *Int Arch Allergy Immunol* (2005) 137:82–92. doi: 10.1159/000085108

2. Jutel M, Watanabe T, Akdis M, Blaser K, Akdis CA. Immune regulation by histamine. *Curr Opin Immunol* (2002) 14(6):735–40. doi: 10.1016/s0952-7915(02)00395-3

3. Akdis CA, Blaser K. Histamine in the immune regulation of allergic inflammation. *J Allergy Clin Immunol* (2003) 112(1):15–22. doi: 10.1067/mai.2003.1585

4. MaGlashan DJr. Histamine: A mediator of inflammation. *J Allergy Clin Immunol* (2003) 112(4 suppl):S53–9. doi: 10.1016/s0091-6749(03)01877-3

5. Morini G, Grandi D, Stark H, Schunack W. Histamine H_3-receptor antagonists inhibit gastroprotection by (R)-alpha-methylhistamine in the rat. *Br J Pharmacol* (2000) 129(8):1579–600. doi: 10.1038/sj.bjp.0703249

6. Haas H, Panula P. The role of histamine and the tuberomamillary nucleus in the nervous system. *Nat Rev Neurosci* (2003) 4(2):121–30. doi: 10.1038/nrn1034

7. Higuchi M, Yanai K, Okamura N, Meguro K, Arai H, Itoh M, et al. Histamine H_1 receptors in patients with alzheimer's disease assessed by positron emission tomography. *Neuroscience* (2000) 99(4):721–9. doi: 10.1016/s0306-4522(00)00230-x

8. Yokoyama M, Yokoyama A, Mori S, Takahashi H, Yoshino T, Watanabe T, et al. Inducible histamine protects mice from p.acnes-primed and LPS-induced hepatitis through H_2-receptor stimulation. *Gastroenterology* (2004) 127(3):892–902. doi: 10.1053/j.gastro.2004.06.020

9. Wake H, Takahashi H, Mori S, Liu K, Yoshino T, Nishibori M. Histamine inhibits advanced glycation end products-induced adhesion molecule expression on human monocytes. *J Parmacol Exp Ther* (2009) 330(3):826–33. doi: 10.1124/jpet.109.155960

10. Brown SG. Cardiovascular aspects of anaphylaxis: implications for treatment and diagnosis. *Curr Opin Allergy Clin Immunol* (2005) 5(4):359–64. doi: 10.1097/01.all.0000174158.78626.35

11. Triggiani M, Patella V, Staiano RI, Granata F, Marone G. Allergy and the cardiovascular system. *Clin Exp Immunol* (2008) 153(Suppl 1):7–11. doi: 10.1111/j.1365-2249.2008.03714.x

12. Faye N, Fournier L, Balvay D, Thiam R, Orliaguet G, Clement O, et al. Macromolecular capillary leakage is involved in the onset of anaphylactic hypotension. *Anesthesiology* (2012) 117(5):1072–9. doi: 10.1097/ALN.0b013e31826d3dc5

13. White MV. The role of histamine in allergic diseases. *J Allergy Clin Immunol* (1990) 86:599–605. doi: 10.1016/s0091-6749(05)80223-4

14. Li H, Burkhardt C, Heinrich UR, Brausch I, Xia N, Förstermann U. Histamine upregulates gene expression of endothelial nitric oxide synthase in human vascular endothelial cells. *Circulation* (2003) 107(18):2348–54. doi: 10.1161/01.CIR.0000066697.19571.AF

15. Thurmond RL, Gelfand EW, Dunford PJ. The role of histamine H_1 and H_4 receptors in allergic inflammation: the search for new antihistamines. *Nat Rev Drug Discovery* (2008) 7(1):41–53. doi: 10.1038/nrd2465

16. Seifert R, Strasser A, Schneider EH, Neumann D, Dove S, Buschauer A. Molecular and cellular analysis of human histamine receptor subtypes. *Trends Pharmacol Sci* (2013) 34(1):33–58. doi: 10.1016/j.tips.2012.11.001

17. Singh M, Jadhav HR. Histamine H_3 receptor function and ligands: recent developments. *Mini Rev Med Chem* (2013) 13(1):47–57. doi: 10.2174/1389557511307010047

18. Thurmond RL. The histamine H_4 receptor: from orphan to the clinic. *Front Pharmacol* (2015) 6:65. doi: 10.3389/fphar.2015.00065

19. Bianchi ME, Agresti A. HMG proteins: dynamic players in gene regulation and differentiation. *Curr Opin Genet Dev* (2005) 15:496–506. doi: 10.1016/j.gde.2005.08.007

20. Pil PM, Lippard SJ. Specific binding of chromosomal protein HMG1 to DNA damaged by the anticancer drug cisplatin. *Science* (1992) 256(5054):234–7. doi: 10.1126/science.1566071

21. Wang H, Bloom O, Zhang M, Vishnubhakat JM, Ombrellino M, Che J, et al. HMG-1 as a late mediator of endotoxin lethality in mice. *Science* (1999) 285(5425):248–51. doi: 10.1126/science.285.5425.248

22. Venereau E, Ceriotti C, Bianchi ME. DAMPs from cell death to new life. *Front Immunol* (2015) 6:422. doi: 10.3389/fimmu.2015.00422

23. Li W, Deng M, Loughran PA, Yang M, Lin M, Yang C, et al. LPS induces active HMGB1 release from hepatocytes into exosomes through the coordinated activities of TLR4 and caspase-11/GSDMD signaling. *Front Immunol* (2020) 11:229. doi: 10.3389/fimmu.2020.00229

24. Liu K, Mori S, Takahashi HK, Tomono Y, Wake H, Kanke T, et al. Anti-high mobility group box 1 monoclonal antibody ameliorates brain infarction induced by transient ischemia in rats. *FASEB J* (2007) 21(14):3904–16. doi: 10.1096/fj.07-8770com

25. Zhang J, Takahashi HK, Liu K, Wake H, Liu R, Maruo T, et al. Anti-high mobility group box-1 monoclonal antibody protects the blood-brain barrier from ischemia-induced disruption in rats. *Stroke* (2011) 42(5):1420–8. doi: 10.1161/STROKEAHA.110.598334

26. Namba T, Tsuge M, Yashiro M, Saito Y, Liu K, Nishibori M, et al. Anti-high mobility group box 1 monoclonal antibody suppressed hyper-permeability and cytokine production in human pulmonary endothelial cells infected with influenza a virus. *Inflammation Res* (2021) 70(10-12):1101–11. doi: 10.1007/s00011-021-01496-5

27. Gao S, Wake H, Sakaguchi M, Wang D, Takahashi Y, Teshigawara K, et al. Histidine-rich glycoprotein inhibits HMGB1-mediated pathway in vascular endothelial cells through CLEC1A. *iScience* (2020) 23(6):101180. doi: 10.1016/j.isci.2020.101180

28. Leurs R, Smit MJ, Meeder R, Laak AM, Timmerman H. Lysine200 located in the fifth transmembrane domain of the histamine H_1 receptor interacts with histamine but not with all H_1 agonists. *Biochem Biophys Res Commun* (1995) 214(1):110–7. doi: 10.1006/bbrc.1995.2263

29. Black JW, Duncan WA, Durant CJ, Ganellin CR, Parsons EM. Definition and antagonism of histamine H_2-receptors. *Nature* (1972) 236(5347):385–90. doi: 10.1038/236385a0

30. Nishibori M. Cyclic AMP increase in canine parotid gland mediated by histamine H2-receptors. *Eur J Pharmacol* (1981) 76(4):309–16. doi: 10.1016/0014-2999(81)90101-1

31. Leurs R, Smit MJ, Timmerman H. Molecular pharmacological aspects of histamine receptors. *Pharmacol Ther* (1995) 66(3):413–63. doi: 10.1016/0163-7258(95)00006-3

32. Guo M, Breslin JW, Wu MH, Gottardi CJ, Yuan SY. VE-cadherin and beta-catenin binding dynamics during histamine-induced endothelial hyperpermeability. *Am J Physiol Cell Physiol* (2008) 294(4):C977–84. doi: 10.1152/ajpcell.90607.2007

33. Zanardo RC, Bonder CS, Hwang JM, Andonegui G, Liu L, Vestweber D, et al. A down-regulatable e-selectin ligand is functionally important for PSGL-1-independent leukocyte-endothelial cell interactions. *Blood* (2004) 104(12):3766–73. doi: 10.1182/blood-2004-02-0578

34. Welsh LC, Dejana E, McDonald DM. Permeability of the endothelial barrier: identifying and reconciling controversies. *Trends Mol Med* (2021) 27(4):314–31. doi: 10.1016/j.molmed.2020.11.006

35. Cyr AR, Huckaby LV, Shiva SS, Zuckerbraun BS. Nitric oxide and endothelial dysfunction. *Crit Care Clin* (2020) 36(2):307–21. doi: 10.1016/j.ccc.2019.12.009

36. Ashina K, Tsubosaka Y, Nakamura T, Omori K, Kobayashi K, Hori M, et al. Histamine induces vascular hyperpermeability by increasing blood flow and endothelial barrier disruption. *vivo. PLoS One* (2015) 10(7):e0132367. doi: 10.1371/journal.pone.0132367

37. Fiuza C, Bustin M, Talwar S, Tropea M, Gerstenberger E, Shelhamer JH, et al. Inflammation promoting activity of HMGB1 on human microvascular endothelial cells. *Blood* (2003) 101(7):2652–60. doi: 10.1182/blood-2002-05-1300

38. Treutiger CJ, Mullins GE, Johansson AS, Rouhiainen A, Rauvala HM, Erlandsson-Harris H, et al. High mobility group 1 b-box mediates activation of human endothelium. *J Intern Med* (2003) 254(4):375–85. doi: 10.1046/j.1365-2796.2003.01204.x

39. Zhao MJ, Jiang HR, Sun JW, Wang ZA, Hu B, Zhu CR, et al. Roles of RAGE/ROCK1 pathway in HMGB1- induced early changes in barrier permeability of human pulmonary microvascular endothelial cell. *Front Immunol* (2021) 12:697071. doi: 10.3389/fimmu.2021.697071

40. Nguyen SMT, Rupprecht CP, Haque A, Pattanaik D, Yusin J, Krishnaswamy G. Mechanism governing anaphylaxis: inflammatory cells, mediators, endothelial gap junctions and beyond. *Int J Mol Sci* (2021) 22(15):7785. doi: 10.3390/ijms22157785

41. Nakamura T, Murata T. Regulation of vascular permeability in anaphylaxis. *Br J Pharmacol* (2018) 175(13):2538–42. doi: 10.1111/bph.14332

42. Ziogas A, Sajib MS, Lim JH, Alves TC, Das A, Witt A, et al. Glycolysis is integral to histamine-induced endothelial hyperpermeability. *FASEB J* (2021) 35(3):e21425. doi: 10.1096/fj.202001634R

43. Wahamaa H, Vallerskog T, Qin S, Lunderius C, LaRosa G, Andersson U, et al. HMGB1-secreting capacity of multiple cell lineages revealed by a novel

HMGB1 ELISPOT assay. *J Leukoc Biol* (2007) 81(1):129–36. doi: 10.1189/jlb.0506349

44. Piao Y, Jiang J, Wang Z, Wang C, Jin S, Li L, et al. Glaucocalyxin a attenuates allergic responses by inhibiting mast cell degranulation through p38MAPK/NrF2/HO-1 and HMGB1/TLR4/NF-κB signaling pathways. *Evid Based Complement Alternate Med* (2021) 2021:6644752. doi: 10.1155/2021/6644751

45. Oschatz C, Maas C, Lecher B, Jansen T, Björkqvist J, Tradler T, et al. Mast cells increase vascular permeability by heparin-initiated bradykinin formation. *vivo. Immun* (2011) 24(2):258–68. doi: 10.1016/j.immuni.2011.02.008

46. Ueno A, Tanaka K, Katori M, Hayashi M, Arai Y. Species difference in increased vascular permeability by synthetic leukotriene C4 and D4. *Prostaglandins* (1981) 21(4):637–48. doi: 10.1016/0090-6980(81)90012-5

47. Francis H, Glaser S, Demorrow S, Gaudio E, Ueno Y, Venter J, et al. Small mouse cholangiocytes proliferate in response to H1 histamine receptor stimulation by activation of the IP3/CaMK I/CREB pathway. *Am J Physiol Cell Physiol* (2008) 295(2):C499–513. doi: 10.1152/ajpcell.00369.2007

48. Clavijo LC, Carter MB, Matheson PJ, Wilson MA, Wead WB, Garrison RN. PAF increases vascular permeability without increasing pulmonary arterial pressure in the rat. *J Appl Physiol* (1985) 90(1):261–8. doi: 10.1152/jappl.2001.90.1.261

49. Carrillo JJ, Pediani J, Milligan G. Dimers of class a G protein-coupled receptors function *via* agonist-mediated trans-activation of associated G proteins. *J Biol Chem* (2003) 278(43):42578–87. doi: 10.1074/jbc.M306165200

50. Galeotti N, Malmberg-Aiello P, Bartolini A, Schunack W, Ghelardini C. H1-receptor stimulation induces hyperalgesia through activation of the phospholipase c-PKC pathway. *Neuropharmacology* (2004) 47(2):295–303. doi: 10.1016/j.neuropharm.2004.03.013

51. Mizuguchi H, Kitamura Y, Takeda N, Fukui H. "Molecular Signaling and Transcriptional Regulation of Histamine H1 Receptor Gene". In: Yanai K, Passani MB editors. *Current Topics in Behavioral Neurosciences*. Heidelberg, Berlin: Springer Press (2021), P91–110.

52. Chen R, Kang R, Tang D. The mechanism of HMGB1 secretion and release. *Exp Mol Med* (2022) 54(2):91–102. doi: 10.1038/s12276-022-00736-w

Frontiers in Immunology

Explores novel approaches and diagnoses to treat immune disorders.

The official journal of the International Union of Immunological Societies (IUIS) and the most cited in its field, leading the way for research across basic, translational and clinical immunology.

Discover the latest Research Topics

See more →

Frontiers

Avenue du Tribunal-Fédéral 34
1005 Lausanne, Switzerland
frontiersin.org

Contact us

+41 (0)21 510 17 00
frontiersin.org/about/contact